AD-A037 037   NAVY ELECTRONICS LAB SAN DIEGO CALIF   F/G 20/4
                PROCEEDINGS TECHNICAL WORKSHOP: HYDRODYNAMIC DESIGN AND EVALUAT--ETC(U)
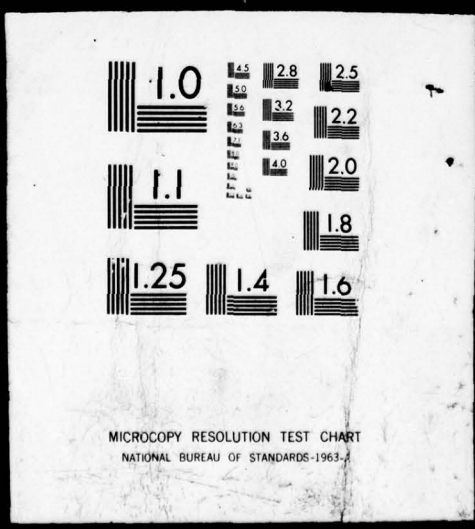   JAN 67

UNCLASSIFIED   NL

                1 OF 4

        AD
        A037037

AD
A037037

MICROCOPY RESOLUTION TEST CHART
NATIONAL BUREAU OF STANDARDS-1963-A

MOST Project – 4

ADA037037

DDC
RECEIVED
MAR 9 1977
C

Proceedings

TECHNICAL WORKSHOP: HYDRODYNAMIC DESIGN AND EVALUATION OF CABLE-TOWED SONAR SYSTEMS (U)

23-27 January 1967

Host: U.S. Navy Electronics Laboratory, San Diego, California 92152

GP. 1

10

6

Proceedings

TECHNICAL WORKSHOP:

Hydrodynamic Design and Evaluation
of Cable-Towed Sonar Systems

D D C
RECEIVED
MAR 9 1977
C

23-27 January 1967

Held at the

U. S. NAVY ELECTRONICS LABORATORY
SAN DIEGO, CALIFORNIA

11   27 Jan 67

12   377 p.

253550

This report contains a collection of papers which were presented at a technical workshop on the Hydrodynamic Design and Evaluation of Cable-Towed Sonar Systems. The workshop was held at the U.S. Navy Electronics Laboratory, 23-27 January 1967.

Statements and opinions contained herein are those of the authors and individual participants, and are not to be construed as reflecting the official opinions of the participating agencies. Papers have been printed in this publication substantially as submitted by the authors.
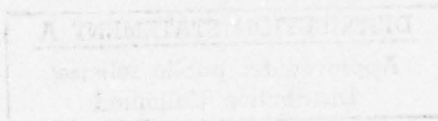
TECHNICAL WORKSHOP STAFF

Chairman

Mr. D. E. Calkins

Coordinator

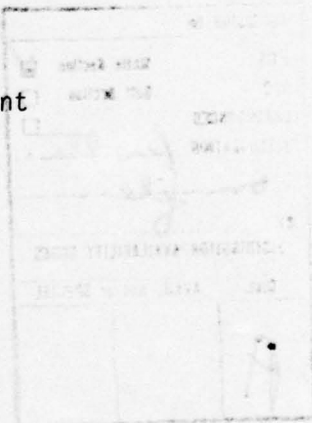Mr. F. D. Parker

Hosts

Mr. D. D. Washburn
Mr. C. N. Miller

PARTICIPATING AGENCIES

HOST	NEL	U.S. Navy Electronics Laboratory San Diego, California
<u>UNITED</u> <u>STATES</u>	DTMB	David Taylor Model Basin Washington, D.C.
	USL	Navy Underwater Sound Laboratory New London, Connecticut
	NUWRES	Naval Underwater Weapons Research and Engineering Station Newport, Rhode Island
		Ballard and Associates Pasadena, California
		The Boeing Company Seattle, Washington
		Hydronautics, Inc. Laurel, Maryland
		Hydrospace Research Corp. Rockville, Maryland
		North American Aviation, Inc. Anaheim, California
<u>CANADA</u>	NRC	National Research Council Ottawa, Canada
	NRE	Naval Research Establishment Halifax, Nova Scotia

CONTENTS

INTRODUCTION

The Technical Workshop on the Hydrodynamic Design and Evaluation of Cable-Towed Sonar Systems represents the third in a series of seminars on the subject of Hydromechanics. The first two gatherings were formally known respectively as the Tripartite Conference on Hydrodynamics of Ship-Towed, Cable-Body Systems, held in May 1958 at the David Taylor Model Basin, and the Tripartite Seminar on the Hydromechanics of High Speed Towing held in October 1965 at the Naval Research Establishment, Dartmouth, Nova Scotia.

The Workshop, although related to the two previous seminars, differed in two respects this year. Representatives from Great Britain were not in attendance (hence deletion of tripartite title), and selected contractors were invited to report on work being performed under present Navy contracts apropos of the aims of the meeting.

The purpose of the workshop was to provide a meeting place among specialists involved in the towed-sonar program for informal discussion on the following subjects:

Towed System Dynamics;

Towed Body Hydrodynamics;

Faired Towline Hydrodynamics; and

Towed System Evaluation.

Representatives of both Canada and the United States were in attendance.

It was agreed that the next Workshop would be held in September of 1969, and would be hosted by the David Taylor Model Basin.

In accordance with recommendation #4 of the 1965 meeting, NEL has prepared bibliographies for each of the four subject divisions. These are included at the end of each session.

blank

SESSION 1
Towed System Dynamics

Dr. J. D. Burroughs
The Boeing Company

<u>Dynamic Analysis and Simulation of Towed Systems</u>

Mr. A. R. Lagasse
Naval Underwater Weapons Research and Engineering
Station

<u>Stability Criteria for Faired Cable</u>

Dr. G. A. Hegemier
Ballard & Associates

<u>Faired Towcable Divergence Criteria</u>

Mr. J. S. Kanno
North American Aviation

<u>The Divergence and Flutter Criteria for Faired Tow</u>

<u>Cables</u>

DYNAMIC ANALYSIS AND SIMULATION OF TOWED SYSTEMS

by Dr. John D. Burroughs
Research Engineer
The Boeing Company
Seattle, Washington

ABSTRACT

An analysis of the static and dynamic behavior of towed systems with freedom to move in three dimensional space has been performed by The Boeing Company for the U. S. Navy. This analysis was performed with the aid of a large active-analog computer. A brief description is presented of the original approach taken and subsequent modifications which have been made to permit a wide range of towed systems to be analyzed. The form of data output that is available from the simulation is presented.

INTRODUCTION

During 1965, The Boeing Company was engaged in the preliminary design of a high performance towed system under U. S. Navy Contract N123(953)52187A. Included in the work of this contract was a dynamic analysis of the resultant towed system. This analysis was performed by means of an analog simulation of the cable and depressor body, which were free to move in three dimensional space. The simulation was used in the selection of the depressor body configuration and in the design of an active control system for the body. The static cable shape and body location as well as the dynamic motion of the system in response to towing ship motion were predicted by the simulation.

During 1966, The Boeing Company was awarded a U. S. Navy contract to extend the capabilities of the simulation developed under Contract N123(953)52187A to allow a wide range of towed systems to be analyzed. This work is currently underway.

This paper presents a brief description of the analytical approach that has been taken by The Boeing Company in analyzing towed systems. Representative results of the simulation operation are presented to demonstrate its capabilities. A complete derivation of equations and a description of the simulation work done in 1965 may be found in Reference (1). A similar report of current Boeing towed system analysis work is given in Reference (2).

DESCRIPTION OF 1965 BOEING TOWED SYSTEM ANALYSIS

MECHANICAL MODEL OF CABLE

A flexible, faired cable presents a difficult problem in dynamic analysis. The exact equations of three dimensional motion of the cable are a set of nonlinear partial differential equations. At the present time there is no direct means for solving equations of this type by either analog or digital computation. Thus, in order to analyze the behavior of the cable it is necessary to describe its motion with either difference or differential equations. The difference equations approximate the motion of the cable at discrete points in space and time while the differential equations approximate the motion at discrete points in space.

The approach taken for all Boeing cable simulation work to date has been to represent the cable at discrete points in space but continuously in time, by the use of a set of nonlinear differential equations. These equations may be thought of as describing the motion of a mechanical model of the cable which consists of n rigid segments. Each segment is allowed three angular degrees of freedom with respect to a coordinate system fixed to the towing craft. Thus it is assumed that elongation of the cable is negligible. The mass of the cable is distributed throughout the mechanical model by placing appropriate point masses at each end of each segment.

The hydrodynamic forces acting on the cable are represented by forces which act at the center of each rigid model segment. These forces are nonlinear functions of the relative water velocities of each segment. Included in these forces are the effects of cable pressure drag, friction drag, and side lift.

The elastic properties of the cable are represented in the mechanical model by springs located at each joint between segments. These springs resist bending or twisting about any of the three axes of motion of each segment relative to its adjacent segments.

Fig. 1 shows a pictorial representation of the cable mechanical model. The spheres represent the points of mass concentration. Included in each sphere is a three axis universal joint with constraining springs to simulate the elastic properties of the cable. The foil shaped segments that connect the spheres are mass-less, rigid links that have hydrodynamic forces F_{xi}, F_{yi}, F_{zi} acting at their midpoints.

The upper end of the cable is assumed to be attached to a towing ship which may change speed and turn rate. In addition, provision is made in the simulation to allow towing ship sway and heave motion to be superimposed on the normal ship maneuvers. Either random or deterministic motion may be used as a disturbance signal. Thus, the behavior of a cable and body system may be studied under a wide variety of simulated towing ship maneuvers and sea state conditions.

The towed body is represented in much the same way as one of the cable model segments in that it is free to roll, pitch, and yaw relative to the last cable segment. However, the hydrodynamic forces acting on the body are more complex. They consist not only of x, y, z, components of force, as considered on the cable segments, but also of moments about each of the three body axes. The forces and moments generated by the vertical and horizontal control surfaces of the towed body are also simulated so that various control schemes and modes of operation may be analyzed.

6

DERIVATION OF EQUATIONS OF MOTION

Having postulated a mechanical model of the cable which consists of rigid segments, point masses, hydrodynamic forces, and springs, the equations of motion of such a mechanical system can be derived. As stated above, these equations will be a set of nonlinear differential equations which may be solved by an active-analog computer.

The mechanical model of the cable consists of n connected, rigid segments. The equations of motion of such a constrained mechanical system may be derived most easily by use of Lagrange's Equations[3]*. Lagrange's equations may be written as:

$$\frac{d}{dt}\left(\frac{\partial T}{\partial \dot{q}_k}\right) - \frac{\partial T}{\partial q_k} + \frac{\partial V}{\partial q_k} = Q_k \tag{1}$$

where:

$T \equiv$ the kinetic energy of the system

$V \equiv$ the potential energy of the system

$q_k \equiv$ the kth generalized coordinate of the system
$k = 1, 2, \ldots m$ where m = the number of degrees of freedom of the system

$Q_K \equiv$ the generalized force corresponding to generalized coordinate q_k

$t \equiv$ time

The m equations given by (1) are the equations of motion of the system.

There are several possible sets of generalized coordinates that may be chosen to describe the motion of the cable model segments. The quantities that were chosen for the 1965 Boeing simulation were three angles defined as roll, pitch, and yaw. These three angles are defined for each of the n cable segments and relate the attitude of each segment to a towing ship coordinate system. These angles are shown in Fig. 2. The coordinates X_s, Y_s, Z_s move with the towing ship with their origin located at mean sea level at the average latitude and longitude of the towing point. The coordinates X_B, Y_B, Z_B are cable segment body axis coordinates with the X_B, Z_B axes in the cable section chord plane and the Z_B axis parallel to the leading edge of the cable section. The order of the application of the angles when going from ship coordinates to body coordinates is significant and must be considered as part of the definition of these quantities. A set of three such angles is defined for each cable segment and for the towed body. Thus the total number of generalized coordinates or degrees of freedom of the system with n cable segments is:

$$m = 3(n + 1)$$

For the cable simulation work that has been done to date, n = 6, so that 21 degrees of freedom are present.

In addition to the ship coordinates, X_s, Y_s, Z_s, and the body axis coordinates X_B, Y_B, Z_B for each segment and the towed body, it is convenient to introduce an additional set of coordinates which are assumed to be fixed to the earth.

----

*Superior numbers refer to similarly numbered references at the end of this paper.

7

This "inertial" set of coordinates is designated as X_I, Y_I, Z_I and is shown in Fig. 3 in relation to the other coordinates described above. We thus see from Fig. 3 that the location of the towed body relative to inertial space, $(\underline{x}_7)_I^*$, is composed of the vector sum of three quantities. These are:

(1) $(\underline{x}_s)_I$, the location of the ship coordinate system origin relative to inertial space which accounts for ship maneuvers;

(2) $(\underline{x}_0)_s$, the location of the tow point relative to the ship origin, which accounts for ship motion due to waves; and

(3) $(\underline{x}_7)_s$, the location of the towed body relative to the tow point.

It is noted that in this case two different coordinate systems are used. Care must be taken when combining quantities in such cases to assure that they have been transformed into a common coordinate system before they are added. The details of these transformations may be found in Reference (1).

The time derivative of the position of the ith mass segment, m_i, of the cable model, $(\underline{\dot{x}}_i)_I$, is the absolute inertial velocity of that element of the cable model. These velocities may be combined to form the kinetic energy** of the system as given by (3).

$$T = \frac{1}{2} \sum_{i=1}^{n+1} m_i \left(\underline{\dot{x}}_i\right)_I^T \left(\underline{\dot{x}}_i\right)_I \tag{3}$$

Differentiation of (3) by each of the 21 generalized coordinates and their time derivatives, as required by (1), forms the acceleration portion of each of the 21 equations of motion.

The potential energy of the system is stated as:

$$V = \frac{1}{2} \sum_{i=1}^{n+1} \left[K_i \left(\phi_{i+1} - \phi_i\right)^2 + L_i \left(\theta_{i+1} - \theta_i\right)^2 + M_i \left(\psi_{i+1} - \psi_i\right)^2 \right] \tag{4}$$

where K_i, L_i, and M_i are spring constants related to the elastic properties of the cable. The effect of gravity on the system could be included as a potential energy effect but it was treated as a generalized force for convenience. Taking partial derivatives of (4) with respect to each of the generalized coordinates, as required by (1), forms the spring terms of the 21 equations of motion.

All that remain to form the equations of motion are the generalized force terms. These terms insert the effects of the hydrodynamic forces of the cable and body,

----

*Vectors will be designated by underlined lower case quantities. Where more than one coordinate system is being used, the subscript outside brackets will be used to identify which coordinate system the vector is defined in.

**This expression for kinetic energy omits the rotational kinetic energy of the cable segments and towed body. These effects are included in the complete derivation[1]. The superscript T designates a transpose.

8

as well as the effects of gravity and buoyancy, into the equations of motion. The generalized forces are derived by Goldstien[3] to be:***

$$Q_k = \sum_{i=1}^{n+1} \left(\underline{F}_i\right)_s^T \frac{\partial\left(\underline{r}_i\right)_s}{\partial q_k} \tag{5}$$

For this problem these quantities are defined as:

$\left(\underline{F}_i\right)_s \equiv$ the hydrodynamic, gravity, or buoyancy force vector of the ith segment, ship coordinates

$\left(\underline{r}_i\right)_s \equiv$ the point of application of force $\underline{F}_i$, ship coordinates

The hydrodynamic forces may be expressed[1] in terms of the generalized coordinates and their time derivatives. These forces are calculated in the body axis coordinates of the particular cable segment upon which they act. In order to apply these forces to other cable model segments as specified by (5), it is necessary to transform the forces to ship coordinates and then back to each of the applicable body axis coordinate system. These transformations are derived in detail in Reference (1).

SIMULATION OF EQUATIONS OF MOTION

For analog solution of the equations of motion, the amount of computer equipment required is proportional to n. The cable model more closely approximates a continuous cable as n becomes larger. Thus one is faced with the problem of selecting n large enough to give a valid representation of the cable but not so large as to require more analog computer equipment than is available. By simplifying the simulation of individual segments, more segments may be included at the risk of less accuracy per segment. A guide in the deliberation of this problem was provided by a conversation with John McKillop of Engineering Research Associates. Mr. McKillop indicated that in studies of towed bodies and flexible faired cables they had found, after trying several numbers, that five segments provided an adequate representation of the cable.

Six segments were used to represent the cable in the Boeing simulation. Two consoles of EASE 2100 active-analog computer equipment were used for the simulation. The equipment requirements were, approximately, as follows: 154 electronic multipliers; 6 electronic resolvers; 288 operational amplifiers; and 328 servo set potentiometers.

Where possible, small angle approximations were made for the trigonometric functions of angles. With the exception of the pitch angles of the upper three cable segments, all cable segment and towed body attitude angles were assumed to be small angles. All towing conditions for which the towed body attitude angles remained within the tolerances specified for the preliminary design resulted in cable and towed body attitude angles which were well approximated by small angles.

Lagrange's equations provide a convenient and rigorous method for deriving the equations of motion of a mechanical system with constraints. The form of the

----

***A slightly more general definition is required for the case of the towed body to include hydrodynamically produced moments.

equations of motion are such that the highest derivative of each generalized coordinate appears in each of the equations of motion. The solution of such a set of equations of motion thus requires that one first solve a set of non-linear algebraic equations for the highest derivatives before proceeding with the integration of the equations of motion. Theoretically, these algebraic equations can be solved on the analog computer by means of high gain integration loops, as described by A. Hausner[4]. In practice, however, it was found that while the nonlinear algebraic equations could be solved by this technique, the rate of solution could not be made fast enough to prevent computational instabilities in the equations of motion. It was, therefore, necessary to neglect the effects of inertial coupling between cable segments. This assumption removed the requirement of solving the set of nonlinear algebraic equations. For slow cable motion and static cable shape solutions, this assumption is valid since the inertia effects in question are zero. Studies were made of the inertial effects by including the inertial coupling terms at reduced levels which permitted stable computer operation. Such studies indicated no significant effect of inertial coupling on the simulation results.

In the process of deriving the equations of motion and simulating the cable and towed body, several assumptions were made in order to reduce the problem to one that could be solved in a practical manner. The more significant of these assumptions have been discussed above. These and other less significant assumptions are listed below.

(1) The cable was assumed to have a constant length for a given analysis. Provision was made to analyze numerous cable lengths.

(2) Inertial cross coupling between cable segments was assumed to be negligible.

(3) The trigonometric functions of the attitude angles of all cable segments and the towed body were approximated by small angle relationships except for the pitch angles of the upper three cable segments.

(4) The cable was represented by six rigid segments.

(5) The effects of towing ship heading accelerations were assumed to be negligible.

(6) The hydrodynamic force down the Z axis of the cable was assumed to be negligible for the lower three cable segments.

(7) Moments due to the products of angular rates (gyroscopic effects) were assumed to be negligible.

DESCRIPTION OF 1966 BOEING TOWED SYSTEM ANALYSIS

MODIFICATIONS TO THE EQUATIONS OF MOTION

The Boeing towing system analysis work done during 1965 was tailored to a specific high performance towed system. The small angle assumptions which were made regarding the cable attitude angles prevented the application of that simulation to most operational towed systems. To simply revoke these assumptions would require a substantial increase in analog equipment beyond that available at the Boeing Company. An alternative approach that has been taken has been to

introduce a new coordinate system which tracks the average motion of the cable system. The attitude angles of the cable model segment relative to this coordinate system are small enough to allow small angle approximations to be applied. The new coordinate system, referred to as the "cable coordinate system", is positioned by the computer so that the average value of the corresponding model segment angles at each end of the cable are equal and opposite. Fig. 4 demonstrates how such a cable coordinate system may be positioned to cause the pitch, roll, and yaw angles of the upper and lower cable segments to be equal and opposite. The cable coordinate angles are obtained by solving the following equations:

$$\dot{\Theta}_c = K(\Theta_1 + \Theta_6)$$
$$\dot{\phi}_c = K(\phi_1 + \phi_6)$$
$$\dot{\psi}_c = K(\psi_1 + \psi_6)$$

(6)

where: $\Theta_c \equiv$ Pitch angle relating ship coordinates to cable coordinates.

$\phi_c \equiv$ Roll angle relating ship coordinates to cable coordinates.

$\psi_c \equiv$ Yaw angle relating ship coordinates to cable coordinates.

$\Theta_i \equiv$ Pitch angle relating cable coordinates to body coordinates.

$\phi_i \equiv$ Roll angle relating cable coordinates to body coordinates.

$\psi_i \equiv$ Yaw angle relating cable coordinates to body coordinates.

$i = 1, 6$ indicates top and bottom cable model segments respectively.

The coordinate positioning gain, K, is selected to cause the cable coordinates to track the gross motion of the cable due to ship or body maneuvers. In this manner, the angles which describe the cable position relative to the cable coordinates are kept small, as are the errors due to small angle approximations for these angles.

By this approach it is possible to simulate a wide range of cable towing attitudes. The introduction of an additional moving coordinate system complicated the derivation of the system equations of motion, and required their complete re-derivation.[2] However, the form of the derivation follows closely that described above.

Nonlinear hydrodynamic force data were originally programmed in the form of analytic approximations to the theoretical force expressions. This information is now programmed by means of nonlinear analog function generators, a more efficient form of data storage for an analog computer. The determination of the nonlinear analog functions is aided by a digital program which performs a least squared error fit to the given analytic or experimental data.

As a result of the assumption that all the generalized coordinate angles describing the cable position relative to the cable axes are small angles, it was found that the set of algebraic equations for the accelerations of these angles becomes linear. Therefore, these equations may be solved for each

cable length by matrix inversion. In this way, the inertial coupling problem which had evaded solution in the 1965 simulation becomes solvable. The result of the approach was to modify the coefficient of the moment producing each angular acceleration and to add to each moment a contribution from the moments of the adjacent model segments.

SIMULATION OPERATION

The set-up and check-out of a large analog simulation of a towed system is a tedious job. The settings of nearly 400 potentiometers must be calculated and are subject to change due to modifications of system parameters, scale factors, or system equations. To aid in the calculation of the potentiometer settings, a digital program was written which not only calculates the potentiometer settings but also punches the results on paper tape which may then be used to servo-set the potentiometers. A second digital program is used to provide static check solutions for verifying the analog computer operation. These two digital programs greatly aid the bookkeeping that accompanies the simulation operation.

Difficulties were encountered in getting the 1966 towed system into operation in addition to those normally experienced with a new simulation. The source of difficulty was traced to the inertial coupling problem that had also plagued the early operation of the 1965 simulation. Although the matrix inversion method described above had removed the unstable d.c. computer loops that otherwise would appear in the simulation of Lagrange's equations, it resulted in a general increase in loop gains. These gain levels exceeded the dynamic capabilities of certain computer components and resulted in computational instability. This was verified by the fact that reducing the solution rate by 10 to 1 time scaling resulted in stable operation. In order to attain practical simulation operation, it again became necessary to neglect the inertial coupling effects. However, by operating at a reduced solution rate, we now have an exact means of examining effects of the inertial coupling. This examination will be done in the near future.

A list of assumptions which are present in the 1966 Boeing towed system analysis is given below:

(1) The cable is assumed to have a constant length for a given analysis. Provision is made to analyze numerous cable lengths.

(2) Inertial cross coupling between cable segments is assumed to be negligible. This assumption may be omitted at the cost of increasing the solution time to 10 times real time.

(3) The trigonometric functions of the attitude angles of all cable segments and the towed body, relative to the cable axes, are approximated by small angle relationships except for the pitch angle of the towed body.

(4) The cable is represented by six rigid segments.

(5) The effects of towing ship heading accelerations are assumed to be negligible.

(6) Moments due to the products of angular rates, (gyroscopic effects), are assumed to be negligible.

12

To date the Boeing towed system analysis has been applied to a high performance preliminary design system. This system was the sole subject of the 1965 work and has been used to check out the 1966 simulation. The simulation results presented below have been taken from Reference (1) describing the 1965 simulation work. The form of data output however, is identical to that available with the improved simulation.

Figs. 5 and 6 present three views of the cable-body system during various steady state turns. In Fig. 5 the body is uncontrolled while in Fig. 6 the roll angle sensed in the body is held to a small value by a roll control system. Projections of cable shape such as these may be recorded by an X-Y plotter or continually observed on a television display which repeats the pictures at a rate of 10 pictures per second. The later form of display is quite helpful in visualizing the three dimensional motion of the cable.

Figs. 7 and 8 present typical analog oscillograph displays of transient time histories. In each figure the transient response of the roll and yaw angles at each model station is presented. In Fig. 7 the depressor body was given an initial roll displacement. An initial body yaw angle transient is shown in Fig. 8. In addition to transient responses, the time history of cable motion in response to various ship maneuvers and distrubances can be readily obtained from the simulation. Either deterministic or random ship towing point motion may be considered. Numerous additional examples of cable and body motion oscillographs may be found in Reference (1).

Fig.9 presents a convenient method of visualizing cable mode shapes. These pictures represent multiple exposures of the cable, taken as the towing point of cable was oscillated sinusoidally along the ship Y axis. The pictures are "rear views" of the cable similar to those of Figs. 5 and 6 but with the horizontal scale expanded to emphasize the mode shape. The envelope of the individual cable shapes gives the mode shape at that particular disturbance frequency. The mode shapes may be recorded by exposing a photograph of the oscilloscope display over the duration of one disturbance frequency period. They may also be conveniently observed during computer operation due to the persistance of the oscilloscope. Additional information concerning Fig. 9 may be found in Reference (1) page 10-54.

In addition to the displays of cable position and motion presented above, the loads distributed along the cable and at the end points are available from the simulation. This information may be presented as plots or as tabular listings.

CONCLUSION

It has been the objective of the Boeing towed system work to provide a means of analyzing the three dimensional behavior of a wide range of towed systems. Due to previous successful system studies, an analog simulation of the towed system was chosen as a practical means of accomplishing these analyses. The simulation has been designed so that both the static and dynamic behavior of a cable system can be evaluated over a wide range of towing vehicle maneuvers and wave disturbances. A simulation of this type provides the designer with a working

model of the system being studied with the following favorable features:

(1) Access to the inner workings of the system.

(2) The ability to artificially hold constant various quantities of the system.

(3) Strict control over the system environment, such as waves.

(4) The ability to readily change the physical parameters of the system.

(5) Numerous displays which realistically depict the operation of the system in real time.

With the aid of such a simulation, various components of the system such as the towed body or control systems may be designed or evaluated, operating procedures may be established, and operational boundaries may be probed. A simulation of this type is also useful in planning sea trials and in aiding the evaluation of the test data taken.

It is believed that the application of this analysis tool to various towed systems will result in better insight into their operation and a better understanding of their capabilities and limitations.

ACKNOWLEDGEMENT

REFERENCES

(1) "Final Report - Development of High Speed Towing Cables/Underwater Towed Body - Part II" (U), Boeing Document D2-89924-2, Volumes I and II (Confidential)

(2) "Advanced Towed Sonar System Dynamics Studies - Part I Report" (U), Boeing Document D2-133017-1 (Confidential)

(3) Classical Mechanics, H. Goldstien, Addison-Wesley, Reading, Mass.

(4) "The Solution of Lagrange's Equations by Analog Computation", A. Hausner, IEEE Transactions on Electronic Computers, February 1965.
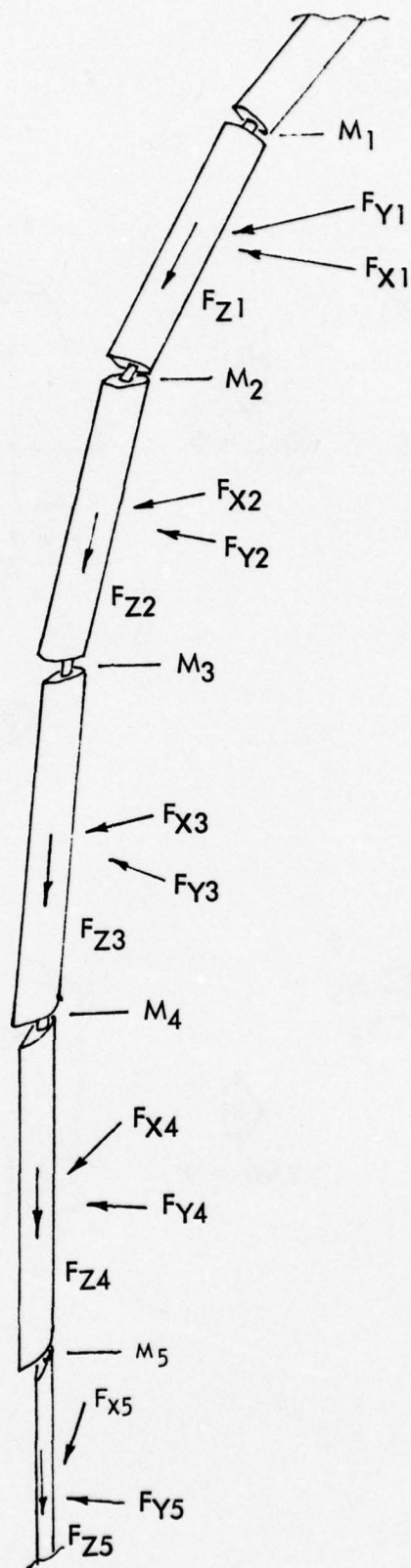
FIGURE 1: PICTORIAL REPRESENTATION OF CABLE MECHANICAL MODEL

15
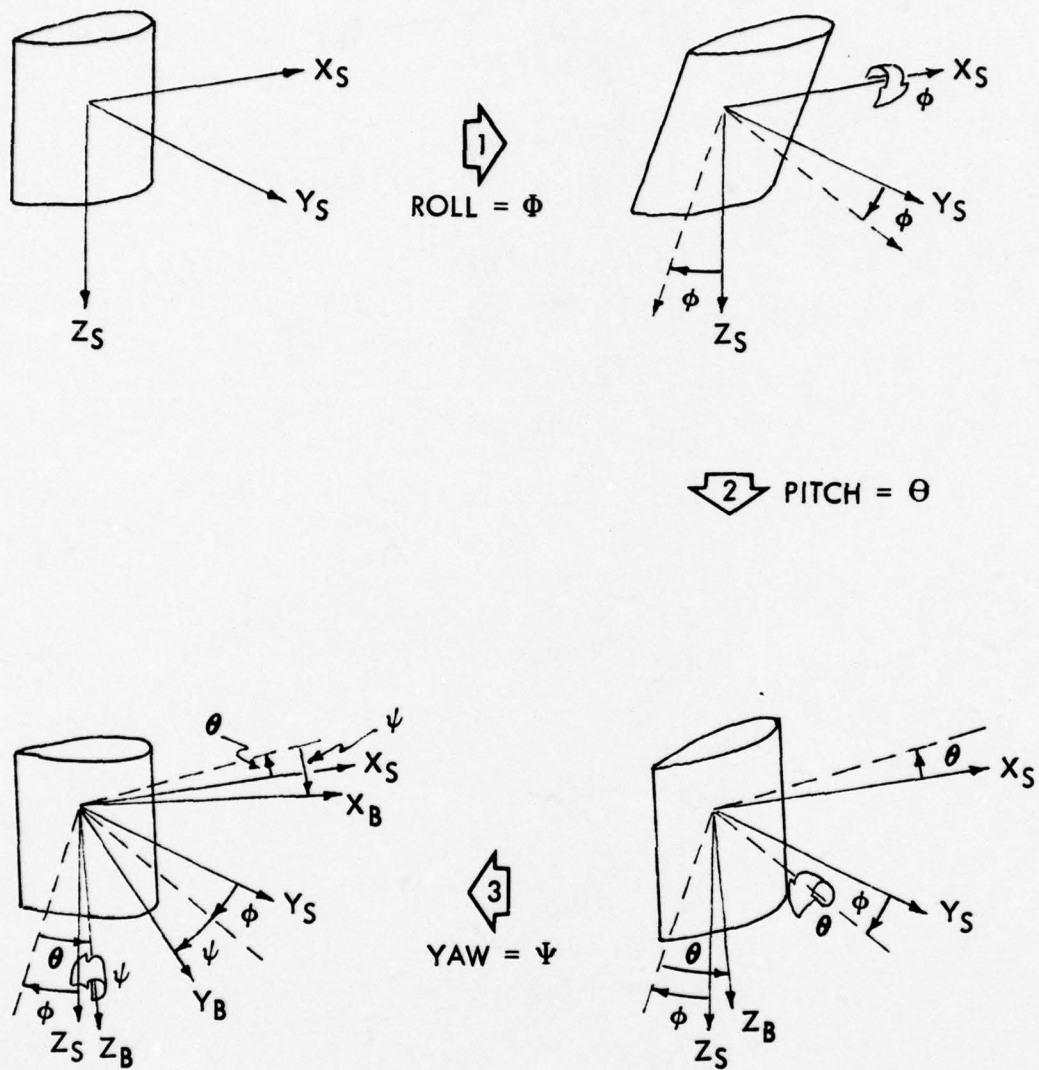
FIGURE 2: DEFINITION OF GENERALIZED COORDINATES OF CABLE
MODEL SEGMENTS
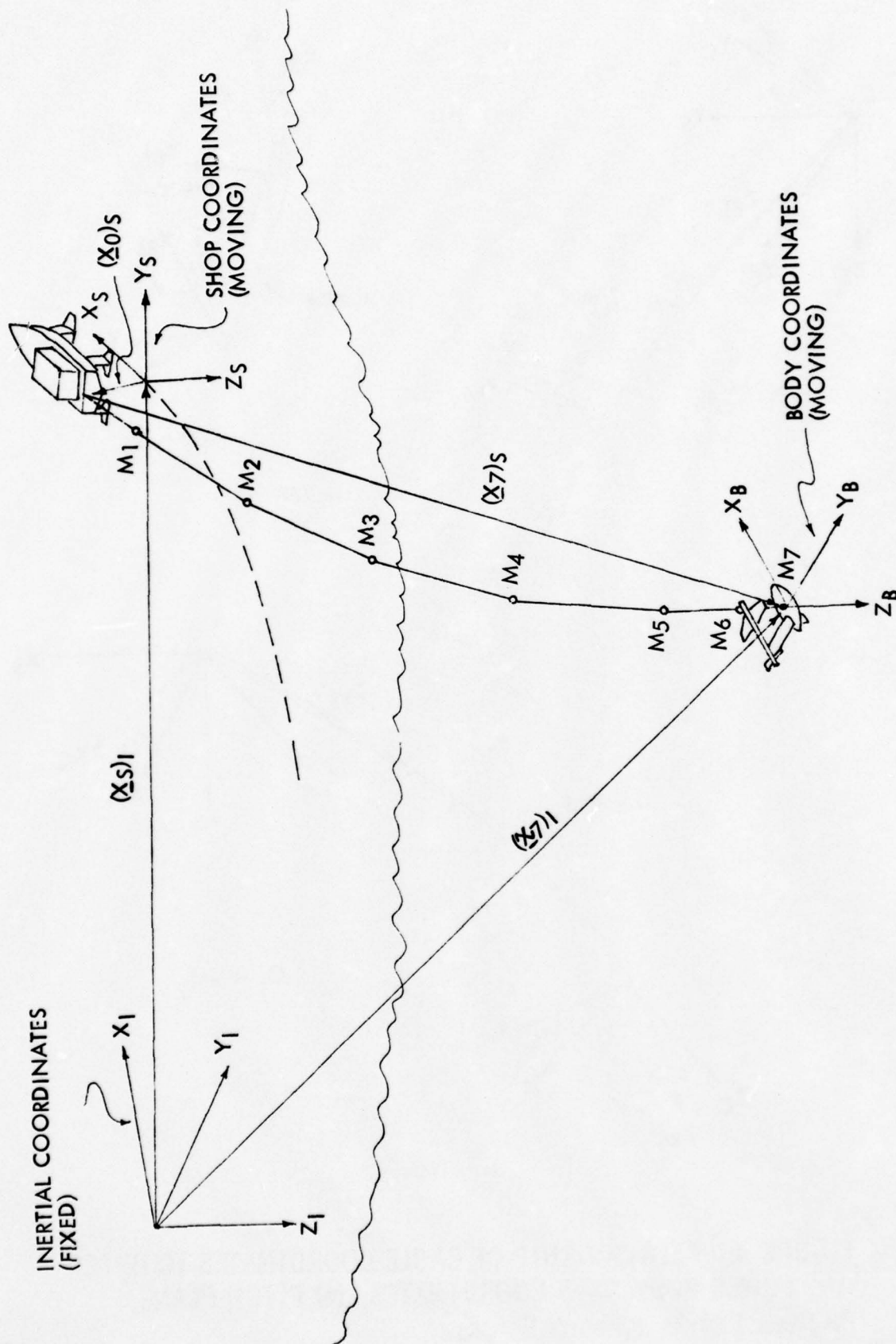
FIGURE 3: RELATIONSHIP OF INERTIAL, SHIP AND BODY AXIS COORDINATE SYSTEMS

17
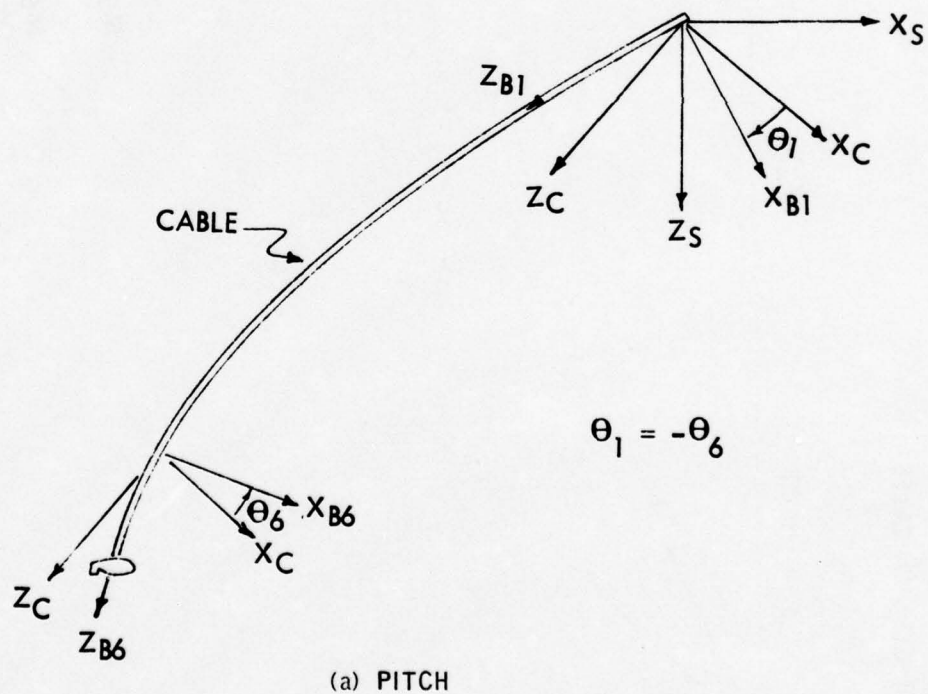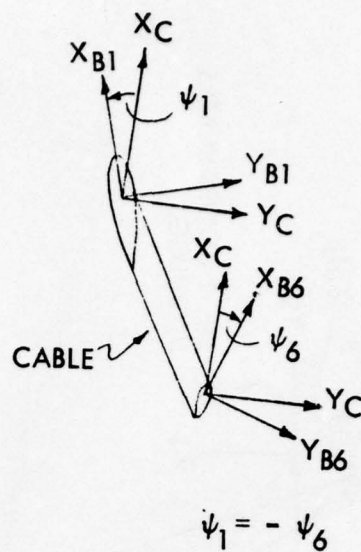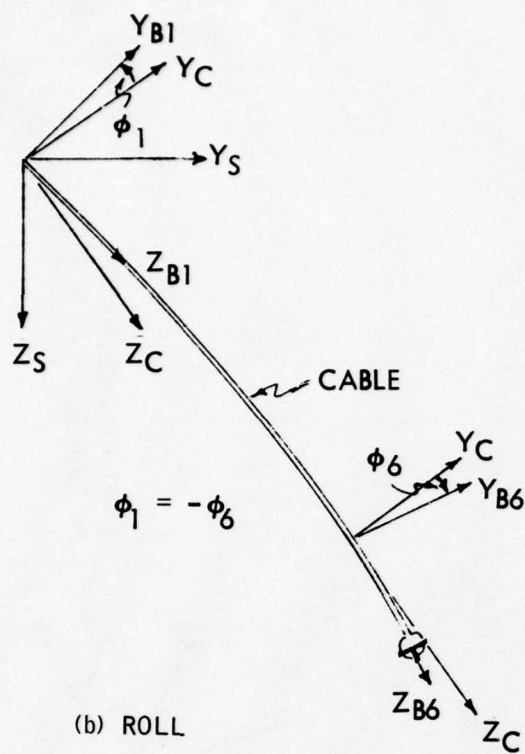
FIGURE 4: RELATIONSHIP OF CABLE COORDINATES TO UPPER
AND LOWER BODY AXIS COORDINATES, (a) PITCH PLANE,
(b) ROLL PLANE, (c) YAW PLANE

18

TOWING CABLE SHAPE, UNCONTROLLED BODY

CABLE LENGTH = 480 FEET

PLAN VIEW

PORT TURN

IDENTIFICATION TABLE

CURVE	TOW SPEED	TURN RADIUS	SIDE ACCEL.
A	45 KNOTS	400 YARDS	0.136 G
B	40 KNOTS	350 YARDS	0.135 G
C	35 KNOTS	200 YARDS	0.129 G
D	25 KNOTS	150 YARDS	0.123 G

STARBOARD VIEW

REAR VIEW

1 IN.

SCALE: 50 FT./IN.
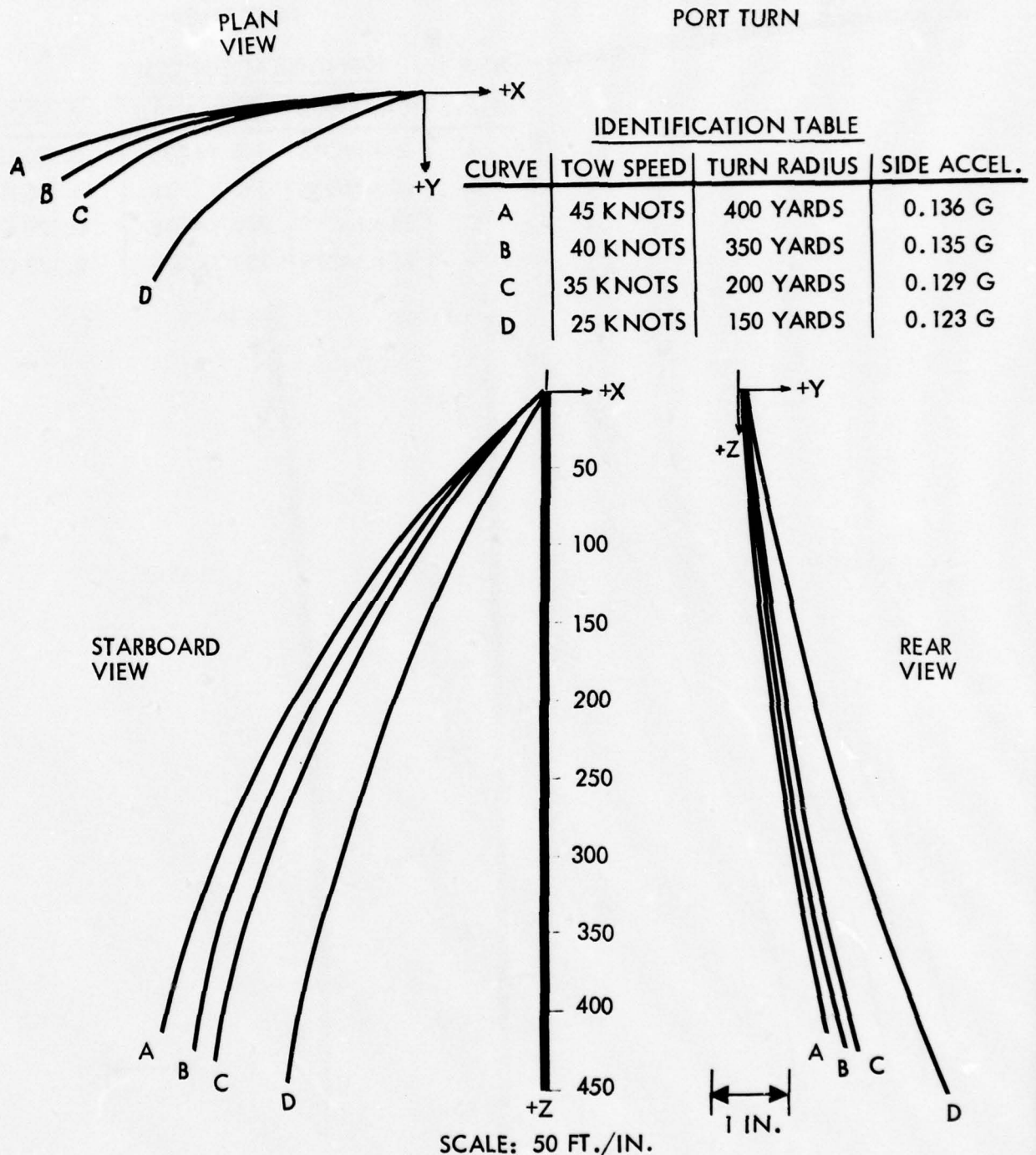
FIGURE 5: TOWING CABLE SHAPE, UNCONTROLLED BODY

CABLE LENGTH = 480 FEET

TOWING CABLE SHAPE, CONTROLLED BODY

PLAN VIEW   CABLE LENGTH = 480 FEET

PORT TURN

A B C   D

+X

+Y

IDENTIFICATION TABLE

CURVE	TOW SPEED	TURN RADIUS	SIDE ACCEL.
A	45 KNOTS	440 YARDS	0.136 G
B	40 KNOTS	350 YARDS	0.135 G
C	35 KNOTS	280 YARDS	0.129 G
D	25 KNOTS	150 YARDS	0.123 G

+X

+Z

50

100

150

200

250

300

350

400

450

+Z

+Y

+Z

STARBOARD VIEW

REAR VIEW

A

B C

D

A

C B

D

SCALE: 50 FT./IN.

FIGURE 6: TOWING CABLE SHAPE, CONTROLLED BODY

CABLE LENGTH = 480 FT.

20

FIGURE 7: TYPICAL TOTAL SYSTEM RESPONSE TO TOWED BODY ROLL DISTURBANCE

CABLE LENGTH = 480 FEET　　　　　SPEED ≈ 45 KNOTS
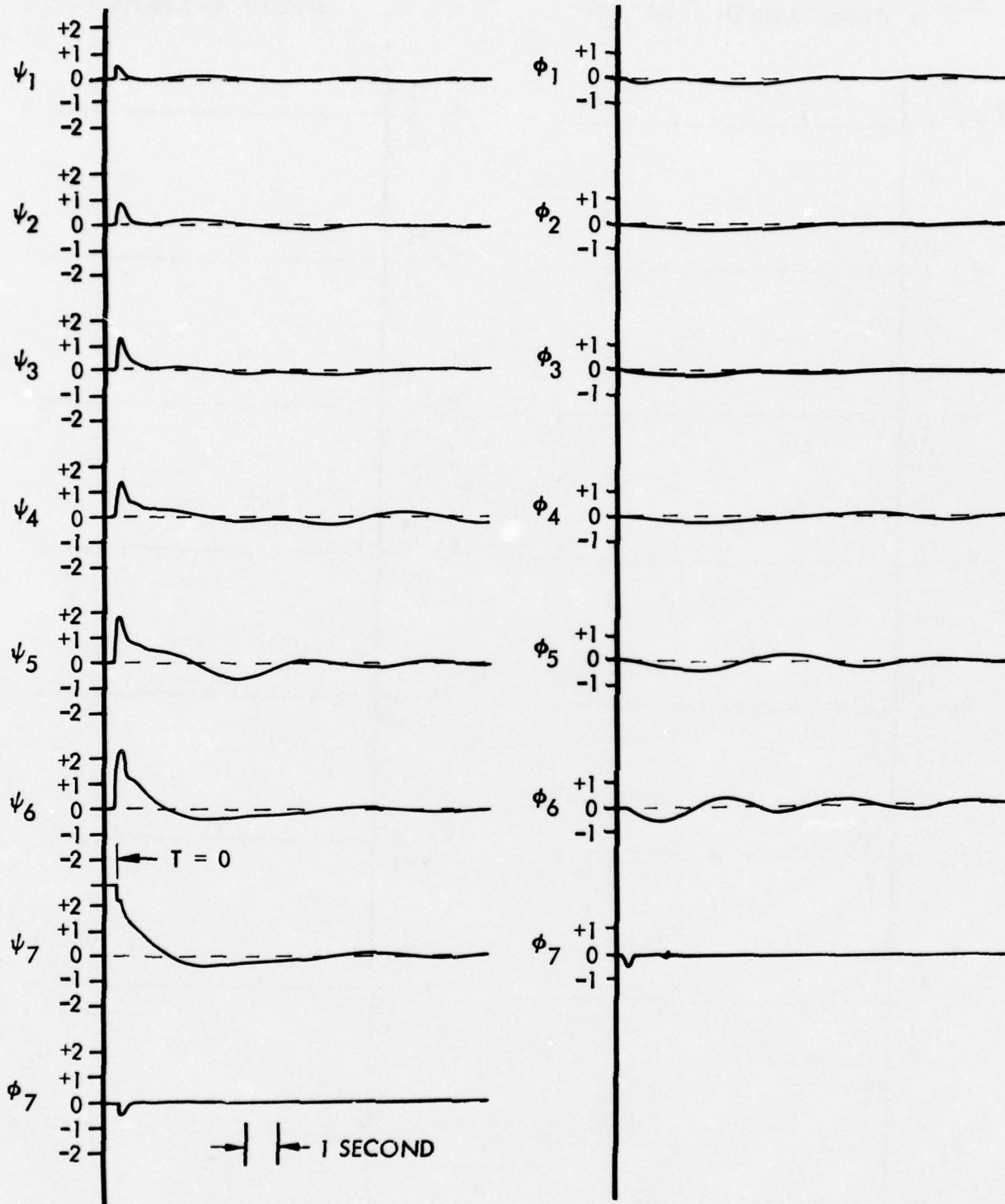
FIGURE 8: TYPICAL TOTAL SYSTEM RESPONSE TO TOWED BODY YAW DISTURBANCE

CABLE
LENGTH
480 FT.
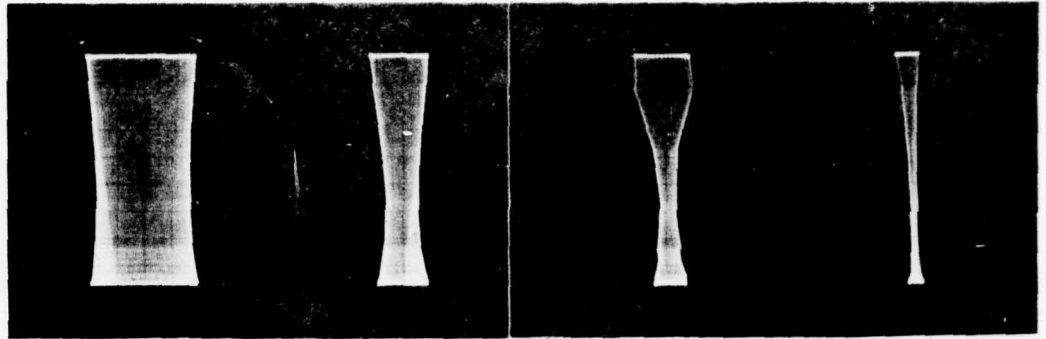
240 FT.
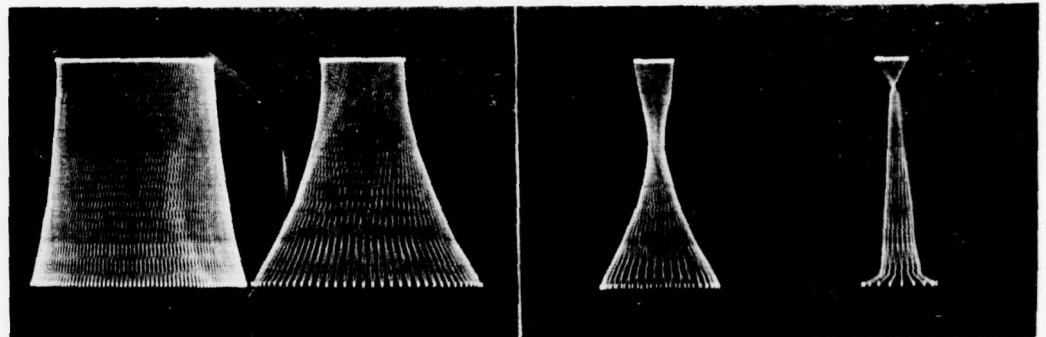
120 FT.
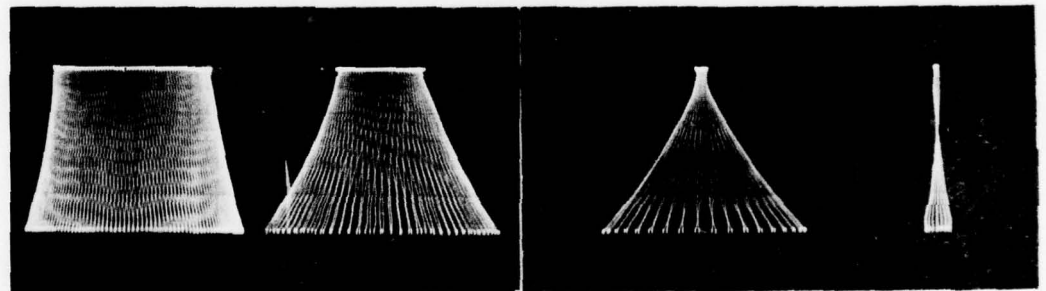
60 FT.
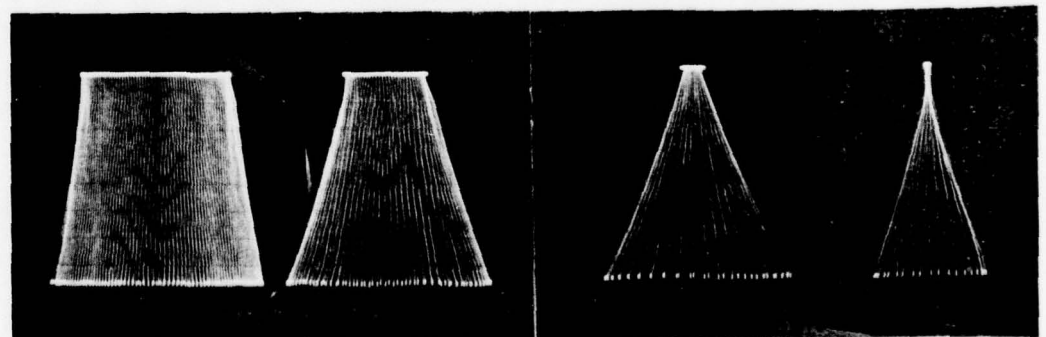
DISTURBANCE
FREQUENCY
0.05 H$_Z$ 0.1 H$_Z$ 0.2 H$_Z$ 0.4 H$_Z$

SPEED = 45 KNOTS

FIGURE 9:   TOWER CABLE MODE SHAPES

23

STABILITY CRITERIA FOR FAIRED CABLE

by Arthur R. Lagasse
Mechanical Engineer
Naval Underwater Weapons Research
    and Engineering Station
Newport, Rhode Island

ABSTRACT

The performance of cables under towing conditions in water has been the subject of many investigations in the past. Theories have been developed which attempt to predict the stability of the cable. These theories are, however, inadequate when the cable is faired or hydrodynamically shaped, or are of such a nature as to be too cumbersome to handle. A set of equations have been developed in this paper which predict the necessary criteria for the stable operation of a continuous faired cable in a tethered system.

INTRODUCTION

One of the major problems in anti-submarine warfare is that of detecting and maintaining contact with a submerged submarine. A tethered* sonar system discussed by Lagasse[1]** might be used for this purpose.

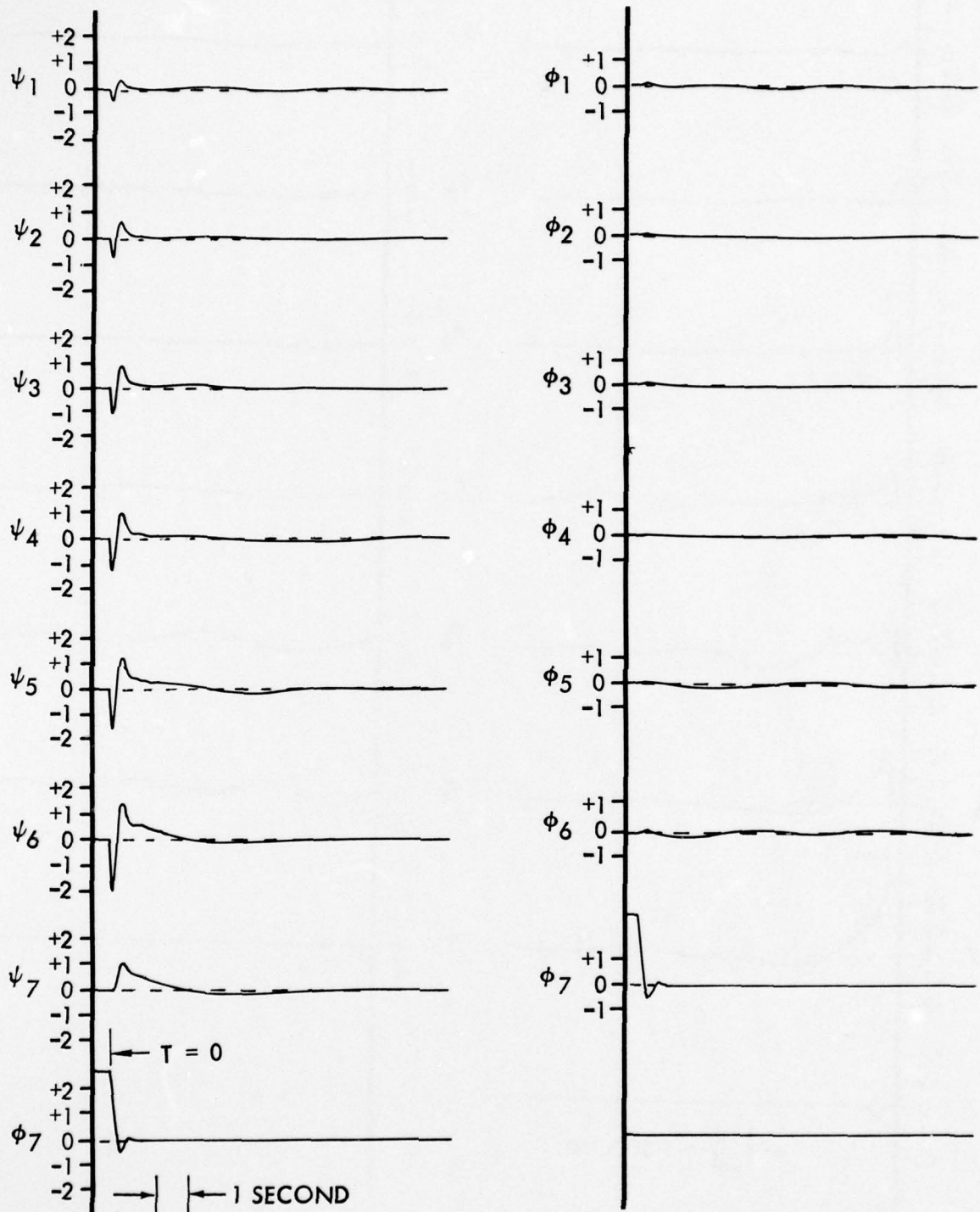The success of the tethered system for deep depth operation depends largely on the use of a faired or hydrodynamically shaped cable. Of primary concern is the performance of the cable. Thus it is the purpose of this paper to present the theory which is necessary for the successful prediction of cable stability.

STATEMENT OF THE PROBLEM

The problem of the stability of an airfoil-shaped cable towed at both ends, if tackled from a completely general standpoint, would certainly be an extremely cumbersome problem. Investigations of the past have mostly involved round cables and were not derived to predict the necessary criteria for the stability of faired cable. Thus it will be the objective of this paper to determine applicable stability criteria. The following assumptions will be made in the stability analysis:

---

*Tethered system in this paper means a system using transmitted electric power to a submerged sonar vehicle to operate the sonar and to propel both the vehicle and tow the lower half of a connecting cable.

**Superior numbers refer to similarly-numbered references at the end of this paper.

1. All situations of the cable crossing over itself or looping around itself will not be permitted.

2. Three force centers will be considered important and defined in the equations:

    a. Center of pressure - the point where the resultant hydrodynamic force due to lift and drag intersects the chord line.

    b. Center of tension - the point where the resultant force produced by both a uniform axial strain in the cable and a bending strain in the cable intersects the chord line.

    c. Center of gravity (or mass) - the point where the resultant of the weights of the component particles intersects the chord line.

3. Rotation being considered here refers only to that which takes place about any axis parallel to the z'-axis of figure 1.

4. The airfoil-shaped cable is symmetric about its longitudinal axis (the chord) so that the three force centers lie on the chord line.

5. The faired cable has a 3.0 inch chord with a maximum thickness of 0.54 inches (NACA 63_3 - 018) and consists of the following materials:

    a. The fairing up to 35% chord consists of a fiberglass strength member with a specific gravity of 3.5 and a modulus of elasticity of $6(10)^6$ pounds per square inch; the remaining portion consists of a material that carries no load and has a specific gravity of 0.5. This aft portion has a modulus of elasticity much less than that of the fiberglass strength member, thus offering no resistance to tension or twist.

STABILITY ANALYSIS

General Equations of Motion

A body moving in a fluid often moves in all six degrees of freedom of motion, i.e., translation along three orthogonal axes and rotation about each of the three axes. Thus in deriving equations of motion it is necessary to choose an axis system that will define these motion freedoms and also conveniently lend itself to the development of a motion analysis. The Society of Naval Architects and Marine Engineers[2] describe a set of equations which apply to a body's motion in the six degrees of freedom if the body has a plane of symmetry and if a rectangular coordinate system is chosen so as to move with the body. The axes of the moving coordinate system are called the body axes. Thus if the body axes x, y, z, coincide with the principal axes of inertia, and the zx - plane is the principal plane of symmetry (Fig. 2), the following equations are obtained:

$$F_x = m \left[\dot{u} + qw - rv - x_g (q^2 + r^2) + y_g (pq - \dot{r}) + z_g (pr + \dot{q}) \right] \tag{1}$$

$$F_y = m \left[\dot{v} + ru - pw - y_g (r^2 + p^2) + z_g (qr - \dot{p}) + x_g (qp + \dot{r}) \right] \tag{2}$$

$$F_z = m \left[\dot{w} + pv - qu - z_g (p^2 + q^2) + x_g (rp - \dot{q}) + y_g (rq + \dot{p}) \right] \tag{3}$$

$$K = I_x \dot{p} + (I_z - I_y) \, qr + m \left[y_g \, (\dot{w} + pv - qu) - z_g \, (\dot{v} + ru - wp) \right] \tag{4}$$

$$M = I_y \dot{q} + (I_x - I_z) \, rp + m \left[z_g \, (\dot{u} + qw - rv) - x_g \, (\dot{w} + pv - qu) \right] \tag{5}$$

$$N = I_z \dot{r} + (I_y - I_x) \, pq + m \left[x_g \, (\dot{v} + ru - pw) - y_g \, (\dot{u} + qw - rv) \right] \tag{6}$$

where F_x, F_y, and F_z are the force components along the x, y, and z axes respectively; K, M, and N are the moment components about these axes respectively; u, v, and w are the components of velocity along these axes respectively; p, q, and r are the components of angular velocity about these axes respectively; I_x, I_y, and I_z are the moments of inertia about these axes respectively; x_g, y_g, and z_g are the components of the location of the center of gravity from the origin; m is the mass of the body; and the dot above the letter symbol designates the derivative with respect to time. These equations are available in numerous textbooks and have been derived by Abkowitz[3] as well as by other investigators.

Application of Equations of Motion to Cable Section

So that the results derived will be applicable for all sections of the cable, an arbitrary cross section designated with the variable subscript "i" will be taken, and the forces will be investigated on this section. The cross-sectional area of the cable to be investigated is that obtained if a plane parallel to the x'y' - plane of Fig. 1 were to cut the cable. Fig. 2 is a sketch of the cross section "i" with the centers and forces acting at the centers indicated.

The stern of the propelled vehicle lies at the origin of the x' and y' axis. The position of the force centers along the axis of symmetry (the chord) was chosen with complete generality; since l_i and h_i could become negative, shifting the relative positions of the centers.

For this case, in order to be consistent with the standard hydrodynamic nomenclature[2], "r", which was previously defined as the angular velocity about the z' axis, is equal to $\dot{\psi}$ where the dot above the letter symbol designates the derivative with respect to time. For this study the motion will be restricted to the horizontal plane without rolling, i.e., $(q = p = \dot{q} = \dot{p} = w = \dot{w} = o)$. This restriction for the cable system thus results in considering only the side and forward velocity components and rotation about the z', or depth axis. In addition, the origin of the moving coordinate system will be placed at the center of gravity of the faired cable, thus making x_g, y_g, and $z_g = o$. The equations (1) to (6) now become:

$$F_x = m \left[\dot{u} - rv \right] \tag{7}$$

$$F_y = m \left[\dot{v} - ru \right] \tag{8}$$

$$N = I_z \dot{r} \tag{9}$$

Forces in an Ideal Fluid

The kinetic energy, S, for an ideal fluid in the fluid medium surrounding the moving body is presented in Lamb[4] as:

$$2S = G_1 u^2 + G_2 v^2 + G_3 w^2 + 2G_4 vw + 2G_5 wu + 2G_6 uv + G_7 p^2 + G_8 q^2$$

$$+ G_9 r^2 + 2G_{10} qr + 2G_{11} rp + 2G_{12} pq + 2 p (G_{13} u + G_{14} v + G_{15} w)$$

$$+ 2 q (G_{16} u + G_{17} v + G_{18} w) + 2 r (G_{19} u + G_{20} v + G_{21} w) \qquad (10)$$

which is a general quadratic function of the velocity components u, v, w, p, q, and r. If the motion is restricted as before, the above equation reduces to:

$$2S = G_1 u^2 + G_2 v^2 + 2G_6 uv + G_9 r^2 + 2G_{19} ru + 2G_{20} rv$$

Since the faired cable is airfoil-shaped, it is symmetric about its longitudinal axis (the chord). Therefore the kinetic energy must be the same when r = o, whether v is positive or negative for a given magnitude of v, thus making $G_6 = 0$. Similarly, because of symmetry, when v = 0, the kinetic energy will be the same for a positive or negative r; therefore $G_{19} = 0$. Thus S can be expressed as:

$$2S = G_1 u^2 + G_2 v^2 + G_9 r^2 + 2G_{20} rv \qquad (11)$$

Further, from Lamb[4] the forces on the cable section in an ideal fluid under the above conditions are:

$$F_x = - \frac{d}{dt} \left[\frac{\partial S}{\partial u} \right] + r \frac{\partial S}{\partial v} \qquad (12)$$

$$F_y = - \frac{d}{dt} \left[\frac{\partial S}{\partial v} \right] - r \frac{\partial S}{\partial u} \qquad (13)$$

$$N = - \frac{d}{dt} \left[\frac{\partial S}{\partial r} \right] + v \frac{\partial S}{\partial u} - u \frac{\partial S}{\partial v} \qquad (14)$$

Carrying out these derivatives, equations (12) to (14) become:

$$F_x = - G_1 \dot{u} + G_2 vr + G_{20} r^2 \qquad (15)$$

$$F_y = - G_2 \dot{v} - G_{20} \dot{r} - G_1 r u \qquad (16)$$

$$N = - G_9 \dot{r} - G_{20} \dot{v} + G_1 u v - G_2 u v - G_{20} u r \qquad (17)$$

By definition, an ideal fluid has mass but no viscosity. Since a real fluid has mass and viscosity, the mass forces of an ideal fluid can be assigned to the real fluid, and viscous effects can be accounted for separately, superimposing the two for a complete solution. The forces due to acceleration are mass forces; thus for the real fluid the following derivatives are obtained:

From equations (15), (16), and (17),

$$\frac{\partial F_x}{\partial \dot{u}} = - G_1 \qquad\qquad \frac{\partial F_y}{\partial \dot{v}} = - G_2$$

$$\frac{\partial N}{\partial \dot{r}} = - G_9 \qquad\qquad \frac{\partial N}{\partial \dot{v}} = - G_{20}$$

Therefore, G_1 represents the fluid virtual mass for longitudinal acceleration, i.e., parallel to the chord of the cable. It can be seen that G_2 represents the fluid virtual mass for lateral acceleration, i.e., perpendicular to the chord of the faired cable and that G_9 represents the virtual moment of inertia of the fluid. Also the coefficient G_{20} represents the moment of the fluid virtual mass for lateral acceleration.

Combining equations (7) to (9) and equations (15) to (17) and superimposing these inertia forces with the viscous forces, where the viscous forces are designated by the symbol ($\mathcal{U}$), the equations of motion become:

$$(m + G_1)\ \dot{u} = F_x\ (\mathcal{U}) + (m + G_2)\ r\ v + G_{20}\ r^2 \tag{18}$$

$$(m + G_2)\ \dot{v} = F_y\ (\mathcal{U}) - (m + G_1)\ r\ u - G_{20}\ \dot{r} \tag{19}$$

$$(I_z + G_9)\ \dot{r} = N\ (\mathcal{U}) - G_{20}\ (\dot{v} + r\ u) - (G_2 - G_1)\ u\ v \tag{20}$$

Derivation of Lift, Drag, and Tension Forces

The lift, drag, and tension forces, indicated in Fig. 2, will now be defined and written as functions of v, u, ψ_i, T_i, μ_i, β_i, and γ_i, the important independent variables. First, the tension components T_{xi} and T_{yi} will be defined. Vertical lines were drawn intersecting the faired cable at each of the cross sections, as indicated in Fig. 3.

Then the angle between the vertical and the length element d_{si} at the ith cross-section was designated γ_i. In addition, the angles that the projection of d_{si} on the x_i' y_i' - plane makes with the x_i' and y_i' axes were designated respectively (β_i) and ($\frac{\pi}{2} - \beta_i$), as indicated in Fig. 4. Then T_{xi} can be expressed as:

$$T_{xi} \approx T_{x(i + 1/2)} = T_{(i + 1)} \sin(\gamma_{(i + 1)}) \cos(\beta_{(i + 1)}) - (T_i) \sin\gamma_i \cos\beta_i$$

and T_{yi} by:

$$T_{yi} \approx T_{y(i + 1/2)} = T_{(i + 1)} \sin(\gamma_{(i + 1)}) \sin(\beta_{(i + 1)}) - (T_i) \sin\gamma_i \sin\beta_i$$

These tension components act at the center of tension as previously defined.

The drag force will act opposite to the direction of motion and will have a magnitude equal to $D_i = D_{oi} C_{Di} V_i^2$ where D_{oi} = a drag constant; V_i = effective velocity of the water past the airfoil shape = $\left[(-u)^2 + (-v)^2\right]^{1/2}$; and C_{Di} = drag coefficient. The drag coefficient can be approximated for an angle of attack varying from 0 to $\pm$ 18 degrees by defining an equation for the curve of experimental data for an N.A.C.A. 0018 airfoil published by the N.A.C.A.[5]. This curve can be defined by a parabola of the following form: $C_{Di} = K_1 \mathcal{F}_i^2 + K_2$ where $\mathcal{F}_i$ is the angle of attack in radians and $K_1 = 1.07$ and $K_2 = 0.01$. From Fig. 2, $\mathcal{F}_i$ is just $(\psi_i - \mu_i)$ and in turn μ_i is given by $\tan^{-1}\left(\frac{v}{u}\right)$. Therefore, the drag can be written as:

$$D_i = D_{oi} \left[K_1 \left(\psi_i - \tan^{-1}\left(\frac{v}{u}\right)\right)^2 + K_2 \right] (u^2 + v^2),$$

28

or letting $\dfrac{K_2}{K_1} = K_3 \approx 0.0093$ and $K_1 D_{o_i} = D_{1_i}$

$$D_i = D_{1i} \left[\left(\psi_i - \tan^{-1}\left(\tfrac{v}{u}\right)\right)^2 + K_3 \right] (u^2 + v^2)$$

The lift force will act perpendicular to the drag force D_i and can be expressed in a manner similar to D_i. The result is:

$$L_i = L_{1_i} \left[\psi_i - \tan^{-1}\left(\tfrac{v}{u}\right) \right] (u^2 + v^2)$$

The differential equation describing the ith cross-section's motion under the action of the above forces can now be written.

Summing forces in the x-direction:

$$F_x = D_{xi} + L_{xi} - T_{-x_i} \tag{21}$$

Summing forces in the y-direction:

$$F_y = -L_{y_i} + D_{yi} + T_{y_i} \tag{22}$$

Taking moments about the center of gravity of the faired cable:

$$N = T_{-x_i}\, l_i \sin\psi_i + T_{yi}\, l_i \cos\psi_i - L_i\, h_i \cos\zeta_i - D_i\, l_i \sin\zeta_i \tag{23}$$

where from Fig. 2:

$$L_{xi} = L_i \sin\mu_i \qquad\qquad L_{-yi} = L_i \cos\mu_i$$

$$D_{xi} = D_i \cos\mu_i \qquad\qquad D_{yi} = D_i \sin\mu_i$$

Rewriting equations (21) to (23) using the expressions previously derived for the lift and drag and utilizing various trigonometric substitutions results in the following:

Equation (21) becomes:

$$F_x = T_{-x_i} + D_{1i} \left[\left(\psi_i - \tan^{-1}\left(\tfrac{v}{u}\right)\right)^2 + K_3 \right] (v^2 + u^2)^{1/2}\, u$$
$$+ L_{1_i} \left[\psi_i - \tan^{-1}\left(\tfrac{v}{u}\right) \right] (v^2 + u^2)^{1/2}\, v \tag{24}$$

Equation (22) becomes:

$$F_y = T_{yi} + D_{1i} \left[\left(\psi_i - \tan^{-1}\left(\tfrac{v}{u}\right)\right)^2 + K_3 \right] (v^2 + u^2)^{1/2}\, v$$
$$- L_{1i} \left[\psi_i - \tan^{-1}\left(\tfrac{v}{u}\right) \right] (v^2 + u^2)^{1/2}\, u \tag{25}$$

Equation (23) becomes:

$$N = T_{-xi}\, l_i \sin\psi_i + T_{yi}\, l_i \cos\psi_i$$
$$- D_{1i} \left[\left(\psi_i - \tan^{-1}\left(\tfrac{v}{u}\right)\right)^2 + K_3 \right] (v^2 + u^2)^{1/2}\, h_i\, (+ u \sin\psi_i - v \cos\psi_i)$$
$$- L_{1i} \left[\psi_i - \tan^{-1}\left(\tfrac{v}{u}\right) \right] (v^2 + u^2)^{1/2}\, h_i\, (+ u \cos\psi_i + v \sin\psi_i) \tag{26}$$

Complete Equations of Motion for a Faired Cable Section

Along with superimposing the viscous force, namely the drag term, on equations (18) to (20), the tension and lift forces that were just described in the previous section must also be superimposed to completely describe the cable forces. Doing this, equations (18) to (20) become:

$$(m + G_1) \, \dot{u} = - T_{-xi} + D_{li} \left[\left(\psi_i - \tan^{-1} \left(\frac{v}{u} \right) \right)^2 + K_3 \right] (v^2 + u^2)^{1/2} \, u$$
$$+ L_{li} \left[\psi_i - \tan^{-1} \left(\frac{v}{u} \right) \right] (v^2 + u^2)^{1/2} \, v + (m + G_2) \, r \, v + G_{20} \, r^2 \qquad (27)$$

$$(m + G_2) \, \dot{v} = + T_{yi} + D_{li} \left[\left(\psi_i - \tan^{-1} \left(\frac{v}{u} \right) \right)^2 + K_3 \right] (v^2 + u^2)^{1/2} \, v$$
$$- L_{li} \left[\psi_i - \tan^{-1} \left(\frac{v}{u} \right) \right] (v^2 + u^2)^{1/2} \, u - (m + G_1) \, r \, u - G_{20} \, \dot{r} \qquad (28)$$

$$(I_z + G_9) \, \dot{r} = T_{-xi} \, l_i \sin \psi_i + T_{yi} \, l_i \cos \psi_i$$
$$- D_{li} \left[\left(\psi_i - \tan^{-1} \left(\frac{v}{u} \right) \right)^2 + K_3 \right] (v^2 + u^2)^{1/2} \, h_i \, (+u \sin \psi_i - v \cos \psi_i)$$
$$- L_{li} \left[\psi_i - \tan^{-1} \left(\frac{v}{u} \right) \right] (v^2 + u^2)^{1/2} \, h_i \, (+u \cos \psi_i + v \sin \psi_i)$$
$$- G_{20} \, (\dot{v} + r \, u) - (G_2 - G_1) \, u \, v \qquad (29)$$

Evaluation of Equations of Motion for Stability

At this point in the analysis assumptions will be made to simplify the equations and thus get a qualitative look at the stability problem. Assume that the towing velocity u is much larger than the velocity which acts 90° to u, that is v, and that the variations in cable ψ_i-orientations are less than 0.5 radians.

Therefore:

$$(v^2 + u^2)^{1/2} \approx u \qquad\qquad \tan^{-1} \left(\frac{v}{u} \right) \approx \frac{v}{u}$$

$$\sin \psi_i \approx \psi_i$$

$$\cos \psi_i \approx 1.0$$

Equation (27) becomes:

$$(m + G_1) \, \dot{u} = - T_{-xi} + D_{li} \left[\left(\psi_i - \frac{v}{u} \right)^2 + K_3 \right] u^2 + G_{20} \, r^2 \qquad (30)$$

Equation (28) becomes:

$$(m + G_2) \, \dot{v} = + T_{yi} - L_{li} \left[\psi_i - \frac{v}{u} \right] u^2 - (m + G_1) \, ru - G_{20} \, \dot{r} \qquad (31)$$

Equation (29) becomes:

$$(I_z + G_9) \, \dot{r} = T_{-xi} \, l_i \, \psi_i + T_{yi} \, l_i - L_{li} \left[\psi_i - \frac{v}{u} \right] u^2 \, h_i - G_{20} \, ru \qquad (32)$$

Rewriting equation (32) as a solution for v:

$$+ \underbrace{\left[\frac{I_z + G_9}{L_{1i}h_i u}\right]}_{K_5} \ddot{\psi}_i + \underbrace{\left[\frac{G_{20} u}{L_{1i}h_i u}\right]}_{K_6} \dot{\psi}_i + \underbrace{\left[\frac{L_{1i}h_i u^2 - T_{-x_i}l_i}{L_{1i} h_i u}\right]}_{K_7} \psi_i - \underbrace{\frac{T_{yi}l_i}{L_{1i}h_i u}}_{K_8} = v$$

$$+ K_5 \ddot{\psi}_i + K_6 \dot{\psi}_i + K_7 \psi_i - K_8 = v \tag{33}$$

Differentiating equation (33) with respect to time and substituting for v and $\dot{v}$ in-to equation (31)

$$(m+G_2) \left[K_5 \dddot{\psi}_i + K_6 \ddot{\psi}_i + K_7 \dot{\psi}_i \right] = + T_{yi} - L_i u^2 \psi_i - (m+G_1) \dot{\psi}_i u - G_{20} \ddot{\psi}_i$$

$$+ L_{1i} u (+ K_5 \ddot{\psi}_i + K_6 \dot{\psi}_i + K_7 \psi_i - K_8)$$

Rearranging terms and substituting new constants, K_9, K_{10}, K_{11}, and K_{12} for various groups of constants results in:

$$\dddot{\psi}_i + K_9 \ddot{\psi}_i + K_{10} \dot{\psi}_i + K_{11} \psi_i + K_{12} = 0 \tag{34}$$

The particular solution of the linear, non-homogeneous equation above is:

$$\psi_i = - \frac{K_{12}}{K_{11}}$$

which reduces to;

$$\psi_i = \frac{T_{yi}}{T_{xi}} \left[\frac{h_i}{l_i} - 1 \right] \tag{35}$$

Equation (35) is the steady state solution to equation (34). The complementary solution of the equation will now be found. Then the complementary solution and the particular solution of equation (34) can be combined to arrive at the general solution. The complementary solution can be found by solving the following homogeneous equation:

$$\dddot{\psi}_i + K_9 \ddot{\psi}_i + K_{10} \dot{\psi}_i + K_{11} \psi_i = 0 \tag{36}$$

Equation (36) will be evaluated for dynamic stability. Using Routh's stability criteria equation (36) becomes

$$b^3 + K_9 b^2 + K_{10} b + K_{11} = 0 \tag{37}$$

where b is a complex number.

From Routh's rules the complete criterion for stability of equation (37) is that K_9, K_{10}, and K_{11} are positive and that $K_9 K_{10} > K_{11}$

$$K_9 = \frac{K_6 (m+G_2) + G_{20} + L_{1i} u K_5}{(m+G_2) K_5} = \frac{G_{20}u}{I_z+G_9} + \frac{G_{20}L_{1i}h_i u}{(m+G_2)(I_z+G_9)} + \frac{L_{1i}u}{m+G_2} \tag{38}$$

$$K_{10} = \frac{K_7 (m+G_2) + (m+G_1) u + L_{1i} u K_6}{(m+G_2) K_5} > 0$$

This reduces to:

$$\left[\frac{m+G_1}{m+G_2} + 1\right]\left[\frac{L_{1i} h_i u^2}{I_z + G_9}\right] - \frac{T_{xi} l_i}{I_z + G_9} + \frac{L_{1i} u^2 G_{20}}{(m+G_2)(I_z+G_9)} > 0 \tag{39}$$

$$K_{11} = \frac{L_{1i} u K_7 - L_{1i} u^2}{(m+G_2) K_5} = \frac{-T_{xi} l_i L_{1i} u}{(m+G_2)(I_z+G_9)} > 0 \tag{40}$$

which in turn states that l_i must be negative for stability, i.e., the center of tension must be forward of the center of gravity on the chord of the airfoil-shaped cable section. The remaining criteria, K_9 $K_{10} > K_{11}$, yields no meaning information.

Examining the coefficients by Routh's criteria as above results only in stating that l_i must be negative, giving no result as to the sign of h_i. At this point the assumption that h_i is also negative will be made, and the coefficients will be evaluated numerically to see if this results in any new conclusions.

The following values will be assigned to the coefficients:

$l_i = h_i = -1.0$ in $= -0.0833$ ft

$T_x = T_{yi} = 1.5$ lbf/ft (due to the displacement of the cable from equilibrium in operation)

$I_z = 56.4(10)^{-6}$ slug-ft^2/ft

$m = 0.0279$ slugs/ft

$G_9 = 160(10)^{-6}$ slug-ft^2/ft

$G_1 = 0.00268$ slugs/ft } Wendel[6]

$G_2 = 0.0983$ slugs/ft

$D_{1i} = D_{oi} K_1 = (1/2 \, \rho \, A_B) K_1 = (1.94/2)(3.0/12)(1.07) = 0.261$ slugs/ft^2

$L_{1i} = L_{oi} K_4 = (1/2 \, \rho \, A_B) K_4 = (1.94/2)(3.0/12)(4.0) = 0.970$ slugs/ft^2

$u = 36$ ft/sec = constant

$G_{20} = (G_2)$(distance between origin of coordinate system, CG, and the point where the virtual mass for lateral acceleration acts)

$G_{20} = (0.0983)(.240/12)$ (assuming the CG is at 58% of the chord and the virtual mass acts at 50% chord)

$G_{20} = 2.0(10)^{-3}$ slugs-ft/ft

The coefficients and terms needed in the equations for a stability analysis are now all defined.

32

From equation (38): $K_9 = 388 > 0$

This criterion is satisfied if h_i if negative; however, it can be shown that it still would be satisfied if h_i was positive.

From equation (39):

$$K_{10} = \left[\frac{m+G_1}{m+G_2} + 1 \right] \left[\frac{L_{li} \, h_i \, u^2}{I_z + G_9} \right] - \frac{T_{xi} \, l_i}{I_z+G_9} + \frac{L_{li} \, u^2 \, G_{20}}{(m+G_2)(I_z+G_9)} > 0$$

$$-566(10)^3 + 0.58(10)^3 + 106(10)^3 > 0$$

$$K_{10} = -460(10)^3 \ngtr 0$$

It appears from this coefficient that we cannot expect to have stability if h_i is negative. However, this is not true if the value that was originally assigned to h_i is changed. The second term of the coefficient K_{10}, i.e., $-\frac{T_{xi} \, l_i}{I_z + G_9}$ will always be positive as long as l_i is negative. The sign of the first term of the coefficient K_{10} depends on the sign of h_i, and if h_i is negative the entire term will be negative. The third term of the coefficient K_{10} will always be positive. Thus if the third term was of such a magnitude as to cancel the negative first term, the entire coefficient K_{10} would be positive. Since G_{20} is dependent on the position of the CG also, we must consider its change in determining the position of the CG that will make the two terms cancel out. If h_i equaled -0.0225 ft or -0.27 in, the first and third term of the coefficient K_{10} would cancel out, thus making K_{10} positive.

From the relation $K_9 K_{10} > K_{11}$:

$$(388)(-460)10^3 > -\frac{T_{xi}(l_i) \, L_{li} \, u}{(m+G_2) \, (I_z+G_9)}$$

$$-1780 (10)^5 \ngtr 1.60(10)^5$$

To satisfy this criterion h_i must be as previously defined since this would make K_{10} positive.

From the preceding stability analysis of the complementary, or transient, solution of equation (34), it can be concluded that if l_i is negative and h_i is positive the system will be stable. Also, if h_i is a relatively small negative number, stability should still be achieved. When this transient solution is combined with the steady-state solution, the result indicates that upon reaching stability the cable will not be oriented parallel to the flow unless T_{yi} is zero, or l_i and h_i are of the same sign and equal. Since the cable has a 3.0 inch chord, 0.27 inches is 9 percent of the chord length. As will be shown later, the center of pressure of the faired cable is approximately at 25% of the chord length, thus making it entirely possible to have l_i and h_i of equal magnitude and the same sign, thus satisfying both the steady-state and transient solutions. However, this would not be advisable since it would be a very marginal operating condition. T_{yi} will be zero if the cable streams out directly in back of the towing vehicles. This situation will arise when the cable is operating in a stable manner, and for this reason it would

seem more advisable to have h_i positive or at worst an extremely small negative number. However, it should be noted that this conclusion is based on the elimination of many terms in the original equations. From the simplified analysis just presented, it can be concluded that for stability the center of tension must be forward of the center of gravity and that both of these centers must be forward of the center of pressure. This is illustrated in Fig. 5.

METHODS FOR THE DETERMINATION OF THE FORCE CENTERS

Equation Defining Airfoil Shape

At this point in the investigation it was decided that a method should be selected which can be applied to the determination of the force centers for the faired shape under consideration. The first step was to determine an algebraic equation approximating the perimeter of the faired cross section. The shape used was that for an NACA 63_3-018 airfoil which is presented in an NACA report[7]. The first 60% of the airfoil[3] (from the leading edge) can be approximated with an error of only $\pm 3.5\%$ by an elliptical equation of the form

$$\frac{x^2}{(35)^2} + \frac{y^2}{(9)^2} = 1 \quad \text{where } x = 0 \text{ at } 35\% \text{ chord}$$

The aft 40% of the shape can be closely approximated by a straight line of the form

$$y = -0.163(x-25) + 6.5 \quad \text{where } x = 0 \text{ at } 35\% \text{ chord}$$

These equations can then be translated so that the variables x and y originate at the leading edge of the airfoil. Let:

$$x + 35 = \phi \text{ and } y = \eta$$

After manipulating the equations, the following form results:

$$\eta_1 \approx 0.257 \, (70 \phi - \phi^2)^{1/2} \qquad\qquad 0 \leq \phi \leq 60 \qquad\qquad (41)$$

and

$$\eta_2 \approx 6.5 - 0.163 \, (\phi - 60) \qquad\qquad 60 \leq \phi \leq 100 \qquad\qquad (42)$$

Equations (41) and (42) can completely describe the perimeter of the airfoil shape.

Center of Twist Calculation

The center of twist, sometimes called the center of flexure, is that point on the foil at which the application of a concentrated vertical force causes only (as dF_y is illustrated in Fig. 6) a vertical displacement without rotation or twisting, as defined by Timoshenko[8]. It should be noted that this center was not considered in the stability equations. This was done because the torsional resistance of the cable compared to the moment of the tension forces taken about the center of gravity and acting in the plane of the cross section of the cable was believed negligible. For this reason the center of tension was considered much more important for stability purposes than the center of twist. However, the center of twist was found to determine its location on the faired cable configuration. The procedure used is presented below.

34

The center of twist can be found by assuming a constant deflection along the strength member of the faired section in the $\phi \eta$ - plane. The cross section $\eta \, d\phi$ can be assumed to be the end of a beam whose deflection under a force dF_y is given by:

$$\Theta \approx \frac{(dF_y) \, B^3}{3 \, E \, I_x}$$

where:

Θ = constant deflection

B = constant length

E = modulus of elasticity

I_x = moment of inertia about the ϕ - axis.

$I_x \approx \dfrac{(2\eta)^3 \, d\phi}{12}$ assuming uniform density in the $\eta \, d\phi$ area

By appropriate manipulation the center of twist (CTT) can then be defined as:

$$CTT \approx \frac{\int_0^{35} \phi \, dF_y}{\int_0^{35} dF_y} = \frac{\int_0^{35} \eta_1^3 \phi \, d\phi}{\int_0^{35} \eta_1^3 \, d\phi} = \frac{\int_0^{35} \phi \, (70\phi - \phi^2)^{3/2} \, d\phi}{\int_0^{35} (70\phi - \phi^2)^{3/2} \, d\phi} \qquad (43)$$

Upon evaluation of the above integrals, the center of twist, CTT, is found to be 23.1% of the chord length of the faired shape.

Center of Tension Calculation

A method for the computation of the center of tension will now be determined. Again, the assumption will be made that the strength member extends to 35% of the chord, and that from 35% to 100% the fairing carries no load. The strain on the strength member will be assumed uniform with a force which acts perpendicular to the $\phi \eta$ - plane as illustrated in Fig. 7. (The effect of bending on the CT will be computed later and superimposed on the following calculation.)

$$dF_z = \sigma \, (d \, A_\phi)$$

where dF = force $\perp$ to the $\phi \eta$ -plane
σ = stress
dA_ϕ = area

or $dF_z = \sigma(2\eta) \, d\phi$

Modulus of elasticity $E = \dfrac{\text{stress}}{\text{strain}} = \dfrac{\sigma}{\epsilon}$

Thus

$$dF_z = E \, \epsilon \, (2\eta) \, d\phi$$

where ϵ = constant
E = constant

35

Therefore, the center of tension (CT_A) can be defined as:

$$CT_A = \frac{\int_0^{35} \phi \, dF_z}{\int_0^{35} dF_z} = \frac{\int_0^{35} \phi \, (70\phi - \phi^2)^{1/2} d\phi}{\int_0^{35} (70\phi - \phi^2)^{1/2} d\phi} \tag{44}$$

Using the integral tables again the integrals of equation (44) can be evaluated in a manner similar to that used for computing the center of twist. The result is that the center of tension is at 20.2% of the chord length with a uniform axial strain. However, the effect of the radius of curvature on the CT must now be considered. Its effect can be determined by computing the center of tension of the faired cable under a bending condition. This was done by making use of the following known bending strain relationship, illustrated in Fig. 8. In this bending situation there is a compression force and a tension force in the cable. Thus it was necessary to determine the magnitude of these forces and to locate the point where the resultant of the tension force and the point where the resultant of the compression force acted.

The same assumptions will be used as before except for the case of uniform strain. The first step is to determine the neutral axis. Since it was assumed that the strength member consisted of an area up to 35% of the chord length, the point must be found at which there is no net force, which is in effect the neutral axis. This is illustrated in Fig. 9.

Force of compression = Force of tension

i.e., $dW_1 = dW_2$

or

$$\int_0^{\phi} \epsilon \, E_1 (2\eta) \, d\phi = \int_0^{35} \epsilon \, E_1 (2\eta) \, d\phi$$

since $\epsilon = \dfrac{x_B}{x_c} = \dfrac{\phi}{x_c}$ and cancelling constants:

$$\int_0^{\phi} \phi \, (70\phi - \phi^2)^{1/2} d\phi = \int_{\phi}^{35} \phi \, (70\phi - \phi^2)^{1/2} d\phi$$

The neutral axis can then be determined by a trial and error procedure. For a 2000 ft operational case it was found to be at 26.2% chord, assuming that the fiberglass has the same properties in tension and in compression. The center of compression for bending for the area between the leading edge of the airfoil and the neutral axis can be found as follows:

$$CT_B = \frac{\int_0^{26.2} E \, \phi \left(\frac{\phi}{x_c}\right) 2\eta \, d\phi}{\int_0^{26.2} E \left(\frac{\phi}{x_c}\right) 2\eta \, d\phi} = \frac{\int_0^{26.2} \phi^2 \, (70\phi - \phi^2)^{1/2} d\phi}{\int_0^{26.2} \phi \, (70\phi - \phi^2)^{1/2} d\phi}$$

Similarly, the center of tension for bending can be found for the area between the 26.2% chord to the 35% chord. The next step was to investigate the relationship between the pure bending forces and the pure tension forces and to combine their

36

effect to find the overall center of tension for the supposed 2000 ft operational case. The forces are illustrated schematically in Fig. 10.

The tension and compression forces for bending are equivalent and can be found as previously illustrated. For the 2000 ft case they were found to be 33.4 lbs (assuming a three inch airfoil chord length) compared to the pure tension force of 27,800 lbs. Since the location of each of the resultant forces is known, the center of tension for this case can be found by simply summing moments about the leading edge of the airfoil.

$$27,800 \ CT = 27,800 \ (20.2) + 33.4(31.2) - 33.4(17.75)$$

$$CT = 20.2\% \text{ chord length}$$

Now the assumption will be made that the system is operating with a 35 ft distance between the underwater vehicle and the surface ship. Further, it will be assumed that the neutral axis of the cable in this case is the same as that in the 2000 ft case. For the 35 ft case the bending force was found to be 1910 lbs and the pure tension force was 550 lbs. Therefore:

$$550(CT) = 550(20.2) + 1910(31.2) - 1910(17.75)$$

$$CT = 67\% \text{ chord length}$$

Center of Gravity Calculation

A method to compute the center of gravity will now be illustrated. Here, the assumption is made that the strength member again consists of 35% of the chord length and that its specific gravity is 3.5, a figure commonly used for glass-reinforced resin. The aft portion of the cable fairing, which will extend from 35% to 100% of the airfoil, will be assumed to have a specific gravity of 0.5, that which is characteristic of buoyant foam materials. The center of gravity (CG) can then be defined as:

$$CG = \frac{\rho_1 \int_0^{35} \phi \, dA_\phi + \rho_2 \, {}_{35}\!\int^{60} \phi \, dA_\eta + \rho_2 \, {}_{60}\!\int^{100} \phi \, dA_\eta}{\rho_1 \int_0^{35} dA_\phi + \rho_2 \int_{35}^{60} dA_\eta + \rho_2 \int_{60}^{100} dA_\eta}$$

where ρ_1 = specific gravity of fiberglass

ρ_2 = specific gravity of foam

These integrals can be evaluated as before, which results in a center of gravity at 26.0% of the chord length.

Center of Pressure Determination

All that now remains is to determine the position of the center of pressure (CP). From the data presented in the NACA report[5], it can be seen that the center of pressure is constant at approximately 25% chord length for an angle of attack varying from 0 to ±18 degrees. Thus 25% of the chord will be used as the figure for the center of pressure.

Discussion of Results with Assumed Hypothetical Airfoil

One of the most critical factors, as can be seen from the force center calculations, is the effect that bending has on the center of tension. For the 2000 ft operational case, the position of the CT is approximately at the best possible location; but when the cable is bent to a 35 ft radius of curvature, the CT moves back too far to hope to achieve stability. However, the system under consideration is intended for deep depth operation, and this effect can thus realistically be ignored.

A design which is presently favored for the internal configuration of the faired cable will be presented. This design places the force centers at their proper position and enables the cable to transmit the required amount of power down to the underwater vehicle to perform its mission. The internal configuration with the location of the force centers is presented in Fig. 11.

CONCLUSIONS

The equations of motion developed from considering a faired cable section indicate that to have stability it is necessary to have the center of tension forward of the center of gravity and both of these force centers ahead of the center of pressure, if possible; however, the CG could be slightly in back of the CP and stability could still be achieved. With this result in mind, and considering the power requirements of the tethered system, a faired cable was designed.

NOMENCLATURE

Symbol	Definition
dA_ϕ	Elemental area of the faired cable cross-sectional strength member in the plane parallel to the xy plane.
dA	Elemental area of the faired cable cross-sectional flexible member in the plane parallel to the xy plane.
b	A complex number, the real part of which determines the damping and the imaginary part of which is the natural frequency.
B	Constant length from a fixed point to a cable cross-section in the $\eta\phi$ plane.
C_D	Drag coefficient of cable when oriented normal to flow.
CG	Center of gravity of cable section.
CP	Center of pressure of cable section.
CT	Center of tension of cable section.
CT_A	Center of tension of cable section for a uniform axial strain only.
CT_B	Center of tension of cable section for bending only.
CTT	Center of twist of cable section.
$\mathcal{C}_L$	Designates centerline.

38

Symbol	Definition
D	Drag of the cable section.
D_o	A drag constant $(1/2 \, f \, A_B)$
D_1	A drag constant $(K_1 \, D_o)$
D_x, D_y	The components of drag acting in the x and y directions of the cable section.
E	Modulus of elasticity
F_x, F_y, F_z	Components of the force on the cable section in the x, y, z coordinate system.
dF_y	Element of force parallel to the ϕm -plane.
dF_z	Element of force perpendicular to the ϕm -plane.
$G_1, G_2, G_3 \ldots G_{21}$	Constants determined by the form and position of the cable surface relative to the coordinate axes.
h	The distance between the CG and the CP on the cable section.
i	Represents an imaginary number.
"i"	When used as a subscript designates an arbitrary cable cross-section.
I_x, I_y, I_z	Moments of inertia of the cable section about the x, y, z axes, respectively.
K	Moment component relative to the x axis.
K_1	A constant (1.07).
K_2	A constant (0.01).
K_3	A constant (0.0093).
K_4	A constant (4.0).
K_5	$\dfrac{I_z + G_9}{L_{1i} \, h_i \, u}$
K_6	$\dfrac{G_{20} \, u}{L_{1i} \, h_i \, u}$
K_7	$\dfrac{L_{1i} \, h_i \, u^2 - T_{-x} \, l_i}{L_{1i} \, h_i \, u}$
K_8	$\dfrac{T_{yi} \, l_i}{L_{1i} \, h_i \, u}$
K_9	$\dfrac{K_6 \, (m + G_2) + G_{20} - L_{1i} \, u \, K_5}{(m + G_2) \, K_5}$
K_{10}	$\dfrac{K_7 \, (m + G_2) + (m + G_1) \, u - L_{1i} \, u \, K_6}{(m + G_2) \, K_5}$

Symbol	Definition
K_{11}	$$\dfrac{-L_{1i}\, u\, K_7 + L_{1i}\, u^2}{(m + G_2)\, K_5}$$
K_{12}	$$\dfrac{L_{1i}\, u\, K_8 - T_{yi}}{(m + G_2)\, K_5}$$
l	The distance between the CG and the CP on the cable section.
L	Lift of the cable section.
L_x, L_y	The lift components in the x and y directions, respectively.
L_o	A lift constant $(1/2\ \int A_B)$.
L_1	A lift constant $(K_4\, L_o)$.
m	Mass of cable section.
M	Moment component relative to the y - axis.
N	Moment component relative to the z - axis.
o, o'	The origin of the moving x, y, z and the fixed x', y', z' coordinate systems, respectively.
p	Angular velocity component about the x axis.
q	Angular velocity component about the y axis.
r	Angular velocity component about the z axis.
ds	Length element of the cable.
S	The kinetic energy for an ideal fluid in the fluid medium surrounding the cable section.
t	Represents time.
T_x, T_y, T_z	The components of tension acting in the x, y, z directions, respectively.
u	Component of the velocity along the x axis.
v	Component of the velocity along the y axis.
V	Effective velocity of the water past the cable section.
W	Component of the velocity along the z axis.
W_1	Total compression force on cable when bent.
dW_1	Elemental force of compression on cable when bent.
W_2	Total tension force on cable when bent.
dW_2	Elemental force of tension on cable when bent.
x	The longitudinal axis in a moving system directed from the leading edge of the cable section to the trailing edge.
x'	The longitudinal axis in a fixed coordinate system.
x_B	Arbitrary distance from neutral axis in a bending situation.
x_c	Radius of curvature.

40

Symbol	Definition

Symbol — **Definition**

Δx_c — Distance from neutral axis to the trailing edge of the airfoil in the bending condition.

x_g — The x-coordinate of the CG of the cable section relative to O.

y — The transverse axis, directed to starboard and in a moving system.

y' — The transverse axis in a fixed coordinate system.

y_B — Amount each fiber of length "y_c" is changed by bending.

y_c — Length of each fiber in airfoil before being bent.

y_g — The y-coordinate of the CG of the cable section relative to O.

z — The normal axis, directed from ocean surface to the ocean bottom and in a moving system.

z' — The normal axis in a fixed coordinate system.

z_g — The z-coordinate of the CG of the cable section relative to O.

Greek Symbols

β — The angle that the projection of ds on the xy plane makes with the x-axis.

γ — The inclination angle of the cable section, i.e., the angle measured counterclockwise from the direction of motion to the element of cable considered.

ϵ — Strain.

η — Corresponds to the y-axis, results from a shift in origin.

η_1 — Refers to η-coordinate for the first 0% to 60% of the airfoil chord starting from the leading edge.

η_2 — Refers to the η-coordinate for 60% to 100% of the airfoil chord starting from the leading edge.

Θ — Deflection produced by a force parallel to the $\eta\phi$ plane.

μ — The angle produced by $\vec{u}$ and $\vec{v}$.

ν — Represents the viscous forces.

ξ — The angle of attack of the cable section ($\psi - \mu$).

ρ — Density of sea water.

ρ_1 — Specific gravity of fiberglass.

ρ_2 — Specific gravity of foam.

σ — Stress.

ϕ — Corresponds to the x-axis, results from a shift in origin.

ψ — The angle of yaw; the angle from the vertical z'x' plane to the vertical zx plane.

REFERENCES

(1) Lagasse, A. R., _Analysis of Three Alternative Propulsion Systems for a Non-Nuclear LEPT Vehicle (U)(CONF)_, U. S. Naval Underwater Weapons Research and Engineering Station, Newport, R.I. ITN No. 97-63 dated 1 October 1963.

(2) Society of Naval Architects and Marine Engineers. _Nomenclature for Treating the Motion of a Submerged Body Through a Fluid._ Hydromechanics Subcommittee, Technical and Research Bulletin No. 1-5, Society of Naval Architects and Marine Engineers, New York, dated April 1952.

(3) Abkowitz, M. A., "Lectures on Ship Hydromechanics - Steering and Maneuverability," Report No. HY-5, Hydro-Og Aerodynamisk Laboratorium, Lyngly, Denmark, dated May 1964.

(4) Lamb, H., _Hydrodynamics_, Dover Publications, New York, 1932.

(5) Goett, H. J., and Bullivant, W. K., _Tests of N.A.C.A. 0009, 0012 and 0018 Airfoils in the Full-Scale Tunnel_, National Advisory Committee for Aeronautics, Report No. 647, dated 1939.

(6) Wendel, K., _Hydrodynamic Masses and Hydrodynamic Moments of Inertia_, David Taylor Model Basin, Translation 260, dated July 1956.

(7) Abbott, I. H., von Doenhoff, A. E., Stivers, L. S., _Summary of Airfoil Data_, National Advisory Committee for Aeronautics, Report No. 824, dated 1945.

(8) Timoshenko, S., _Strength of Materials_, Part II, Advanced Theory and Problems, D. Van Nostrand Company, Inc., New York, 1938.

BIBLIOGRAPHY

(1) Den Hartog, J. P., _Mechanical Vibrations_, McGraw Hill Book Co., Inc., New York, 1947.

(2) Hodgman, C.D., _Handbook of Chemistry and Physics_, Chemical Rubber Publishing Company, Cleveland, Ohio, 1950.
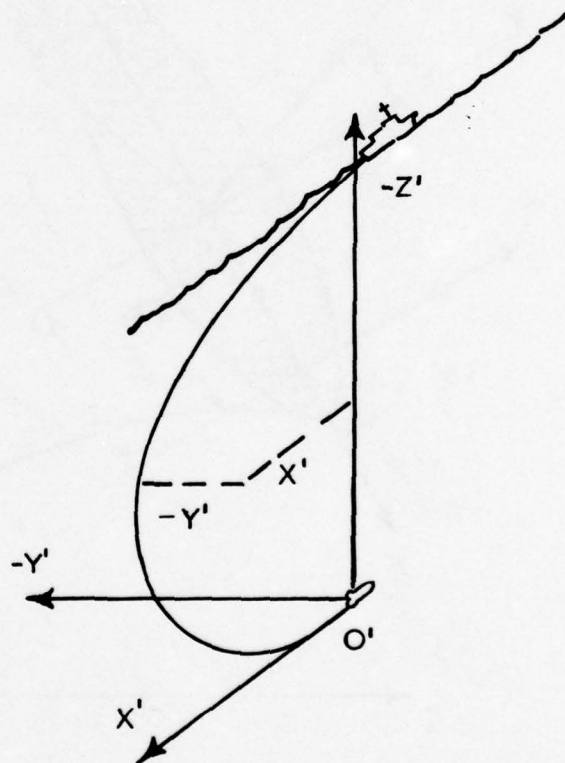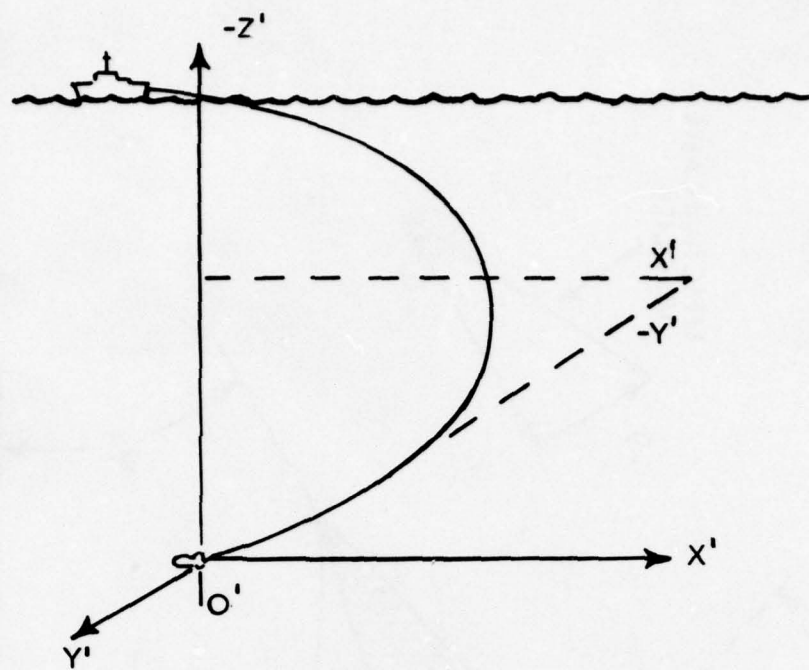
Cable System

Figure 1

43
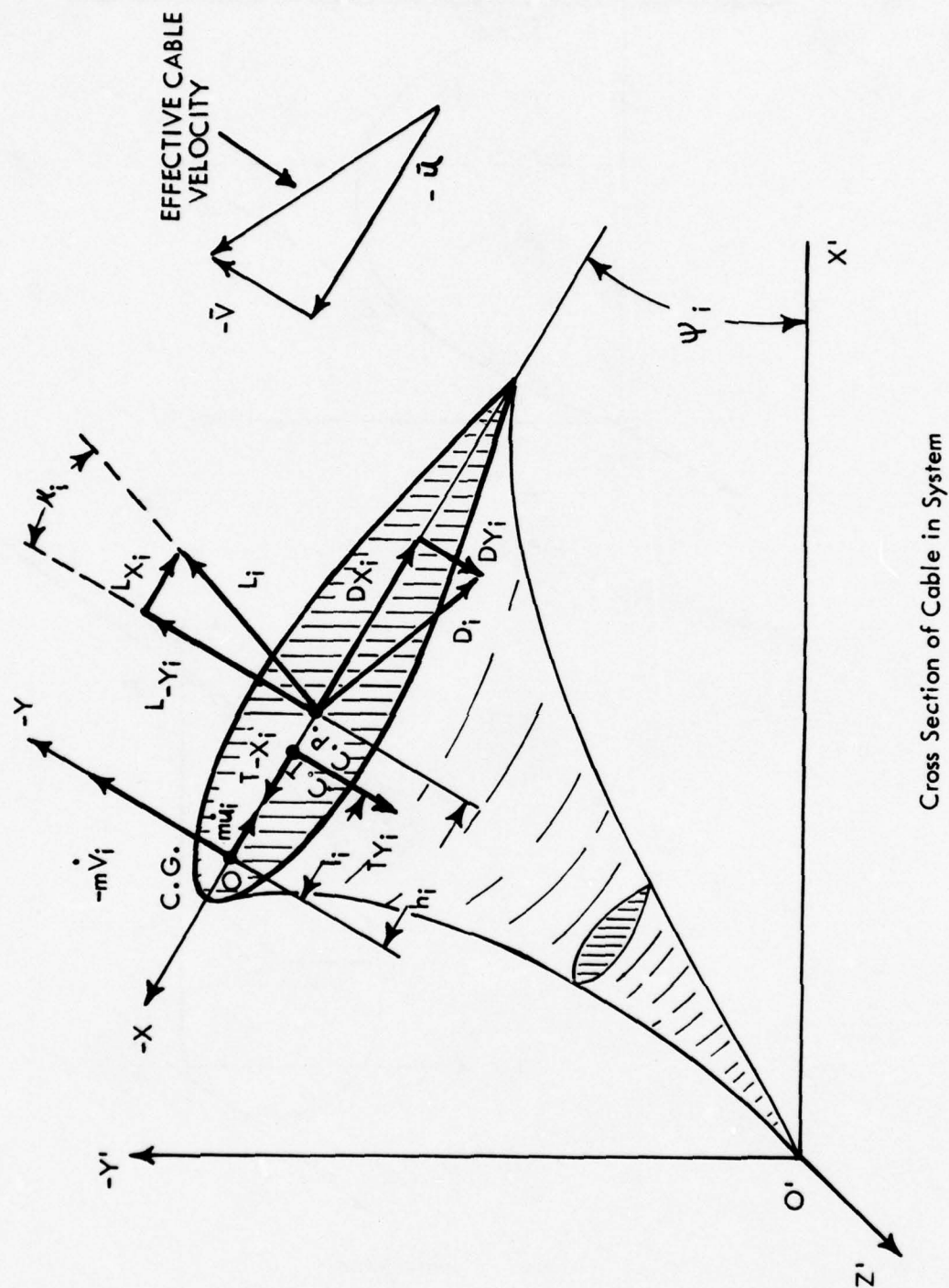
Figure 2

Cross Section of Cable in System

44
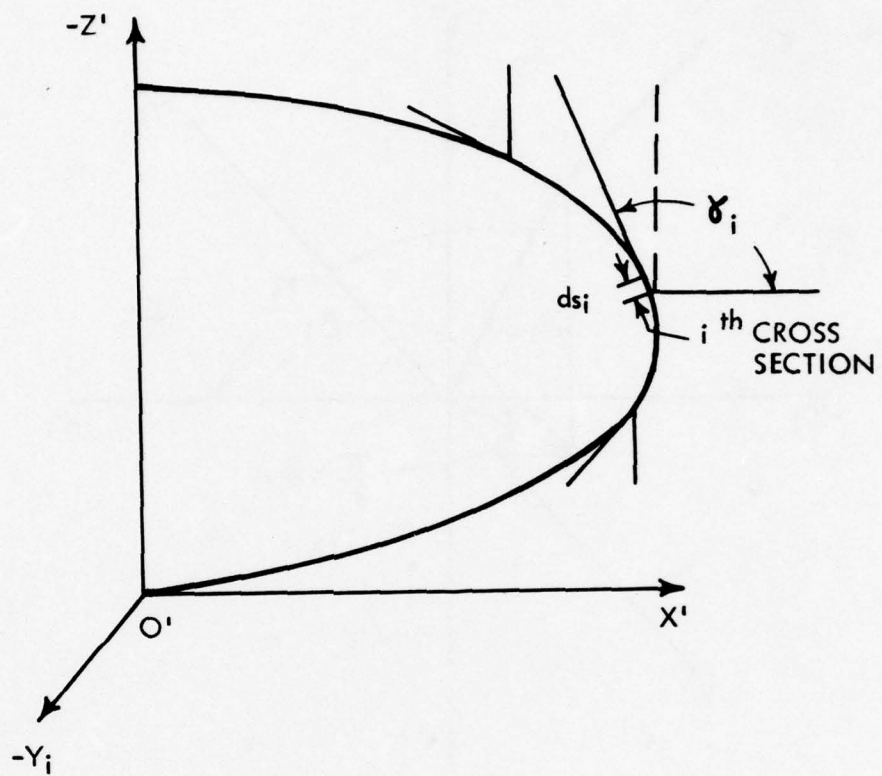
Locating Cable Segment in System

Figure 3
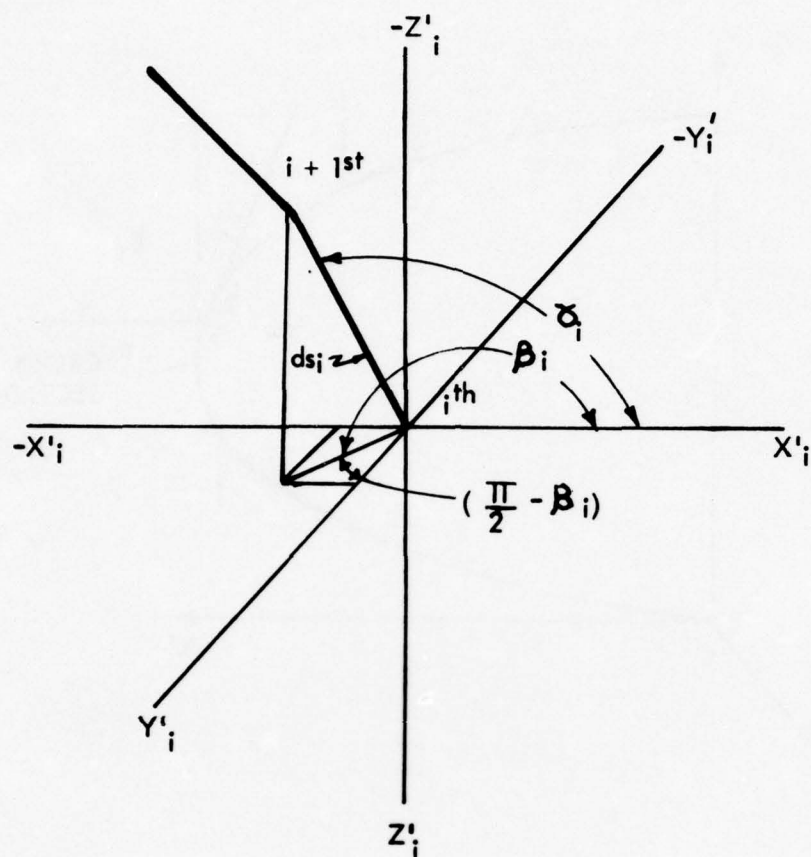
Projection of Cable Segment in System

Figure 4
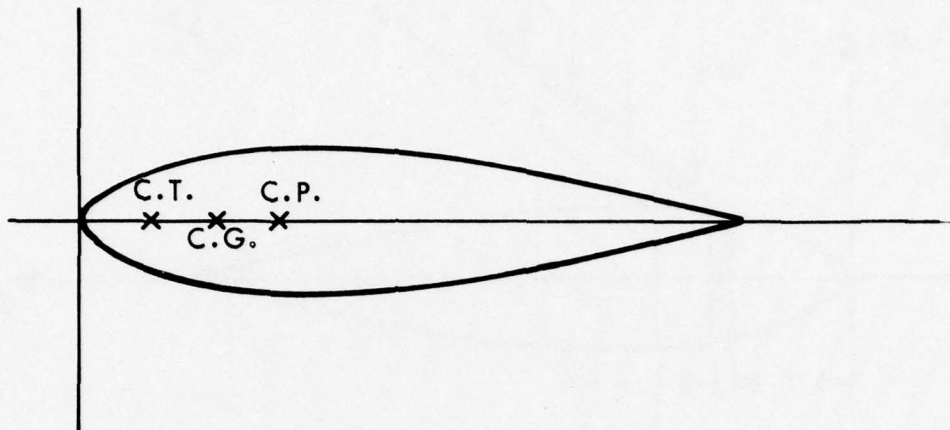
Location of Force Centers on Cable Cross Section

Figure 5
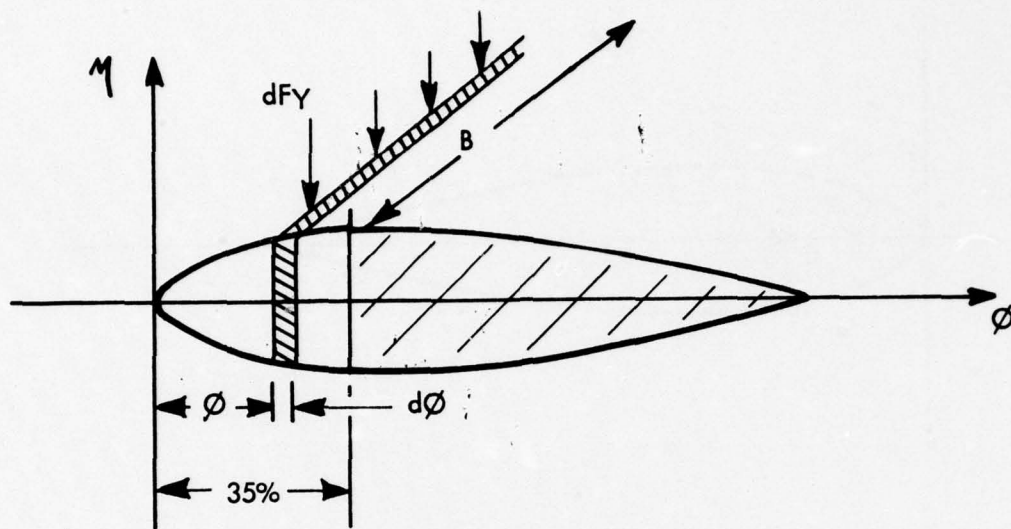
Cable Cross Section Illustrating Center of Twist

Figure 6

48
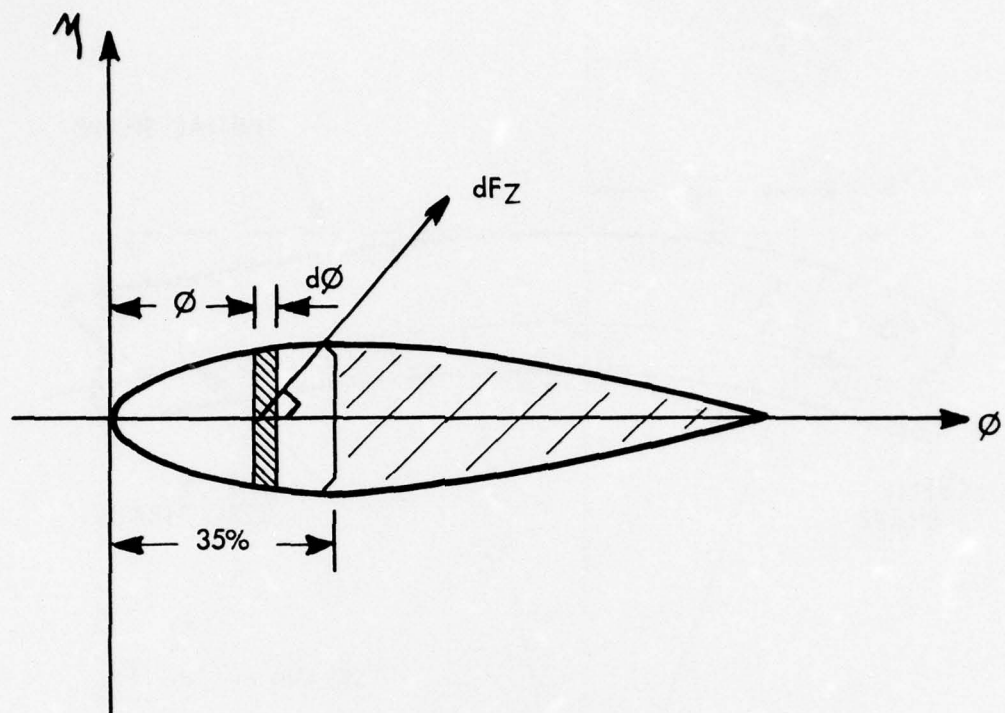
Cable Cross Section Illustrating Center of Tension for Uniform Axial Strain Only

Figure 7

49

STRAIN $= \epsilon = \dfrac{Y_B}{Y_C}$

BY SIMILAR TRIANGLES:

$$\dfrac{Y_B}{X_B} = \dfrac{Y_C}{X_C}$$

$$\dfrac{Y_B}{Y_C} = \dfrac{X_B}{X_C} = \epsilon$$
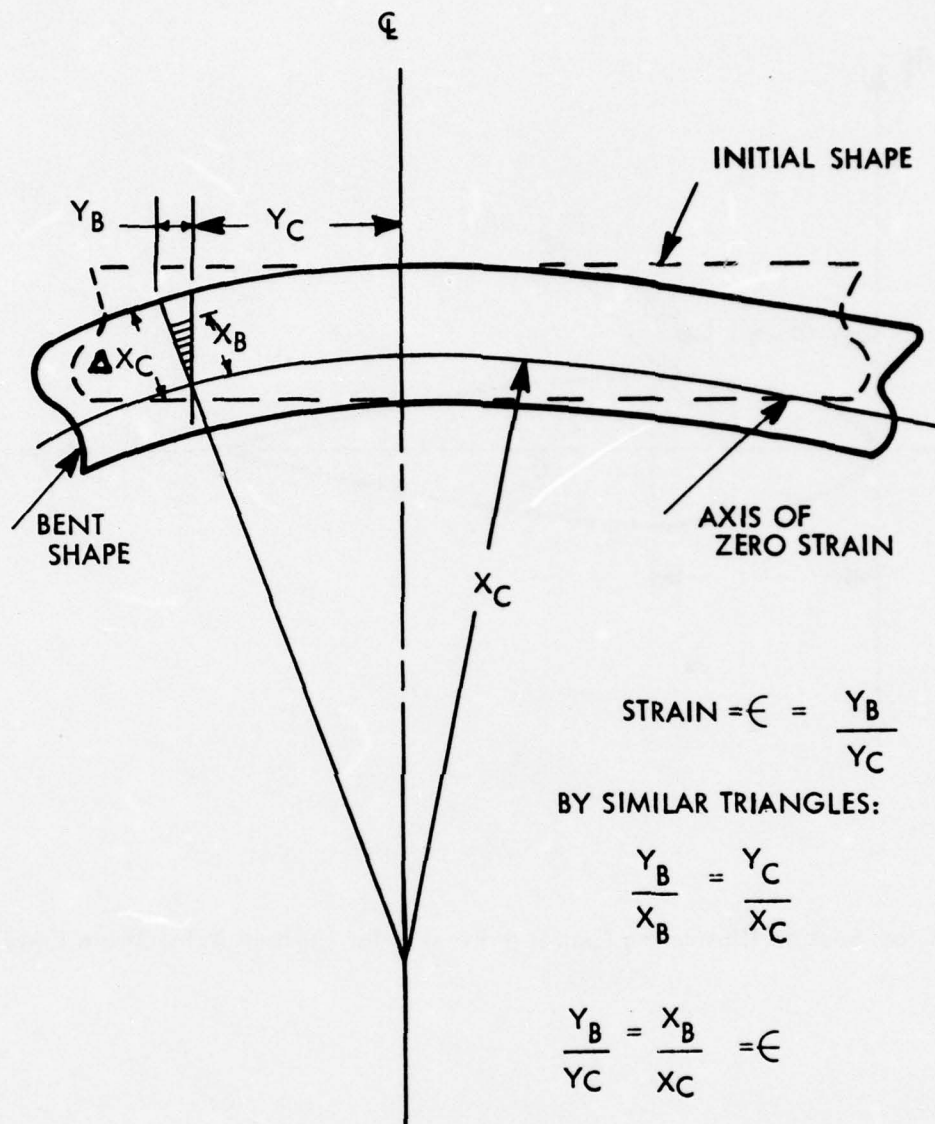
Bending Strain Relationship

Figure 8
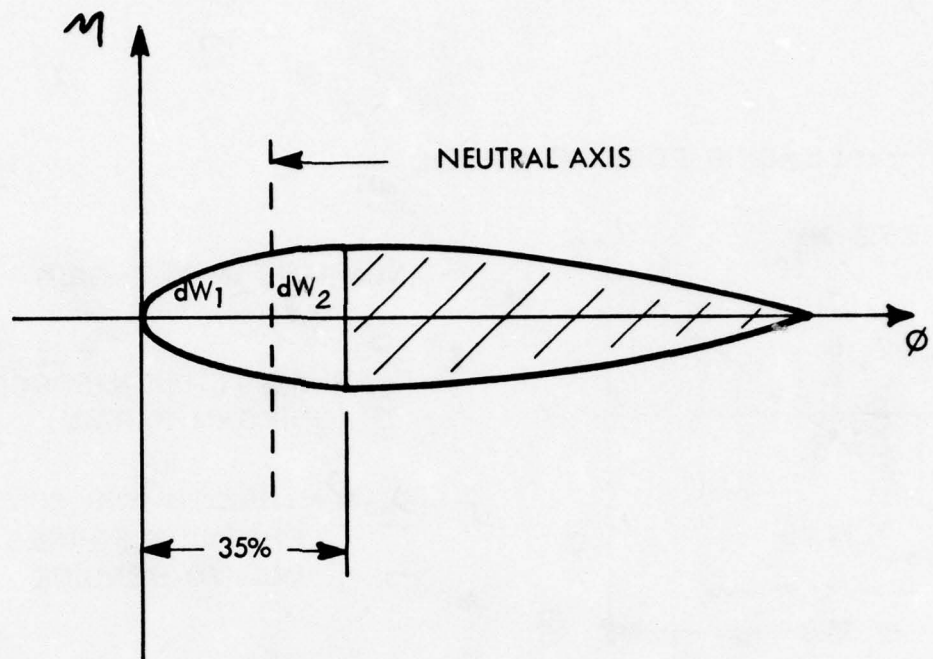
Neutral Axis on Cable Cross Section

Figure 9
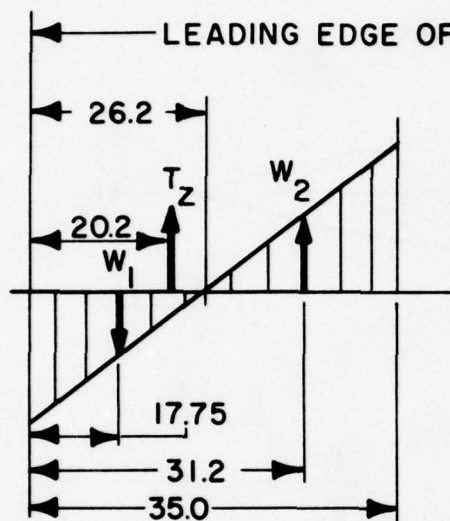
Figure 10. Combined Effect of Pure Tension Force and Bending Forces.

WIREWAY FOR COPPER CONDUCTOR

FIBERGLASS STRENGTH
MEMBER

5%

2.93%

ELASTOMER FAIRING

30%

35%

NACA $63_3 - 018$
CHORD LENGTH = 3.0"
NUMBER IN % CHORD
MAX THICKNESS = d = 0.54"
C. T. = 20.7%
C. G. = 25.8%
C. P. = 25.0%

AREA OF STRENGTH MEMBER = 0.361 IN^2
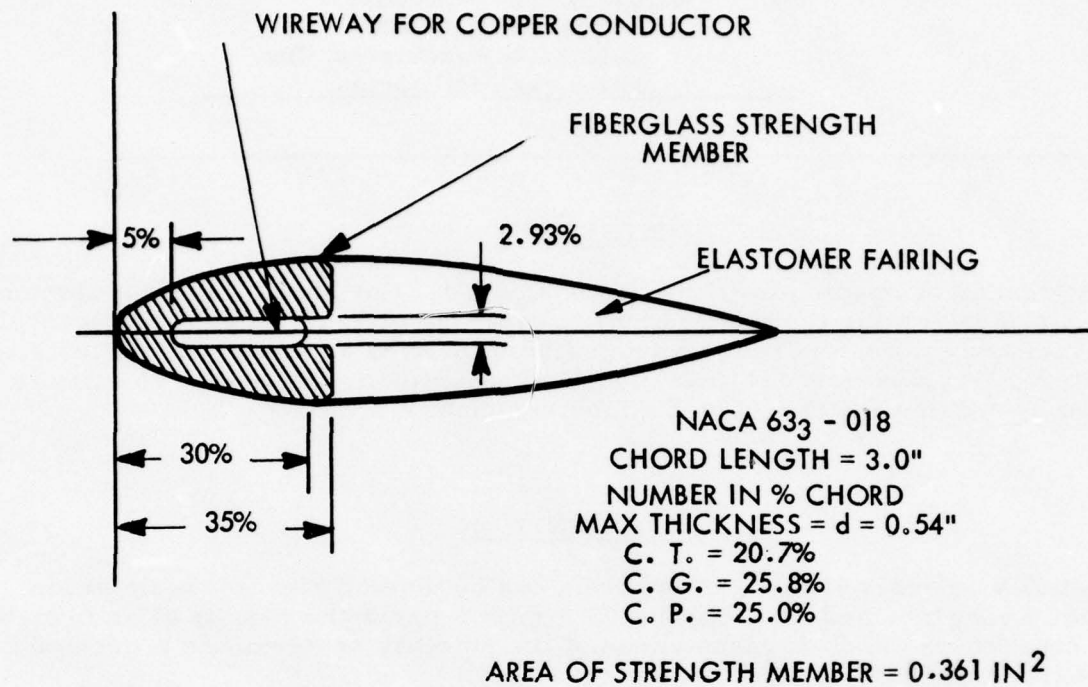
Internal Configuration of Favored Cable Cross Section

Figure 11

53

FAIRED TOWCABLE DIVERGENCE CRITERIA

by Dr. G. A. Hegemier
Research Consultant
Ballard & Associates, Inc.
Pasadena, California

ABSTRACT

The divergence of a faired towcable is considered. For long cables an elementary relation governing the minimum divergence velocity is derived and several sufficiency conditions for freedom from divergence for all towing velocities are presented. For cables of arbitrary length the minimum divergence velocity is obtained by seeking the zero of a 2 x 2 determinant.

INTRODUCTION

The stability analysis of a faired towcable can be divided into two basic areas: 1) cable divergence and 2) cable flutter. In this paper the results of an investigation concerning the divergence phase of the stability problem are presented and discussed.

The intended meaning of "cable divergence" as used here parallels "wing divergence" in the theory of aeroelasticity. However, while wing divergence and aeroelasticity are mentioned, we note that an analysis of a cable differs considerably from that of a conventional wing. For example the deflections of a wing in the chordwise direction can usually be ignored. This is not possible in the case of a cable since it is flexible enough (by virtue of its length) to permit large chordwise deflections. While an airplane wing resists loads in shear and torsion, a cable carries its load primarily in tension, although bending and torsional effects may not be negligible. Further, the influence of drag, which is neglected in a classical aeroelastic treatment, plays a major role in the cable problem due to the large aspect ratios involved.

The mathematical cable model considered in this paper includes the affects of tension, the bending rigidities in both principal directions, torsional rigidity (including the increase in the cable torsional rigidity due to tension), drag, and lift. The deflection field investigated comprises chordwise angular rotation, chordwise deflection, and lateral deflection.

In the discussion to follow an effort is made to arrive at simple but meaningful relations concerning the minimum divergence velocity and sufficient conditions for stability. For cables of arbitrary length, the final results are obtained in the form of a 2 x 2 determinant, the zeros of which define the divergence criteria. For sufficiently long cables this determinant is simplified considerably and an

54

elementary equality is found to govern the minimum divergence velocity. In the case of long cables several useful inequalities are obtained that guarantee freedom from divergence for all towing velocities and clearly indicate the importance of certain parametric combinations.

FORMULATION OF THE PROBLEM

Consider a towed cable as illustrated in Fig. 1. Let us assume the cable is initially untwisted with all chordwise sections at zero angle of attack with respect to the normal flow velocity component V_n. This state of deflection will be referred to in the following as the undisturbed state.

Next, let us introduce small disturbances into the system. The objective of the divergence analysis is to determine if the undisturbed position of the cable is statically stable with respect to such disturbances.

Stability Concept

As is customary, we shall define a divergence velocity as that towing velocity for which, under a small static perturbation in deflection from the undisturbed configuration, the hydrodynamic forces and moments acting on the cable exactly balance the restoring forces and moments of the cable. For velocities slightly above the minimum divergence velocity the cable can be expected to deviate from the undisturbed position; below the minimum divergence velocity the cable will be stable with respect to divergence. Although there may exist multiple regions of stable and unstable behavior (with respect to towing velocity), only the lowest divergence speed is usually of practical interest.

Basic Assumptions

In the sequel the cable will be modeled as an elastic beam of airfoil shaped cross section (symmetric) with tension and fluid forces applied as external forces. Where more than one material is involved the various constituents will be assumed securely bonded, thus allowing an equivalent beam analysis. Any warping of the cross sections during deformation will be assumed small and neglected. The hydrodynamic forces will be calculated from classical strip theory. The latter appears justified in view of the essentially infinite aspect ratio of the cable.

Center of Tension, Shear, Pressure

Several terms will be referred to repeatedly in the text. Among these are the cross sectional shear center, center of pressure (or aerodynamic center) and the center of tension. The algebraic positive signs of these quantities are noted in Fig. 2. The center of pressure and shear center have their usual meaning and do not deserve comment here. The center of tension, as used here, refers to that point on the chord corresponding to the centroid of a stress field resulting from a cable under tension only. By definition then, the first moment of the tensile stress field vanishes at the center of tension. If one assumes the various cables materials are bonded together, and hence that a linear strain distribution is the result of cable deformation, the center of tension is obtained in terms of the cable material and geometric properties, via an elementary calculation, as

$$x_T' = \frac{\int_A x' E(x', y') \, dA}{\int_A E(x', y') \, dA} \tag{1}$$

Here x_T' is a point on the chord, measured from the origin of the x', y' coordinates (see Fig. 2). The quantity A represents the cross sectional area of the cable. A further calculation indicates the center of tension is coincident with the neutral axis for bending about the y' axis.

Beam Equations

Let x, y, z be a rectangular coordinate frame, attached to the cable in the undisturbed state as illustrated in Fig. 2. The z axis lies along the locus of local shear centers (elastic axis). This line will be selected as a reference line. In addition, let x', y', z' be a set of deformed coordinates, attached to the cable during a deformation from the undisturbed configuration. According to classical beam theory we have

$$\frac{B_1}{R_1} = M_{x'} \; ; \qquad \frac{B_2}{R_2} = (M_{y'})_T \; ; \qquad C\theta = M_{z'} \tag{2a}$$

Here B_1, B_2 are the bending rigidities about the x' and y' axes respectively; R_1, R_2 are radii of curvature in the y', z' and z', x' planes respectively; R_1 refers to the elastic axis and R_2 to the neutral axis (center of tension) for bending in the z', x' plane. The sign convention for moments $M_{x'}$, $M_{y'}$, $M_{z'}$ is defined in Fig. 2. The quantity $(M_{y'})_T$ in (2a) is the moment at the center of tension about an axis parallel to the y' axis. The quantity θ is the angle of twist per unit length.

It should be noted that the torsional constant C, in the presence of tension, depends on the cable tensile force T. This, of course, is not part of classical beam theory. (The reader is referred to[1,2] for a discussion of elastic torsion in the presence of initial axial stress.) In general C has the form

$$C = (C)_{T=0} + \int \int_A \sigma_{z'z'} \, r^2 \, dx' dy' \tag{2b}$$

where $\sigma_{z'z'}$ is the axial stress due to tension, $r^2 = x'^2 + y'^2$, and $(C)_{T=0}$ denotes the torsional rigidity under zero tension (classical torsional rigidity). For any given cable one can write

$$C = (C)_{T=0} + \alpha T \; , \quad \alpha > 0 \tag{2c}$$

where α is a parameter depending on the geometry and distribution of Young's modulus.

Curvature - Displacement

Consider now displacements u, v and a rotation β, as illustrated in Fig. 2. Here u, v are, respectively, the displacements of the elastic axis in the x, y directions as measured from the undisturbed configuration, and β represents a rotation of the chord about the z axis. Within the context of a local stability analysis (we consider only the initiation of divergence) u, v and β will be assumed small (infinitesimal). For small u, v and β one has approximately[3]

$$\frac{1}{R_1} = \frac{\beta}{R_e} - \frac{d^2 v}{ds^2}$$

$$\frac{1}{R_2} = \frac{1}{R_T} + \frac{u}{R_T{}^2} + \frac{d^2u}{ds^2} \tag{3}$$

$$\theta = \frac{d\beta}{ds} + \frac{1}{R_e}\frac{dv}{ds}$$

where R_e and R_T refer to the radii of curvature of the elastic axis and the center of tension, respectively, in the undisturbed state.

Substituting equations (3) into equations (2a) we obtain the displacement - moment relations

$$B_1\left(\frac{\beta}{R_e} - \frac{d^2v}{ds^2}\right) = M_{x'}$$

$$B_2\left(\frac{1}{R_T} + \frac{u}{R_T{}^2} + \frac{d^2u}{ds^2}\right) = (M_{y'})_T \tag{4}$$

$$C\left(\frac{d\beta}{ds} + \frac{1}{R_e}\frac{dv}{ds}\right) = M_{z'}$$

Undisturbed State

In the undisturbed configuration one has

$$M_{x'} = M_x = M_{z'} = M_z = 0$$

$$u = v = \beta = 0 \tag{5a}$$

$$\frac{B_2}{R_T} = (M_y)_T = M_y + Te \tag{5b}$$

Perturbation Equations

The moments in the x', y', z' system are related to the undisturbed moments and the displacements u, v, β by

$$M_{x'} = (M_y)_T\,\beta + M_{x'}^* + O(u^2, v^2, \beta^2)$$

$$M_{y'} = M_y + O(u^2, v^2, \beta^2) \tag{6}$$

$$M_{z'} = (M_y)_T\frac{dv}{ds} + M_{z'}^* + O(u^2, v^2, \beta^2)$$

The terms in equation (6) arise from two sources: 1) undisturbed moments (which do not change direction and magnitude to the first order in v, v, β)

having components along x', y', z' and 2) moments induced by u, v, β; e.g., from fluid forces and tension.

The induced moments $M_{x'}^{*}$ and $M_{z'}^{*}$, are given by

$$\frac{d \ M_{x'}^{*}}{ds^2} = -\frac{1}{2} \ \rho \ V_n^2 \ c\beta C_{\ell\beta} - T \ \frac{d^2}{ds^2} \ (v + e\beta)$$

(7)

$$\frac{d \ M_{z'}^{*}}{ds} = -\frac{1}{2} \ \rho V_n^2 \ ca\beta C_{\ell\beta} - T \ \frac{d^2}{ds^2} \ (v + e\beta) \ e$$

In deriving (7), the airfoil cross section of the cable was assumed efficient, i.e., the drag coefficient was assumed much smaller than the sectional left coefficient. Classical strip theory was used to represent the fluid forces.

After differentiating equations (4) and (5) with respect to s and combining the resulting equations with equations (5b) and (7), one obtains

$$\frac{d^2}{ds^2} \left(B_1 \ \frac{d^2 v}{ds^2} \right) - T \ \frac{d^2}{ds^2} \ (v + e\beta) + \frac{d^2}{ds^2} \left[\left((M_y)_T - \frac{B_1}{R_e} \right)\beta \right] = \frac{1}{2} \ \rho V_n^2 \ c \beta \ C_{\ell\beta}$$

$$\frac{d^2}{ds^2} \left[B_2 \left(\frac{u}{R_T^2} + \frac{d^2 u}{ds^2} \right) \right] = 0$$

(8)

$$\frac{d}{ds} \left(C \ \frac{d\beta}{ds} \right) + T \ \frac{d^2}{ds^2} \ [(v + e\beta) \ e] + \frac{d}{ds} \left[\left(\frac{C}{R_e} - (M_y)_T \right) \frac{dv}{ds} \right] = -\frac{1}{2} \rho V_n^2 \ c a\beta C_{\ell\beta}$$

The second of equations (8) implies $u \equiv 0$ to first order in the perturbation quanties. We need therefore only consider the first and third equations. Now,

$$(M_y)_T = \frac{B_2}{R_T} = \frac{B_2}{R_e + e} = \frac{B_2}{R_e} \ \left(1 - \frac{e}{R_e} + \dots \right)$$

(9)

and since, in general, $e/R \ll 1$, one has approximately

$$(M_y)_T \doteq \frac{B_2}{R_e}$$

(10)

Employing equation (10), the first and third of equations (8) can be written

$$\frac{d^2}{ds^2}\left(B_1 \frac{d^2v}{ds^2}\right) - T \frac{d^2}{ds^2} (v + e\beta) + \frac{d^2}{ds^2}\left[\beta\left(\frac{B_2 - B_1}{R_e}\right)\right] = q_n c \beta C_{\ell\beta}$$

(11)

$$\frac{d}{ds}\left(C \frac{d\beta}{ds}\right) + T \frac{d^2}{ds^2}(v + e\beta) e + \frac{d}{ds}\left[\left(\frac{C - B_2}{R_e}\right)\frac{dv}{ds}\right] = -q_n c a \beta C_{\ell\beta}$$

Here $q_n \equiv \frac{1}{2} \rho v_n^2$.

Equations (11) are perturbation equations governing small cable deformations from the undisturbed state. They are quite general, e.g., they admit variable cable properties with respect to the span coordinate s; the undisturbed curvature can be large and vary with s; the tension field can vary with s, etc. We note that the influence of tangential drag has been implicitly included and manifests itself through the distribution of T along the span.

SOLUTION OF THE PERTURBATION EQUATIONS

Boundary Conditions

For the purpose of this analysis the cable ends will be assumed hinged with respect to the v displacement and fixed with respect to a rotation about the z' axis. These boundary conditions can be written as

$$v(0) = v(\ell) = 0$$

$$\frac{d^2v}{ds^2}(0) = \frac{d^2v}{ds^2}(\ell) = 0$$

(12)

$$\beta(0) = \beta(\ell) = 0$$

Solution Method

We formally expand v and β into the following series, each term of which satisfies the boundary conditions (12)

$$v = \sum_{n=1}^{\infty} a_n \sin \frac{n\pi s}{\ell}$$

(13)

$$\beta = \sum_{n=1}^{\infty} b_n \sin \frac{n\pi s}{\ell}$$

As an approximation to the lowest mode, leading to the minimum divergence velocity, only the first (n = 1) terms of equations (13) are retained. A substitution of the resulting relations for v and ß into the differential equations (11) leads to the following errors for the first and second of (11) respectively.

$$\epsilon_1(s) = -a_1\left(\frac{\pi}{\ell}\right)^2 \frac{d^2}{ds^2}\left(B_1 \sin \frac{\pi s}{\ell}\right) + T(a_1 + eb_1)\left(\frac{\pi}{\ell}\right)^2 \sin \frac{\pi s}{\ell}$$

$$+ b_1 \frac{d^2}{ds^2}\left[\left(\frac{B_2 - B_1}{R_e}\right) \sin \frac{\pi s}{\ell}\right] - q_n cb_1 C_{\ell\beta} \sin \frac{\pi s}{\ell}$$

$$(15)$$

$$\epsilon_2(s) = b_1\left(\frac{\pi}{s}\right) \frac{d}{ds}\left(C \cos \frac{\pi s}{\ell}\right) + T\left(\frac{\pi}{\ell}\right)^2 e(a_1 + eb_1) \sin \frac{\pi s}{\ell}$$

$$+ \left(\frac{\pi a_1}{\ell}\right) \frac{d}{ds}\left[\left(\frac{C - B_2}{R_e}\right) \cos \frac{\pi s}{\ell}\right] - q_n ca C_{\ell\beta} b_1 \sin \frac{\pi s}{\ell}$$

Galerkin's method[4] is now utilized. Accordingly the errors are averaged by

$$\int_o^\ell \epsilon_1(s) \sin \frac{\pi s}{\ell} \, ds = 0 \quad ; \quad \int_o^\ell \epsilon_2(s) \sin \frac{\pi s}{\ell} \, ds = 0 \qquad (16)$$

Following a few integrations by parts we obtain two equations for the two unknowns, a_1 and b_1

$$\left|\bar{B}_1\left(\frac{\pi}{\ell}\right)^4 + \bar{T}\left(\frac{\pi}{\ell}\right)^2\right| a_1 + \left|\bar{T}e\left(\frac{\pi}{\ell}\right)^2 - \left(\frac{\pi}{\ell}\right)^2 \bar{B}_{12} - c\,C_{\ell\beta}\,q\right| b_1 = 0$$

$$(17)$$

$$\left|-\bar{T}e\left(\frac{\pi}{\ell}\right) - \bar{C}_{12}\left(\frac{\pi}{\ell}\right)\right| a_1 + \left|-\left(\frac{\pi}{\ell}\right)^2 \bar{C} - \left(\frac{\pi}{\ell}\right)^2 \bar{T}e^2 + c\,C_{\ell\beta}\,a\bar{q}\right| b_1 = 0$$

Here

$$\bar{T} \equiv \frac{2}{\ell} \int_o^\ell T(s) \sin^2 \frac{\pi s}{\ell} \, ds$$

$$\bar{B}_1 \equiv \frac{2}{\ell} \int_o^\ell B_1 \sin^2 \frac{\pi s}{\ell} \, ds$$

$$(18)$$

$$\bar{B}_{12} \equiv \frac{2}{\ell} \int_o^\ell \left(\frac{B_2 - B_1}{R_e}\right) \sin^2 \frac{\pi s}{\ell} \, ds$$

$$\bar{q} \equiv \frac{2}{\ell} \int_o^\ell q_n(s) \sin^2 \frac{\pi s}{\ell} \, ds$$

$$\bar{C}_{12} \equiv \frac{2}{\ell} \int_o^\ell \left(\frac{C - B_2}{R_e}\right) \sin^2 \frac{\pi s}{\ell} \, ds$$

STABILITY CONDITIONS

Equations (17) possess nontrivial solutions if and only if the determinant of the coefficients vanish; the latter condition leads to the stability determinant:

$$\begin{vmatrix} \bar{B}_1 \left(\dfrac{\pi}{\ell}\right)^2 + \bar{T} & \left(\dfrac{\pi}{\ell}\right)^2 (\bar{T}e - \bar{B}_{12}) - c\, C_{\ell\beta}\, \bar{q} \\[2ex] \bar{T}e + \bar{C}_{12} & \left(\dfrac{\pi}{\ell}\right)^2 (\bar{C} + \bar{T}e^2) - c\, a\, C_{\ell\beta}\, \bar{q} \end{vmatrix} = 0 \qquad (19)$$

An expansion of (19) yields

$$\bar{q}\, c\, C_{\ell\beta} \left[\, \bar{T}(a - e) - \bar{C}_{12} \right]$$

$$+ \left(\frac{\pi}{\ell}\right)^2 \left[\, \bar{B}_1\, c\, C_{\ell\beta}\, a\, \bar{q} - \bar{C}\bar{T} - \bar{T}e\bar{B}_{12} + \bar{C}_{12}\bar{T}e - \bar{C}_{12}\bar{B}_{12} \right] \qquad (20)$$

$$+ \left(\frac{\pi}{\ell}\right)^4 \left[\, -\bar{B}_1\bar{C} - \bar{T}e^2 \right] = 0$$

Considerable insight into the divergence problem can be obtained at this point by observing equation (20) in the limit as $(\pi/\ell)^2 \to 0$, i.e., for long cables. In this case it is evident that the first group of terms in (20) dominate and the divergence condition is governed by

$$\bar{q}\, c\, C_{\ell\beta} \left[\, \bar{T}(a - e) - \bar{C}_{12} \right] = 0 \qquad (21)$$

whereby, for non trivial q, the minimum divergence velocity is obtained from

$$\bar{T}(a - e) = \bar{C}_{12} \qquad \text{(defines divergence velocity)} \qquad (22)$$

By virtue of equation (22) and the geometry of the problem, one concludes that a sufficient condition for freedom from divergence at all towing velocities for long cables is

$$\bar{T}(e - a) > -\bar{C}_{12} \qquad \text{(sufficient condition for stability)} \qquad (23)$$

The term $(e - a)$ in (23) represents the distance between the center of tension and the center of pressure; its sign is positive if the center of tension lies ahead of the center of pressure. Equation (23) implies optimum first mode conditions (with respect to divergence) occur when 1) $(e - a)$ is a large as possible with positive sign, 2) B_2 is as small as possible, and 3) C is as large as possible.

Several other more restrictive, but useful sufficiency conditions for stability can be derived from (23). For example, since

$$|\bar{C}_{12}| = \frac{2}{\ell} \left| \int_{o}^{\ell} \left(\frac{C-B_2}{R_e} \right) \sin^2 \frac{\pi s}{\ell}\, ds \right| \leq \frac{2}{\ell} \int_{o}^{\ell} \left| \frac{C-B_2}{R_e} \right| \sin^2 \frac{\pi s}{\ell}\, ds$$

$$\leq \max_{s} \left| \frac{C-B_2}{R_e} \right|$$

one concludes the system is stable if

$$(e-a) > \max_{s} \left| \frac{C-B_2}{(R_e)(\bar{T})} \right| \qquad \begin{array}{l}\text{(sufficient condition} \\ \text{for stability)}\end{array} \tag{24}$$

A further sufficiency condition is obtained from equation (23) if one notes that C takes on a minimum value (according to equation (2c)) when $T = 0$. This condition is

$$e-a > 0 \quad ; \quad (C)_{T=0} - B_2 \geq 0 \qquad \begin{array}{l}\text{(sufficient condition} \\ \text{for stability)}\end{array} \tag{25}$$

CONCLUSION

We conclude by noting the following results of the analysis:

1) For sufficiently long cables the minimum divergence velocity is governed by the relation: $\bar{T}(e-a) = \bar{C}_{12}$.

2) Any one of the following are sufficient conditions for freedom of divergence of long cables.

   a) $\bar{T}(e-a) > -\bar{C}_{12}$

   b) $(e-a) > \max_{s} \left| \dfrac{C-B_2}{(R_e)(T)} \right|$

   c) $e-a > 0$, $(C)_{T=0} - B_2 \geq 0$

3) In general, optimum stability conditions for long cables occur when

   a) the center of tension e is forward of the center of pressure a;

   b) the distance $(e-a)$ is a maximum;

   c) the chordwise bending rigidity B_2 is a minimum and

   d) the torsional rigidity is a maximum.

4. The minimum divergence velocity for all cable lengths can be obtained by determining the minimum q yielding a zero of the determinant (19).

NOMENCLATURE

a	distance from elastic axis to aerodynamic center
c	chord
e	distance from elastic axis to center of tension
q_n	$(1/2)\,\rho\,V_n^2$
s	running coordinate
u, v	small displacements from the undisturbed position in the x, y directions respectively
x, y, z	coordinates of undisturbed state
x', y', z'	coordinates of perturbed state
B_1	bending rigidity about x' axis (bending in y', z' plane)
B_2	bending rigidity about center of tension (neutral axis for bending x', z' plane)
C	effective torsional rigidity
R_1	radius of curvature of elastic axis in z', y' plane
R_2	radius of curvature of tension axis in x', z' plane
R_e	radius of curvature of elastic axis in x, z plane
R_T	radius of curvature of tension axis in x, z plane
T	tension force
V_n	(See Figs. 1 and 2)
$\overline{T}, \overline{B}_1, \overline{B}_{12}, \overline{q}, \overline{C}_{12}$	See equation (18)
β	angle of rotation about the z axis
θ	angle of twist per unit length
ρ	fluid density
$C_{\ell\beta}$	sectional lift curve slope

REFERENCES

(1) Goodier, J. N., "Elastic Torsion in the Presence of Initial Axial Stress", J. Appl. Mech., 17, (1950)

(2) Engel, H. L. and J. N. Goodier, "Measurements of Torsional Stiffness Changes and Instability Due to Tension, Compression, and Bending", J. Appl. Mech., 20, (1953)

(3) Timoshenko, S., Theory of Elastic Stability, McGraw-Hill, (1936).

(4)   Kantorovich, L. V. and V. I. Krylov, <u>Approximate Methods of Higher Analysis</u>, P. Noordhoff, ltd., (1958).

(5)   Fung, Y. C., <u>The Theory of Aeroelasticity</u>, John Wiley & Sons, Inc., (1955).

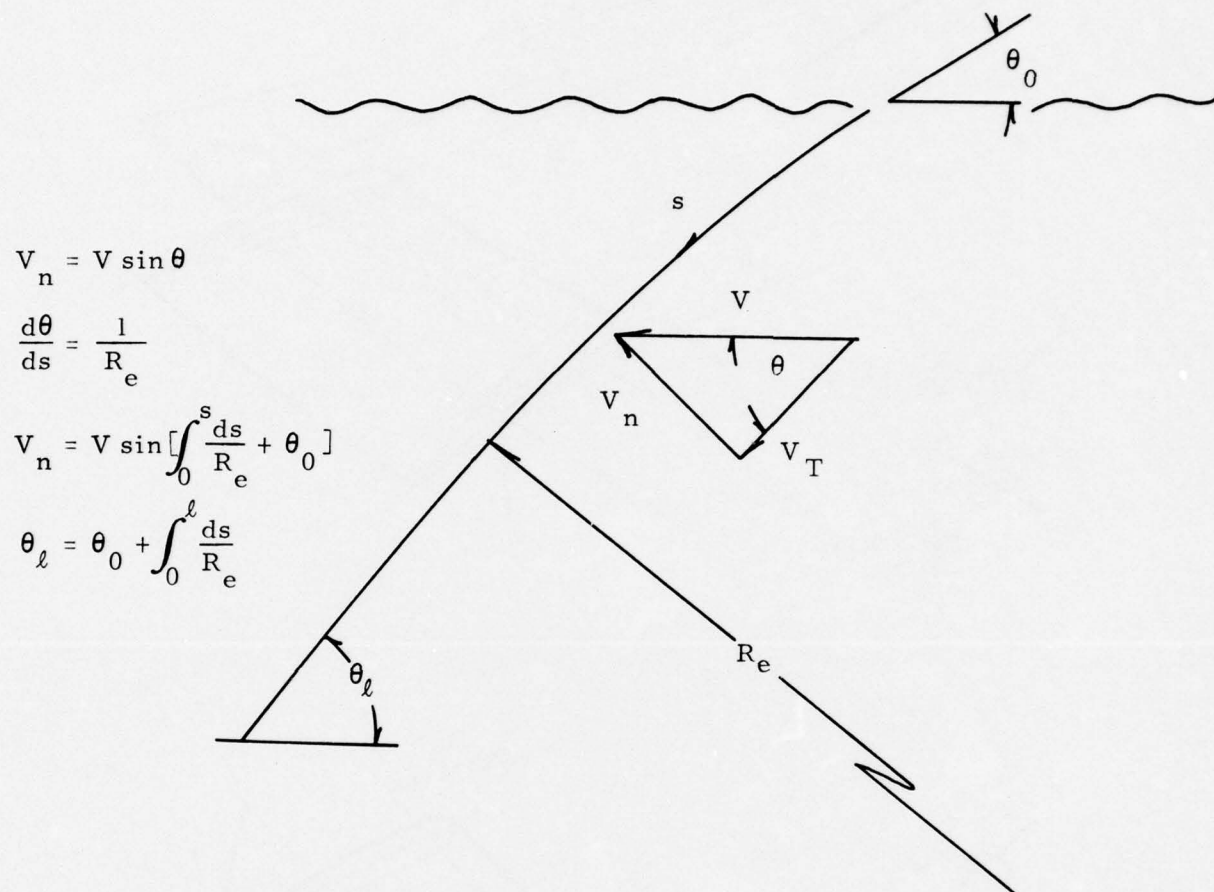$$V_n = V \sin \theta$$

$$\frac{d\theta}{ds} = \frac{1}{R_e}$$

$$V_n = V \sin \left[\int_0^s \frac{ds}{R_e} + \theta_0 \right]$$

$$\theta_\ell = \theta_0 + \int_0^\ell \frac{ds}{R_e}$$

Fig. 1 Undisturbed Configuration

65

Fig. 2   Coordinate System

THE DIVERGENCE AND FLUTTER CRITERIA FOR FAIRED TOW CABLES

by J. S. Kanno
Senior Technical Specialist
Space and Information Systems
North American Aviation, Inc.

ABSTRACT

During 1965, the Ocean Systems Operations organization of North American Aviation, Inc. designed and fabricated two test sections of a faired tow cable for the US Navy Electronics Laboratory (Contract N123(935)-52188A). This paper reviews the highlights of the theoretical analysis of the hydroelastic behavior of marine faired tow cables which was formulated and carried out in compliance with the contracted requirements. The discussion of the basic phenomena, the mathematical model, the criteria and the conclusions pertinent to the prevention of flutter, torsional divergence, and cable attachment sway angle divergence is presented. Calculated stability boundaries reflecting the hydroelastic performance of the NAA-faired tow cable are also presented. Only material prepared for and submitted in the final report[1] of the contracted work is reviewed in this paper.

INTRODUCTION

The potential high-speed capability of a marine tow cable faired to reduce the hydrodynamic drag loading and applied to the towing of a deeply submerged sonar instrument platform is drastically impaired by the occurrence of hydroelastic torsional divergence and flutter. A well designed tow cable must trail behind the towing vehicle keeping the faired cross-section always aligned in the direction of the towing velocity. Lateral angles of attack of the cable section, due to the torsional deformations of the tow cable, cause large lateral hydrodynamic loads to occur. This, in turn, disrupts the intended trim state of the towed body, because of the change of inclination of the cable tension force at the towed body. In the extreme case, the accompanying unstable response culminates either with the towed system at the surface of the sea or with a severed tow cable.

As depicted in Fig. 1, the deformed state of the faired tow cable is characterized by large cable drag loads, large cable tension and inplane bending moments. The external load is maintained in equilibrium by the cable tension acting in conjunction with the elastically deformed inplane curvature of the tension axis. For a continuous cable, the chordwise shear is generally ineffective because of the significant deformation of the tension axis. From the structural standpoint, the faired tow cable is a long flat ribbon that is forced to bend in the plane of the ribbon. From the hydrodynamic standpoint, the faired tow cable is a symmetrically sectioned and laterally oriented lifting surface of infinite aspect ratio. The former point of view suggests torsional buckling, whereas the latter suggests hydroelastic instabilities.

The fundamental structural response properties characteristic of the faired tow cable are depicted in Figs. 2 and 3. In Fig. 2, the lateral displacement, v, and the torsional displacement, ψ, due to an imposed lateral load, F, are depicted. The cable is forced to bend in the plane of the cable and is also presumed to be simply supported at the two ends. The structural reference axis (SRA), used to define the torsional angular displacement, is the

axis of the cable center of twist for the cable exhibiting no inplane bending curvature. For no cable tension, the SRA is the elastic axis, that is, the line of sectional shear centers. For predominant cable tension, the SRA is the tension axis, that is, the line of the sectional tension stress resultants. For most practical tow cable structures, the elastic and the tension axes are located very close to each other. Throughout this work they are presumed to be essentially one and the same.

The lateral displacement and the twist caused by a constant lateral load placed at various chordwise locations are depicted in terms of influence functions in Fig. 3. The imposed inplane curvature is presumed to be less than that required to buckle the tow cable. Two chordwise points denoted by (t) and (r) and designating the zero angular displacement and the zero transverse displacement load locations, respectively, characterize the structural response and the imposed inplane curvature. It is apparent that the center of twist which for the straight cable is defined by the SRA is located for the cable arched in the plane of the cable behind the SRA at the point denoted by (t). As the intensity of the imposed inplane curvature is increased, the point (t) moves farther aft and the point (r) moves farther forward. At the imposed inplane curvature, for which the two points coalesce, the structure buckles torsionally and no longer resists any lateral load. More critical than the structural torsional buckling, however, is the hydroelastic torsional divergence of the tow cable. Hydroelastic torsional divergence, for which the required chordwise shift of the center of twist is less, occurs when the center of twist moves aft of the center of pressure of the lateral static hydrodynamic lift. Generally, this center of pressure is located at the quarter-chord point. The chordwise movement of the center of twist is proportional to the intensity of the imposed inplane bending moment. Although both the shear center and the tension center may be designed well forward of the quarter-chord point to prevent hydroelastic torsional divergence, the operational towing loads may still be encountered which cause the center of twist to move far enough aft toward the quarter-chord point such that marginally stable behavior and hydroelastic divergence occur.

The fundamental dynamic lateral translational and torsional behaviors associated with flutter are depicted in Fig. 4. The lateral translation and twist exhibit coupled oscillations. The torsional oscillation leads the transverse oscillation essentially by the phase angle of a quarter of a cycle. The reduced frequency, k, due to the low frequency of the coupled oscillation and the small chord length of the tow cable, is generally a very small value. The coupling between the transverse and the torsional behaviors governed by the interaction attributable to the sectional elastic, inertial and hydrodynamic properties determines the amplitude ratios of the transverse and torsional oscillations and, consequently, the occurrence of flutter. It is apparent in Fig. 4 that the torsional amplitudes of the stable and unstable oscillations are, respectively, less and greater than the torsional amplitude of the neutrally stable oscillation. In the former case, fluid forces are generated which damp the oscillation whereas, in the latter case, fluid forces are generated which cause the amplitude of the oscillation to grow. Binary hydroelastic flutter is generally prevented by maintaining the center of mass of the cable structure noticeably forward of the midchord point.

MATHEMATICAL MODEL OF THE TOW CABLE

An accurate simulation of the dynamics of the overall towed system would involve the mathematical representations of both the tow cable and the towed body. The dynamic behavior of one cannot be realistically separated from the dynamic behavior of the other. However, from the standpoint of preventing torsional divergence and flutter, it can be safely presumed that the cable proper must be stable regardless of the nature of the dynamic behavior of the towed body. A reasonable torsional divergence and flutter prevention criteria can be formulated by stipulating that the standing wave dynamic response of all conceivable spatial wavelengths of the tow cable be stable.

The mathematical model formulated to examine the hydroelastic behavior of a faired tow cable must at least include (a) the structural behavioral relationships describing the lateral buckling of a flat ribbon which is initially deformed in the plane of the ribbon; (b) structural behavioral relationships describing the structural stiffening due to the steady state tension of both the transverse displacement and the twist of the tow cable; and (c) distributed hydrodynamic lateral forces and twisting moments usually associated with the incompressible and invicid fluid flutter and divergence theory of high aspect ratio lifting surfaces. Since the torsional behavior is of fundamental concern, the formulation should include sufficient detail to show how the torsional rigidity and the chordwise location of the structural center of twist are influenced by the interaction reflected by the cross-sectional transverse distortions and stresses. The formulation of such a mathematical model does not require the development of any new fundamental theory. In fact, all pertinent theoretical considerations are found in readily available reference textbooks. Timoshenko[2], Goodier[3], and Bisplinghoff, Ashley and Halfman[4] constitute, respectively, excellent sources for the basic theories pertaining to the lateral buckling behavior of a flat ribbon, the structural torsional behavior including the stiffening effects of tension, and the hydrodynamic transverse forces and twisting moments.

The highlights of the formulation of the mathematical model of the faired tow cable and the corresponding simplifying assumptions and solution are reviewed in Fig. 5 and Tables 1 through 5. In Fig. 5 the structural sectional stress resultants and the lateral perturbations pertinent to the mathematical model are reviewed. The vectors, $\bar{P}$ and $\bar{M}_y$, consistent with the right-hand rule, respectively denote the steady state tension and the inplane bending moment. The vectors, v and ψ, also consistent with the right-hand rule, denote the transverse and torsional perturbations, respectively. All other quantities designated by the upper case letters, M, V and T, denote the stress resultants attributable to the strains of the lateral perturbations.

The equations of motion of the lateral perturbations are presented in Tables 1 and 2. It is apparent that the elastic relationships of these equations reflect beam-type flexural and torsional behavior of the theory of the strength of materials. Aerodynamic two-dimensional strip theory based on the cross flow component of the free stream velocity is presumed to apply. The partial differential equations of the system are linearized by assuming that the transverse and torsional displacements constitute small perturbations about the steady deformed state. The small perturbations do not alter the steady state curvature nor the intensities of the steady state external and internal inplane tow cable loads. The tow cable, however, in changing its orientation by virtue of the lateral perturbations twists and bends in accordance with the imposed steady state curvature. The stress and the stress distribution across the section of the cable changes in accordance with the imposed steady state loads. The influence of the imposed steady deformed state in the derived elastic laws is reflected essentially by the terms $\bar{P}$ and $\bar{M}_y$ – that is, the steady state tension and the inplane bending moment, respectively. It is apparent in the equations of motion that the structural coupling between the transverse and the torsional perturbations entails the terms

$$\bar{M}_y \left(1 - \frac{B_\xi}{B_\eta}\right) \text{ and } \bar{M}_y \left(1 - \frac{C}{B_\eta}\right).$$

Additional coupling, namely, the cable mass static unbalance, $m\xi_0$, and that reflected by the hydrodynamic derivatives tabulated in Table 2, is also apparent in these equations.

The format of Table 2 is used to identify the various hydrodynamic derivatives pertinent to the lateral force and twisting moment. Quite often, the quasi-steady stability derivatives of the airfoil section are known. These are established by experimental measurements, and in such instances, these values may be used in place of the theoretical thin airfoil values.

In this study, except for the known $C_{l\alpha} = 5.3$ per radian, Theodorsen's thin airfoil stability derivatives were used throughout. The three-quarter chord point downwash velocity noted in Table 2 is

$$w_{3/4} = -\dot{v} + \frac{1}{2}\left(\frac{1}{2} - a\right)c\dot{\psi}.$$

Where a denotes the chordwise location of the midchord with respect to the SRA, in terms of the half-chord length. Positive values of a signify that the SRA is behind the midchord point. For chordwise locations of the SRA in front of the quarter-chord point, $a < -1/2$.

The assumptions pertaining to a simplified solution of the equations of motion are tabulated in Table 3. The assumed mode flutter equations of motion and the flutter characteristic equations derived consistently with these assumptions are presented in Table 4. The coefficients of the characteristic equation reflect the structural, inertial and hydrodynamic sectional properties as well as the towing speed and the spatial half-wavelength, l, of the presumed dynamic behavior. In this study, the coefficients and the roots, λ, as functions of the spatial half-wavelength were calculated and examined. Fortunately, the stability requirements can also be established from the inequalities of the Routh-Hurwitz stability criterion[5] — cf, Table 4 — and therefore a large amount of calculated dynamic response data is not needed. The results of the analytical analysis of the Routh-Hurwitz inequalities are presented in Table 5.

The two inequalities tabulated in Table 9 reflect (a) the sectional structural mass balancing required to prevent flutter and (b) the static stability margin with respect to the structural twist axis required to prevent torsional divergence. Both inequalities must be satisfied. The first relationship pertains to the prevention of adverse dynamic coupling between the transverse and torsional behaviors. It reveals that a forward location of the structural center of mass must be maintained in the design of the tow cable. The second relationship pertains to the maintenance of the center of pressure of the lateral static hydrodynamic lift behind the structural center of twist. Although both the elastic axis and the tension axis may be designed well forward of the quarter-chord point, the twist axis shifts toward the trailing edge because of the imposed steady state towing loads. The movement of the twist axis is governed essentially in accordance with the equation shown in Table 5.

FLUTTER AND DIVERGENCE BOUNDARIES OF THE TOW CABLE

The sectional mass balancing required to prevent the occurrence of flutter is depicted in Fig. 6. The equation of the boundary is established by the first relationship of Table 5. Superimposed in Fig. 6 is the point representing the inertial properties of the NAA tow cable. Calculations of the dynamic behavior representative of the NAA tow cable reflect free oscillations which damp to half-amplitude in 1/4 to 3/2 cycles of vibration.

The static stability margin with respect to the structural twist axis for the NAA tow cable is depicted in Fig. 7. These curves reflect in accordance with the second equation of Table 5, the influence of the steady state internal cable loads, $\bar{P}$ and $\bar{M}_y$. The ratio $(\bar{M}_y/\bar{P}_c)$, for a continuous tow cable, is largest at the lower terminal and decreases slowly over the length of the tow cable. The extent of the chordwise shift of the twist axis at the lower terminal described in terms of the cable drag load and the steady state towed body loads is

$$\left(\frac{\xi_T}{c}\right)_1 \cong -\frac{\left(C_d\right)_c (B\eta - C)}{W' C_D S} \cdot G\left(x, \frac{C_L}{C_D}\right)$$

where

$$\left(C_d\right)_c \equiv \frac{\text{running cable drag load, lbs/ft}}{\frac{1}{2} \rho \bar{V}^2 c}$$

$$G\left(x, \frac{C_L}{C_D}\right) \equiv \frac{x\left(\frac{C_L}{C_D} + x\right)}{\left[1 + \left(\frac{C_L}{C_D} + x\right)^2\right]^{3/2}}$$

$$x \equiv \frac{W'}{C_D \frac{1}{2} \rho \bar{V}^2 S}$$

It is apparent in Fig. 7 that the loss of the static stability margin is small at both low and high towing velocities. The loss of the static stability margin is greatest at an intermediate towing velocity. It is not enough to achieve by appropriate structural and hydrodynamic design a substantial initial static stability margin, $-1/2 (a + 1/2)$. Torsional divergence of the tow cable will still occur if the trim state of the towed body is not maintained at high lift-drag ratios. Unfortunately, the curves of Fig. 7 do not reveal the destabilizing influence of having an excessively small weight of the towed body in water. This information is readily established by the analytical determination of the properties that are related to the maximum destabilizing chordwise movement of the twist axis.

The dimensionless parameters describing the properties of the maximum chordwise shift of the twist axis are depicted in Fig. 8. Both the dimensionless movement of the twist axis and the towing velocity squared at which it occurs are shown plotted as functions of the trim state lift-drag ratio of the towed body. As implied in Fig. 8, the chordwise shift of the twist axis is maintained small by designing the towed system such that the value of the parameter

$$\frac{\left(C_d\right)_c (B\eta - C)}{W' C_D S}$$

is made as small as possible. Since $C_D S$ affects the drag performance of the towed system this property of the towed body can not be increased. The only towed body property which is easily adjusted without unduly penalizing the towed system is the weight of the towed body in water. It is apparent that the weight of the towed body in water can not be allowed to become too small.

Another source of tow cable hydroelastic divergence is that caused by the mechanical behavior of the towed body cable attachment assembly acting in conjunction with the sway angular perturbation of the tow cable. The pertinent elements of the problem associated with the hook's joint attachment assembly are depicted in Fig. 9. The assembly is free to pitch with respect to the towed body and is connected to the tow cable through an axial bearing which is aligned with the cable cross flow velocity. The inclination of the tow cable with respect to the towed body wind reference axis is denoted by the angle, θ_1. If the tow cable sways from a lateral disturbance as shown in Fig. 9, it is apparent that a lateral angle of attack of the cross flow is generated. This lateral angle of attack in turn generates a

corresponding lateral static hydrodynamic load. The lateral hydrodynamic load cannot be sustained by the structure without significant transverse deformations of the tow cable. The tow cable deforms in the direction of the load and increases the sway angular displacement of the tow cable at the attachment; the lateral angle of attack in turn is further increased and so is the corresponding lateral load.

The sway angular displacement of the tow cable at the lower attachment can diverge. Whether it does or does not depends on the dynamic pressure, the trim state of the towed body, the lateral flexibility of the tow cable, the hydroelastic static stability margin of the tow cable, and the torsional rigidity of the tow cable. If the tow cable is soft torsionally, and the hydroelastic static stability margin is large, the tow cable twists into the direction of the local freestream and tends to close the angle of attack opened by the sway angle perturbation. The criterion for stable behavior reflecting these properties is presented in Fig. 10. Curves pertaining to the NAA tow cable typical of the terms of the inequality which must be maintained for stable behavior are also depicted in Fig. 10. Although the cable proper is free of torsional divergence, it still exhibits cable attachment sway angle divergence over a brief interval of intermediate towing velocities.

The occurrence of torsional divergence and cable attachment sway angle divergence may be summarized in terms of the stability regimes of towed body trim state lift-drag ratios and towing velocities. Such a chart appropriate for the Lake Washington tow tests of the NAA tow cable conducted during 1966 is depicted in Fig. 11. The unstable regime for cable attachment sway angle divergence is a great deal larger than the unstable regime for cable torsional divergence. It is apparent that the attachment fitting should be modified so that either the torsional behavior of the tow cable is not mechanically constrained at the attachment fitting, or the constrained mechanical behavior of the tow cable as it sways does not generate a lateral angle of attack.

The torsional divergence preventive measures reviewed thus far involve, (1) designing the elastic axis and the tension axis well forward of the center of pressure of the lateral static hydrodynamic lift and, (2) maintaining the trim states of the towed body such that the twist axis does not shift chordwise too far aft towards the center of pressure. The chordwise shift of the twist axis is additionally governed by two design principles. These principles entail reducing the structural coupling parameter, $(1 - C/B_\eta)$, and the inplane bending moment, $\bar{M}_y$. The relationship between the parameter, $(1 - C/B_\eta)$, and the effective base-to-thickness ratio of the primary tension member of the tow cable is depicted in Fig. 12. The point representing the NAA tow cable is also shown superimposed on this relationship. Although the calculated sectional structural properties of the NAA tow cable include the contribution of the polypropylene trailing edge, the percentage contribution of the soft trailing edge — that is, 16.2 percent for B_η, and 0.6 percent for C — is too small to be significant. It is apparent in Fig. 12 that a moderate reduction of the structural coupling parameter, $(1 - C/B_\eta)$, is realized by a minor reduction of the effective base-to-thickness ratio of the steel leading edge section.

The reduction of the inplane bending moment, $\bar{M}_y$, achieved by using a linked tow cable is depicted in Figs. 13 and 14. Because of the short length of the basic cable link (Fig. 13) the cable drag load of the link is maintained in equilibrium by the chordwise shear as well as by the cable tension. The corresponding inplane bending deformation of the cable proper is less than the inplane bending deformation that is exhibited by an equivalent sectioned continuous cable. The reduction of the inplane bending moment of the linked tow cable as shown in Fig. 14 depends on the length of the link, L, the cable tension, $\bar{P}$, and the inplane bending flexural rigidity, B_η. It is apparent in Fig. 14 that very significant moment reductions are realized by the NAA linked tow cable especially at the intermediate and lower cable tensions at which torsional divergence of the tow cable occurs — cf., Fig. 11.

Unfortunately, in order to complete the theoretical analysis at the earliest possible date in the contracted work, the torsional divergence of the NAA tow cable was examined assuming that the tow cable is essentially continuous, and divergence properties of the linked tow cable per se were not examined at all. Additional analysis may reveal that for most practical towing missions the NAA linked tow cable is completely free of torsional divergence. If this is not the case, minor modifications of both the tow cable and the towed body will make it so.

CONCLUSIONS

Fundamental binary flutter is avoided by maintaining a forward chordwise location of the center of mass. This is not difficult to achieve because the structural design requirements for the prevention of torsional divergence places most of the primary structural material at the leading edge. Torsional divergence of the tow cable is avoided by maintaining the chordwise locations of the elastic and the tension axes well forward of the center of pressure of the lateral static hydrodynamic lift. Adverse chordwise movement of the structural twist axis, in view of the towed body, is avoided by maintaining an appreciable weight of the towed body in water and moderately high towed body trim lift-drag ratios and, in view of the tow cable, is avoided by reducing the sectional structural coupling and the imposed structural inplane bending moment. The imposed structural inplane bending moment exhibited by a continuous cable is significantly reduced by using the moment relieving pin jointed cable links. Tow cable sway angle divergence caused primarily by poor design of the towed body cable attachment assembly is prevented by designing the attachment assembly so that either the torsional response of the tow cable is not constrained by the fitting or the constrained mechanical behavior of the tow cable as it sways exhibits no cross flow angle of attack at the fitting.

NOMENCLATURE

SRA	The structural reference axis used to define the structural centers of twist of the tow cable exhibiting no inplane bending effect.
s, θ	The distance along the tow cable from the lower terminal and the inclination of the tow cable, respectively.
ξ, η, ζ	Cable attached Cartesian reference coordinate used to define the structural stress resultants – cf., Fig. 9.
v, ψ	Transverse and torsional lateral perturbation of the SRA at s.
K_ξ	Transverse flexural curvature of the tow cable.
V_η, M_ξ, T_ζ	Transverse shear, transverse bending moment and torsional moment of the tow cable.
$\bar{P}$	Steady state cable tension.
$\bar{M}_y$	Steady state inplane bending moment of which the positive sign denotes tension of the leading edge fibers.
B_ξ, B_η, C	Flexural and torsional structural rigidities of the tow cable with respect to the ξ, η and ζ axes, respectively – cf., Fig. 9.

F_y, M_T	Externally applied running transverse and torsional loads.
m	Structural mass per unit length of the tow cable.
ξ_0	Chordwise location of the structural mass center with respect to the SRA.
x_0	Chordwise location of the structural mass center behind the leading edge.
I'_0	Mass moment of inertia per unit length of the tow cable with respect to the center of mass.
C'_y	Sectional transverse lift coefficient.
$C'_{m\zeta}$	Sectional twisting moment coefficient with respect to the SRA.
c	Chordlength
ρ	Fluid mass density.
$\bar{V}$	Steady state towing velocity.
$\bar{V}_n$	Steady state cross flow velocity.
$w_{3/4}$	Downwash component of velocity at the 3/4 chordline.
ω	Oscillation frequency.
K	Reduced frequency, $(c\omega/2\,\bar{V}_n)$.
$C(k)$	Theodorsen's function representing unsteady wake effects.
a	Location of the midchord ahead of the SRA in terms of half-chordlengths.
$-1/2\,(a + 1/2)$	Location of the static lift center of pressure behind the SRA in terms of chordlengths.
ℓ	Vibrational half-wavelength exhibited along the tow cable axis.
μ	Hydrodynamic mass ratio, $m/\rho\pi\,(c/2)^2$.
ξ_T	Location of the twist axis with respect to the SRA.
$\left(c_d\right)_c$	Sectional drag coefficient of the tow cable based on the chordlength.
W'	Weight of the towed body in water.
C_L, C_D	Lift and drag coefficients of the towed body.
S	Reference area of the hydrodynamic forces of the towed body.
ν	Sway angular displacement of the tow cable – cf., Fig. 9.

REFERENCES

(1) "High Speed Towing Cable Development," Phase I, Volume II, Appendix C, SID 65-1279-2, Space and Information Systems Division, North American Aviation, Inc., 29 Oct. 1965.

(2) Timoshenko, S., Theory of Elastic Stability, McGraw-Hill Book Co., Inc., New York, 1966.

(3) Goodier, J. N., Torsion, "Handbook of Engineering Mechanics" edited by N. Flugge, McGraw-Hill Book Co., Inc., New York, 1962.

(4) Bisplinghoff, R. L., Ashley, H. and Halfman, R. L., Aeroelasticity, Addison-Wesley Publishing Co., Inc., Cambridge, 1942.

(5) Fung, Y. C., The Theory of Aeroelasticity, John Wiley and Sons, New York, 1955.

TABLE 1. EQUATIONS OF MOTION OF THE TOW CABLE

THE ELASTIC LAWS

Transverse

$$\frac{\partial^2}{\partial s^2}\left(B_\xi \frac{\partial^2 v}{\partial s^2}\right) - \frac{\partial}{\partial s}\left(\bar{P}\frac{\partial v}{\partial s}\right) - \frac{\partial^2}{\partial s^2}\left[\bar{M}_y\left(1 - \frac{B_\xi}{B_\eta}\right)\psi\right] = F_y, \text{ Lbs/Ft.}$$

Torsion

$$\frac{\partial}{\partial s}\left[\bar{M}_y\left(1 - \frac{C}{B_\eta}\right)\frac{\partial v}{\partial s}\right] + \frac{\partial}{\partial s}\left[(C+J)\frac{\partial \psi}{\partial s}\right] = -M_T, \text{ Lbs Ft./Ft.}$$

THE APPLIED DISTRIBUTED STRUCTURAL LOADS

Transverse

$$F_y = -m\left(\frac{\partial^2 v}{\partial t^2} + \xi_o \frac{\partial^2 \psi}{\partial t^2}\right) + c'_y \frac{1}{2}\rho \bar{V}_n^2 c$$
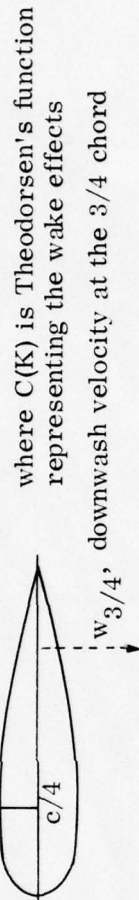
Torsion

$$M_T = -m\xi_o \frac{\partial^2 v}{\partial t^2} - (I'_o + m\xi_o^2)\frac{\partial^2 \psi}{\partial t^2} + c'_{m\zeta} \frac{1}{2}\rho \bar{V}_n^2 c^2$$

TABLE 2. LATERAL HYDRODYNAMIC DERIVATIVES, c'_y AND c'_{m_ζ} OF THE TOW CABLE

1. Quasi-Steady $c_{\iota\alpha}$

$K \approx 0,\quad (K) \approx 1$

$$c_{\iota\alpha}\left(\psi + \frac{w_{3/4}}{V_n}\right) \cdot C(K),$$

where C(K) is Theodorsen's function representing the wake effects

$w_{3/4}$, downwash velocity at the 3/4 chord

2. Quasi-Steady c_{mf} Load

$$\frac{\pi}{2} \cdot \frac{c}{V_n}\dot{\psi},\quad c_{\iota f} \cong \frac{\pi}{2}$$

3. Quasi-Steady $c_{m\dot{\alpha}}$ Load

$$-\frac{\pi}{2} \cdot \frac{c}{V_n}\frac{\ddot{v}}{V_n},\quad c_{\iota\dot{\alpha}} \cong \frac{\pi}{2}$$

4. Virtual Mass Terms

$$-\frac{\pi}{2}\frac{a}{2}\frac{c^2}{V_n^2}\ddot{\psi}$$

$$-\frac{\pi}{4}\frac{1}{2}(1/8 + a^2)\ c^2/\overline{V}_n^2\ \ddot{\psi}$$

Remaining virtual mass hydrodynamic derivatives

Structural Reference Axis

$a\frac{c}{2}$

0   c/4   c/2   3c/4   c

TABLE 3. ASSUMPTIONS PERTINENT TO SIMPLIFIED SOLUTION

1. The tension axis and the elastic axis used to define the structural reference axis are located at essentially the same chordwise position.

2. The steady state tension $\bar{P}$ and the steady state inplane bending moment $\bar{M}_y$ vary slowly along the length of the tow cable.

3. No appreciable unsteady hydrodynamic wake effects – i.e., reduced frequency, $K \approx 0$ and $C(K) \approx 1$.

4. The cross flow component of velocity, $\bar{V}_n = \bar{V} \sin \theta$ (where θ denotes the inclination of the tow cable) is also essentially constant over the length of the tow cable.

5. The significant behavior of the tow cable is of the form

$$v(s, t) = V(t) \sin \pi \frac{s}{\ell} \quad , \quad \psi(s, t) = \Psi(t) \sin \pi \frac{s}{\ell}$$

where ℓ denotes the spatial half wavelength of the lateral perturbation and $V(t)$ and $\Psi(t)$ denote the amplitudes of the dynamic behavior.

78

TABLE 4. REDUCED EQUATIONS OF MOTION OF THE LATERAL DISPLACEMENT
AND TWIST AMPLITUDES (FLUTTER EQUATIONS OF MOTION)

$$\begin{bmatrix} M_{11}, & M_{12} \\ M_{21}, & M_{22} \end{bmatrix} \begin{bmatrix} \ddot{V} \\ \ddot{\Psi} \end{bmatrix} + \begin{bmatrix} D_{11}, & D_{12} \\ D_{21}, & D_{22} \end{bmatrix} \begin{bmatrix} \dot{V} \\ \dot{\Psi} \end{bmatrix} + \begin{bmatrix} K_{11}, & K_{12} \\ K_{21}, & K_{22} \end{bmatrix} \begin{bmatrix} V \\ \Psi \end{bmatrix} = \begin{bmatrix} 0 \\ 0 \end{bmatrix}$$

- The matrix coefficients reflect the sectional hydrodynamic, structural and inertial properties as well as the towing speed and the spatial half wavelength of the vibration.

The Characteristic Equation Associated with the Behavior, $V(t) = V_o$ (Constant) $e^{\lambda t}$ and $\Psi(t) = \Psi_o$ (Constant) $e^{\lambda t}$.

$$a_4 \lambda^4 + a_3 \lambda^3 + a_2 \lambda^2 + a_1 \lambda + a_o = 0$$

- The roots λ reveal the frequency and damping of the response as a function of the half wavelength.

- Routh-Hurwitz stability criterion: The roots λ reflect stable behavior if the cable properties are such that

$$a_4 > 0, \ a_3 > 0, \ a_2 > 0, \ a_1 > 0, \ a_o > 0 \quad \text{and} \quad a_1 a_2 a_3 - a_o a_3^2 - a_4 a_1^2 > 0$$

TABLE 5. SIMPLIFIED FLUTTER AND DIVERGENCE CRITERIA RESOLVED ANALYTICALLY FROM THE ROUTH-HURWITZ INEQUALITIES

- For freedom from flutter

$$\frac{\chi_o}{C} < \frac{1}{4}\left(1 + \frac{1}{\mu}\right)$$

Where:

$\frac{\chi_o}{C}$ is the chordwise location of the structural mass center in terms of chordlengths with respect to the leading edge.

$$\mu \equiv \frac{m}{\rho \pi \left(\frac{C}{2}\right)^2}$$ is the mass ratio parameter.

- For freedom from torsional divergence

$$\frac{\xi T}{c} - \frac{1}{2}\left(a + \frac{1}{2}\right) > 0$$

Where:

$\frac{\xi T}{c} \cong \frac{\overline{M}_V}{\overline{P}c}\left(1 - \frac{C}{B_\eta}\right)$ is the chordwise shift of the structural twise axis in terms of chordlengths.

$-\frac{1}{2}\left(a + \frac{1}{2}\right)$ is the chordwise location of the center of pressure of the static lateral lift in terms of chordlengths behind the structural reference axis.
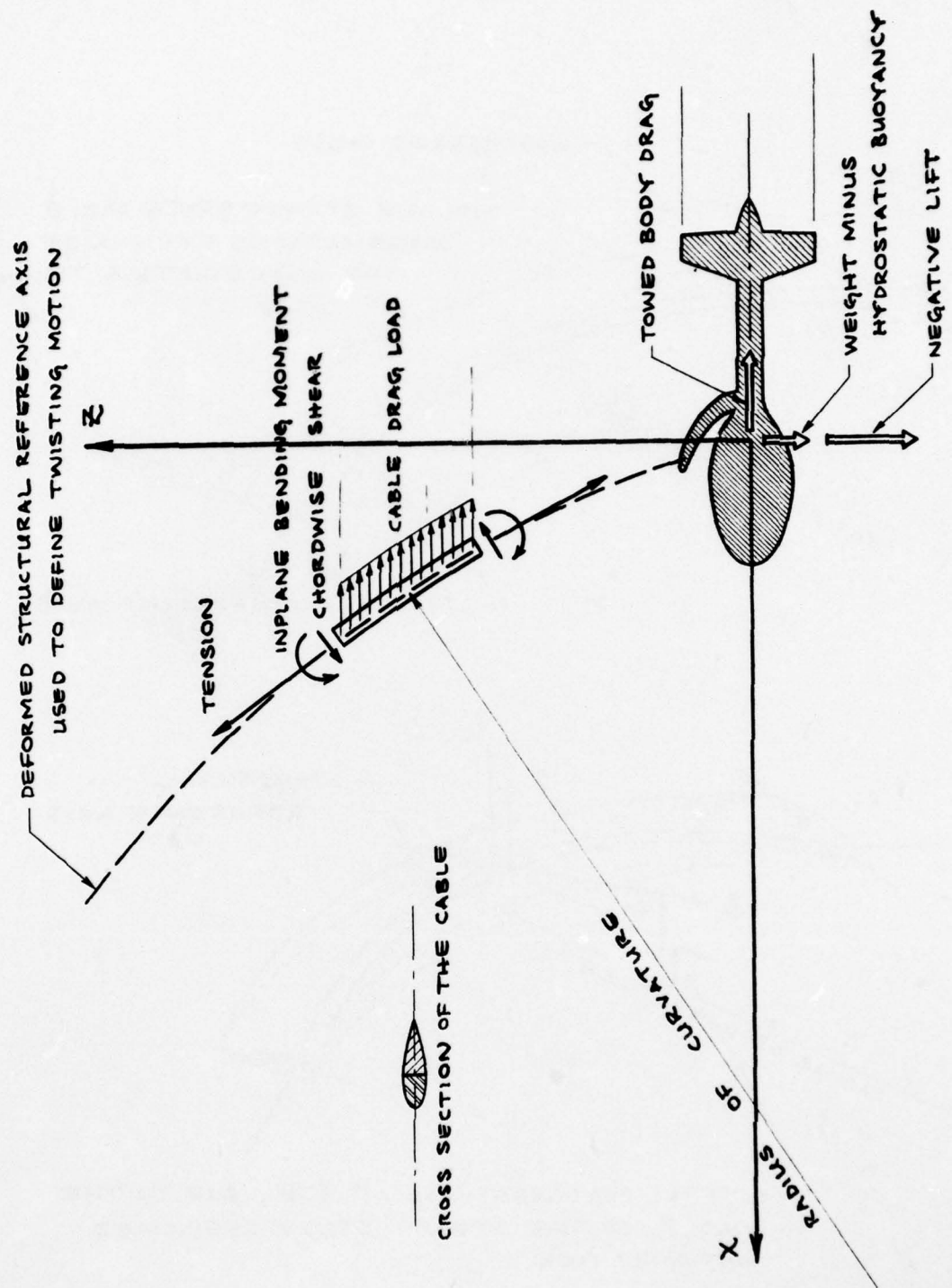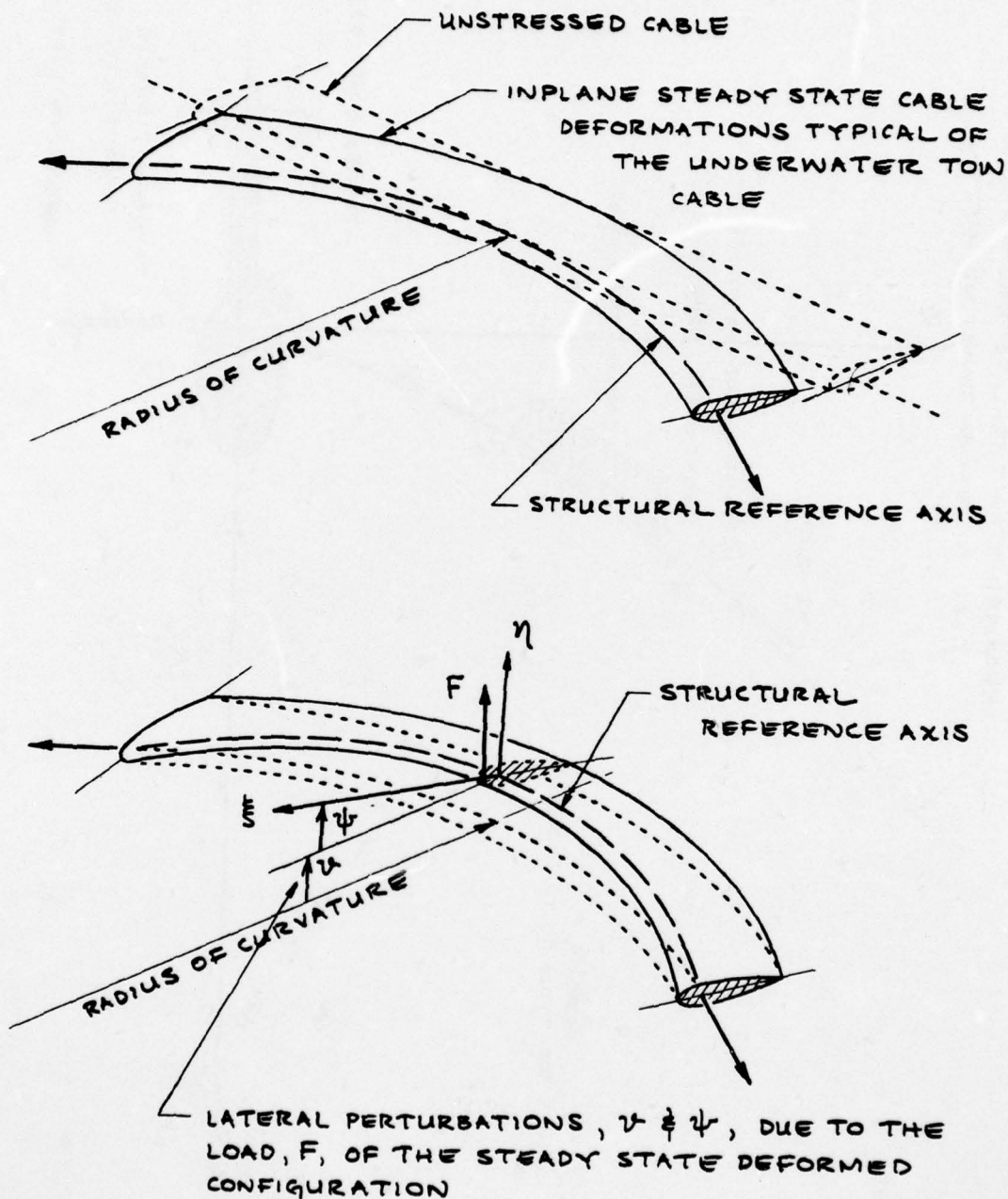
FIGURE 1.   STEADY STATE LOADS ACTING ON THE TOW CABLE

FIGURE 2.   LATERAL LOAD–DISPLACEMENT PROPERTIES TYPICAL
OF THE TOW CABLE (PART 1)

82
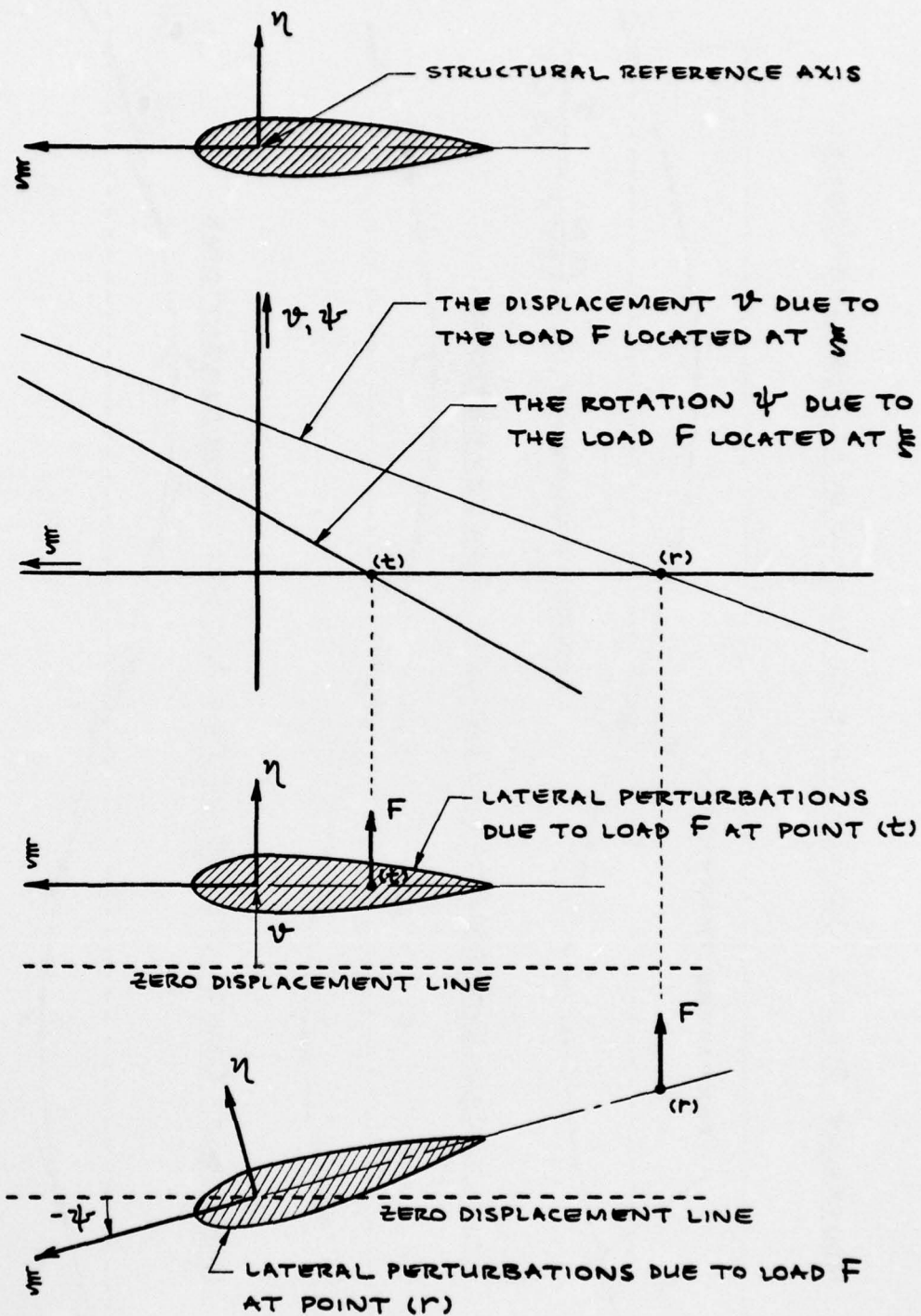
FIGURE 3.   LATERAL LOAD-DISPLACEMENT PROPERTIES
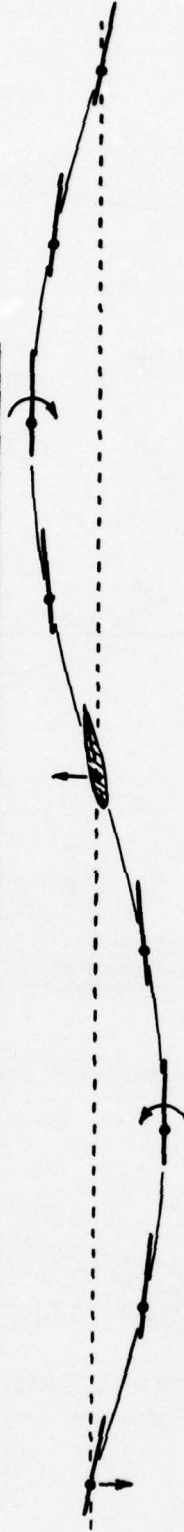TYPICAL OF THE TOW CABLE (PART 2)
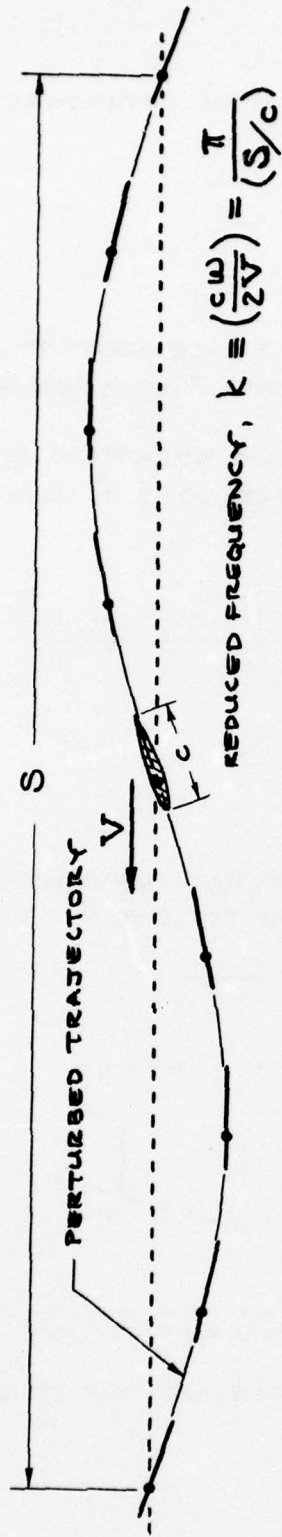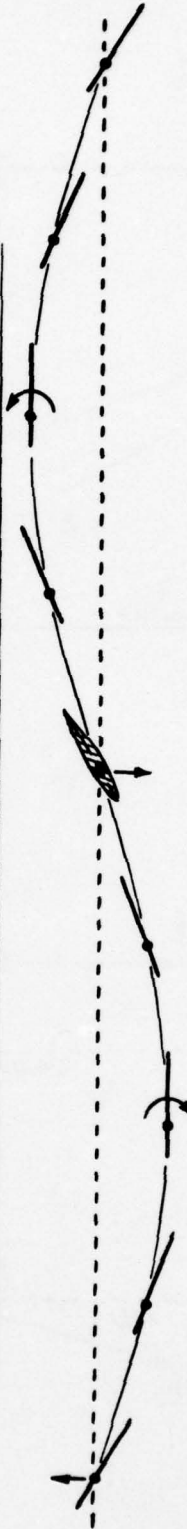
FIGURE 4. FUNDAMENTAL LATERAL TRANSLATIONAL AND TWISTING AMPLITUDE
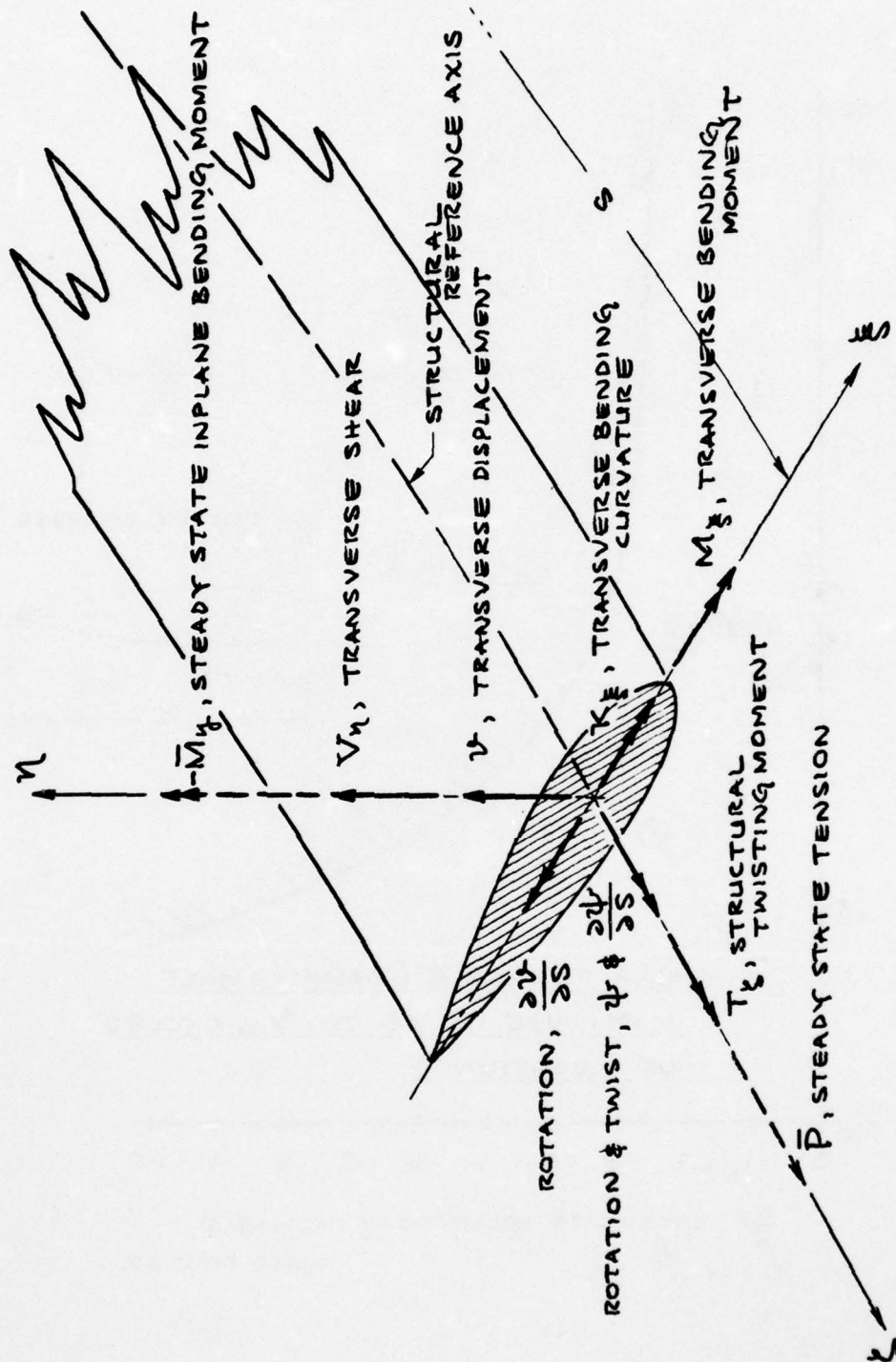RATIOS PERTINENT TO FLUTTER TYPE PERTURBATIONS

FIGURE 5. STRUCTURAL FORCES AND PERTURBATIONS PERTINENT TO THE MATHEMATICAL MODEL OF THE TOW CABLE

670811-0175

MASS RATIO , $\mu \equiv \dfrac{m}{\rho \pi \left(\frac{U}{2}\right)^2}$

100

BOUNDARY , $\left(4\dfrac{X_0}{C}-1\right)^{-1}$

10

CENTER OF MASS

UNSTABLE

STABLE

m

X_0

C

1

NAA TOW CABLE (DAMP TO HALF
AMPLITUDE IN 1/4 TO 3/2 CYCLES
OF VIBRATION)

1/10

0   ·1   ·2   ·3   ·4   ·5   ·6   ·7   ·8   ·9   1·0
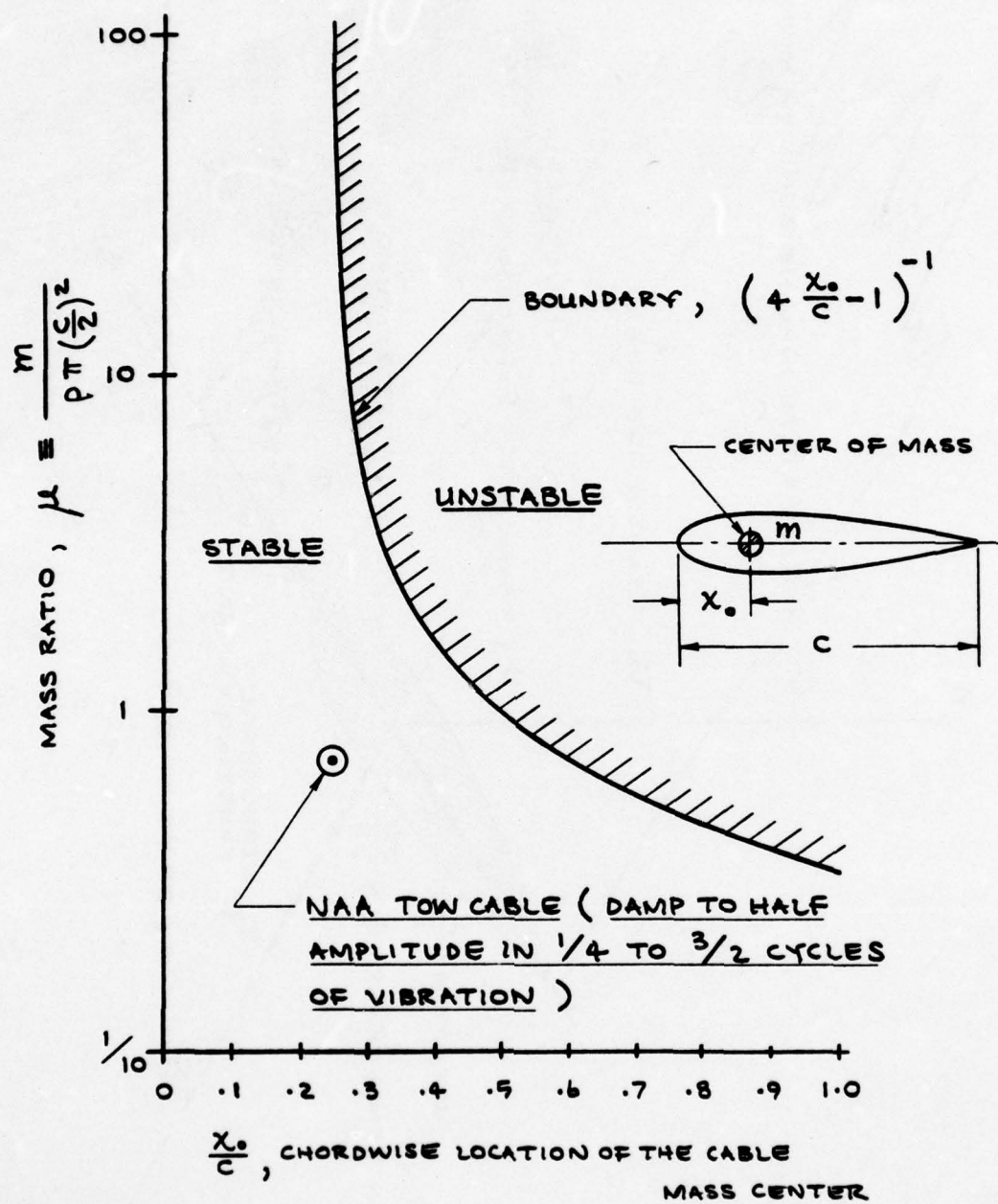
$\dfrac{X_0}{C}$, CHORDWISE LOCATION OF THE CABLE

MASS CENTER

FIGURE 6. SIMPLIFIED FLUTTER CRITERION: $\dfrac{X_0}{C} \prec \dfrac{1}{4}\left(1+\dfrac{1}{\mu}\right)$
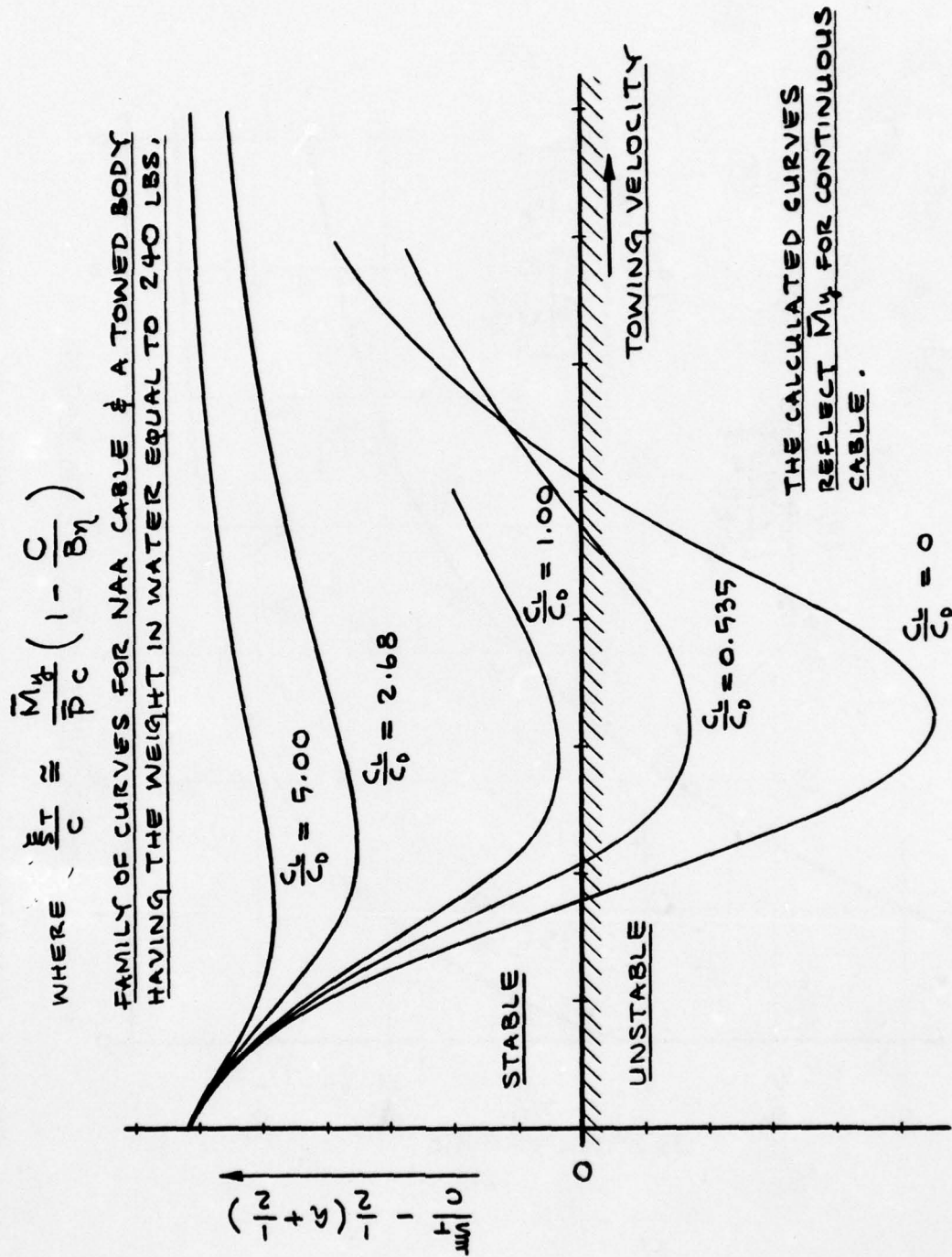
FIGURE 7. SIMPLIFIED TORSIONAL DIVERGENCE CRITERION: $\dfrac{\xi_T}{C} - \dfrac{1}{2}\left(a + \dfrac{1}{2}\right) > 0$
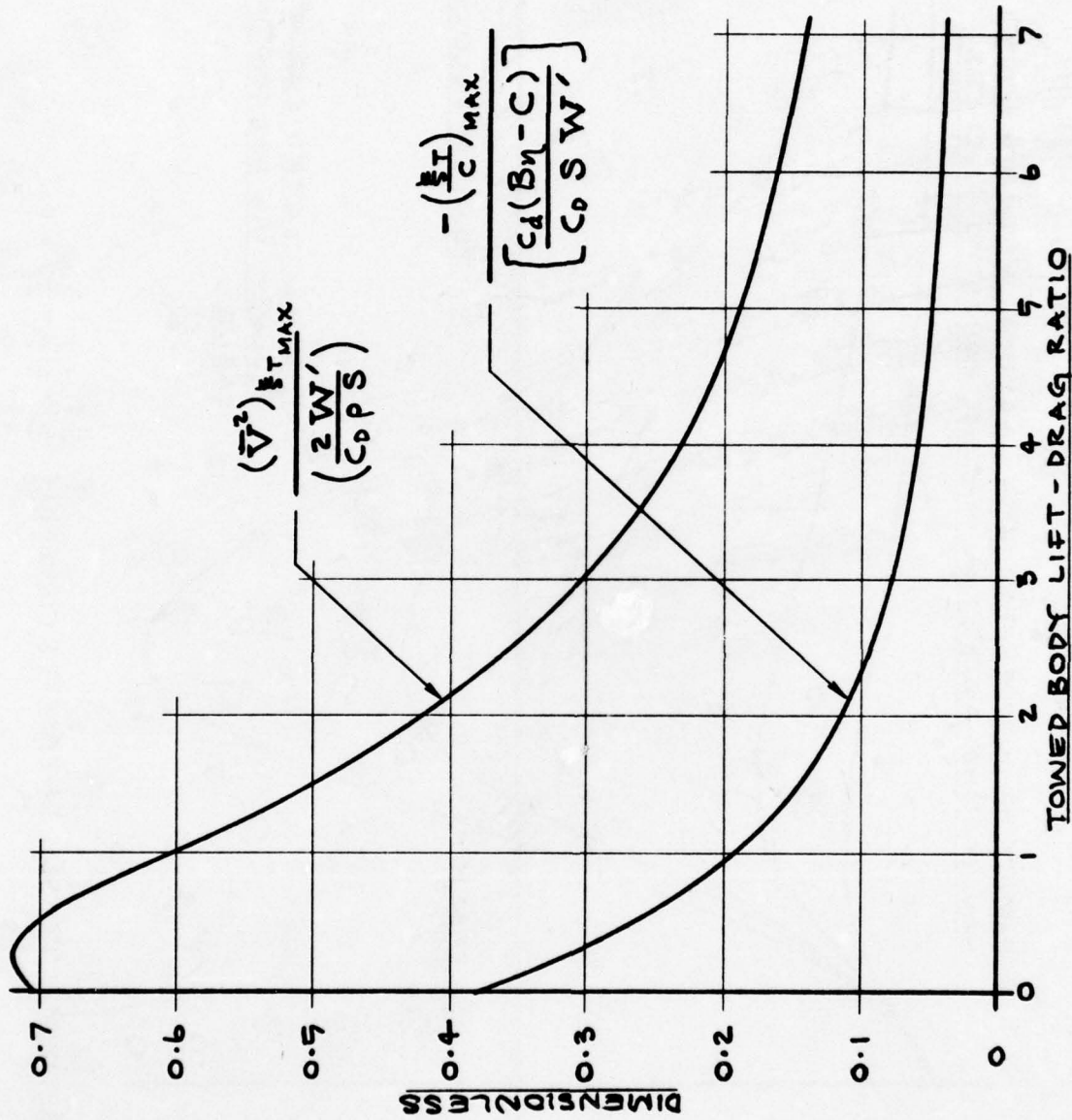
FIGURE 8. MAXIMUM CHORDWISE SHIFT OF THE TWIST AXIS AND THE TOWING VELOCITY AT WHICH IT OCCURS

SWAY ANGLE OF THE TOW CABLE

ν

$\bar{V} \cos \theta_1 \cos \nu$

$\bar{V} \cos \theta_1 \sin \nu$

DISTRIBUTED LATERAL LOAD DUE TO THE ANGLE OF ATTACK

$\bar{V}$

HOOKE'S JOINT

θ_1

$\bar{V} \sin \theta_1$

$\alpha \cong \nu \cot \theta_1$

ANGLE OF ATTACK OF THE CROSS FLOW

PITCH AXIS OF THE CABLE ATTACHMENT ASSEMBLY FIXED TO THE TOWED BODY

$\bar{V}$

FIGURE 9. HYDROMECHANICAL BEHAVIOR IMPOSED BY THE MECHANICAL BEHAVIOR OF THE CABLE ATTACHMENT ASSEMBLY IN CONJUNCTION WITH THE SWAY ANGULAR DISPLACEMENT OF THE TOW CABLE

CRITERION FOR STABLE BEHAVIOR:

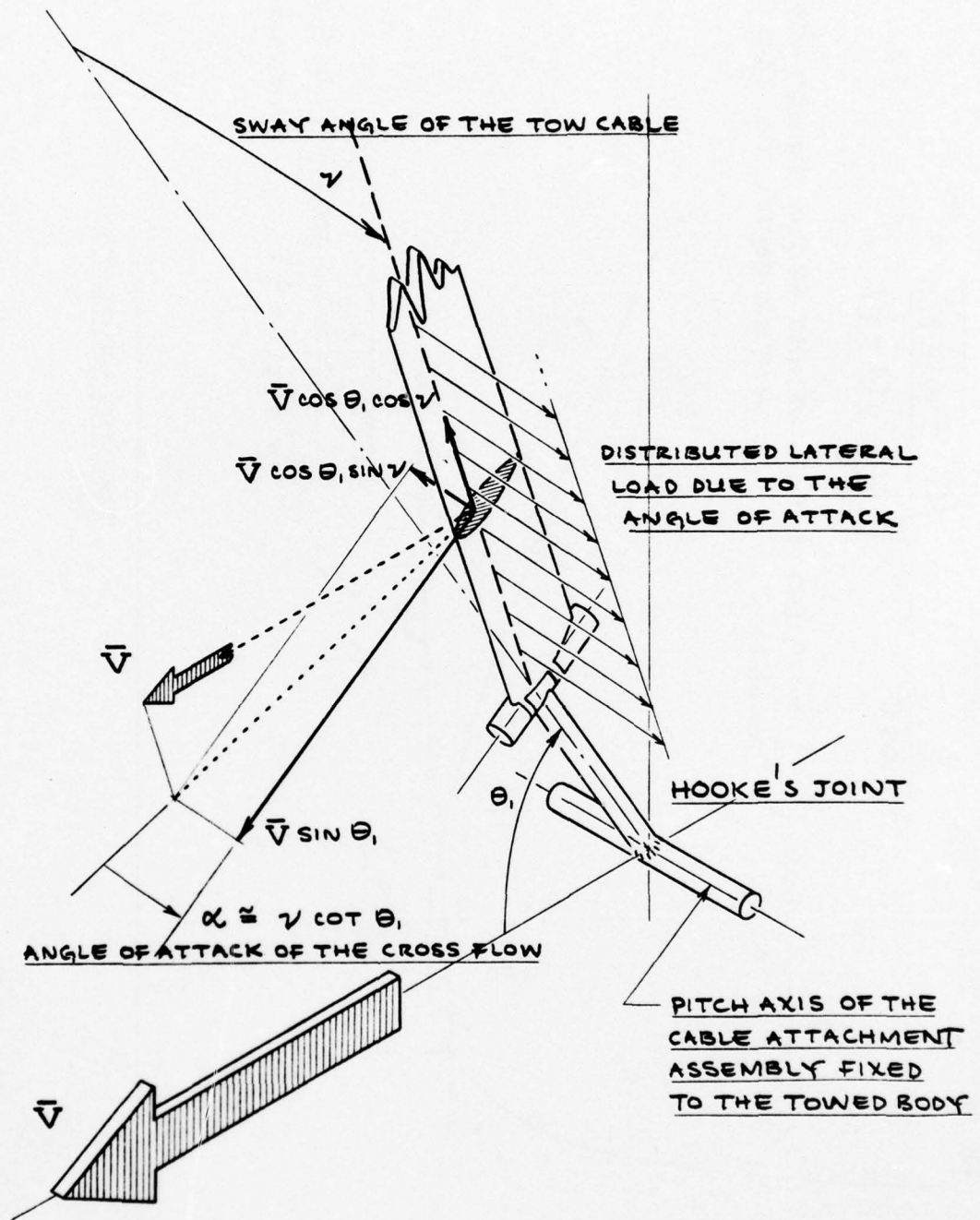$$\frac{\bar{P}_1}{\bar{V}\cos\theta_1} > \sqrt{\frac{C \cdot C_{L\alpha} \frac{1}{2}\rho}{\frac{\xi_T}{C} - \frac{1}{2}\left(a + \frac{1}{2}\right)}}$$

FOR $\left(\frac{C_L}{C_D}\right)_{TOWED\ BODY} = 5.00$ & THE WEIGHT OF THE TOWED BODY IN WATER EQUAL TO 240 LBS.

$$\frac{\bar{P}}{\bar{V}\cos\theta_1}$$

FOR $\left(\frac{C_L}{C_D}\right)_{TOWED\ BODY} = 5.00$

UNSTABLE

$$\sqrt{\frac{C \cdot C_{L\alpha} \frac{1}{2}\rho}{\frac{\xi_T}{C} - \frac{1}{2}\left(a + \frac{1}{2}\right)}}$$

FOR $\left(\frac{C_L}{C_D}\right)_{TOWED\ BODY} = 5.00$

TOWING VELOCITY
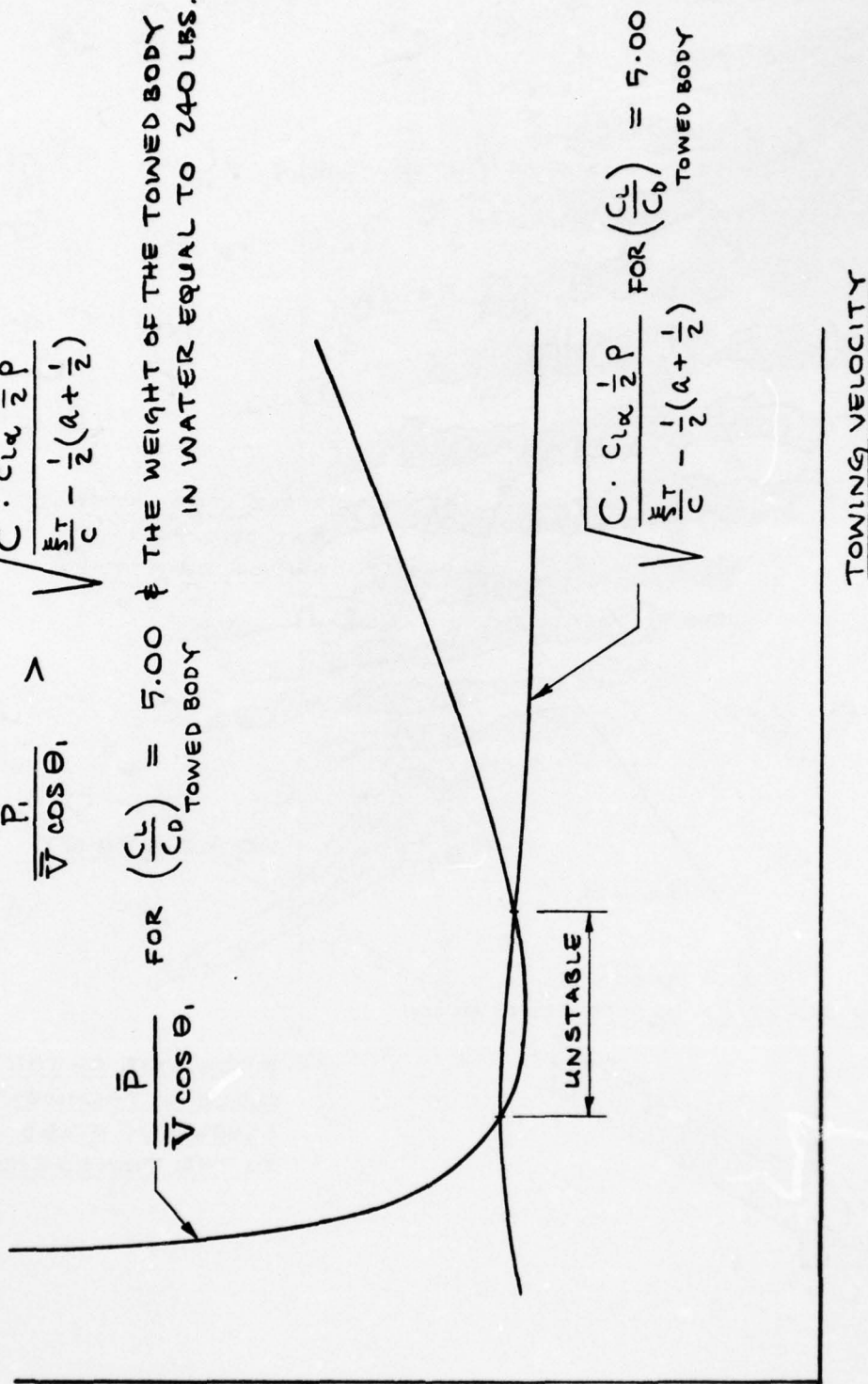
FIGURE 10. FREEDOM FROM CABLE ATTACHMENT SWAY ANGLE DIVERGENCE

AD
A037037

MICROCOPY RESOLUTION TEST CHART
NATIONAL BUREAU OF STANDARDS-1963-
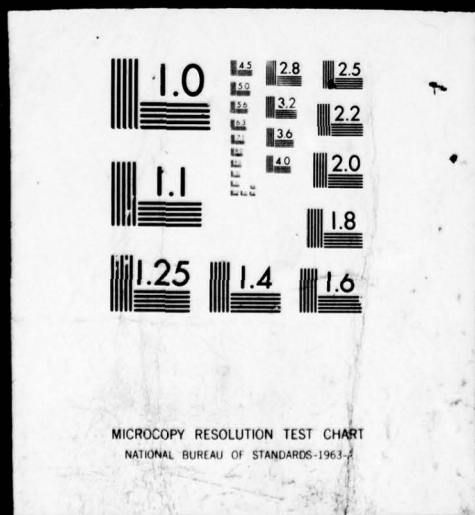
FIGURE 11. DIVERGENCE BOUNDARIES

NOTE : $\dfrac{\xi_T}{c} \cong \dfrac{\bar{M}_{\not{y}}}{\bar{P}c}\left(1 - \dfrac{c}{B_{\eta}}\right)$

STEEL LEADING EDGE

POLYPROPYLENE TRAILING EDGE

NAA TOW CABLE

$B_{\eta} = 1,791$ LBS·FT.^{2} , $C = 525$ LBS·FT.^{2}.

CURVE CALCULATED FOR A RECTANGULAR CROSS SECTION

$(G = \frac{4}{10} E)$

EFFECTIVE BASE TO THICKNESS RATIO OF THE PRIMARY TENSION

MEMBER OF THE CABLE -

$\left(1 - \dfrac{c}{B_{\eta}}\right)$

FIGURE 12. RELATIONSHIP BETWEEN THE SECTIONAL GEOMETRY OF THE PRIMARY TENSION MEMBER OF THE CABLE AND THE STRUCTURAL COUPLING PARAMETER INFLUENCING THE CHORDWISE SHIFT OF THE TWIST AXIS.
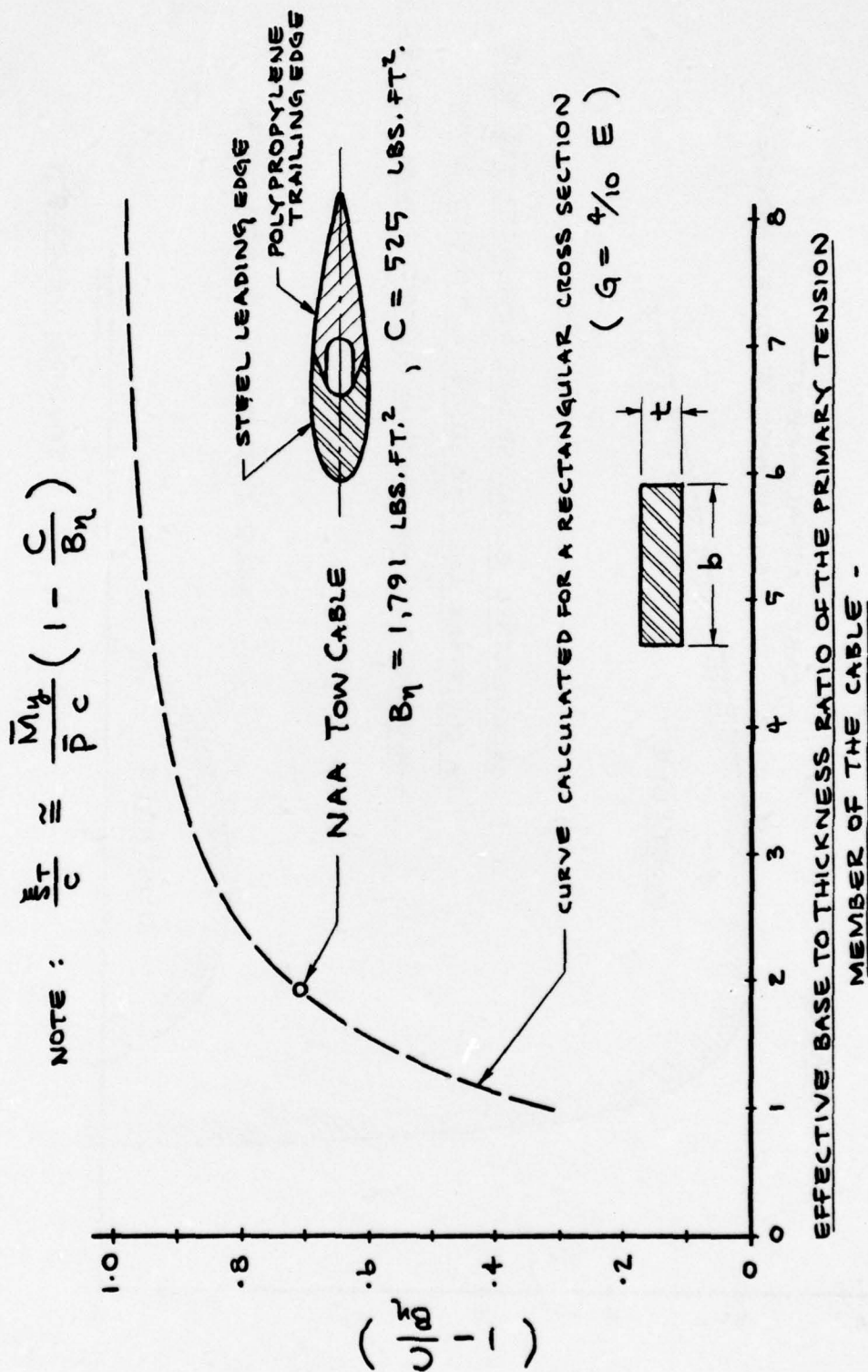
NOTE: $\dfrac{\xi_T}{c} \simeq \dfrac{\bar{M}_{\chi}}{P c}\left(1 - \dfrac{c}{B\eta}\right)$

DEFORMED STRUCTURAL REFERENCE AXIS OF A CONTINUOUS CABLE

DEFORMED STRUCTURAL REFERENCE AXIS OF THE NAA CABLE LINK

DISTRIBUTED DRAG LOAD

CHORDWISE SHEAR

CHORDWISE SHEAR

TENSION

TENSION

L = 4 FT.
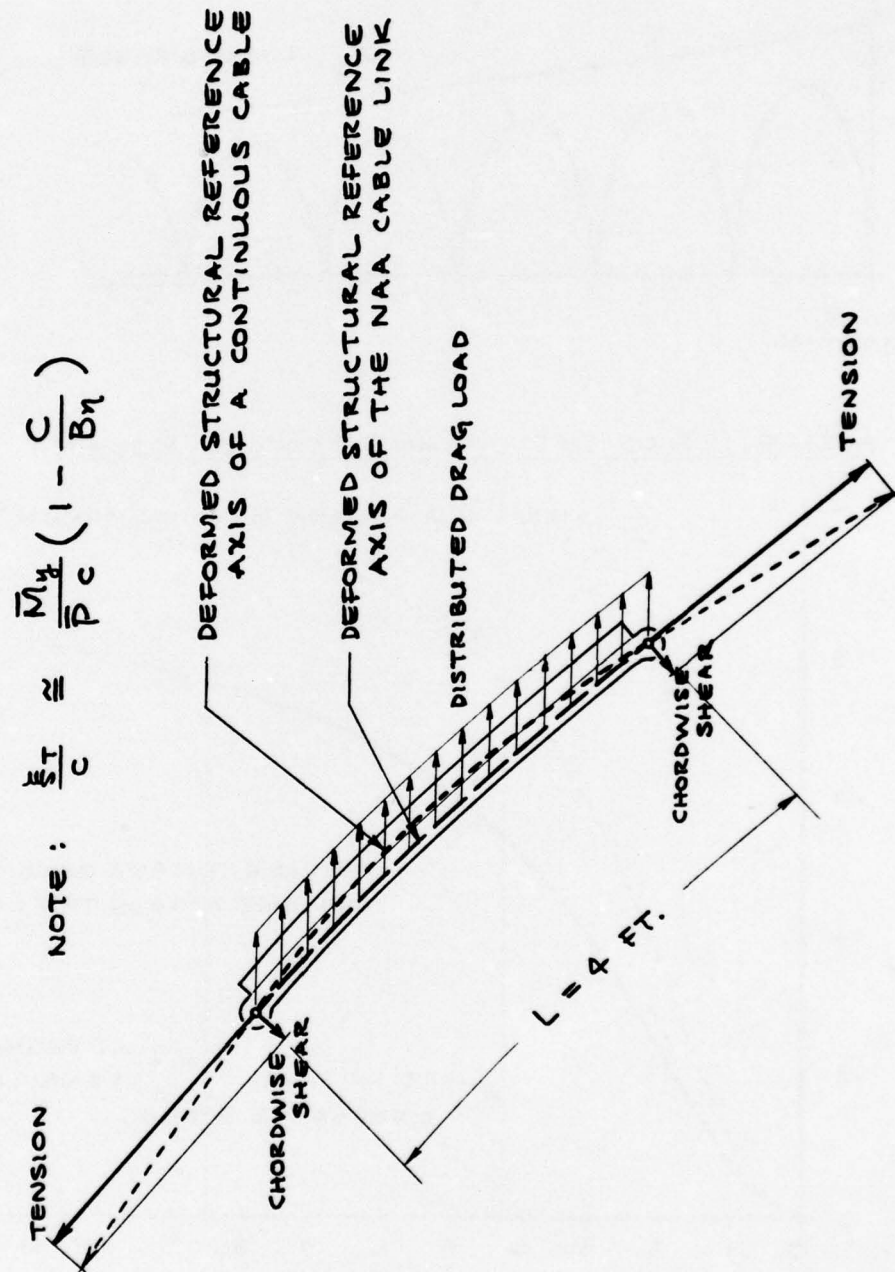
FIGURE 13. REDUCTION OF THE INPLANE BENDING MOMENT WHICH AFFECTS THE CHORDWISE SHIFT OF THE TWIST AXIS BY USING A LINKED TOW CABLE.

FIGURE 14. STEADY STATE INPLANE BENDING MOMENT OF THE
NAA LINKED TOW CABLE.

SESSION 1

TOWED SYSTEM DYNAMICS

Bibliography

Summary of Discussion
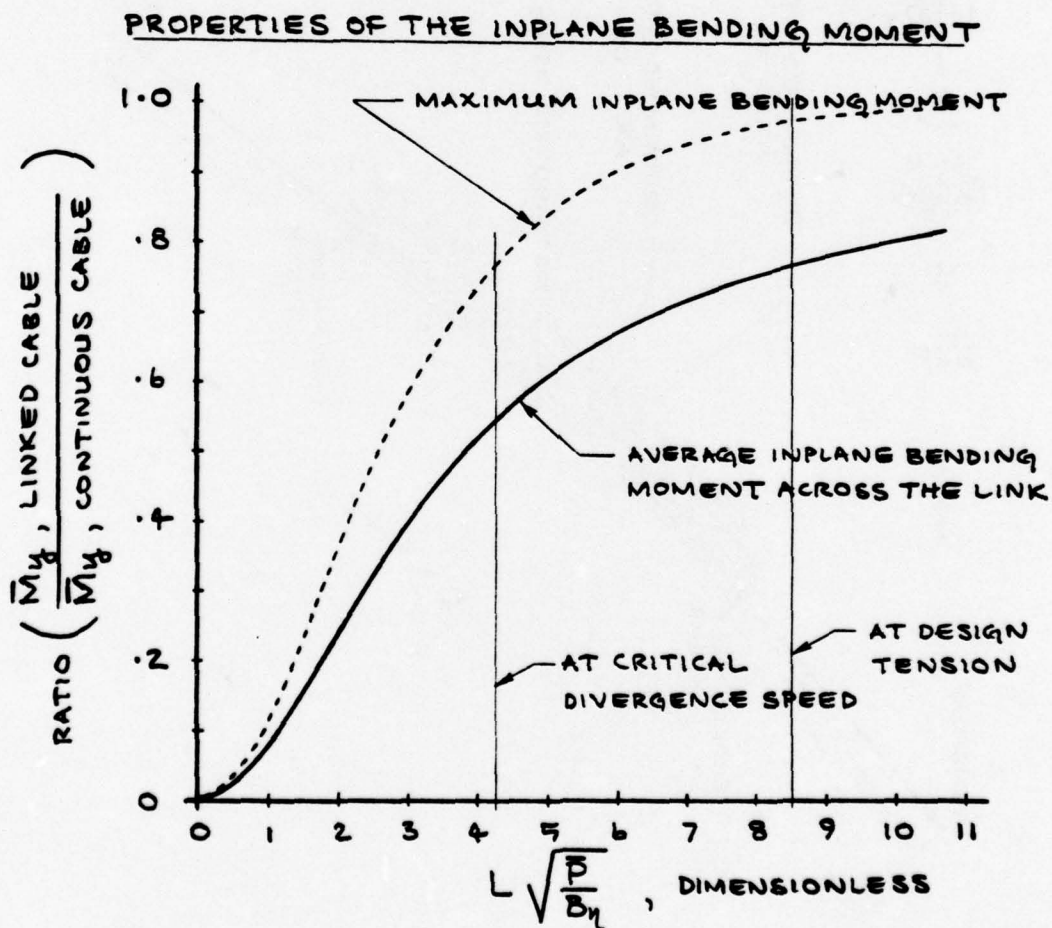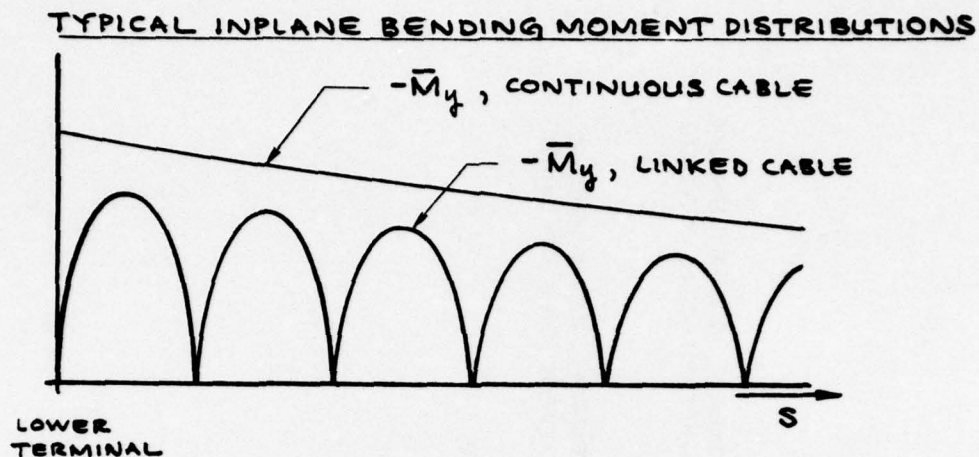
1.0 TOWED SYSTEM DYNAMICS

1.1 Boeing Company D2-89924-1; Final Report, Development of High-Speed Towing Cables; Underwater Towed Body, Part 1, CONFIDENTIAL 12 January 1966

1.2 Boeing Company D2-89924-2; Final Report, Development of High-Speed Towing Cables; Underwater Towed Body, Part 2, CONFIDENTIAL, 12 January 1966

1.3 Canada. Engineering Research Assoc. Report 56-1, Dynamics of Towed Underwater Systems Part 1, Stability of the System, by J.R. Richardson. Apr 65

1.4 Canada. Naval Research Establishment, Dartmouth Technical Note FM/65/12, Analog Computer Simulation of Towed Body Longitudinal Symmetric Motion. Part 1: Constant Coefficient Linear Equations, by N.E. Jeffrey, W.T. Swyer and J.M.Rozee. June 1965

1.5 Canada. Naval Research Establishment, Dartmouth TN FM/65/18, Analog Computer Simulation of Towed Body Lateral-Directional Antisymmetric Motion Part 1 - Constant Coefficient Linear Equations, by N.E. Jeffrey, W.T.Swyer and J.M.Rozee. Oct 65

1.6 Canada. Naval Research Establishment, Dartmouth TN FM/65/19 MOBY 4 Lateral Directional Dynamics, by N.E. Jeffrey, W.T. Swyer and J.M. Rozee. Oct 65

1.7 Canada. Toronto. University, Institute of Aerophysics, Technical Note 65. Aerodynamic Instability of Non-lifting Bodies Towed Beneath an Aircraft, by B. Etkin and J.C. Mackworth, January 1963.

1.8 Canada. Toronto University. Institute of Aerophysics Technical Note 65. Aerodynamic Instability of Non-lifting Bodies Towed Beneath an Aircraft, by B. Etkin and J.C. Mackworth, January 1963

1.9 Douglas Aircraft Co. Report SM-18593, On the Motion of a Finite, Towed Cable, by J.W. Miles, October 1954.

1.10 David Taylor Model Basin Report 1279, Calculation of Nonlinear Transient Motion of Cables, by T.S. Walton and H. Polachek. July 1959

1.11 Great Britain Aeronautical Research Council R+M 1312, The Stability of a Body Towed by a Light Wire, by H. Glauert, February 1930

1.12 National Advisory Committee on Aeronautics TN 1796. Theoretical Analysis of Oscillations of a Towed Cable, by W.H. Phillips, January 1949

1.13 Navy Mine Defense Laboratory Rept 219. Dynamics of Towed Underwater Vehicles, by A.G. Strandhagen and C.F. Thomas. Nov 63

1.14 Navy Mine Defense Laboratory Rept i-77, <u>Specialized Equations of Motion</u> <u>of a Towed Underwater Vehicle,</u> by H. M. Lacey, May 65

1.15 Naval Ordnance Laboratory TR 64-116, <u>Stability of a Towed Object,</u> by W. P. Reid. 4 Aug 64

1.16 Naval Ordnance Test Station Technical Publication 2378, Pt. 1, <u>Steady-</u> <u>State Motion of Cables in Fluids, Part 1: Tables of Neutrally</u> <u>Buoyant Cable Functions</u>, by C.J. Thorne, G.E. Blackshaw and R.W. Claassen. Sep 1962

1.17 North American Aviation SID 65-1279, 1 thru 4; Final Report, <u>High-</u> <u>Speed Towing Cable Development</u> (Phase I-II, Vols. 1-4) CONFIDENTIAL 29 October 1965

1.18 Rutgers University. Contract N70024-1366, <u>Equilibrium and Dynamic</u> <u>Motion of a Towline and a Towed Body</u>, by S.P. Reyle and J.W. Schram

1.19 Navy Underwater Sound Laboratory Rept 736, <u>Equations of Motion for a</u> <u>Towed Body Moving in a Vertical Plane</u>, by K.T. Patton and J.W. Schram 15 June 66

1.20 Whicker, L.F., <u>The Oscillatory Motion of Cable-Towed Bodies</u>, (Ph.D. Thesis, University of California), 1957

DISCUSSION SUMMARY

SESSION 1. Towed System Dynamics

1) It was suggested that Mr. Lagasse's stability analysis might be improved if the velocity potential, ϕ, of the towline section were established. The acceleration pressures over the surface could then be integrated in the sway direction about the center of cable rotation.

   Mr. Lagasse explained that only a small section of the towline had been examined for stability, resulting in what might be termed a section analysis. This approach had been necessary since the analysis had to be performed by hand. The so-called swept wing portions of the cable were not examined, although it was recognized that the dominant problem was the stability of the entire towline configuration. It was hoped that by stabilizing the center section, where the towline angle was $90°$, the entire towline would be stable.

2) Present investigations, Dr. Burroughs pointed out, are concerned with correlating computer simulation output with measured sea trial data. This comparative analysis encompasses several existing Navy towed sonar systems.

   Boeing's choice of the analog over the digital computer was explained by Dr. Burroughs. Under the current state of Boeing's equipment, there would be little gained in the use of the digital computer, either in data display or in observing the intricacies of the problem. Analog simulation, on the other hand, made it possible to work for long periods on the problem and at the same time to observe the phenomena being analyzed. This was in contrast to digital simulation in which you were fortunate if the questions you had formulated were answered by the following day because of turn-around time.

3) Dr. Hegemier's analysis was originally derived for use on the Boeing-II-type continuous faired towlines. He explained it would be possible, however, to apply it to discontinuous faired towlines such as the hinged North American design. This could be done by first examining the entire system, and then looking at each link separately.

   In the towline configurations under consideration, it was assumed that the towed body was attached to the end of the towline in a manner that prevented its movement in the event of towline divergence. It was pointed out that this assumed arrangement was in contrast to a possible alternative in which the towed body would be allowed lateral displacement. Further work exploiting a system allowing lateral displacement might well be the next step in Dr. Hegemier's studies.

4) Figure 7 of Mr. Kanno's paper was the subject of lengthy discussion. The illustration showed the stability ratio (the distance of the twist center forward of the hydrodynamic center) as a function of towing velocity. The example given in the illustration assumed the towline to be the North American design and the towed body to have a weight in water of 240 pounds. The lift/drag ratio was indicated as a third parameter. Unstable (divergent) operation was shown to take place as the $\frac{L}{D}$ of the body decreased past a certain critical value. It was pointed out that although the abcissa and ordinate were not scaled, the graph represented the properties of a physical system - that is, a faired towline of a specific size and a towed body with certain physical characteristics. The confusion centered on the inference, on first examination, that the only variable was the angle between the towline and the towed body at their juncture. Actually, through variation of the parameter $\frac{L}{D}$, other physical characteristics of the cable body system were also being varied.

SESSION 2
Towed Body Hydrodynamics

Mr. N. E. Jeffrey
Naval Research Establishment

Influence of Body Design Features on Towing Stability

Mr. P. A. Hamill
National Research Council

Hydrodynamic Design, Model and Full Scale Tests of a Towed Sonar Body

Mr. K. T. Patton
Navy Underwater Sound Laboratory

On the Hydrodynamic Mass and Damping of Bodies Oscillating in a Viscous Fluid

Mr. M. Gertler
David Taylor Model Basin

The Hydrodynamic Coefficients of Cable-Towed Bodies

INFLUENCE OF BODY DESIGN FEATURES ON TOWING STABILITY

Michael C. Eames and Norman E. Jeffrey
Fluid Mechanics Section
Naval Research Establishment
Dartmouth, N.S., Canada

ABSTRACT

This paper is a first progress report on a parametric study of very simple towed systems, intended to provide physical insight into the factors influencing their dynamic stability. It should be treated qualitatively and not employed for practical design, since the mathematical models are over-simplified. These early results identify three significant and three unimportant modes of motion. Of the former, one mode essentially depends on body design features, a second depends on towing configuration parameters, and the third is influenced by both groups of variables.

INTRODUCTION

A simple mathematical model has been proposed for simulating the behaviour of towed systems, based on linear equations of motion.[1,2]* Although this model requires much development, initial results of its use[3] have been sufficiently encouraging to warrant its application in a parametric study, to determine the broad influence of design features on dynamic stability.

This study is not intended for practical design purposes, but rather to provide physical insight into the principal mechanisms involved in the stability of towed bodies, in the simplest possible terms. Practical bodies and cables will involve additional mechanisms and in some cases these may override the trends indicated by the present academic study of simple models.

Following a description of the hypothetical parent towed system and of the nine series of parameter variations studied, root-locus plots are discussed for each Series in turn (Figs. 3 to 16). In every case, only the named parameter is changed; all other variables retain the design value of the parent system. The parent design conditions are identified on all diagrams by the solid spots.

Finally, the essential characteristics of each mode of motion are summarized. An appendix discusses root-locus plots for readers unfamiliar with their use.

This work is continuing and the paper should be regarded as an early progress report.

PARENT SYSTEM

The parent body is a simplified model of MOBY II[4], designed to achieve 250 ft. depth at 40 knots with a limiting steady cable tension of 25000 lb.

* Superior numbers refer to similarly numbered references at the end of this paper.

As shown in Fig. 1, the housing is of prismatic form, the halves of an 8.0 ft. long, 2.0 ft. diameter body of revolution being separated by a 2.0 ft. deep window section. It is ballasted to a weight of 3000 lb. in water, while the flooded weight (in air) is 5000 lb.

The body has moments of inertia of 320, 1500 and 1300 slug ft.^{2} about axes through its centre of gravity parallel to the Ox, Oy, Oz axes respectively. The centres of gravity and buoyancy and the hydrodynamic centre of the housing are assumed coincident, located 1.0 ft. vertically below the towpoint. This distance is known as the "housing lever" (z_G). A drag coefficient of 0.1 based on a frontal area of 8.0 ft^2 is taken to cover housing, tail and parasitic effects.

The vertical tail has an area of 16.0 ft^2 (S_V) and an aspect ratio of 1.0. Its hydrodynamic centre is located 6.0 ft. abaft the towpoint (x_V) and 1.2 ft. above the towpoint (z_V). The horizontal tail has an area of 5.0 ft^2 (S_H) and an aspect ratio of 0.8. Its hydrodynamic centre is located 8.4 ft. abaft and in line with the towpoint (x_H).

The depressing wing is designed to achieve a total downforce (A) of 12,000 lb. at 40 knots. It has a lift/(speed)^2 of 2.0 lb. sec^2/ft^2 (L/V^2), a net area of 8.0 ft^2 (S_W) and a net aspect ratio of 2.0. Its hydrodynamic centre coincides with the towpoint and a lift/drag ratio of 10 is used for the additional drag of the wing.

The parent body is referred to as the DEPRESSED BODY. When the wing is removed, the WINGLESS BODY is obtained, which represents a simplified model of MOBY IV[4]. The steady-state performance of these two bodies is compared in Fig. 2, at the design speed of 40 knots.

A third hypothetical body is also used. This WEIGHT BODY is an idealized high density weight having negligible volume and hydrodynamic form, except that it is assumed to have the same drag as the Wingless Body. Weights of 3000 lb. and 12000 lb. are used for comparison with the Wingless and Depressed Bodies respectively.

The basic cable used with all bodies has a normal drag coefficient (C_R) of 0.2 based on a diameter of 0.75 in, and a friction ratio (μ) of 0.75. Standard towing conditions are with 400 ft. of cable immersed at 40 knots.

SYSTEM VARIATIONS

Using the simple linear equations of motion for three degress of freedom in space axes, with the cable represented by a single system of damped springs[1], stability roots have been calculated for longitudinal and lateral-directional motions of these bodies. For each oscillatory mode, root-locus plots have been drawn to illustrate how the damping and frequency varies as particular features of body geometry or other parameters are varied one at a time.

Series I and II study variations of speed from 20 to 60 knots and cable length from 200 to 600 ft. Series I covers longitudinal modes, Series II covers lateral-directional modes.

<u>Series III and IV</u> study variations of cable drag coefficient from 0.1 to 0.3 and body downforce from 3000 to 12000 lb. Downforce of the Depressed Body is decreased by reducing L/V^2, maintaining a constant 3000 lb. weight. Series III covers longitudinal modes, Series IV covers lateral-directional modes.

<u>Series V and VI</u> study variations of tail area and tail lever arm on the Depressed Body only. Series V covers longitudinal modes with horizontal tail areas from 2.5 to 7.5 ft^2 (at constant aspect ratio) and lengths (x_H) from 6.4 to 10.4 ft. abaft the tow point. Series VI covers lateral-directional modes with vertical tail areas from 8.0 to 24.0 ft^2 (at constant aspect ratio) and lengths (x_V) from 4.0 to 8.0 ft. abaft the tow point.

<u>Series VII</u> studies variations of tail vertical location and housing lever on the Depressed Body, in lateral-directional modes. The hydrodynamic centre of the vertical tail is varied from 1.8 ft. above the towpoint to 0.6 ft. below the towpoint. Housing levers from 0 to 1.5 ft. are covered, the zero case corresponding to a body of revolution.

<u>Series VIII and IX</u> study variation of wing lift coefficient. Assuming constant area, L/V^2 values from 2.67 to 0 are taken in conjunction with body weights from 0 to 12,000 lb, such that the total downforce remains constant. Series VIII covers longitudinal modes, Series IX covers lateral-directional modes.

<div align="center"><u>SERIES I</u></div>

HEAVILY DAMPED SURGE MODE

In general there are three longitudinal modes, of which one is non-oscillatory in all Series studied. This comprises a pair of heavily damped convergences, mainly in surge but with some heave coupling. Damping in this mode is strongly affected by body drag-area. If drag-area is significantly reduced from the design value the motion may become oscillatory. However, for bodies of the type studied this mode is unlikely to result in significant motion and is not considered further.

SHORT PERIOD PITCH MODE

The two oscillatory modes are plotted in Fig. 3. Of these, one has a high frequency (of order 5 rad/sec damped) and is well damped. It is not influenced by cable length and essentially involves the body pitching about its towpoint. This mode does not exist for the hypothetical Weight Bodies, of course. Its damping ratio lies between 0.7 and 1.0, and increases when the wing is fitted, indicating a favourable effect associated with a large increase in heave damping. The damping ratio is unaffected by speed, but the natural frequency is strongly speed dependent, particularly when the wing is fitted. In fact, the natural frequency increases roughly linearly with speed. Because of the high damping, this mode is unlikely to be significant in practice.

LONG PERIOD HEAVE MODE

The most important mode is a damped oscillation having a low frequency (of order 0.5 rad/sec.) and a damping which varies greatly with cable length. This is primarily a heaving motion, although surge and pitch coupling can be important.

Damping increases rapidly with cable length, going supercritical by 600 ft. in the case of the Wingless Body and the 3000 lb. Weight. Conversely, in the case of the Depressed Body and the 12000 lb. Weight, the damping is becoming unsatisfactorily light at short cable lengths. Clearly the angle of depression of the cable plays an important role in this mode. It is interesting that cable length has a comparatively minor effect on the undamped natural frequency.

The effect of speed differs radically with the Depressed and the Wingless Bodies. In the latter case, damping increases rapidly with speed, becoming super-critical by 60 knots, while there is little change in natural frequency. With the Depressed Body, however, the primary effect is an increase of frequency with speed, while damping actually decreases slightly. This difference is mainly due to the angle of depression of the cable, which decreases much more rapidly with speed in the case of the Wingless Body.

SERIES II

SHORT PERIOD YAW MODE

In general there are three lateral modes, all of which are oscillatory. They are plotted in Figs. 4 and 5. One has a high frequency (of order 5 rad/sec, damped) and is nearly critically damped. It is not influenced by cable length and essentially involves the body yawing about its towpoint. This mode does not exist for the hypothetical Weight bodies, of course. The damping ratio is unaffected by speed, but the natural frequency is strongly speed dependent. In fact, the natural frequency increases roughly linearly with speed. Presence or absence of the wing has little effect on this mode except for a slight favourable contribution due to roll damping. Because of the high damping, this mode is unlikely to be significant in practice.

COUPLED ROLL-YAW MODE

The second mode has an intermediate frequency (of order 1 rad/sec) and a damping which varies greatly with speed. This is a coupled roll-yaw motion, somewhat analagous to the Dutch roll of an aircraft, and is essentially a body mode, being affected little by cable length.

The Wingless Body exhibits instability in this mode at all speeds, the rate of divergence increasing with speed. When a hypothetical skeg is added to increase the roll damping, this characteristic is reversed and the locus becomes similar to that shown for the Depressed Body, the wing of which provides the necessary roll damping. The damping ratio for the Depressed Body increases rapidly with speed, becoming supercritical by 60 knots. The effect of speed on natural frequency is not large. Cable length has a very minor influence on the Depressed Body and a negligible effect on the Wingless Body.

It is likely that this will be found to be the mode most sensitive to detailed design features of a towed body, and it requires further study.

106

LONG PERIOD KITING MODE

The third mode is a damped oscillation having a low frequency (of order 0.5 rad/sec) and relatively light and variable damping. This is primarily a swaying motion, although roll and yaw coupling can be important; pendulous kiting is perhaps the best description.

The primary effect of cable length is on damping, which is becoming unsatisfactorily light at short cable lengths, particularly in the case of the Depressed Body. There is a secondary effect on the undamped natural frequency, which decreases with increasing cable length.

For the realistic bodies the primary effect of speed is on the natural frequency, which increases with speed. However, in the case of the Depressed body, beyond 40 knots there is a sudden collapse of damping, and the mode goes unstable at about 50 knots. This is mainly the result of unfavourable sway-roll coupling, caused by the fact that wing lift rolls with the body, and this lift dominates the downforce at high speeds. It is this effect in this mode which is most likely to impose a limit on towing speeds attainable in practice without the use of automatic controls; the mode demands further study.

SERIES III

SHORT PERIOD PITCH MODE

As indicated in Fig. 6, this mode is unaffected by cable drag coefficient, and affected very little by downforce.

LONG PERIOD HEAVE MODE

The effect of cable drag coefficient is quite similar to the effect of speed discussed in Series I. At low depression angles of ballasted bodies, damping increases rapidly with cable drag, becoming supercritical by a C_R of 0.3. With the Depressed Body, however, the primary effect is an increase of natural frequency with cable drag coefficient.

The importance of depression angle in this mode is well illustrated by the effect of downforce, particularly in the case of the hypothetical Weight Bodies. These show a rapid decrease of damping as downforce increases, with negligible change in natural frequency. There is an indication that very heavily ballasted bodies may encounter inadequate damping if towed with very low drag cables. When added to the effect of short cable lengths at low speeds discussed in Series I, this is clearly a point to watch in future system designs.

SERIES IV

SHORT PERIOD YAW MODE

Fig. 7 shows that neither cable drag coefficient nor body downforce have any noticeable influence on this mode, as might be expected.

COUPLED ROLL-YAW MODE

Since this is also essentially a mode governed by body characteristics, it is not surprising to find that cable drag coefficient has little effect. There is a small decrease in natural frequency as cable drag increases.

On the other hand, reduction of downforce, which is a reduction of wing lift on the Depressed Body, causes an important decrease in damping and increase in frequency, similar to that caused by reduction of speed. It is interesting to note that the only difference between the Depressed Body at a downforce of 3000 lbs. and the Wingless body is the damping effect of the wing, since this is not developing any lift in this condition; yet the Depressed Body remains stable at 3000 lbs. whereas the Wingless Body was badly unstable at 40 knots. (Fig.4)

LONG PERIOD KITING MODE

Fig. 8 indicates that the major effect of increased cable drag coefficient on this mode is to increase the natural frequency. There is a secondary increase in damping with cable drag.

It appears that changes of downforce have a negligible effect on the damping, but this could be a misleading conclusion. If the downforce of the Depressed Body had been increased beyond 12000 lbs. by increasing wing lift, it is expected that the damping would begin to fall off rapidly, the curve turning over in a similar manner to the effect of high speed shown in Fig. 5.

Comparison of the effect of increased downforce on natural frequency on the Weight Body and the Depressed Body shows opposite trends. For the Weight Body the decrease of natural frequency with mass is the dominant effect. However, in the case of the Depressed Body there is no change in mass since the additional downforce is achieved with wing lift alone. The increased cable spring constant and increased sway-roll coupling are, therefore, the important effects.

No plot is shown for the Wingless Body. The results are not meaningful because of the instability of the body in the roll-yaw mode.

SERIES V

SHORT PERIOD PITCH MODE

The primary effect of increasing horizontal tail length and area on this mode is a moderate increase in natural frequency. Damping increases a small amount as length or area are reduced below the design value but becomes relatively constant for increases in length and area above the design point.

In any event the effect of large changes in horizontal tail length and area are probably not significant since the Depressed Body is so well damped in this mode.

LONG PERIOD HEAVE MODE

Fig. 9 shows that increased horizontal tail length results in increased

natural frequency with little effect on damping from 6.4' to 10.4', with this effect becoming less significant at the higher values.

Increased horizontal tail area leads to a reduction in damping, but this becomes less sensitive as area is increased beyond the design value.

However, these design features of the Depressed Body appear comparatively unimportant in this mode. This may not be true of ballasted bodies having significantly less heave damping.

SERIES VI

SHORT PERIOD YAW MODE

Fig. 10 shows that this mode is not sensitive to vertical tail length around the design value, but damping increases with excessive length, becoming supercritical by 8 ft. Large changes in vertical tail area have little significant effect but a trend to slightly decreased damping is evident with increase in area. In any event, this mode is not likely to be of practical importance since it is well damped.

COUPLED ROLL-YAW MODE

As expected, this mode is very sensitive to vertical tail length and area. The body goes unstable when the length is reduced to 5.6 ft., or the area to 13 ft^2, and around and below these values the effect is wholly on damping. Beyond 5.7 ft. or 14 ft^2 however, natural frequency increases rapidly with tail length or area and the change in damping is not so significant.

The overall shape and trend of the root loci are similar to those which arise with changing static directional stability and the effect of tail length and area on this fundamental derivative appears to be the significant factor.

LONG PERIOD KITING MODE

The effect of vertical tail length or area on this mode is almost opposite to the effect on the coupled roll-yaw mode, as seen in Fig. 11. At small tail lengths or areas, damping decreases rapidly with increasing tail length or area, but beyond 5.7 ft or 14 ft^2, it reaches a minimum value and it is then the natural frequency which decreases with increasing tail length or area. Practical design will demand a careful comparison of behaviour in the long kiting and roll-yaw modes, and further study of the above effects is required.

SERIES VII

SHORT PERIOD YAW MODE

Fig. 12 shows that the depth of the body housing has a small and unimportant effect on the damping and natural frequency of the short yaw mode.

Damping tends to decrease initially with vertical tail height but beyond + 0.6' remains relatively constant while natural frequency increases. Overall effect of tail height appears relatively unimportant in this mode since it is well damped for all cases considered.

COUPLED ROLL-YAW MODE

Housing depth has an important effect on the coupled roll-yaw mode, as would be expected. From the zero value appropriate to a body of revolution, up to the design value, the change is essentially one of decreasing natural frequency, but beyond the design value, damping is improved as the frequency continues to decrease.

The trend for vertical tail height variation is, not surprisingly, very similar to that for housing depth, for positive values. Increasing negative values cause an increase in damping and frequency.

LONG PERIOD KITING MODE

Fig. 13 shows that housing depth has an important effect on the damping of the long kiting mode, which decreases continuously with increasing housing lever, going unstable by 1.5 ft. The effect on natural frequency is secondary. Again it is noted that the effects on this and the roll-yaw mode tend to be opposite, requiring careful study and compromise in practical design.

The effect of vertical tail height is similar except for an initial increase in frequency with little change in damping ratio for positive values. Note that the mode becomes unstable at approximately + 1.4 ft.

Instability resulting from too much vertical tail height or body housing depth can be readily explained by increased rolling moment due to sideslip.

A similar instability can be expected at negative values of tail height beyond those studied. In fact, this effect has been demonstrated in an NRE towing trial of a body with inverted vertical tail.

SERIES VIII

SHORT PERIOD PITCH MODE

Fig. 14 shows that the proportion of the downforce taken by the wing has a moderate effect on the short pitch mode. Both frequency and damping are influenced by cross coupling effects with surge and heave. Since damping is close to critical for all values of L/V^2, these effects are unlikely to have practical significance.

LONG PERIOD HEAVE MODE

The influence of L/V^2 on the long period heave mode is surprisingly moderate. Both damping and natural frequency decrease as L/V^2 is increased, due to cross-coupling with surge and pitch. As will be seen in the next series, these effects are of little importance compared with corresponding effects on the lateral modes.

110

SHORT PERIOD YAW MODE

Fig. 15 shows that the proportion of downforce taken by the wing has no effect on the short period yaw mode.

COUPLED ROLL-YAW MODE

The proportion of down-force taken by the wing has a radical effect on the damping of this mode, and a significant effect on natural frequency. Indeed the damping changes all the way from negative values below an L/V^2 of about 1.0, to super-critical at an L/V^2 of about 2.2. The effect is similar to that of speed shown in Series II, and it demonstrates almost the same order of instability at $L/V^2 = 0$ as shown by the Wingless Body under design conditions.

As L/V^2 is decreased, the corresponding addition of weight causes a large increase in the rolling moment due to roll, which decreases the damping ratio and increases natural frequency.

LONG PERIOD KITING MODE

Fig. 16 shows that the effect of L/V^2 is similar to that of speed, and again opposes its effect on the roll-yaw mode. Up to the design value an increasing natural frequency is the primary effect, but beyond the design value the curve turns over rapidly and damping ratio drops off, producing instability beyond an L/V^2 of about 2.15. Careful design will be required to achieve satisfactory behaviour in both the roll-yaw and the kiting modes.

SUMMARY OF MODES

HEAVILY DAMPED SURGE MODE

One of the longitudinal modes is non-oscillatory in all cases studied. This mode is unlikely to result in any significant motion, unless future bodies achieve drags much lower than the assumed values.

SHORT PERIOD PITCH MODE

One of the two oscillatory longitudinal modes has a high frequency (of order 5 rad/sec, damped) and is always well damped (ratio greater than 0.7). It is independent of cable length and cable drag coefficient and involves the body pitching about its own towpoint. Its damping is affected by wing L/V^2, horizontal tail length and area, but none of these variations are too significant for the Depressed Body, being confined to the region of high damping. Removing the wing completely shows the largest reduction in damping.

The undamped natural frequency of this mode is most sensitive to speed, increasing roughly linearly with speed. It also increases somewhat with increasing wing L/V^2, horizontal tail length and area, but these effects are unlikely to be significant.

In summary, this is a body mode. Its damping is always satisfactory.

not significantly affected by any of the variables studied. Its undamped natural frequency is a linear function of speed, the only variable significantly influencing this mode.

LONG PERIOD HEAVE MODE

The most important longitudinal mode is an oscillation having a low frequency (of order 0.5 rad/sec) and a damping which varies significantly with towing conditions. This is primarily a heave motion, although surge and pitch coupling can be important.

This mode is not very sensitive to Depressed Body design features such as horizontal tail length and area or wing L/V^2. Its damping is mainly controlled by cable configuration parameters. Specifically, damping falls off with body trail, as cable length decreases or as the depression angle is increased by downforce, or by reduced speed or cable drag in the case of ballasted systems. The damping can vary from super-critical with long cable lengths at shallow depression angles, to barely adequate with short cable lengths at deep depression angles. Very heavy bodies may be inadequately damped at low speed when towed with very low drag cables. Moreover, body design features may have a greater effect on ballasted bodies. The effect of all variables on undamped natural frequency is comparatively unimportant.

This is a towing configuration mode which demands further study; its behaviour is complex, even for the simple models adopted here.

SHORT PERIOD YAW MODE

Of the three oscillatory lateral-directional modes, one has a high frequency (of order 5 rad/sec, damped) and is nearly critically damped. It is independent of cable length, cable drag coefficient, body downforce and wing L/V^2, and involves the body yawing about its own towpoint. Its damping is affected by vertical tail length, height and area, and by housing lever, but none of these variations are too significant, for the Depressed Body, being confined to the region of near-critical damping.

The undamped natural frequency of this mode is most sensitive to speed, increasing roughly linearly with speed. Other effects on natural frequency are not significant.

In summary, this is a body mode. Its damping is always near critical, not significantly affected by any of the variables studied. Its undamped natural frequency is a linear function of speed, the only variable significantly influencing this mode.

COUPLED ROLL-YAW MODE

An important lateral-directional mode has an intermediate frequency (of order 1 rad/sec) and a damping which varies greatly with speed and body design features. This is a coupled roll-yaw motion, similar to aircraft Dutch roll, and is essentially a body mode, affected little by cable length or cable drag coefficient.

112

Damping is very sensitive to wing L/V^2, ranging from negative with no wing fitted, to super-critical for L/V^2 values slightly greater than the design value. A similar trend is obtained by varying speed at constant L/V^2. Both damping and frequency are also sensitive to vertical tail length, height and area, and to housing lever, in a complex manner which requires further study.

This appears to be the mode which is most sensitive to detailed design features of the body, and must be carefully studied in any practical design because the effect of many features on this mode is opposite to their effect on the Long Period Kiting Mode, and careful compromise may be demanded.

LONG PERIOD KITING MODE

Of equal importance is an oscillation having a low frequency (of order 0.5 rad/sec) and relatively light and variable damping. This is primarily a swaying or kiting motion, although roll and yaw coupling are important, and the mode is influenced almost equally by cable configuration parameters and body design features.

For the Depressed Body, the primary influence on damping is cable length, and wing lifts exceeding the design value, obtained either through high speed or increased L/V^2. Large vertical tail height (positive or negative) or housing lever can also cause serious loss of damping.

Below design values, speed and wing L/V^2 primarily affect natural frequency, but as wing lift becomes a large fraction of the total downforce a rapid damping loss occurs, and it is this effect which is most likely to impose a limit on towing speeds attainable without the use of automatic controls. This decrease of damping with high lift is opposite to the effect in the Coupled Roll-Yaw mode, demanding careful compromise in the selection of wing size. The vertical tail effects are similar in that they too cause opposite trends in the damping of the two modes.

In summary, this mode cannot be attributed to either the body or the towing configuration. Its behaviour is influenced equally by both groups of variables, and body variables tend to produce opposing effects in this and the Coupled Roll-Yaw Mode. It demands careful further study.

CONCLUDING REMARKS

Although this work is incomplete and the models employed are greatly over-simplified, some tentative conclusions can be reached for depressed bodies, at least in a qualitative sense.

1) Of the six modes of motion exhibited by these models, three are likely to be significant, and three insignificant, for depressed bodies of the type studied.

2) The three insignificant modes are:-
   (a) Heavily Damped Surge Mode, which is non-oscillatory under all conditions investigated.
   (b) Short Period Pitch Mode, which is a well damped body mode, its undamped natural frequency varying linearly with speed.

(c) **Short Period Yaw Mode**, which is a well damped body mode, its undamped natural frequency varying linearly with speed.

3) **The Long Period Heave Mode** is a towing configuration mode, affected little by body design details. Its damping is sensitive to cable length and other parameters affecting body trail or system depression angle. Heavily ballasted bodies towed at low speeds on low drag cables may be inadequately damped at short cable lengths.

4) **The Coupled Roll-Yaw Mode** is the most sensitive body design mode, affected little by cable configuration variables. Its damping is sensitive to wing and vertical surface parameters, and bodies with low roll damping have shown instabilities in this mode. Since trends tend to oppose those in the Long Period Kiting Mode, careful study is demanded.

5) **The Long Period Kiting Mode** is sensitive to both towing configuration and body design variables. Its damping is sensitive to cable length and to wing and vertical surface parameters. In particular, large wing lift (in relation to ballast) can cause instability in this mode, as can excessive vertical surfaces. Since trends tend to oppose those in the Coupled Roll-Yaw Mode, careful study is demanded.

APPENDIX

(For readers unfamiliar with root-locus plots.)

Consider a simple second order dynamic system such as:-

$$m\ddot{x} + \mu\dot{x} + kx = 0$$

where m is the system mass, μ the damping coefficient and k the spring constant.

Define,

$$\omega_n = \sqrt{\frac{k}{m}} \quad , \quad \zeta = \frac{\mu}{2\sqrt{mk}}$$

then the equation may be written,

$$\ddot{x} + 2\zeta\omega_n\dot{x} + \omega_n^2 x = 0$$

This has solutions in the form, $x = x_0 e^{pt}$, where p is a root of the characteristic equation,

$$p^2 + 2\zeta\omega_n p + \omega_n^2 = 0$$

These "stability roots" are, therefore,

$$p = -\zeta\omega_n \pm i\omega_n\sqrt{1 - \zeta^2}$$

A system of simultaneous linear equations will have pairs of roots of this form, each pair defining a mode of motion. The complex plane is a

convenient means of displaying these roots, ie, a plot of the imaginary part $\omega_n\sqrt{1 - \zeta^2}$ against the real part $-\zeta\omega_n$. The location of the root on this diagram immediately indicates the nature of the mode. For example:-

(a) If $\zeta \leq -1.0$, no imaginary part exists, and the real part is positive. A root on the positive real axis thus represents a non-oscillatory divergence.

(b) If $-1.0 < \zeta < 0$, there are positive real and imaginary parts. A root in the first quadrant thus represents a divergent oscillation, of frequency $\omega_n\sqrt{1 - \zeta^2}$, and exponential coefficient $-\zeta\omega_n$.

(c) If $\zeta = 0$, there is a positive imaginary part ω_n, but the real part is zero. A root on the imaginary axis thus represents an undamped oscillation of frequency, ω_n.

(d) If $0 < \zeta < 1.0$, there is a positive imaginary part and a negative real part. A root in the second quadrant thus represents a convergent oscillation, of frequency $\omega_n\sqrt{1 - \zeta^2}$, and exponential coefficient $-\zeta\omega_n$.

(e) If $\zeta \geq 1.0$, no imaginary part exists and the real part is negative. A root on the negative real axis thus represents a non-oscillatory convergence.

In summary, the abscissa $(-\zeta\omega_n)$ measures the rate of divergence if positive, or convergence if negative, and the ordinate $(\omega_n\sqrt{1 - \zeta^2})$ is the actual frequency of oscillation. It will also be seen that, if the diagram is read in polar coordinates, the radius vector is the natural or undamped frequency (ω_n), while the vectorial angle is a measure of damping (ζ) in the second quadrant. Specifically, if the radius vector is inclined at ϕ to the negative real axis, $\zeta = \cos \phi$.

REFERENCES

1. Eames, M.C.   "Summary of the Linear Equations of Motion and Stability Derivatives for Towed Bodies", Naval Research Establishment, Technical Note FM/66/2, February 1966.

2. Jeffrey, N.E.   "Analog and Digital Computer Simulation of Cable Towed Body Systems", Naval Research Establishment Technical Note FM/66/6, December, 1966.

3. Earle, D.H.   "The NRE MOBY IV High Speed Underwater Towed Body", Naval Research Establishment, Technical Note FM/66/DR 1, April 1966.

4. Eames, M.C.   "The NRE MOBY Bodies for High-Speed Underwater Towing Research", Naval Research Establishment, Technical Note FM/65/DR 1, August 1965.
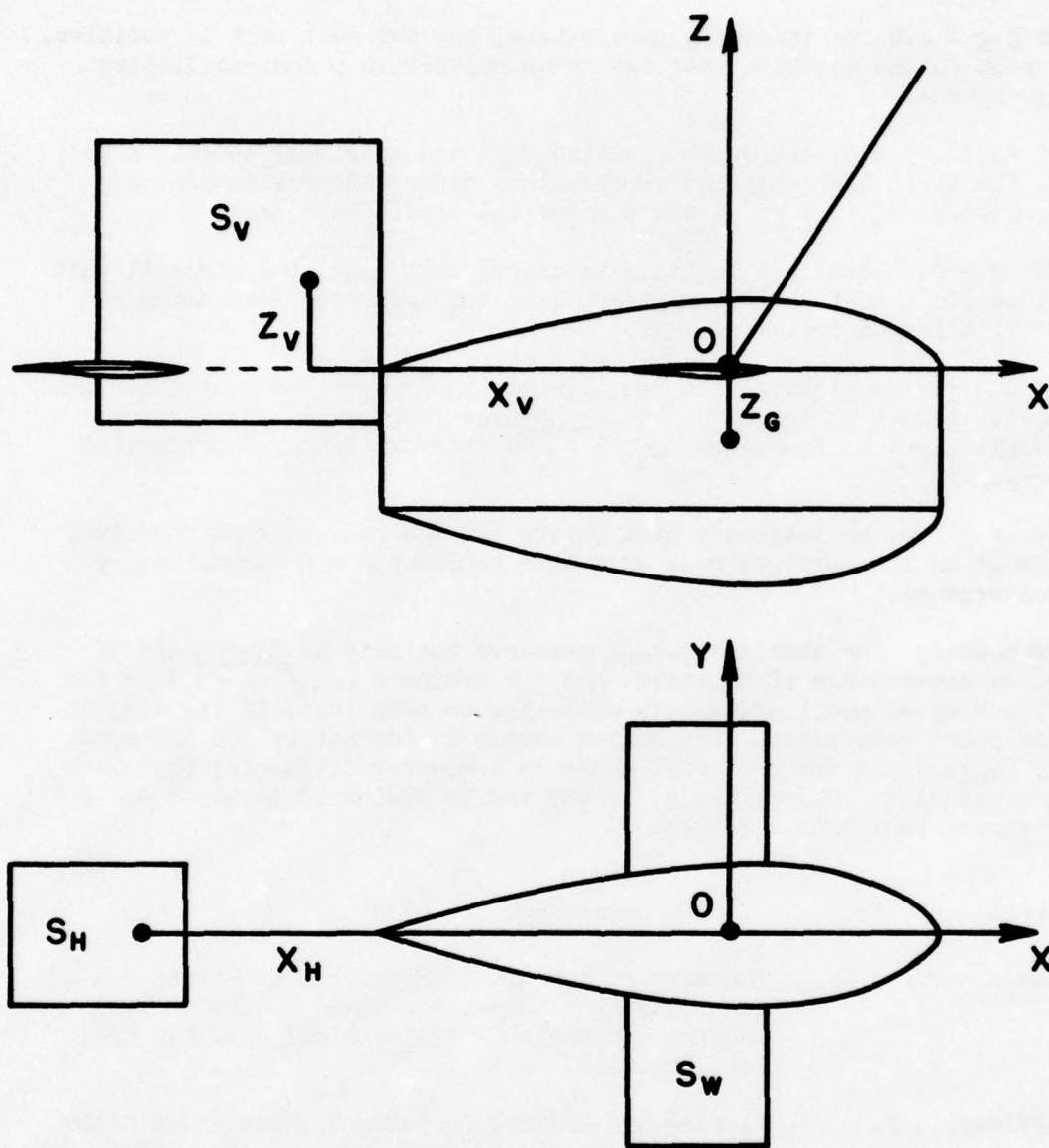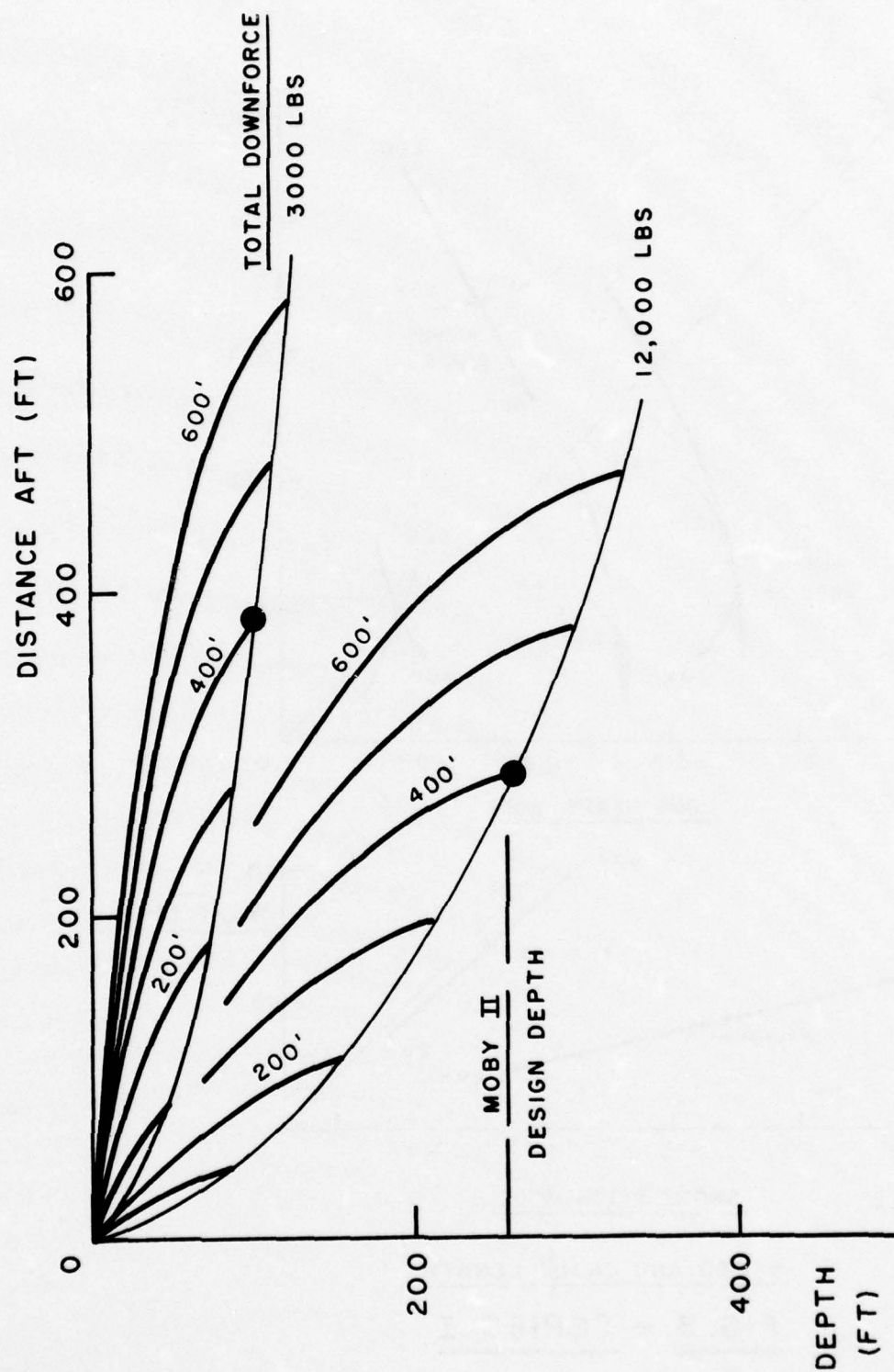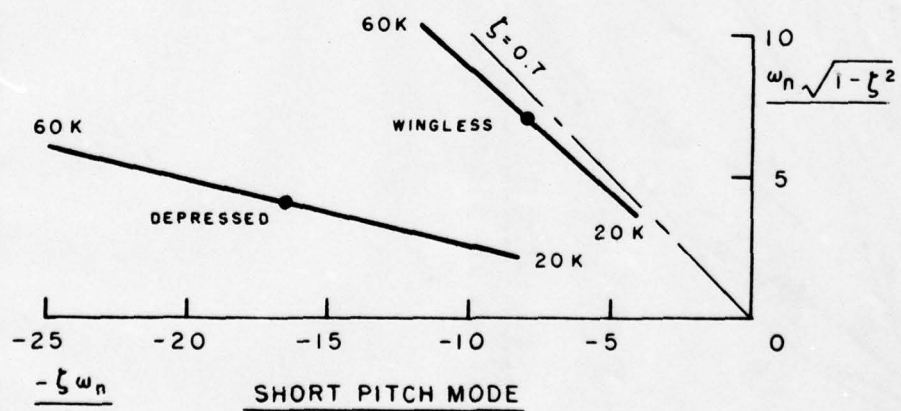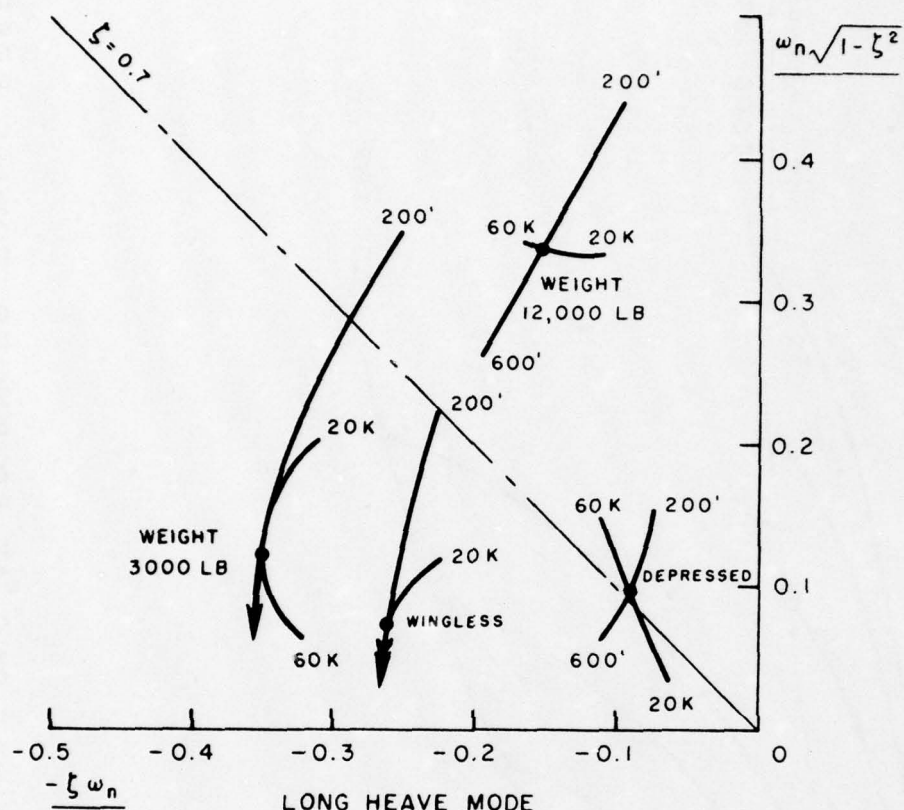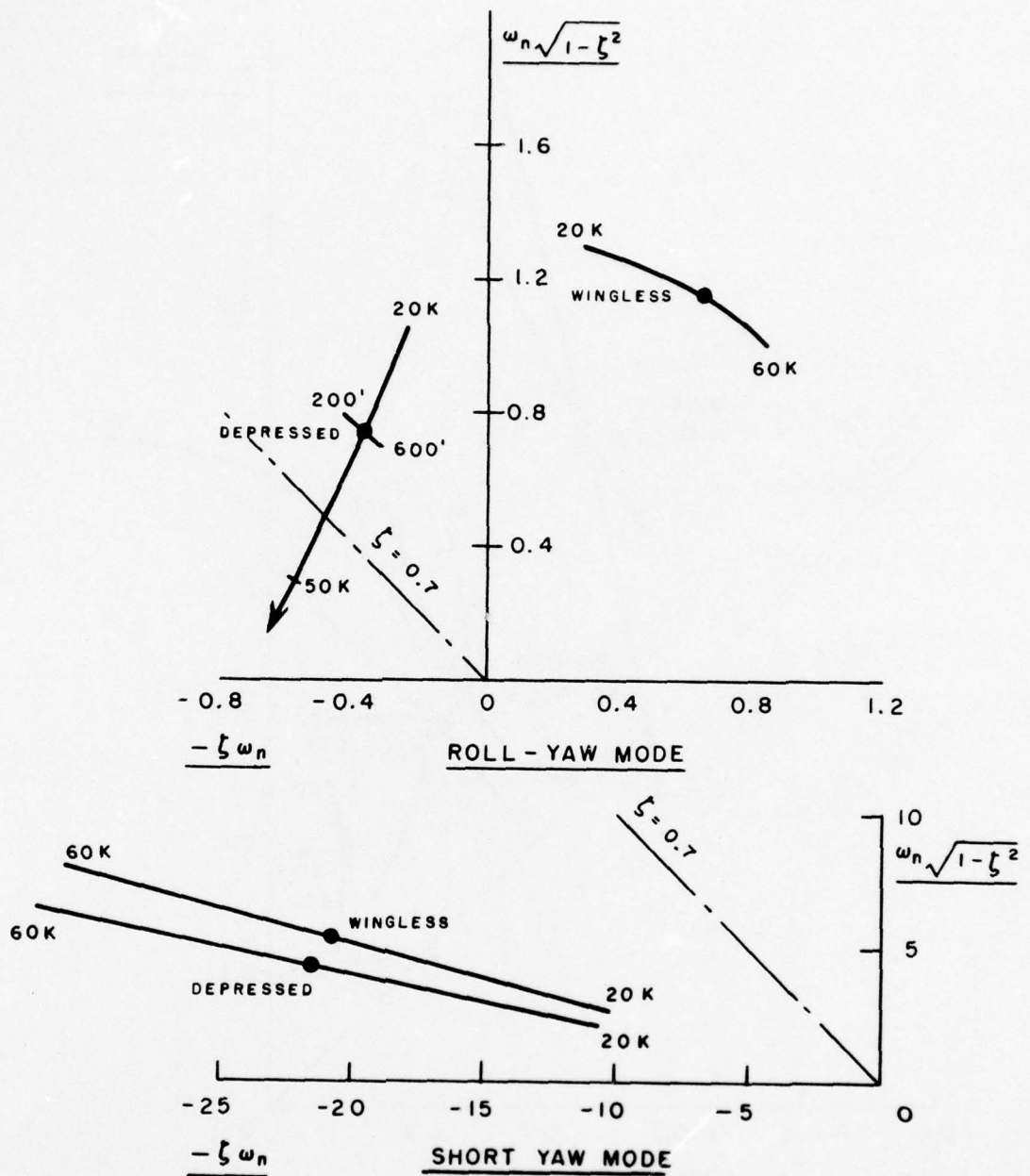
FIG. I PARENT BODY

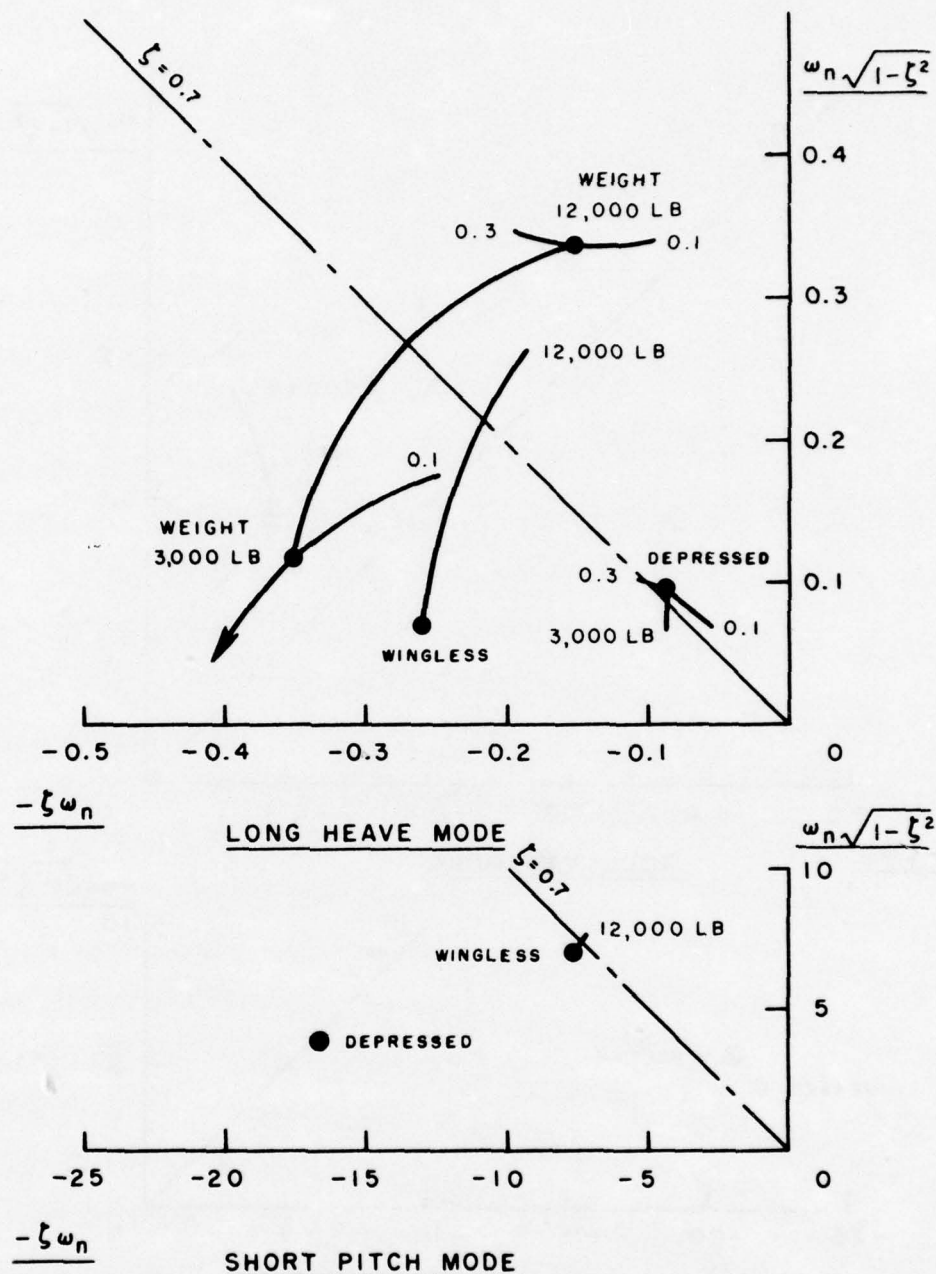FIG. 2 CABLE CONFIGURATIONS AT 40 KNOTS TOWING SPEED

117

SPEED AND CABLE LENGTH

FIG. 3 — SERIES I

SPEED AND CABLE LENGTH

FIG. 4 — SERIES II
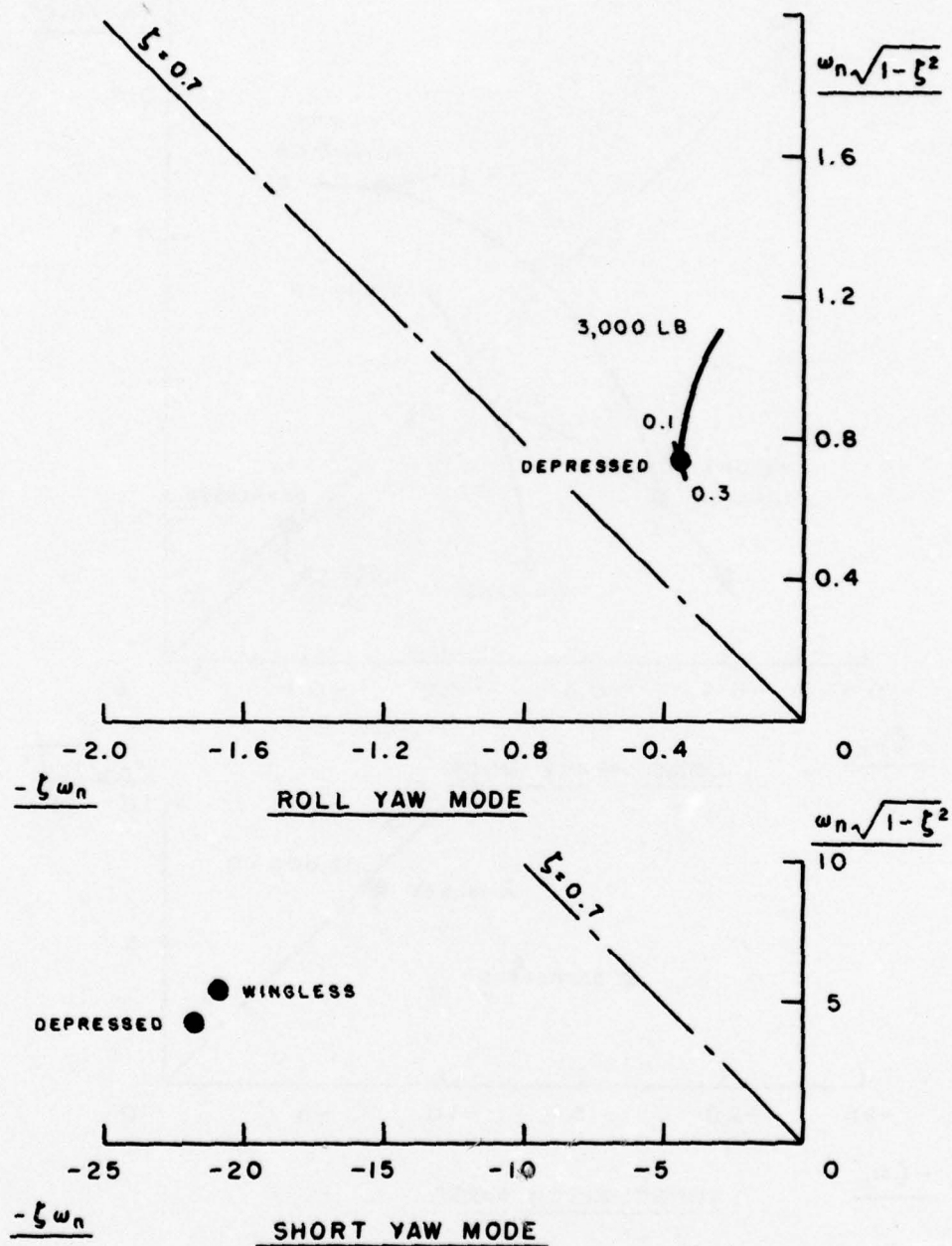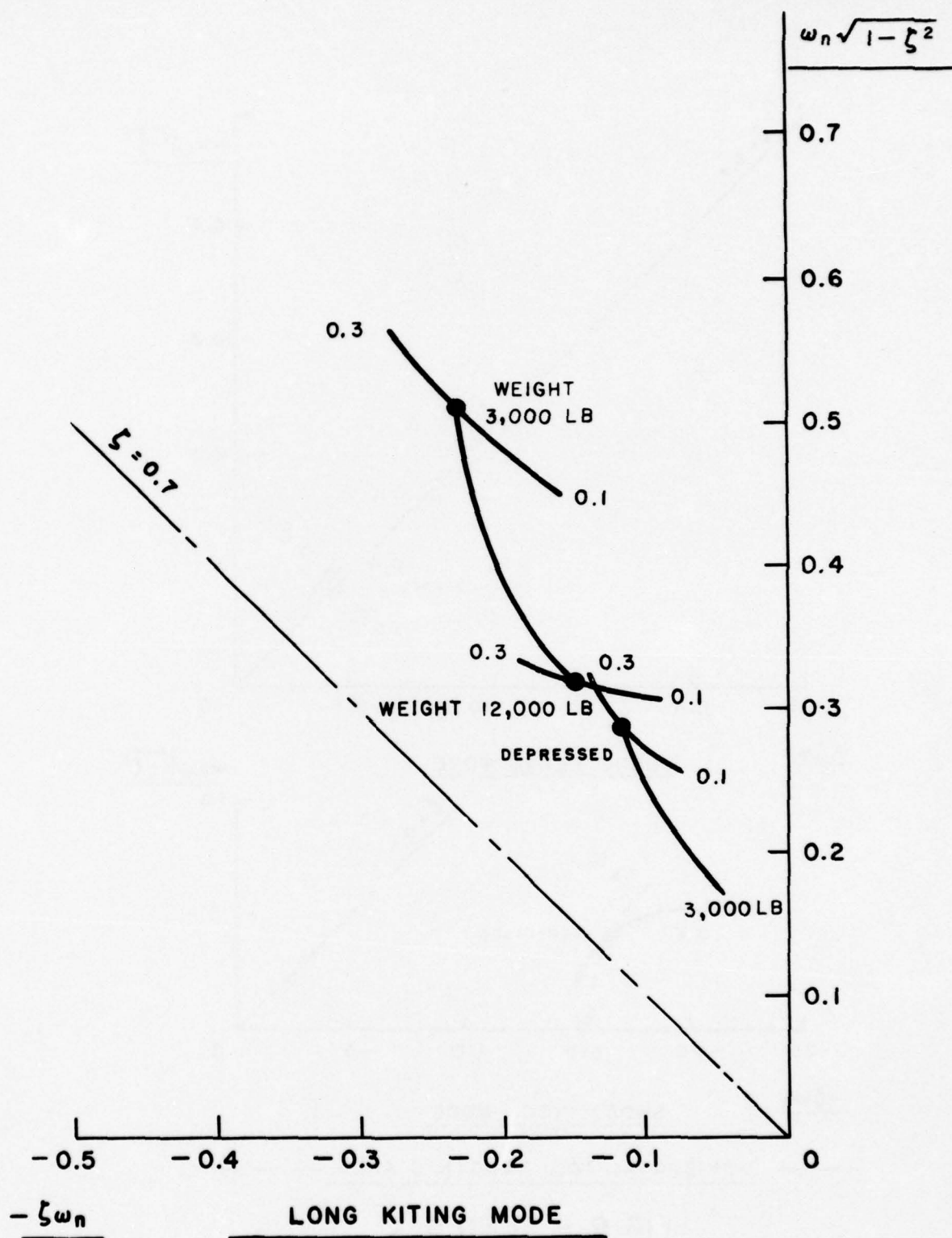
119

$$\omega_n \sqrt{1-\zeta^2}$$

60 K

200'

0.7

0.6

WEIGHT
3000 LB

0.5

60 K

$\zeta = 0.7$

600'

60 K   200'

50 K

0.4

200'

WEIGHT
12000 LB

DEPRESSED

0.3

600'

20 K   60 K

600'

200'

20 K

0.2

WING
-LESS

600'

20 K   20 K   0.1

−0.5   −0.4   −0.3   −0.2   −0.1   0

$-\zeta\omega_n$ LONG KITING MODE

SPEED AND CABLE LENGTH

FIG 5 — SERIES II

LONG HEAVE MODE

SHORT PITCH MODE

DOWNFORCE & CABLE DRAG

FIG. 6 — SERIES III

121

DOWNFORCE & CABLE DRAG

FIG. 7 — SERIES IV

LONG KITING MODE

DOWNFORCE AND CABLE DRAG

FIG 8 — SERIES IV
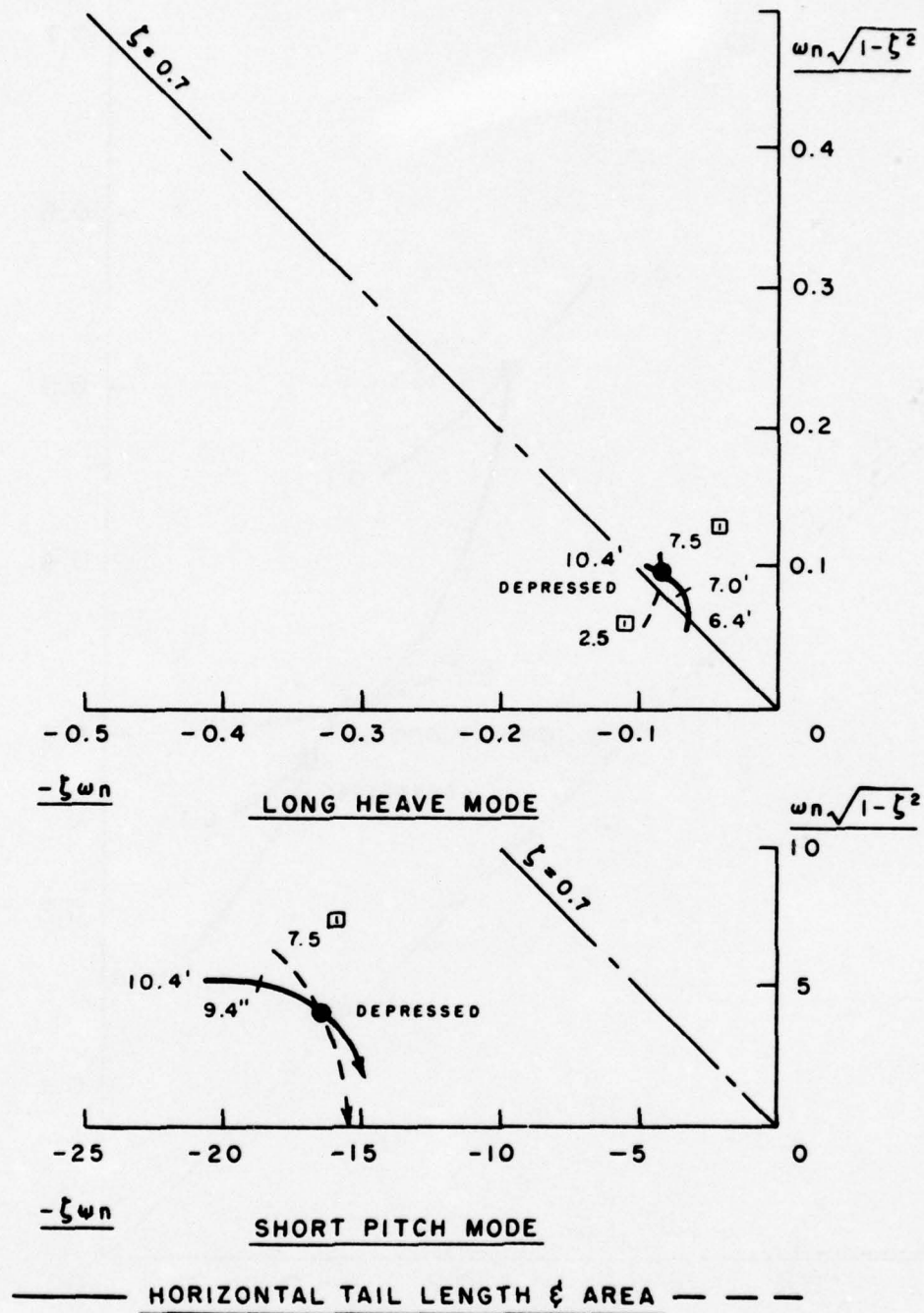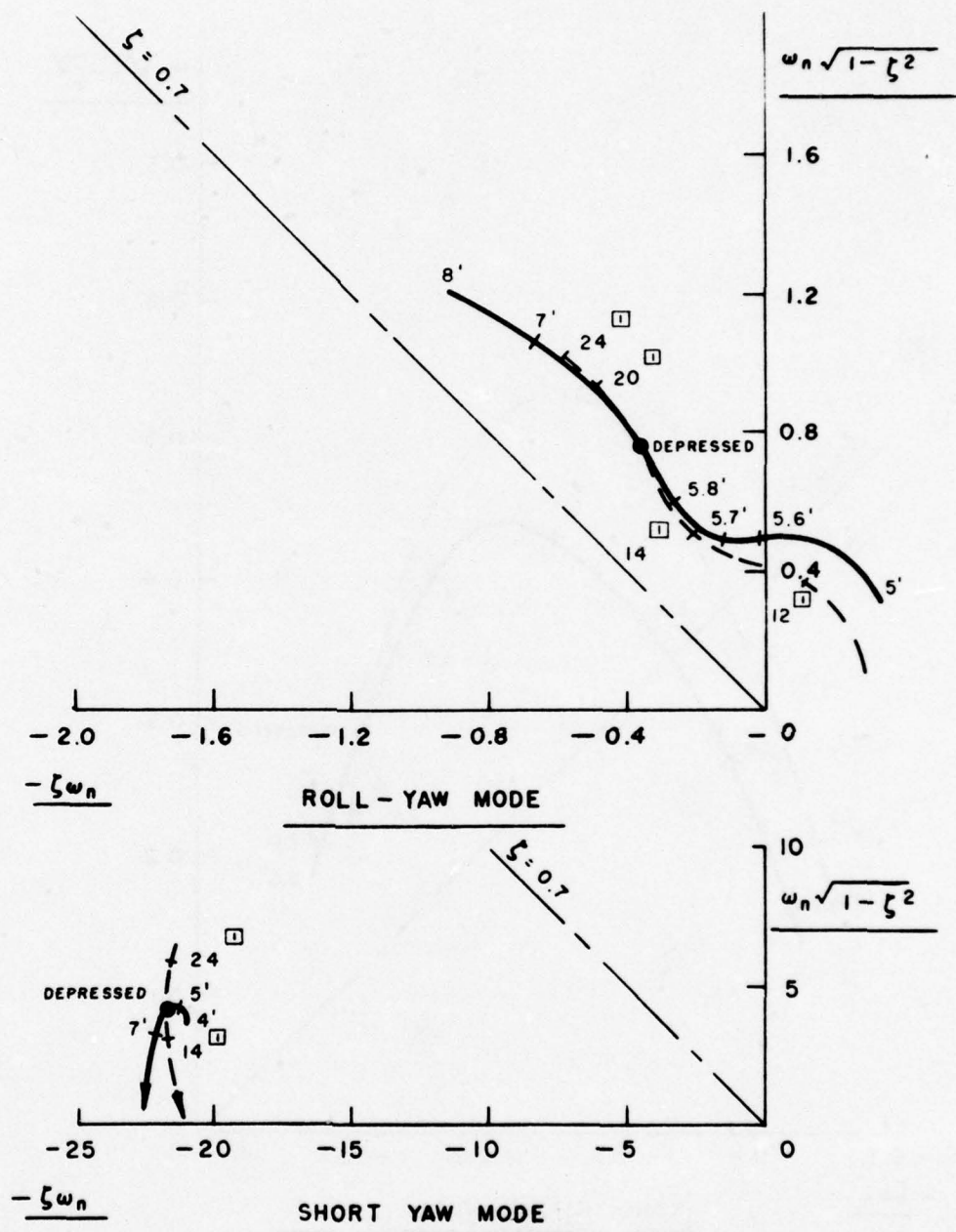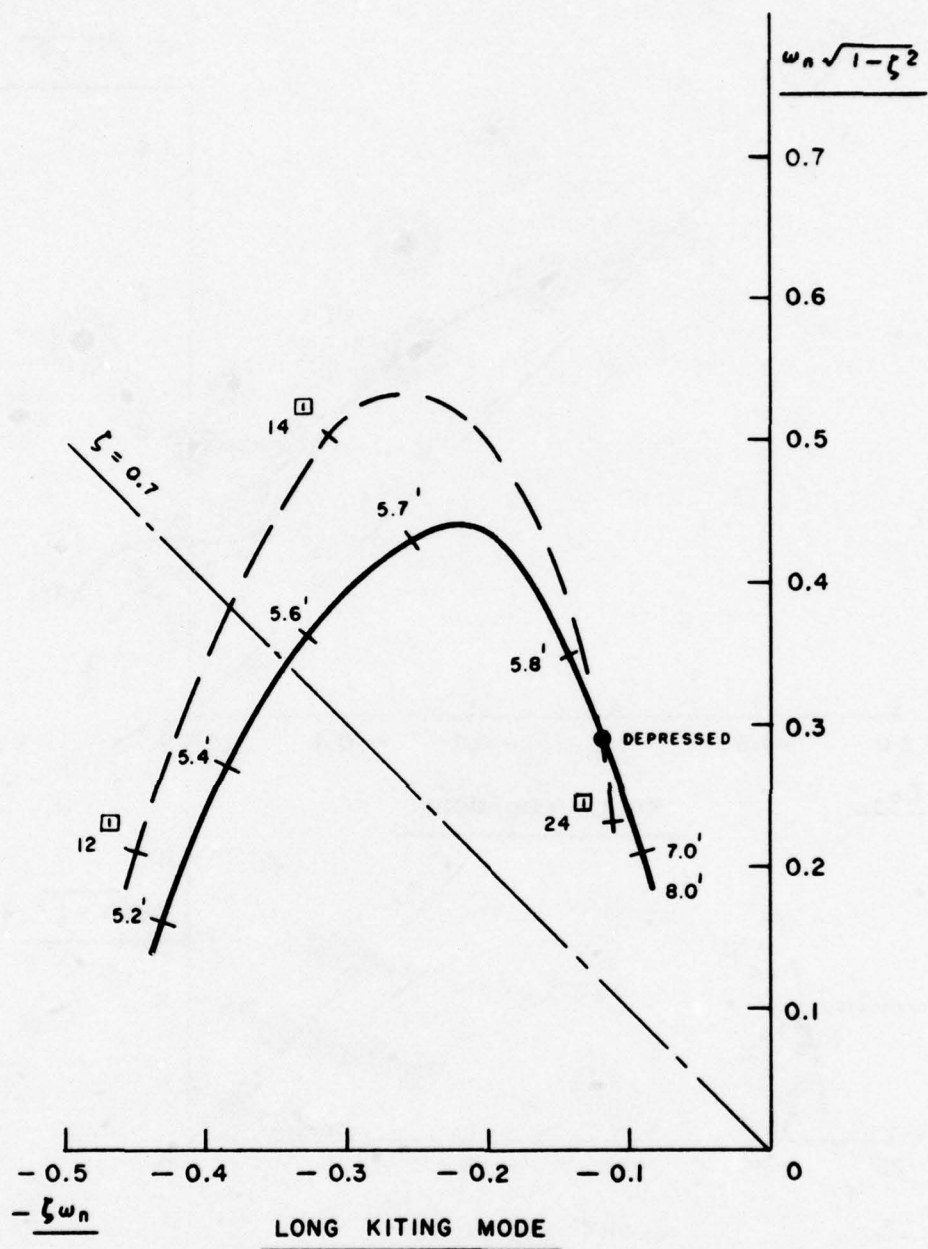
123

FIG. 9 – SERIES Ⅴ

124

FIG 10 – SERIES VI

FIG 11 – SERIES VI

126

FIG. 12 – SERIES VII

127
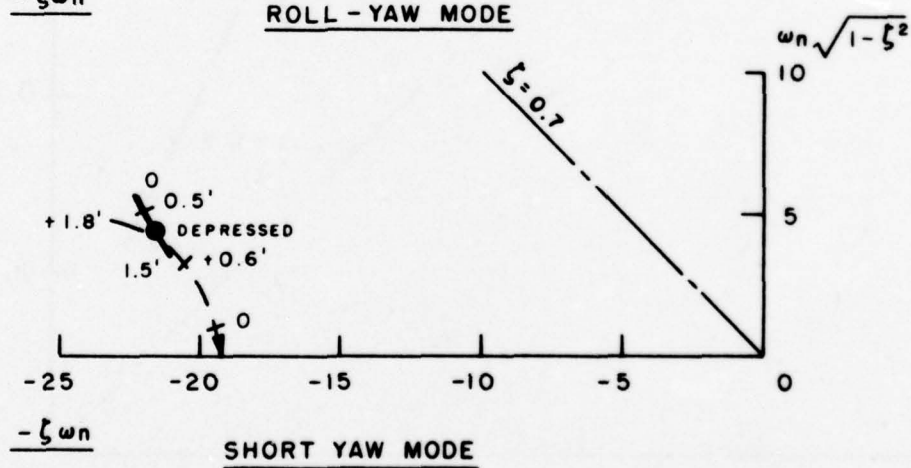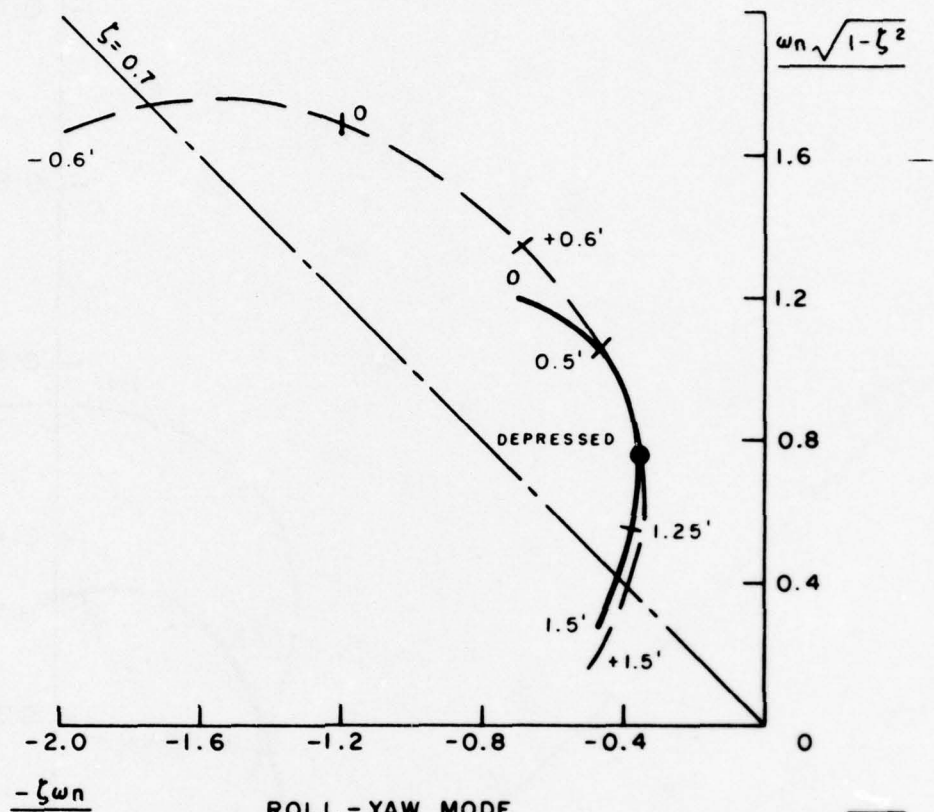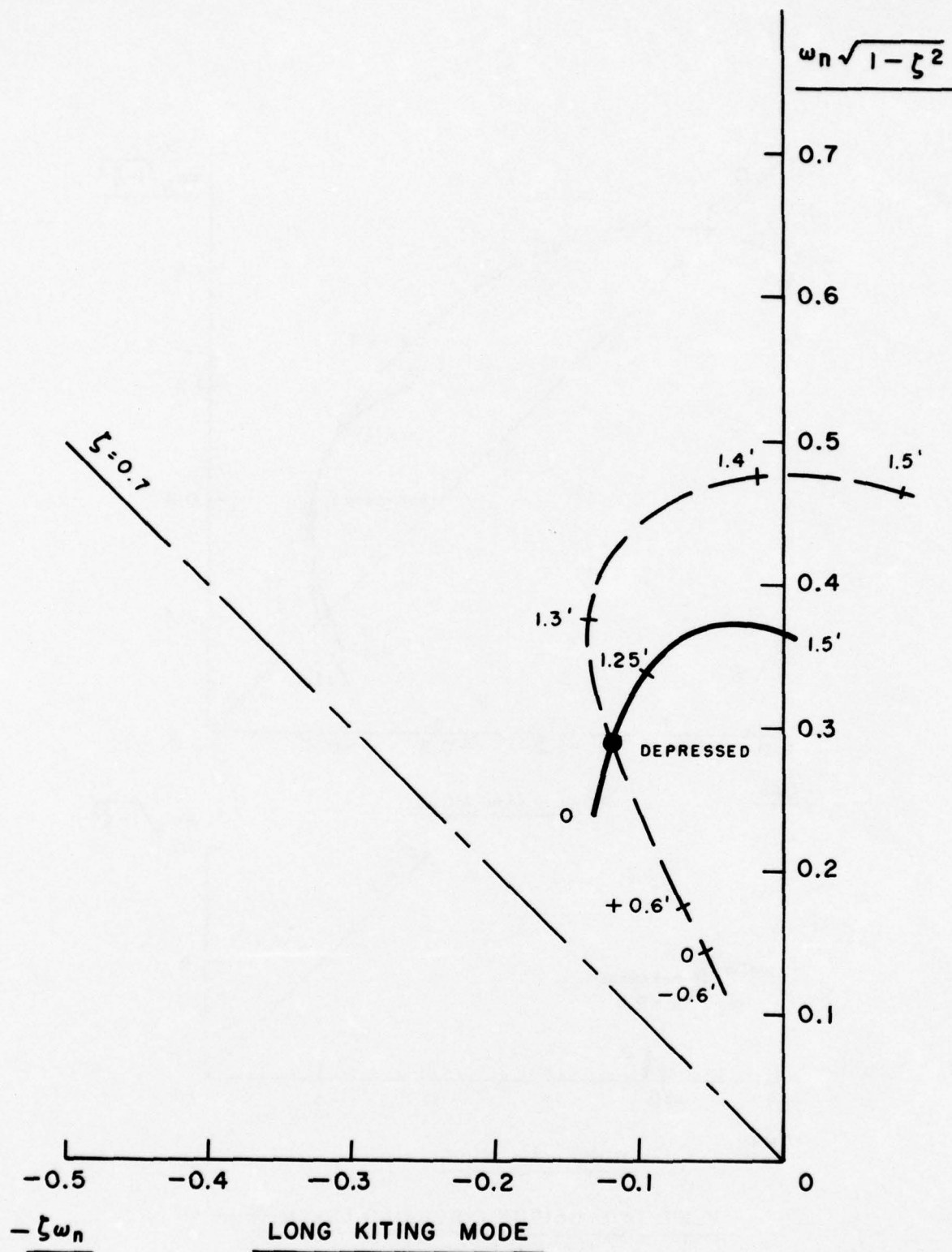
FIG 13 — SERIES VII

FIG. 14 — SERIES VIII

$\zeta = 0.7$

0

0.67

$\omega_n \sqrt{1-\zeta^2}$

1.6

1.33

1.2

0.8

● DEPRESSED

2.1

0.4

−2.0   −1.6   −1.2   −0.8   −0.4   0

$-\zeta\omega_n$ ROLL − YAW MODE

$\zeta = 0.7$

10

$\omega_n \sqrt{1-\zeta^2}$

5

● DEPRESSED

−25   −20   −15   −10   −5   0

$-\zeta\omega_n$ SHORT YAW MODE
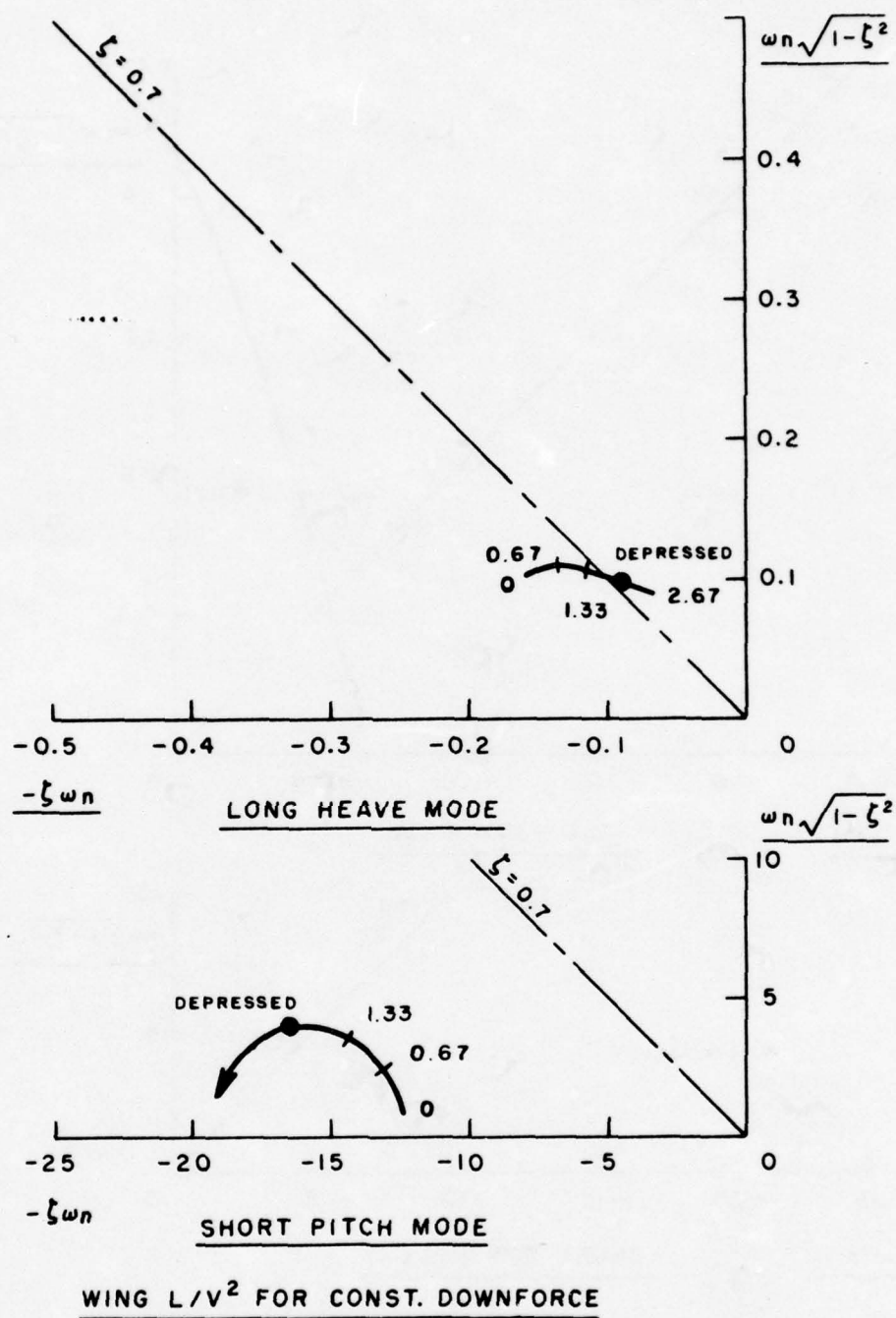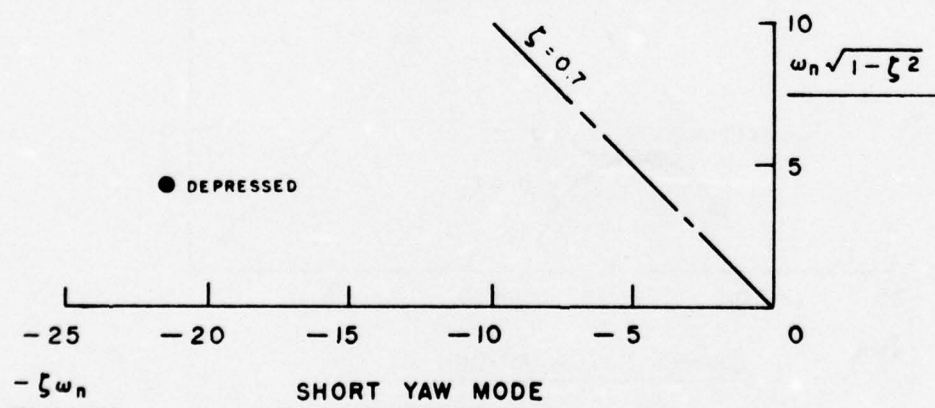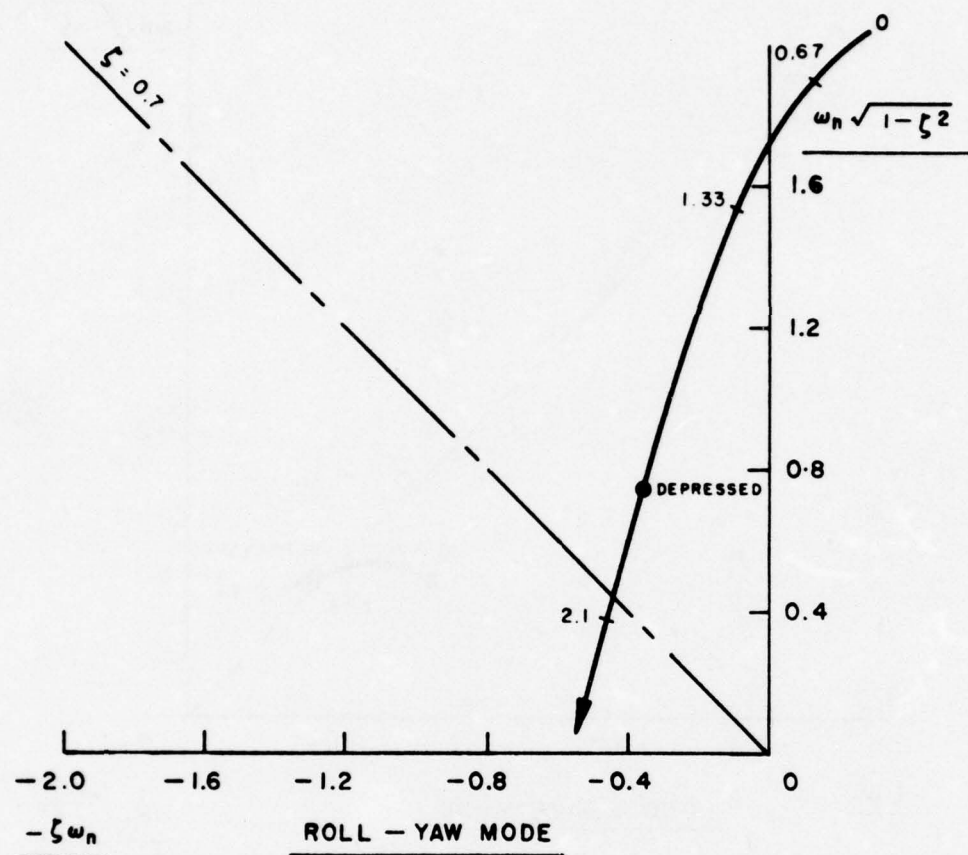
WING L/V^2 FOR CONST. DOWNFORCE

FIG 15 − SERIES IX

130

LONG KITING MODE

WING L/V² FOR CONST. DOWNFORCE
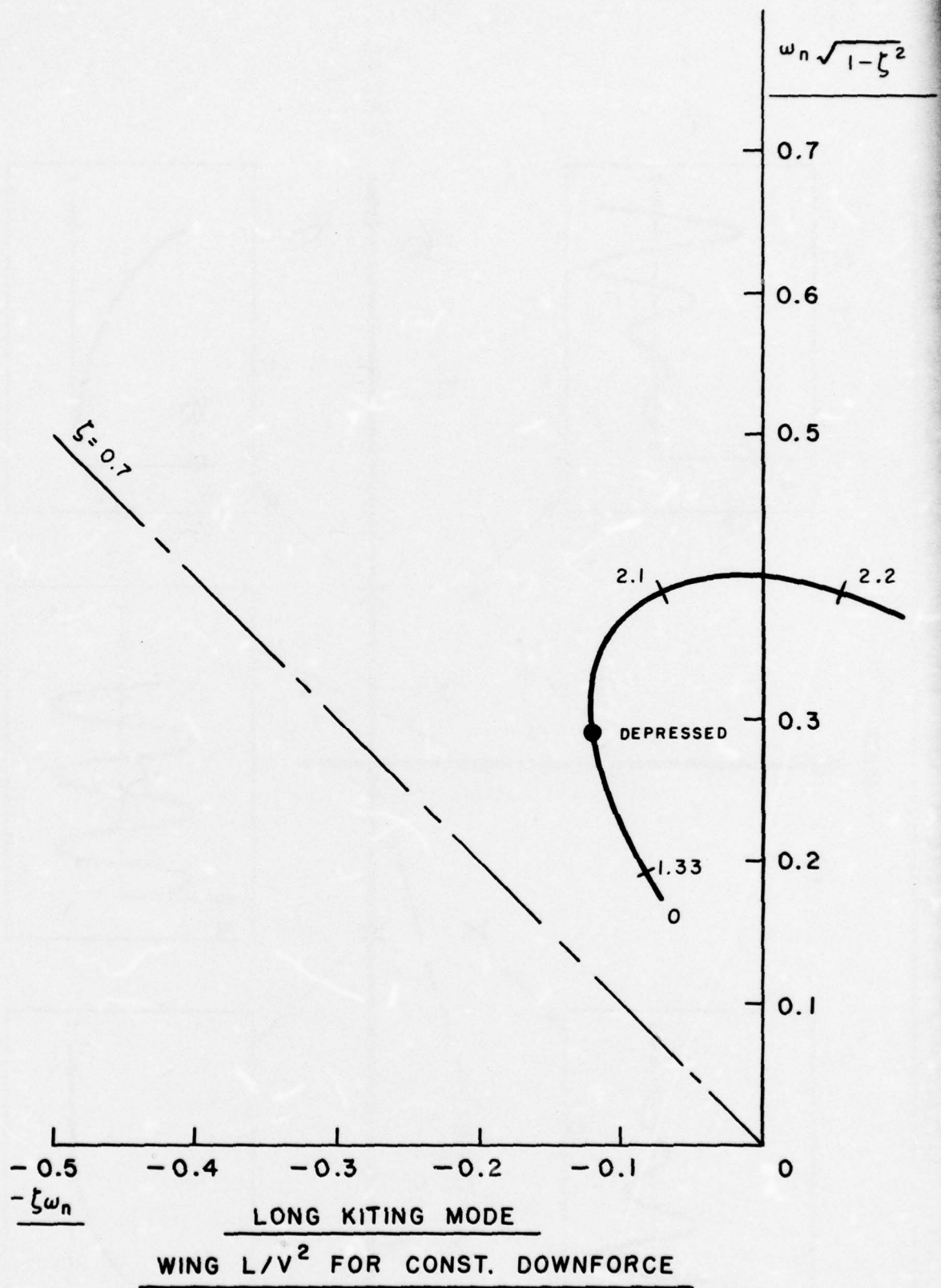
FIG 16 – SERIES IX

FIG. 17 CHARACTERISTICS OF COMPLEX PLANE ROOTS
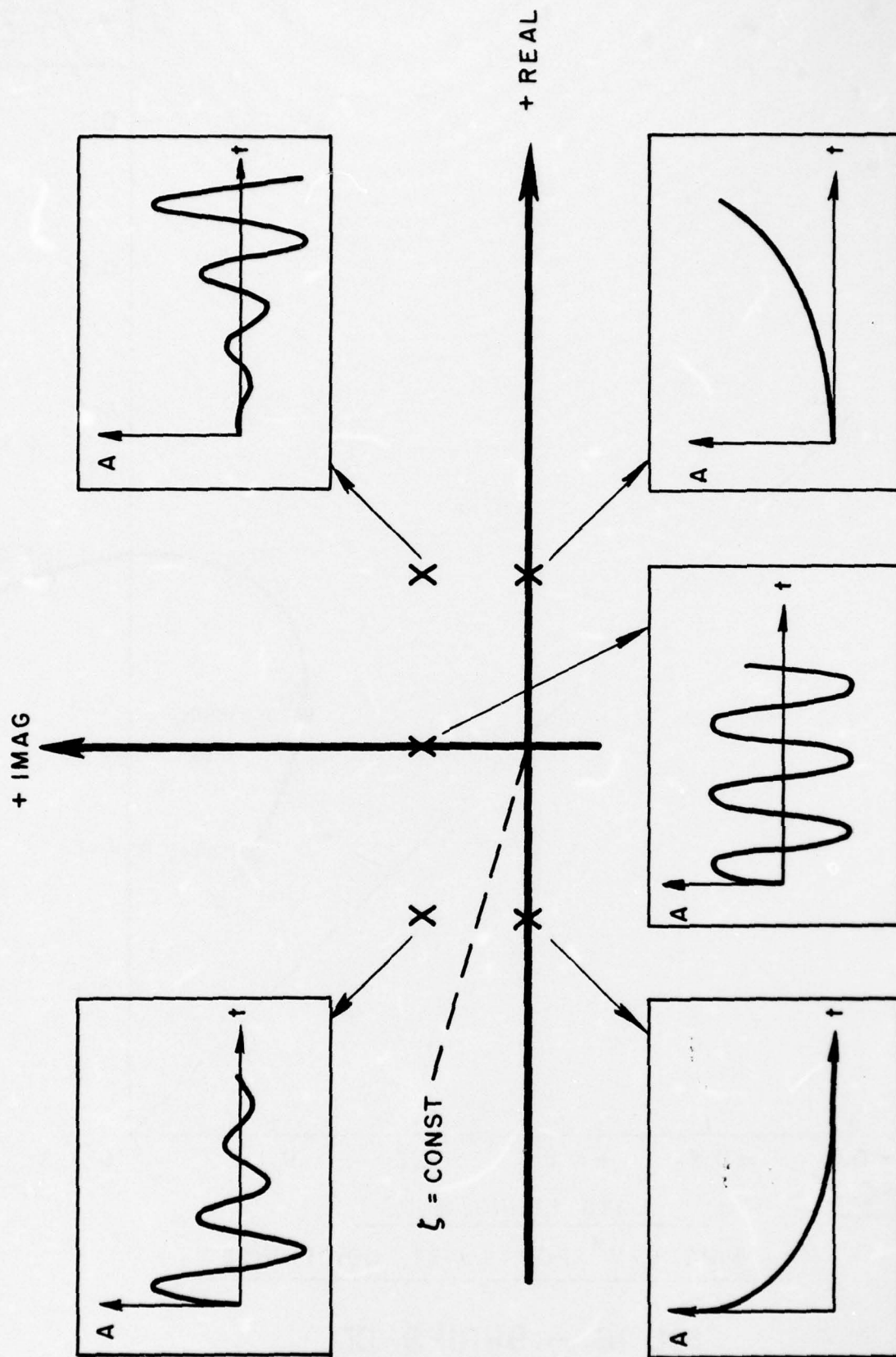
HYDRODYNAMIC DESIGN, MODEL AND FULL SCALE TESTS

OF A TOWED SONAR BODY, AN/SQS-505 XP-I

P. A. Hamill

Ship Section
National Research Council
Ottawa, Canada.

SUMMARY

Development of a towed body is described in
some detail. Relevant model and full scale
results are presented. It is concluded that
the design should meet all of the hydro-
dynamic requirements.

JANUARY, 1967

1.0   INTRODUCTION

   The Sonar Improvement Program for R.C.N. Destroyer Escort Vessels, designated DIANA I, has many aspects. One of these is a research and development project on a towed body to house the transducer. Following a request from the Canadian Department of National Defence, dated 25 March, 1963, the Ship Section of the National Research Council undertook to carry out Phase I of this project, i.e., the hydrodynamic design and model testing of the towed body.

   The preliminary design, small model tests (1/24 scale) and analog computer studies were complete in February 1964 and industrial contract was placed by the Department of National Defence for the construction of two bodies. In parallel with the construction extensive 1/4 scale model tests were carried out. These included drag and static derivative measurements, evaluation of dynamic derivatives using an oscillating mechanism and finally, in October 1965, an instrumented 1/4 scale model towing trial.

   In February 1965, DND requested that Ship Section, NRC, should prepare instrumentation and carry out the full scale hydrodynamic evaluation. The first phase, essentially a calm water trial, was completed in December 1966. Further trials, in rough seas, are scheduled for early 1967.

2.0   SPECIFIED DESIGN REQUIREMENTS

   The basic requirement was to design a hydrodynamically suitable body to contain a transducer 4 ft in diameter x 4 ft high. Essentially the hydrodynamic specifications were:

   (a)   Low drag (about 3200 lbs at 25 knots).
   (b)   Minimum pitch response (3 degrees r.m.s. pitch amplitude in sea state 5).
   (c)   Good tracking in high speed ship manoeuvers
   (d)   Directional stability in semi-submerged state.

   However there were additional restrictive physical requirements. The maximum length was limited to 18 ft, maximum width and height to 6-1/2 ft, maximum weight in water 10,000 lbs. To isolate the transducer from ship propeller noise a horizontal accoustic baffle was required above the transducer and extending as far as possible ahead

of it. As an ultimate design goal a baffle extension
approaching 100" ahead of the transducer mid-point was
stated to be desirable although it was noted that this was
likely to be impractical within the size limitations. A
spillway, capable of emptying all the entrained water in
5 seconds, was also to be incorporated in the design.

3.0   DESIGN PHILOSOPHY

Faced with the above requirements it is clear that
there could be as many solutions as there are designers.
In practice important guidelines tend to be set, in the
early stages, on the basis of organisational experience
and preference. Also, in context with the complete DIANA I
program, accoustic and operational handling aspects were
monitored by other groups. Thus the hydrodynamic
considerations were dominant in the NRC approach to the
problem and it was viewed primarily as a requirement for
a low drag body which would have a dynamic behaviour that
could be estimated, in advance, with reasonable certainty.
For both these reasons and because of the obvious
structural and dynamic load advantages it was decided, in
the first instance, to start with a body of revolution.

The requirement for good tracking during high speed
ship manoeuvers, it was intuitively felt, also favoured a
body of revolution since it appeared less susceptible to
side loading than the more usual slab sided body.

Requirements of accoustic baffle length and static
stability indicated that the maximum 18 ft length should
be used. Preliminary drag estimates were obtained by
extrapolating the data (1) on the TMB Series 58 shapes and
it appeared that a body with maximum diameter 6 ft would
meet the requirements and provide an acceptable accoustic
baffle.

The available towed body literature offered little
guidance on what constitutes good design practice from the
viewpoint of minimum pitch response. Preliminary estimates
of fin requirements were based on the unsophisticated but
reasonable premise that, in the pitch mode, by analogy with
a damped spring-mass system the body should have a soft
spring with high damping. Following detailed estimates of

"Superior numbers refer to similarly-numbered references
  at the end of this paper."

fin requirements for static stability and drag of the body plus fins it was decided to proceed with a design based on the TMB Series 58-40-05-01-30 body (Fig. 1).

The approach adopted was basically experimental and wherever possible, throughout the entire development, model tests were carried out to confirm or refine analytical estimates. This experimental approach was possible because the required facilities were readily available and was considered necessary at the current state of the art in this complex field.

4.0 DEVELOPMENT

4.1 Model Tests 1/24 Scale:

The first series of tests were made in the NRC Water Tunnel on a brass model of maximum diameter 3 inches. The tunnel has a 20 inch x 20 inch working section and a maximum speed of 42 ft/sec. A three-component balance was set up to measure drag, side force and yawing moment. The bare body and a variety of fin geometries, simply constructed of 1/16 inch brass plate, were tested. From this series a fin arrangement evolved which appeared to have acceptable drag and stability characteristics, and which, it was thought, would give high damping in both pitch and roll.

A 1/24 scale mahogany model with flat plate 1/16 inch bakelite fins (Fig. 2) of this arrangement was then constructed. The purpose of this model was to obtain qualitative confirmation of stability and an assessment of the general behaviour of the body when it was towed. The model was hollow to allow suitable weight disposition for correct vertical and longitudinal centre of gravity. The scaling was such that the ratio of gravity to hydrodynamic forces was the same as full scale with 10 ft/sec on the model corresponding to the maximum full scale towing speed of 25 knots. The cable model was 1/64 inch diameter braided steel fishing line.

A series of runs were made in the towing tank covering the speed range and depths to 8 ft. Generally the cable was held by hand on the towing carriage and a variety of disturbances introduced by oscillating the cable. It was observed that even with very large perturbations it was

difficult to induce perceptible angular body motions in pitch or yaw. Except for very low speeds where the natural pendulum frequency could be excited the model behaved very well.

The near surface and semi-submerged stability was also examined in detail and the behaviour of the model was excellent for large disturbances.

Because of the small scale and qualitative nature of these towing tests it was clearly impossible to draw any hard conclusions about the full scale body. Nevertheless the model looked very good even with disproportionally large excitations through the cable and was accepted as a positive indication for the future of the design.

4.2 Analog Computer Study:

In parallel with with these experiments the equations of motion of the body in the vertical plane, the coupled heave and pitch equations, were set up on the analog computer. The first analog was a very simple one with the cable equilibrium tensions assumed to act at the tow point and to remain constant for small disturbances in pitch and vertical displacement. Static force and moment derivatives were available from the tunnel tests. Acceleration and damping force and moment derivatives were calculated by available methods (2).

This simple analog was used to study the effect on the body pitch response of gross variations from the best available estimates of the acceleration and damping terms. It was found that even with very large, ± 50%, variations in these terms the basic character of the pitch response remained unchanged. The body pitch response was heavily damped at all speeds; the damping increased with speed and approached critical damping at 25 knots.

A digital computer program was written for quick determination of steady state cable body conditions. The Heavy General Cable Solution (3) was used.

Further analog computer experiments were made to assess the influence on body motion of the cable. A very simple cable spring term, linear in vertical displacement was introduced. The spring strength was calculated by considering the change in vertical tension and displacement for a small perturbation about the steady state condition

with constant cable scope. It was tentatively assumed, on
the basis of the small effect which resulted from the gross
variations in the body velocity and acceleration terms,
that cable damping and inertia might be ignored. They
would in any case, it was felt, tend to decrease the spring
effect.

In general it was concluded that the effect of the
cable would probably increase the stability of the body
in the sense that it would act as a spring tending to
restore the cable-body system to its steady state equi-
librium position. The results from the analog, which is
obviously over simplified, indicated that the cable effect
could be important at low speeds but would be small at
speeds of 15 knots and above. In the pitch mode it showed
up as an increase in stiffness at low speeds and appeared
to justify the premise that the body itself should be a
soft spring in the pitch mode.

4.3 Detailed Body Geometry:

Figure 3 shows the full scale body and is a convenient
reference for a brief description of the detailed geometry.
It consists of the main Series 58 body of maximum diameter
6 feet and length 18 feet. The towpoint is at the maximum
diameter which is at a distance 0.4 of the length from the
fore end. Four cruciform fins, faired fore and aft of
thickness 3 inches, start at 7.2 feet from the end and
extend out to the body's enveloping cylinder. Each of
these fins carries an end plate. The end plates have
modified NACA 16009 sections with chord length 3 feet at
the centre adjacent to the fin and tapering to 2 feet chord
over a span width of 2 feet on each side. The 16009 section
is modified to a 1/16 inch trailing edge thickness on the
outer (2 ft. chord) section and all outer sections are
faired with half bodies of revolution. Except for the top
one, which has 26 degree dihedral all of the end plates
are perpendicular to the fins. As a result of flow
visualisation tests all end plates are aligned 2 degrees
trailing edge inboard with respect to the body axis.

The top end plate dihedral was introduced to increase
static stability in yaw and to counter roll moments in a
turn.

Adjustable trim tabs are fitted on the trailing edge
at all four fins.

4.4 Model Tests 1/4 Scale:

Two detailed fiberglass models were constructed to 1/4 full scale. The first model was fitted out for installation on the Model Testing Basin static and dynamic balance (Fig. 4) which is an oscillating mechanism similar in principle and operation to that of the David Taylor Model Basin (4). The second model was intended as a mechanical development model and was used primarily for towing tests. From the large body of experimental data collected only those results of immediate relevance will be presented at this time.

Figure 5 shows the predicted full scale drag. In coefficient form based on body frontal area S_F and, perhaps more significant, transducer frontal area S_T,

$$\frac{D}{1/2\rho U^2 S_F} = 0.067 \qquad \frac{D}{1/2\rho U^2 S_T} = 0.118 \quad .$$

Non-dimensional static force, and moment coefficients in the notation of (4) were, in the vertical plane:

$$Z'_w = -0.261 \qquad\qquad M'_w = -0.026$$

and in the horizontal plane:

$$Y'_v = 0.301 \qquad\qquad N'_v = 0.037$$

The ratios $M'w/Z'w = 0.10$ and $N'v/Y'v = 0.12$ give the location aft of the tow point, in terms of the body length of the hydrodynamic centre of effort in the two planes.

One quarter scale towing trials carried out with an instrumented model (Fig. 6) substantially confirmed the drag measurements in the Model Basin tests and the heavily damped pitch response indicated by the analog simulation. The tests were made with the equivalent of 200 feet full scale cable length and measurements of body vertical acceleration, pitch and roll were recorded. Since the trials were made in calm water it was necessary to apply excitation through the cable. An attempt was made to excite an approximate impulse response by applying a jolt at the ship end of the cable equivalent to an 8 ft. full scale

motion of the stern. It was possible to transmit a vertical acceleration to the model of approximately 0.5 g excursion. Figure 7 shows typical acceleration and pitch records at speeds equivalent to 10 knots and 19 knots. The resultant body pitch angles are 7.5 and 4.5 degrees and obviously very well damped.

In addition approximately sinusoidal excitations equivalent to ± 4 feet stern motion were applied over a range of frequencies and speeds. The results are shown on Fig. 8. Pitch amplitude in degrees per foot amplitude stern motion is plotted on excitation frequency for speeds of 10, 15 and 19 knots full scale. Using these curves applied to Neumann Sea Spectra for 23 knots wind speed and assuming the stern motion to follow the encountered waves 1 to 1 at all frequencies, the r.m.s. pitch amplitudes were calculated to be 4.7, 2.9 and 2.0 degrees at 10, 15 and 19 knots respectively. For the 19 knot case actual stern motion response to model waves was available (6) and using this data the r.m.s. pitch was calculated to be 1.3 degrees.

Detailed qualitative towing trials were carried out with the 1/4 scale model from the Model Basin Towing Carriage to check on the stability of the body in the near surface and semi-submerged condition. It was concluded that with some reservation as to the body's behaviour in coming through the highly disturbed propeller race, there should not be any stability problems in the launch-recovery condition.

5.0 FULL SCALE TESTS

The body and the towpoint at the ship were both instrumented by stable platforms which measured, with respect to fixed space axes, three axial accelerations and three angles (Pitch, Roll and Yaw). In addition the cable angle at the body and the body depth were recorded.

At three cable lengths, 200, 400 and 600 feet, measurements were made on straight course and variety of circle manoeuvers up to the maximum ship rudder angle. The speeds ranged from 12 to 28 knots. The data was recorded on a 14-channel analog magnetic tape unit with paper chart monitoring of the most important variables. Digital

computer programs are available for power spectral density analysis of the magnetic tapes but this has not yet been carried out. For this presentation limited results have been obtained by hand analysis of paper charts.

Figure 9 shows body depth versus speed for different cable lengths; the curves are calculated and the points are full scale measurements.

Sea conditions were generally low throughout the trials (Sea State 1 with Swell 2 - 3 feet), with r.m.s. stern amplitudes of less than 1 ft being typical. Pitch r.m.s. varied from 1-1/2 degrees at 12 knots to less than 1/2 degree at 24 knots and above. On straight course runs the largest pitch amplitude recorded was 5 degrees, the largest roll was 3-1/2 degrees. Generally pitch decreased rapidly with increase in speed and also with increase in cable length. Preliminary results shown on Figure 10 demonstrate this trend. Pitch r.m.s.(degrees) per stern motion amplitude (feet) is plotted against cable length for speeds of 12 and 20 knots. It is emphasized that these results should be interpreted for trend rather than absolute numerical accuracy which should await rough sea data with power spectral density analysis of substantial inputs and body motions.

In steady state turns the body tracked well lagging the ship yaw by 20 to 40 degrees for rates of turn from 0.8 to 2.2 degrees per second. Steady state roll in turns varied from 3 to 18 degrees over the same range. The maximum depth change in a turn was 75 feet with 600 feet of cable out. This was recorded in a 24 knot approach speed 25 degrees rudder manoeuver where the steady state rate of turn was 2.4 degrees per second.

In summary the first ship trials showed that the body tows well at predicted depths and has satisfactory stability in the launch and recovery condition. It tracks well in severe manoeuvers and appears to have very satisfactory dynamic behaviour in pitch and roll.

6.0   CONCLUSION

Present indications are that the body will meet all of the hydrodynamic requirements. From the point of view of dynamic response the design shows exceptional promise in the higher speed range.

7.0   ACKNOWLEDGEMENT

8.0   REFERENCES

1. Gertler, M.   "Resistance Experiments on a Systematic Series of Streamlined Bodies of Revolution for Application to the design of High Speed Submarines." DTMB Report C-297, April 1950.

2. Paster, D.L. "Hydrodynamic Stability and Control
        and   Derivatives." U.S. NUOS Tech. Memo 120,
    Abkowitz, M.A.Feb. 1957.

3. Eames, M.C.   "The Configuration of a Cable Towing a Heavy Submerged Body from a Surface." NRE, PHx 103, November 1956.

4. Gertler, M.   "The DTMB Planar Motion Mechanism System Proc. of Symposium on Towing Tank Facilities.", Zagreb, Yugoslav Ship Hydrodynamics Institute Publication. September 1959.

5. SNAME   "Nomenclature for Treating the Motion of
    Technical   a Submerged Body Through a Fluid."
    and   April 1952.
    Research
    Bulletin
    No.1-5

6. Straszak, J.S.C., "DE 266 Model Experiments in Regular Head Waves of Ship Speed 18 knots." NRC, MET-468, January 1965.

DIM X	RAD Y		DIM X	RAD Y
.00	.00		112.32	35.15
8.64	14.82		120.96	34.55
17.28	21.12		129.60	33.78
25.92	25.67		138.24	32.81
34.56	29.06		146.88	31.00
43.20	31.60		155.52	30.05
51.84	33.42		164.16	28.12
60.48	34.67		172.80	25.68
69.12	35.46		181.44	22.66
77.76	35.87		190.08	18.94
86.40	36.00		198.72	14.40
95.04	35.90		207.36	8.80
103.68	35.99		216.00	00

NOSE SPHERICAL RADIUS 12.00 INCHES

TAIL SPHERICAL RADIUS 2.40 INCHES

BASIC BODY SHAPE

T.M.B. SERIES 58-40-05-01-65-30

FIG. 1

143
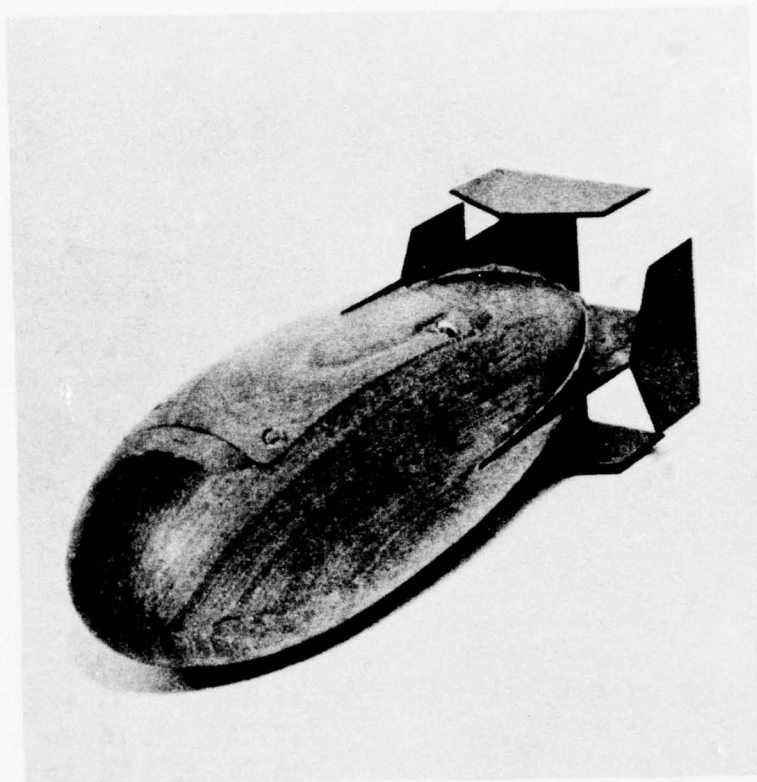
¼ SCALE TOWING MODEL

FIG. 2

144
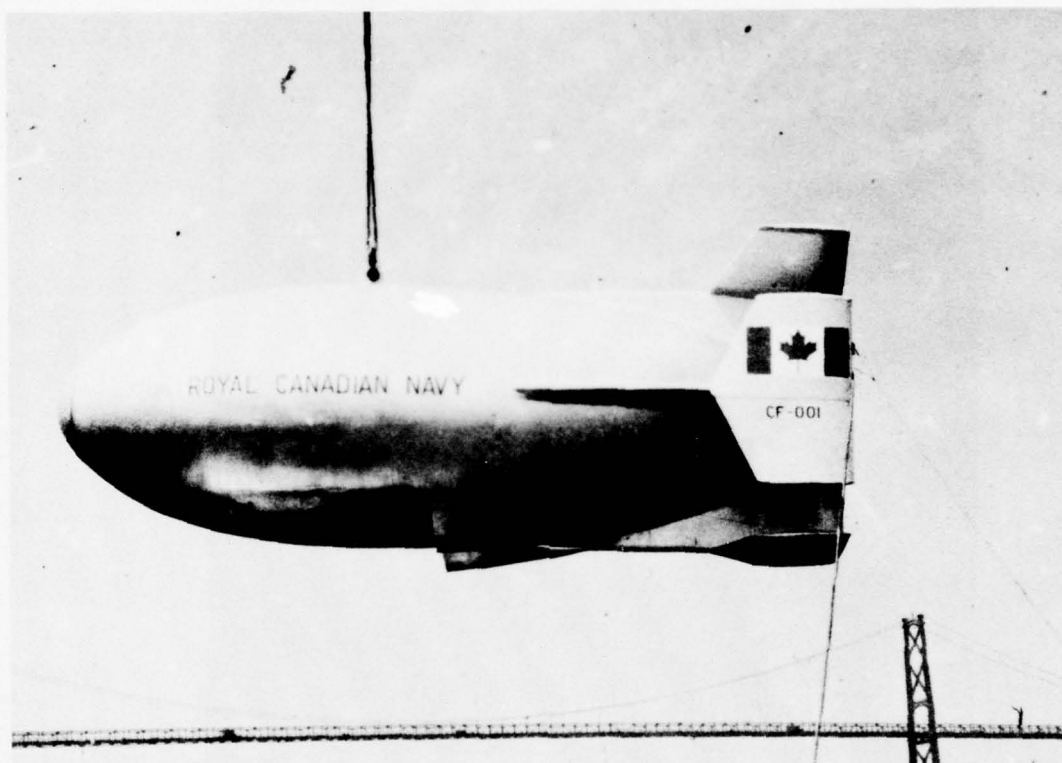
FULL SCALE BODY

FIG. 3
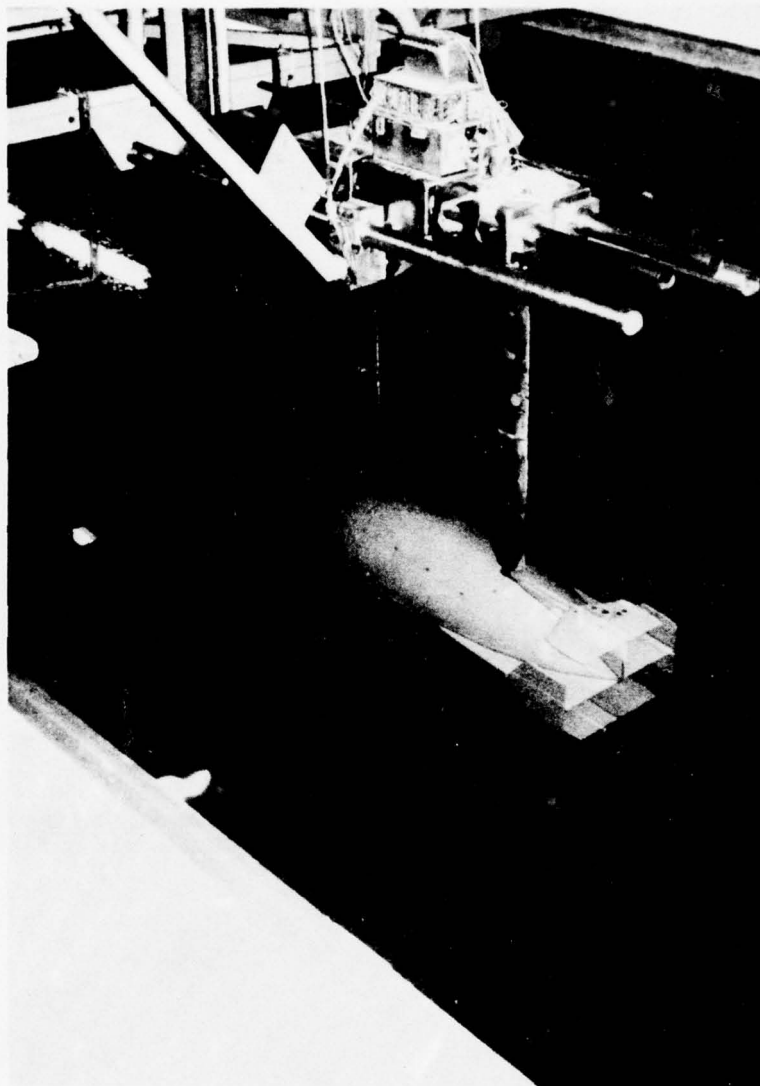
¾ SCALE MODEL ON TOWING TANK OSCILLATING
MECHANISM

FIG. 4

FULL SCALE DRAG vs. SPEED
BASED ON ¼ SCALE MODEL TESTS
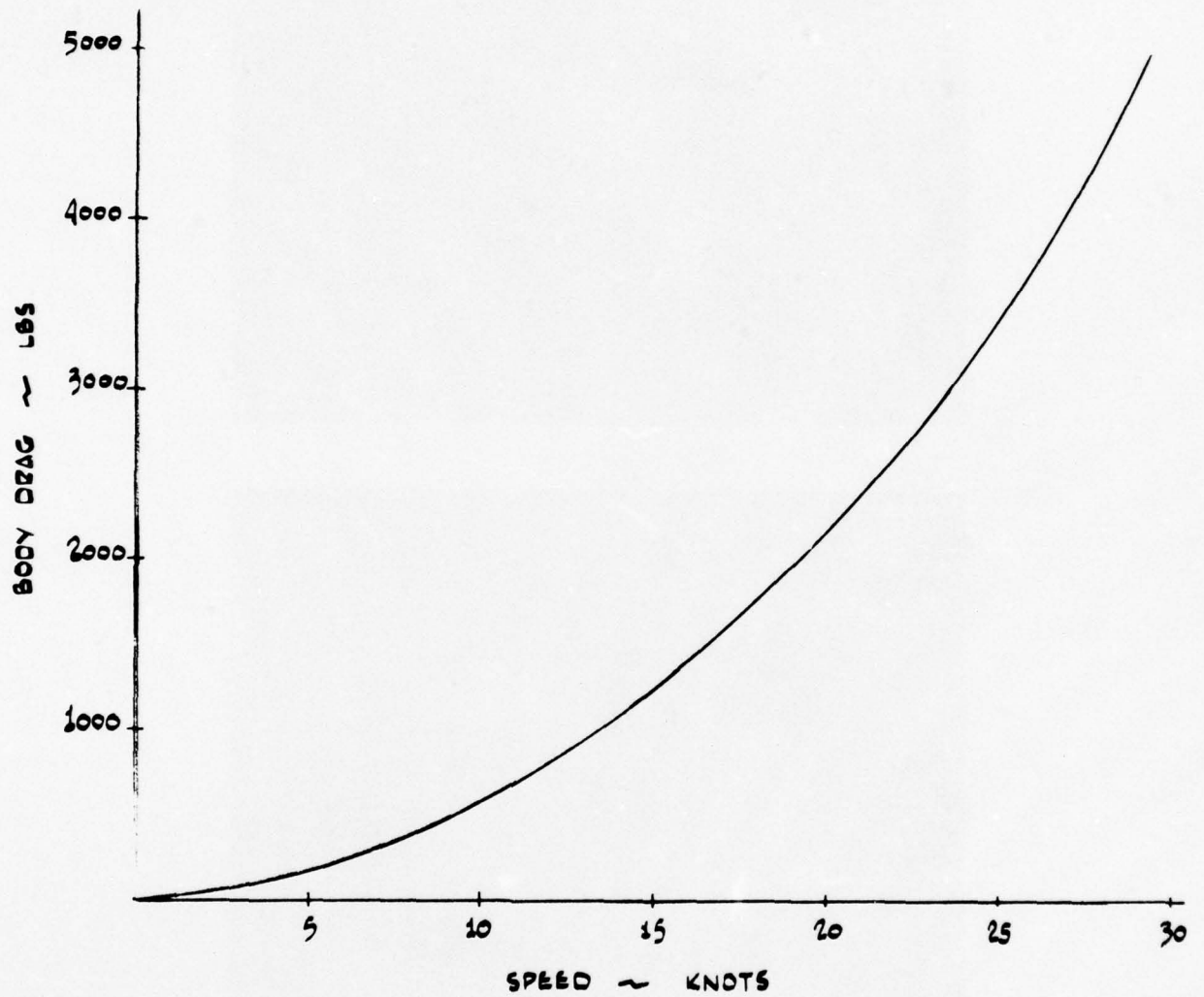
FIG. 5
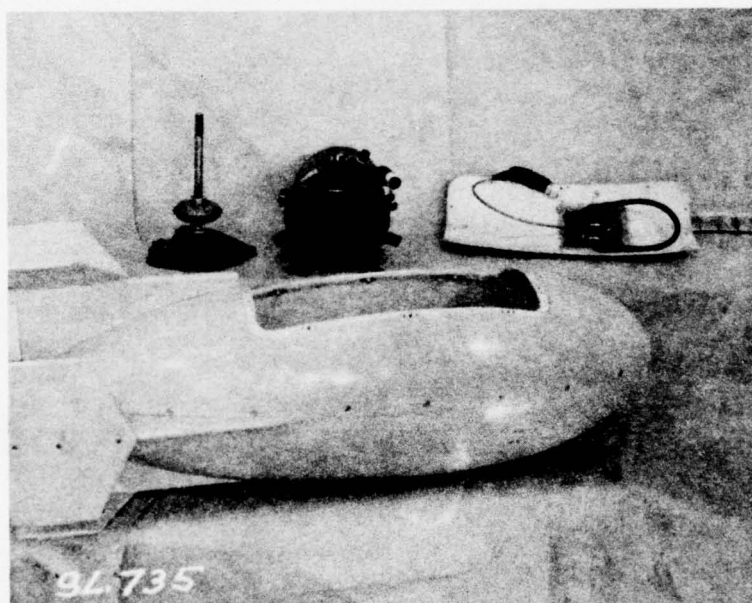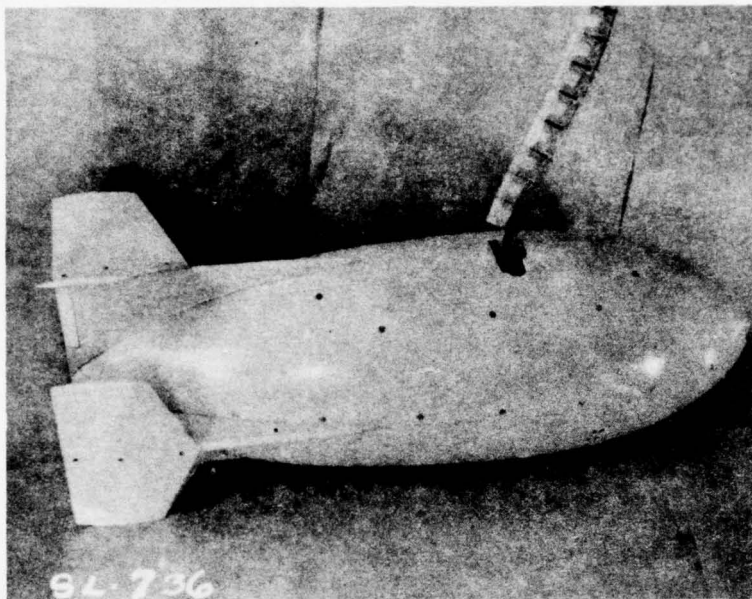
¼ SCALE INSTRUMENTED TOWING MODEL

FIG. 6
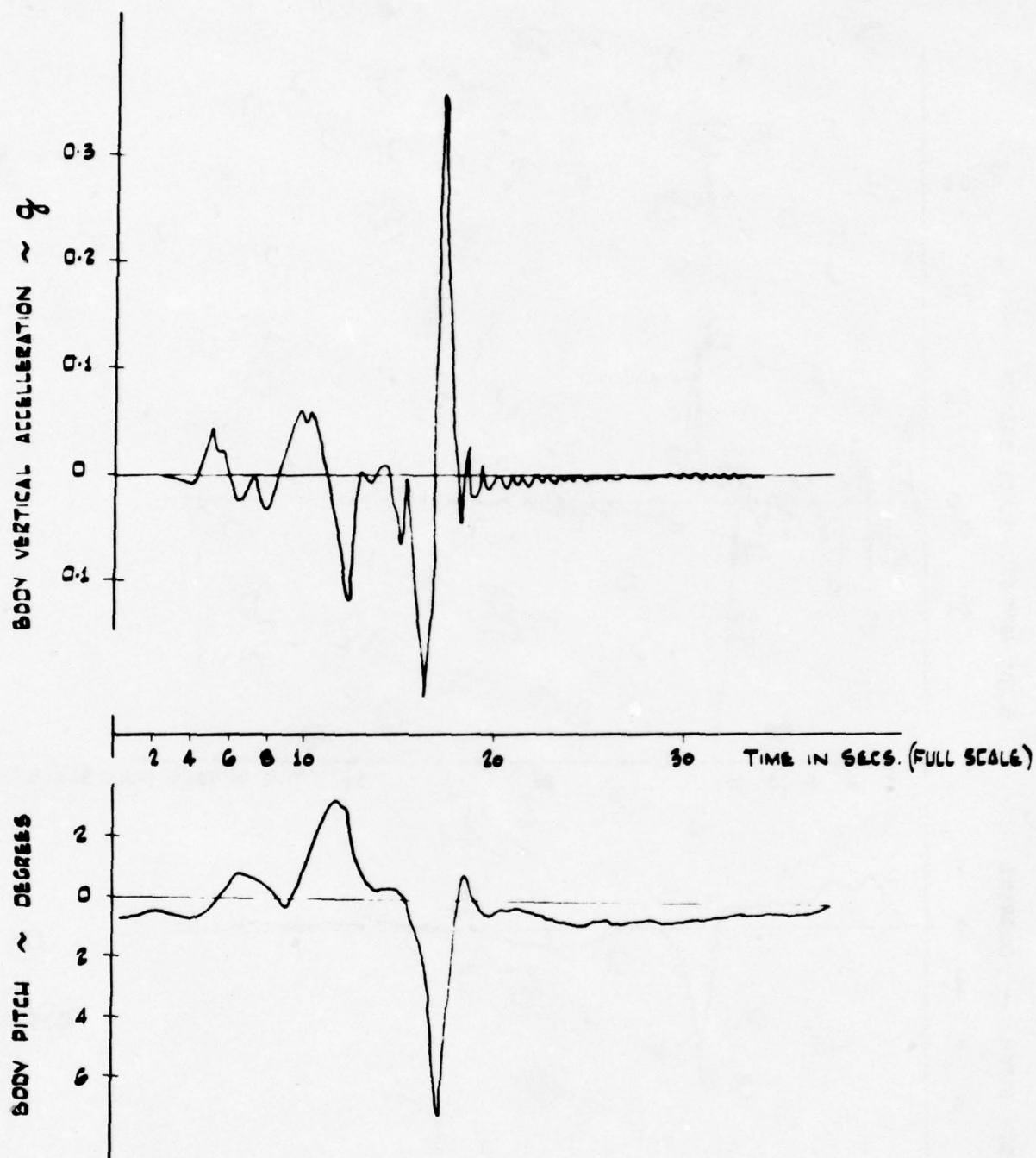
SIMULATED "IMPULSE" RESPONSE AT
10 KNOTS   200 FT. OF CABLE

FIG. 7 A

149
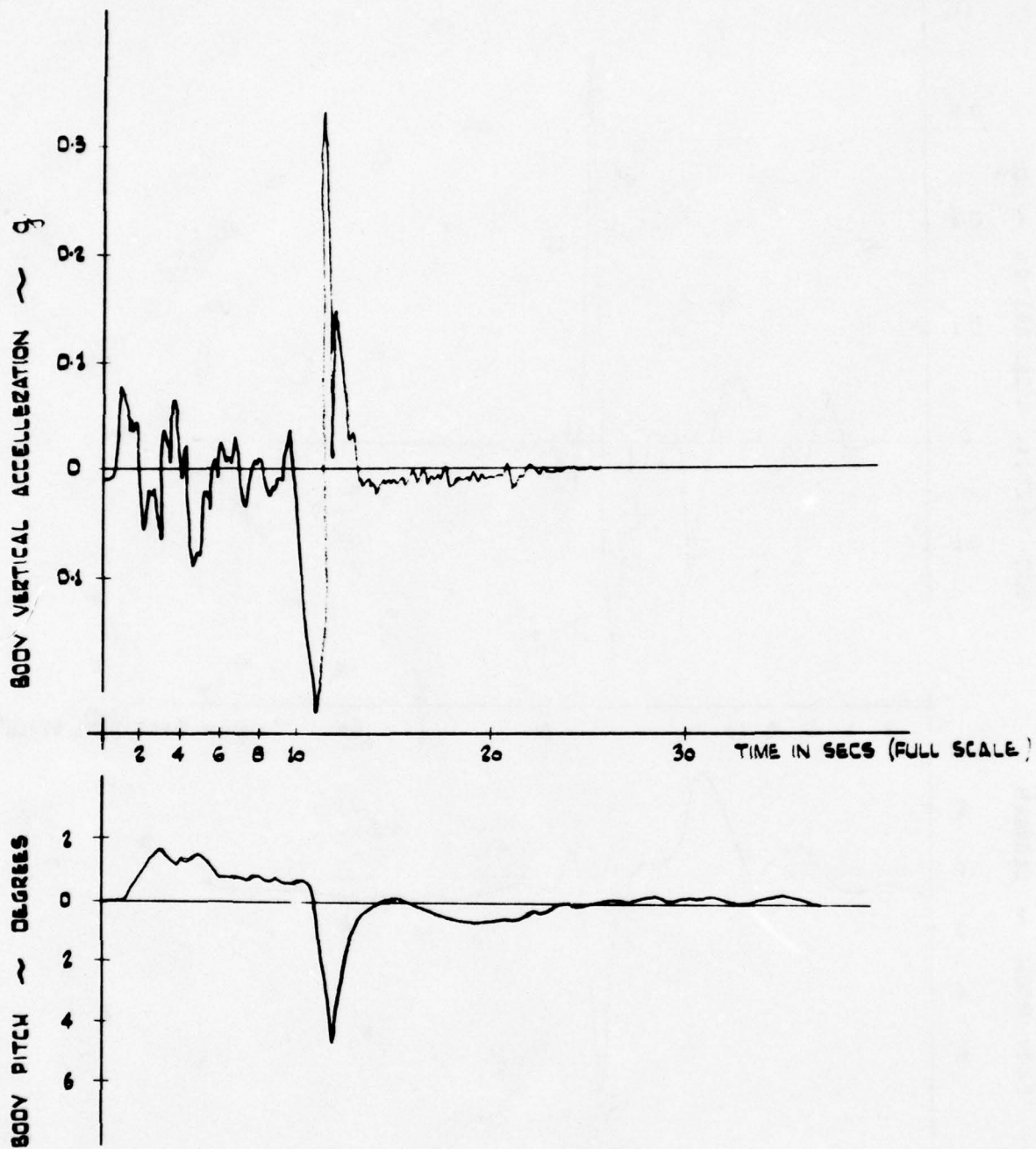
SIMULATED "IMPULSE" RESPONSE AT 19 KNOTS

200 FEET OF CABLE

FIG. 7 ᵇ

BODY PITCH PER FT. AMPLITUDE SHIP STERN MOTION
vs
EXCITATION FREQUENCY

FORCED PITCHING OF 1/4 SCALE TOWED MODEL.
EXCITATION EQUIVALENT TO 4 FT. AMPLITUDE SHIP MOTION
CABLE LENGTH EQUIVALENT TO 200 FT.

x 10 KNOTS
+ 15 KNOTS
⊙ 20 KNOTS

FIG. 6

ω$_E$ EXCITATION FREQUENCY ~ RAD/SEC   (FULL SCALE)

PITCH AMPLITUDE ~ DEGREES / STERN MOTION AMPLITUDE ~ FEET.

151

BODY DEPTH vs. SPEED

FIG. 9

152

PRELIMINARY ANALYSIS OF FULL SCALE TRIALS DATA
SHOWING THE TREND OF BODY PITCH RESPONSE TO SHIP STERN MOTION WITH INCREASE OF SPEED AND CABLE LENGTH.
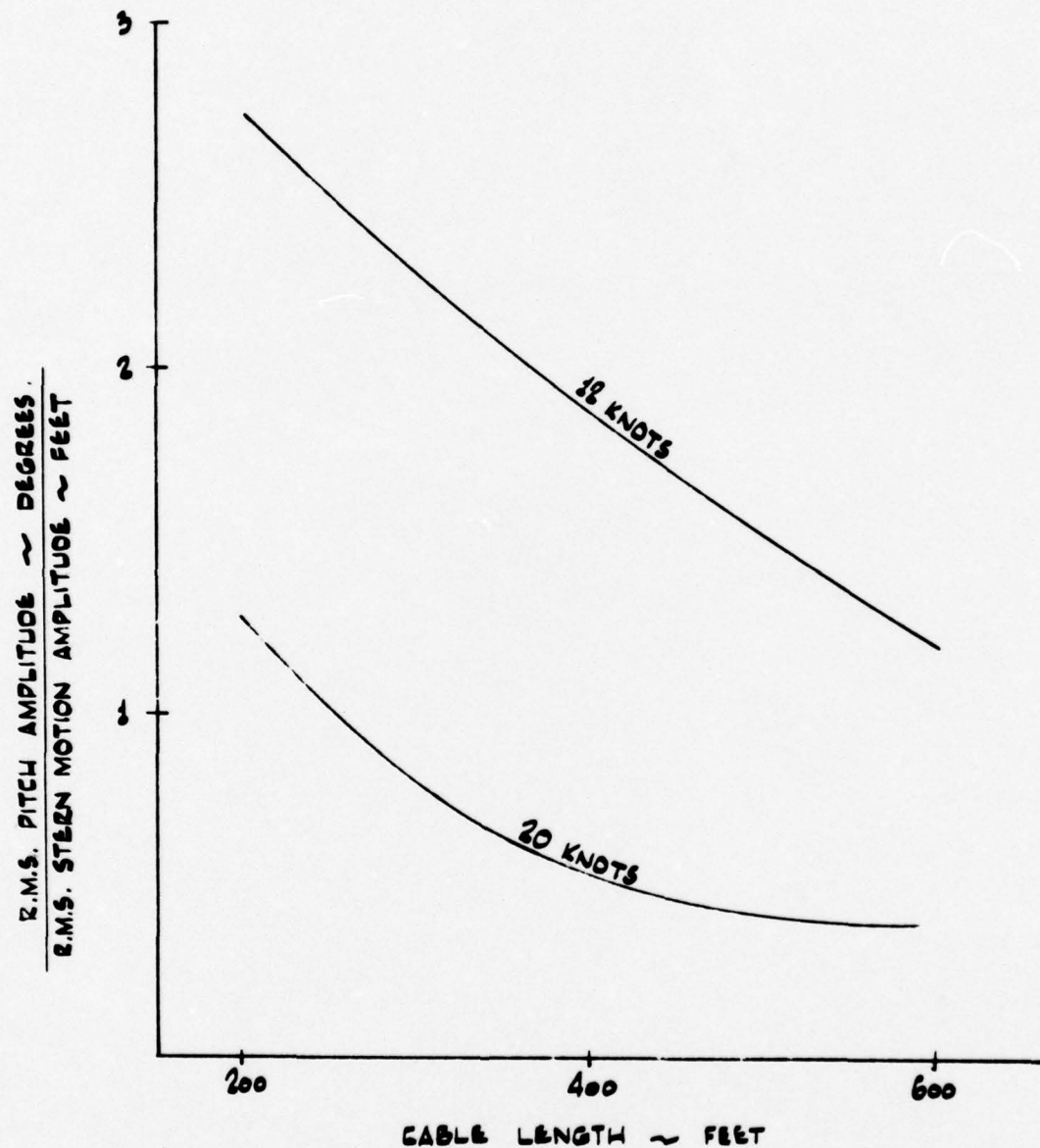
FIG. 10

ON THE HYDRODYNAMIC MASS AND DAMPING OF BODIES OSCILLATING IN A VISCOUS FLUID

by Kirk T. Patton   - ASME Associate Member
Mechanical Engineer
U. S. Navy Underwater
Sound Laboratory
New London, Connecticut

ABSTRACT

The sonar performance of cable-towed transducer systems is affected significantly by the motions of the towed body. Consequently, the dynamic simulation of towed-sonar system response to towing-platform excitation is of utmost importance to the sonar system designer. The mathematical model used to simulate the towed system must include forces acting on the body due to the body's oscillatory motion in the fluid. This paper discusses two of these forces....hydrodynamic inertial force and damping force.

INTRODUCTION

Because it has been used extensively in the past to facilitate mathematical analysis, the sphere is used here to illustrate the types of forces encountered by a non-lifting body oscillating in a viscous fluid. Odar [1] has shown that the fluid forces acting on a non-lifting, non-translating body undergoing small oscillations in a viscous fluid can be written:

$$- F = F_I + F_H + F_V \tag{1}$$

where: F_I - Inertial force (hydrodynamic mass times body acceleration)

F_H - Hydrodynamic inertial history force (particles of fluid set in motion by previous motion of the fluid now acting on the body)

F_V - Viscous force acting on the body

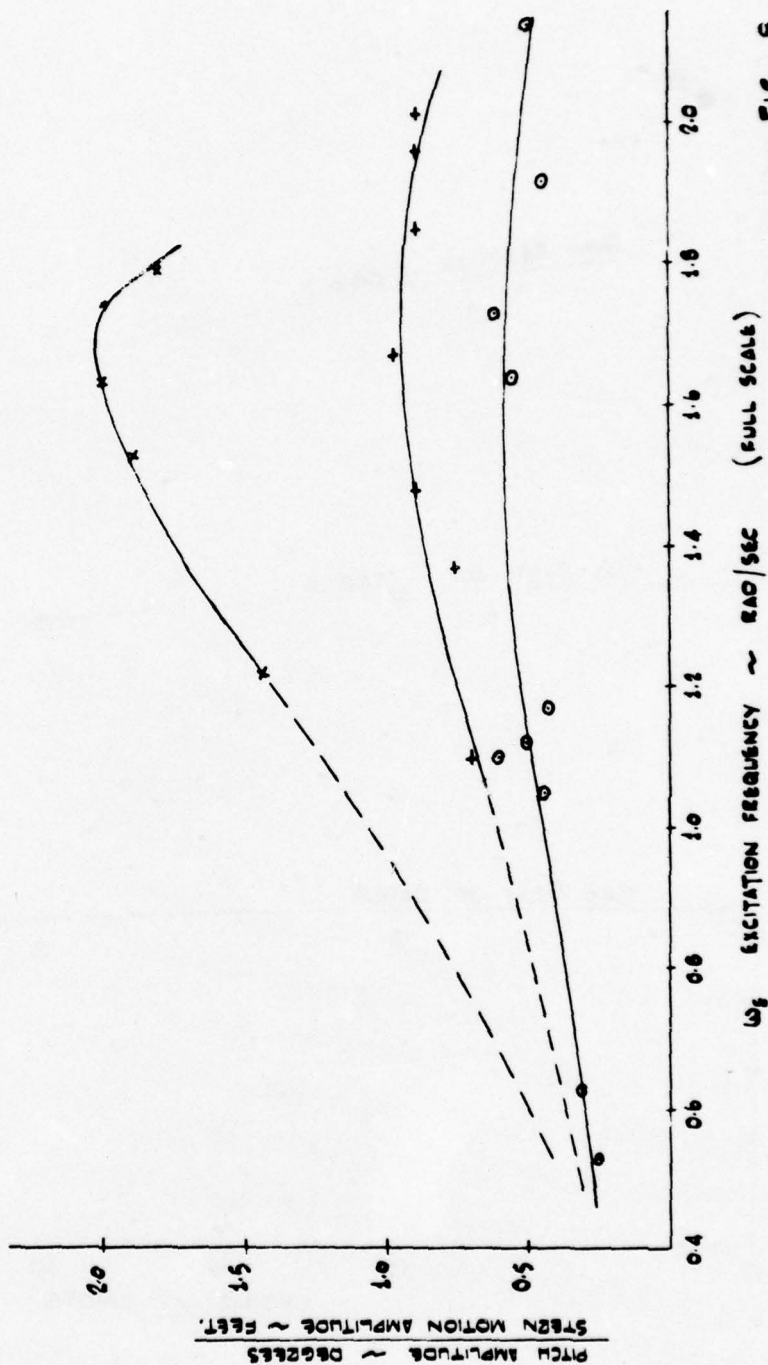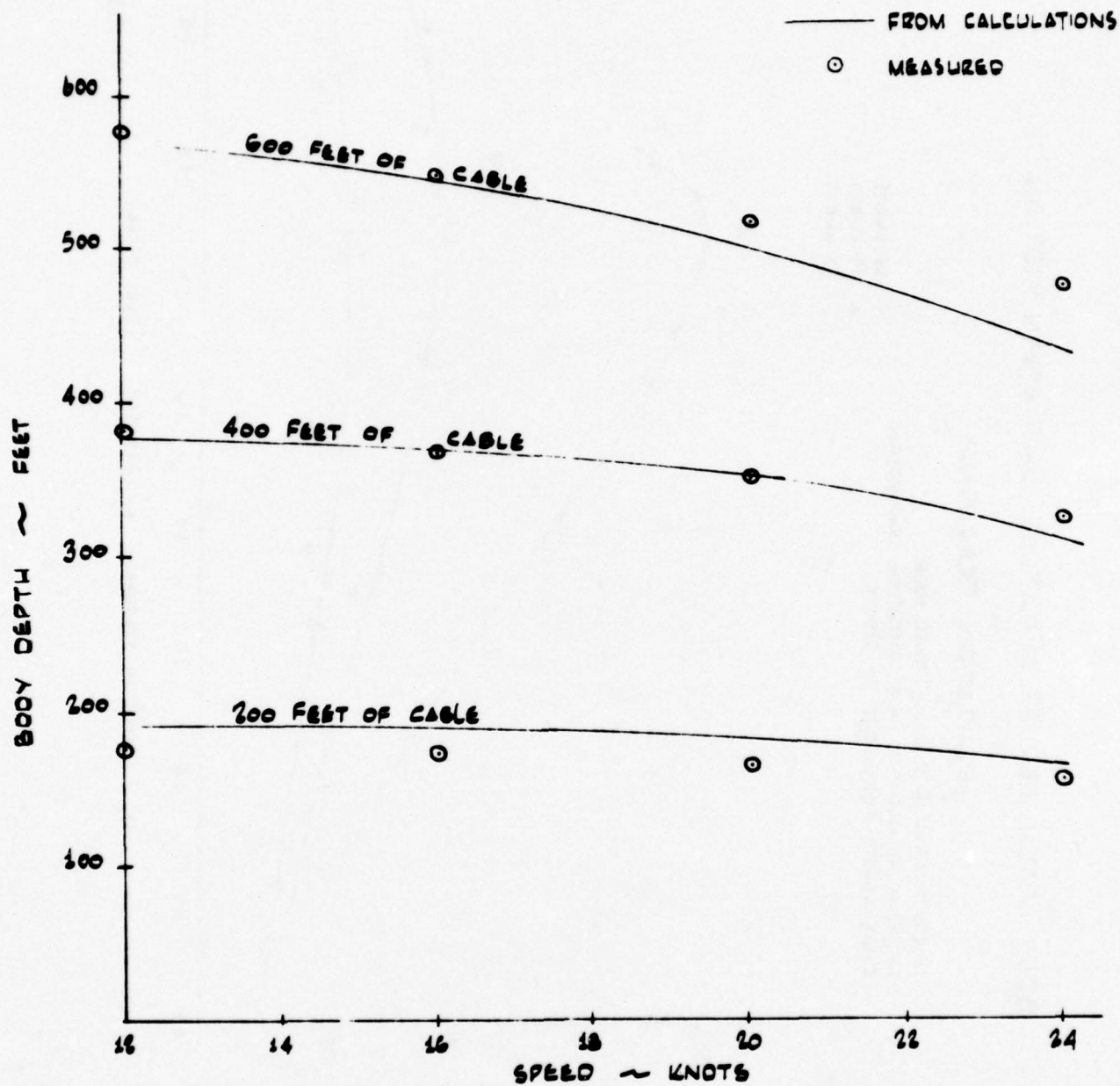After Basset (1888), Boussinesq (1885), and Oseen (1927), Odar wrote, for the force exerted by the fluid on a smooth sphere performing rectilinear oscillations:

$$- F = C_I \frac{4}{3} \pi a^3 \rho \ddot{q} + C_H a^2 (\pi \rho \mu)^{1/2} \int_o^t \frac{\ddot{q}(t')}{(t - t')^{1/2}} \, dt' + \frac{1}{2} C_V \pi a^2 \rho \, |\dot{q}| \, \dot{q}. \tag{2}$$

Utilizing the work of Stokes (1843) and Basset, eq'n (2) can be rewritten:

$$\tag{3}$$

$$- F = \left[0.50 + \frac{3.1815}{\sqrt{\omega a^2 / \nu}} \right] \frac{4}{3} \pi a^3 \rho \ddot{q} + 6 a^2 (\pi \rho \mu)^{1/2} \int_o^t \frac{\ddot{q}(t')}{(t - t')^{1/2}} \, dt' + 2.25 \left[\left(\frac{2}{\omega a^2 / \nu} \right)^{1/2} + \left(\frac{2}{\omega a^2 / \nu} \right) \right] \frac{4}{3} \pi a^3 \rho \omega \dot{q}.$$

"Superior numbers refer to similarly-numbered references at the end of this paper."

PRECEDING PAGE BLANK NOT FILMED

For sinusoidal motion, let
$$q = \delta \cos \omega t$$
$$\dot{q} = - \omega \delta \sin \omega t$$
$$\ddot{q} = - \omega^2 \delta \cos \omega t$$

$$F = \left[0.50 + \frac{3.1815}{(\text{Re})^{1/2}} \right] \frac{4}{3} \pi a^3 \rho \omega^2 \delta \cos \omega t + 6 \pi a^2 (1/2 \, \mu \rho)^{1/2} \omega^{3/2} \delta (\sin \omega t + \cos \omega t)$$
$$+ 2.25 \left[\left(\frac{2}{\text{Re}} \right)^{1/2} + \left(\frac{2}{\text{Re}} \right) \right] \frac{4}{3} \pi a^3 \rho \omega^2 \delta \sin \omega t. \tag{4}$$

Equation (4) has been derived from the Navier-Stokes equation; consequently, it is valid only for laminar, non-separating flows, i.e., small-amplitude body oscillations.

EXPERIMENTAL WORK WITH SPHERES

Dimensional analysis indicates that the hydrodynamic mass factor for a smooth body in an infinite, viscous fluid is a function of the Stokes Number and of the displacement parameter:

$$k = f_1 (\pi_2, \pi_6) \tag{5a}$$

$$k = f_1 (\omega a^2 / \nu, \, a/\delta) \tag{5b}$$

Experimentation performed by K. T. Patton[2] and C. B. Basye[3] indicates that the Stokes expression for hydrodynamic mass factor is valid over the range of Stokes Numbers from 110 to 165,000 (see Fig. 1, below).
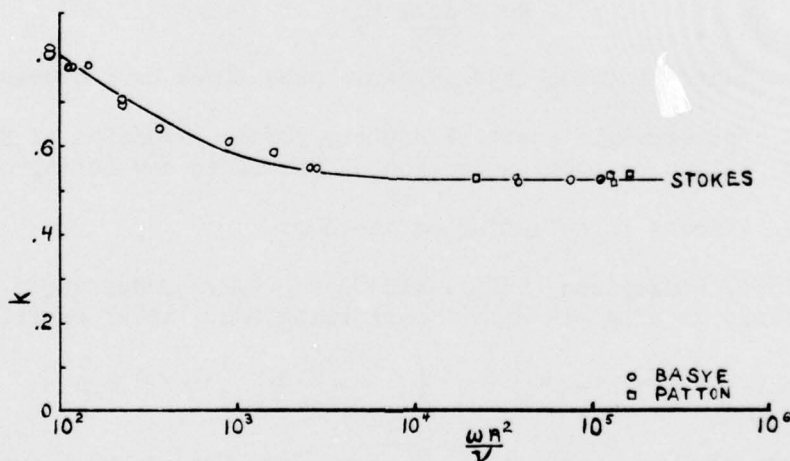
Fig. 1
HYDRODYNAMIC MASS FACTOR
vs
STOKES NUMBER
FOR SPHERES UNDERGOING SMALL OSCILLATIONS

Bayse found hydrodynamic mass to be independent of displacement amplitude in the range of displacement parameters from 2.25 to 93. However, Basye postulates that the convective acceleration terms in the Navier-Stokes equations will become significant with decreasing amplitude parameter. Also, separation may occur and a different phenomenon would be encountered; with the hydrodynamic mass factor showing a heavy dependence on displacement parameter.

The author found the above to be true while performing experiments in the displacement parameter range of 0.5 to 3.0. Data illustrating the effect of displacement amplitude on hydrodynamic mass is shown in Fig. 2, below.
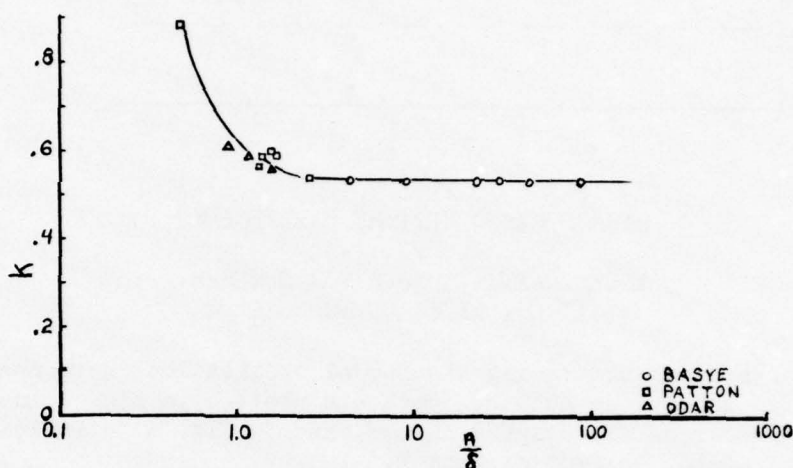
Fig. 2
HYDRODYNAMIC MASS FACTOR
vs
DISPLACEMENT AMPLITUDE PARAMETER
FOR SPHERES AT A STOKES NUMBER = 10^5

Fig. 2 was used to develop an empirical equation for hydrodynamic mass factor as a function of displacement parameter. The author suggests that the hydrodynamic mass factor of a sphere be expressed as a function of Stokes Number and displacement parameter, as shown in equation (6).

$$k = .50 + \frac{3.18}{(Re)^{1/2}} + \frac{.125}{(a/\delta)^{3/2}} \tag{6}$$

Odar has determined experimentally the hydrodynamic mass factor and hydrodynamic history coefficient of spheres for sinusoidal oscillations in oil. Unfortunately, he did not discuss tank effects of Reynolds effects in his paper. Fig. 3 illustrates the effect of acceleration number (the inverse of displacement parameter) on the hydrodynamic history coefficient.
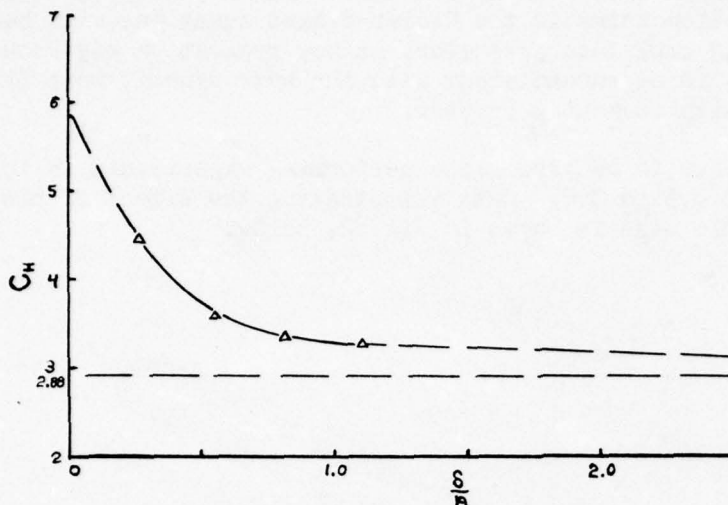
Fig. 3
HYDRODYNAMIC HISTORY COEFFICIENT
vs
ACCELERATION NUMBER FOR SPHERES
AT LOW REYNOLDS NUMBERS

Damping forces for spheres undergoing sinusoidal oscillations were measured
separately by Basye and by the author. Data are plotted in Fig. 4 to indicate the
effect of Stokes Number on the damping factor, and in Fig. 5 to indicate the effect
of displacement parameter on damping factor.
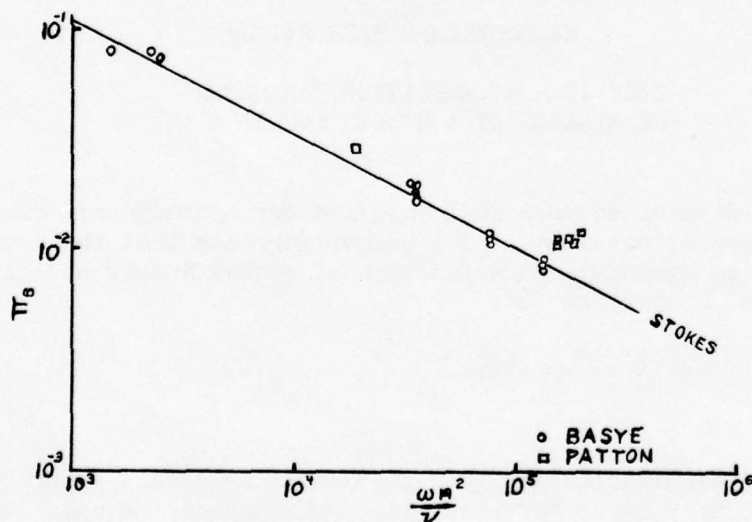
Fig. 4
DAMPING FACTOR
vs
STOKES NUMBER
FOR SPHERES UNDERGOING SMALL OSCILLATIONS
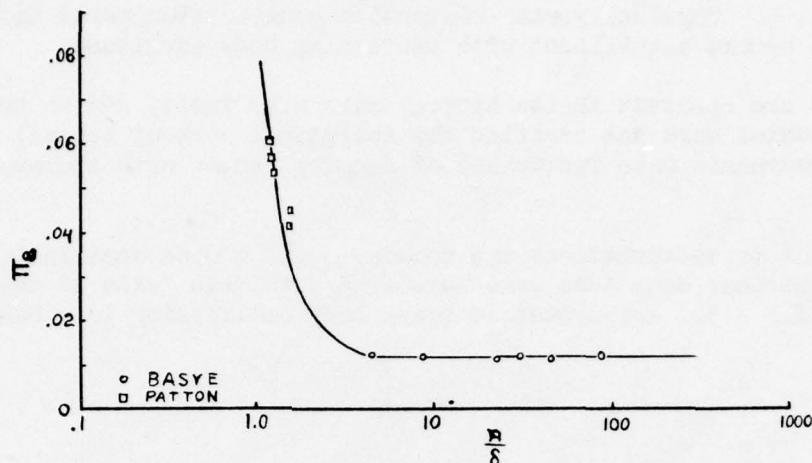
Fig. 5
DAMPING FACTOR
vs
DISPLACEMENT PARAMETER FOR SPHERES

Figs. 4 and 5 were used to derive equation (7) empirically, which equation expresses damping factor as a function of Stokes Number and displacement parameter.

$$\pi_8 = \frac{4.50}{Re} + \frac{3.18}{(Re)^{1/2}} + \frac{.12}{(a/\delta)^3} \tag{7}$$

Note that when the oscillations are small, equation (7) reduces to the Stokes expression.

This writer proposes the following empirical equation for the forces acting on a smooth sphere oscillating harmonically in an infinite viscous fluid, with no net translation.

$$F = \left[0.50 + \frac{3.1815}{(Re)^{1/2}} + \frac{0.125}{(a/\delta)^{3/2}} \right] \frac{4}{3} \pi a^3 \rho \omega^2 \delta \cos \omega t \tag{8}$$

$$+ \left[2.88 + 3.12 \, e^{-\frac{2.25}{a/\delta}} \right] \pi a^2 \, (1/2 \, \mu \rho)^{1/2} \, \omega^{3/2} \, \delta (\sin \omega t + \cos \omega t)$$

$$+ \left[\frac{4.50}{Re} + \frac{3.1815}{(Re)^{1/2}} + \frac{0.12}{(a/\delta)^3} \right] \frac{4}{3} \pi a^3 \rho \omega^2 \delta \sin \omega t$$

159

Equation (8) indicates that the hydrodynamic mass, the hydrodynamic history force, and the hydrodynamic damping are influenced significantly by the displacement amplitude parameter, (a/δ). Physically, the convective acceleration terms in the Navier-Stokes equations become significant with increasing body amplitude.

Reynolds effects are apparant in the hydrodynamic mass factor and in the damping factor. Experimental work has verified the analytical work of Stokes, indicating a decrease of hydrodynamic mass factor and of damping factor with increasing Stokes Number.

To illustrate that these variations are common to all bodies oscillating in a fluid, the following empirical equations were developed from data taken at the University of Rhode Island for a 5:1 axi-symmetric towed body oscillating in a heave mode.

$$k = \frac{23.25}{(Re)^{1/3}} + 0.14\left(1.0 - \frac{2.67}{a/\delta}\right) \tag{9}$$

$$\pi_8 = (2.12 \times 10^{-4})(Re)^{0.63} + \frac{1.14}{(a/\delta)^3} \tag{10}$$

The above equations are valid over a Stokes Number range of 4×10^4 to 3×10^5, and over a displacement parameter range of 2.0 to 32.0.

HYDRODYNAMIC FORCES ACTING ON TOWED BODIES

As soon as the body deviates from a spherical shape, the variations in the hydrodynamic forces due to the shape of the body must be accounted for. This is usually accomplished by displaying the hydrodynamic coefficients in matrix form....the order of the matrix being dictated by the number of degrees of freedom possessed by the body. For a completely asymmetrical, non-lifting body, equation (3) becomes:

$$
\begin{bmatrix} F_1 \\ F_2 \\ F_3 \\ F_4 \\ F_5 \\ F_6 \end{bmatrix} =
\begin{bmatrix}
k_{11} & k_{12} & k_{13} & k_{14} & k_{15} & k_{16} \\
k_{21} & k_{22} & k_{23} & k_{24} & k_{25} & k_{26} \\
k_{31} & k_{32} & k_{33} & k_{34} & k_{35} & k_{36} \\
k_{41} & k_{42} & k_{43} & k_{44} & k_{45} & k_{46} \\
k_{51} & k_{52} & k_{53} & k_{54} & k_{55} & k_{56} \\
k_{61} & k_{62} & k_{63} & k_{64} & k_{65} & k_{66}
\end{bmatrix}
\frac{4}{3}\pi a^3 \rho
\begin{bmatrix} \ddot{q}_1 \\ \ddot{q}_2 \\ \ddot{q}_3 \\ \ddot{q}_4 \\ \ddot{q}_5 \\ \ddot{q}_6 \end{bmatrix}
+
\begin{bmatrix}
C_{H_{11}} & C_{H_{12}} & C_{H_{13}} & C_{H_{14}} & C_{H_{15}} & C_{H_{16}} \\
C_{H_{21}} & C_{H_{22}} & C_{H_{23}} & C_{H_{24}} & C_{H_{25}} & C_{H_{26}} \\
C_{H_{31}} & C_{H_{32}} & C_{H_{33}} & C_{H_{34}} & C_{H_{35}} & C_{H_{36}} \\
C_{H_{41}} & C_{H_{42}} & C_{H_{43}} & C_{H_{44}} & C_{H_{45}} & C_{H_{46}} \\
C_{H_{51}} & C_{H_{52}} & C_{H_{53}} & C_{H_{54}} & C_{H_{55}} & C_{H_{56}} \\
C_{H_{61}} & C_{H_{62}} & C_{H_{63}} & C_{H_{64}} & C_{H_{65}} & C_{H_{66}}
\end{bmatrix}
a^2(\pi\mu\rho)^{1/2}
\begin{bmatrix}
\int_o^t \frac{\ddot{q}_1(t')}{(t-t')^{1/2}} dt' \\
\int_o^t \frac{\ddot{q}_2(t')}{(t-t')^{1/2}} dt' \\
\int_o^t \frac{\ddot{q}_3(t')}{(t-t')^{1/2}} dt' \\
\int_o^t \frac{\ddot{q}_4(t')}{(t-t')^{1/2}} dt' \\
\int_o^t \frac{\ddot{q}_5(t')}{(t-t')^{1/2}} dt' \\
\int_o^t \frac{\ddot{q}_6(t')}{(t-t')^{1/2}} dt'
\end{bmatrix}
$$

$$+ \begin{bmatrix} \pi_{8_{11}} & \pi_{8_{12}} & \pi_{8_{13}} & \pi_{8_{14}} & \pi_{8_{15}} & \pi_{8_{16}} \\ \pi_{8_{21}} & \pi_{8_{22}} & \pi_{8_{23}} & \pi_{8_{24}} & \pi_{8_{25}} & \pi_{8_{26}} \\ \pi_{8_{31}} & \pi_{8_{32}} & \pi_{8_{33}} & \pi_{8_{34}} & \pi_{8_{35}} & \pi_{8_{36}} \\ \pi_{8_{41}} & \pi_{8_{42}} & \pi_{8_{43}} & \pi_{8_{44}} & \pi_{8_{45}} & \pi_{8_{46}} \\ \pi_{8_{51}} & \pi_{8_{52}} & \pi_{8_{53}} & \pi_{8_{54}} & \pi_{8_{55}} & \pi_{8_{56}} \\ \pi_{8_{61}} & \pi_{8_{62}} & \pi_{8_{63}} & \pi_{8_{64}} & \pi_{8_{65}} & \pi_{8_{66}} \end{bmatrix} \frac{4}{3}\pi a^3 \rho \omega \begin{bmatrix} \dot{q}_1 \\ \dot{q}_2 \\ \dot{q}_3 \\ \dot{q}_4 \\ \dot{q}_5 \\ \dot{q}_6 \end{bmatrix}$$

Extrapolating from the case of the sphere, it is predicted that each of the coefficients in the above equation, k_{mn}, $C_{H_{mn}}$, and $\pi_{8_{mn}}$, is a function of Stokes Number and of the displacement amplitude parameter.

Because the convective acceleration terms in Navier-Stokes equations and the separating and turbulent flows over the body are influenced by the mean translational velocity of the body, variation of the hydrodynamic coefficients with body Reynolds Number is also expected. If the body Reynolds Number is identified as Ry (the Stokes Number is Re), the expressions for the hydrodynamic coefficients become:

$$k_{mn} = f_{K_{mn}} (Re, Ry, a/\delta) \tag{10a}$$

$$C_{H_{mn}} = f_{H_{mn}} (Re, Ry, a/\delta) \tag{10b}$$

$$\pi_{8_{mn}} = f_{\pi_{8_{mn}}} (Re, Ry, a/\delta) \tag{10c}$$

To describe completely the hydrodynamic forces acting on an asymmetrical, non-lifting body oscillating in an infinite fluid, 21* of each of the above expressions are needed, a total of 63 functions. If dynamic lift forces are included, 84 functions are needed to describe the hydrodynamic coefficients. Unfortunately, data of this type are relatively scarce in the literature.

AN APPROXIMATE TECHNIQUE FOR THE COMPUTATION
OF TERMS IN THE HYDRODYNAMIC MASS FACTOR MATRIX

Lewis[6] introduced the concept of representing a three-dimensional body as a series of short cylindrical sections in order to simplify computation of hydrodynamic coefficients. This technique can be used to compute all the terms in the matrix representing the hydrodynamic mass dyadic of a three-dimensional body of arbitrary shape. It is assumed that the two dimensional hydrodynamics of the sections are mathematically tractable. The basic operating premise of this sectionalization technique is the assumption that the three-dimensional forces and moments can be found by summing the corresponding two-dimensional forces and moments acting on the cylindrical sections.

The force acting on the cylindrical section in the h direction, for acceleration in the k direction in an ideal fluid, is:

$$F_{hk} = \int_S (p_B)_k \ (\cos \theta)_h \ dS \tag{11}$$

where: $(p_B)_k$ = the acceleration pressure acting on the surface of the body due to acceleration in the k direction.

$(\cos \theta)_h$ = the component in the h direction of the unit vector normal to the surface of the body.

The hydrodynamic mass of the cylinder is:

$$m_{hk} = \frac{F_{hk}}{d\dot{q}_k/dt} = \frac{1}{d\dot{q}_k/dt} \int_S (p_B)_k \ (\cos \theta)_h dS \tag{12}$$

The computation of hydrodynamic mass is now reduced to the task of determining the acceleration pressure distribution over the surface of the body....relatively simple job for two-dimensional bodies.

The acceleration pressure distributions over cylinders of various cross-sectional shapes have been reported by Wendel[7]. Using these pressure distributions, the hydrodynamic masses and mass moment of inertia can be computed by substitution in equation (12). This writer has extended Wendel's work and uses the pressure distributions for computation of cross-coupled translational-rotational masses and of cross-coupled translational-rotational mass moments of inertia. It is of interest to note that if the cylinder contains a plane of symmetry, the cross-coupled translational hydrodynamic mass vanishes. Also, if the cylinder contains two orthogonal planes of symmetry and is rotated about their point of intersection, the cross-coupled rotational-translational hydrodynamic mass vanishes.

In the summation of hydrodynamic masses or hydrodynamic mass moments of inertia for the cylindrical sections and tails, the mass moments of inertia must undergo a co-

* Birkhoff[5] has shown that the coefficient matrices are symmetric.

ordinate transform in order to refer their mass moment of inertia to the axis of rotation passing through the center of mass of the body.

If we consider a typical towed body, i.e., one possessing two orthogonal planes of symmetry, and select a co-ordinate system with surge motions represented by the index 1, heave by 2, sway by 3, roll by 4, yaw by 5 and pitch by 6; the elements in the hydrodynamic mass factor matrix are computed by the following method:

Birkhoff has shown that a body possessing this type if symmetry is described by eleven terms, as compared to the usual twenty-one terms for an asymmetric body. Because of symmetry, the following off-diagonal terms vanish:

$$k_{12} = 0$$
$$k_{13} = 0$$
$$k_{43} = 0$$
$$k_{53} = 0$$
$$k_{23} = 0$$
$$k_{24} = 0$$
$$k_{25} = 0$$
$$k_{36} = 0$$
$$k_{46} = 0$$
$$k_{56} = 0$$

If the body is "sliced" in planes parallel to the 1-3 plane, the hydrodynamic mass factor in the 1 direction is:

$$k_{11} = \frac{\sum_{n=o}^{n} m_{n_{11}}}{\pi \rho a^3} \tag{13}$$

The hydrodynamic mass moment of inertia factor in the 5 direction is:

$$k_{55} = \frac{\sum_{n=o}^{n} \left(J_{on_{55}} + m_{n_{33}} r_n^2 \right)}{\pi \rho a^5} \tag{14}$$

The cross-coupled mass moment of inertial factor in the 5 direction for motion in the 3 direction is given by:

$$k_{35} = \frac{\sum_{n=o}^{n} \left(J_{n_{53}} \right)}{\pi \rho a^5} \tag{15}$$

163

"Slicing" the body in planes parallel to the 2-3 plane enables computation of the hydrodynamic mass factor in the 2 direction and in the 3 direction.

$$k_{22} = \frac{\sum\limits_{n=o}^{n} m_{n_{22}}}{\pi \rho a^3} \qquad (16)$$

$$k_{33} = \frac{\sum\limits_{n=o}^{n} m_{n_{33}}}{\pi \rho a^3} \qquad (17)$$

The cross-coupled mass moment of inertia factor in the 4 direction for motion in the 3 direction is:

$$k_{43} = \frac{\Sigma \left(J_{n_{43}} \right)}{\pi \rho a^3} \qquad (18)$$

The mass moment of inertia factor in the 4 direction is:

$$k_{44} = \frac{\sum\limits_{n=o}^{n} \left(J_{on_{44}} + m_{n_{33}} r_n^2 \right)}{\pi \rho a^5} \qquad (19)$$

"Slicing" the body in planes parallel to the 1-2 plane enables computation of the mass moment of inertia factor in the 6 direction.

$$k_{66} = \frac{\sum\limits_{n=o}^{n} \left(J_{on_{66}} + m_{n_{22}} r_n^2 \right)}{\pi \rho a^5} \qquad (20)$$

The cross-coupled mass moment of inertia factor in the 6 direction for motion in the 2 direction is:

$$k_{62} = \frac{\sum\limits_{n=o}^{n} J_{n_{62}}}{\pi \rho a^5} \qquad (21)$$

The cross-coupled mass moment of inertia factor in the 6 direction for motion in the 1 direction is given by:

$$k_{61} = \frac{\sum\limits_{n=o}^{n} J_{n_{61}}}{\pi \rho a^5} \qquad (22)$$

Finally, the mass moment of inertia factor in the 4 direction for motion in the 5 direction is given by:

$$k_{45} = \frac{\sum\limits_{n=o}^{n} m_{n_{33}} r_{n_4} r_{n_5}}{\pi \rho a^5} \qquad (23)$$

A towed body with a shape similar to an existing variable-depth sonar towed body was studied, using the above method. The co-ordinate system is shown in Fig. 6.
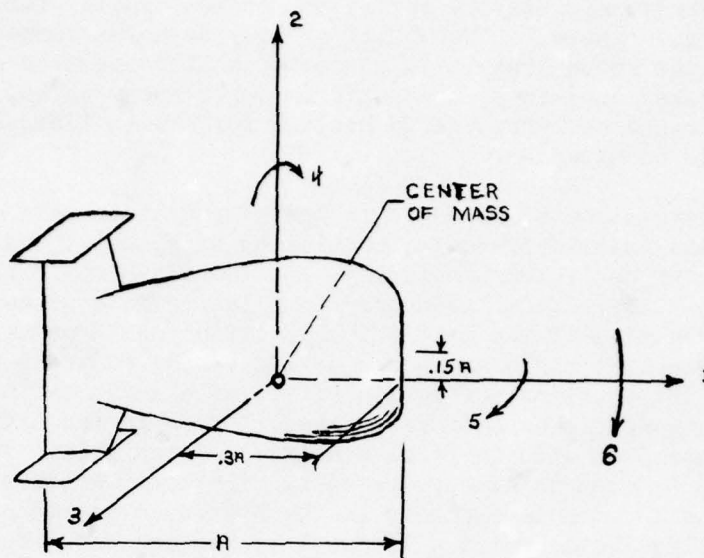
Fig. 6

The hydrodynamic mass matrix for the body at high Stokes Numbers, small oscillations, and no net translation is shown in Fig. 7.

$$\overline{m} \approx \begin{bmatrix} .002358 & 0 & 0 & 0 & 0 & -.00001326 \\ 0 & .008206 & 0 & 0 & 0 & -.001422 \\ 0 & 0 & .02656 & .0001492 & .001585 & 0 \\ 0 & 0 & .0001492 & .000136 & -.000398 & 0 \\ 0 & 0 & .001585 & -.000398 & .009129 & 0 \\ -.00001326 & -.001422 & 0 & 0 & 0 & .001747 \end{bmatrix} \pi \rho a^3$$

Fig. 7
COMPUTED HYDRODYNAMIC MASS MATRIX

The inertial stability derivative matrix for the AN/SQA-13 body[8], as determined on a planar motion machine, is shown in Fig. 8. These derivatives were measured in a towing tank with a net body translation, and, therefore, dynamic lift and drag force components would appear in the off-diagonal terms. Also, the Stokes Number, the displacement amplitude parameter, and tank correction factors were not compensated for in the values shown in Fig. 8.

$$F_{\ddot{q}} = \begin{bmatrix} - & 0 & 0 & 0 & 0 & - \\ 0 & .01092 & 0 & 0 & 0 & -.00077 \\ 0 & 0 & .0352 & - & -.002145 & 0 \\ 0 & 0 & - & - & - & 0 \\ 0 & 0 & .000298 & - & .002254 & 0 \\ - & -.00077 & 0 & 0 & 0 & .000482 \end{bmatrix} \pi \rho a^3$$

Fig. 8
MEASURED ACCELERATION STABILITY DERIVATIVE COEFFICIENT MATRIX

CONCLUSIONS

The hydrodynamic forces acting on a body due to the body's oscillatory motion in a viscous fluid were illustrated by discussing analytical and experimental studies performed on spheres. The influence of Reynolds effects (Stokes Number) and convective acceleration effects (displacement amplitude parameter) on the hydrodynamic inertia force, the hydrodynamic history force, and on the damping force is shown in an empirical equation for spheres. The effect of body Reynolds Number (Ry) on these forces for spheres is not known, but it is suspected that convective acceleration terms in the Navier-Stokes equations would gain in importance. Also, by the same reasoning, a sharp decrease of hydrodynamic history force with increasing body translational velocity would be expected.

A technique for the computation of elements in the hydrodynamic mass matrix has been presented. Although the example presented considered a typical towed body oscillating in an ideal fluid with no net forward velocity, the technique could be used to extend the computation for the case of the towed body oscillating in a viscous fluid, if the two-dimensional hydrodynamics of the cylindrical sections could be described. This writer prefers to handle lift and drag forces acting on the body due to body motions as a separate term in the equations of motion (i.e., as elastic restoring or upsetting forces). Some institutions prefer to include these forces in the hydrodynamic mass matrix for ease of comparison with inertial stability derivatives. The sectionalization technique could be used in either approach. The sectionalization of the towed body could also be used to compute elements in the hydrodynamic history coefficient matrix and in the damping factor matrix, if these forces are known for the cylinders of which the towed body is assumed to be composed.

166

NOMENCLATURE

a — A characteristic body dimension, i.e., sphere radius or towed body length (feet)

C_H — Hydrodynamic history coefficient (dimensionless)

C_I — Hydrodynamic mass factor (dimensionless)

C_V — Drag constant (dimensionless)

F — Total force exerted by the fluid on a non-lifting body oscillating in the fluid (lbs.)

F_{II} — Hydrodynamic inertial history force (lbs.)

F_I — Hydrodynamic inertial force (lbs.)

F_V — Resistive force (lbs.)

J — Hydrodynamic mass moment of inertia relative to center of mass of towed body (lb-sec^2-ft)

J_o — Hydrodynamic mass moment of inertia relative to center of cylindrical section (lb-sec^2-ft)

k — Hydrodynamic mass factor (dimensionless)

m — Hydrodynamic mass (lb-sec^2/ft)

P_B — Acceleration pressures on surface of body accelerating in a quiescent fluid (lb/ft^2)

$q, \dot{q}, \ddot{q}$ — Body oscillatory displacement, velocity and acceleration (ft, ft/sec, ft/sec^2)

Re — Stokes Number (a form of Reynold's Number $\omega a^2/\nu$ (dimensionless)

Ry — Reynold's Number, Ua/ν (dimensionless)

t — time (sec)

t' — A dummy variable (sec)

U — Body translational velocity (ft/sec)

δ — Body displacement amplitude (ft)

θ — Angle between component in h direction and unit vector normal to surface of the body (dimensionless)

μ — Absolute viscosity of fluid (lb-sec/ft^2)

ν — Kinematic viscosity of fluid (ft^2/sec)

θ — Phase angle (dimensionless)

π — 3.1416 …

π_1 — Hydrodynamic mass factor (dimensionless)

π_2 — Stokes Number (dimensionless)

π_6 — Displacement amplitude parameter, a/δ (dimensionless)

π_8 — Damping factor (quotient of damping coefficient and product of the angular frequency and a characteristic mass (dimensionless)

ρ — Fluid density (lb-sec^2/ft^4)

ω — Angular frequency (rad/sec)

REFERENCES

(1) Odar, F. and Hamilton, W. S., <u>Forces on a Sphere Accelerating in a Viscous Fluid.</u>, Journal of Fluid Mechanics, Vol. 18, pp 302-314, 1963

(2) Patton, K. T., <u>An Experimental Determination of Hydrodynamic Masses and Mechanical Impedances.</u> U. S. Navy Underwater Sound Laboratory Report No. 677, 1965

(3) Basye, C. B. and Young, D. F., <u>Oscillations of a Sphere in a Cylindrical Tube Containing a Viscous Liquid</u>, A. S. M. E. paper No. 66 WA/UNT-5, 1966

(4) Miller, R. R. and Hagist, W. M., <u>Experimental Determination of the Hydrodynamic Mass</u>, Final Report to Navy Underwater Sound Laboratory on Contract N70024-1162, 1965

(5) Birkhoff, G., <u>Hydrodynamics</u>, Princeton University Press, Princeton, N. J., 1960 p 161

(6) Lewis, F. M., <u>The Inertia of the Water Surrounding a Vibrating Ship</u>, Trans. SNAME Vol. 37, 1929, pp 1-20

(7) Wendel, K., <u>Hydrodynamic Masses and Hydrodynamic Moments of Inertia</u>, David Taylor Model Basin, translation No. 260, 1956

(8) Walton, C. O. and Brillhart, R. E., <u>The Stability Derivatives of the Scheme A Body Used with the AN/SQA-13 (XN-1) Variable-Depth Sonar System</u>, David Taylor Model Basin Hydromechanics Laboratory, Report No. 153-H-01, 1966

THE HYDRODYNAMIC COEFFICIENTS OF CABLE-TOWED BODIES

by Morton Gertler
  Head, Stability and Control Division
  David Taylor Model Basin
  Washington, D.C. 20007

ABSTRACT

This paper briefly describes how the hydrodynamic coefficients for bodies associated with cable-towed-body systems are determined by experiments with the DTMB Planar-Motion-Mechanism System and how these coefficients can be utilized to solve a variety of problems in advance of construction of the prototype system. Included, is their use to optimize the body design from the standpoint of static stability, dynamic stability, and minimum response to disturbance, as well as their ultimate use in simulation studies to predict the dynamic behavior of the cable-towed-body system under various operational conditions and to establish the design of automatic controls in activated systems.

INTRODUCTION

The traditional method for evaluating hydrodynamic characteristics of bodies associated with cable-towed systems has been based on tests with dynamically scaled models or prototypes which were towed either by a short scope of cable in a model basin or by representative scopes of cable at sea. This technique leaves much to be desired since its very nature usually requires that the tests be conducted late in the developmental stage after certain commitments have been made on the design of the body form, stabilizers, wings, weight distribution, etc. Furthermore, the information derived from such tests provides little more than a limited evaluation of the specific design tested and does not provide fundamental data that may be needed to improve the design. The modern tendency, therefore, is to employ captive-model techniques to determine hydrodynamic coefficients for the body independent of the cable. These coefficients can serve as a basis for establishing the complete hydrodynamic design of the body alone, and when they are combined ultimately with pertinent data for the cable, the resulting mathematical model can be used to obtain computer predictions of the expected dynamic performance of the proposed cable-towed-body system at sea.

One such captive-model technique which has been employed extensively during the past ten years to study the hydrodynamic characteristics of submerged bodies is the DTMB Planar-Motion-Mechanism System (PMM). Complete sets of hydrodynamic coefficients have been acquired on hundreds of different configurations including miscellaneous bare bodies, specific designs completely equipped with appendages, and systematic series of streamlined bodies of revolution. However, nearly all of the data are applicable to self-propelled vehicles such as submarines and torpedoes. In fact, complete sets of hydrodynamic coefficients obtained from PMM tests are available only for two cable-towed bodies; the AN/SQA-13(XN-1) Variable-Depth-Sonar (VDS) body[1] and the DTMB Mark 46 Air-Towed-Sonar Body.[2] Three models, extending Series 58 down to a fineness ratio (L/D) of 2.5 have been constructed for tests with the PMM. The results of these

"Superior numbers refer to similarly-numbered references at the end of this paper."

tests should at least provide a start toward acquiring fundamental hydrodynamic data applicable to cable-towed bodies.

The primary purpose of this paper is to impart an understanding of the DTMB Planar-Motion-Mechanism System and to indicate how the data obtained by means of this powerful experimental technique can be used to solve a variety of problems pertaining to the hydrodynamic design of cable-towed-body systems early in the preliminary design stage. To accomplish this, the pertinent hydrodynamic coefficients and derivatives are identified and described; the methods and procedures for obtaining these data with the PMM System are outlined; and the results of PMM tests of the Scheme A Body of the AN/SQA-13 VDS System[1] are used to illustrate how such data can be applied to solve some of the hydrodynamic problems related to cable-towed-body systems.

HYDRODYNAMIC COEFFICIENTS AND DERIVATIVES

General differential equations for treating the motions of a deeply submerged body moving in six degrees of freedom through a fluid have been developed over the years until they have now reached a high degree of sophistication. These equations are comprised of numerous coefficients or derivatives of hydrodynamic origin. Therefore, to take full advantage of these equations, it is necessary to know the numerical values of these coefficients with reasonable accuracy for the specific configuration being investigated.

The hydrodynamic forces and moments which enter into the equations of motion as coefficients are usually classified into three kinematic categories: "static", "rotary", and "acceleration". The static coefficients are due to components of linear velocity of the body relative to the fluid; the rotary coefficients are due to angular velocity components; and the acceleration coefficients are due to either linear or angular acceleration components. Within limited ranges, the coefficients are linear with respect to the appropriate variables and thus may be treated as static, rotary, and acceleration derivatives in linearized equations of motion. Typical static derivatives are Z_w', M_w', Y_v', N_v', and K_v'; typical rotary derivatives are Z_q', M_q', Y_r', N_r', K_r', and K_p' ; and typical acceleration derivatives are $Z_{\dot{w}}'$, $M_{\dot{w}}'$, $Z_{\dot{q}}'$, $M_{\dot{q}}'$, $K_{\dot{v}}'$, $K_{\dot{r}}'$, and $K_{\dot{p}}'$.

The acceleration derivatives are often called "added mass" coefficients. These derivatives can be determined on the basis of potential flow theory, at least for conventional types of bodies. However, many of the body-configurations associated with cable-towed systems are so unusual and so far off the beaten track, it would probably be desirable to rely on experimental means for determining the acceleration derivatives for these bodies. On the other hand, the static and rotary derivatives and coefficients are primarily due to viscous flow and cannot be obtained reliably with existing theory even for simple body shapes. Thus, it is necessary to conduct experiments to determine these coefficients. If the PMM system is employed, the acceleration derivatives should be experimentally determined at the same time to ensure that their values are compatible with the other experimentally determined coefficients.

DTMB PLANAR-MOTION-MECHANISM SYSTEM

The DTMB Planar-Motion-Mechanism System is a complete system for determining explicity by means of model tests all of the hydrodynamic coefficients required in the equations of motion for six degrees of freedom. This includes coefficients of all three types, namely static, rotary, and acceleration coefficients. The system embraces all mechanical, electrical, and electronic components necessary to carry out the complete investigation including preparing the model prior to testing, conducting the static and oscillation tests, sensing and recording the test data, and processing the data as a direct tabulation or as an input to high-speed computers. Two PMM Systems are in current use at the Model Basin. Both systems are functionally the same but the Mark I has a measurement capacity of ±1000 pounds for each of the three force components and the Mark II has a measurement capacity of ±4000 pounds for each of the three force components. A detailed description of the PMM System, its principles of operation, and procedures for its use are given in References 3 and 4. Therefore, only a brief account of the PMM System is given in the following paragraphs to explain how it is used to obtain the coefficients for bodies associated with cable-towed systems.

The major features of PMM Mark I are shown schematically in Figure 1. The model, supporting apparatus, angle positioning mechanism, and forced motion mechanism are transferred as a single unit and mounted on a support bracket which, in turn, is mounted on vertical rails on the east end of either Towing Carriage 2 or Towing Carriage 1. Discrete angles in the pitch plane can be set on the model by rotating the tilt table, tow strut, and model assembly about the tilt axis. Sinusoidal motion can be imparted to the model by activating the forced-motion-mechanism, which drives the pistons to which the tow struts are attached. The phase changer inserted in the common drive shaft can be used to adjust the phase of the motion of one strut relative to the other.

The forces and moments acting on the model are measured by means of two gage assemblies. Each gage assembly is composed of three modular force balances which are oriented in series to be sensitive (without interactions) to only X-, Y-, or Z-force, respectively. In addition, one assembly contains a balance to measure roll moment. Each gage assembly is fixed to the model on one side and is attached to a tow strut through a gimbal bearing on the other. The gimbals centers are aligned with the body x-axis and arranged so that their centers are equidistant from the reference point (usually taken as the prototype center of gravity). Since the force components are sensed as pure reactions at the gimbal centers, the moments M, and N can be obtained by taking the vector differences between the Z- and Y- forces, respectively, and multiplying them by the distance between the reference point and one gimbal center. The roll moment K is read directly from the roll balance. The gage readings are transmitted by electrical cables through the tow struts to recorders on the towing carriage.

It should be noted that both PMM Mark I and PMM Mark II are designed for large models ranging from 8 to 25 feet in length depending on fullness. This means that, in most cases for towed bodies, models of a scale of at least 1:1 and sometimes as high as 4:1 are required for tests of such bodies.

Three basic types of tests called static stability (or steady-state) tests, pure heaving (or sideswaying) tests, and pure pitching (or yawing) tests are required to obtain all of the necessary coefficients. The types of motion produced by the
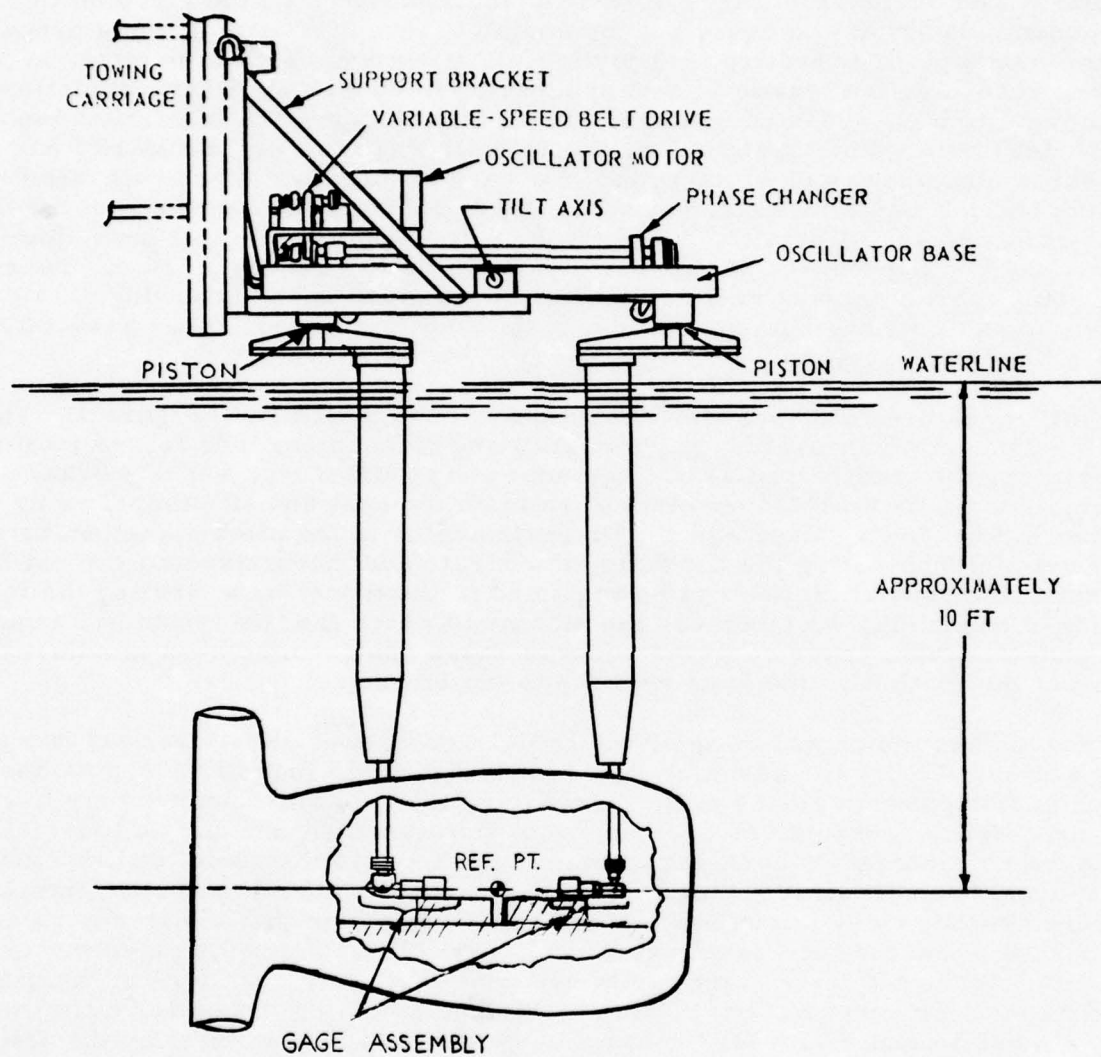
Figure 1 - Sketch of DTMB Planar Motion Mechanism with VDS
Body Attached

PMM for these tests are shown schematically for the vertical-plane case in Figure 2.

Figure 2a shows the mode of motion used to obtain static coefficients. This kind of motion is commonly used by wind tunnels and, therefore, does not have to be explained in detail. The PMM produces this motion by using the towing carriage to tow the model in a straight path at constant velocity. Then, discrete angles are set on the model by means of the tilt table and, when steady conditions have been reached, the readings on the gages are recorded digitally. Since the tilt table can be set at discrete angles remotely, data for several different angle settings can be obtained during one pass of the towing carriage along the length of the basin. If it is desired to obtain control coefficients (associated with various incidence angles on wings, stabilizers, trim tabs etc.), a similar procedure is followed except that the discrete angles are set on the lifting surfaces involved.

Figure 2b shows the mode of motion associated with a pure heaving test. The PMM produces this motion by towing the model at steady speed and then sinusoidally oscillating both tow struts in phase with each other. The resulting motion is one in which the model CG moves in a sinusoidal path while the model pitch angle θ remains at zero. The time history of the forces sensed at each of the gages during the test run is automatically resolved and integrated into in-phase and out-of-phase (quadrature) components which are recorded digitally. The in-phase components of force at each gage are directly related to the linear acceleration of the model and, therefore, can be used to compute explicitly the associated acceleration derivatives. For example, the nondimensional acceleration derivative $Z_{\dot{w}}'$ which defines the added mass in heave can be obtained as follows:

$$Z_{\dot{w}}' = \frac{\partial[(Z_1')_{in} + (Z_2')_{in}]}{\partial \dot{w}_o'} + m_m'$$

where $(Z_1')_{in}$ and $(Z_2')_{in}$ are the nondimensional in-phase components of normal force at each gimbal point,
$\dot{w}'$ is the nondimensional amplitude of the linear acceleration, and
m_m' is the nondimensional mass of the model.

The out-of-phase components of force at each gage are directly related to the linear velocity and can be used to obtain static derivatives. However, these derivatives are more accurately obtained from the static stability tests (Figure 2a).

Figure 2c shows the mode of motion associated with a pure pitching test. The PMM produces this motion by towing the model at steady speed and then sinusoidally oscillating the struts with a prescribed phase angle between them. The phase angle is dependent upon frequency of oscillation, forward speed, and distance of each strut from the reference point (CG). The relationship is as follows:

$$\cos \phi_s = \frac{1 - (\frac{\omega x}{U})^2}{1 + (\frac{\omega x}{U})^2}$$
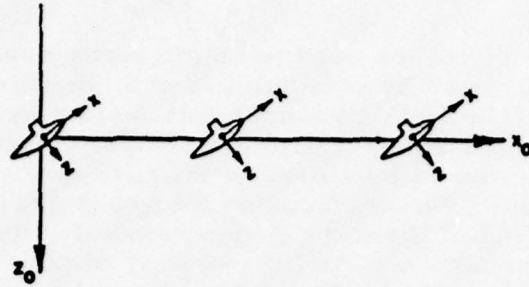
(a) - Straight-line Pitched Motion for Steady-State Tests
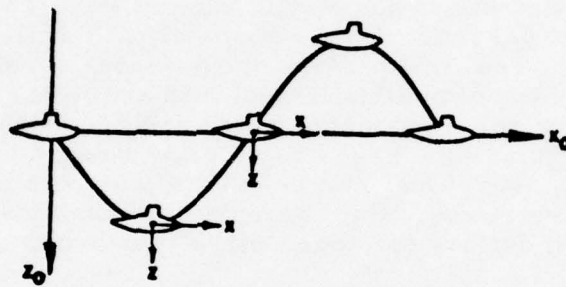
(b) - Pure Heaving
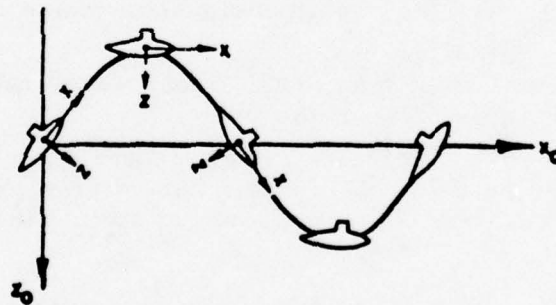
(c) - Pure Pitching

Figure 2 - Modes of Motion Used in PMM Tests

where

ϕ_s is the phase angle between struts,

ω is the frequency of oscillation,

x is the distance of each gimbal center from the reference point, and

U is the forward speed of the model.

The resulting motion is one in which the model CG moves in a sinusoidal path with the model x-axis tangent to the path (angle of attack $\alpha = 0$). As for the heaving tests, the forces sensed at each gage are processed into in-phase and out-of-phase components. The in-phase components of force are directly related to the angular acceleration and the quadrature components are directly related to the angular velocity. Thus both the angular acceleration derivatives and rotary derivatives, respectively, can be computed explicitly. As an example of the latter, the nondimensional rotary (or damping) derivative M_q' can be obtained as follows:

$$M_q' = \frac{x}{\ell} \frac{[(Z_2')_{out} - (Z_1')_{out}]}{\partial q_o'}$$

where

$(Z_1')_{out}$ and $(Z_2')_{out}$ are the nondimensional quadrature components of normal force at each gimbal center,

q_o' is the nondimensional amplitude of angular velocity, and

ℓ is the model length.

Coefficients similar to those illustrated for vertical-plane motions are obtained on PMM Mark I and Mark II by rotating the model 90 degrees about the x-axis and reattaching it to the tow struts.

APPLICATION OF DATA TO SOLUTION OF CABLE-TOWED-BODY PROBLEMS

The hydrodynamic coefficients determined from PMM tests can be used directly with existing equations of motion to perform computer-simulation studies of the motions of the free body in six degrees of freedom. Such studies can include investigations of the effects of changes in size and location of appendages, location of towpoint, distribution of weight, etc. to arrive at a suitable hydrodynamic design for the body independent of the cable. Furthermore, when an adequate means for representing the dynamics of the cable becomes available, the cable representation can be combined with the body representation to form a complete mathematical model which can be used to make computer predictions of the expected behavior of the complete cable-towed-body system under various environmental conditions at sea. Unfortunately, the state of the art on the coefficients defining the dynamics of cables (both bare and faired) has not yet reached an adequate stage of development. However, this should not act as a deterrent against taking full advantage of the use of the hydrodynamic coefficients to establish the hydrodynamic design of the body early in the preliminary design stage.

Short of conducting sophisticated analog or digital computer studies, the hydrodynamic coefficients for the body can be utilized to make preliminary analyses which can effect design decisions. Some examples of problems which can be solved in this manner are given in the following paragraphs. A few of the examples given are problems which have been solved traditionally on basis of tests of dynamic models towed by cables. It is submitted, however, that the proposed

approach is more direct and informative. Furthermore, it eliminates the trial and error type of testing and prevents needless delay in establishing the hydrodynamic design of the body.

To illustrate the examples and to provide coefficients for a cable-towed body-type, the data obtained from FMM tests of a 1:1 model of the AN/SQA-13 (XN-1) VDS body, which are reported in Reference 2, are reproduced in Table 1. Pertinent geometric and inertial characteristics for the prototype body are presented in Table 2. Unfortunately, these tests were carried out primarily to characterize the specific design to provide a mathematical model for later simulation studies of the system and, therefore, most of the design decisions already had been made. Ideally, for preliminary design studies, the test program should be somewhat more extensive and include tests of the bare body and build-up tests to determine the contributions of separate appendages such as stabilizers, wings, etc.

Certain design judgments can be based directly on an analysis of individual hydrodynamic coefficients or derivatives. To illustrate, the question of whether or not the body is statically stable with respect to a given reference point can be answered by noting the sign of the values of static-moment derivatives such as M_w' and N_v' ; the body is statically stable if M_w' is negative or N_v' is positive (or N_β is negative). The degree of static stability or static instability is indicated by the magnitude of these derivatives. It is generally believed that for good performance, a cable-towed body should be at least statically stable about the towpoint, but the degree of static stability required is a matter of conjecture. One rule of thumb which seems to have become engrained in the hydrodynamic design process is that the stable static-moment derivative (about the towpoint) of the body equipped with stabilizers should be 0.5 times the unstable static-moment derivative of the bare body. This rule leads to the incongruity that, if the original bare body is marginally statically unstable or is neutrally statically stable, it would require little or no static stability when equipped with stabilizers. It is felt, therefore, that there is an urgent need for the establishment of more significant static stability criteria for cable-towed bodies. Such criteria could be one outgrowth of systematic computer-simulation studies in which the degree of static stability, as indicated by the magnitude of M_w' or N_v', is related to the dynamic responses of the body alone and of ultimately the cable-towed body system. For the case in Table 1, the Scheme A body has static stability in pitch and neutral stability in yaw about the reference point. Since the towpoint is forward of the reference point, the body is statically stable about the towpoint in both pitch and yaw (M_w' = -0.0580 and N_v' = + 0.0716). It is to be noted that, about the towpoint, the body is more statically stable in yaw than in pitch.

Another single quantity that can be interpreted in terms of hydrodynamic design is the drag coefficient. It is true that the steady-state drag of the body is not too important in cable-towed-body systems such as those in which a deeply submerged body is towed from a surface ship. Nevertheless, a high drag coefficient may have other implications. For example, a high total drag coefficient which is caused by a large amount of residual resistance can be indicative of excessive flow separation. This may mean that there will be flow noise which may affect the performance of the sonar transducer, or that there is associated periodic vortex shedding which will result in unsteady body motions. These unsteady motions may be a source of concern in regard to the transducer as well as the life of the cable, fittings, etc. The residual-resistance coefficient C_r for the smooth Scheme A body is about 0.0014 compared with its frictional-resistance coefficient at 20 knots of about 0.0026. Thus, although some improvement

TABLE 1

Nondimensional Derivatives, Coefficients and Hull Constants
Applicable to Prototype Scheme A AN/SQA-13 (XN-1) VDS Body

Hydrodynamic Quantities				Hull Quantities	
Longitudinal		Lateral			
Z_w'	-0.1427	Y_v'	-0.4928	I_y'	0.0125
M_w'	-0.0372	N_v'	0.0	I_z'	0.0125
Z_q'	-0.0269	Y_r'	0.1366	m'	0.2886
M_q'	-0.0457	N_r'	-0.0802	m_o'	0.1179
$Z_{\dot{w}}'$	-0.0686	$Y_{\dot{v}}'$	-0.2214	x_T'	0.1440
$M_{\dot{w}}'$	0.0059	$N_{\dot{v}}'$	-0.0019	x_B'	0.0099
$Z_{\dot{q}}'$	0.0048	$Y_{\dot{r}}'$	0.0135	x_G'	0.0094
$M_{\dot{q}}'$	-0.0030	$N_{\dot{r}}'$	-0.0142	z_T'	-0.2340
X_{uu}'	-0.0049	K_v'	-0.0255	z_B'	0.0
X_{vv}'	0.2520	K_r'	0.0790	z_G'	0.0051
X_{ww}'	0.0821	$K_{\dot{v}}'$	-0.0425		
Z_*'	0.0038	$K_{\dot{r}}'$	0.0159		
M_*'	0.0004				

NOTE: All quantities are referred to a point 3.5 feet aft of the nose on the longitudinal centerline of the body. The values of I_y' and I_z' were estimated based on the model airswing tests. The value of z_G was assumed.

TABLE 2

Geometric and Inertial Characteristics of Scheme A
AN/SQA 13 (YN-1) VDS Body

Length overall, feet	8.12
Maximum width, feet	2.17
Maximum height, feet	4.04
Height of tail, feet	4.62
Displacement, pounds	2000
Weight in standard sea water, pounds	2951
Weight in air, pounds	3825
Total weight (including free-flooding water), pounds	4951
Static trim angle in water, degrees	0
Longitudinal distance from nose to towpoint, feet	2.33
Longitudinal distance from nose to CG, feet	2.74
Longitudinal distance from nose to CB, feet	3.42
Height of CG above baseline, feet	2.12
Height of CB above baseline, feet	2.08
Total wetted surface area, square feet	80.0
Frontal area, square feet	7.14
Horizontal planform area of bare body, square feet	7.84
Planform area of vertical tail surface, square feet	5.54
Planform area of upper horizontal tail surface, sq ft	1.50
Planform area of lower horizontal tail surface, sq ft	2.0
Planform area of each vertical trim tab, square feet	0.22
Planform area of each horizontal trim tab, square feet	0.09
Volume, cubic feet	31.35

NOTE: The location of the center of gravity (CG) is for the
body immersed in water and includes the contribution of
free-flooding water.

could be made by further streamlining, it is believed that this body would not have the aforementioned flow separation problems.

The static coefficients can be used in various combinations to determine pertinent quantities such as cable tension at the body T_O, cable angle at the body ϕ_O, and equilibrium body pitch angle θ. These quantities play an important role in making judgments as to towpoint location, total weight of body including water ballast, location of the center of gravity (both longitudinal and vertical), and trim-tab settings, if required. The values T_O and ϕ_O can be used as end conditions with existing cable formulations to compute steady-state cable configurations and tensions. To illustrate, the static equilibrium equations for the body in the vertical plane for the case where the towpoint, center of gravity, and center of buoyancy are not coincident are:

$$X = \tfrac{1}{2}\rho \ell^2 U^2 \left[X_{uu}{}' \cos^2 \gamma + X_{ww}{}' \sin^2 \gamma \right] + (B - W) \sin \theta = -T_O \cos \phi_O$$

$$Z = \tfrac{1}{2}\rho \ell^2 U^2 \left[Z_w{}' \cos \alpha \sin \gamma + Z_*{}' \cos^2 \alpha \right] + (W - B) \cos \theta = T_O \sin \phi_O$$

$$M = \tfrac{1}{2}\rho \ell^3 U^2 \left[M_w{}' \cos \alpha \sin \gamma + M_*{}' \cos^2 \alpha \right]$$
$$+ (x_B B - x_G W) \cos \theta + (z_B B - z_G W) \sin \theta$$
$$= -z_T T_O \cos \phi_O - x_T T_O \sin \phi_O$$

where $\theta = \alpha$ and, for small angles, $\cos \gamma \approx 1$

Taking the numerical values listed in Tables 1 and 2 for the Scheme A body, and solving the foregoing equations for a speed of 20 knots:

$$T_O = 3322 \text{ pounds}$$
$$\phi_O = 84.1 \text{ degrees}$$
$$\theta = -0.4 \text{ degree}$$

The static equilibrium equations can be simplified for the special case where the towpoint, center of gravity, and center of buoyancy are longitudinally coincident ($x_B = x_G = x_T$). In such a case, it can be shown that the body will have a zero equilibrium pitch angle at all towing speeds if the following relationship is satisfied:

$$M_*{}' = \frac{z_T}{\ell} X_{uu}{}'$$

The dynamic characteristics of the free body can be studied best with an analog or digital computer. However, an indication of dynamic stability in various modes of motion can be obtained by using the values of the static, rotary, and acceleration derivatives to solve for the roots of the characteristic stability equations.

Of course, if a deeply submerged body is shown to be statically stable on basis of the signs of the static-moment derivatives $M_w{}'$ and $N_v{}'$, it will certainly be dynamically stable as well, in the pitching and yawing modes, respectively. However, stability indices and other criteria such as damping ratio, time to damp to half amplitude, etc may provide an indication of the degree of dynamic

stability. Again, as in the case of static stability, the degree of dynamic stability that is desirable for cable-towed bodies is presently a matter of speculation, but could be defined eventually on basis of systematic computer-simulation studies. In the case of the Scheme A body, the stability indices are $\sigma_{iv} = -1.3810$ and $\sigma_{ih} = -1.0726$ for the vertical and horizontal planes of motion, respectively.

CONCLUDING REMARKS

There is a strong need for fundamental hydrodynamic data and design criteria to aid in the solution of many complex problems attendant with the use of cable-towed-body systems. Captive-model techniques such as the DTMB Planar-Motion-Mechanism System that have been developed in recent years offer a direct, expedient, and relatively economical method of providing this information. Ultimately, it would be desirable to obtain fundamental hydrodynamic coefficients on systematic series of representative types of bodies that are or should be used in various cable-towed-body applications. Meanwhile, until such systematic design data become available, it is urged that captive-model techniques be applied on a regular basis, to specific designs of at least major cable-towed-body systems.

NOMENCLATURE

Symbol	Dimensionless Form	Definition
B	$B' = \dfrac{B}{\frac{1}{2}\rho \ell^2 U^2}$	Buoyancy force
I_x, I_y, I_z	$I_x' = \dfrac{I_x}{\frac{1}{2}\rho \ell^5}$	Moment of inertia of body about x-, y-, and z-axis, respectively
K_r	$K_r' = \dfrac{K_r}{\frac{1}{2}\rho \ell^4 U}$	Derivative of rolling moment component with respect to r
$K_{\dot{r}}$	$K_{\dot{r}}' = \dfrac{K_{\dot{r}}}{\frac{1}{2}\rho \ell^5}$	Derivative of rolling moment component with respect to $\dot{r}$
K_v	$K_v' = \dfrac{K_v}{\frac{1}{2}\rho \ell^3 U}$	Derivative of rolling moment component with respect to v
$K_{\dot{v}}$	$K_{\dot{v}}' = \dfrac{K_{\dot{v}}}{\frac{1}{2}\rho \ell^4}$	Derivative of rolling moment component with respect to $\dot{v}$
ℓ	$\ell' = 1$	Characteristic body length
M	$M' = \dfrac{M}{\frac{1}{2}\rho \ell^3 U^2}$	Hydrodynamic moment about y-axis (pitching moment)
M_*	$M_*' = \dfrac{M_*}{\frac{1}{2}\rho \ell^3 U^2}$	Hydrodynamic pitching moment at zero body angle
M_q	$M_q' = \dfrac{M_q}{\frac{1}{2}\rho \ell^4 U}$	Derivative of pitching moment component with respect to angular velocity component q
$M_{\dot{q}}$	$M_{\dot{q}}' = \dfrac{M_{\dot{q}}}{\frac{1}{2}\rho \ell^5}$	Derivative of pitching moment component with respect to angular acceleration component $\dot{q}$
M_w	$M_w' = \dfrac{M_w}{\frac{1}{2}\rho \ell^3 U}$	Derivative of pitching moment component with respect to velocity component w
$M_{\dot{w}}$	$M_{\dot{w}}' = \dfrac{M_{\dot{w}}}{\frac{1}{2}\rho \ell^4}$	Derivative of pitching moment component with respect to acceleration component $\dot{w}$

Symbol	Dimensionless Form	Definition
M_θ	$M_\theta' = \dfrac{M_\theta}{\frac{1}{2} \rho \ell^3 U^2}$	Derivative of pitching moment component with respect to pitch angle component θ
m	$m' = \dfrac{m}{\frac{1}{2} \rho \ell^3}$	Mass of body, including water in free-flooding spaces
m_o	$m_o' = \dfrac{m_o}{\frac{1}{2} \rho \ell^3}$	Mass of displaced volume of water
N	$N' = \dfrac{N}{\frac{1}{2} \rho \ell^3 U^2}$	Hydrodynamic moment about z-axis (yawing moment)
N_r	$N_r' = \dfrac{N_r}{\frac{1}{2} \rho \ell^4 U}$	Derivative of yawing moment component with respect to angular velocity component r
$N_{\dot{r}}$	$N_{\dot{r}}' = \dfrac{N_{\dot{r}}}{\frac{1}{2} \rho \ell^5}$	Derivative of yawing moment component with respect to angular acceleration component $\dot{r}$
N_v	$N_v' = \dfrac{N_v}{\frac{1}{2} \rho \ell^3 U}$	Derivative of yawing moment component with respect to velocity component v
$N_{\dot{v}}$	$N_{\dot{v}}' = \dfrac{N_{\dot{v}}}{\frac{1}{2} \rho \ell^4}$	Derivative of yawing moment component with respect to acceleration component $\dot{v}$
q	$q' = \dfrac{q\ell}{U}$	Angular velocity component relative to y-axis
$\dot{q}$	$\dot{q}' = \dfrac{\dot{q}\ell^2}{U^2}$	Angular acceleration component relative to y-axis
r	$r' = \dfrac{r\ell}{U}$	Angular velocity component relative to z-axis
$\dot{r}$	$\dot{r}' = \dfrac{\dot{r}\ell^2}{U^2}$	Angular acceleration component relative to z-axis
U	$U' = 1$	Velocity of origin of body axis relative to fluid

Symbol	Dimensionless Form	Definition
v	$v' = \dfrac{v}{U}$	Component along y-axis of velocity of origin of body axes relative to fluid
$\dot{v}$	$\dot{v}' = \dfrac{\dot{v}\,\ell}{U^2}$	Component along y-axis of acceleration of origin of body axes relative to fluid
w	$w' = \dfrac{w}{U}$	Component along z-axis of velocity of origin of body axes relative to fluid
$\dot{w}$	$\dot{w}' = \dfrac{\dot{w}\,\ell}{U^2}$	Component along z-axis of acceleration of origin of body axes relative to fluid
X	$X' = \dfrac{X}{\frac{1}{2}\,\rho\,\ell^2\,U^2}$	Hydrodynamic longitudinal force, positive forward
X_{uu}	$X_{uu}' = \dfrac{X_{uu}}{\frac{1}{2}\,\rho\,\ell^2}$	Derivative of longitudinal force component with respect to the square of the velocity component u
X_{vv}	$X_{vv}' = \dfrac{X_{vv}}{\frac{1}{2}\,\rho\,\ell^2}$	Derivative of longitudinal force component with respect to the square of the velocity component v
X_{ww}	$X_{ww}' = \dfrac{X_{ww}}{\frac{1}{2}\,\rho\,\ell^2}$	Derivative of longitudinal force component with respect to the square of the velocity component w
x_B	$x_B' = \dfrac{x_B}{\ell}$	Longitudinal distance to center of buoyancy measured from reference point, positive forward

Symbol	Dimensionless Form	Definition
x_G	$x_G' = \dfrac{x_G}{\ell}$	Longitudinal distance to center of gravity measured from reference point, positive forward
x_T	$x_T' = \dfrac{x_T}{\ell}$	Longitudinal distance to towpoint measured from reference point, positive forward
Y	$Y' = \dfrac{Y}{\frac{1}{2}\rho\,\ell^2\,U^2}$	Hydrodynamic lateral force, positive starboard
Y_r	$Y_r' = \dfrac{Y_r}{\frac{1}{2}\rho\,\ell^3\,U}$	Derivative of lateral force component with respect to angular velocity component r
$Y_{\dot{r}}$	$Y_{\dot{r}}' = \dfrac{Y_{\dot{r}}}{\frac{1}{2}\rho\,\ell^4}$	Derivative of lateral force component with respect to angular acceleration component $\dot{r}$
Y_v	$Y_v' = \dfrac{Y_v}{\frac{1}{2}\rho\,\ell^2\,U}$	Derivative of lateral force component with respect to velocity component v
$Y_{\dot{v}}$	$Y_{\dot{v}}' = \dfrac{Y_{\dot{v}}}{\frac{1}{2}\rho\,\ell^3}$	Derivative of lateral force component with respect to acceleration component $\dot{v}$
Z	$Z' = \dfrac{Z}{\frac{1}{2}\rho\,\ell^2\,U^2}$	Hydrodynamic normal force, positive downward
Z_*	$Z_*' = \dfrac{Z_*}{\frac{1}{2}\rho\,\ell^2\,U^2}$	Hydrodynamic normal force at zero body angle
Z_q	$Z_q' = \dfrac{Z_q}{\frac{1}{2}\rho\,\ell^3\,U}$	Derivative of normal force component with respect to angular velocity component q
$Z_{\dot{q}}$	$Z_{\dot{q}}' = \dfrac{Z_{\dot{q}}}{\frac{1}{2}\rho\,\ell^4}$	Derivative of normal force component with respect to angular acceleration component $\dot{q}$

Symbol	Dimensionless Form	Definition
Z_w	$Z_w' = \dfrac{Z_w}{\frac{1}{2}\rho \ell^2 U}$	Derivative of normal force component with respect to velocity component w
$Z_{\dot{w}}$	$Z_{\dot{w}}' = \dfrac{Z_{\dot{w}}}{\frac{1}{2}\rho \ell^3}$	Derivative of normal force component with respect to acceleration component $\dot{w}$
z_B	$z_B' = \dfrac{z_B}{\ell}$	Vertical distance to center of buoyancy measured from reference point, positive downward
z_G	$z_G' = \dfrac{z_G}{\ell}$	Vertical distance to center of gravity measured from reference point, positive downward
z_T	$z_T' = \dfrac{z_T}{\ell}$	Vertical distance to tow-point measured from reference point, positive downward
γ		Angle of attack
β		Angle of drift
θ		Angle of pitch
ρ		Mass density of water
ψ		Angle of yaw
ω	$\omega' = \dfrac{\omega \ell}{U}$	Circular frequency of oscillation
Φ_0		Cable angle at body
T_0		Cable tension at body

NOTE: All derivatives with respect to angular quantities are given as "per radian."

REFERENCES

(1) Walton, C.O. and Brillhart, R.E., "The Stability Derivatives of the Scheme A Body Used with the AN/SQA-13 (XN-1) Variable Depth Sonar System," David Taylor Model Basin Hydromechanics Laboratory Report 153-H-01 (May 1966).

(2) Feldman, Jerome P., and Magnuson, Alan H., "Model Investigation of the Stability and Control Characteristics of the DTMB MK-46 Body," David Taylor Model Basin Hydromechanics Laboratory Report C-034-H-01 (November 1964) CONFIDENTIAL.

(3) Gertler, Morton, "The DTMB Planar-Motion-Mechanism System," David Taylor Model Basin Paper, Published in Proceedings of Symposium on Towing Tank Facilities, Instrumentation and Measuring Techniques, Zagreb, Yugoslavia (September 1959).

(4) Goodman, Alex, "Experimental Techniques and Methods of Analysis Used in Submerged Body Research," Paper Presented at Office of Naval Research Third Symposium on Naval Hydrodynamics, The Hague, Netherlands (September 1960).

SESSION 2

TOWED BODY HYDRODYNAMICS

Bibliography

Summary of Discussion

2.0 TOWED BODY HYDRODYNAMICS

2.1 DESIGN

2.1.1 Boeing Company D2-89924-1; Final Report, Development of High-speed Towing Cables, Underwater Towed Body, Part 1 CONFIDENTIAL, 12 January 1966

2.1.2 Boeing Company D2-89924-2, Final Report, Development of High-speed Towing Cables; Underwater Towed Body, Part 2 CONFIDENTIAL, 12 January 1966

2.1.3 Canada. Naval Research Est., Dartmouth TN FM/66/4, 1966 Series of MOBY Wind Tunnel Tests at N.A.E., by J.A.Tremills

2.1.4 Canada. Naval Research Est., Dartmouth TN FM/66/DR-1, NRE "MOBY IV" High Speed Underwater Towed Body, by D.H.Earle. Apr 66

2.1.5 David Taylor Model Basin Report No. 495, Calculated and Observed Speeds of Cavitation About Two- and Three- Dimensional Bodies in Water, by H.B. Freeman. November 1942

2.1.6 David Taylor Model Basin Report No. 647, Cavitation Method for the Development of Forms having Specified Critical Cavitation Numbers, by P. Eisenberg. September 1947

2.1.7 David Taylor Model Basin Report 661, An Analysis of Cable and Housing Requirements for a Deep-Towed Body at High Speed, by L. Pode, November 1948

2.1.8 David Taylor Model Basin Report No. 819, The Pitching Moment Acting on a Body of Revolution Moving Under a Free Surface, by H.L. Pond. May 1952

2.1.9 David Taylor Model Basin Report 933, Free-Stream Characteristics of a Family of Low-Aspect-Ratio, All-Movable Control Surfaces for Application to Shop Design, by L.F. Whicker and L.F. Fehlner, December 1958

2.1.10 David Taylor Model Basin Report 1389, The Hydrodynamic Design of a Cable-Towed Body Suitable for Economical Production, by S.M. Gay. Dec 1959

2.1.11 David Taylor Model Basin Report No. C-76, Hydrodynamic Properties of the Air-Towed Sonar Housing, by L. F. Fehlner, April 1948

2.1.12 David Taylor Model Basin Report No. C-318, Development of the Disk-Nose Air-Towed Sonar Housing, by R.A. Ebner. December 1950

2.1.13 David Taylor Model Basin Report No. C-297, Resistance Experiments on a Systematic Series of Streamlined Bodies of Revolution - for Application to the Design of High-Speed Submarine, by M. Gertier. April 1950

2.1.14 David Taylor Model Basin Report No. C-523, A Bibliography of Reports on Low-Aspect-Ratio Lifting Surfaces and Elongated Bodies in Subsonic Flow, by J.L. Johnson, November 1952

2.1.15 Ellsworth, W. M., Model-Prototype Relations in the Study of Cable-Towed Buoy Systems, p. 245-271 in Hydraulics conference. 7th, State University of Iowa, 1958 Proceedings; edited by Arthur Toch and G.R. Schneider. Iowa City, 1959.

2.1.16 Germany Technische Hochschule Hannover. Institute for Aero-mechanik und Flugtechnils. Longitudinal Stability of Bodies of Revolution with Tail Fins, by W. Albring (Translation AII 3732)

2.1.17 Great Britain. Admiralty Underwater Weapons Est. Tech Note 109/63 Assessment of Stability and Drag of Certain Under-water Bodies when Towed in Line Ahead Formation, by E.H. Constable. Jan 63

2.1.18 Navy Mine Defense Laboratory Rept i-77, Specialized Equations of Motion of a Towed Underwater Vehicle, by H. M. Lacey May 65

2.1.19 North American Aviation, P.O. 953/10623/65, Computer Study to Establish the Lower Limit of Length to Diameter Ratio Advis-able for Low Drag Bodies, by B.H. Carmichael and O. Niehuss 12 October 1964

2.1.20 North American Aviation. P.O. 953/14002/64, Body of Revolution Drag Calculations, 6 May 1964

2.1.21 North American Aviation, SID 65-1279, 1 thru 4; Final Report High-Speed Towing Cable Development (Phase I-II, Volumes 1-4) CONFIDENTIAL, 29 October 1965

2.1.22 North Atlantic Treaty Organization, Advisory Group for Aero-nautical Research and Development Report 108, Some Effects of Shed Vortices on the Flow Fields Around Stabilizing Tail Surfaces, by R.W. Stone and E.C. Polhamus, April-May 1957

2.1.23 Patton, K.T., Tables of Hydrodynamic Mass Factors for Transla-tional Motion, American Society of Mechanical Engineers Winter Annual Meeting, Chicago, Ill., November 7-11, 1965 Paper 65-WA/UnT-2.

2.1.24 Pennsylvania State University, Ordnance Research Laboratory Technical Memorandum 5.2420.13, Real Flow Over-Body of Revolution at Angle of Attack, by E.J. Rodgers, 24 May 1963

2.1.25 Pneumodynamics Corp Report TN-SEDU-6634-1, General Design Criteria for Cable-Towed Body Systems Using Faired and Un-faired Cable, by W.M. Ellsworth. Oct 1960

2.1.26 U.S. Rubber Co. Rept EP-605-65, Comments on the Development of a Towed Variable Depth Sonar Body. Undated, Rec'd. Dec 65
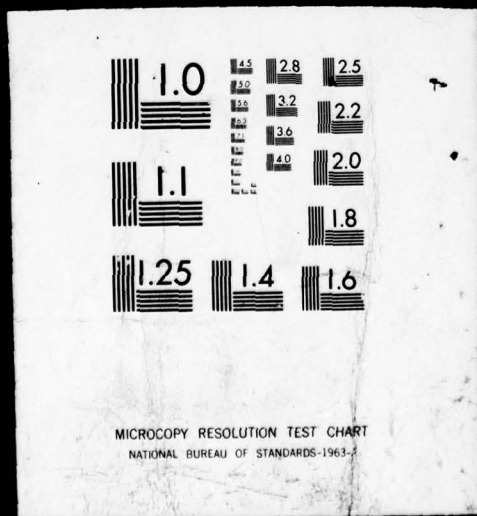
AD
A037037

2.1.27 Underwater Sound Lab Pub 765, Guide for Designing Towed Bodies and Towlines for Variable Depth Sonar, by K.T. Patton. 30 June 66

2.2 STABILITY AND CONTROL (DYNAMICS)

2.2.1 Abkowitz, M.A., The Motion of a Body in a Fluid in the Range of Non-Linear Forces, (Ph.D. Thesis, Harvard University), 1958

2.2.2 Boeing Company D2-89924-1; Final Report, Development of High-Speed Towing Cables; Underwater Towed Cables, Part I, CONFIDENTIAL, 12 January 1966

2.2.3 Boeing Company D2-89924-2; Final Report, Development of High-Speed Towing Cables; Underwater Towed Body, Part 2 CONFIDENTIAL, 12 January 1966

2.2.4 Canada. Naval Research Est., Dartmouth TN FM/66/1, Towed Body Behaviour in Steady Turns, by D.H. Earle, Jan 66

2.2.5 David Taylor Model Basin, Report No. 553 (rev. ed.), Dynamical Stability of Torpedoes, by M.A. Garstens. February 1949

2.2.6 David Taylor Model Basin, Report 796, A Theoretical Analysis of the Dynamical Stability of Towed Models, by W.H. Roach.

2.2.7 David Taylor Model Basin, Report 1369, A Theoretical Investigation of the Body Parameters Affecting the Open-Loop Pitch Response of a Submerged Towed Body, by S.M.Y.Lum. Feb 1960

2.2.8 David Taylor Model Basin, Report No. C-358. The Design of Control Surfaces for Hydrodynamic Applications, by L.F. Fehlner. January 1951

2.2.9 David Taylor Model Basin, Report No. C-359. Prediction of Dynamic Stability Derivatives of an Elongated Body of Revolution, by L. Landweber and J.L. Johnson.

2.2.10 David Taylor Model Basin Rept C-2230, Predicted Steady Towing Characteristics of the Scheme a Body and Cable Configurations for the AN/SQA-13(XN-1) Variable Depth Sonar System, by C.O.Walton and J.P.Ramsey. June 66

2.2.11 David Taylor Model Basin Hydromechanics Lab Report 153-H-01 Stability Derivatives of the Scheme a Body Used With the AN/SQA-12(XN-1) Variable Depth Sonar System, by C.O. Walton and R.E. Brillhart. May 66

2.2.12 Naval Ordnance Test Station Report 1107. Hydrodynamic Coefficients of Torpedo Bodies, by T.G. Lang, CONFIDENTIAL, 27 April 1955

2.2.13 North American Aviation SID 65-1279, 1 thru 4; Final Report High-Speed Towing Cable Development (Phase I-II, Volumes 1-4) CONFIDENTIAL, 29 October 1965

2.2.14 Pennsylvania State University Ordnance Research Laboratory Technical Memorandum 6.2461-06 The Lift on an Oscillating Body of Revolution, by M. Sevik, 23 September 1963

2.2.15 Underwater Sound Lab Rept 736. Equations of Motion for a Towed Body Moving in a Vertical Plane, by K.T. Patton and J.W. Schram. 15 June 66

2.3 MODEL TESTS

2.3.1 Boeing Co. D2-23504, High-Speed Towing Cable Development, Final Report. CONFIDENTIAL 31 July 1964

2.3.2 Boeing Co. D2-89924-1; Final Report, Development of High-Speed Towing Cables; Underwater Towed Body, Part 1, CONFIDENTIAL 12 January 1966

2.3.3 Boeing Company D2-89924-2; Final Report; Development of High-Speed Towing Cables; Underwater Towed Body, Part 2 CONFIDENTIAL 12 January 1966

2.3.4 Canada. National Research Council. National Aeronautical Establishment Report 5x5/0010, Vols. 1-4 N.R.E. Moby Series of Towed Bodies, by R.D. Galway 16 August 1965

2.3.5 David Taylor Model Basin Report No. 504. Effect of Rigid Guide Vanes on the Vibration and Drag of a Towed Circular Cylinder, by C. Grimminger. April 1945

2.3.6 David Taylor Model Basin Report 1339. Subsonic Stability and Control Investigation of a Full-Scale Model Project "Position" Towed Body July 1959

2.3.7 David Taylor Model Basin Rept 1475 Modifications to Stabilize the "O" Type, Size 5, Minesweeping Depressor, by P.K. Spangler. Dec 60

2.3.8 David Taylor Model Basin Report 1488. Evaluation of the Static Yawing Stability of the AN/SQS-22 Sonar Vehicle with Three Different Tail Configurations, by S.M.Y.Lum and R. Folb, January 1961

2.3.9 David Taylor Model Basin Report C-899. Towing Characteristics of a 1/4-Scale Model of the NADL Towed-Wing, by T. Gibbons and C.O. Walton, CONFIDENTIAL, December 1957

2.3.10 David Taylor Model Basin Report C-905. Towing Characteristics of the 1/4-Scale AN/SQA-S Sonar Body, by T. Gibbons and L.F. Whicker, CONFIDENTIAL, January 1958

2.3.11 David Taylor Model Basin Report C-1172. An Investigation of the 1/3 Scale AN/SQS-17 Variable-Depth-Sonar Body Based on Constrained-Model and Calm-Water Cable-Towing Tests, by S.M.Y.Lum. May 1960

2.3.12 David Taylor Model Basin Report C-1872. Predicted Hydrodynamic Characteristics of the AN/SQA-11 (XN-1) Variable Depth Sonar Vehicle, by L.G. Avelyra. July 64

2.3.13 David Taylor Model Basin Rept C-1976. Predicted Hydrodynamic Characteristics of the AN/SQA-10 Variable Depth Sonar Vehicle by P.K. Spangler Feb 65

2.3.14 David Taylor Model Basin Rept C-2230. Predicted Steady Towing Characteristics of the Scheme a Body and Cable Configurations for the AN/SQA-13(XN-1) Variable Depth Sonar System, by C.O. Walton and J.P. Ramsey. June 66

2.3.15 David Taylor Model Basin Aerodynamics Lab Test Rept 2 Low-Speed Wind Tunnel Tests on a 1/5-Scale Model Underwater Towed Wing, by S. Loezos. Aug 64

2.3.16 David Taylor Model Basin Hydromechanics Lab. Rept 073-H-01 Response of two AN/SQA-11 Variable Depth Sonar Vehicle Designs to Towcable Heaving Inputs, by C. O. Walton May 65

2.3.17 David Taylor Model Basin. Hydromechanics Lab Rept 153-H-01 Stability Derivatives of the Scheme a Body Used With the AN/SQA-12(XN-1) Variable Depth Sonar System, by C.O. Walton and R.E. Brillhart. May 66

2.3.18 North American Aviation SID 65-1279, 1 thru 4; Final Report High-Speed Towing Cable Development (Phase I-II, Volumes 1-4) CONFIDENTIAL 29 October 1965

2.3.19 Pennsylvania State University Ordnance Research Laboratory Technical Memorandum 21.3361-OS Water Tunnel Tests of Half-Scale CW 272/AQ Sonar Housing, by J.H. McGinley CONFIDENTIAL 23 May 1955

SESSION II. Towed Body Hydrodynamics

1) Mr. Jeffrey was asked if, when making the parametric variations in one sta-
bility derivative, its attendant effect on the other stability derivatives
was considered. It was pointed out that since this was a digital analysis,
corrections were applied to all derivatives for variations in one.

Mr. Jeffrey pointed out that only two degrees of the freedom, roll and pitch,
were assumed for the coupling between the towline and body. The towline was
assumed to be constrained in yaw.

The single towline link at the body was simulated by a spring and damper along
each of the three orthogonal axes. The spring constants and damping coeffi-
cients were obtained by differentiating the equations for the towline con-
figuration.

Present analysis, it was explained, assumes that the lateral and longitudinal
modes are decoupled and are therefore examined separately. Future plans,
however, call for coupling these modes in complete six-degree of freedom
system study.

2) Mr. Hamill was questioned on the comparison of the full-scale towing results
with the model tests. He stated that comparison was made only for pitch re-
sponse. This comparison indicated that the full-scale system was pitching
somewhat more than the model. This was attributed to the fact that the model
tests were conducted with a very large amplitude sinusoidal disturbance, and
nonlinearity of the body forces would give less response. Response from the
full-scale body, on the other hand, was the result of insignificant excita-
tion at the tow point.

3) Mr. Gertler was asked whether the support strut spacing was fixed or variable.
He answered that the spacing can be varied between 3 1/2 and 7 1/2 feet.
A 6-foot spacing is generally used. To accommodate lateral work, the PPM
model is rotated 90° so that the struts protrude through the side of the model.

REVERSE SIDE BLANK

SESSION 3
FAIRED TOWLINE HYDRODYNAMICS

Mr. M. C. Eames
Naval Research Establishment

Steady-State Towing Theory - A Designer's Summary

Mr. D. E. Calkins
Navy Electronics Laboratory

Faired Towline Loading Functions from Boundary
Layer Considerations

Dr. L. F. Whicker
Hydrospace Research Corp.

Investigation of Hydrodynamic Loading Functions
on Faired Towlines

Mr. R. Folb
David Taylor Model Basin

Reynolds Number Effects on Faired Towline Function

Mr. T. Gibbons
David Taylor Model Basin

Correlation Studies of Cable-Towed Systems Using
Bare Cable

Mr. A. Goodman
Hydronautics, Inc.

The Experimental Determination of the Dynamic Co-
efficients for Faired Cables

STEADY-STATE TOWING THEORY - A DESIGNER'S SUMMARY

Michael C. Eames
Head, Fluid Mechanics
Naval Research Establishment
Dartmouth, N.S., Canada

ABSTRACT

This paper summarizes the steady-state theory of towing cables in a general form applicable to all types of cable. Intended as a manual for the towed system designer, it emphasizes practical methods and simple approximations which have proved useful for preliminary design.

FUNDAMENTALS

ASSUMPTIONS

The fundamental theory, as originated by Glauert[1*] and developed by Landweber[2] and Pode[3], is based on the following assumptions.

1. The cable is uniform and moving at constant horizontal velocity.
2. The cable lies wholly in a plane containing the direction of motion and, unless all gravity forces are negligible, the vertical direction.
3. The cable ends are subjected to constant forces acting in the plane of the cable, and the cable generates no force outside this plane.
4. The cable is completely flexible, sustaining no internal forces other than tension.
5. The hydrodynamic force acting on an element of cable depends only on the angle of that element to the flow, and is unaffected by neighbouring elements.
6. Free surface effects are negligible.

EQUILIBRIUM CONDITIONS

Fig. 1 shows an element of cable of length ds, inclined at an angle ϕ to the flow at its centre, where the tension is T. Let the resultant of the external hydrodynamic and gravity forces on the element have components $P(\phi)$ and $Q(\phi)$ per unit length, respectively tangential and normal to the cable as shown. Then the changes in tension and cable angle over the length of the element, dT, $d\phi$, necessary to maintain equilibrium are,

$$dT = -P(\phi) \, ds \qquad (1)$$

$$Td\phi = -Q(\phi) \, ds \qquad (2)$$

These are the fundamental differential equations describing the steady-state behaviour of a cable.

---

* Superior numbers refer to similarly numbered references at the end of this paper.

CRITICAL ANGLE

When a cable is towed without a body on the end, it lies in a straight line inclined at the "critical angle", ϕ_c, to the flow. This angle is such that the net external force normal to each cable element is zero. Hence it is the root of the equation,

$$Q(\phi_c) = 0 \qquad (3)$$

When a body is added, exerting a force inclined at ϕ_o to the flow, it pulls the end of the cable away from this line, but remote from the body influence the cable tends towards its critical angle, and all cable configurations are asymptotic to a straight line inclined at ϕ_c to the flow. The following facts follow.

1. When $\phi_o > \phi_c$, the cable configuration is concave downwards.
2. When $\phi_o < \phi_c$, the cable configuration is concave upwards.
3. The curvature of a configuration maintains its sign and decreases to zero as the cable length is increased indefinitely.

In practice, applications requiring faired cable involve $\phi_o > \phi_c$, with $0 < \phi \leq \pi/2$. Since the treatment of Pode[3] appears adequate for bare cable applications, the current paper describes only this "first quadrant" case to simplify the geometry.

CABLE FUNCTIONS

It is convenient to adopt axes as shown in Fig. 2, with the origin at the point where the cable, or its imagined extension, has a cable angle of 90°. The positive Ox axis defines the direction of motion, with Oy positive upwards. The body is at (x_o, y_o) where the tension is T_o and the cable angle is ϕ_o. The surface is at (x_1, y_1) where the tension is T_1 and the cable angle is ϕ_1. The scope is $s' = s_1 - s_o$, where s_1 and s_o are the curved lengths measured from the origin. Similarly, the trail is $x' = x_1 - x_o$ and the body depth is $y' = y_1 - y_o$. Let the tension in the imagined extension of the cable be Λ_i at the origin.

The tension at any point in the cable may be obtained by summing the forces along the cable from any reference point where the tension and cable angle are known. In practice, it is convenient to refer all such integrations to the origin, even though Λ_i must first be determined. Combining (1) and (2) to eliminate ds,

$$\frac{dT}{T} = \frac{P(\phi)}{Q(\phi)} \, d\phi$$

and, integrating from the origin to any point along the cable,

$$\tau = \exp \int_{\pi/2}^{\phi} \frac{p(\phi)}{q(\phi)} \, d\phi \qquad (4)$$

where T, $P(\phi)$ and $Q(\phi)$ have been expressed non-dimensionally as

$$\tau = T/\Delta_1 \qquad\qquad p(\phi) = P(\phi)/R \qquad\qquad q(\phi) = Q(\phi)/R$$

where R is the drag of the cable per unit length when it is normal to the flow.

The cable length from the origin to any point along the cable, and the corresponding coordinates, may be obtained by integrating (2) in the form,

$$ds = -Td\phi/Q(\phi)$$

and by using,

$$dx = \cos\phi \, ds$$

$$dy = \sin\phi \, ds$$

In the non-dimensional form, the resulting cable functions are,

$$\sigma = \int_{\pi/2}^{\phi} \frac{\tau d\phi}{-q(\phi)} \tag{5}$$

$$\zeta = \int_{\pi/2}^{\phi} \frac{\tau \cos\phi}{-q(\phi)} \, d\phi \tag{6}$$

$$\eta = \int_{\pi/2}^{\phi} \frac{\tau \sin\phi}{-q(\phi)} \, d\phi \tag{7}$$

where $\sigma = sR/\Delta_1$ $\qquad\qquad \zeta = xR/\Delta_1 \qquad\qquad \eta = yR/\Delta_1$

These differ from Pode's functions[3] only in that they specify the origin at $\phi = \pi/2$.

The usual procedure for applying these functions is as follows. Body characteristics determine the tension and cable angle at the body, T_o and ϕ_o. Equation (4) is used to find τ_o, then $\Delta_1 = T_o/\tau_o$. All the cable functions can then be scaled.

The cable functions completely specify the configuration and may be evaluated numerically for any form of the functions $p(\phi)$ and $q(\phi)$, which specify the forces acting on a cable element. The essential problem of cable theory lies in the selection of $p(\phi)$ and $q(\phi)$.

Except in special cases, the cable functions can only be integrated numerically, and practical methods of calculation have used function tables, such as those of Pode[3] for bare cable, and Eames[4] for faired cable. Digital computer programs are now replacing tables when numerical integration is necessary. However, the direct integration of special cases remains of equal interest for

approximate design and analysis, and for providing that physical insight which is denied by numerical solution.

LOADING FUNCTIONS

DEFINITIONS

To define the loading functions, the force components $P(\phi)$ and $Q(\phi)$ are first separated into hydrodynamic and gravity terms. In Fig. 3, $F(\phi)$ and $G(\phi)$ are the normal and tangential components of the drag per unit length of a cable element. Then if W is the weight of the cable per unit length (in water),

$$P(\phi) = -G(\phi) -W \sin \phi \qquad , \qquad Q(\phi) = +F(\phi) -W \cos \phi$$

or, in non-dimensional form,

$$p(\phi) = -g(\phi) -\tan \phi \sin \phi \quad , \qquad q(\phi) = +f(\phi) - \tan \phi \cos \phi$$

where the hydrodynamic loading functions are defined by

$$f(\phi) = F(\phi)/R \qquad , \qquad g(\phi) = G(\phi)/R$$

and the "weight angle", ϕ, is defined by

$$\tan \phi = W/R$$

The exact nature of the hydrodynamic drag of a cable element is unknown and assumptions must be made. The assumption underlying the proposed theory is that the drag can be separated into two additive terms which, when the cable is normal to the stream, are written,

μR, the component due to friction effects, per unit length,

$(1-\mu)R$, the component due to pressure effects, per unit length.

The papameter μ is called the "friction ratio".

PRESSURE DRAG

When the element is inclined to the flow, the tangential component of velocity is assumed to have negligible effect on the pressure distribution round the cable, so that pressure drag will result only from the normal velocity component. This is the "crossflow principle" of aerodynamics. Since pressures act normal to their surface, and are proportional to velocity squared, the pressure drag will be $(1 - \mu)R \sin^2 \phi$, normal to the cable.

FRICTION DRAG

The friction drag is assumed unaffected by the pressure distribution, so that, as first suggested by Reber[5], it will act in the direction of the flow and be independent of cable angle. This will be a valid assumption only in the case of a well faired cable of small thickness chord ratio, and it neglects changes in Reynolds Number which may become significant at very small cable angles. A

refinement is considered below under FORM DRAG THEORY, but the present assumption appears adequate for most practical purposes.

PROPOSED FUNCTIONS

A major advantage of the above formulation is that direct integration of the cable functions is possible in many cases. It must be appreciated however, that this proposal is strictly a simplifying assumption justified by experience, and it must be applied with caution. However, this remark applies almost equally to the underlying assumption that friction and pressure components are separate and additive. Seeking too much refinement in terms of simple functions is thus unlikely to be profitable.

On this basis, then, the proposed loading functions are,

$$f(\phi) = (1-\mu) \sin^2 \phi + \mu \sin \phi$$

$$g(\phi) = \mu \cos \phi \tag{8}$$

The two extreme cases represented by $\mu = 0$ and $\mu = 1$ are of interest.

When $\mu = 0$, the cable is called BLUFF. An ordinary bare cable approaches this condition, but a BLUFF cable has no tangential force component and its tension does not increase along its length. When tension estimates are important it is essential to include the small value of μ appropriate to bare cable. The BLUFF cable closely approximates the configuration of a bare cable, however, and was the form adopted by Glauert[1] in the earliest theory.

When $\mu = 1$, the cable is called FINE. A fully-enclosed fairing of small thickness-chord ratio approaches this ideal. In this case the tension of a practical cable is overestimated, so the FINE cable is useful for conservative preliminary design. It is particularly useful for faired cable when cable weight is important, as will be appreciated later, and tables of the cable functions are available[4].

FORM DRAG THEORY

There is some evidence that values of $g(\phi)$ drop significantly below the cosine form at cable angles lower than 30°. This is the expected result of neglected form drag and Reynolds Number effects.

Pending further experimental evidence it is premature to suggest a refinement to the proposed theory for practical engineering purposes, particularly when this would cause a less conservative result. However, it is an interesting theoretical exercise to examine the effects of reduced tangential drag at small angles.

To do this a third additive drag component is assumed. This is called form drag, although it is a hypothetical concept only. When the cable is normal to the stream, the forces per unit length are now, μR due to friction, νR due to form, and $(1 - \mu - \nu)R$ due to pressure. The parameter ν is called the "form ratio".

The form drag is assumed to act in the direction of the flow, but to decrease linearly with the effective horizontal thickness-ratio as cable angle decreases. Thus it follows a sine law and the "improved" loading functions are,

$$f(\phi) = (1 - \mu) \sin^2 \phi + \mu \sin \phi$$

$$g(\phi) = \mu \cos \phi + \nu \sin \phi \cos \phi \tag{9}$$

Note that $f(\phi)$ has not been affected because the normal component of form drag follows the sine squared law.

The third extreme case which arises when $\mu = 0$, $\nu = 1$ represents another type of ideal fairing called MODIFIED FINE cable. Tensions are again overestimated, but this case yields a configuration which is particularly convenient for some engineering approximations.

CABLE FUNCTION SOLUTIONS

CABLE CLASSIFICATION

At this stage, it is convenient to classify the various cable types according to the values of the parameters φ, μ, and ν.

Any case in which φ is assumed zero is called a LIGHT cable; otherwise the cable is HEAVY. It should be noted that absolute cable weight is not the criterion here. Negligible φ requires W to be very small compared with R, and this is usually determined by the towing speed rather than by cable weight.

Fig. 4 shows how the types of LIGHT cable are classified by their assumed loading functions, values of (μ, ν) being shown in parentheses. All vectors in Fig. 4 are to be multiplied by $R \, ds$ to obtain the appropriate forces. The same types of HEAVY cable exist, of course.

The following paragraphs list and consider solutions of the cable functions for the various types, when these can be integrated directly.

LIGHT BLUFF CABLE ($\mu = 0$, $\nu = 0$)

$$f_B(\phi) = \sin^2\phi, \qquad g_B(\phi) = 0 \tag{10}$$

$$\tau_B = 1 \tag{11}$$

$$\sigma_B = \cot \phi \tag{12}$$

$$\zeta_B = \operatorname{cosec} \phi - 1 \tag{13}$$

$$\eta_B = \ln \cot \frac{\phi}{2} \tag{14}$$

LIGHT FINE CABLE ($\mu = 1$, $\nu = 0$)

$$f_F(\phi) = \sin \phi \qquad , \qquad g_F(\phi) = \cos \phi \tag{15}$$

$$\tau_F = \operatorname{cosec} \phi \tag{16}$$

$$\sigma_F = \sigma_B \quad , \qquad \zeta_F = \zeta_B, \qquad \eta_F = \eta_B \tag{17}$$

<u>LIGHT GENERAL CABLE</u> ($\mu = x$, $v = 0$)

$$f_G(\phi) = (1 - \mu) \sin^2 \phi + \mu \sin \phi \quad , \quad g_G(\phi) = \mu \cos \phi \tag{18}$$

$$\tau_G = 1 + \mu (\operatorname{cosec} \phi - 1) \tag{19}$$

$$\sigma_G = \sigma_B \quad , \quad \varsigma_G = \varsigma_B \quad , \quad \eta_G = \eta_B \tag{20}$$

The fact that σ_G, ς_G and η_G are independent of μ might suggest that the cable configuration is identical in the three cases considered above. It is important to appreciate that this is only true of the non-dimensional configuration starting from the origin. The scaling of the actual configuration (and hence also the position of the towed body from the origin) is governed by Λ_i/R which depends on τ. Thus the effect of μ is to control the tension distribution according to (19), and to adjust the scale of the configuration. In practice, this scale adjustment is small if the towed body has a low drag-downforce ratio.

The function τ_G is particularly useful, and is plotted in Fig. 5. The basic non-dimensional configuration defined by σ_B, ς_B, η_B is equally important. Eliminating ϕ between ς_B and η_B yields,

$$\varsigma_B = \cosh \eta_B - 1 \tag{21}$$

which is the equation of a catenary. This basic catenary is plotted in Fig. 6.

It should be noted that R does not appear in the cable functions. This implies that towing speed, cable normal drag coefficient and cable diameter serve only as scaling factors, except that towing speed usually also governs the body cable angle and hence the position of the body along the catenary.

<u>MODIFIED LIGHT FINE CABLE</u> ($\mu = 0$, $v = 1$)

$$f_M(\phi) = \sin^2 \phi \quad , \quad g_M(\phi) = \sin \phi \cos \phi \tag{22}$$

$$\tau_M = \tau_F \tag{23}$$

$$\sigma_M = \frac{1}{2} \ln \cot \frac{\phi}{2} + \operatorname{cosec} \phi \cot \phi \tag{24}$$

$$\varsigma_M = \frac{1}{2} \cot^2 \phi \tag{25}$$

$$\eta_M = \cot \phi \tag{26}$$

The non-dimensional configuration in this case has changed from the basic catenary to the simple parabola,

$$\varsigma_M = \frac{1}{2} \eta_M^2 \tag{27}$$

which is also plotted in Fig. 6. Since this case is not as versatile or realistic as the LIGHT GENERAL cable, it is seldom used in its own right. However, the resulting "parabolic approximation" to the catenary is frequently assumed for

special purposes because of the simple geometrical properties of a parabola.

IMPROVED LIGHT FINE CABLE $(\mu = x, \quad v = 1 - x)$

$$f_{IF}(\phi) = (1 - \mu) \sin^2\phi + \mu \sin\phi, \quad g_{IF}(\phi) = \mu \cos\phi + (1 - \mu) \sin\phi \cos\phi$$

(28)

$$\tau_{IF} = \tau_F$$

(29)

$$\sigma_{IF} = \frac{1}{\mu} \cot\phi - \frac{1 - \mu}{\mu^2} \left[\ln \cot \frac{\phi}{2} - (1 - \mu)X \right]$$

(30)

$$\zeta_{IF} = \frac{1}{\mu} (\csc\phi - 1) - \frac{1 - \mu}{\mu^2} \ln(1 + \mu (\csc\phi - 1))$$

(31)

$$\eta_{IF} = \frac{1}{\mu} \ln \cot \frac{\phi}{2} - \frac{1 - \mu}{\mu} X$$

(32)

where $X = \frac{2}{\sqrt{2\mu - 1}} \tan^{-1}\left[\sqrt{2\mu - 1} \ (\sec\phi - \tan\phi) \right]$, for $\mu > \frac{1}{2}$

$$= \frac{2}{\sqrt{1 - 2\mu}} \ln \frac{(1 - \mu) + \mu \sin\phi + \sqrt{1 - 2\mu} \cos\phi}{\mu + (1 - \mu) \sin\phi}, \text{ for } \mu < \frac{1}{2}$$

(33)

$$= 2 (\sec\phi - \tan\phi) \qquad\qquad \text{for } \mu = \frac{1}{2}$$

The second terms in σ_{IF} , ζ_{IF} , η_{IF} represent corrections causing the non-dimensional configuration to deviate from the basic catenary as μ decreases. The eventual parabolic form of the MODIFIED FINE cable cannot be recognized because the solution is not valid at $\mu = 0$. The entire configuration is scaled by μ , and in this case it is the non-dimensional tension distribution which is independent of μ .

The above expressions are cumbersome and probably offer little advantage over a numerically integrated solution. However, the special case given by $\mu = 1/2$, $v = 1/2$, physically representing good high-speed faired cable, is of particular interest. Its solution reduces to,

$$\sigma_{1/2\ F} = 2 \left[\cot\phi - \ln \cot \frac{\phi}{2} + (\sec\phi - \tan\phi) \right]$$

(34)

$$\zeta_{1/2\ F} = 2 \left[(\csc\phi - 1) - \ln \frac{\csc\phi + 1}{2} \right]$$

(35)

$$\eta_{1/2\ F} = 2 \left[\ln \cot \frac{\phi}{2} - (\sec\phi - \tan\phi) \right]$$

(36)

This configuration is shown dotted in Fig. 6.

204

MODIFIED LIGHT GENERAL CABLE ($\mu = 0$, $v = x$)

This case is of little interest. Only one function can be integrated,

$$\tau_{MG} = \operatorname{cosec}^v \phi \tag{37}$$

and if numerical integration must be programmed, it is sensible to adopt the most general case of IMPROVED HEAVY GENERAL cable.

IMPROVED LIGHT GENERAL CABLE ($\mu = x$, $v = y$)

Similiarly, this case yields only,

$$\tau_I = \operatorname{cosec} \phi \left[\mu + (1 - \mu) \sin \phi \right]^{1 - \frac{v}{1 - \mu}} \tag{38}$$

by direct integration. This might be usefully employed to refine the tension estimate in cases employing LIGHT GENERAL cable, but the validity of the refinement has yet to be established experimentally.

HEAVY CABLES - CRITICAL ANGLES

Taking the most general case, the equation for the critical angle (3) becomes,

$$(1 - \mu)\sin^2 \phi_c + \mu \sin \phi_c - \tan \psi \cos \phi_c = 0 \tag{39}$$

Since $f_I(\phi) = f_G(\phi)$, form drag has no effect on the critical angle and this equation is independent of v. Solutions are presented in Fig. 7.

Explicit solutions can be written for the two extreme cases:-

$$\phi_{co} = \cos^{-1} \frac{1}{2} \left(\sqrt{\tan^2 \psi + 4} - \tan \psi \right), \quad \text{when } \mu = 0 \tag{40}$$

$$\phi_{cl} = \psi \qquad\qquad\qquad , \quad \text{when } \mu = 1 \tag{41}$$

Thus the weight angle ψ is seen to be the critical angle of HEAVY FINE cable.

For all HEAVY cables, towing speed, cable normal drag coefficient and cable diameter cannot be regarded merely as scaling factors. The non-dimensional cable configuration itself depends on these variables because ψ is a function of R.

On substituting the appropriate loading functions for HEAVY cable, it is found that the cable functions can be directly integrated in only one special case. This is the HEAVY FINE cable, discussed at length in an earlier report[4].

HEAVY FINE CABLE ($\mu = 1$, $v = o$, $\psi = x$)

$$\tau_{HF} = \frac{1}{\sin \phi - \tan \psi \cos \phi} \tag{42}$$

$$\sigma_{HF} = \cos \psi \cos \phi \operatorname{cosec}(\phi - \psi) \tag{43}$$

$$\zeta_{HF} = \cos^3 \theta \left[\operatorname{cosec}(\phi - \theta) - \tan\theta \ln\cot\frac{\phi - \theta}{2} \right.$$

$$\left. - \sec\theta + \tan\theta \ln(\tan\theta + \sec\theta) \right] \qquad (44)$$

$$\eta_{HF} = \cos^3 \theta \left[\ln\cot\frac{\phi - \theta}{2} + \tan\theta \operatorname{cosec}(\phi - \theta) \right.$$

$$\left. - \ln(\tan\theta + \sec\theta) - \tan\theta \sec\theta \right] \qquad (45)$$

The effect of θ on ζ and η is similar to that which would result from a rotation of the configuration through the angle θ. This might be expected, since θ is the critical angle in this case. The tension function and non-dimensional configurations are plotted in Figs. 8 and 9.

IMPROVED HEAVY GENERAL CABLE ($\mu = x$, $\nu = y$, $\theta = z$)

In all other cases numerical integration is necessary and it is sensible to programme this for the most general case, even though it is currently proposed that ν should be assumed zero for practical purposes. The functions to be substituted in (4) (5) (6) and (7) are:-

$$p(\phi) = -\mu\cos\phi - \nu\sin\phi\cos\phi - \tan\theta\sin\phi$$

$$q(\phi) = (1 - \mu)\sin^2\phi + \mu\sin\phi - \tan\theta\cos\phi \qquad (46)$$

PRACTICAL APPLICATIONS

CABLE TYPE SELECTION

At speeds above 20 knots it is usually permissible to neglect cable weight and use a LIGHT cable. Below 12 knots a HEAVY cable should always be used. Between 12 and 20 knots, the value of θ should be calculated and the curves presented in Figs. 8 and 9 for the HEAVY FINE cable can then be used as a guide to the significance of cable weight.

The LIGHT GENERAL cable is advocated for all practical calculations when θ can be neglected. It is as simple to use as the LIGHT FINE and LIGHT BLUFF cases, while the improved form drag theory cannot yet be recommended. This suggestion assumes that practical cases will not employ cable angles appreciably below 30°. Noting that at 30°, $\tau_G = 1 + \mu$, an approximate criterion for this is,

$$\frac{sR}{T} < \frac{2}{1 + \mu} \qquad (47)$$

For very low cable angles, no recommendation can be backed by experience, but the special case of IMPROVED LIGHT FINE cable with $\mu = 1/2$, $\nu = 1/2$, appears a reasonable representation of well faired cables at very high speeds.

Thus the most useful functions for LIGHT CABLES are τ_G, σ_B, ζ_B, η_B, plotted in Figs. 5 and 6. For certain purposes the "parabolic approximation" to

the basic catenary, given by ϵ_M, η_M is useful, and Fig. 6 will show the errors incurred by its use.

When ϕ cannot be neglected, the HEAVY FINE cable is the only simple case available. This will overestimate the tension but will provide a reasonable estimate of the cable configuration in all practical cases. Figs. 8 and 9 are analagous to Figs. 5 and 6 for this case. Tables of HEAVY FINE cable functions are also available[4].

All the cable functions for these simple cases are readily obtained from trigonometrical tables. For convenience a table of $\ln \cot \frac{\theta}{2}$ is appended as Table I. In addition, Pode's tables are available[3], but can be recommended only for bare cables.

CABLE PARAMETER VALUES

There remains the question of selecting appropriate values of the cable normal drag coefficient, C_R, and friction ratio μ. C_R is based on cable diameter, thus,

$$R = C_R \frac{\rho}{2} d V^2 \quad , \quad \text{per unit length,} \quad (48)$$

where d is the cable diameter, V the towing speed and ρ the mass density of the water.

For bare cable, C_R varies with strand size and Reynolds Number, but experience suggests that a value of 1.2 is a good compromise and is suggested when specific test data are unavailable. Similarly a μ value of .05 is recommended for bare cable operating at cable angles above about 30°. For very low cable angles a μ value of .02 can be adopted to compensate for inaccuracies in the theory. These values yield results in close agreement with Podes tables for his f = .02.

The drag coefficients of typical types of faired cable are listed in Table II, together with μ values obtained from analysis of sea trials results. Although the accuracy of such analysis is open to question, it is the best technique available pending further loading function experiments on faired cable.

TABLE II

TYPICAL CABLE CHARACTERISTICS

	NORMAL DRAG COEFFICIENT (C_R)	FRICTION RATIO (μ)
BARE CABLE (STRANDED)	1.20	0.05
TRAILING FAIRING - SHORT TYPE	0.45	0.40
TRAILING FAIRING - BEST TYPE	0.30	0.50
SECTIONAL FAIRING	0.20	0.75
ENCLOSED FAIRING - FLEXIBLE	0.12	0.80
ENCLOSED FAIRING - STRUT TYPE	0.08	0.80

207

OPTIMUM TOWING

A technique for determining the optimum configuration, that which provides maximum depth and speed for a given cable tension, has been described at the previous seminar . For completeness, Figs. 10 and 11 are repeated here and will be found useful for preliminary design.

Both are plots of "depression ratio" against a normalized depth, defining an optimum line which determines the depression ratio required to attain maximum depth under given conditions. Depression ratio is the ratio of the total body downforce (Δ) to the design surface cable tension (T_1). The technique assumes that the breaking strength of the cable, T max, is proportional to its cross section area. The effective ultimate stress is defined by,

$$q = T_{max}/d^2$$

and a safety factor, f, is introduced, such that the design tension is

$$T_1 = q\, d^2/f.$$

Fig. 10 is appropriate for very deep towing at modest speeds, using good cable fairing. In this case it is assumed that body drag is negligible and that cable weight (in water) is proportional to its cross-section area. The effective density is defined by,

$$\omega = W/d^2$$

HEAVY FINE cable is used in Fig. 10 so that depths predicted for a given design tension will be conservatively underestimated. The normalizing factor for body depth is ($\omega f/q$) and curves are plotted for discrete values of critical angle (ϕ) and surface cable angle (ϕ_1). To use as a speed term, the critical angle can be written,

$$\cot \phi = (\rho C_R/2\omega d)V^2$$

Fig. 11 is appropriate for high speed towing at moderate depth, using good cable fairing. In this case it is assumed that cable weight is negligible, but body drag (D) is taken into account, in terms of the drag-downforce ratio,

$$D/\Delta = \cot \phi_o$$

LIGHT FINE cable is used in Fig. 11 so that depths predicted for a given design tension will be conservatively underestimated. The normalizing factor for body depth is (R/T_1) and curves are plotted for discrete values of body drag-downforce ratio (D/Δ) and surface cable angle (ϕ_1). Noting that,

$$R/T_1 = (\rho C_R f/2qd)V^2$$

the abscissa can be used to find the maximum speed for a given depth, as well as the reverse.

A word of caution on the practical application of optimum configurations is in order. In both cases considered, it will be seen that a sizeable reduction in Δ/T_1 and in ϕ_1 can be made from the optimum without too great a loss of depth. Reduced Δ implies smaller wings or a lighter body. Reduced ϕ_1 means that less of the ship's motion in rough water will be transferred to the body.

Some relaxation from the steady-state optimum configuration may frequently be good design practice, to ease dynamic problems or body handling considerations.

CURRENT ENGINEERING POSSIBILITIES

Nevertheless, the optimum configuration concept provides a valid means of assessing current possibilities. To illustrate this in the broadest sense, the number of variables will be reduced to the minimum and a conservative approach adopted. Thus cable weight will be neglected and a μ value of 1.0 adopted. Body drag will also be neglected on the assumption that depressing wings will be used at high speed to maintain a reasonable drag ratio. Calculations show that body drag effects are more than offset by the conservative μ value adopted, and the extreme depth indicated in Fig. 11 may be taken. Then,

$$(V^2 y)_{Max} = \frac{2}{3} \frac{q}{f} \frac{d}{C_R} \tag{49}$$

An analysis of cables used in many towed systems[6] suggests that a typical value of q is 1.2×10^7 lbs/ft^2, while common practice is to use a safety factor of 3. The best faired cables now operational have a normal drag coefficient of about 0.2. On this basis, an estimate of current towing possibilities is given by

$$(V^2 y)_{Max} = \frac{4}{3} d \times 10^7$$

which is plotted in Fig. 12 as towing speed versus body depth, for various cable diameters.

This is strictly based on current engineering. Developments now in hand offer potential for halving the cable drag coefficient and increasing cable strength by 50%. Improved design for system dynamics should also permit safety factors to be relaxed. The maximum value of $(V^2 y)$ could therefore be multiplied by a factor of 3 to 5 over the next few years.

TABLE I

$$\ln \cot \frac{\phi}{2}$$

ϕ	$\ln \cot \frac{\phi}{2}$	ϕ	$\ln \cot \frac{\phi}{2}$	ϕ	$\ln \cot \frac{\phi}{2}$	ϕ	$\ln \cot \frac{\phi}{2}$
90	0	50	.7629	32.2	1.2426	24.8	1.5147
89	.0175	49	.7863	32.0	1.2491	24.7	1.5189
88	.0349	48	.8092	31.8	1.2558	24.6	1.5231
87	.0524	47	.8328	31.6	1.2624	24.5	1.5273
86	.0699	46	.8569	31.4	1.2691	24.4	1.5315
85	.0874	45	.8812	31.2	1.2758	24.3	1.5357
84	.1049					24.2	1.5399
83	.1225	44.5	.8937	31.0	1.2826	24.1	1.5442
82	.1401	44.0	.9063	30.8	1.2894		
81	.1577	43.5	.9189	30.6	1.2962	24.0	1.5485
		43.0	.9316	30.4	1.3031	23.9	1.5528
80	.1755	42.5	.9445	30.2	1.3100	23.8	1.5571
79	.1932	42.0	.9575	30.0	1.3170	23.7	1.5615
78	.2110	41.5	.9706	29.8	1.3239	23.6	1.5659
77	.2289	41.0	.9838	29.6	1.3310	23.5	1.5702
76	.2468	40.5	.9971	29.4	1.3381	23.4	1.5746
75	.2648			29.2	1.3452	23.3	1.5790
74	.2829	40.0	1.0107			23.2	1.5834
73	.3011	39.5	1.0243	29.0	1.3524	23.1	1.5879
72	.3195	39.0	1.0381	28.8	1.3596		
71	.3378	38.5	1.0521	28.6	1.3669	23.0	1.5923
		38.0	1.0661	28.4	1.3742	22.9	1.5968
70	.3563	37.5	1.0804	28.2	1.3816	22.8	1.6013
69	.3750	37.0	1.0948	28.0	1.3890	22.7	1.6058
68	.3937	36.5	1.1094	27.8	1.3964	22.6	1.6103
67	.4126	36.0	1.1242	27.6	1.4039	22.5	1.6149
66	.4317	35.5	1.1391	27.4	1.4115	22.4	1.6194
65	.4508			27.2	1.4191	22.3	1.6240
64	.4702	35.0	1.1542			22.2	1.6287
63	.4897	34.8	1.1603	27.0	1.4268	22.1	1.6333
62	.5094	34.6	1.1665	26.8	1.4345		
61	.5292	34.4	1.1726	26.6	1.4423	22.0	1.6379
		34.2	1.1789	26.4	1.4501	21.9	1.6425
60	.5493	34.0	1.1851	26.2	1.4580	21.8	1.6467
59	.5695	33.8	1.1913	26.0	1.4659	21.7	1.6520
58	.5900	33.6	1.1976	25.8	1.4739	21.6	1.6567
57	.6107	33.4	1.2039	25.6	1.4819	21.5	1.6615
56	.6316	33.2	1.2103	25.4	1.4900	21.4	1.6663
55	.6528			25.2	1.4981	21.3	1.6711
54	.6742	33.0	1.2166			21.2	1.6759
53	.6960	32.8	1.2231	25.0	1.5063	21.1	1.6807
52	.7180	32.6	1.2295	24.9	1.5105		
51	.7403	32.4	1.2361				

TABLE I
(Continued)

ϕ	$\ln \cot \frac{\phi}{2}$	ϕ	$\ln \cot \frac{\phi}{2}$	ϕ	$\ln \cot \frac{\phi}{2}$	ϕ	$\ln \cot \frac{\phi}{2}$
21.0	1.6856	17.0	1.9009	13.0	2.1721	9.0	2.5421
20.9	1.6905	16.9	1.9068	12.9	2.1800	8.9	2.5534
20.8	1.6954	16.8	1.9128	12.8	2.1878	8.8	2.5646
20.7	1.7003	16.7	1.9189	12.7	2.1957	8.7	2.5763
20.6	1.7052	16.6	1.9249	12.6	2.2036	8.6	2.5878
20.5	1.7102	16.5	1.9311	12.5	2.2118	8.5	2.5996
20.4	1.7152	16.4	1.9372	12.4	2.2198	8.4	2.6113
20.3	1.7203	16.3	1.9435	12.3	2.2280	8.3	2.6235
20.2	1.7253	16.2	1.9497	12.2	2.2361	8.2	2.6356
20.1	1.7303	16.1	1.9560	12.1	2.2445	8.1	2.6480
20.0	1.7354	16.0	1.9623	12.0	2.2528	8.0	2.6610
19.9	1.7406	15.9	1.9687	11.9	2.2613	7.9	2.6731
19.8	1.7457	15.8	1.9750	11.8	2.2697	7.8	2.6857
19.7	1.7509	15.7	1.9815	11.7	2.2784	7.7	2.6989
19.6	1.7560	15.6	1.9879	11.6	2.2870	7.6	2.7118
19.5	1.7612	15.5	1.9945	11.5	2.2958	7.5	2.7252
19.4	1.7665	15.4	2.0010	11.4	2.3045	7.4	2.7385
19.3	1.7718	15.3	2.0076	11.3	2.3135	7.3	2.7523
19.2	1.7771	15.2	2.0142	11.2	2.3223	7.2	2.7660
19.1	1.7824	15.1	2.0209	11.1	2.3314	7.1	2.7802
19.0	1.7877	15.0	2.0276	11.0	2.3404	7.0	2.7942
18.9	1.7931	14.9	2.0344	10.9	2.3497	6.9	2.8089
18.8	1.7985	14.8	2.0412	10.8	2.3587	6.8	2.8233
18.7	1.8041	14.7	2.0481	10.7	2.3684	6.7	2.8384
18.6	1.8094	14.6	2.0549	10.6	2.3777	6.6	2.8532
18.5	1.8149	14.5	2.0619	10.5	2.3878	6.5	2.8688
18.4	1.8204	14.4	2.0689	10.4	2.3977	6.4	2.8840
18.3	1.8259	14.3	2.0760	10.3	2.4071	6.3	2.9000
18.2	1.8315	14.2	2.0830	10.2	2.4164	6.2	2.9158
18.1	1.8371	14.1	2.0902	10.1	2.4264	6.1	2.9324
18.0	1.8427	14.0	2.0973	10.0	2.4362	6.0	2.9487
17.9	1.8485	13.9	2.1045	9.9	2.4464	5.9	2.9658
17.8	1.8541	13.8	2.1119	9.8	2.4565	5.8	2.9826
17.7	1.8599	13.7	2.1193	9.7	2.4670	5.7	3.0004
17.6	1.8656	13.6	2.1266	9.6	2.4773	5.6	3.0178
17.5	1.8714	13.5	2.1341	9.5	2.4879	5.5	3.0362
17.4	1.8772	13.4	2.1415	9.4	2.4984	5.4	3.0542
17.3	1.8831	13.3	2.1492	9.3	2.5093	5.3	3.0733
17.2	1.8889	13.2	2.1567	9.2	2.5200	5.2	3.0920
17.1	1.8949	13.1	2.1644	9.1	2.5312	5.1	3.1099
						5.0	3.1313

C_R Drag coefficient of cable, when cable is normal to the stream, based on cable diameter; $R/\frac{1}{2} \rho d V^2$.

D   Drag of towed body.

d   Diameter of cable.

$F(\phi)$ Normal component of cable drag per unit length.

$f(\phi)$ Normal cable loading function; $F(\phi)/R$.

f   Safety factor of cable; $T \max/T_1$.

$G(\phi)$ Tangential component of cable drag per unit length.

$g(\phi)$ Tangential cable loading function; $G(\phi)/R$.

$P(\phi)$ Tangential component of external forces per unit length.

$p(\phi)$ Non-dimensional $P(\phi)$; $P(\phi)/R$.

$Q(\phi)$ Normal component of external forces per unit length.

$q(\phi)$ Non-dimensional $Q(\phi)$; $Q(\phi)/R$.

q   Effective ultimate stress of cable; T_{max}/d^2.

R   Drag per unit length of cable, when cable is normal to the stream.

s   Length of cable, measured from the origin.

s'   Scope of cable; $s_1 - s_o$.

T   Tension in cable.

T_{max} Breaking strength of cable.

V   Steady velocity of towing ship or stream.

W   Weight per unit length of cable, in water

x   Coordinate of cable configuration in direction of motion.

x'   Trail of towed body; $x_1 - x_o$.

y   Coordinate of cable configuration vertically upwards.

y'   Depth of towed body; $y_1 - y_o$.

212

Δ	Total down-force of towed body
Δ_i	Tension in imagined extension of cable at the origin
η	Non-dimensional depth function; yR/Δ_i.
θ	Depression angle of towed body.
μ	Friction ratio of cable
ν	Form ratio of cable
ξ	Non-dimensional trail function; xR/Δ_i.
ρ	Mass density of sea water
σ	Non-dimensional scope function; sR/Δ_i.
τ	Non-dimensional tension function; T/Λ_i.
ϕ	Angle of cable to the horizontal.
ϕ_c	Critical angle of cable
ψ	Weight angle of cable; $\tan^{-1}(W/R)$
ω	Effective density of cable; W/d^2.

SUBSCRIPTS

0	At the towed body	) Applicable to s, T, x, y, η, ξ, σ, τ, ϕ.
1	At the water surface	)
B	LIGHT BLUFF CABLE	
F	LIGHT FINE CABLE	
G	LIGHT GENERAL CABLE	
HF	HEAVY FINE CABLE	
I	IMPROVED LIGHT GENERAL CABLE	
IF	IMPROVED LIGHT FINE CABLE	
M	MODIFIED LIGHT FINE CABLE	
MG	MODIFIED LIGHT GENERAL CABLE	

213

REFERENCES

1. Glauert, H.   "The form of a heavy flexible cable used for towing a heavy body below an aeroplane", Advisory Committee for Aeronautics, Reports and Memoranda, 1592, February 1934.

2. Landweber, L. and Protter, M.H. "The shape and tension of a light flexible cable in a uniform current", David Taylor Model Basin, Report 533, October 1944.

3. Pode, L.   "Tables for computing the equilibrium configuration of a flexible cable in a uniform stream", David Taylor Model Basin, Report 687, March 1951.

4. Eames, M.C.   "The configuration of a cable towing a heavy submerged body from a surface vessel", Naval Research Establishment, Report PH_x-103, November, 1956.

5. Reber, R.K.   "The configuration and towing tension of towed sweep cables supported by floats", USN Bureau of Ships, Report 75, February 1944.

6. Ellsworth, W.M.   "General design criteria for cable towed body systems using faired and unfaired cable", Pneumodynamics Corporation, TN-SEDU-6634-1, October 1960.
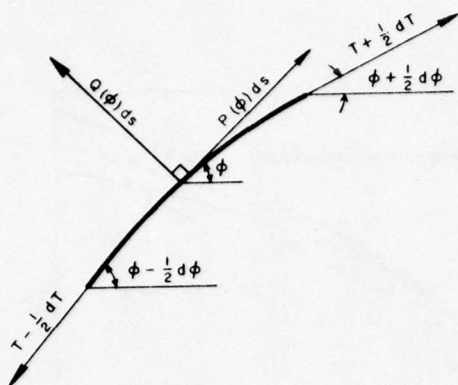
Fig.1 Forces on a cable element
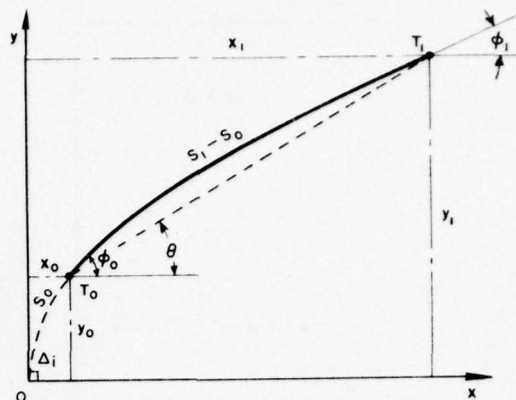
Fig.2 Axis system for configuration
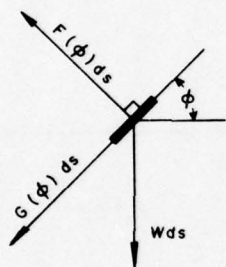
Fig.3 Cable force components
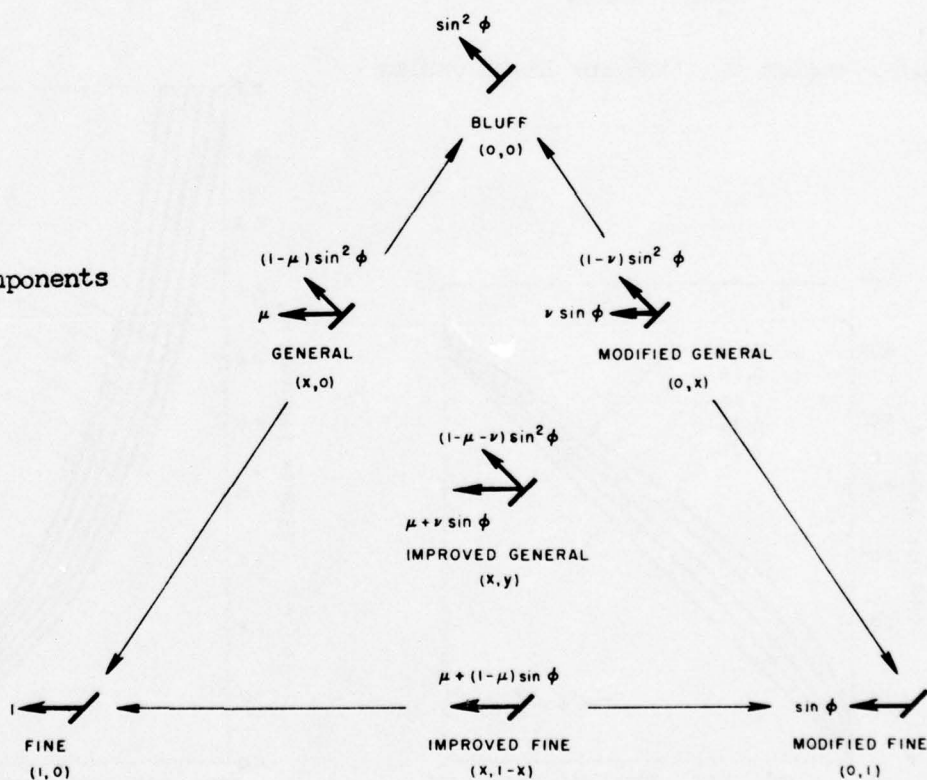
Fig.4 Classification of Light Cables

215
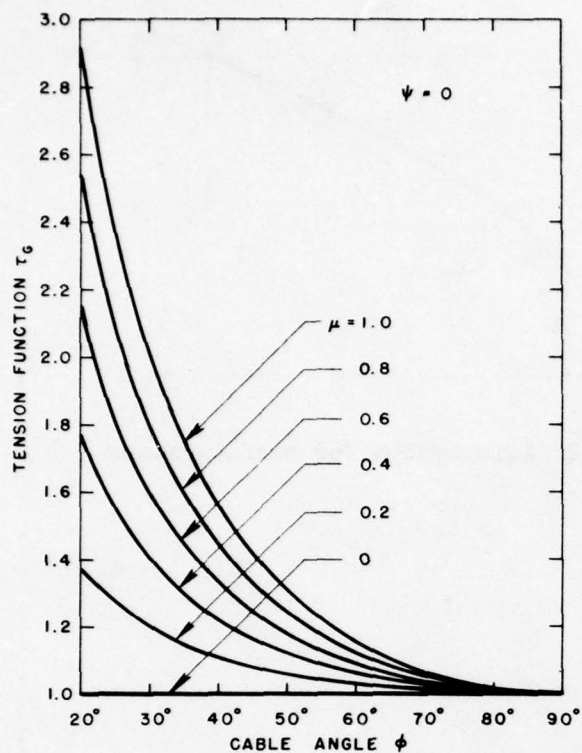
Fig.5 Tension function for Light Cables

Fig.6 Configuration of Light cables

Fig.7 Critical angle of Heavy Cables
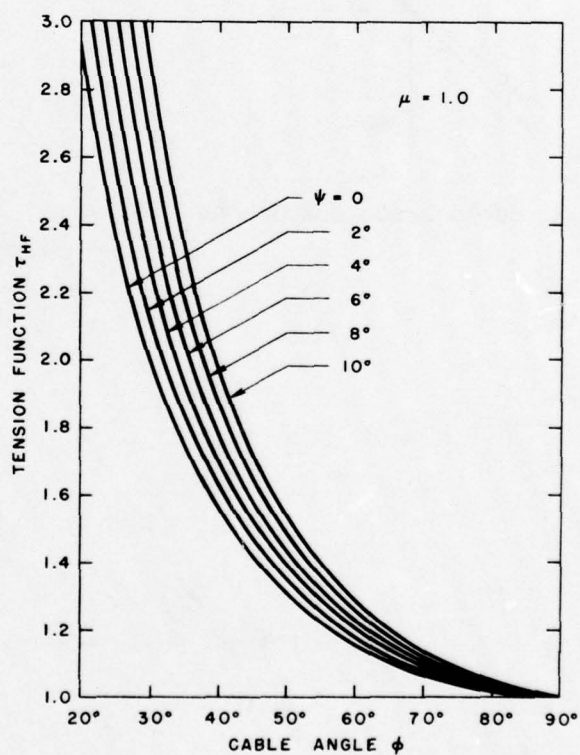
Fig.8 Tension function for Heavy Fine cable

216
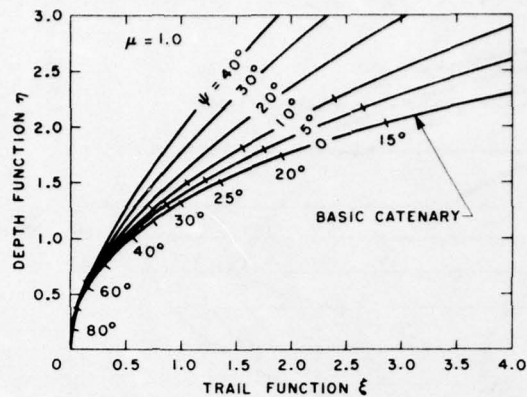
Fig.9   Configuration of Heavy Fine cable
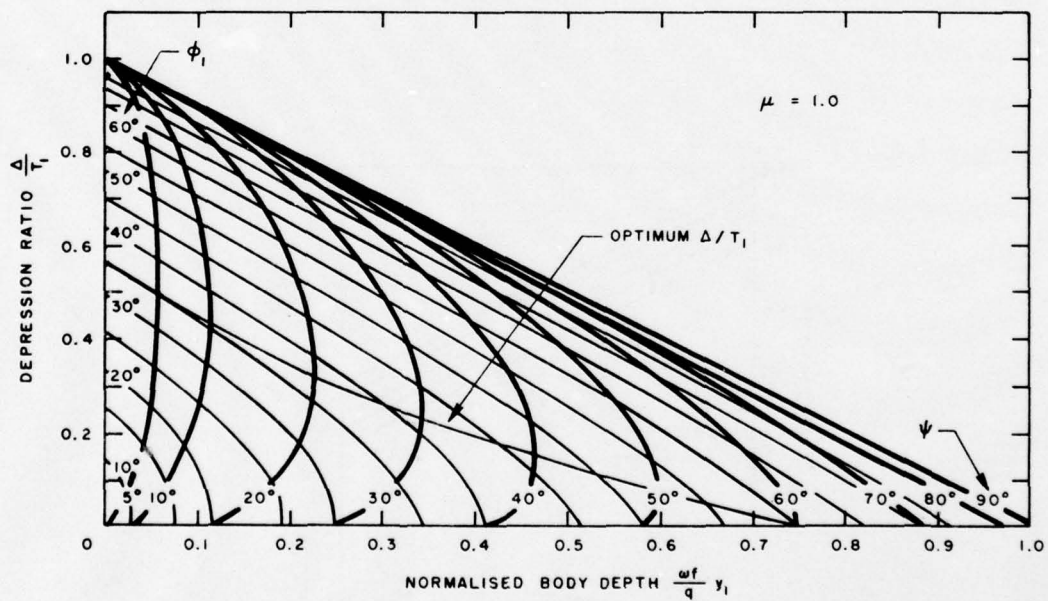
Fig.10 Depression ratio vs. normalized body depth - large depths

217
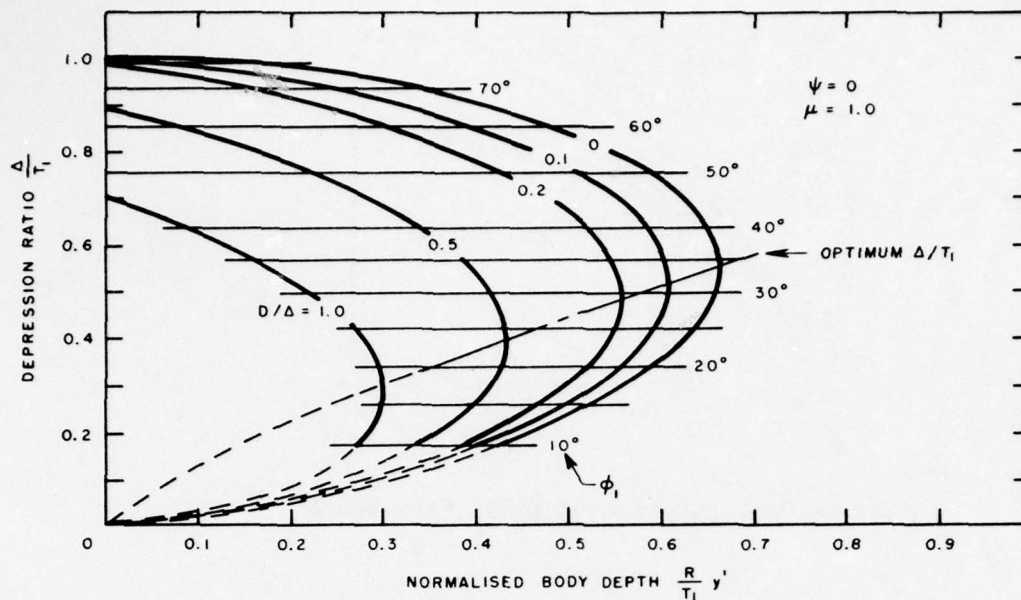
Fig.11 Depression ratio vs. normalized body depth - high speeds
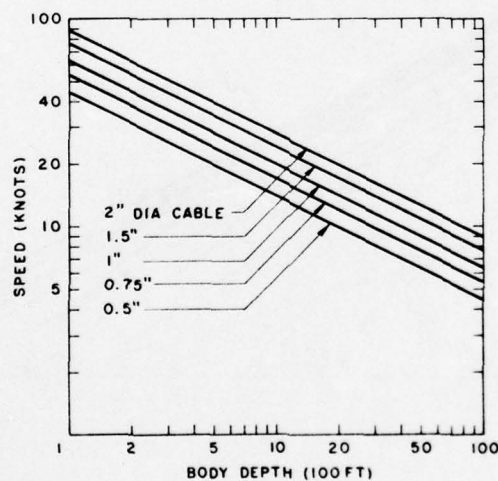
Fig.12 Current towing limits

FAIRED TOWLINE LOADING FUNCTIONS FROM BOUNDARY LAYER CONSIDERATIONS

by D. E. Calkins
U.S. Navy Electronics Laboratory
San Diego, California

1.0 ABSTRACT

A method for determining the variation in the Normal and Tangential hydro-dynamic forces on a faired towline is presented. The loading functions are obtained from consideration of the boundary layer, and are termed BLLF (boundary layer loading functions). The computations are based on the most up-to-date methods available from swept wing boundary layer theory. Only the planar (side force = zero) case is considered.

The computational procedure resulting may be performed using only a desk calculator, although a simple digital program could be written.

The BLLF are determined for a faired towline with an NACA 63A022 section, a three inch chord, and operating at 15 and 45 knots. The results are seen to be reasonable when compared with existing theories for determining the load-ing functions. The BLLF show that the boundary layer transition location and Reynolds Number effects do not result in a "universal" loading function law.

2.0 INTRODUCTION

In an effort to improve the performance of cable towed systems, faired towlines of several different designs have appeared over the past decade. The capability of accurately defining the effect of variations in the local towline angle, ϕ, on the hydrodynamic force field is necessary for accurate prediction of the tensions and configuration of the faired towline. Several authors have advanced theories for defining the relationship between the Normal and Tangential forces (loading functions) and their variation with towline angle. The most widely quoted are Clark(1),* Eames(2), and Whicker(3). None of the theories have approached the problem from pure boundary layer considerations, so that the correct effect of Reynolds Number might be taken into account.

It was therefore decided to approach the problem of defining the loading functions on a 3-dimensional faired towline by examining the boundary layer bearing in mind the necessity of keeping the computations required simple enough to perform with the aid of a desk calculator. The analysis is based on the most up-to-date swept wing theories which have been validated by experi-ment.

The following assumptions were made concerning the scope of the analysis.

1. The cable section is uncambered.

2. The chord and thickness ratio are constant in the spanwise direction (along the towline).

3. There are no discontinuities along the towline.

4. The angle of yaw is zero; i.e. no side forces are considered.

5. The boundary layer is not separated in either the laminar or turbu-lent region.

*Numbers in parentheses refer to similarly numbered references at the end of the text.

3.0 PRESENT LOADING FUNCTION THEORIES

For purpose of comparison, a capsule discussion of the three existing faired towline loading function theories is included. The comparison is included not to criticize these theories, nor to discount their use in practical applications, but rather to point out the differences between them and the boundary layer loading functions (BLLF).

3.1 Clark Analysis

Clark assumed that the flow over the deflected towline was two-dimensional in the streamwise direction; i.e., that local spanwise flow in the boundary layer of the swept but unyawed towline would have a negligible effect on the hydrodynamic force. As a result of this assumption, the local hydrodynamic force is directed in the streamwise direction and can be resolved into the Normal and Tangential components F and G. It was assumed that the magnitude of the local hydrodynamic force varied with cable angle ϕ, and could be approximated by the drag of the two-dimensional foil section obtained by passing a plane through the towline in the streamwise direction. Except for a small difference in leading-edge radius, the coordinates in percent chord for the hypothetical foil in the streamwise direction are those of the basic foil (ϕ = 90 deg) multiplied by sin ϕ. The Reynolds Number based on chord length of this hypothetical airfoil is then Reynolds Number for ϕ = 90 deg divided by sin ϕ.

Figure 1 summarizes the procedure used in the Clark analysis, and presents data for an NACA 4-digit series section, which will be used later for the comparison with the proposed BLLF. The 4-digit series was selected for analysis because of the complete data matrix available for this section.

3.2 Eames Analysis

The Eames "Light General" analysis was selected as most representative of the type of faired towline that is being considered. The term "Light" implies that the towline weight in water is negligible, and is therefore neglected in the analysis. Eames separates the total force acting on the towline, when the towline angle (ϕ) is 90°, into two components F and P, where F is the frictional force and P is the pressure force.

Eames assumes that the pressure force is the result of the velocity component normal to the leading edge. Therefore, the pressure drag will vary as $\sin^2\phi$, and will always act normal to the leading edge. The frictional component F is assumed to be invariant with towline angle, and to be equal to the value of F at ϕ = 90°. The form of the loading functions is shown in Figure 2.

The constant, μ is introduced as the ratio of the friction force to the total force at ϕ = 90°. 1-μ is the percent of total drag due to the pressure force. μ may be evaluated from an emperical equation derived by Hoerner(4) for the total drag coefficient:

$$C_R = C_f [1 + 2(t/c) + 60 (t/c)^4]$$

total   friction   pressure

where: C_f = Schoenherr friction coefficient

t/c = thickness/chord

$$\mu = \frac{1+2(t/c)}{60(t/c)^4} = \frac{F}{R} \qquad [1]$$

Graphs of μ (friction ratio) and $1-\mu$ (pressure ratio) are included in Figure 2. Data derived theoretically by Squire and Young(5) are included for various locations of the boundary layer transition location. For the section under consideration, t/c = 0.22, μ is seen to lie between 0.75 and 0.9.

3.3 Whicker Analysis

Whicker derives the Normal and Tangential loading functions in terms of the Normal and Tangential components of the free stream velocity, U_∞ Figure 3. The resultant loading functions are assumed to be portional to the square of the respective velocities and neglects any spanwise pressure gradient. Force coefficients are considered to be composed of two parts, the pressure and friction drag. Whicker assumes that the components of the drag coefficients due to the pressure forces, a and d, are independent of variation in Reynolds Number along the towline, and that the components of the drag coefficients due to the friction forces, i.e., $b/\sin\phi$ and $e/\cos\phi$ are functions of the components of velocity parallel to the leading edge. The final form of the loading functions are shown as equations 6 and 7 in Figure 3. The constants a, b, d and e were evaluated from test data on a strut with t/c = 0.25. The values are presented in equation 8 where a linear ratio was assumed for the various t/c values. The coefficients are expressed as functions of t/c, the section thickness to chord ratio.

4.0 BOUNDARY LAYER DEFINITIONS

The following definitions, taken from Schlicting(6), are considered essential for an understanding of the analysis.

4.1 δ-Boundary Layer Thickness

In a real fluid, a thin layer of the flow is retarded because of its adhesion to the wall. This layer is called the boundary layer or friction layer. The boundary layer thickness, δ, is usually defined as that distance from the surface where $u = 0.99 \ U_\infty$

4.2 δ^*-Displacement Thickness

The displacement thickness, δ^*, is the thickness of the layer by which the potential flow; i.e. the streamlines are displaced because of the reduction of velocity within the boundary layer. The deficiency of flow in the boundary layer as a result of the shear stresses is:

$$\int_{y \ = \ 0}^{\infty} (U_\infty - u)dy$$

consequently, δ^* as shown in Figure 4, is defined as

$$\delta^* = \int_0^\delta \left[1 - \frac{u}{U_\infty}\right] dy \qquad [2]$$

4.3 θ - Momentum Thickness

The momentum thickness, θ, is based on the reduction of momentum due to the frictional resistance of the surface. For the control surface given in Figure 5, the resistance of a piece of the plate of length x and width b wetted on one side is given by the momentum equation to be

$$R_f(x) = b\rho \int_{y=0}^\infty u(U_\infty - u) dy$$

in which u(x,y) denotes the velocity distribution in the boundary layer at the point x. If one introduces the momentum thickness θ into the equation and writes in the form

$$R_f(x) = \rho b\, U_\infty\; \theta(x)$$

then the momentum thickness is defined as

$$\theta = \int_0^\delta \frac{u}{U_\infty} \left(1 - \frac{u}{U_\infty}\right) dy \qquad [3]$$

4.4 H - Shape Factor

The shape factor is defined as the ratio of the displacement thickness to the momentum thickness

$$H = \delta^*/\theta \qquad [4]$$

5.0 2-DIMENSIONAL CASE

The essential physical difference between the flow of inviscid (friction-less) fluids and viscous fluids is exhibited in the fact that in the former, two contacting layers experience only normal forces (pressures) while in the latter, tangential shearing stresses also exist. These tangential or friction forces cause adhesion of the fluid to a wall wetted by it; that is, both the normal and tangential velocity components are uniformly zero at a boundary. This is depicted in Figure 6, in which the upper half shows the slip of an in-viscid fluid, while the lower half shows the adhesion of a viscous fluid (no slip condition).

For small Reynolds Numbers the flow and wake proceeds in well ordered parallel layers. This flow is called laminar. For increasing Reynolds Num-bers irregular transverse movements are formed more strongly in the wake causing an intermixture of the neighboring layers. This flow is called turbulent.

In general, the drag of a foil is dependent not only on the pressure differences (normal stresses) on the surface of the body but also on the tangential (shearing) stresses which emanate from the viscosity. These two parts of the drag may be computed separately by integrating the pressure and shear stresses over the surface of the body. If p denotes the pressure on the surface element dA of the body, and α is the angle between the direction of flow and the normal to the surface element, integration of the pressure yields the form drag Dp.

$$Dp = \oint (P \cos \alpha) dA \qquad [5]$$

in which the integration is carried out over the entire surface. Likewise, the skin friction drag is obtained through integration of the shearing stress, τ_0, at the wall

$$D_f = \oint (\tau_0 \sin \alpha) dA \qquad [6]$$

The total drag day is the sum of the form drag and the skin friction drag

$$D_{Total} = D_p + D_f \qquad [7]$$

6.0 3-DIMENSIONAL CASE

6.1 Pressure Stresses

It has been theorized by Jones(7) that the pressure forces on a swept wing of constant chord are determined solely by the component of velocity normal to the leading edge. This has been verified experimentally by Lippisch and Beuschausen(8), and Dannenberg(9).

In essence, this means that in the case of the faired towline, the Normal Force is composed of pressure forces (determined solely by the chordwise velocity component) and frictional forces, while the Tangential Force is the result only of frictional stresses due to the spanwise velocity component.

6.2 Frictional Stresses

The investigations of Jones(7), and Sears(10) have shown that the laminar boundary layer on a yawed infinite wing (faired towline) may be determined in a simple manner. Outside the boundary layer in the inviscid region, see Figure 7, the flow is obtained by superposition of a two-dimensional flow perpendicular to the wing leading edge (chordwise flow) and a (spanwise flow) parallel to the leading edge with a velocity, V_0, which is invariant. The chordwise velocity component, U, outside the boundary layer is given as a function of x from the two dimensional case. z is the coordinate in the spanwise direction; i.e. in the direction of the cable axis.

The boundary layer problem becomes soluble after recognizing that any quantity, inside as well as outside the boundary layer is independent of z. Let us consider the case of vanishing chordwise flow. Then, in a purely spanwise flow, we would expect a growth of the boundary layer in the z direction and thus no independence of z. Actually, we must exclude the special case of vanishing chordwise flow; if the chordwise flow exists, it will remove fluid contained in the spanwise layer so that a constant thickness in the z direction (and also an independence of any quantity of z) becomes possible.

The spanwise component of the velocity in the boundary layer, v, then becomes a function of x alone. Once this is recognized, it may be concluded that the chordwise flow may be calculated as if no spanwise flow were present.

Recently, it was theorized by Young and Booth(11) and supported by experimental evidence for a flat plate that the "independence principle" for yawed infinite wings is also valid for the turbulent boundary layer. Altman and Hayter(12) gave further experimental evidence in support of this theory for the case of a swept wing (at zero lift) in turbulent flow. Further discussion by Rott and Crabtree(13) give credibility to the "independence principle."

7.0 NORMAL FORCE CHORDWISE FLOW DETERMINATION

As indicated, the Normal Force may be determined from examination of the chordwise velocity, U_o, alone. The problem reduces, then, to one of determining the forces of a two-dimensional foil section. From section 5.0, the Normal Force, F, is the sum of the integrals of the pressure and shear stresses over the contour of the foil.

The computation of the chordwise force begins with the potential solution for inviscid flow over the two-dimensional section. Several methods are available for this solution. However, one which is particularly attractive is that developed by Weber(14). Its usefulness lies in the fact that only knowledge of the section coordinates are necessary, and the computation may be readily handled with a desk calculator.

The method involves evaluation of the section y coordinate at N stations along the chord, which are in turn operated on by constants available from tables for N = 8, 16, or 32. Of course, the computation takes longer for larger N, however the results are more accurate.

The velocity ratio is evaluated as

$$\frac{U}{U_o} = \frac{U}{U_\infty \sin\phi} = \frac{1 + S^{(1)}(X)}{\sqrt{1 + (S^{(2)}(X))^2}} \qquad [8]$$

where

$$S^{(1)}(X) = \sum_{\mu=1}^{N-1} S_{\mu\nu}^{(1)} Y_\mu \qquad [9]$$

$$S^{(1)}(X) = \sum_{\mu=1}^{N-1} S_{\mu\nu}^{(2)} Y_\mu \qquad [10]$$

$S_{\mu\nu}^{(1)}$ and $S_{\mu\nu}^{(2)}$ are constants taken from Tables II and III (N = 8) and Y_μ is the section coordinate evaluated at X_μ. Tables for N = 16 and 32 may be found in reference [14].

With knowledge of the velocity ratio, U/U_0, it is now possible to evaluate the shear stresses and hence the total skin friction drag. It is pointed out that the pressure, or form drag, is zero at this point because of the utilization of the potential solution. The distortion of this pressure distribution from that occurring in the actual fluid arises from the formation of the boundary layer which increases in thickness from the leading edge to the trailing edge. The form drag may be evaluated by solving for the displacement thickness, δ^*, adding this thickness to the section coordinates, and recomputing the pressure distribution. However, this would be tedious and a better procedure is based on the fact that the skin friction and form drag are together manifested finally by a loss of momentum at infinity downstream.

Consider the two dimensional flow past the foil section shown in Figure 7. The flow pressure is constant in the fluid field except in the boundary layer and in the wake, which are shown shaded. Starting from the stagnation point, L, boundary layers are present on the upper and lower surfaces of the foil. Boundary layers are generally laminar for some distance to transition which occurs at the point x_t. After a transition region, fully turbulent boundary layers are formed to the trailing edge, T. The boundary layers of the upper and lower surface coalesce to form a wake which extends downstream to infinity.

The wake has a minimum thickness a short distance downstream of the trailing edge and then becomes gradually broader. Static pressure in the wake is greatest at the trailing edge and decreases downstream. The static pressure in the wake eventually becomes equal to the static pressure of the free stream. For a section of the wake sufficiently downstream for this to be true, it is easy to show from momentum considerations that the Normal Force, F, per unit length is:

$$F = \rho \int_{-\infty}^{\infty} u(U_0 - u)dy \qquad [11]$$

$$F = C_R \, 1/2 \, \rho U_0^2 c \qquad [12]$$

where U_0 = Chordwise freestream velocity = $U_\infty \sin\phi$

   u = Velocity in the wake parallel to the direction of motion

   c = Foil Chord

   ρ = Fluid Density

The momentum thickness of the wake far downstream, θ_∞, is defined as:

$$\theta_\infty = \int_{-\infty}^{\infty} \frac{u}{U_0} \left(1 - \frac{u}{U_0}\right) dy \qquad [13]$$

so that $C_R = \dfrac{2\theta_\infty}{c}$ $\qquad [14]$

The momentum thickness, θ_∞, may now be evaluated in terms of the momentum thickness at the trailing edge of the foil, θ_{xx}.

$$\theta_\infty = \theta_{xx} \left[\frac{U_t}{U_0} \right]^{(H_t+5)/2} \tag{15}$$

Where U_t = velocity outside of the boundary layer at the trailing edge

   H_t = shape parameter at trailing edge

If a value of $H_t = 2.0$ is used, according to Thwaites(15), equation [14] becomes:

$$C_R = 2 \left[\left(\frac{\theta_{xx}}{c} \right)^{6/5} \left(\frac{U_t}{U_0} \right)^{21/5} \right]^{5/6} \tag{16}$$

Where θ_{xx} is the sum of the momentum thicknesses on the upper and lower surfaces.

The momentum thickness, θ_{xx}, is dependent on the extent of both the laminar and turbulent boundary layers, and may evaluate according to Thwaites as

$$C_R = 2.0 \left[\frac{1.422}{R^{3/5}} \left\{ \frac{U_t}{U_0} \int_0^{\frac{X_t}{c}} \left(\frac{U}{U_0} \right)^5 d\left(\frac{X}{c} \right) \right\}^{3/5} + \frac{0.02429}{R^{1/5}} \int_{\frac{X_t}{c}}^{1} \left(\frac{U}{U_0} \right)^4 d\left(\frac{X}{c} \right) \right]^{5/6} \tag{17}$$

where   R = Chord Reynolds Number = $U_0 c / \nu$

   $\frac{X_t}{c}$ = Chordwise position of boundary layer transition

8.0 TANGENTIAL FORCE (SPANWISE FLOW) DETERMINATION

Since, as assumed, the foil section is constant along the towline length, the Tangential force, G, has no form or pressure drag component and is strictly the result of the frictional stress, τ_{yz}. Therefore the Tangential force, G, per unit length is:

$$G = \int_0^c (\tau_{yz}) dx \tag{18}$$

where $\tau_{yz} = \rho V_0^2 (\partial\theta_{zx}/\partial X) dx$ $\tag{19}$

θ_{zx} - Cross momentum thickness

V_0 = Spanwise velocity component = $U_\infty \cos \phi$

So that $G = \rho V_0^2 \int_0^c \left(\frac{\partial\theta_{zx}}{\partial x} \right) dx$ or $G = \rho V_0^2 \left[\theta_{zx} \right]_{L.E.}^{T.E.}$ $\tag{20}$

θ_{zx} is assumed to vary from zero at the leading edge, L.E., to (θ_{zx})T at the trailing edge, T.E.

$$\theta_{zx} = \int_0^\delta \frac{u}{V}\left(1-\frac{u}{V}\right)dy$$

$$\theta_{zx} = \frac{U}{V}\int_0^\delta \frac{u}{U}\left(1-\frac{v}{V}\right)dy \qquad [21]$$

or θ_{zx} may be expressed in terms of the total momentum thickness, θ_{xx}, at the trailing edge.

$$\theta_{zx} = \frac{U_t}{V_0}\ K\ \theta_{xx} \qquad [22]$$

where $K = \dfrac{1}{\theta_{xx}}\displaystyle\int_0^\delta \frac{u}{U}\left(1-\frac{v}{V}\right)dy \qquad [23]$

Under the assumption of a turbulent boundary layer at the trailing edge, K may be determined if the following assumptions are made.

(1) The distribution of v/V_0 is the same for any X where the boundary layer is turbulent, and is independent of the chordwise pressure gradient.

(2) $v/V_0 = \left(\dfrac{y}{\delta}\right)^{1/7}$ as for a flat plate in turbulent flow.

now since $\dfrac{u}{U} = \left(\dfrac{y}{\delta}\right)^{(H_t-1)/2} = \left(\dfrac{y}{\delta}\right)^n \qquad n = (H_t-1)/2 \qquad [24]$

$$K = \frac{\delta}{\theta_{xx}}\int_0^1 \left(\frac{y}{\delta}\right)^n\left[1-\left(\frac{y}{\delta}\right)^{1/7}\right]d\left(\frac{y}{\delta}\right)$$

$$K = \frac{\delta}{\theta_{xx}}\left[\frac{1}{n+1} - \frac{1}{n+1+(1/7)}\right]$$

since $\dfrac{\delta}{\theta_{xx}} = \dfrac{(n+1)(2n+1)}{n}$

then $K = \left(\dfrac{1/7}{n}\right)\left(\dfrac{2n+1}{1+n+1/7}\right)$

$$K = \frac{4H_t}{7H_t^2 + 2H_t - 9}$$ [25]

Following the assumption of $H_t = 2.0$ at the trailing edge, $K = 0.348$. K is shown as a function of H_t in Figure 8.

Now the Tangential force may be expressed as

$$G = \rho V_o^2 \; \frac{U_t}{V_o} \; K \; \theta_{xx}$$

or $\quad G = \rho V_o \; U_t \; K \; \theta_{xx}$ [26]

However, from equations [12] and [16]

$$\theta_{xx} = \left(\frac{F(\phi)}{\rho U_o^2}\right)\left(\frac{U_o}{U_t}\right)^{(H_t+5)/2}$$ [27]

Where $F(\phi)$ is the Normal force at ϕ, so that G may be expressed in final form as:

$$G = \rho V_o \; U_t \; K \; \frac{F(\phi)}{\rho U_o^2} \left(\frac{U_o}{U_t}\right)^{(H_t+5)/2}$$

or $\quad G = K \; F(\phi) \left(\frac{U_\infty \cos\phi}{U_\infty \sin}\right)\left(\frac{U_t}{U_o}\right) \left(\frac{U_o}{U_t}\right)^{(H_t+5)/2}$

$$G = F(\phi) \left(\frac{4H_t}{7\,H_t^2 + 2H_t - 9}\right) \cot\phi \left(\frac{U_o}{U_t}\right)^{(H_t+3)/2}$$ [28]

Therefore substituting the value of $H_t = 2.0$ as used in the Normal force derivation we obtain:

$$G = 0.348 \; F(\phi) \cot\phi \left(\frac{U_o}{U_t}\right)^{2.5}$$ [29]

9.0 EXAMPLE

For illustration of the procedure, the NACA 63A022 section was selected, since the loading functions for this section are presently being evaluated in a series of model tests. Full-scale evaluation test data are also available from recent trials. These data will be used in a future evaluation of the present theory.

Two Reynolds Numbers were selected as being representative of a working range of speeds. Reynolds Numbers of 0.5 and 1.5×10^6 are equivalent to a towline with a three inch chord operating at 15 and 45 knots.

10.0 BOUNDARY LAYER TRANSITION LOCATION

The determination of the location of the boundary layer transition is at best a difficult problem even in the two-dimensional case. It generally is true that:

(1) Transition occurs near the minimum pressure point.

(2) Transition moves toward the trailing edge with decreasing Reynolds Number.

However, it has been observed by Gregory, Stuart, and Walker[16] that in the three-dimensional case, transition moves forward with increasing sweep. This trend would therefore seem to contradict the previous statement (2). In addition, the ambient stream turbulence level will affect transition causing it to occur nearer to the leading edge as the level increases in intensity.

Since time did not allow for a more thorough analysis of the transition location, it was decided to use experimental data from Silverstein and Becker[17] that were obtained on a series of NACA 4-digit air foil sections. The transition location, Figure 9 was extrapolated to the t/c value of 0.22 which was used for the example analysis.

11.0 ANALYSIS PROCEDURE

11.1 Evaluate y_μ at each x_ν, table I, for the section shape under consideration.

11.2 For $\nu = 1, 2, \ldots 7$, list $S_{\mu\nu}(1)$ from table II and find $S^{(1)}(X_\nu)$ from equation [2].

11.3 For $\nu = 1, 2, \ldots 7$, list $S_{\mu\nu}(2)$ from table III and find $S^{(2)}(X_\nu)$ from equation [3]. Table IV presents steps 11.2 and 11.3 for $\nu = 4$, $X_\nu = 0.5$.

11.4 Find $(U/U_0)_\nu$ for $\nu = 1, 2, \ldots 7$ from equation [8].

11.5 Plot $(U/U_0)^4$ and $(U/U_0)^5$ versus x/c, Figure 10. The solid lines represent the exact potential solution from Abbott and Von Doenhorf[18], with the Weber solution for $N = 8$ shown for comparison. The results agree well with the exact solution, although more points ($N = 16$ or 32) would be necessary for an accurate description.

11.6 Locate the boundary layer transition as function of Reynolds Number, Fig. 11.

11.7 With $R = R_\infty \sin\phi$, plot $X_{t/c}$ versus ϕ from 11.6, Figure 12.

11.8 Choose range of increments of ϕ for force computations, Table V. For the present analysis, computations were carried out down to $\phi = 30°$, in $15°$ increments.

11.9 Perform integrations on $\dfrac{U}{U_0}^4$ and $\dfrac{U}{U_0}^5$ using the result from 11.7 for the limits of the laminar and turbulent areas. Table V contains data for the $R = 1.5 \times 10^6$ case. Graphical integration was performed in this analysis using a planimeter.

11.10 Find C_R using equation [17] and the data from step 11.9,   Table V.

Note that C_R is based on the chord area.

11.11 Find F (Normal force per unit length) using equation [12], see Table V.

11.12 Find G (Tangential force per unit length) using equation [29], see Table V.

11.13 Non-dimensionalize F and G by dividing by $\phi=90°$, see Table V.

12.0 RESULTS

The normal drag coefficient, C_R, is shown as a function of Reynolds Number in Figure 13. Note that C_R has been based on the frontal area. The results show the anticipated decrease with Reynolds Number.

In order to show the full range of dependence on transition location, computations were carried out for both of the examples (R = 0.5 and 1.5×10^6) assuming three transition locations:

(1) $X_{t/c}$ = 1.0 (Full laminar)

(2) $X_{t/c}$ = f(R) (laminar/turbulent)

(3) $X_{t/c}$ = 0   (Full turbulent)

The Normal (F) and Tangential (G) forces as functions of ϕ are shown in Figures 14 (R = 0.5×10^6), and 15 (R = 1.5×10^6). It must be pointed out that for application of the BLLF method, the computations need go no farther than finding F and G as a function of ϕ. The use of F and G would then require numerical integration techniques for the solution of the towline configuration and tension equations.

The non-dimensional loading functions, F/R and G/R are shown in Figures 16 through 19.

Case I (R = 0.5×10^6) shows some rather interesting results. Both F/R and G/R show that the boundary layer transition location will affect the shape of the curves. This in essence means that there can be no "universal" loading function law. For comparison, the $\sin\phi$, $\sin^2\phi$, Clark, Eames, and Whicker loading functions are included.for the normal loading function comparison.

F/R, Figure 16, is seen to follow approximately the shape of the $\sin^2\phi$ curve, although displaced to the left. Data from Clark's method are seen to fall across the range of the BLLF, while the $\sin\phi$ Whicker and Eames curves fall to the left of the BLLF. The same trends are seen for F/R (R = 1.5×10^6) Figure 17. However, the laminar/turbulent and full turbulent BLLF are seen to collapse to one curve.

G/R, Figure 10 shows a much wider spread between the compared curves. The Clark data is seen to follow Eames, the upper bound, down to $\phi = 60°$, and then drop off, while Whicker represents the lower bound. The BLLF fall approximately midway between the bounds. Again, the same trends are noted for the R = 1.5×10^6 case, Figure 19, with the laminar/turbulent and full turbulent curves collapsing. The effect of Reynolds Number is seen to be small, with the exception of the laminar/turbulent case.

13.0 CONCLUSIONS

Within the limits of the assumptions, the BLLF method is seen to represent a reasonable approach to the determination of the loading functions. However, several areas of work must be completed beofre its value may be truely assessed, namely:

13.1 Compare the velocity distribution computation method with experimental results.

13.2 Compare the loading functions measured on models with the BLLF.

13.3 Compare the data from the full-scale sea trials with results computed using the BLLF.

13.4 Investigate the effects of ambient stream turbulence and sweep on the transition location.

TABLE I - NACA 63A022		
N = 8		
ν	X_ν	Y_μ
0	1.000(T.E.)	0
1	0.9619	0.0085
2	0.8536	0.0325
3	0.6913	0.0675
4	0.5000	0.1005
5	0.3087	0.108
6	0.1464	0.0845
7	0.03806	0.047
8	0 (L.E.)	0

TABLE II

(1)

$\underline{s}_{\mu\nu}$ for N = 8

μ \ ν	1	2	3	4	5	6	7	8
1	20.905	-4.072	0	-0.224	0	-0.072	0	-0.052
2	-7.524	11.314	-3.359	0	-0.298	0	-0.133	0
3	0	-4.389	8.659	-3.154	0	-0.389	0	-0.242
4	-0.586	0	-3.414	8.000	-3.414	0	-0.586	0
5	0	-0.389	0	-3.154	8.659	-4.389	0	-1.212
6	-0.133	0	-0.298	0	-3.359	11.314	-7.524	0
7	0	-0.072	0	-0.224	0	-4.072	20.905	-33.022

TABLE III

$$S_{\mu\nu}{}^{(2)} \underline{\text{ for N = 8}}$$

μ \ ν	1	2	3	4	5	6	7
1	6.309	4.993	-1.531	0.828	-0.634	0.664	-1.082
2	-17.048	1.414	4.718	-2.000	1.405	-1.414	2.266
3	8.922	-8.055	0.448	4.828	-2.613	2.398	-3.696
4	-5.657	4.000	-5.657	0	5.657	-4.000	5.657
5	3.696	-2.398	2.613	-4.828	-0.448	8.055	-8.922
6	-2.266	1.414	-1.405	2.000	-4.718	-1.414	17.048
7	1.082	-0.664	0.634	-0.828	1.531	-4.993	-6.309

TABLE IV

	$\nu = 4;$		$X_\mu = 0.50;$	
μ	$S^{(1)}_{\mu\nu}$	$S^{(1)}_{\mu\nu} \cdot Y_\mu$	$S^{(2)}_{\mu\nu}$	$S^{(2)}_{\mu\nu} \cdot Y_\mu$
0	0	0	0	0
1	-0.224	-0.0019	0.828	0.007
2	0	0	-2.000	-0.065
3	-3.154	-0.2126	4.828	0.326
4	8.000	0.804	0	0
5	-3.154	-0.3402	-4.828	-0.5216
6	0	0	2.000	0.169
7	-0.224	-0.0105	-0.828	-0.0384
8	0	0	0	0

$$S^{(1)}(X_\nu) = \sum_{\mu = 1}^{N = 1} S^{(1)}_{\mu\nu} \cdot Y_\nu = 0.2598 \quad ; \quad S^{(2)}_{\mu\nu}(X_\nu) = -0.1235$$

$$\left(\frac{U}{U_0}\right)_{\nu = 4} = \frac{1 + S^{(1)}(X)_\nu}{\sqrt{1 + [S^{(2)}(X)]^2}} = 1.25$$

TABLE V – EXAMPLE FOR RN = 1.5X10^6
LAMINAR/TURBULENT CASE

ϕ - DEG	RN(ϕ)	x_t/c	$\int_o^{x_t/c}\left[\frac{U}{U_o}\right]^5 d\left(\frac{x}{c}\right)$	$\int_{x_t/c}^{1.0}\left[\frac{U}{U_o}\right]^4 d\left(\frac{x}{c}\right)$	$\frac{C}{R}$ Based on Chord	F(#/Ft.)	G(#/Ft.)	F/R	G/R
90	1.5x10⁶	0.34	1.058	1.05	0.01043	14.74	0	1.0	0
75	1.449	0.343	1.060	1.04	0.01045	13.78	1.95	0.935	0.132
60	1.299	0.348	1.072	1.025	0.01062	11.26	3.43	0.764	0.233
45	1.06	0.355	1.088	1.005	0.01102	7.78	4.10	0.528	0.278
30	0.75	0.365	1.112	0.975	0.01179	4.17	3.80	0.283	0.258

1. $RN' = \dfrac{(RN)_{\phi = 90°}}{\sin\phi}$

2. $t/c' = (t/c)_{\phi = 90°} \sin\phi$

3. $\dfrac{F}{R} = \dfrac{C_R \sin\phi}{(C_R)_{\phi = 90°}} = $ NORMAL LOADING FUNCTION

4. $\dfrac{G}{R} = \dfrac{C_R \cos\phi}{(C_R)_{\phi = 90°}} = $ TANGENTIAL LOADING FUNCTION

NACA 4-DIGIT SERIES SECTION

EX. $\begin{cases} RN_{90} = 0.5 \times 10^6; \quad RN_{90} = 1.5 \times 10^6 \\ 0020 \text{ SECTION} \end{cases}$
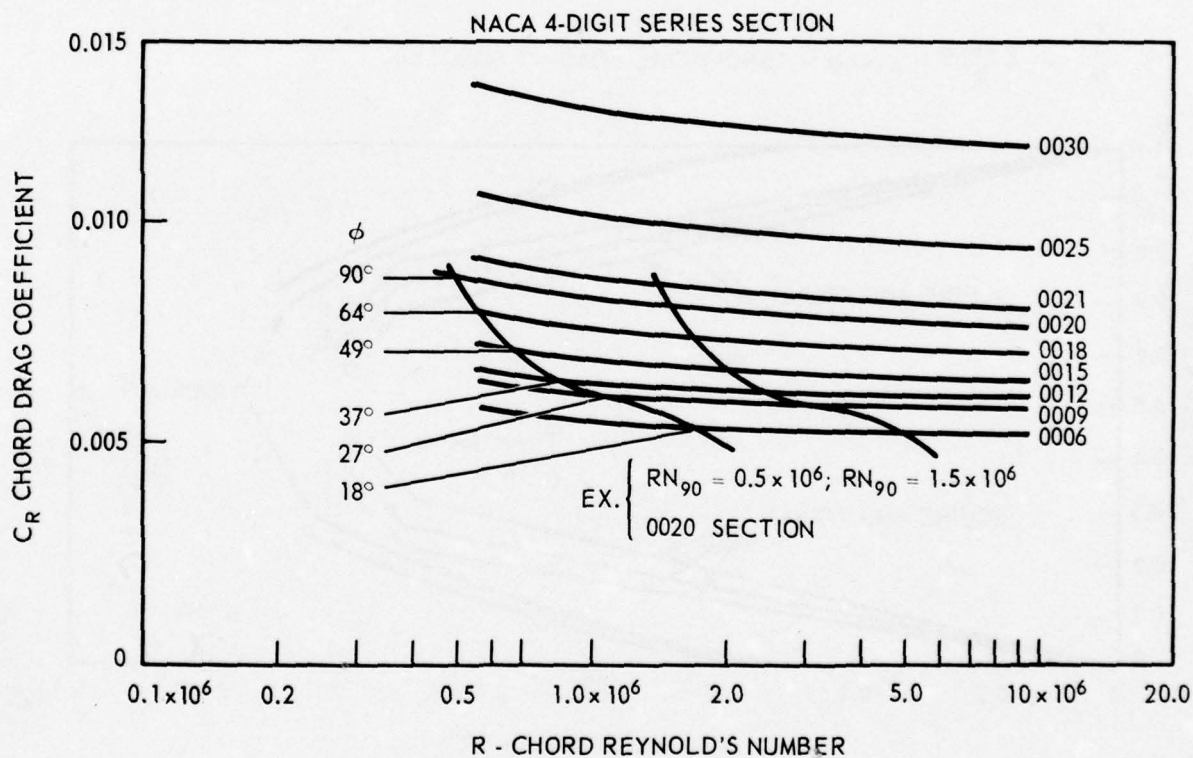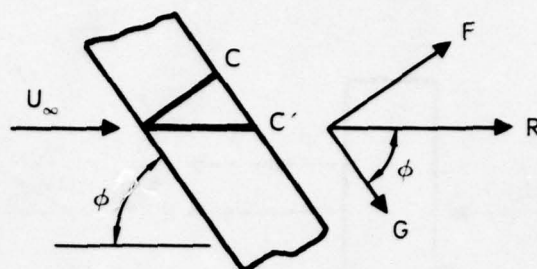
Figure 1. Clark analysis.
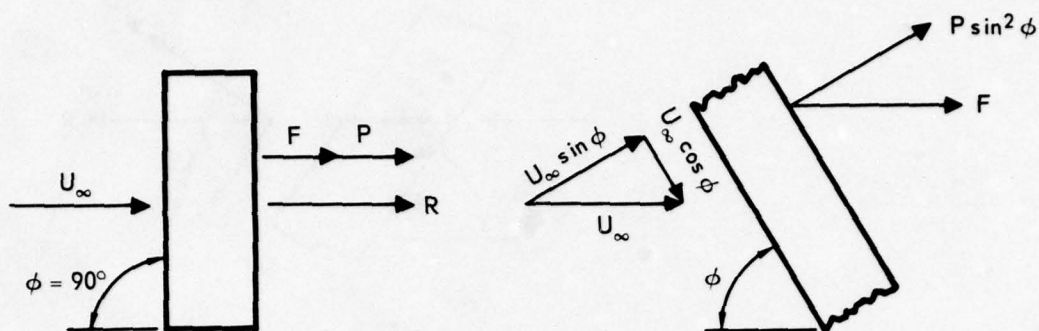
1. $R = F + P @ \phi = 90°$

2. $F = \mu R$

3. $P = (1 - \mu) R$

4. $\dfrac{F}{R} = \dfrac{P \sin^2 \phi + F \sin \phi}{R} = (1 - \mu) \sin^2 \phi + \mu \sin \phi$ = NORMAL LOADING FUNCTION

5. $\dfrac{G}{R} = \dfrac{F \cos \phi}{R} = \mu \cos \phi$ = TANGENTIAL LOADING FUNCTION
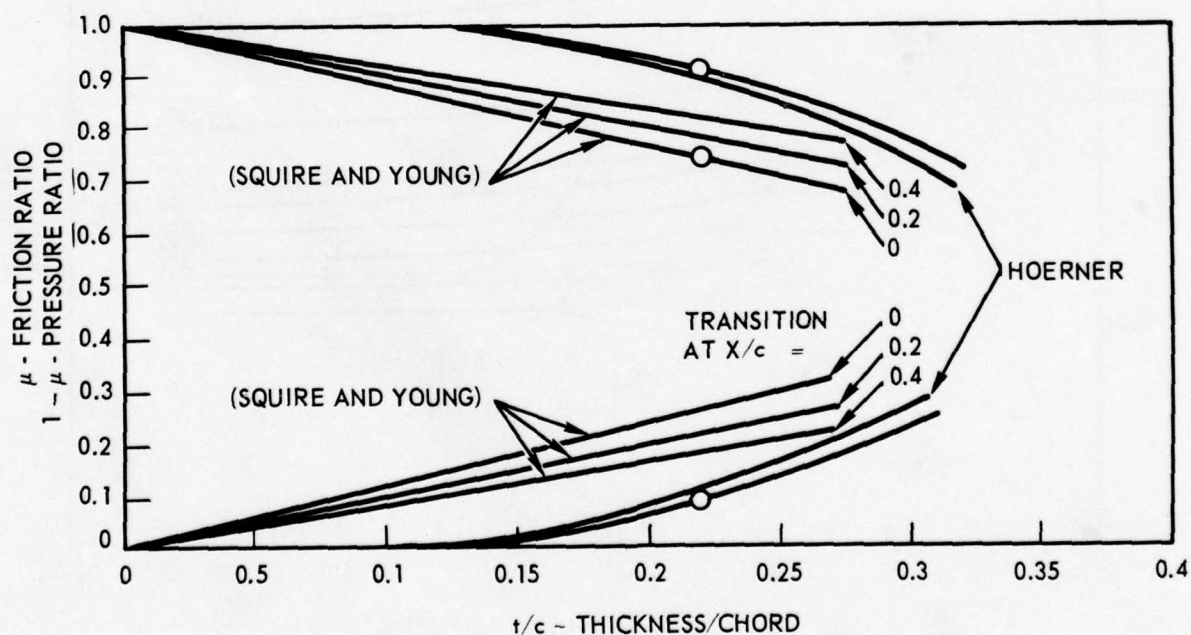
Figure 2. Eames analysis.

$U = U_\infty \sin\phi$ $V = U_\infty C_R \phi$ U_∞
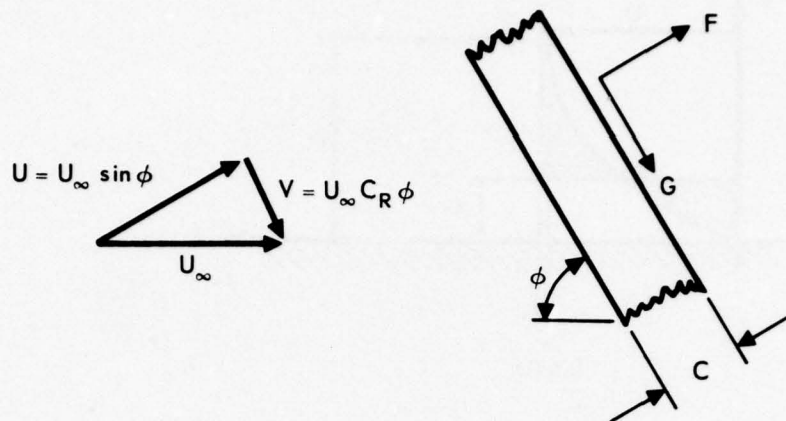
1. $F = C_N \dfrac{\rho U^2}{2} C = C_N \dfrac{\rho U_\infty^2 \sin^2\phi\, C}{2}$

2. $G = C_T \dfrac{\rho V^2}{2} C = C_T \dfrac{\rho U_\infty^2 \cos^2\phi\, C}{2}$

3. $C_N = C_R \left[a + \dfrac{b}{\sin\phi} \right]$

4. $C_T = C_R \left[d + \dfrac{e}{\cos\phi} \right]$

5. $C_R = \dfrac{R}{\dfrac{\rho U_\infty^2 C}{2}}$

6. $\dfrac{F}{R} = [\, a\sin^2\phi + b\cos\phi \,] = $ **NORMAL LOADING FUNCTION**

7. $\dfrac{G}{R} = \cdot\, [\, d\cos^2\phi \div e\cos\phi \,] = $ **TANGENTIAL LOADING FUNCTION**

$$\begin{bmatrix} a = t/c & ; & d = -[0.055 - 0.020\ t/c] \\ b = 1 - t/c & ; & e = [0.386 - 0.303\ t/c] \end{bmatrix}$$

Figure 3.   Whicker analysis.
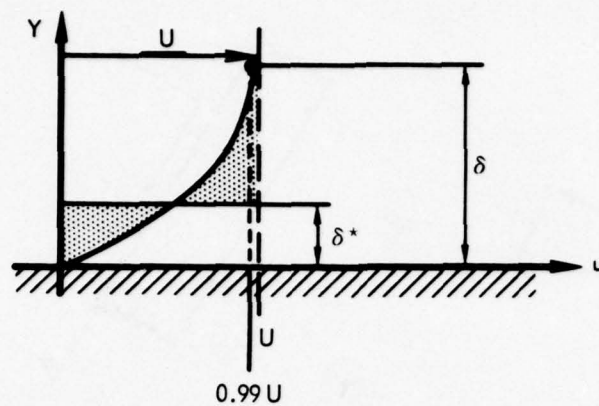
Figure 4. δ^* - Displacement thickness.
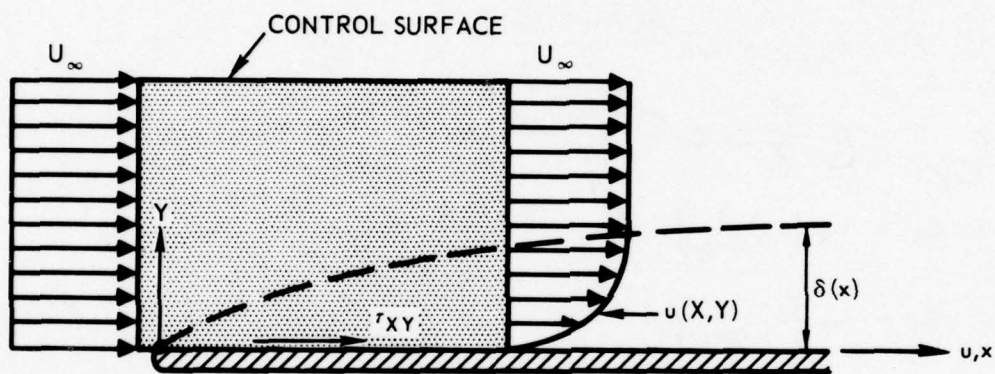
Figure 5. Application of momentum equation.
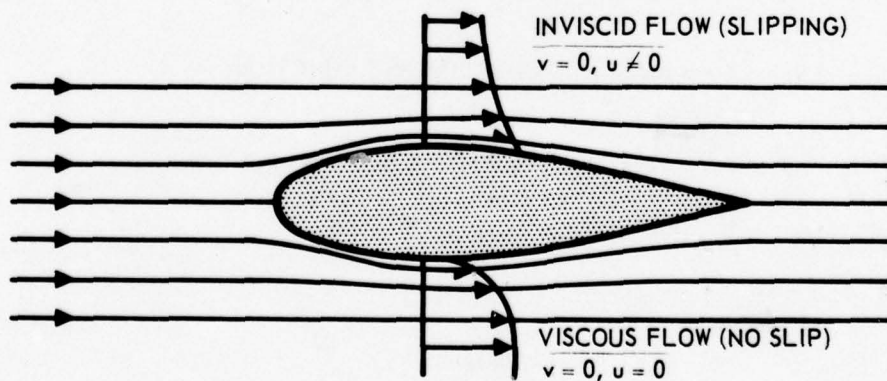
Figure 6. Boundary conditions for flow past body.

238
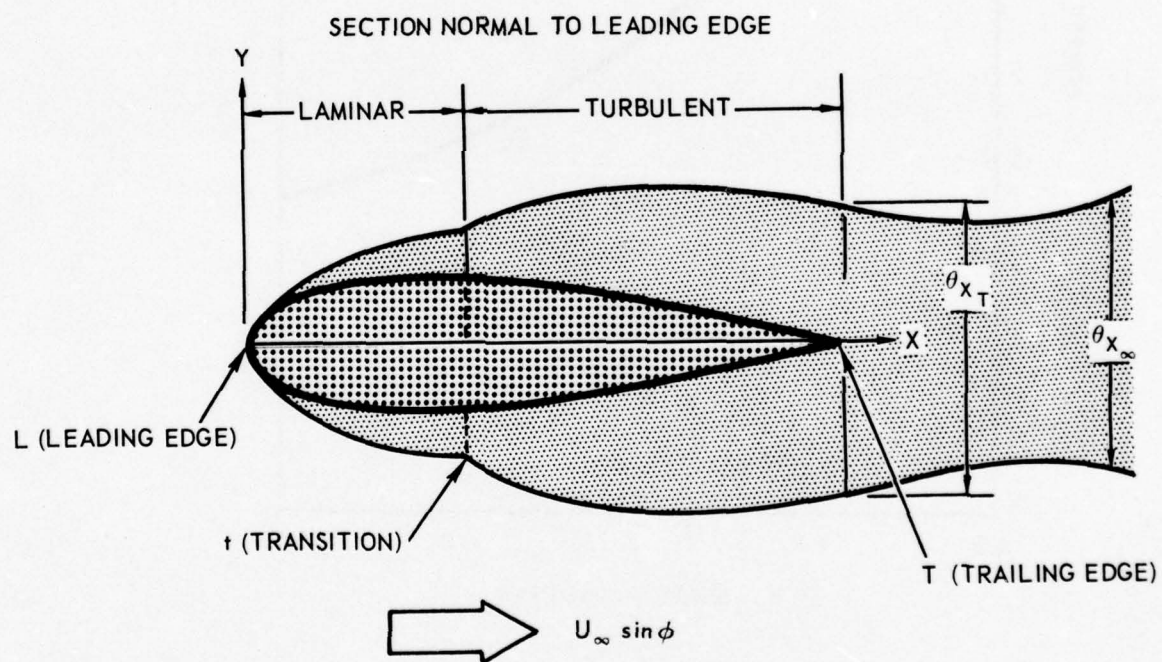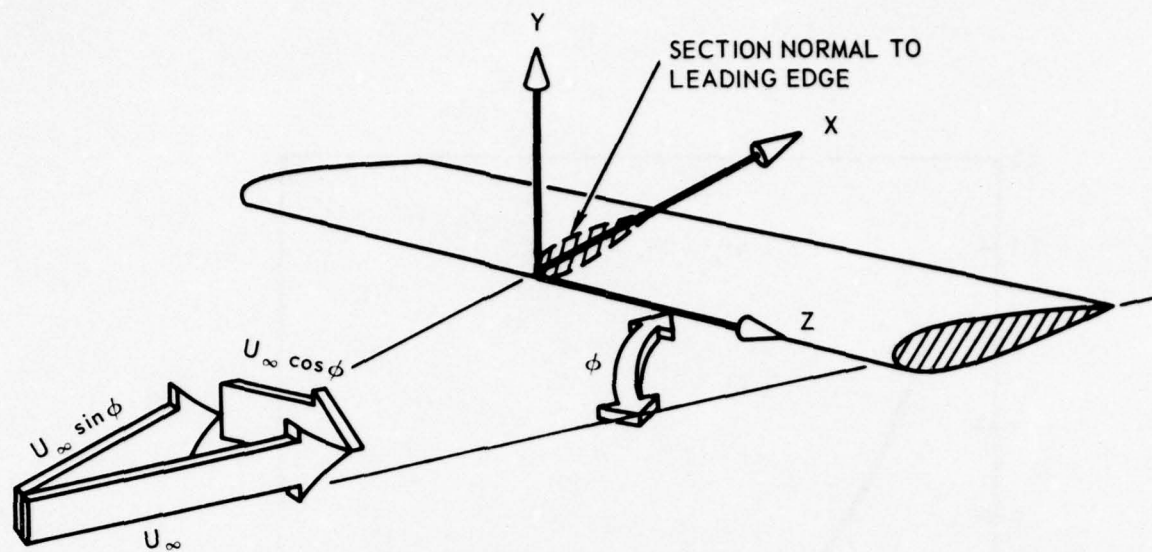
Figure 7.   Coordinate system.

239

$$K = 7H_x{}^2 + 2H_x - 9$$

K ~ CORRECTION FACTOR

H_x - SHAPE PARAMETER
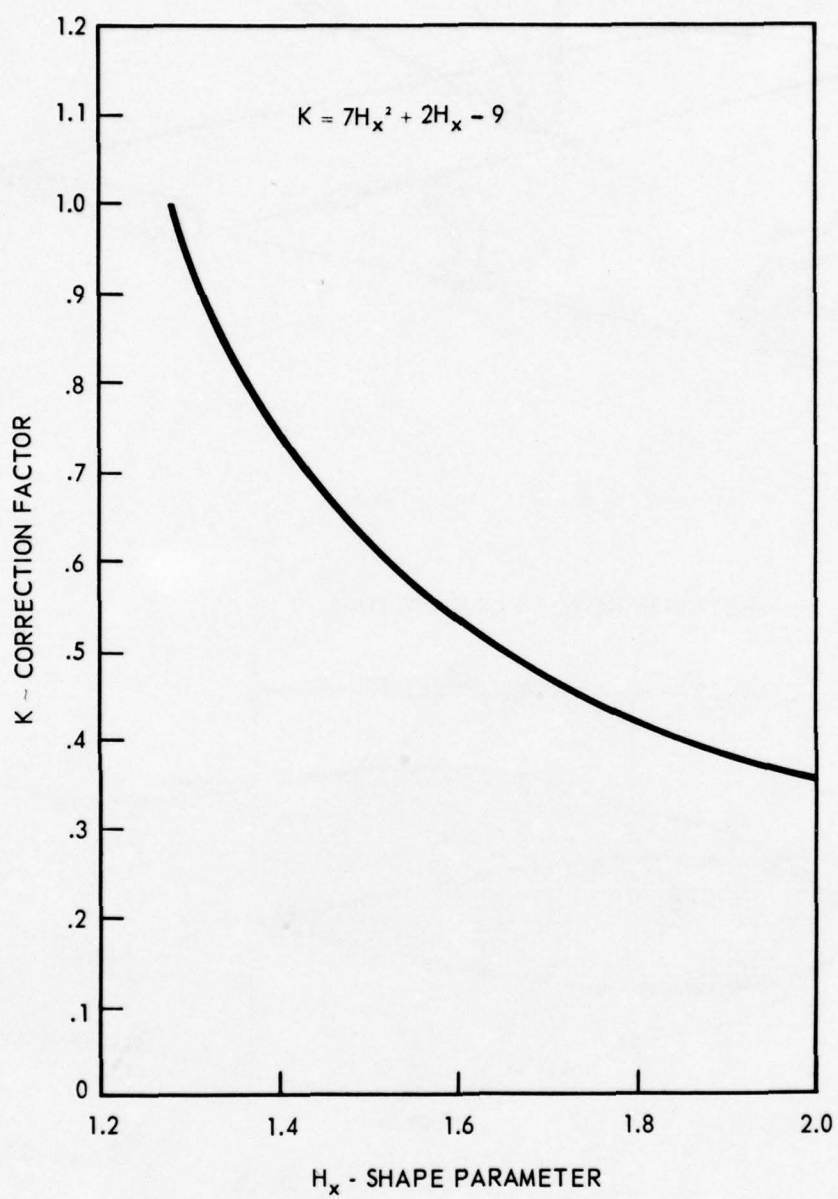
Figure 8. Mixed-momentum thickness correction factor.

240
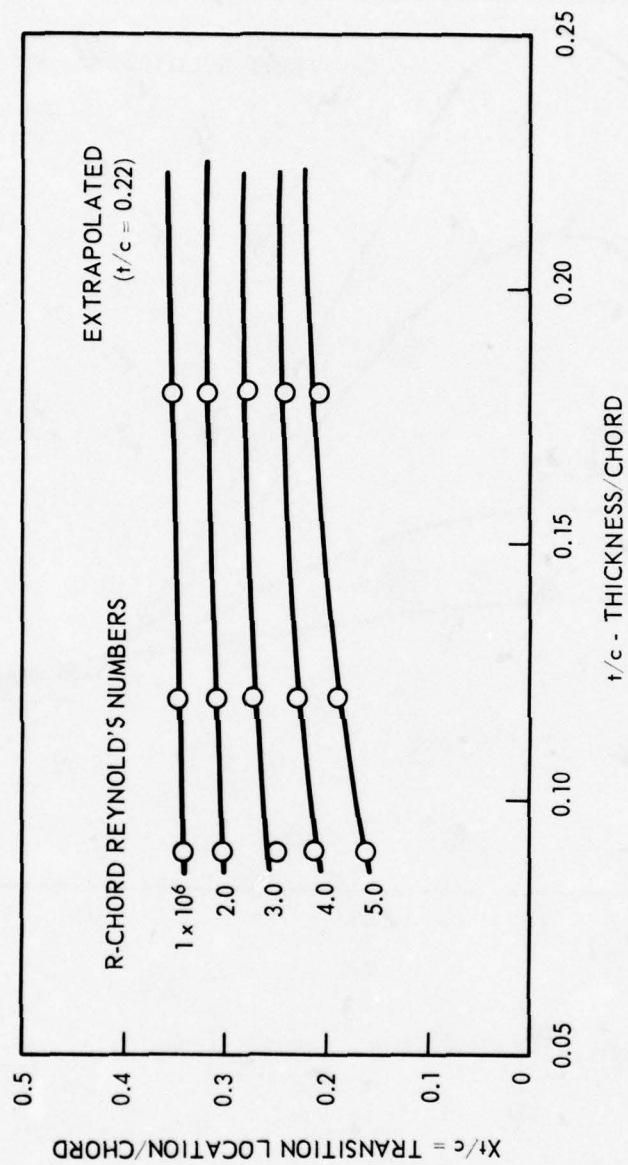
Figure 9. Transition location NACA-4 digit series section.
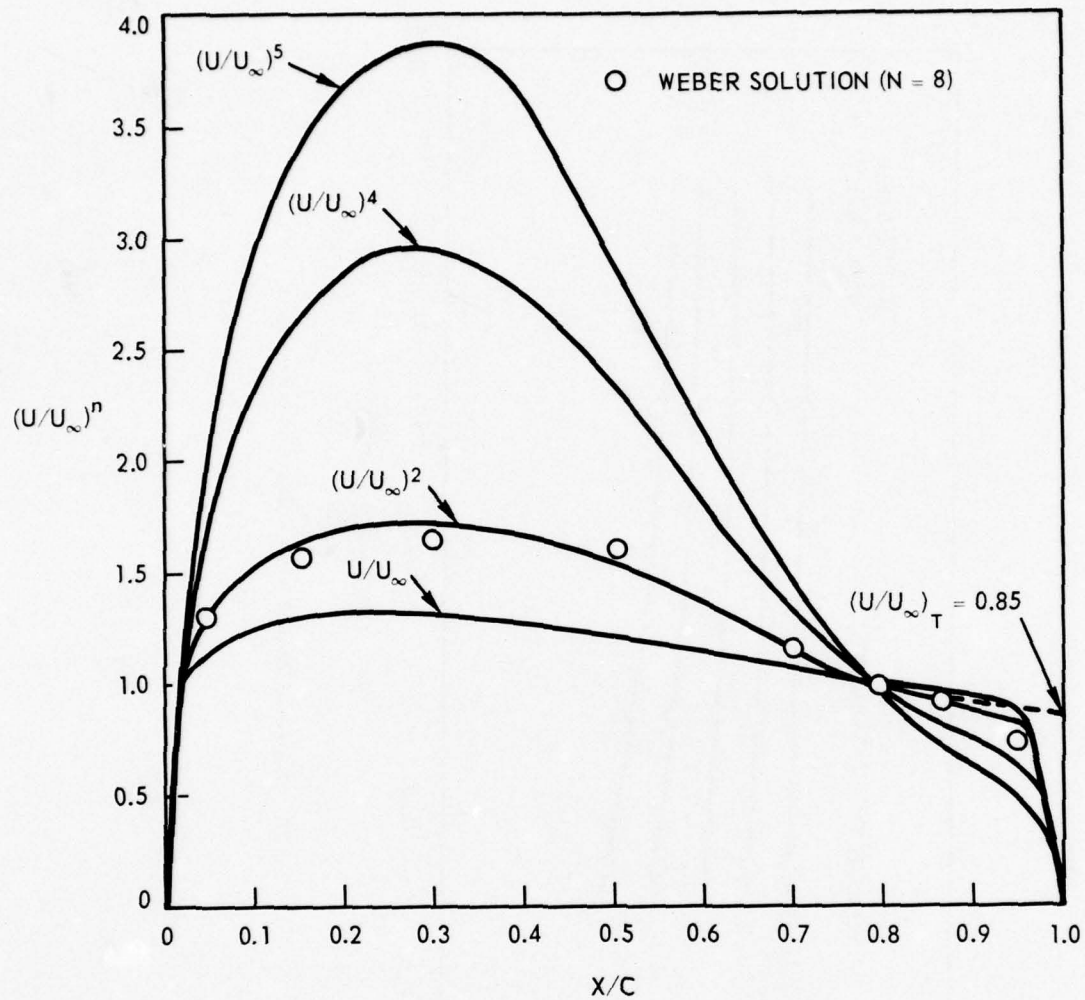
Figure 10. NACA 63A022 section ~ velocity distribution.
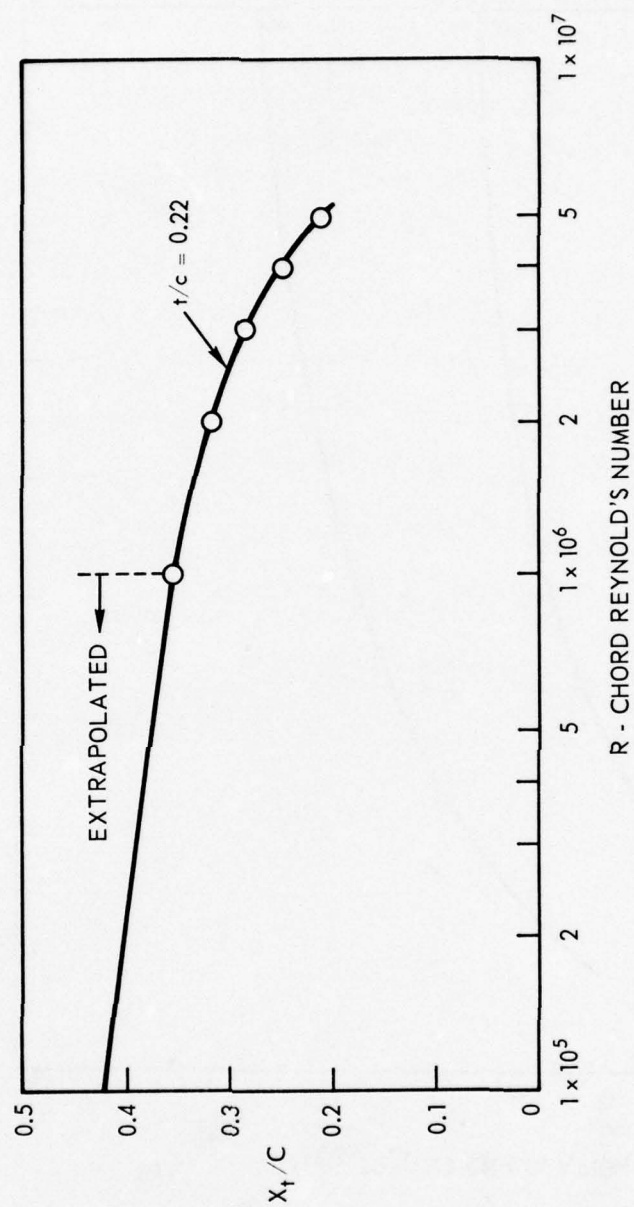
Figure 11. Boundary layer transition location.

t/c = 0.22

EXTRAPOLATED

X_t/C

R - CHORD REYNOLD'S NUMBER

0.5
0.4
0.3
0.2
0.1
0

1×10^5
2
5
1×10^6
2
5
1×10^7
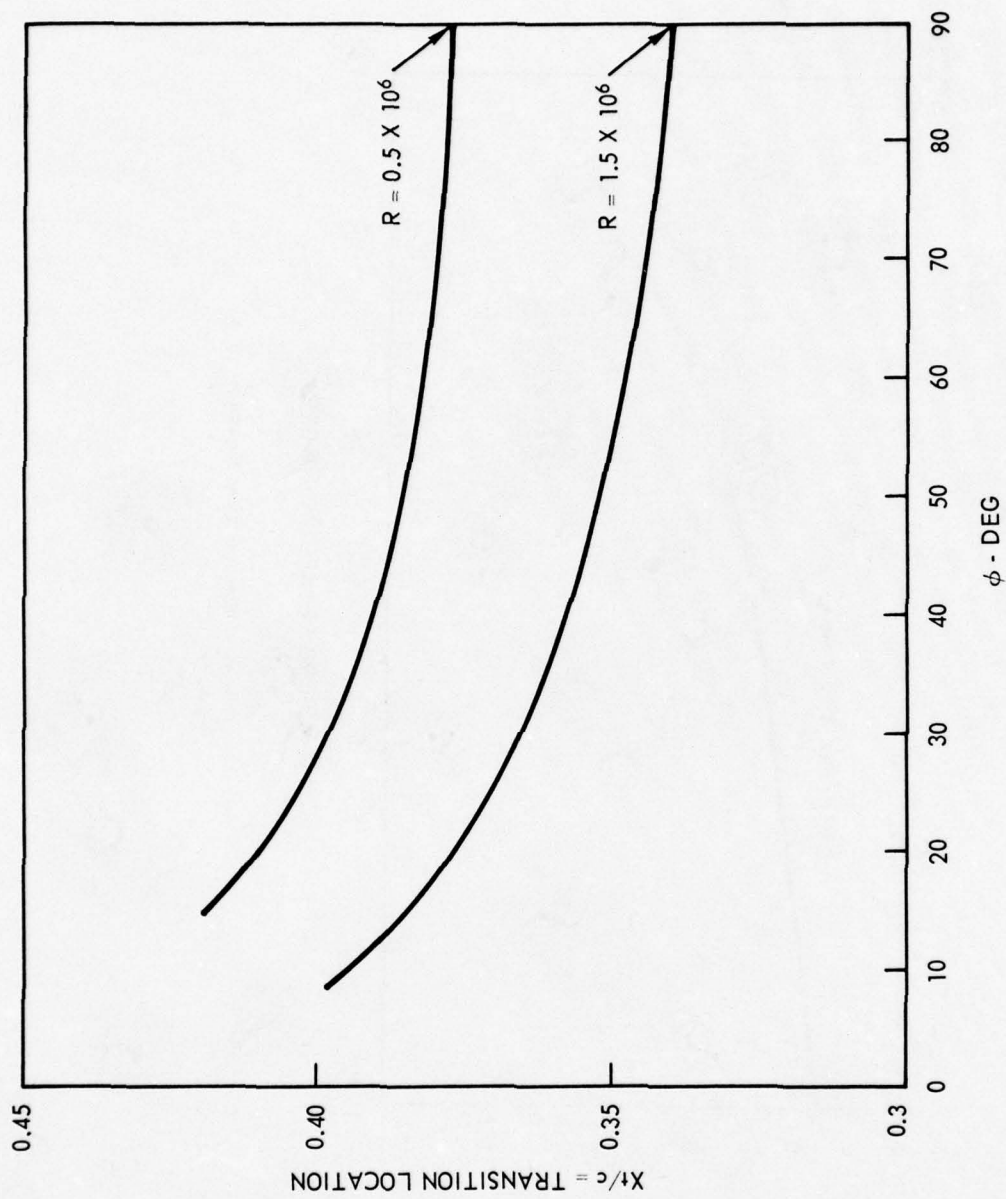
Figure 12.   Boundary layer transition location.
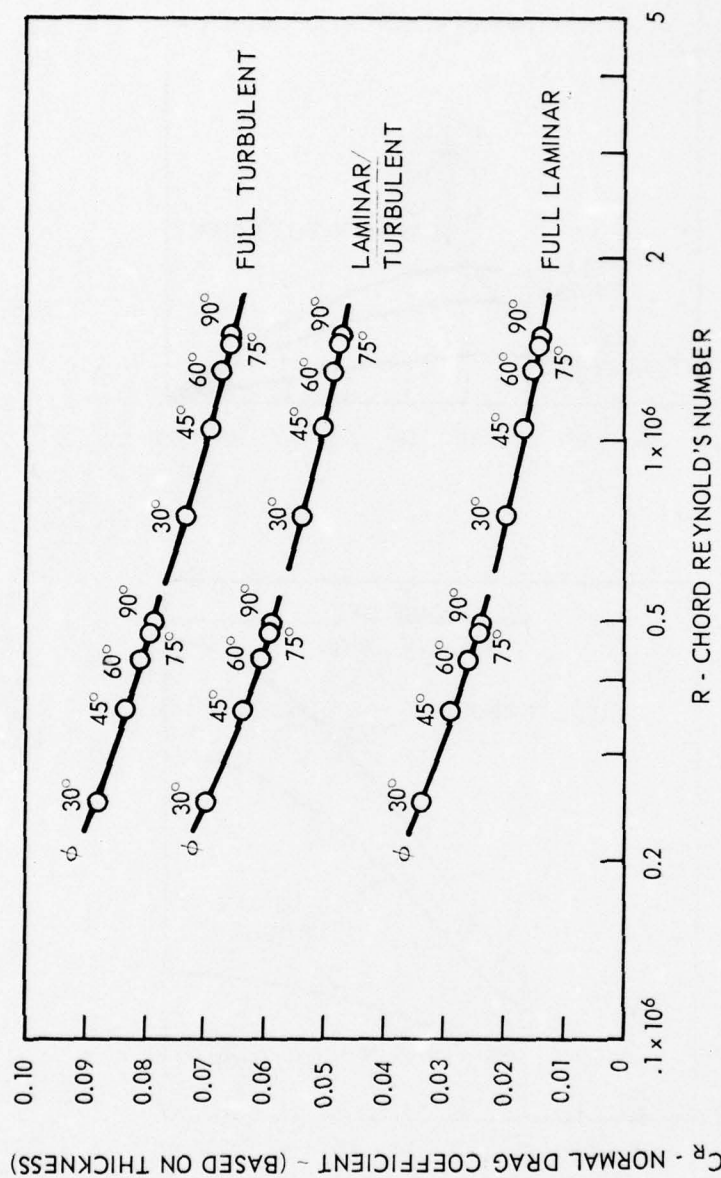
Figure 13. Computed normal drag coefficients.
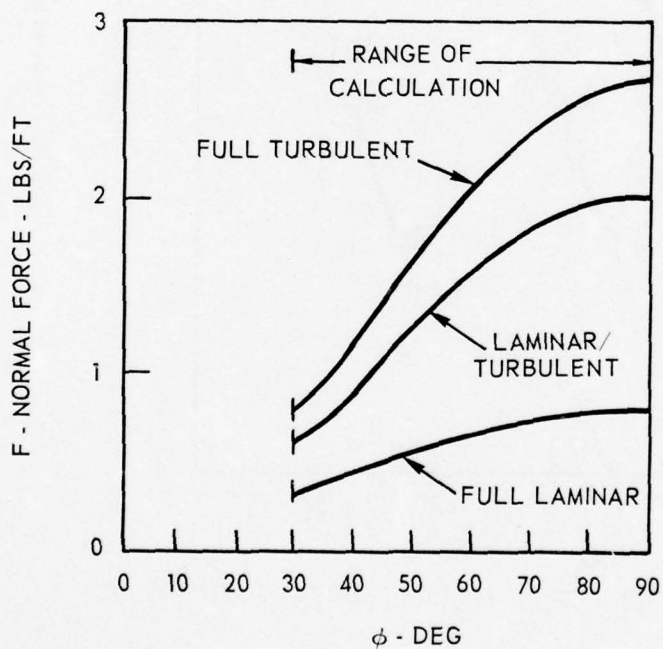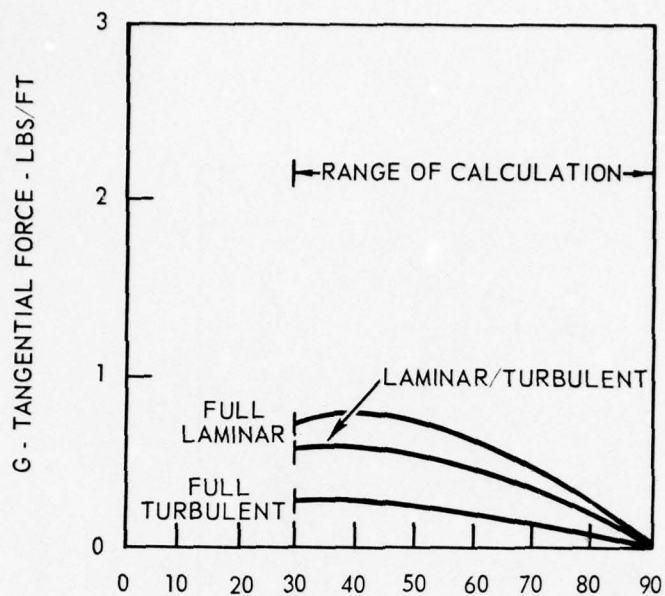
Figure 14. Computed BLLF forces (R = 0.5 x 10⁶ CASE).
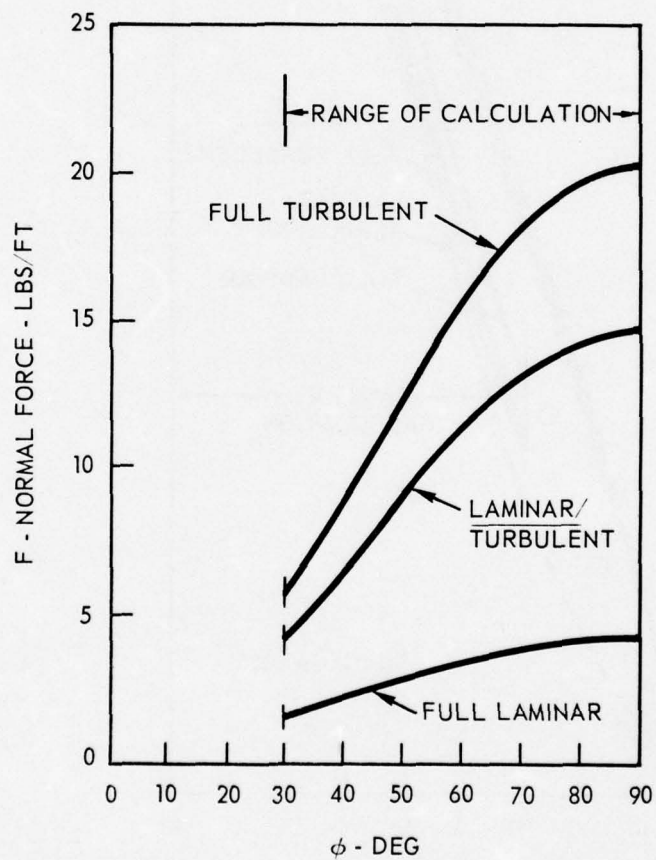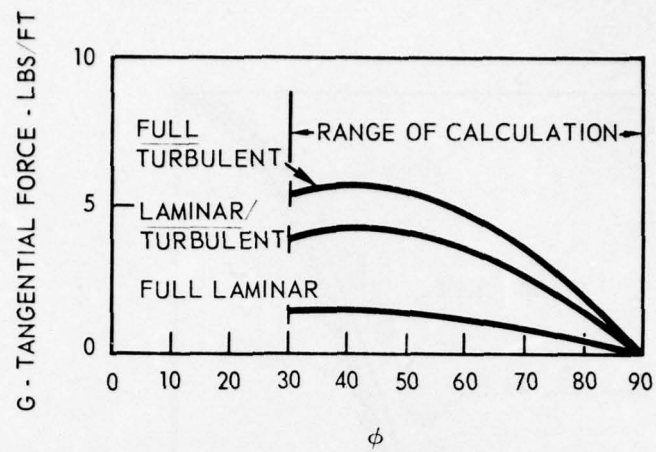
Figure 15. Computed BLLF forces (R = 1.5x10⁶ CASE).
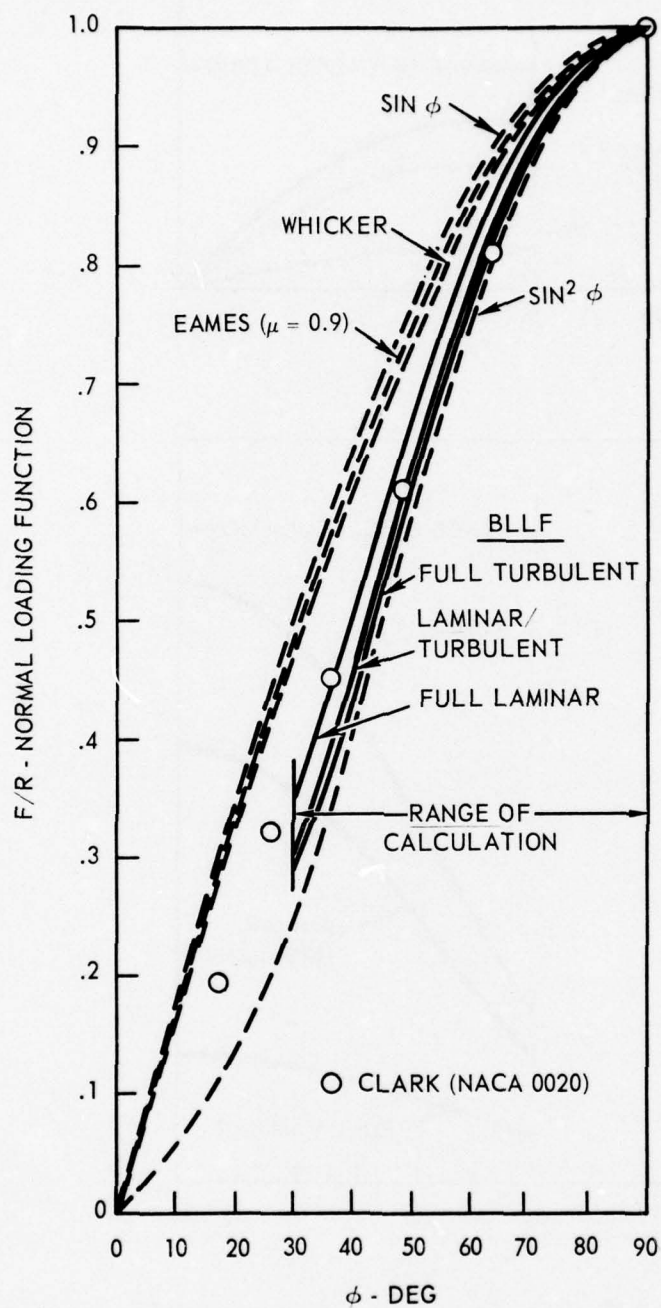
Figure 16.   Normal loading function comparison
(R = 0.5 × 10⁶ CASE).
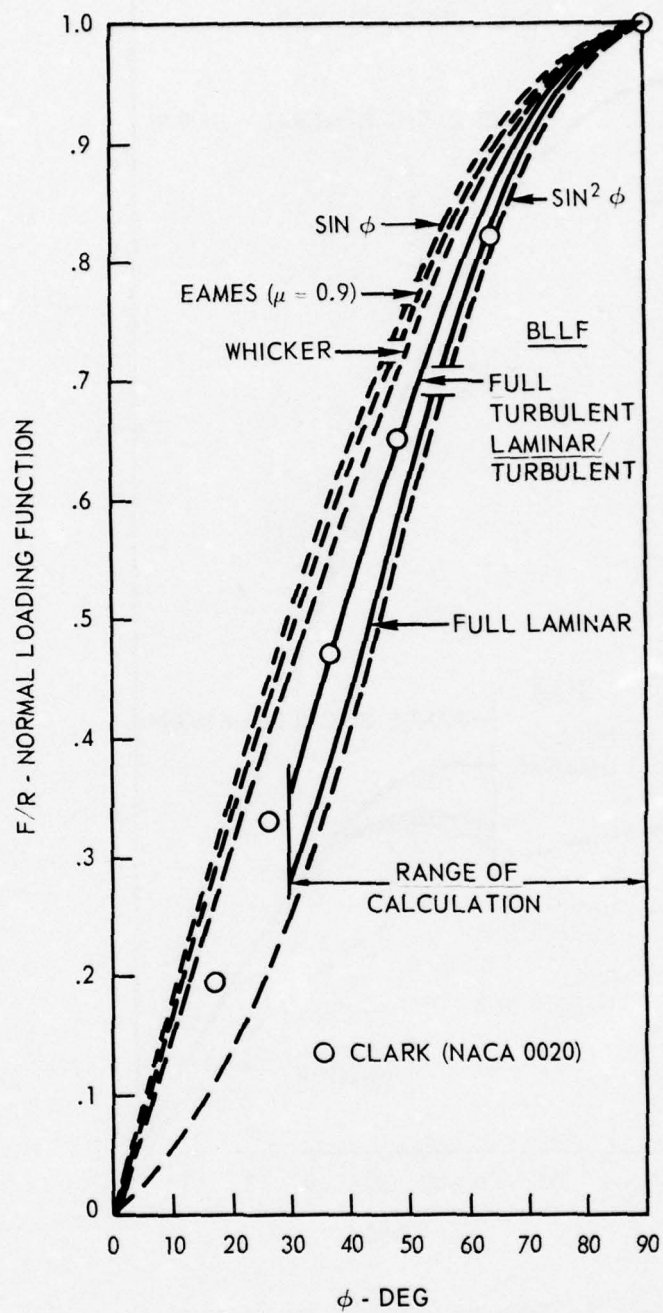
Figure 17. Normal loading comparison
$(R = 1.5 \times 10^6 \text{ CASE})$.
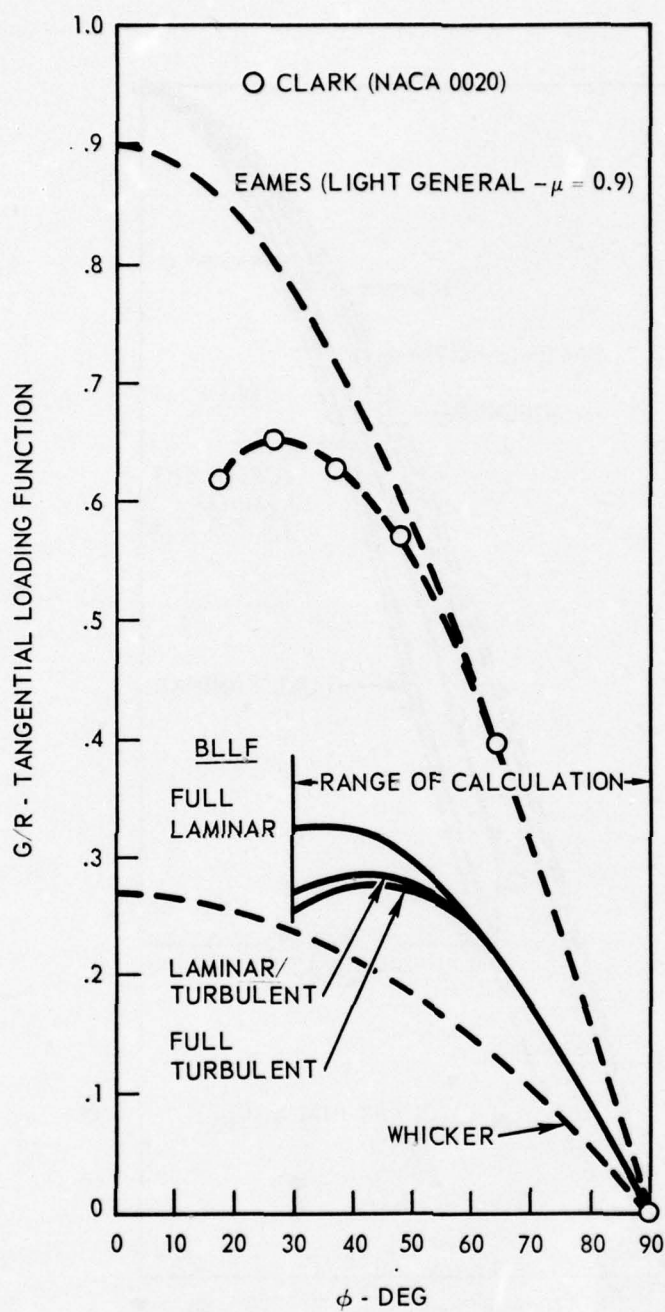
Figure 18. Tangential loading function comparison
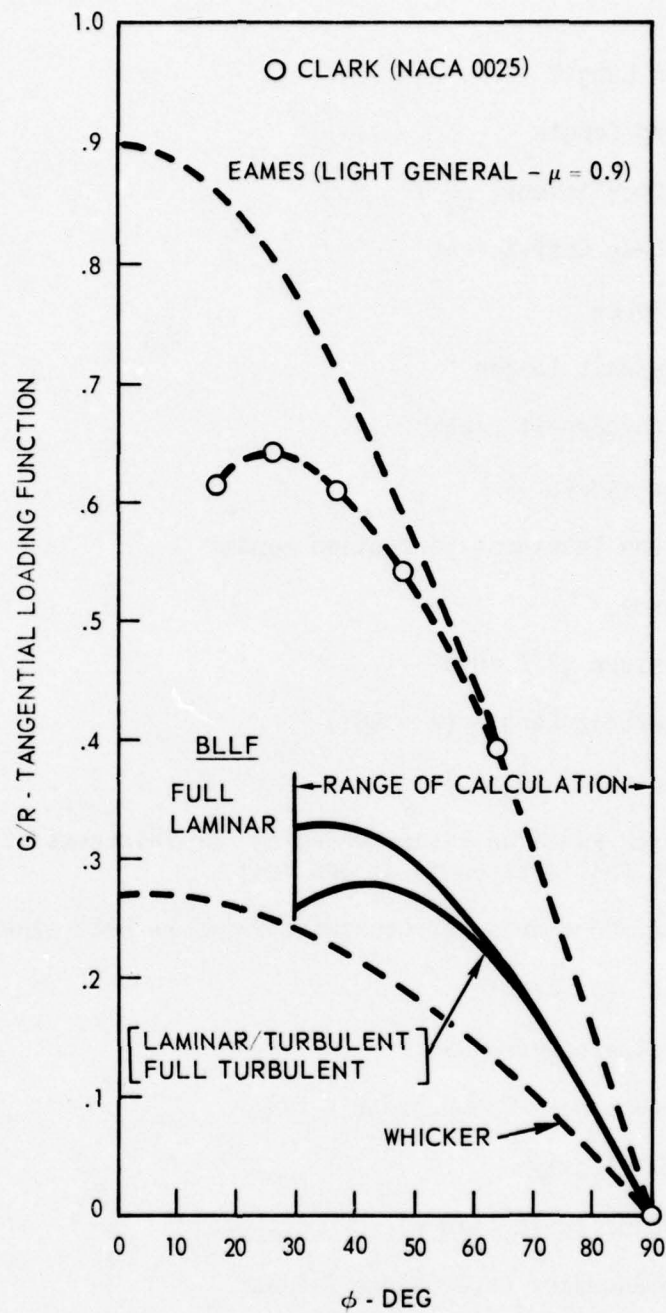(R = 0.5 x 10⁶ CASE).

Figure 19. Tangential loading function comparison
(R = 1.5 × 10⁶ CASE).

251

15.0 NOMENCLATURE

b - Towline Span Length

c - Towline Chord Length

C_R - Total Drag Coefficient($\frac{R}{qS}$)

C_f - Frictional Drag Coefficient

F' - Frictional Force

F - Normal Force/Unit Length

G - Tangential Force/Unit Length

H - Shape Factor (δ^*/θ)

K - Mixed Momentum Thickness Correction Factor

P - Pressure Force

Q - Dynamic Pressure ($1/2\ \rho U_\infty^2$)

R - Normal Force/Unit Length ($\phi = 90°$)

RN - Reynold's Number = ($U_\infty c/\nu$)

S - Reference Area Based on Either Chord(c), or Thickness (t)
     Where Length (b) is taken to be One Foot

$S^{(1,2)}$ (X) - Weber Constants For Chordwise Pressure Determination

t - Towline Thickness Length

t/c- Towline Thickness/Chord Ratio

u - Velocity in Boundary Layer Along X-Axis

U_∞ - Free Stream Velocity

U_0 - Chordwise Velocity ($U_\infty \sin \phi$)

v - Velocity in Boundary Layer Along Z-Axis

V_0 - Spanwise Velocity ($U_\infty \cos \phi$)

X - Distance Along Towline Chord

Y - Distance Normal to XZ Plane

Z - Distance Along Towline Length

δ - Boundary Layer Thickness

δ* - Boundary Layer Displacement Thickness

θ - Boundary Layer Momentum Thickness

μ - Friction Ratio (Eames Analysis)

ν - Fluid Kinematic Viscosity

ρ - Fluid Density

τ - Shearing Stress

φ - Local Towline Angle Measured From Horizontal

16.0 REFERENCES

16.1 United Aircraft Corporation, Report B110128-1, _Extension of Underwater Towing Cable Theory to High Speeds,_ by James W. Clark, September 1963

16.2 Naval Research Establishment, PHx-103, _The Configuration of a Cable Towing a Heavy Submerged Body from a Surface Vessel_, by Michael C. Eames, November 1956

16.3 University of California, _The Oscillatory Motion of Cable-towed Bodies_, by Lester Folger Whicker, Doctor of Engineering, Jul 16, 1957

16.4 Hoerner, Sighard F., _Fluid-Dynamic Drag_, Published by the Author, 1958

16.5 Royal Aircraft Establishment, Reports and Memoranda No. 1838, _The Calculation of the Profile Drag of Aerofoils_, by H. B. Squire, M.A. and A. D. Young, B.A., 18th November, 1937

16.6 Schlichting, Dr Hermann, _Boundary Layer Theory_, New York: McGraw-Hill Book Co. Inc, 1955

16.7 National Advisory Committee for Aeronautics, Technical Report No. 863 _Wing Plan Forms for High-Speed Flight_, by Robert T. Jones

16.8 National Advisory Committee for Aeronautics, _Technical Memorandum_ No. 1115, _Pressure Distribution Measurements at High Speed and Oblique Incidence of Flow_, by A. Lippisch and W. Beuschausen, March 1947

16.9 National Advisory Committee for Aeronautics, Technical Note 2160, _Measurements of Section Characteristics of a 45° Swept Wing Spanning a Rectangular Low-Speed Wind Tunnel as Affected by the Tunnel Walls_, by Robert E. Dannenberg, August 1950

16.10 _Journal of Aeronautical Sciences_, Vol. 15, No. 1, pp.49-52, _The Boundary Layer of Yawed Cylinders_, by W. R. Sears, January 1948

16.11 Aeronautical Quarterly, v.3, _The Profile Drag of Yawed Wings of Infinite Span_, by A. D. Young, M.A., F.R.Ae.S. and T. B. Booth, B.A., D.C.Ae., Nov.3, 1951

16.12 National Advisory Committee for Aeronautics, Technical Note 2500, _A Comparison of the Turbulent Boundary-Layer Growth on an Unswept and a Swept Wing_, by John M. Altman and Nora-Lee F. Hayter, September 1951

16.13 Journal of the Aeronautical Sciences, v.19, _Simplified Laminar Boundary-Layer Calculations for Bodies of Revolution and for Yawed Wings_, by Nicholas Rott and L. F. Crabtree, 1952

16.14 Royal Aircraft Establishment Report No: AERO.2497, <u>The Calculation of the Pressure Distribution Over the Surface of Two-Dimensional and Swept Wings with Symmetrical Aerofoil Sections</u>, by J. Weber, Dr.rer.nat.,

16.15 Thwaites, Bryan, <u>Incompressible Aerodynamics</u>, Oxford at the Clarendon Press, 1960

16.16 Aerodynamics Division, National Physical Laboratory, Phil. Trans., A, 248, 155-199, <u>On The Stability of Three-Dimensional Boundary Layers With Application to the Flow Due to a Rotating Disk</u>, by N. Gregory, J. T. Stuart and W. S. Walker

16.17 National Advisory Committee for Aeronautics, Report No. 637, <u>Determination of Boundary-Layer Transition on Three Symmetrical Airfoils in the N. A. C. A. Full-Scale Wind Tunnel</u>, by Abe Silverstein and John V. Becker

16.18 Abbott, Ira H. and Von Doenhoff, Albert E., <u>Theory of Wing Sections</u>, Dover Publications, Inc. New York

INVESTIGATION OF HYDRODYNAMIC LOADING FUNCTIONS ON FAIRED TOWLINES

By:

Dr. Lowell Collier
Arthur Brisbane
Leonard Davis
Hydrospace Research Corporation
Rockville, Maryland

ABSTRACT

Hydrospace Research Corporation conducted instrumented towing tests on two three-dimensional towlines, one with a fully enclosed sectional fairing and the other with a trailing clip-type fairing. Normal and tangential loading functions were derived as functions of cable angle. The normal loading functions were extrapolated to $\varphi = 90°$ to determine C_R for each fairing. These values of C_R were plotted as functions of Reynold's number and compared with measured two-dimensional data. The normal loading functions were non-dimensionalized by R and the ratios of F/R were analyzed as functions of cable angle. This analysis showed further Reynold's number dependencies.

INTRODUCTION

The faired towcable appears to be the key hydromechanical component of Variable Depth Sonar (VDS) Systems. It is this component that serves to transmit propulsive forces and surface generated disturbances to the housing, transmits electrical power to the transducer and the electrical analog of the acoustic information back to the surface, resists attainment of depth, establishes maximum system forces, and complicates handling and storage. A clear understanding of the hydromechanics of towcables is thus a prerequisite to the satisfactory resolution of the many problems involved in sonar-system design.

One of the more important and timely aspects of this topic is the true nature of the hydrodynamic loads imposed on the towline by the flow. The magnitude and direction of this force determines the local rate of change of its inclination and tensile load. The hydrodynamic load is in turn affected by the shape, size, and inclination of the cable. A description of the variation of the hydrodynamic loads acting on a length of towline is called a "cable loading function," or simply, "loading function." It is evident that the prediction of towline characteristics, i.e., the forces, the depth, and horizontal distance spanned, and the inclination, depends on the accuracy with which the force variation is described by the loading function.

Loading functions in current use are based on a combination of theoretical conjecture and limited experimental data. They are essentially two-dimensional

in nature; a postulate fundamental to their derivation being that the flow about any section is identical with that existing on a rigid cylinder having the same shape and cross section. The results obtained on application of the various forms do not agree, and discrepancies between predicted and measured performance have been observed in the field.

This paper summarizes the results of test on three types of faired towlines. The three types are as follows:
1. Continuous, fully enclosed;
2. Trailing type, and
3. Fully enclosed sectional.
The characteristics of the three fairings are listed in Figure 1.

BASIC CONSIDERATIONS AND TEST THEORY

We restrict our considerations to steady-state (no time dependence), plane configurations. The plane is that one defined by the direction of gravity and the direction of translation of the towing vessel. The towed system is thus considered to translate rectilinearly in the direction normal to gravity. Configurations not lying wholly within this plane are of practical interest. Such configurations are said to "kite." "Kiting," however, is an undesirable phenomenon and the interest in this area is only to understand its effect on the system geometry in order to correct the situation rather than to predict the degree.

The scope of this problem is thus reduced to consideration of an idealized towing configuration in equilibrium. Computation of the equilibrium configuration of a cable-towed system in terms of its geometry and towline tension involves consideration of both the towline and the towed body. The individual forces acting on these components must be determined and the way in which they combine to produce the configuration must be defined. Gravitational, displacement, and hydrodynamic forces are involved.

In treating the problem of computing the configuration, the body and towline are separable. *

Consider the requirement for specification of the boundary condition in the solution of the problem. The boundary condition (T_o, φ_o) represents the force developed by the body and establishes the reference point from which the integration of the towline equations may commence.
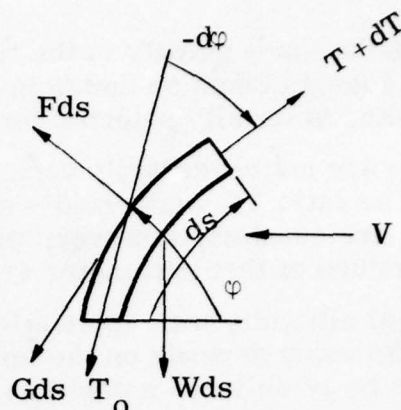
Examining the towline, the equations describing the equilibrium of an incremental segment may be written:

---

*With the exception, perhaps, of that small region of towline immediately adjacent to the body.

258

$$F = -T \frac{d\varphi}{ds} + W \cos \varphi$$

and

$$G = \frac{dT}{ds} - W \sin \varphi ,$$

where the F and G represent the hydrodynamic force components per unit length resolved in the directions normal and tangential to the element, T is the tension in the line, and W is the unit weight of towline in water. These equations express the static force balance on the assumption of a plane configuration containing the gravitational vector and negligible bending moments in the fairing and cable. As such, they are independent of any assumption regarding the nature of F and G.

The solution to the problem now depends on specification of the hydrodynamic loading functions, F and G. From what is known of the nature of hydrodynamic forces a list of probably influencing parameters can be formed:

1. Velocity of tow,
2. Fairing type, thickness, chord length, surface roughness,
3. Fluid density and viscosity, and
4. Angle of inclination to the flow.

These represent a minimum listing of the important parameters. The influence of other factors is suspected, e.g., the effect of the flow over neighboring elements on the hydrodynamic force on a particular element. We observe that if F and G are functions <u>only</u> of the angle and speed, we may write,

$$F = F(\pi/2) \, F'(\varphi)$$

and

$$G = G(0) \, G'(\varphi) ,$$

where $F'(\varphi)$ and $G'(\varphi)$ are functions of the angle only. Now $F(\pi/2)$ is the resistance per unit length of the towcable when normal to the stream. It is, then, just the drag per unit length. This value is typically designated by the symbol "R." The similarity principle mentioned earlier permits the measure of R to be taken from a strut of similar cross-sectional shape. Similarly, G(0) is the tangential force per unit length when the cable is parallel to the stream.

In general, the values of R and G(0) depend on the velocity of tow and the shape and size of the fairing. We may define force coefficients, C_R and C_G, as follows:

$$C_R = R/(1/2 \, \rho \, V^2 \, d) \quad \text{and} \quad C_G = G(0)/(1/2 \, \rho \, V^2 \, d),$$

Where ρ is the mass density of the fluid (e.g., sea water) and d is a typical measure of length taken on the right-section of the fairing. The breadth, or frontal width, is usually selected for this measure.

C_R and C_G are not necessarily constant. Values of C_R measured at identical values of the ratio Vd/ν (Reynold's number), where ν is the kinematic viscosity, are constant, however, whereas values of C_G measured at identical values of that parameter are not necessarily constant.

An essential difficulty with application of the concept of G(0) is immediately evident. Its value depends on the length of cable parallel to the flow. Since this cannot be established a priori for any given configuration, the value of the measure of G(0) is doubtful.

If, then, values of tension and angle can be measured as a function of distance along a faired towline of known weight and at a known speed, all values necessary for the solution of F and G are available.

On the basis of the foregoing, it was decided that the most direct approach to resolution of the loading function problem was to obtain measures of the hydromechanical loads directly from a real configuration. As with all experimental work, certain practical considerations impose limitations on the experimental technique.

The ideal experiment would consist of obtaining simultaneous measures of the tension and angle at closely spaced intervals along a long cable towed at constant speed. This procedure would require depths obtainable only at sea and a very expensive specially designed and constructed, instrumented, test fairing.

An alternate approach consists of obtaining the desired measures at the surface and changing the scope for each run. This procedure is as valid as the one outlined above, provided that no element of the fairing is affected by the presence of the elements situated farther up the towline. But the latter is an effect we seek to discern.

Of even greater importance, it is absolutely necessary that the test fairing be steady and stable under tow and give repeatable results.

A determination of the required test conditions necessary for conducting a meaningful test program was made. Steady-state towing, or as close to steady-state conditions as possible, was needed. The size and the incremental length of the cable and fairing used had to be large enough to produce measurable forces, yet small enough to produce closely spaced data and to facilitate practical handling techniques and equipment. Forces, on the other hand, had to be small enough to permit obtainment of a good range of cable angles and towing speeds. Based on these considerations, it was decided that the Hydrospace Research Corporation test facility in Martinsburg, West Virginia, would give close to steady-state conditions, and would be suitable to conduct such a program. It was also decided that 0.3 inch and 0.5 inch diameter cables and fairing, tested in 10-foot increments, would provide suitable test models.

In order to tow such a faired cable, a multi-purpose depressor was needed. This depressor had to meet the following requirements: be stable under steady tow; produce downward forces large enough to control the behavior of the towline; produce constant T_o and φ_o at constant speed; and be large enough to house required bottom end instrumentation.

The instrumentation for the test program included that required to measure tension and towline angle at the surface and tension and angle at the body, body depth and attitude, and towing speed.

The body used in the investigation was a hull of revolution, designed by Hydrospace Research Corporation. It had a fineness ratio of 5 and used both a shroud ring tail and boundary layer wedges to provide high stability in pitch and yaw. Roll stability was provided by a low center of gravity, with the towpoint attached 1.5 feet from the nose, and two inches above the body centerline.

The body housing contained two watertight containers, one of which housed pitch and roll pendulum pots, a pressure transducer to measure depth, and the associated electronics for the bridge type transducer. The second can contained the 26 volt battery pack which supplied the power to the electronics in the body. Additional body instrumentation included a pendulum pot attached to the towstaff to measure towstaff angle, and a strain gaged flexure to measure tension at the body. Figure 3 shows the arrangement of these various items.

TEST PROCEDURES

With the body trimmed and ballasted to its test weight it was towed over the full range of speed for each scope to assure no kiting of the system. This was done for each towline.

The system at this point was considered ready for data acquisition. At dockside, before each test, the body and the length of test scope were lowered into the water and the cable angle potentiometer was clamped to the fairing at the proper location between the towline storage drum and the water surface.

With the towline hanging vertically in the water and the towboat tied to the dock, the instrument operator, to assure that the instruments were functioning correctly, checked and recorded:

1. battery voltage
2. reference voltage
3. calibration voltage
4. roll, pitch, and towstaff angles
5. body tension
6. top tension
7. depth
8. cable angle

The readings recorded for roll, pitch, and towstaff angle were then checked against known readings for each of these potentiometers. The body tension reading was checked against the known weight of the body in water. The top tension was checked against the known body weight in water plus the weight of the cable angle potentiometer and its clamp, plus the known weight of the length of test scope. The depth reading was checked against the length of scope payed out for the test.

During a run, the instrument operator used a nulling voltage to bring the pens into the range of the recorder as quickly as possible. At the end of each run, each channel on the recorder was monitored and a plus or minus value was assigned to the difference between the actual pen trace and the preselected null position of each channel. This value was then added or subtracted from the null reading for each channel and recorded along with the knotmeter reading.

An immediate conversion of this data was made before the next run to insure the consistency of the data taken. At the end of each run, the instrument operator checked all the electrical calibrations. This procedure was repeated for every run until the entire speed range for the particular scope was completed. The above procedure was used on all speeds and scopes tested.

PRESENTATION OF DATA

Figures 4, 5, 6, and 7 show the data recorded for the trailing type fairing. The data recorded for the other two fairings is similar in form and is not shown here.

Delta top tension is defined here as the difference between tension at the upper end of the towline at a particular speed and the top tension at zero speed for the same scope, or in other words, the top tension increase due to speed. Delta bottom tension is the towline tension at the body at a particular speed minus body weight in water, which was 241 pounds. Figures 4 and 5, since they are a measure of the body characteristics, define the lower boundary conditions of both towlines, and as such they are expected to remain constant and repeatable for a given speed. A review of Figures 4 and 5 shows that this data is both repeatable and free of any influence due to cable scope except the tension data for the 10-foot scope (dashed curve on Figure 5). This discrepancy was determined to be due to effects produced on the body by the nearness of the towboat for the short scope tow. A correction on top tension was made for this effect.

Figures 6 through 7 are presented as an illustration of the quality of the data. The scatter of the angle data is nearly all within plus or minus one degree of a fitted curve and the tension data is within plus or minus two pounds, but with a few exceptional points which are as much as six pounds from the curve. These tolerances are approaching the basic accuracy of the transducer-recorder system. Therefore, the data is considered to be the best that can practically be obtained with the present experimental system.

DATA REDUCTION

The loading function coefficients were calculated from the equations

$$F = -T \frac{d\varphi}{dS} + \underline{w} \cos \varphi ,$$

$$G = \frac{dT}{dS} - \underline{w} \sin \varphi .$$

The top angle vs speed and top tension vs speed curves for all scopes were used to obtain cross-plots of φ vs S and T vs S from which the derivatives in the above equations could be computed. However, since φ and T were measured at discrete scopes, a method of interpolating between these points was needed. A finite polynomial curve was fitted to the data in order to carry out the interpolation. The method of least squares was used to obtain this fit. In Figures 8 and 9 the data points are indicated by the symbols and the curves are the mathematical fits to these data points. The percent difference between any datum point and the curve is much less than the 1% accuracy of the measuring instruments.

A second degree polynomial fits both φ vs S and T vs S data. This is not meant to imply that φ and T are actually quadratic functions of S, but that this was the method used to evaluate the functions and the derivatives over the scopes tested. The fitted curves cannot be extrapolated to longer scopes since the quadratic is an approximation good only for the scopes tested. The justification for using a quadratic equation is that the experimental data indicated that φ and T were monotonically increasing functions of S and a quadratic polynomial gave such a fit. A higher degree polynomial would fit each data point more exactly but would also give inflection points between the data points, a situation which is contrary to the experimental evidence.

The fitted curves were used to calculate $\frac{d\varphi}{dS}$ and $\frac{dT}{dS}$. Knowing tension and angle and their derivatives with respect to scope, the hydrodynamic forces per unit length, F and G, were then calculated from the equations of equilibrium. The coefficients C_F and C_G are non-dimensionalized by

$$C_F = \frac{F}{q d}$$

$$C_G = \frac{G}{q d}$$

where q is the dynamic pressure and d is the frontal width of each assembled towline.

Figures 10 and 11 show C_F versus φ for the three fairings tested. Notice that the curves for each speed are quite distinct from each other, indicating C_F is a function of Reynold's number.

Curves of C_G versus φ for two fairings tested are shown in Figure 12. Notice that for the enclosed sectional fairing at 4 and 6 knots the C_G is negative. This would indicate that the tangential force is directed up the cable and this could only be caused by a flow up the cable. The cable is at a steep angle and the Reynold's number is low. The G forces are about one order of magnitude less

than the F forces. Also, the G forces are not measured directly but are determined indirectly by measurement on tension and angle. Consequently, the negative forces may not be real but may only be artifacts of the experiment. However, just as there may be a reversal of flow on a swept wing aircraft so there may be a reversal of flow on this fairing at angles close to 90 degrees. Surface effect may be very important in this low Reynold's number range. Future experiments along with some theoretical investigation of the hydrodynamic forces on a catenary are needed to resolve this question. The trailing fairing does not show a negative G force for 6 through 12 knot speeds, but the 4 knot speed did indicate that G was negative. Above 6 knots the C_G curve is almost independent of speed for the trailing fairing. However, the 4 knot curve is not shown as the curve fitting technique for the tension curve did not give a good fit to the data.

Many tests have been conducted on faired cables in wind tunnels and water channels in order to deduce a drag coefficient for various angles of inclination of the cable. The results of these tests are difficult to compare with data obtained for catenary shaped cables. The data obtained in the HRC tests were extrapolated to $\varphi = 90^O$ in an effort to compare these results with the data obtained from two dimensional tests. The extrapolation is necessary since all data obtained in the tests were for angles less than 90°. Two methods of extrapolation were used. The methods are as follows:
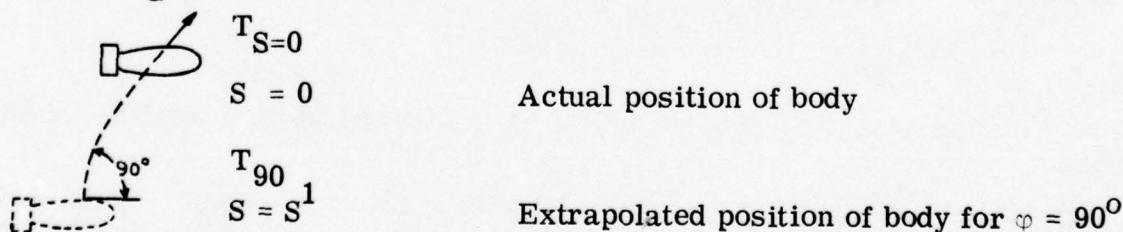
1. The curves of angle versus scope were individually extrapolated to $\varphi = 90^O$ and

$$C_R = \frac{T}{qd} \left. \frac{d\varphi}{dS} \right|_{\varphi = 90^O}$$

The tension was calculated from the equation

$$T_{90} = T_{S=O} - \int_{S=0}^{S=S^1} W \sin \varphi \, ds + \int_{S=0}^{S=S^1} G \, dS$$

and the integral involving G is neglected. The G integral would change T_{90} by only a few percent, the C_G range being 0.0 to 0.02 over the interval. See Figure 12 C_G vs φ. The notations S and S^1 are explained in the following figure:

$T_{S=0}$

$S = 0$ Actual position of body

T_{90}

$S = S^1$ Extrapolated position of body for $\varphi = 90^O$

2. The second method used was to fit a curve to C_F versus φ plots of the form

$$C_F = A + B \sin \varphi + C \sin^2 \varphi$$

and

$$C_R = C_F \left. \right|_{\varphi = 90}$$

264

The constants A, B, and C would then be functions of speed. The method of least squares was again used to determine the equation.

The two methods gave C_R's that were within about 5% of each other except for the 10 knot and 12 knot speeds on the plastic fairing. Only the first method was used to calculate C_R for these two speeds, as the second method did not give a good fit to the data.

The curves of C_R versus Reynold's number, Figure 13, indicate that for speeds less than 8 knots on the enclosed fairing C_R is related to Reynold's number by

$$C_R = \frac{Const}{Rey}$$

The same relationship is approximately true for the trailing type fairing. C_R for the trailing fairing is approximately constant above a Reynold's number of 5×10^4. The general form of the two curves are similar and they are also similar to the curves obtained from a two-dimensional fairing test, which was run in the DTMB water channel and was reported in Ref. 10. Figure 13 also contains data for Model B, an identical shape but different size enclosed fairing, and Model E, a trailing type fairing, taken from that reference.

The fully enclosed fairing is a more streamlined body than the trailing type fairing as is indicated by the lower values of C_R at all Reynold's numbers. A parameter indicative of the amount of streamlining of the fairing and cable should, therefore, be considered in analyzing the data, i.e., ratio of fairing thickness to cable diameter diameter. The trailing fairing in this study is then "rougher" than the enclosed fairing. Rough in this context means a body that is not well streamlined, or one that may have separation near the junction of the back side of the cable and the leading edge of the fairing.

Notice that for the enclosed fairing C_R decreases with Reynold's number from 4 to 10 knots but after 10 C_R begins to increase with Reynold's number. This increase in C_R around 10 knots could be interpreted as a transition range from laminar to turbulent flow. C_R would increase if the flow changed from laminar to turbulent due to the increase in the shear stress. The separation point on this well streamlined body would probably not change appreciably in the transition range and thus the pressure drag would not decrease as is the case for a circular cylinder. The total increase in C_R would then be due only to the increased shear stress.

The trailing fairing does not show a transition range, indicating that the flow is probably fully established turbulent. This would, of course, be due to the roughness of the fairing.

Many investigators have assumed loading functions of the form

$$C_F = C_R \, f(\varphi)$$

where C_R is the normal force coefficient for $\varphi = 90^O$ and $f(\varphi)$ is a function of cable angle usually in the form of $\sin \varphi$ and $\cos \varphi$. This means that the Reynold's number dependence (speed effect) for C_F is the same as that for C_R. Under this assumption

$$F/R = \frac{C_F}{C_R} = f(\varphi)$$

265

and f (φ) is independent of speed. Figure 14 of F/R versus φ indicates that this assumption is only partially true. There is an indication that F/R does depend on Reynold's number and, as mentioned previously, the degree of streamlinedness of the cable and fairing.

Let us consider the following in analysis of the F/R versus φ curves for both trailing type fairing and enclosed fairing.

      1. For the trailing type fairing, F/R is almost independent of speed for 6 through 12 knots but the curve for 4 knots is different from the other four speeds.

      This seems to indicate that below a certain speed for this fairing F/R depends on Reynold's number while above this speed F/R is almost independent of speed. Notice that all of the independent data falls completely above the $\sin^2 \varphi$ curve, which is included in Figure 14.

      2. For the enclosed fairing the same reasoning applies except that the 4, 6, and 8 knot curves are separate while only the 10 and 12 knot curves are almost independent of speed. The enclosed fairing is a better streamlined body than the trailing type fairing. Thus, the transition from F/R dependent on Reynold's number to F/R as only a function of angle takes place at a higher Reynold's number.

These two considerations indicate that F/R depends not only on angle but also on Reynold's number and roughness, and that above a critical Reynold's number, the assumption that F/R is only a function of angle is probably good. The critical Reynold's number depends on the roughness of the cable and fairing. The theory that there exists a critical Reynold's number dependent on the shape of the fairing above which F/R is only a function of angle should be investigated in future tests, along with a wider range of cable angle to see if F/R is only a function of angle above that critical Reynold's number.

CONCLUSIONS

Reynold's number effects were observed on both towlines. Since only a small portion of the data appeared to be free of such effects, no attempt was made to derive general expressions for the loading functions. It is evident that data taken at Reynold's numbers above the transition range are needed to permit the fit of a mathematical expression to the loading functions.

For both towlines, extrapolated values of C_R show the same general trend as two dimensional test results obtained with geometrically similar fairing. However, each set of three dimensional data was consistently higher than the corresponding set of two dimensional data. This difference is believed to be real and due to effects of curvature and possible cable-body interaction.

Above the Reynold's number at which transition occurs the limited data of these tests indicate loading functions that are close to the F/R = $\sin^2 \varphi$ law. However, the trailing fairing values were greater than the $\sin^2 \varphi$ law and there utilization would result in predictions of shallower tows with higher tensions.

The enclosed sectional fairing data would predict deeper tows and lower tensions than those given by a F/R = $\sin^2 \varphi$ loading function.

The negative values of G were due either to an upward vertical component of flow or to difficulty in measuring tangential components when the towline is at steep angles and low Reynold's numbers. The latter is the more likely.

The questions concerning the dependence of the forces on the shape of the catenary and the effect of upstream sections on the forces at a given point have not been settled.

NOMENCLATURE

F	normal hydrodynamic force per unit length
G	tangential hydrodynamic force per unit length
R	drag/unit length of cable when cable is normal to the direction of motion
V	horizontal velocity component
C_R	normal force coefficient when cable is normal to the direction of motion
C_F	normal hydrodynamic force coefficient
C_G	tangential hydrodynamic force coefficient
T	cable tension
W	cable weight in water
φ	angle of inclination to the flow
d	frontal width of fairing
ρ	mass density of the fluid
ν	kinematic viscosity
T_o	resultant force developed by the body
φ_o	cable angle at the body (e.g., towstaff angle)
S	length of cable in water (scope)

ACKNOWLEDGEMENT

BIBLIOGRAPHY

(1) Gay, S. M., Brisbane, A., Davis, L. I., and Nelligan, J. J., "Investigation of Hydrodynamic Loading on Faired Towline," Hydrospace Research Corporation, Report 119, Jan. 15, 1965.

(2) Relf, E. F., and Powell, C. H., "Tests on Smooth and Stranded Wires Inclined to the Wind Direction, and a Comparison of Results on Stranded Wires in Air and Water," R&M 307, January 1917.

(3) Glauert, H., "Heavy Flexible Cable for Towing a Heavy Body Below an Aeroplane," R&M 1952, February 1934.

(4) Pode, Leonard, "Tables for Computing the Equilibrium Configuration of a
     Flexible Cable in a Uniform Stream," David Taylor Model Basin
     Report No. 687, March 1951.

(5) Reber, R. K., "The Configuration and Towing Tension of Towed Sweep
     Cables Supported by Floats," Report No. 75, Mine-Sweeping Section,
     Bureau of Ships, Department of the Navy, Washington, D.C.
     February 18, 1944.

(6) Eames, M.C., "The Configuration of a Cable Towing a Heavy Submerged
     Body from a Surface Vessel," Naval Research Establishment (Canada),
     Report No. PHx-103, November 1956.

(7) Whicker, L.F., "The Oscillatory Motion of Cable-towed Bodies,"
     University of California Report Series No. 82, Issue No. 2, 1957.

(8) Powell, C.H., "The Resistance of Inclined Struts," R&M 599, March, 1919.

(9) Lofft, R.F., "Variable Depth Asdic Resistance and Lift of Cable Fairing
     When Inclined to Direction of Flow," Admiralty Experimental Works,
     Report No. 31/58, July 1958. (SECRET)

(10) Nelligan, J.J., and Gibbons, T., "Evaluation of Six Types of Cable-Fairing
     for the Ship-Towed Sonar Program," David Taylor Model Basin
     Report C-1015, December 1958. (CONFIDENTIAL)

(11) Collier, Lowell, Brisbane, A.P., Davis, L.I., "Investigation of Hydro-
     dynamic Loading Functions on Two Faired Towlines," Report No. 142,
     November, 1966.

FAIRING CHARACTERISTICS

Parameter	Trailing Fairing Towline	Enclosed Sectional Fairing Towline	Continuous Fully Enclosed Towline
1. Shape	Mod. DTMB No. 7	DTMB No. 7	DTMB No. 7
2. Frontal Width	0.46 inch Max.	0.44 inch Max.	0.50 inches Max.
3. Fineness Ratio	6	6	6
4. Wt. Water	0.55 lb/ft	0.53 lb/ft	0.2 lb/ft
5. Length	10 ft/Section	4 inches/Section	Continuous
6. Cable Diameter	0.53"	0.3"	0.3"
7. Material	Rubber & Stainless Steel Clips	Stainless Steel Nose and Plastic After Body	Rubber
8. Breaking Strength*	20,000 lbs	6,000 lbs	6,000 lbs

* Of Cable

Figure 1

$$F = -T \frac{d\varphi}{ds} + W \cos \varphi$$

$$G = \frac{dT}{ds} - W \sin \varphi \, ,$$
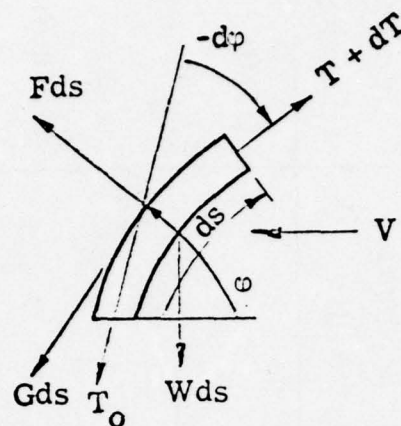
The coefficients C_F and C_G are non-dimensionalized by

$$C_F = \frac{F}{qd}$$

$$C_G = \frac{G}{qd}$$

where q is the dynamic pressure and d is the frontal width of each assembled towline.

Figure 2
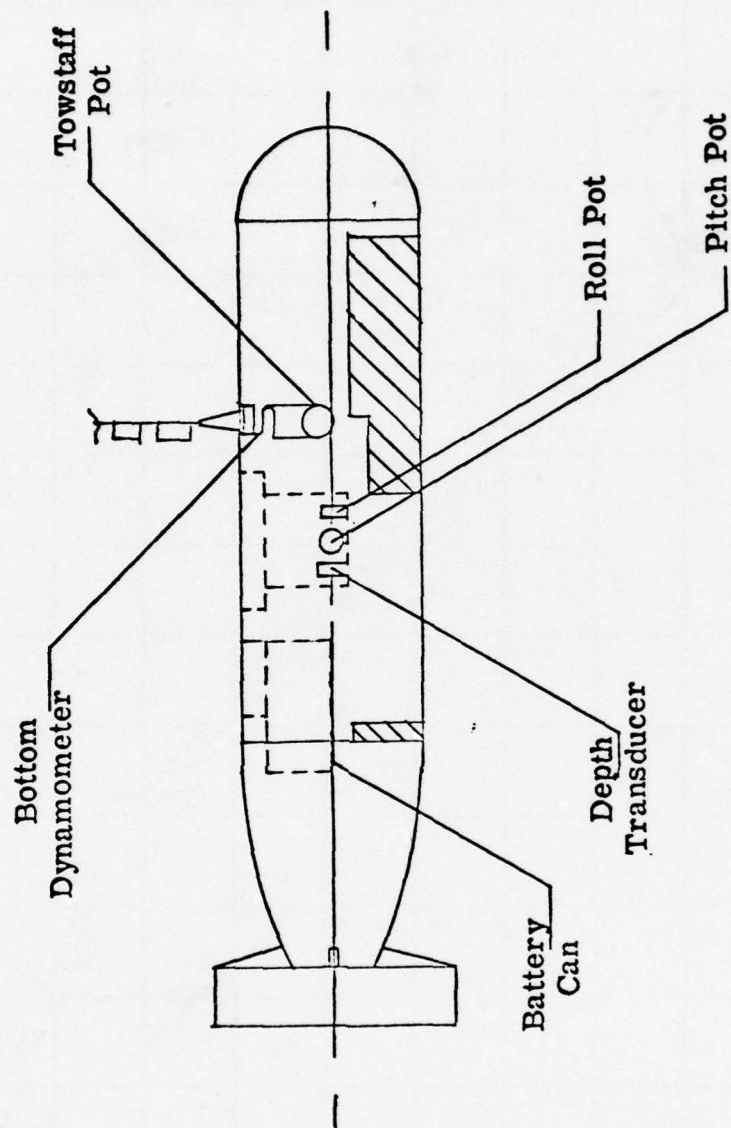
Figure 3. Body Instrumentation

Towstaff
Pot

Roll Pot

Pitch Pot

Bottom
Dynamometer

Depth
Transducer

Battery
Can
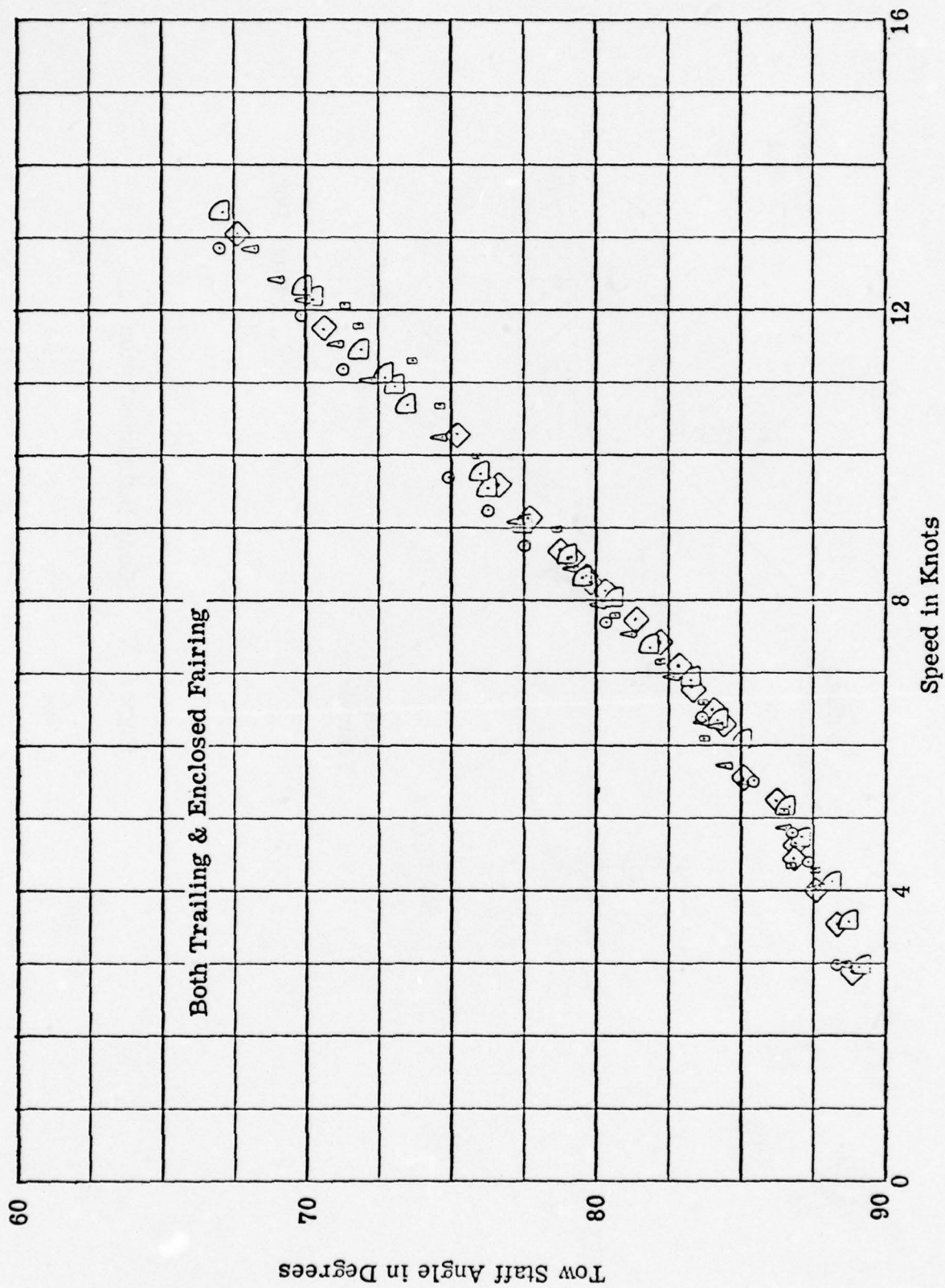
Figure 4.   Tow Staff Angle vs. Speed for Various Scopes of Both Trailing and Enclosed Fairing
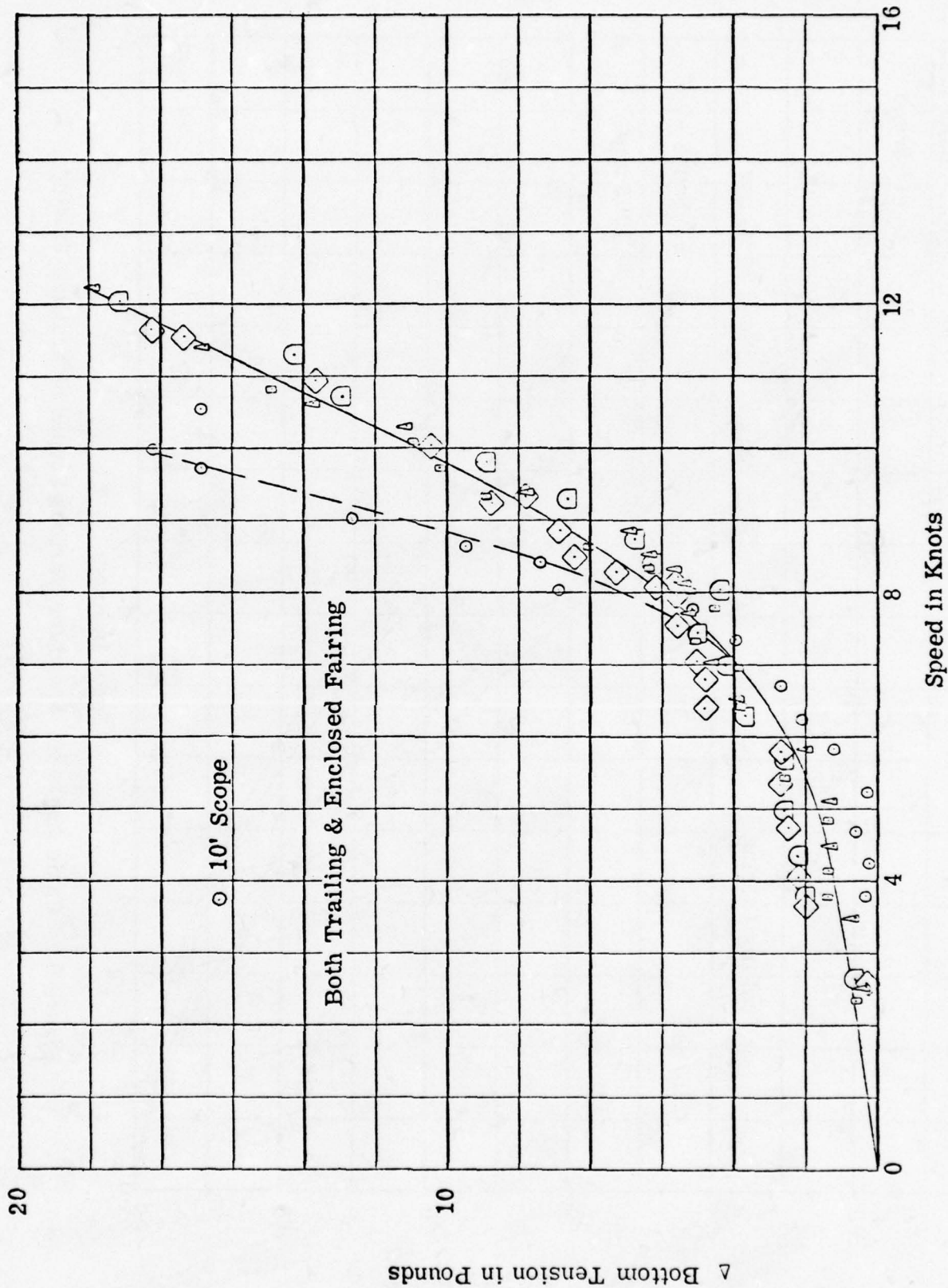
Figure 5. △ Bottom Tension vs. Speed for Various Scopes of Both Trailing and Enclosed Fairing

273
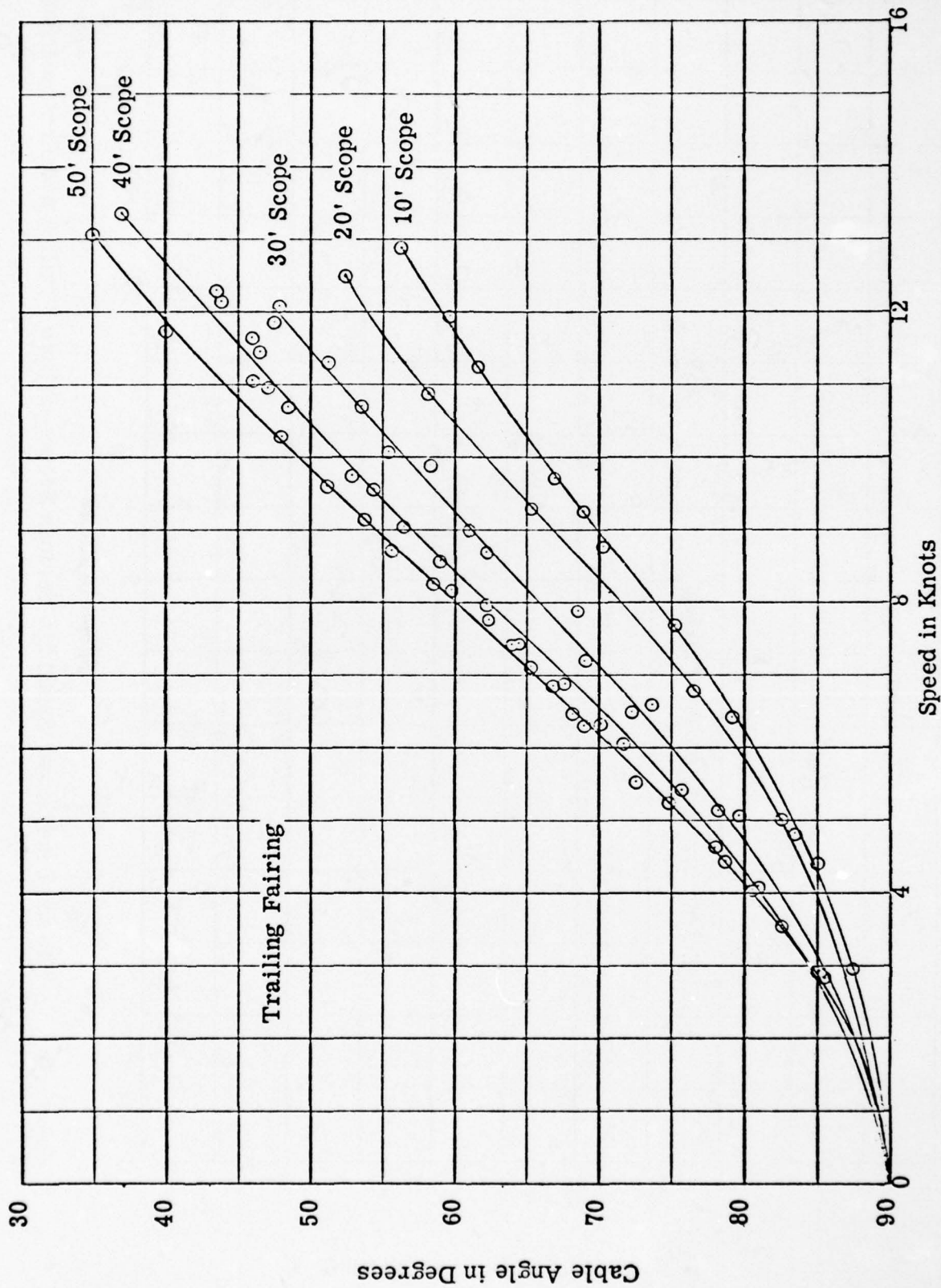
Figure 6. Cable Angle vs. Speed for Various Scopes of Trailing Fairing
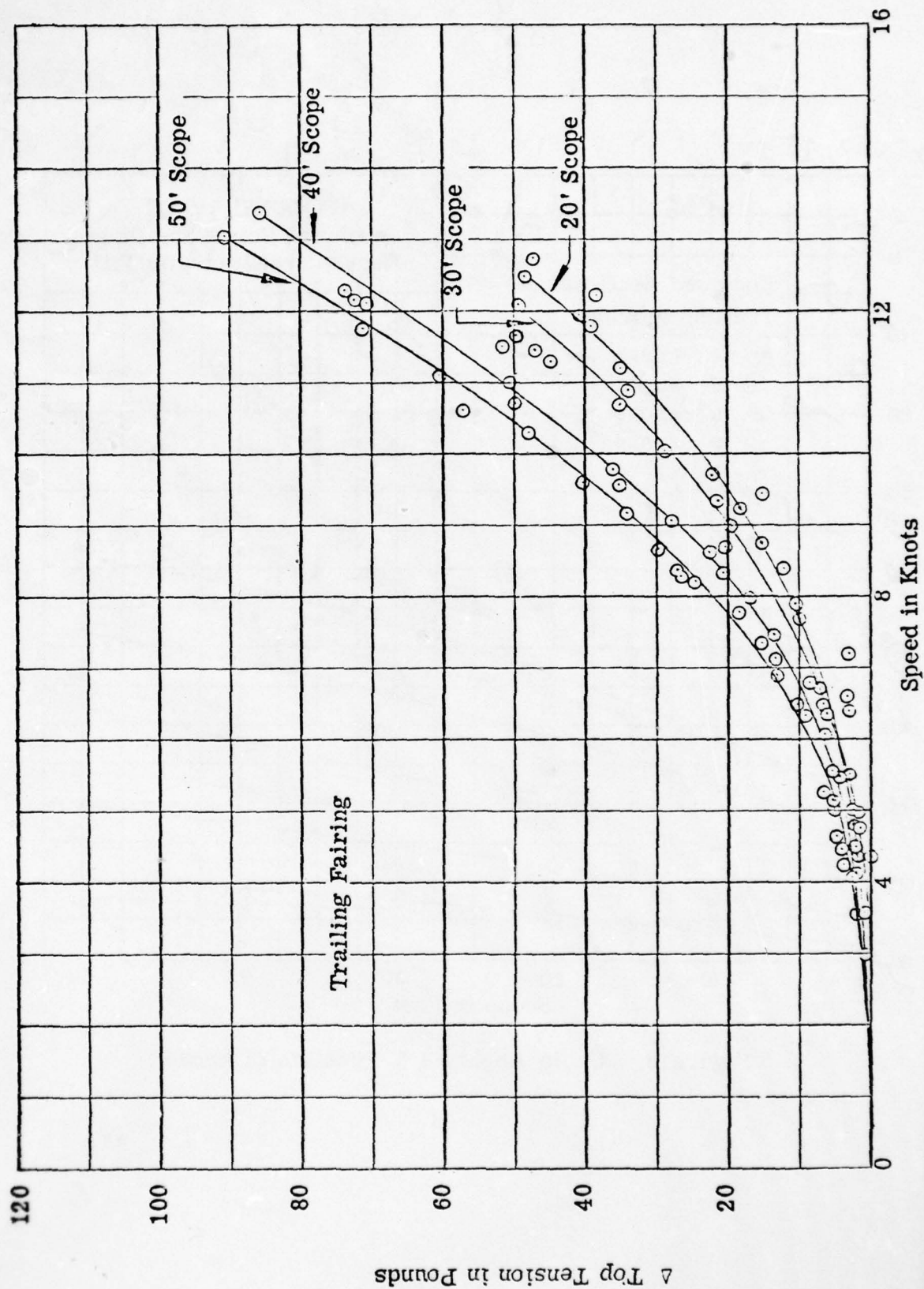
Figure 7. Δ Top Tension vs. Speed for Various Scopes of Trailing Fairing
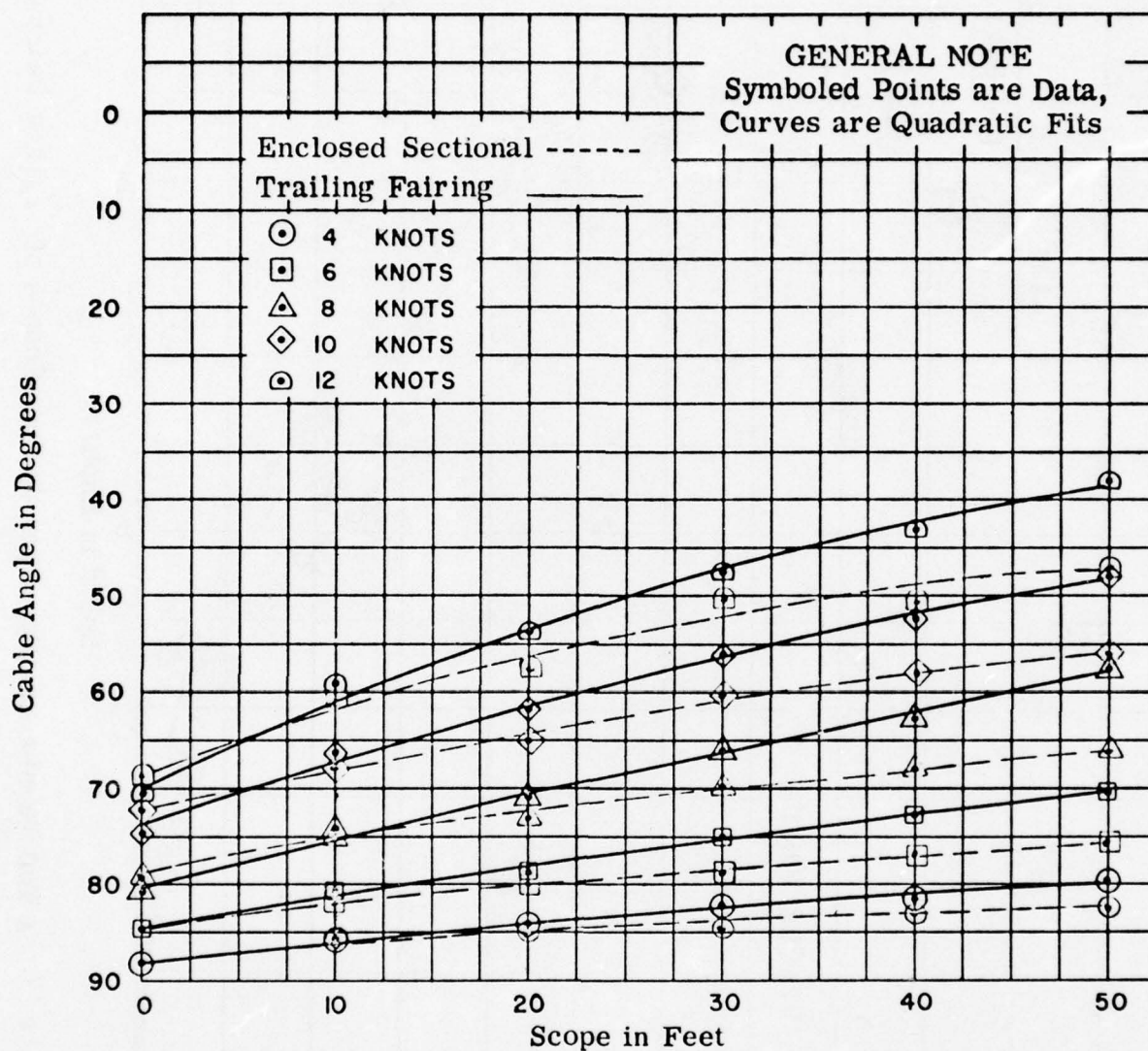
Figure 8. Cable Angle as a Function of Scope

276
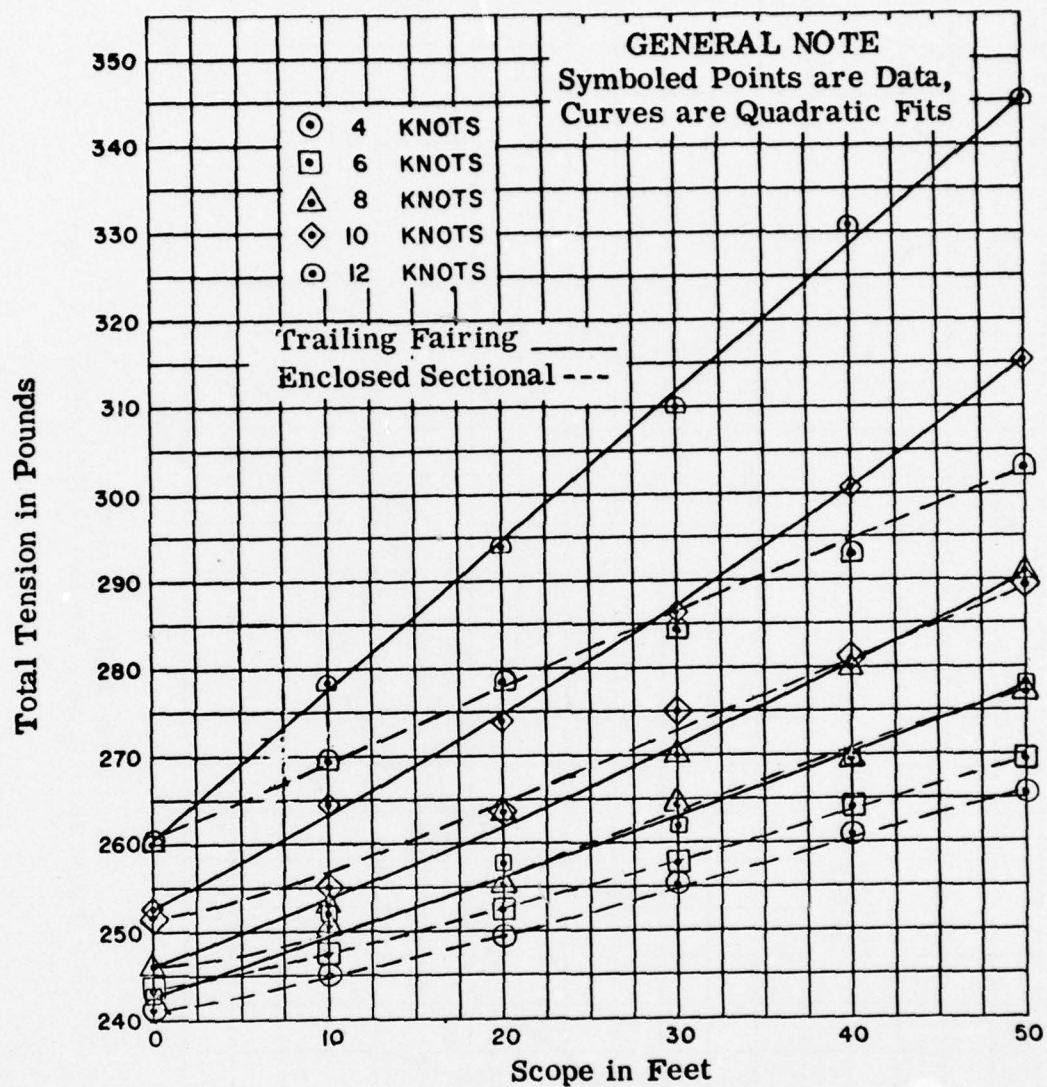
Figure 9.   Total Tension as a Function of Scope

Figure 10. C_F as a Function of Cable Angle

Figure 11. C_F as a Function of Cable Angle
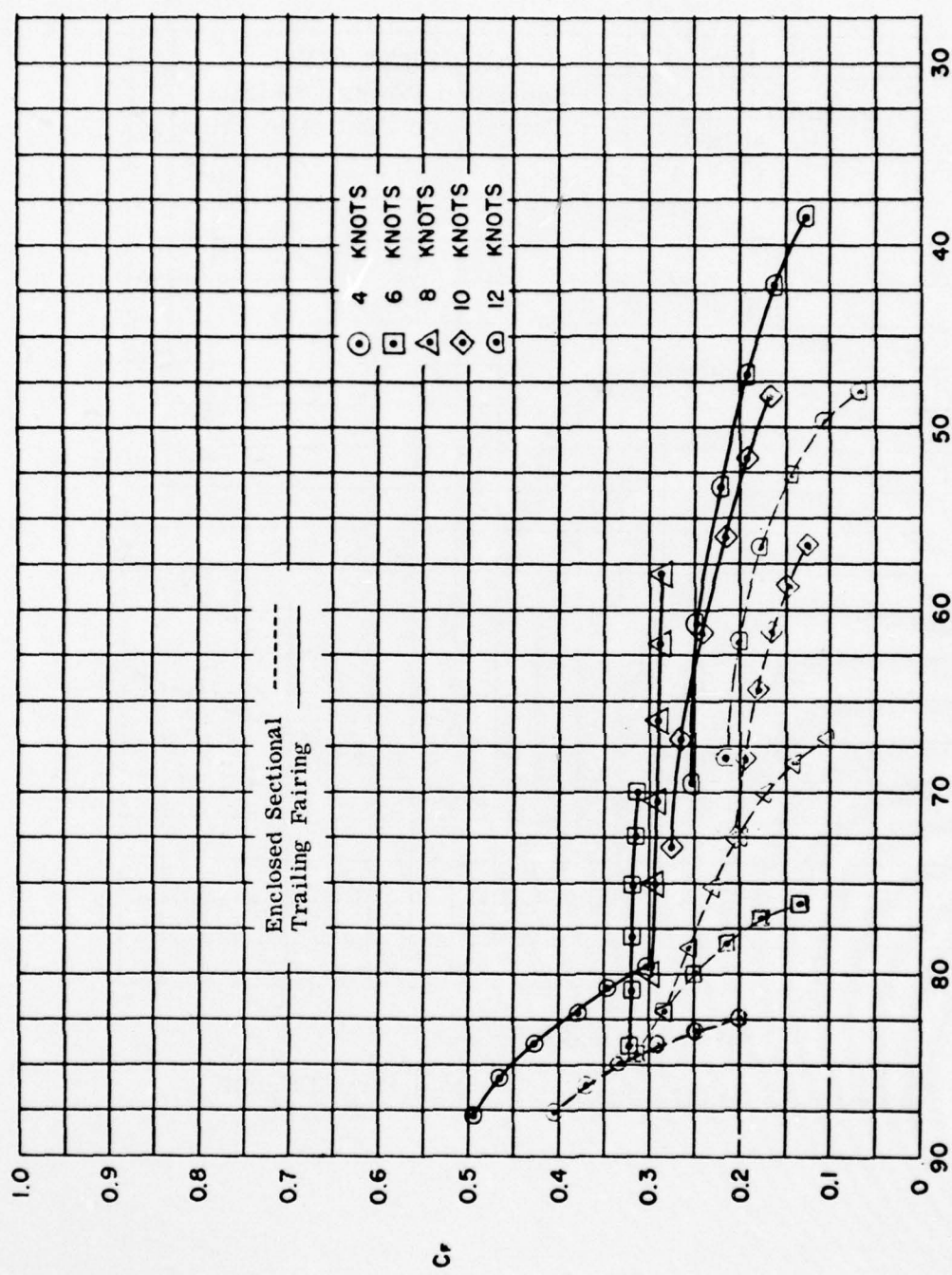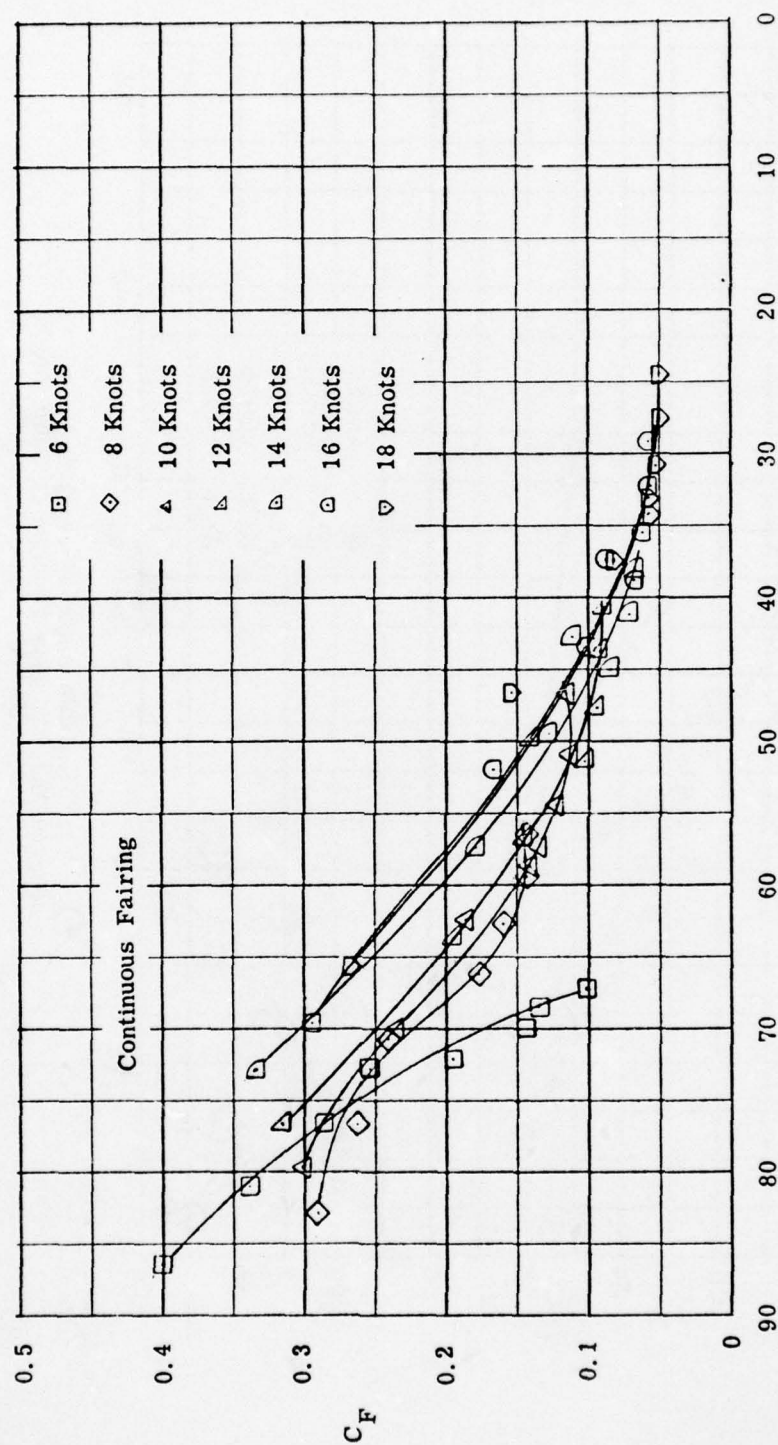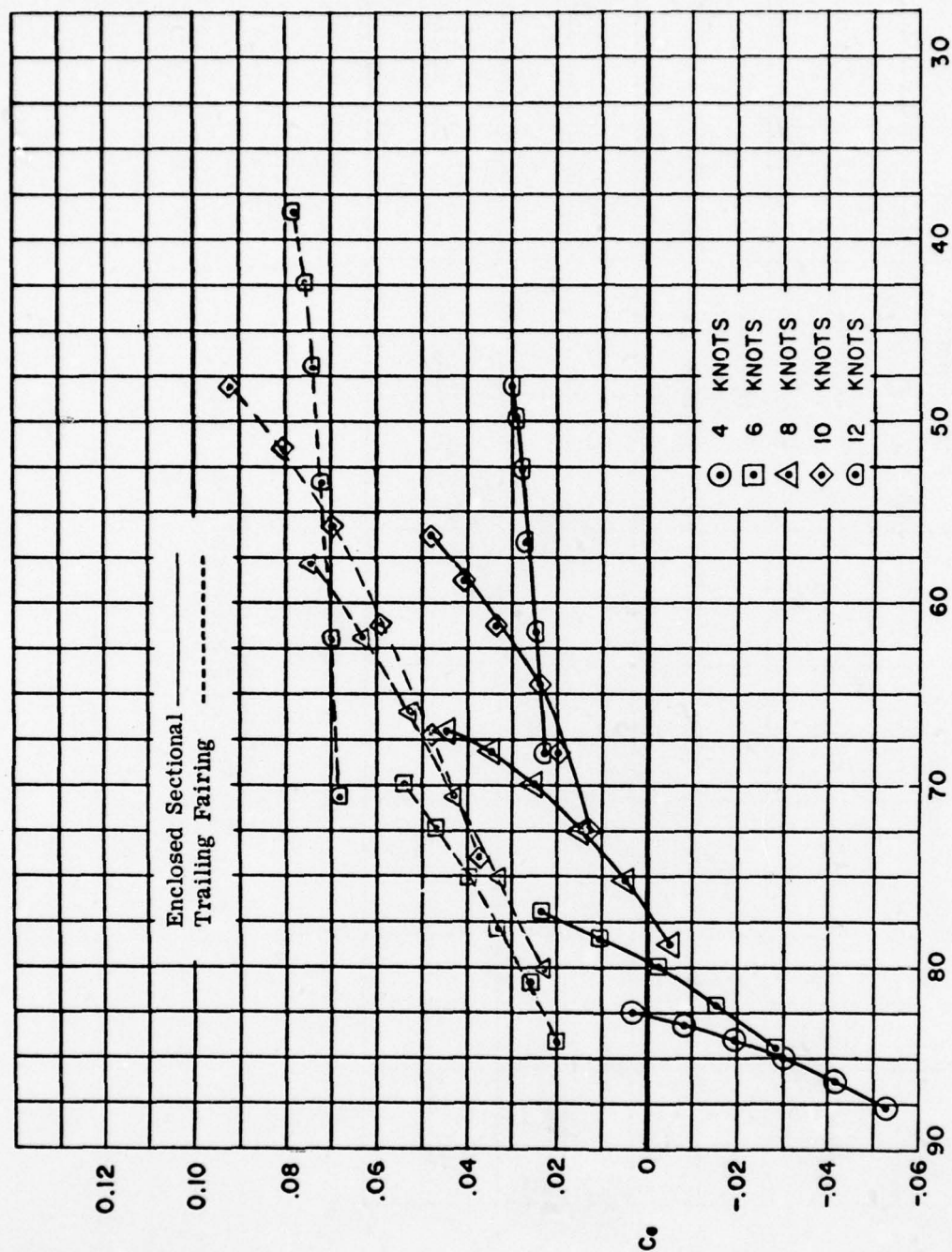
Cable Angle in Degrees

Figure 12. Cable Angle in Degrees
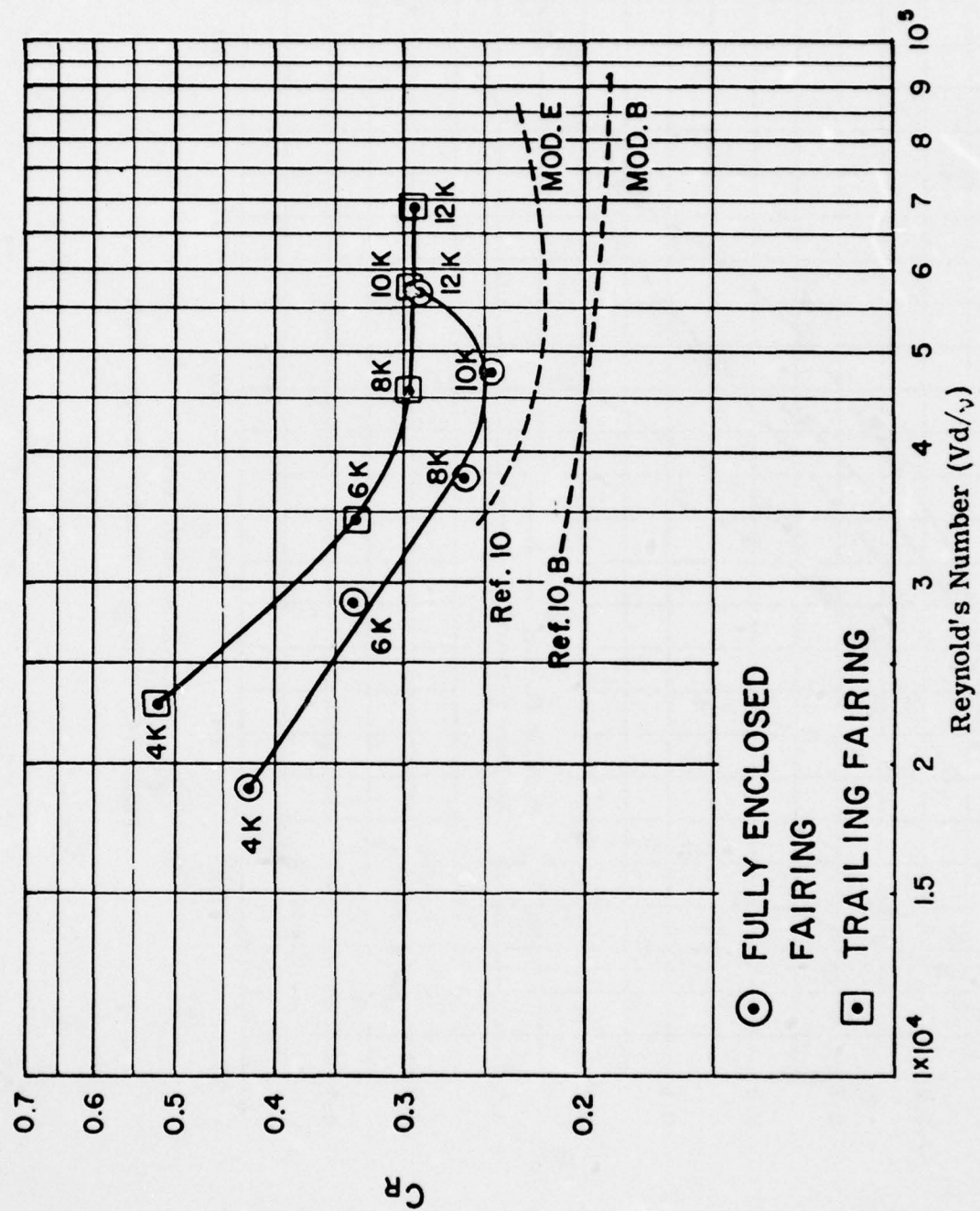C_G as a Function of Cable Angle

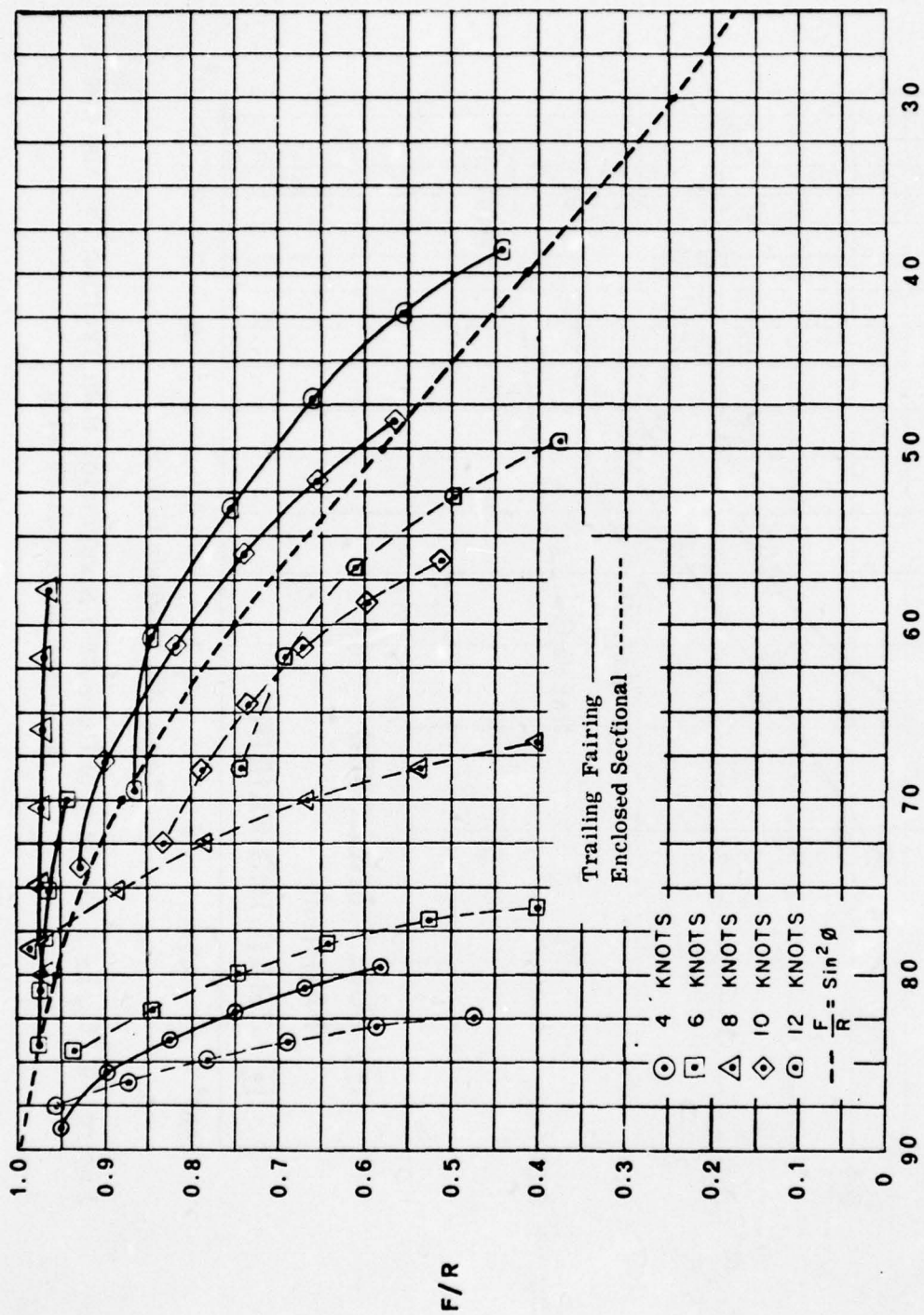Figure 13. C_R as a Function of Reynold's Number for Both Trailing Fairing and Enclosed Sectional Fairing

Figure 14. F/R as a Function of Cable Angle

Cable Angle in Degrees

F/R

Trailing Fairing ——————
Enclosed Sectional - - - - - - - -

⊙ 4 KNOTS
▣ 6 KNOTS
△ 8 KNOTS
◇ 10 KNOTS
⬢ 12 KNOTS

- - - $\frac{F}{R}$ = Sin² ∅

REYNOLDS NUMBER EFFECTS ON FAIRED TOWLINE LOADING FUNCTIONS

by Reece Folb
Head, Towed Countermeasures Section
Hydromechanics Laboratory
David Taylor Model Basin
Washington, D. C. 20007

ABSTRACT

Laboratory tests on a trailing fairing model using the DTMB Cable-Fairing Dynamometer have shown a significant Reynolds number effect on the tangential loading function. The quantitative effects of Reynolds number are shown for the model and a method for collapsing the data is described.

INTRODUCTION

To predict with reasonable accuracy the steady-towing tensions and configurations of systems consisting of a towed body and a faired towcable, the normal and tangential hydrodynamic loading functions for an element of the particular cable-fairing combination must be known. The David Taylor Model Basin has developed a test facility, the DTMB Cable-Fairing Dynamometer, to provide a means of determining these loading functions by laboratory tests of relatively short cable-fairing models[1]. The accuracy of predictions based on loading functions obtained by this facility has not yet been evaluated, but the accuracy will be evaluated as sea trial data are accumulated. Recent tests on a particular fairing model using the Dynamometer have revealed an apparent Reynolds number effect that cannot be neglected when using the tangential loading function in the calculation of cable tensions and configurations.

TEST APPARATUS AND PROCEDURE

Prior to describing the effects of Reynolds number on the loading functions, a brief description of the test apparatus and procedure is in order. The DTMB Cable-Fairing Dynamometer, described briefly in Reference 1, is designed to measure the normal, tangential, and transverse forces acting on a rigid cable-fairing model for cable angles from 90 to 30 degrees in 5-degree increments and for cable-fairing immersions from 0 to 80 inches. The normal and tangential forces sensed by the gages are recorded by integrating digital voltmeters, and the transverse force is monitored so that this force can be minimized. The cable and fairing model used for the tests described in this report was a modified DTMB TF-84. The cable model has a diameter of 2 inches; the fairing has a maximum thickness equal to 80 percent of the cable diameter; and the cable-fairing combination has a chord length equal to 3.875 cable diameters.

[1]Superior numbers refer to similarly-numbered references at the end of this paper.

With the model at 90 degrees to the flow, the normal and tangential forces were measured for various submergences up to 80 inches at speeds from 1 to 9 knots in 1-knot increments. The normal and tangential forces were then measured at cable angles from 90 to 30 degrees in 10-degree increments for various submergences at speeds of 2, 4, 6, 7, and 8 knots.

ANALYSIS TECHNIQUE TO OBTAIN LOADING FUNCTIONS

To obtain the two-dimensional forces acting on the model, the following technique was used. The normal and tangential forces for each cable angle and speed were plotted as a function of submergence. When the force increased linearly with increasing submergence, the end effects were assumed to have become constant with increasing submergence. The slope of the linear portion of this curve is the force per unit length (unit force) acting on the cable-fairing model, independent of length, for each speed and cable angle.

The unit normal force at 90 degrees was put in coefficient form based on wetted area and plotted as a function of Reynolds number based on chord length as shown in Figure 1. The ATTC Turbulent Friction Line is also presented to show the relation between friction drag and total drag; the friction drag is seen to be 10 to 15 percent of the total drag for this particular model.

The hydrodynamic loading functions are defined as the ratio of the steady-state, two-dimensional, hydrodynamic forces acting on an element of cable at an angle ϕ to the free stream to the force when the element is normal to the free stream ($\phi = 90$ degrees). The method then to obtain the loading functions is to non-dimensionalize the unit normal force (X) and unit tangential force (Z) at each cable angle and speed by dividing each unit force by the unit normal force at 90 degrees (R) at the corresponding speed. Both non-dimensionalized forces are then plotted as a function of cable angle and the resultant curves, one for the normal and one for the tangential, are the loading functions. Using this non-dimensionalizing technique for the normal force results in the plot shown in Figure 2 for the model being discussed. The curve X/R equals $\sin^2\phi$ also is shown on the graph, and the data points are in very close agreement with the "sine squared law".

Using the same non-dimensionalizing technique for the unit tangential force to obtain the tangential loading function results in the plot shown in Figure 3. The points plotted for each speed show a considerable spread. Therefore, a single equation independent of speed cannot be written to describe their form. A curve describing the points for 2 knots is 30 to 40 percent higher than the one to describe the points for 8 knots. Thus, a different mathematical expression for the nondimensional tangential loading function is required at each Reynolds number. Although it is possible to write an expression for this loading function at each Reynolds number, it seems more desirable to write one expression which includes the effects of Reynolds number.

MODIFIED TECHNIQUE TO COLLAPSE THE
TANGENTIAL LOADING FUNCTION

Because of the consistent variation with speed of the nondimensional unit tangential force for each angle, the force was assumed to be Reynolds number dependent. To account for the dependency, a different non-dimensionalizing

284

force was used; e.g., the frictional component of the total drag based on the effective chord which is described by the distance from leading edge to trailing edge as measured coincidental to the free-stream velocity vector. This is the distance that effectively dictates the boundary-layer build-up. To obtain the frictional drag, the Reynolds number is first computed from the relation

$$R_n = \frac{Vc}{\nu \sin \phi},$$ [1]

where V is the towing speed,
     c is the chord (distance from the front of the cable, measured perpendicular to the longitudinal axis of the cable, to the trailing edge of the fairing),
     ν is the kinematic viscosity of the fluid,
and ϕ is the acute angle between the longitudinal axis of the cable and the direction of motion.

The frictional drag coefficient was then obtained from the ATTC Turbulent Friction Line described by Schoenherr's Friction Formulation, which is tabulated in Reference 2 or may be computed from

$$\frac{0.242}{\sqrt{C_f}} = \log_{10}(C_f R_n),$$ [2]

where C_f is the frictional drag coefficient.

Then, for each speed and cable angle, the frictional drag was computed using

$$D_{f_\phi} = C_f Q S,$$ [3]

where Q is the dynamic pressure,
and   S is the wetted area per unit length of cable.

The unit tangential force for each cable angle and speed is divided by the corresponding computed friction drag. The results of this analysis are shown in Figure 4. The data collapse very well and can now be described by a single curve and a single equation that accounts for Reynolds number.

For a cable angle of 90 degrees, there is no tangential force, thus the value of the loading function is 0. For very clean fairing (one having a minimum of surface imperfections along length) inclined parallel to the stream (a cable angle of 0 degrees), the tangential force can be assumed all frictional drag and the value of the loading function is unity. This is equivalent to considering the fairing as an infinitesimally thin flat plate that has no pressure drag (Eames[3] "general fine" case), in which case the loading function is equal to the cosine of the cable angle. As a component of pressure drag is added to the component of frictional drag in the tangential direction, the loading function should rise above "cosine" line as is seen to be the case for the modified TF-84 fairing.

CONCLUDING REMARKS

The results of the tests on this fairing model show that there is a significant Reynolds number effect on the tangential loading that should be taken into account when predicting cable configurations and tensions using this type of fairing.

The Model Basin feels that it would be premature at this time to recommend adoption of the modified technique for expressing the tangential loading function, but wishes to alert future investigators that this Reynolds number effect should be expected and taken into account when the state of the art warrants this requirement. The technique discussed here may provide a convenient means for accomplishing this end.

REFERENCES

(1) Gibbons, T. and Gray, D., "Experimental Determination of the Hydro- dynamic Loading Functions for a Special Faired Towcable," David Taylor Model Basin Hydromechanics Laboratory Test Report 155-H-01 (May 1966).

(2) Gertler, M., "The Prediction of the Effective Horsepower of Ships by Methods in Use at David Taylor Model Basin," David Taylor Model Basin Report 576 (December 1947).

(3) Eames, M. C., "The Configuration of a Cable Towing a Heavy Submerged Body from a Surface Vessel," Naval Research Establishment (Canada) Report PHX-103 (November 1956).
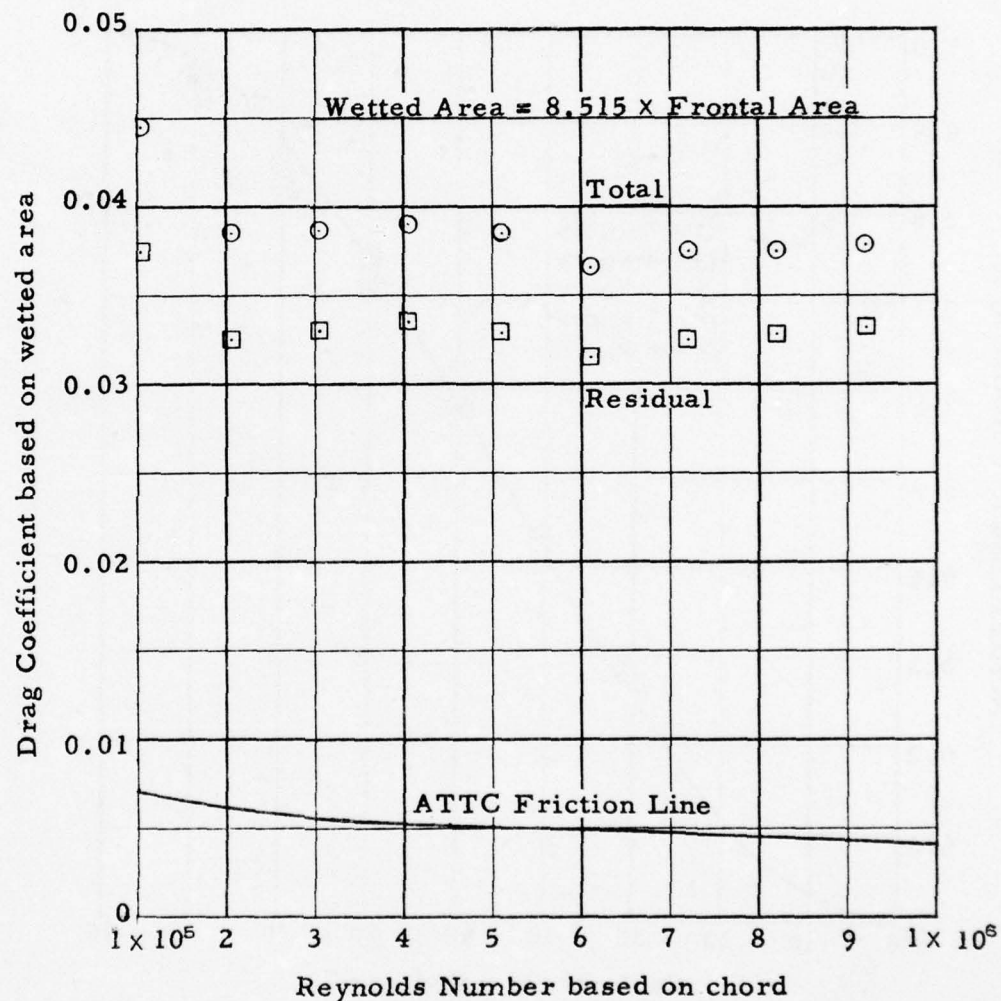
Figure 1 - Drag Coefficient as a Function of Reynolds
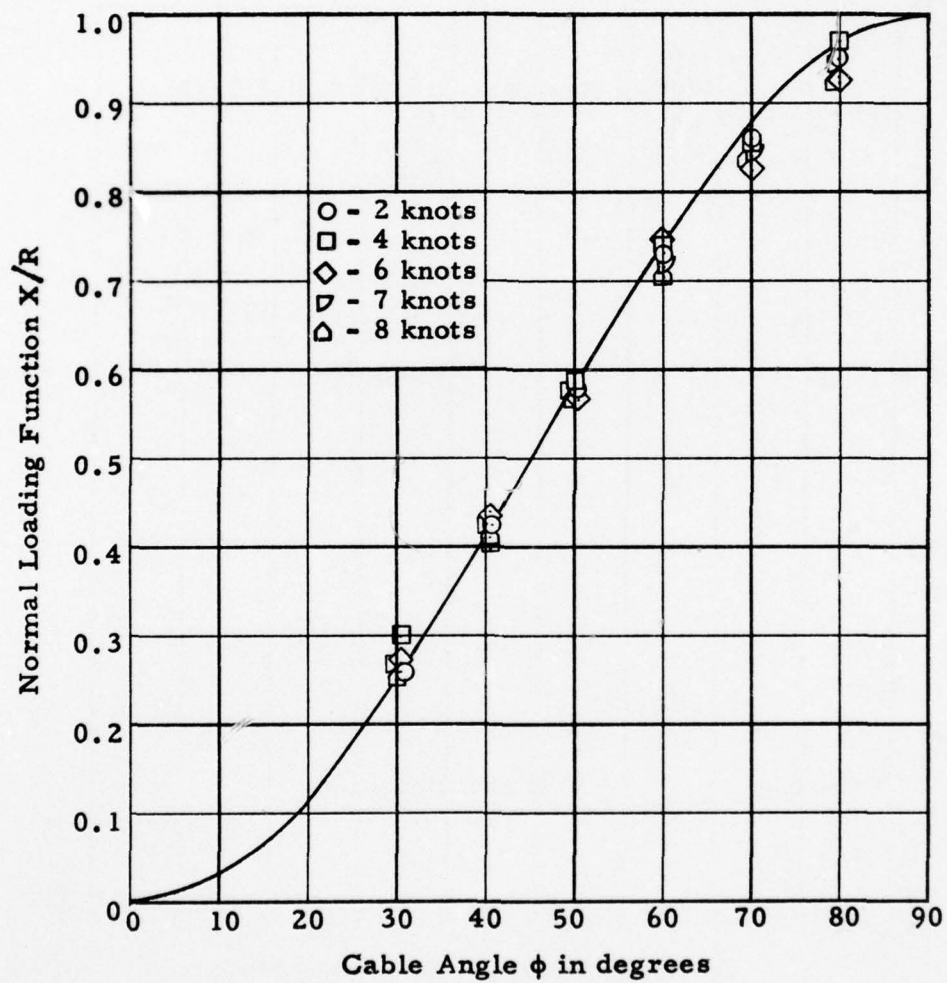Number for a Cable Angle of 90 Degrees

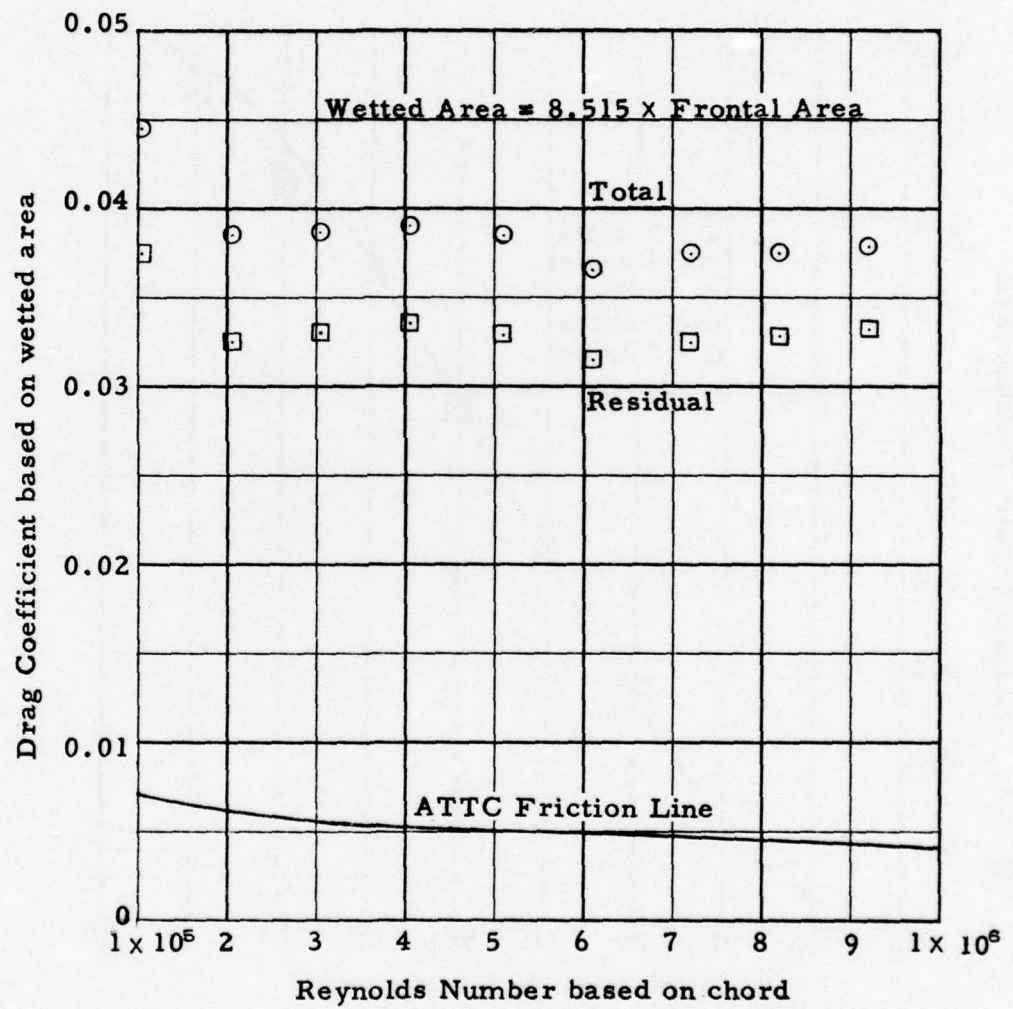Figure 2 – Normal Loading Function

END

DATE
FILMED
4-77

F 4

037

Figure 1 - Drag Coefficient as a Function of Reynolds
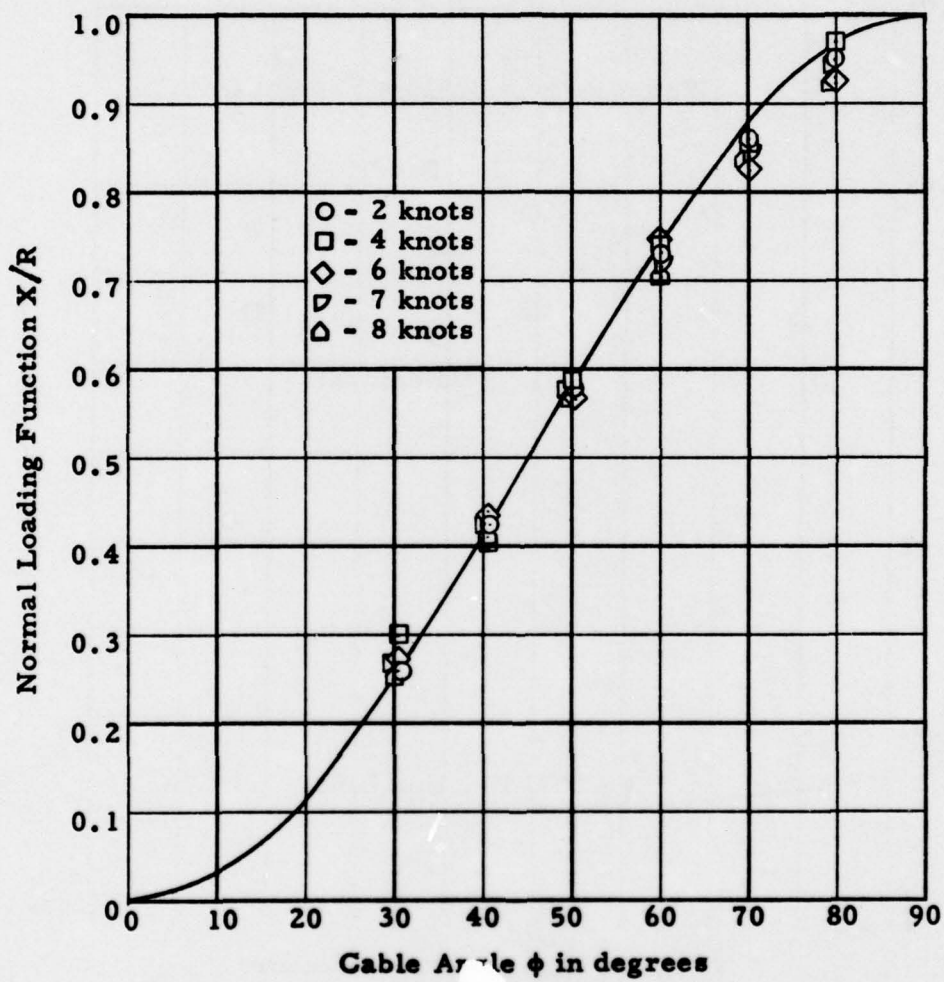Number for a Cable Angle of 90 Degrees
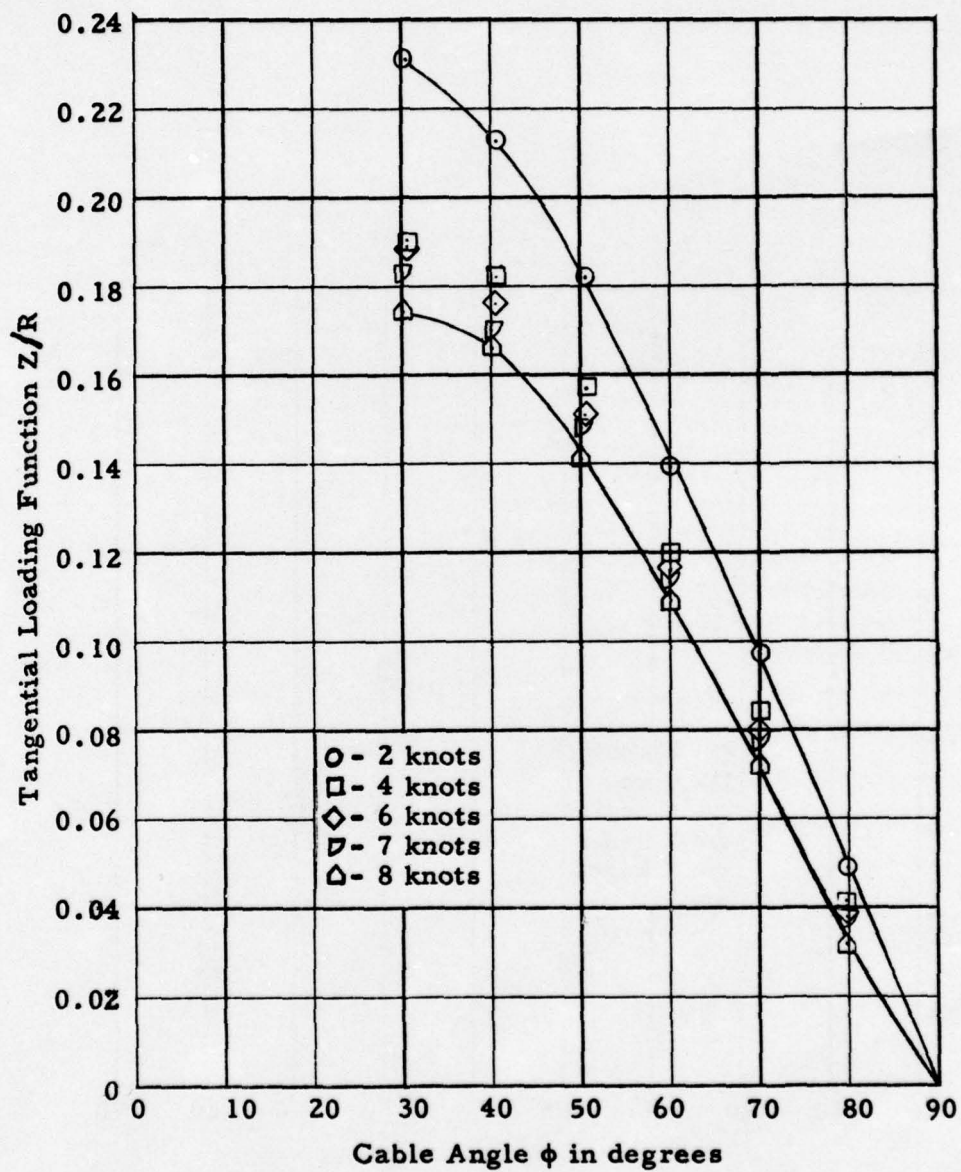
Figure 2 - Normal Loading Function
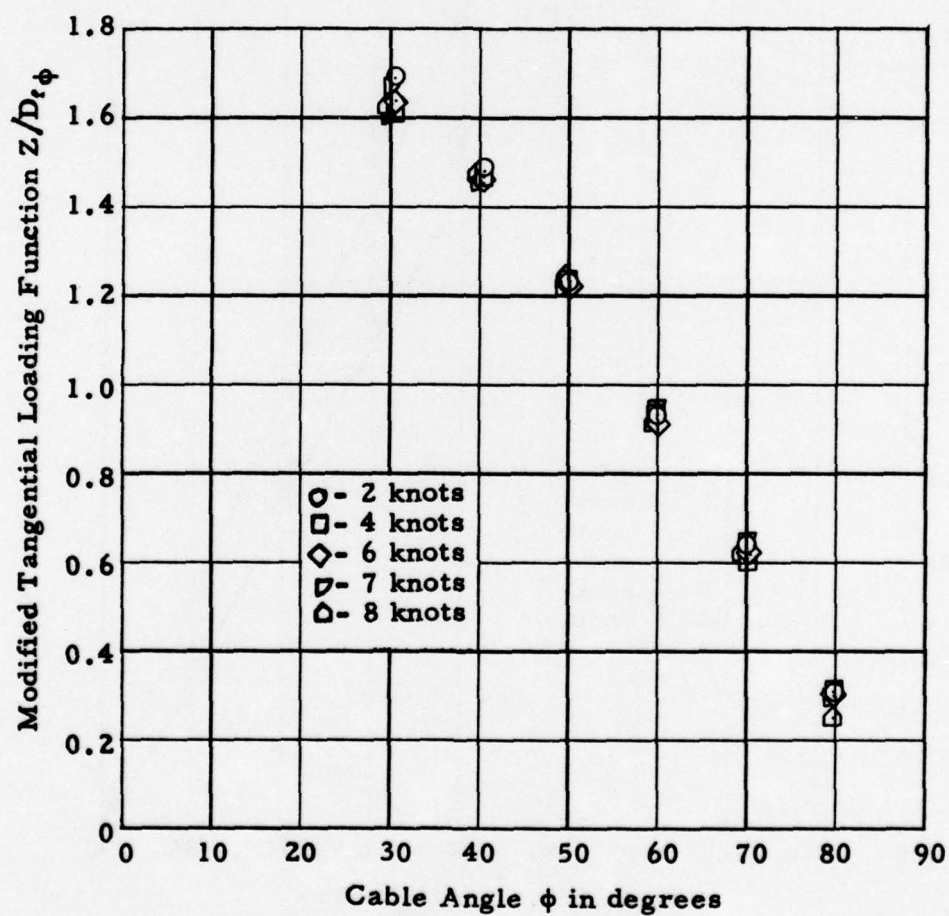
Figure 3 - Tangential Loading Function

Figure 4 - Modified Tangential Loading Function

CORRELATION STUDIES OF CABLE-TOWED SYSTEMS USING BARE CABLE

by Thomas Gibbons
Head, Special Systems Section
Hydromechanics Laboratory
David Taylor Model Basin
Washington, D. C. 20007

ABSTRACT

Two alternative methods for predicting steady-state configurations and towline tensions are evaluated by comparing predicted data with experimental data. Between the two methods, Method 1 is shown to provide better overall predictions of cable tension, cable angle at towing vessel, and body depth for the bare-cable case. The best agreement between the experimental data and the data predicted by Method 1 is obtained with a cable drag coefficient of 1.5 and a tangential force factor of 0.02.

INTRODUCTION

The David Taylor Model Basin is engaged in a broad research program directed toward the development of improved experimental and analytical techniques for predicting the steady-state and dynamic characteristics of cable-towed systems. Pursuant thereto, a project was initiated to determine which of the various existing methods would provide the most accurate predictions of the steady-state configurations and associated towline tensions for cable-towed bodies. The project is being carried out in two phases; one involving the use of bare cables and the other involving the use of faired cables. This paper deals with the first phase[1], and is confined to an evaluation of the two methods most commonly used by the Model Basin.

To carry out the objectives of the subject program, the Model Basin equipped an existing body with special purpose instrumentation and towed it at sea by bare cable to obtain steady-state configuration data. The experimental data were then compared with corresponding values obtained by means of each of the two prediction methods. Based on these comparisons, a set of "loading functions" was selected that should result in reasonably accurate predictions of steady-state configurations and tensions for body-dominated towed systems.

GENERAL CONSIDERATIONS

The steady-state equations of a cable-body system expressed in terms of the hydrodynamic and hydrostatic forces acting on an element of cable are given in Reference 2. A diagram showing how these forces are resolved is

[1]Superior numbers refer to similarly-numbered references at the end of this paper.

reproduced as Figure 1. Once the hydrodynamic characteristics of the towed body and the towing cable are known, the cable configuration and tension can be determined from the equations. Generally, the hydrodynamic characteristics of the towed body are known or can be readily obtained. However, there are little data concerning the exact magnitude of the hydrodynamic forces acting on the element of cable. Consequently, the usual practice is to assume that these forces are some predetermined function of the angle that the cable makes to the stream. Furthermore, such factors as cable strands, roughness, and cable vibration may affect the forces on a cable. The cable strands and roughness may cause turbulent flow over the element of cable which could either increase or decrease the hydrodynamic forces. If the cable is vibrating, the effective frontal area is increased and hence, the forces are increased. Severe vibration usually occurs in bare-cable towing operations.

In spite of the aforementioned uncertainties, the basic differential equations have been generally accepted and used, but various agencies have developed different expressions for the hydrodynamic loading forces on an element of cable. The two methods most commonly used by the Model Basin to predict the steady-state characteristics of the cable-towed body system are described in References 2 and 3 and are designated herein as Methods 1 and 2, respectively. The two methods are essentially the same but differ in the loading functions which are used. Both methods resolve the hydrodynamic force into normal and tangential components, as shown in Figure 1. The expression used for the hydrodynamic force components for each method are compared in Table 1. It may be noted that the tangential force in Method 1 is independent of the cable angle whereas, in Method 2, it is a function of cable angle.

TABLE 1

Assumed Expressions for Hydrodynamic Force Components Used
in Methods 1 and 2

Method	Normal Force	Tangential Force
1	$R \sin^2 \phi$	$+Rf$
2	$R \sin^2 \phi$	$R[\,0.083 \cos \phi - 0.035 \cos^2 \phi\,]$

The Model Basin has a computer program for calculating the equilibrium configuration of a flexible cable in a uniform stream[4]. The program is based on the differential equations of Reference 2 which assume that the velocity at the element is constant and is not affected by curvature of the cable. It further assumes that the cable is inelastic and offers no resistance to bending. When the hydrodynamic forces acting on the cable-body system are known, the predicted configuration may be computed to an accuracy of ± 0.001 percent for each integration step. The exact configuration, then, is primarily dependent upon the accuracy of the input data used in the program. The computer program was set up to allow a choice of the two methods to predict the cable configuration and towline forces.

PARAMETRIC STUDIES WITH TWO PREDICTION METHODS

Prior to making direct comparisons between measured and predicted results, computations were made to determine the effect of arbitrary parametric variations on the cable configurations and tensions computed by each of the two methods using the hydrodynamic characteristics of the body. The cases considered were for scopes of 100, 200, and 280 feet. For Method 1, cable drag coefficients C_R of 0.8, 1.5, and 1.8 in combination with f values of 0.01, 0.02, and 0.03 were used for the computations. For Method 2, cable drag coefficients of 0.8, 1.5, and 1.8 were used.

For Method 1, the variation in C_R has a significant influence on the body depth, cable angle, and tension at the ship. However, the variation in f has little effect on depth and cable angle but has considerable influence on the net tension. Thus, if a drag coefficient is selected to give good agreement between predicted and measured values of depth and cable angle, a value of f can be selected which will give good agreement on net tension as well.

For Method 2, the variation in C_R also has a significant influence on the body depth, cable angle, and tension at the ship. In this case, the only value that can be changed in any given computation is the cable drag coefficient. Consequently, if good agreement cannot be obtained with one value of drag coefficient for all three quantities, then changes in the drag coefficient to improve the agreement with one of the quantities will result in poorer agreement with one or both of the other two quantities.

On this basis, a C_R of 1.5 in combination with an f value of 0.02 was found to be best for Method 1 and a C_R of 1.5 was found best for Method 2. The predictions based on the selected values for each method are compared with the measured data in Figures 2, 3, and 4 for a nominal cable scope of 280 feet.

CONCLUSIONS

Based on an evaluation of two alternative methods of predicting steady-state towing configurations and towline tensions of a cable-body system towed by bare cable, and comparisons made between predictions and measurements obtained from towing experiments conducted at sea on a body dominated cable towed body system, the following conclusions are drawn:

1. Within the range investigated, Method 1 is the best of the two methods from the standpoint of providing good predictions of both the steady-state tensions and configurations for a towed-body system utilizing bare cable.

2. Using a cable drag coefficient $C_R = 1.5$ and a tangential force factor f = 0.02, Method 1 can be used with reasonable accuracy to predict the cable tension, the cable angle at the towing ship, and the body depth for towed body systems utilizing bare cable.

3. Using a cable drag coefficient $C_R = 1.5$, Method 2 can be used to predict the body depth and the cable angle at the towing ship, but will tend to predict cable tensions that are too high for towed body systems utilizing bare cable.

NOMENCLATURE

C_R Drag coefficient, $\dfrac{R}{\frac{1}{2}\rho d V^2}$

d   Diameter of cable

F   Drag per unit length of cable when cable is parallel to the stream

f   Ratio F/R

R   Drag per unit length of cable when cable is perpendicular to the stream

s   Scope (length) of cable

T   Cable tension at the ship

T_o Cable tension at the towed body

V   Speed

W   Weight in water per unit length of cable

y   Depth

ρ Mass density of fluid

ϕ Cable angle

REFERENCES

(1) Gibbons, T. and Walton, C., "Evaluation of Two Methods for Predicting Towline Tensions and Configurations of a Towed Body System Using Bare Cable," David Taylor Model Basin Report 2313 (December 1966).

(2) Pode, L., "Tables for Computing the Equilibrium Configuration of a Flexible Cable in a Uniform Stream," David Taylor Model Basin Report 687 (March 1951).

(3) Whicker, L. F., "The Oscillatory Motion of Cable-Towed Bodies," Institute of Engineering Research, University of California, Series 82, Issue 2 (May 1957).

(4) Cuthill, E., "A FORTRAN Program for the Calculation of the Equilibrium Configuration of a Flexible Cable in a Uniform Stream," David Taylor Model Basin Report 1806 (March 1964).
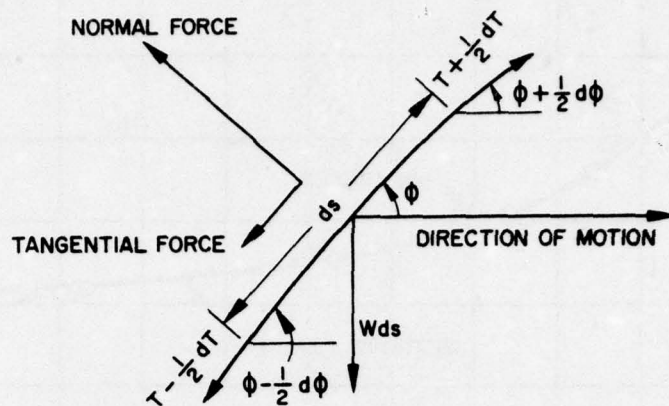
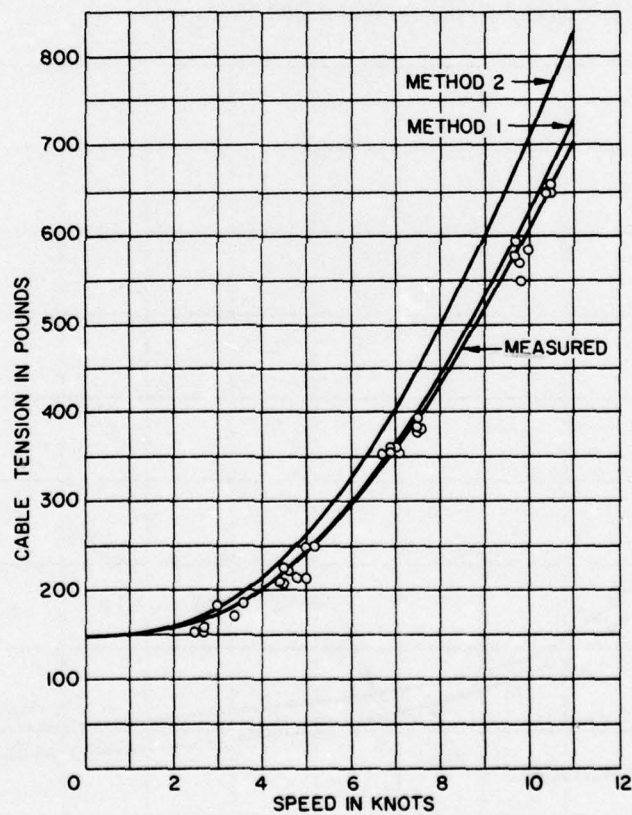Figure 1 – Forces Acting on an Element of Cable

Figure 2 – Comparison of Measured and Predicted Cable Tension
at the Towing Ship as a Function of Speed for a
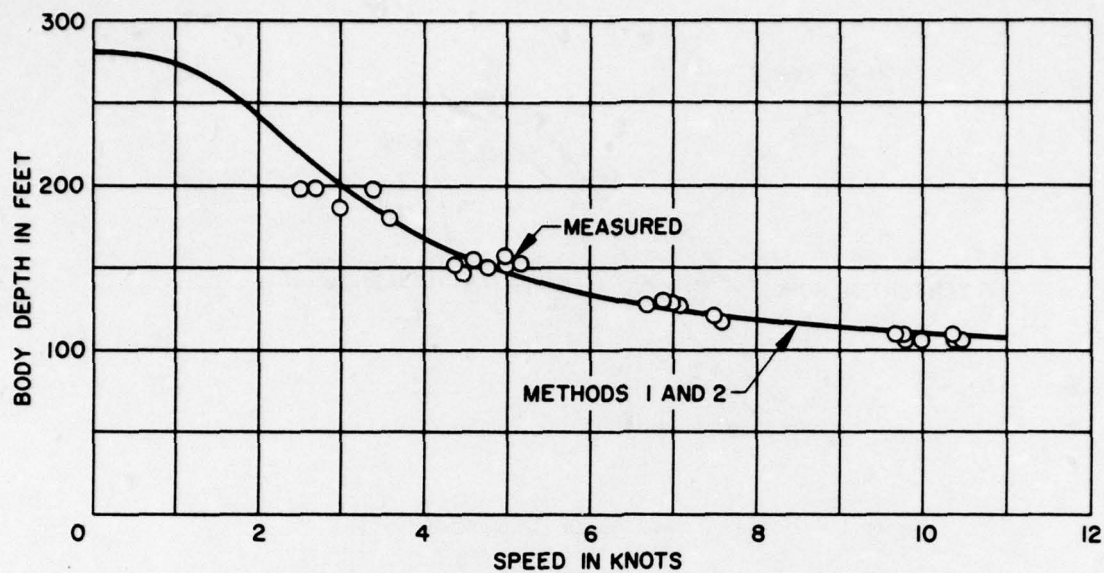Nominal Cable Scope of 280 Feet

Figure 3 — Comparison of Measured and Predicted Body Depth as a Function of Speed
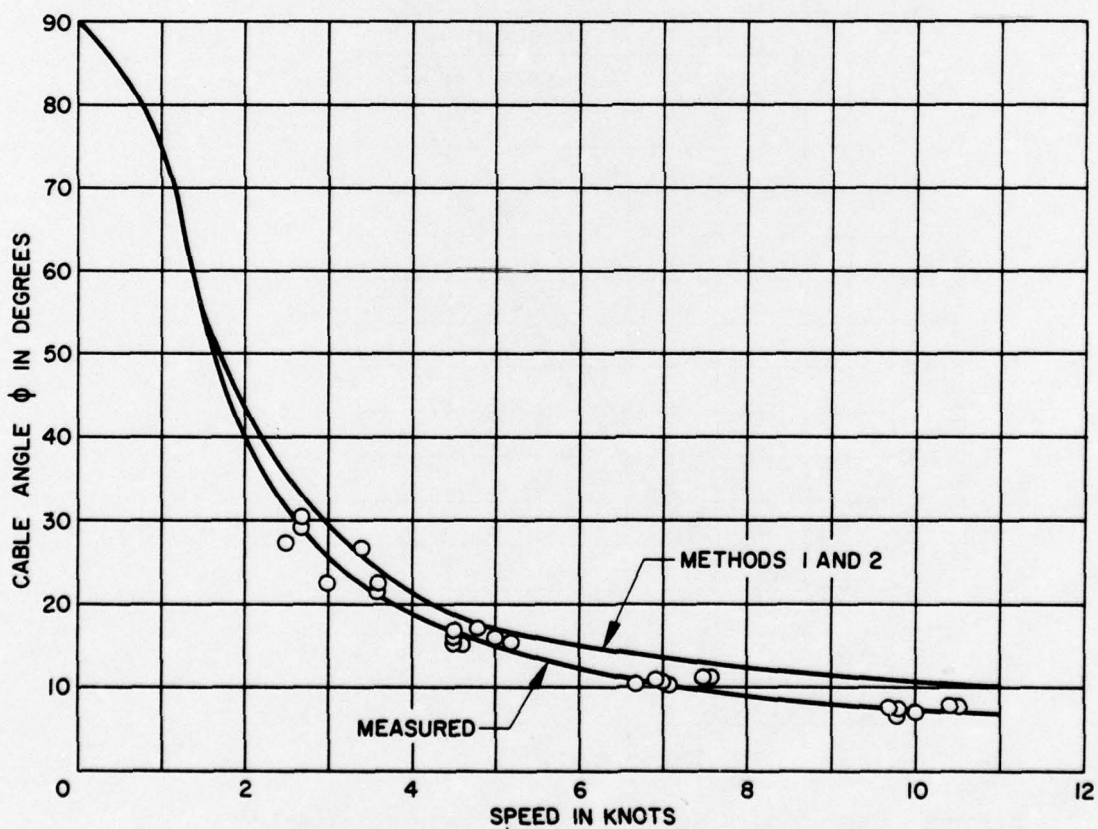for a Nominal Cable Scope of 280 Feet

Figure 4 — Comparison of Measured and Predicted Cable Angle at the Towing Ship
as a Function of Speed for a Nominal Cable Scope of 280 Feet

296

EXPERIMENTAL DETERMINATION OF THE
DYNAMIC COEFFICIENTS APPLICABLE TO
FAIRED CABLES

By

Alex Goodman, T. T. Huang and R. J. Etter

NOTATION

The nomenclature defined in DTMB Report 1319 is used herein where applicable. The positive direction of axes, angles, forces, moments and velocities are shown in the accompanying sketch. Sketches defining pure swaying and pure yawing motions are also included. The coefficients and symbols are defined as follows:

Symbol	Dimensionless Form	Definition
A		Planform area of a section of faired cable
AR	$\dfrac{b^2}{A}$	Aspect ratio
a	$\dfrac{ac}{2}$	Distance between reference axis and midchord of faired cable, percent of semichord positive aft of midchord
a_o		Section lift curve slope
b		Span of faired cable section
c		Chord of faired cable
C(k)	F(k) + iG(k)	Theodorsen Function
$C_{L\alpha}$	$\dfrac{\partial C_L}{\partial \alpha}$	Three dimensional lift curve slope
D	$C_D = \dfrac{D}{\frac{1}{2}\rho U^2 A}$	Drag coefficient
F(k)		Real part of C(k)

Symbol	Dimensionless Form	Definition
f		Frequency in cycles per second
$G(k)$		Imaginary part of $C(k)$
Im		Imaginary part of
I_z	$I_z' = \dfrac{I_z}{\frac{1}{2}\rho c^5}$	Moment of inertia of faired cable section about z axis
k	$\dfrac{\omega c}{2U}$	Reduced frequency parameter
L	$C_L = \dfrac{L}{\frac{1}{2}\rho U^2 A}$	Lift coefficient
m	$m' = \dfrac{m}{\frac{1}{2}\rho c^3}$	Mass of faired cable section
N	$C_N = \dfrac{N}{\frac{1}{2}\rho U^2 A c}$	Hydrodynamic yawing moment about z axis; positive from x to y
p_o		Free stream static pressure
p_v		Vapor pressure of water
Q	$\frac{1}{2}\rho U^2$	Dynamic pressure
Re		Real part of
R	$\dfrac{Uc}{\nu}$	Renolds number
r	$r' = \dfrac{rc}{2U} = k\,\psi_m$	Angular velocity about z axis

Symbol	Dimensionless Form	Definition
$\dot{r}$	$\dot{r}' = \dfrac{\dot{r}c^2}{4U^2} = k^2 \psi_m$	Angular acceleration about z axis
t	$\dfrac{t}{c}$	Maximum thickness of faired cable section
U		Velocity, relative to fluid, of origin of body axes x,y,z; in feet per second
v	$v' = \dfrac{v}{U} = k\,\dfrac{2y_m}{c}$	Component of velocity along y axis
$\dot{v}$	$\dot{v}' = \dfrac{\dot{v}c}{2U^2} = k^2\,\dfrac{2y_m}{c}$	Linear acceleration along y axis
X	$C_X = \dfrac{X}{\frac{1}{2}\rho U^2 A}$	Longitudinal force
x		Reference length for PMM system
x_R	$\dfrac{x}{c}$	Distance along x axis from leading edge of faired cable section to reference axis
x_o, y_o		Inertial axes fixed in space
Y	$C_Y = \dfrac{Y}{\frac{1}{2}\rho U^2 A}$	Lateral force
y	$\dfrac{2y}{c}$	Displacement along y axis

| Symbol	Dimensionless Form	Definition
β	$\beta = -\sin^{-1} \dfrac{v}{U}$	Sideslip angle
ν		Kinematic viscosity
ρ		Mass density of water
σ	$\dfrac{p_o - p_v}{\frac{1}{2}\rho U^2}$	Cavitation number
θ	$\tan^{-1}\left(\dfrac{Im}{Re}\right)$; $\tan^{-1}\left(\dfrac{\text{OUT-PHASE}}{\text{IN-PHASE}}\right)$	Phase angle
φ		Cable angle, angle between leading edge of faired cable and horizontal reference plane
φ_s	$\cos^{-1} = \dfrac{1 - \left(\dfrac{\omega x}{U}\right)^2}{1 + \left(\dfrac{\omega x}{U}\right)^2}$	Phase angle between PMM cranks required for pure yawing
ψ		Yaw angle about y axis
$\dot{\psi}$		Yawing angular velocity
$\ddot{\psi}$		Yawing angular acceleration
ω		Circular frequency of oscillation

Subscripts:

|	
IN	In-phase component of force or moment
OUT	Out-of-phase or quadrature component of force or moment
m	Maximum amplitude
F	Associated with forward gage
A	Associated with aft gage
m	Value for model (affected quantity to be enclosed in parentheses)
s	Associated with swaying
y	Associated with yawing
R	Resultant

Note: All derivatives with respect to angular quantities are given as "per radian."
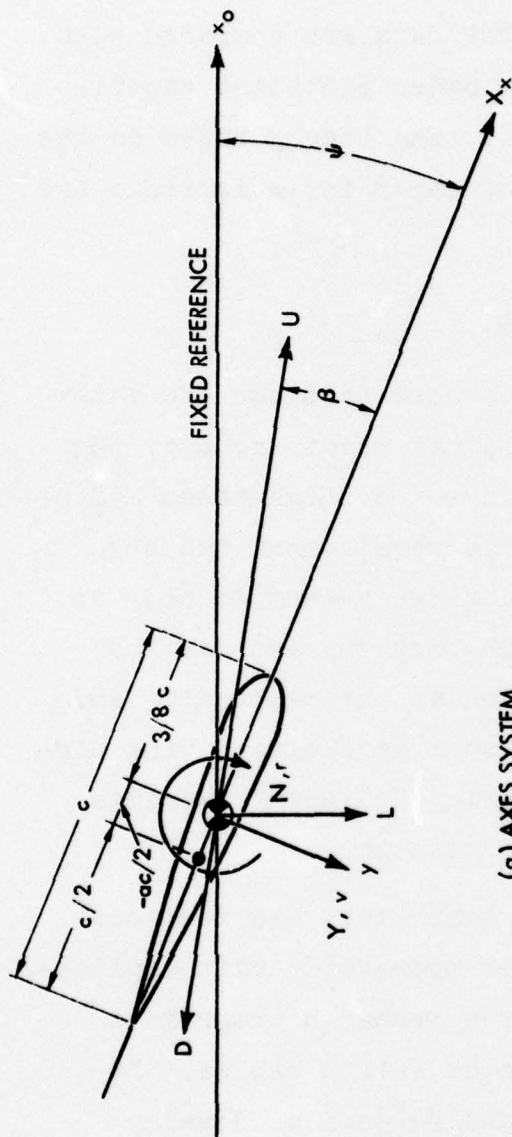
(a) AXES SYSTEM
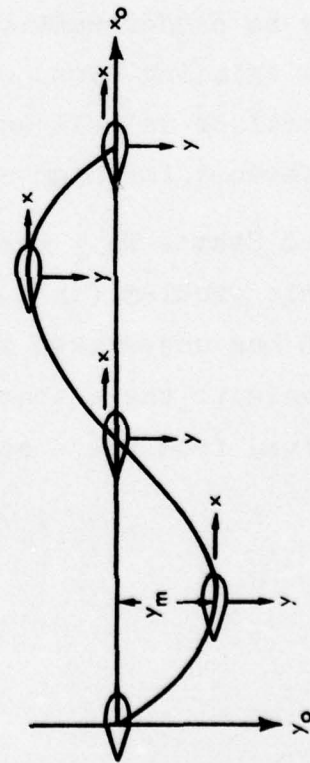
(b) PURE SWAYING ; $\psi = 0$
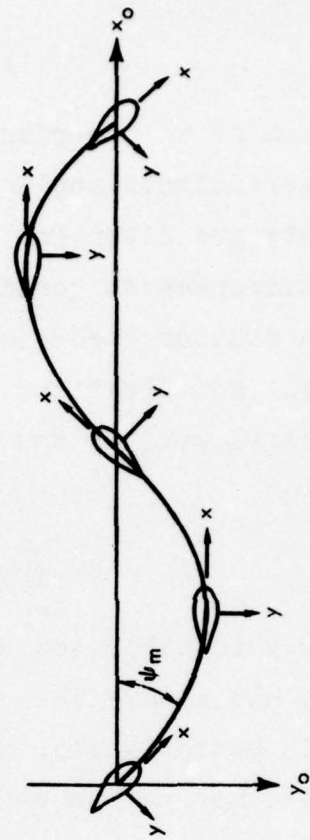
(c) PURE YAWING ; $\beta = 0$

SKETCHES SHOWING POSITIVE DIRECTIONS OF AXES, ANGLES, DISPLACEMENTS, VELOCITIES, FORCES, MOMENTS, AND DEFINITIONS ASSOCIATED WITH PURE-SWAYING AND PURE-YAWING MOTIONS

ABSTRACT

The results of an experimental study performed to determine the dynamic coefficients applicable to faired cables are presented. The coefficients are given for a range of reduced frequencies and for several environmental conditions. The data are compared with the Theodorsen flutter theory as well as other pertinent experimental results. Modifications to the existing theory based on the present results as well as the results of other investigations are suggested.

INTRODUCTION

The ability to cable tow submerged bodies from surface ships at high speeds has always been an operational requirement of the U. S. Navy. In recent years, with the advent of high-speed hydrofoil craft and other marine vehicles, this requirement has been reenforced. The power required to tow a given submerged body at high speeds is not only a function of the body characteristics (drag) but may be predominantly a function of the cable drag and behavior. The existing types of cables such as cables having circular cross-sections as well as those having "clip-on" fairings are not satisfactory for high-speed applications.

The United States Navy Electronics Laboratory has been concerned with this problem for a particular hydrofoil craft application. The NEL has undertaken to sponsor a research program to develop and evaluate the characteristics of faired cables. Information derived from these studies could be used to develop

304

design criteria for such cables. As part of this program HYDRO-
NAUTICS, Incorporated, under Contract No. 123(953)53212A, has
undertaken a systematic experimental study to determine the hydro-
dynamic characteristics of several specific faired-cable sections
(having standard NACA cross-sections) which were being considered
by the NEL. These studies[1,2] consisted of determining the static
and dynamic characteristics of the specified sections operating
under various environmental conditions. In addition, studies in-
volving boundary flow visualization were performed to provide a
better physical understanding of the measured data.

The present report presents the results of the dynamic tests
that were performed. It is believed that the results presented
herein are unique. A search of existing literature has failed to
reveal comparable information. Results are presented for a sim-
ulated faired cable having an NACA 63A020 section. The data are
compared with existing theory and modifications to the theory are
discussed.

DESCRIPTION OF MODEL

The simulated faired-cable model used for the dynamic tests
was the A-3 model of Reference 1. The geometric characteristics
of this model are presented in Table 1.

------

[1] References are listed on page 142

TABLE 1

Geometric Characteristics of Simulated Faired Cable

Chord, ft.	0.333
Span, ft. (effective submerged)	1.5
Taper ratio	1.0
Sweep angle, degrees	90
Projected area, sq.ft.	0.5
NACA Section	63A020
Section maximum thickness, percent chord	20
Distance to Reference point from leading edge, percent chord	37.5

The models were machined from 7075-T6 aluminum plate to the required section offsets using the HYDRONAUTICS, Incorporated profile-milling machine and airfoil cutting techniques.

TEST APPARATUS AND PROCEDURES

The experimental study was conducted in the HYDRONAUTICS, Incorporated High-Speed Channel (HSC) using a Planar Motion Mechanism and associated instrumentation. The channel and PMM are described in detail in Reference 3. Briefly, the HSC is a free-surface, variable-pressure, high-speed channel. The HSC tests section is twelve feet long and two feet wide. Generally, the HSC is operated with a free-surface. The water depth in the test section can be varied remotely, from 6-inches to 24 inches. In addition, the ambient pressure in the HSC is adjustable from about 2-inches of

water absolute to 1 atmosphere. This feature allows models to be tested at the proper cavitation number. The HSC is also equipped with a large heat exchanger-cooling tower system. Thus the water temperature can be varied over a wide range (up to 120 degrees Fahrenheit). A view of the HSC test section and control console is shown in Figure 1.

For the two-dimensional test carried out as part of the present study, the HSC test-section was equipped with an aluminum roof to eliminate the free surface. The forward part of the roof was equipped with a smooth elliptical transition section so that smooth flow would be obtained in the test section. A pitot-static tube was mounted upstream of the model location to record the flow velocity with the roof installed.

The Planar Motion Mechanism (PMM) described in Reference 3 was modified for the present experimental investigation. The PMM is integral with the HSC test section cover and is normally used for static and dynamic tests of hydrofoils, submarine models, and other marine vehicles. These types of models are normally tested in the vertical plane of motion. For the faired-cable studies a mechanism was designed which transformed the PMM vertical-plane motions (heaving and pitching) into horizontal plane motions (swaying and yawing).

The model was attached to the modified PMM by means of a five-component balance system made up of modular force gages. These gages are described in detail in Reference 3. The electrical output signal from this gage is displayed in digital form by an
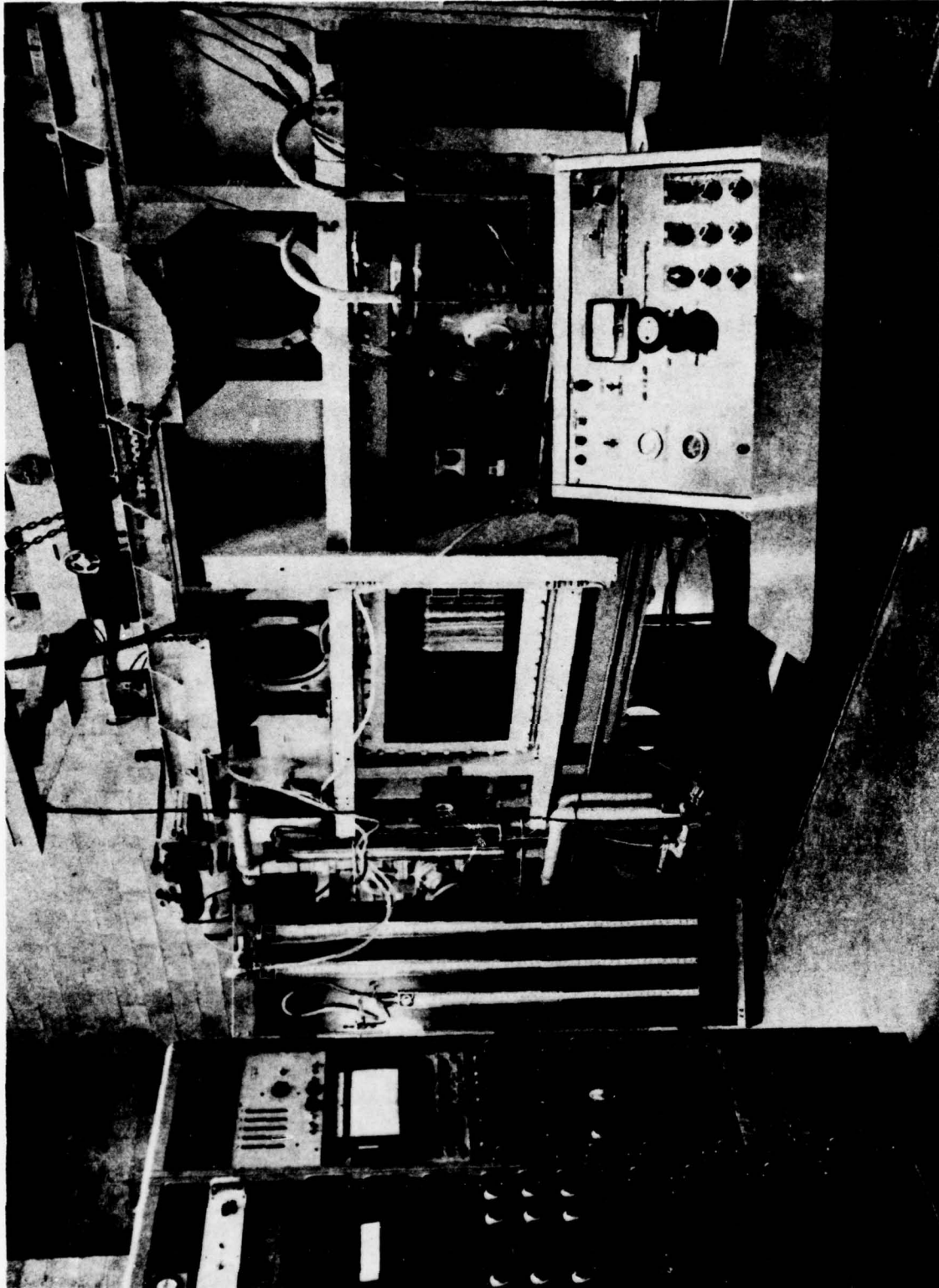
FIGURE 1 – TEST SECTION AREA OF HIGH SPEED, FREE SURFACE WATER CHANNEL

electronic null-balance servo system. A view of the model, balance system, HSC cover and PMM mechanism is shown in Figure 2.

The pure swaying and pure yawing tests (as defined in the Notation) were carried out using the A-3 model in two phases; namely without a free-surface and with a free surface in the HSC test section. The various test conditions covered in the present study are outlined in Table 2.

TABLE 2

Outline of Various Test Conditions

| Test Condition | Test Variable | Type of Test | |
		Pure Swaying	Pure Yawing
1. Without Free Surface	Speed, fps Ambient pressure	15, 20 atmospheric	15, 20 atmospheric
	Reduced frequency range	0.05-0.37	0.05-0.37
	Amplitude of oscillation, percent semichord	0.125	0.125
	Average water temp. degrees F	85	85
2. With Free Surface	Speed, fps Ambient pressure	15, 20 atmospheric, $\sigma = 0.37$	15, 20 atmospheric, $\sigma = 0.37$
	Reduced frequency range	0.05-0.37	0.05-0.37
	Amplitude of oscillation, percent semichord	0.125	0.125
	Average water temp. degrees F	85	85
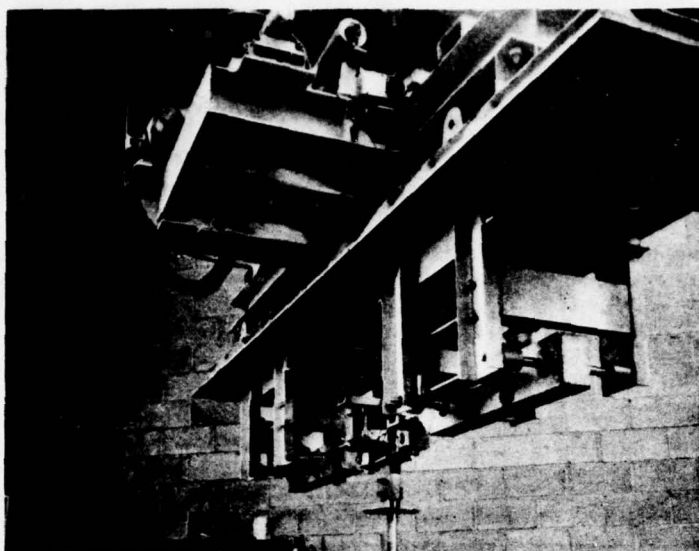
(a) MODEL ATTACHED TO PMM
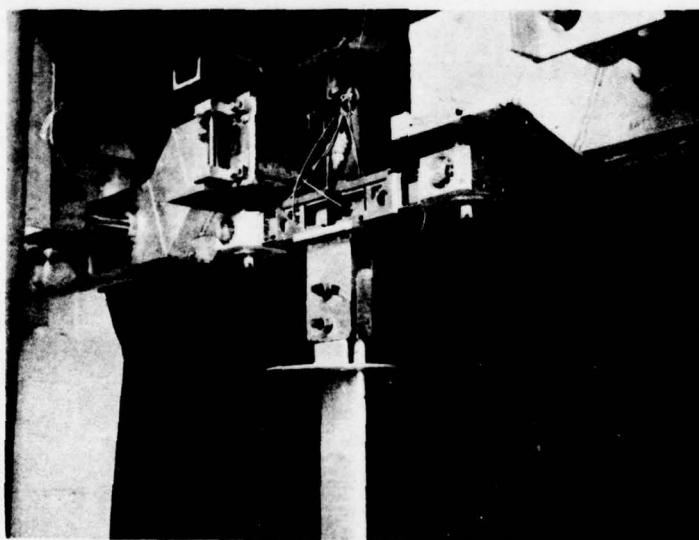
(b) MODEL AND FORCE BALANCE SYSTEM

FIGURE 2 – VIEW OF MODEL AND PLANAR MOTION MECHANISM SYSTEM

310

For each type of test, the speed in the HSC test section was kept constant and the oscillation frequency of the PMM was varied over the test range. The pure yawing and swaying motions were obtained by the techniques outlined in Reference 4. The results from the dynamic tests were obtained in the form of "In-Phase" and "Out-of-Phase" components of the lateral force and yawing moment. Tare tests were performed in air to obtain the "model mass" and moment of inertia corrections.

REDUCTION, CORRECTION AND PRESENTATION OF DATA

The results of the pure swaying and pure yawing tests are plotted in Figures 3 through 10 of Appendix A and B, respectively, as curves of nondimensional In-Phase and Out-of-Phase lateral force and yawing moment coefficients versus the appropriate velocity and acceleration parameters. In addition, results are presented to show the variations of the resultant forces and moment coefficients due to pure swaying and pure yawing and the phase angles between these forces and the imposed motion as a function of the reduced frequency parameter.

The results have been corrected for the nonhydrodynamic forces and moments associated with the model mass and the internal friction of the system. Such tares were determined experimentally from tests conducted in air. However, the data are uncorrected for possible blockage, wall interference, and boundary layer effects

The data have been reduced to coefficient form in accordance with the definitions presented in the Notation Section.

DISCUSSION OF RESULTS

A great deal of experimental and theoretical work has been carried out over the years to predict aeroelastic phenomena (flutter) of airfoils. Such theoretical and experimental studies as presented in References 5, 6, and 7 on oscillating two-dimensional airfoil are most inclusive. A review and re-evaluation of work in this field is presented in Reference 8. However, some of the aerodynamic data do not necessarily apply to the case of hydrofoils or faired cables for the following reasons:

      (a) The added mass effects are much more important to oscillating foils in water than oscillating foils in air,

      (b) Cavitation can occur in water, producing a departure from normal flow patterns,

      (c) Effects of the free surface on the coefficients could be an important factor, and

      (d) Foils in water generally operate at higher reduced frequencies than foils in air.

The ability of the designer to predict the behavior of a towed faired-cable-submerged combination, strongly dependent on understanding and being able to predict the dynamic coefficients of the cable configuration. One of the main purposes of this study is to provide such needed information for computer-simulation studies.

The applicable theory of Reference 5 is presented and compared with the experimental results of the present study as well as with the results of Reference 7.

Applicable Theory

The two-dimensional theory presented in Reference 5 may be used to calculate the lateral force and yawing moments per unit span acting on a faired cable, moving with velocity U, which is performing a simple harmonic swaying and yawing oscillation. The equations presented in Reference 5 may be expressed in the notation of the presented report as:

$$\frac{Y}{b} = -\operatorname{Re}\left\{\rho\pi\left(\frac{c}{2}\right)^2\left[(\ddot{y}_0 - U\dot{\psi}) - \frac{ac}{2}\ddot{\psi}\right]\right.$$

$$\left. + a_0\left(\tfrac{1}{2}\rho U_c\right)C(k)\left[(\dot{y}_0 - U\psi) + \frac{c}{2}\left(\tfrac{1}{2} - a\right)\dot{\psi}\right]\right\} \qquad [1]$$

$$\frac{N}{b} = -\operatorname{Re}\left\{\rho\pi\left(\frac{c}{2}\right)^2\frac{ac}{2}\left[(\ddot{y}_0 - U\dot{\psi}) - \frac{ac}{2}\ddot{\psi}\right]\right.$$

$$+ a_0\left(\tfrac{1}{2}\rho U_c\right)C(k)\frac{c}{2}\left(a + \tfrac{1}{2}\right)\left[(\dot{y}_0 - U\psi) + \frac{c}{2}\left(\tfrac{1}{2} - a\right)\dot{\psi}\right]$$

$$\left. - \rho\pi\left(\frac{c}{2}\right)^2\left[\frac{Uc}{4}\dot{\psi} + \frac{c^2}{32}\ddot{\psi}\right]\right\} \qquad [2]$$

where the moment expressed by Equation [2] is about a point a distance (ac/2) aft of the mid-chord. Equations [1] and [2] are written with respect to a fixed axis system.

To obtain the effect of oscillation frequency on the dynamic coefficients of a periodically oscillating faired cable, the following substitutions are made in Equation [1] and [2] transferring from a fixed to a moving axis system[6]

$$v = \dot{y}_o - U\psi$$

$$\dot{\psi} = r$$

$$iv = \frac{c}{2kU} \dot{v}$$

$$ir = \frac{c}{2kU} \dot{r}$$

Equation [1] then becomes in real form

$$\frac{Y}{b} = - \left[a_o (\tfrac{1}{2}\rho Uc)F(k) \right] v - \rho\pi \left(\frac{c}{2} \right)^2 \left[1 + \frac{a_o}{2\pi} \frac{2G(k)}{k} \right] \dot{v}$$

$$+ [a_o (\tfrac{1}{2}\rho Uc)F(k) \frac{c}{2} (a - \tfrac{1}{2})] r$$

$$+ \rho\pi \left(\frac{c}{2} \right)^3 \left[a + \frac{a_o}{2\pi} \frac{2G(k)}{k} (a - \tfrac{1}{2}) \right] \dot{r} \qquad [3]$$

and for the yawing moment

$$\frac{N}{b} = - \left[a_o \left(\tfrac{1}{2}\rho Uc \right) \frac{c}{2} \left(a + \tfrac{1}{2} \right) F(k) \right] v$$

$$- \rho\pi \left(\frac{c}{2} \right)^3 \left[a + \frac{a_o}{2\pi} \left(a + \tfrac{1}{2} \right) \frac{2G(k)}{k} \right] \dot{v}$$

$$+ \rho\pi \left(\frac{c}{2} \right)^2 Uc \left[\frac{1}{4} + \frac{a_o}{2\pi} F(k) \left(a^2 - \tfrac{1}{4} \right) \right] r$$

$$+ \rho\pi \left(\frac{c}{2} \right)^4 \left[a^2 + \frac{a_o}{2\pi} \frac{2G(k)}{k} \left(a^2 - \tfrac{1}{4} \right) + \frac{1}{8} \right] \dot{r} \qquad [4]$$

In non-dimensional form Equation [3] and [4] become

$$C_Y = - a_o F(k) \, v' - \pi \left[1 + \frac{a_o}{2\pi} \frac{2G(k)}{k} \right] \dot{v}'$$

$$+ \left[a_o F(k) \left(a - \tfrac{1}{2} \right) \right] r' + \pi \left[a + \frac{a_o}{2\pi} \frac{2G(k)}{k} \left(a - \tfrac{1}{2} \right) \right] \dot{r}' \quad [5]$$

$$C_N = - \frac{a_o}{2} \left(a + \tfrac{1}{2} \right) F(k) \, v' - \frac{\pi}{2} \left[a + \frac{a_o}{2\pi} \frac{2G(k)}{k} \left(a + \tfrac{1}{2} \right) \right] \dot{v}'$$

$$+ \pi \left[\frac{1}{4} + \frac{a_o}{2\pi} F(k) \left(a^2 - \tfrac{1}{4} \right) \right] r'$$

$$+ \frac{\pi}{2} \left[a^2 + \frac{a_o}{2\pi} \frac{2G(k)}{k} \left(a^2 - \tfrac{1}{4} \right) + \frac{1}{8} \right] \dot{r}' \qquad [6]$$

315

where

$$v' = k \frac{2y_m}{c} \qquad \text{(Out-of-phase with motion)}$$

$$\dot{v}' = k^2 \frac{2y_m}{c} \qquad \text{(In-phase with motion)}$$

$$r' = k \psi_m \qquad \text{(Out-of-phase with motion)}$$

$$\dot{r}' = k^2 \psi_m \qquad \text{(In-phase with motion)}$$

and

$$\psi_m = \frac{y_m}{k} \sin \frac{\phi_s}{2}$$

Thus, the terms of Equations [5] and [6] can be separated into quadrature (out-of-phase) and in-phase components as follows:

$$(C_{YS})_{OUT} = - [a_o F(k)] v' \qquad [7]$$

$$(C_{YS})_{IN} = - \pi \left[1 + \frac{a_o}{2\pi} \frac{2G(k)}{k} \right] \dot{v}' \qquad [8]$$

$$(C_{Yy})_{OUT} = [a_o F(k)(a - \tfrac{1}{2})] r' \qquad [9]$$

$$(C_{Yy})_{IN} = \pi \left[a + \frac{a_o}{2\pi} \frac{2G(k)}{k} (a - \tfrac{1}{2}) \right] \dot{r}' \qquad [10]$$

$$(C_{NS})_{OUT} = - \left[\frac{a_o}{2} (a + \tfrac{1}{2}) F(k) \right] v' \qquad [11]$$

316

$$(C_{NS})_{IN} = -\frac{\pi}{2}\left[a + \frac{a_o}{2\pi}\frac{2G(k)}{k}\left(a + \tfrac{1}{2}\right)\right]\dot{v}' \qquad [12]$$

$$(C_{Ny})_{OUT} = \pi\left[\frac{1}{4} + \frac{a_o}{2\pi}F(k)\left(a^2 - \tfrac{1}{4}\right)\right]r' \qquad [13]$$

$$(C_{Ny})_{IN} = \frac{\pi}{2}\left[a^2 + \frac{a_o}{2\pi}\frac{2G(k)}{k}\left(a^2 - \tfrac{1}{4}\right) + \frac{1}{8}\right]\dot{r}' \qquad [14]$$

The variation of the Theodorsen functions $F(k)$ and $G(k)$ with the reduced frequency parameters is presented in Table 3.

Comparison of Theory with Experimental Results

The comparison of the pure swaying data presented in Appenxix A with theory[5] and data from other studies[7] indicates good agreement for the atmospheric two-dimensional case at low and moderate values of the linear velocity parameter. However, in the case of the free-surface conditions studied (faired cable ventilating and cavitating) the theory, as expected, does not predict the variations of the force and moment coefficients with the velocity and acceleration parameters. The data from Reference 7 for the two-dimensional case seems to indicate trends similar to those obtained in the present study. Also, improvements in the agreement between theory and experiment are obtained if the measured lift-curve slope (obtained from Reference 1 for the A-3 faired cable) is used in the theoretical equations instead of 2π.

TABLE 3

Tabulation of Theodorsen Functions
For Various Values of the Reduced
Frequency Parameter

k	F(k)	-G(k)	$-\dfrac{2G(k)}{k}$
∞	0.5000	0	0
10.00	0.5006	0.0124	0.00248
6.00	0.5017	0.0206	0.00687
4.00	0.5037	0.0305	0.0153
3.00	0.5063	0.0400	0.0267
2.00	0.5129	0.0577	0.0577
1.50	0.5210	0.0736	0.0981
1.20	0.5300	0.0877	0.1461
1.00	0.5394	0.1003	0.2006
0.80	0.5541	0.1165	2.9123
0.66	0.5699	0.1308	0.3903
0.60	0.5788	0.1378	0.4593
0.56	0.5857	0.1428	0.51
0.50	0.5979	0.1507	0.6028
0.44	0.6130	0.1592	0.7259
0.40	0.6250	0.1650	0.8250
0.34	0.6469	0.1738	1.0223
0.30	0.6650	0.1793	1.1953
0.24	0.6989	0.1862	1.5558
0.20	0.7276	0.1886	1.886
0.16	0.7628	0.1876	2.345
0.12	0.8063	0.1801	3.0017
0.10	0.8320	0.1723	3.446
0.08	0.8604	0.1604	4.01
0.06	0.8920	0.1426	4.7533
0.05	0.9090	0.1305	5.22
0.04	0.9267	0.1160	5.80
0.025	0.9545	0.0872	6.976
0.01	0.9824	0.0482	9.64
0	1.000	0	

The force and moment coefficients presented in Figure 4 are a measure of the added mass and associated moments about the reference point (a = - 1/4). The measurements show a large negative added mass. The agreement with theory is poor. A similar trend was obtained from the studies presented in Reference 7.

The resultant force coefficient presented in Figure 5 is in excellent agreement with both theory and results of Reference 7. This is to be expected because the out-of-phase component predominates. However, as shown in Figure 6, the measured phase angle between the motion and the resultant force is some 20 degrees lower then predicted by theory. Similar results have been postulating by other investigators[9] in order to obtain good correlation with flutter results.

The pure yawing results are believed to be unique, in that all other investigators have obtained data on airfoils and hydrofoils performing combined motions (swaying and yawing). This did not permit a true evaluation of the separate effects of angular velocity and acceleration on the force and moment coefficients. The results presented in Appendix B shows that the agreement between the yawing results and the modified theory is in general fair. The effects of ventilation and cavitation in some cases are quite marked. For the atmospheric, two-dimensional case, the results presented in Figure 9 indicates that the theory can predict the resultant force reasonably well. However, the theory does not accurately predict the phase angles at low values of reduced frequency.

CONCLUDING REMARKS

Dynamic coefficients, determined from tests of a simulated, unswept, faired cable having an NACA 63A020 section are presented and compared with existing theory and other experimental results. Based on these comparisons, the following concluding remarks can be made regarding the applicability of the existing theory and the need for additional experimental results.

In general, it appears that the existing thin-airfoil theory cannot be relied upon to estimate the forces, moments and phase angle information required for accurate motion predictions. The effects of ventilation and cavitation further compound the discrepancies between experiment and theory.

The results of the present study were obtained using a rigid model. It can be expected that moderately different results would be obtained if the model had a greater degree of flexibility (similar to actual faired cable). Pending the development of improved theories which would account for the effects of thickness, flexibility, ventilation and cavitation, reliance should be placed on carefully conducted experimental programs. A similar conclusion has been reached by many investigators in an allied area; namely, the prediction of hydrofoil flutter.
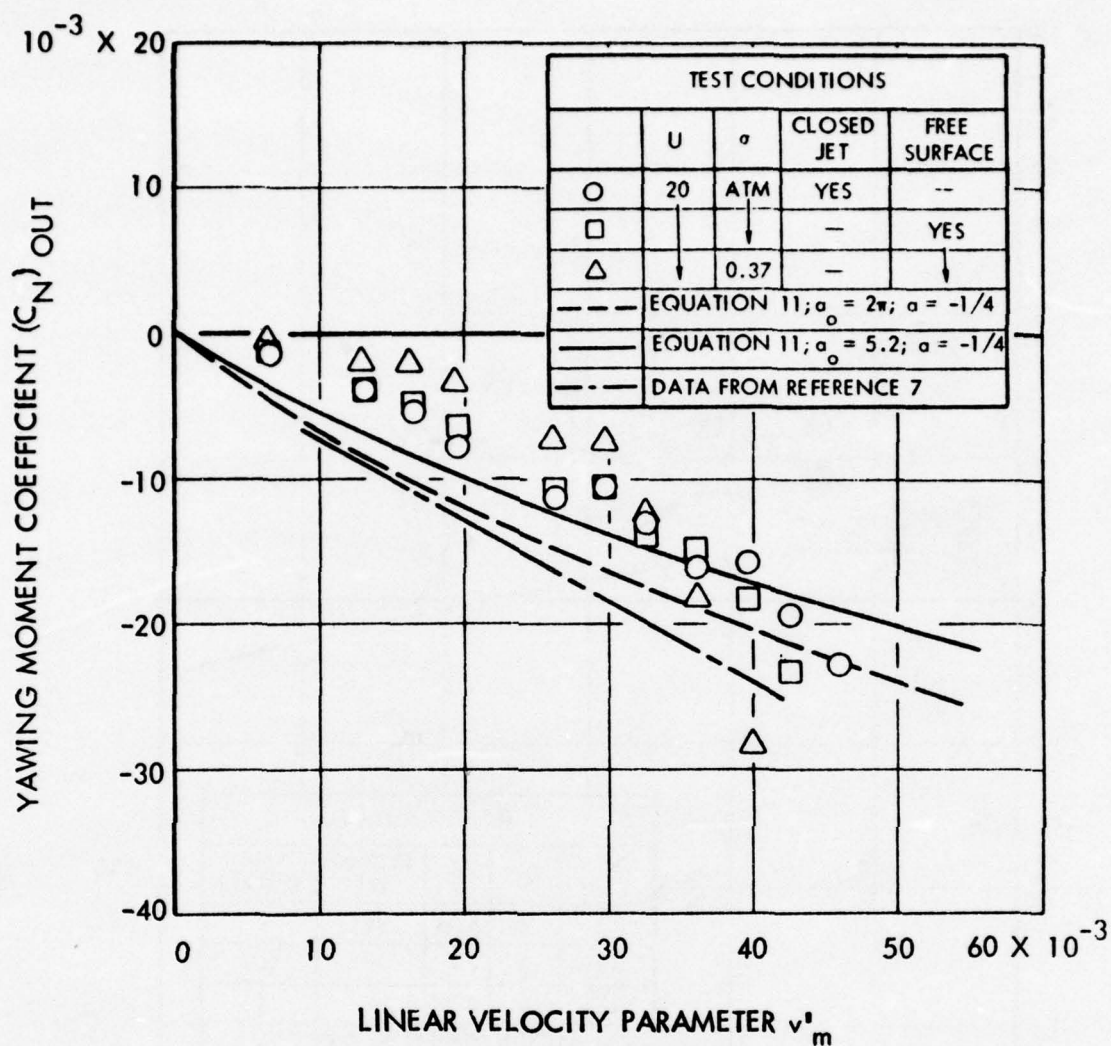
APPENDIX A

RESULTS OBTAINED FROM PURE-SWAYING TESTS
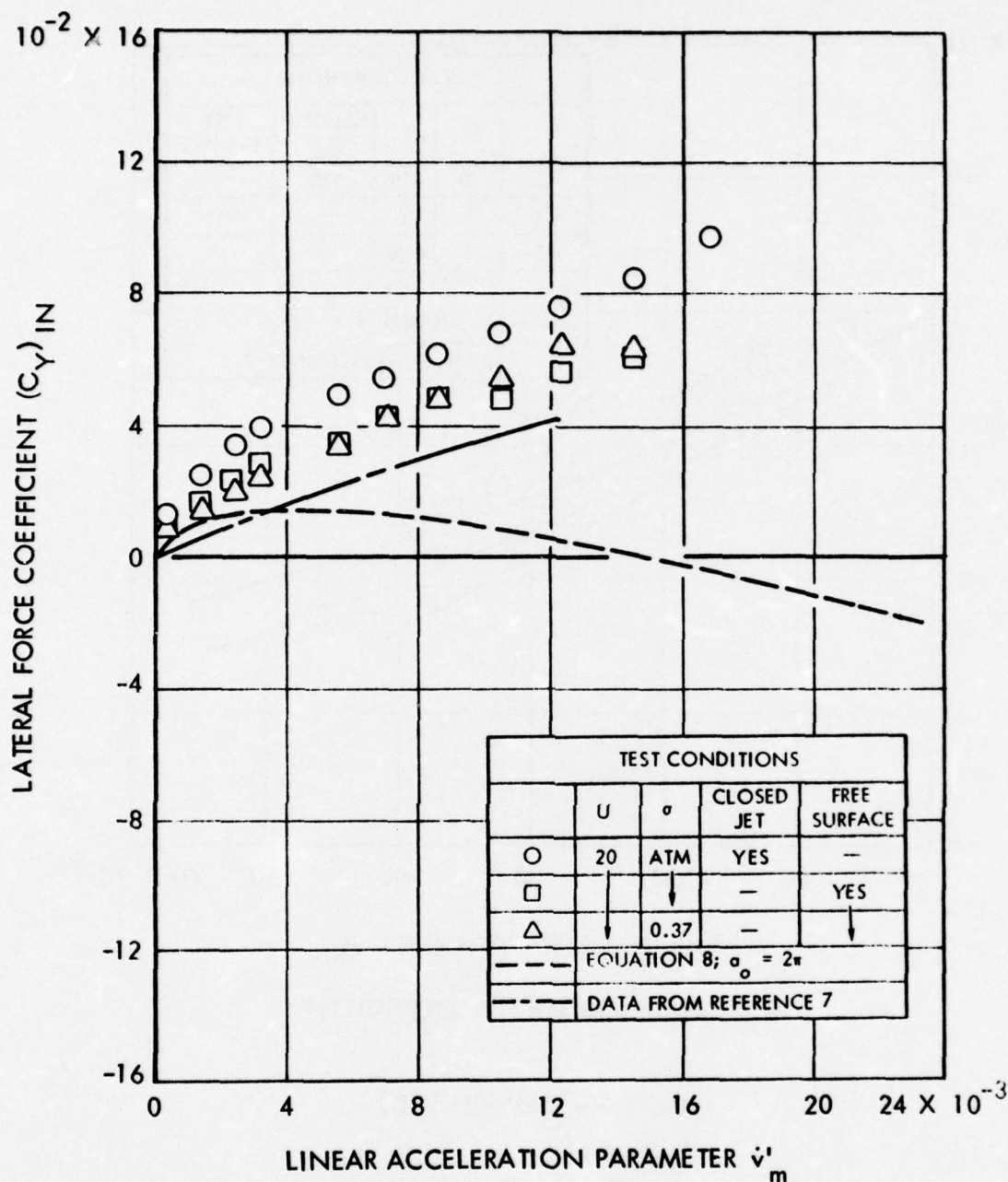
(Figures 3 - 6)
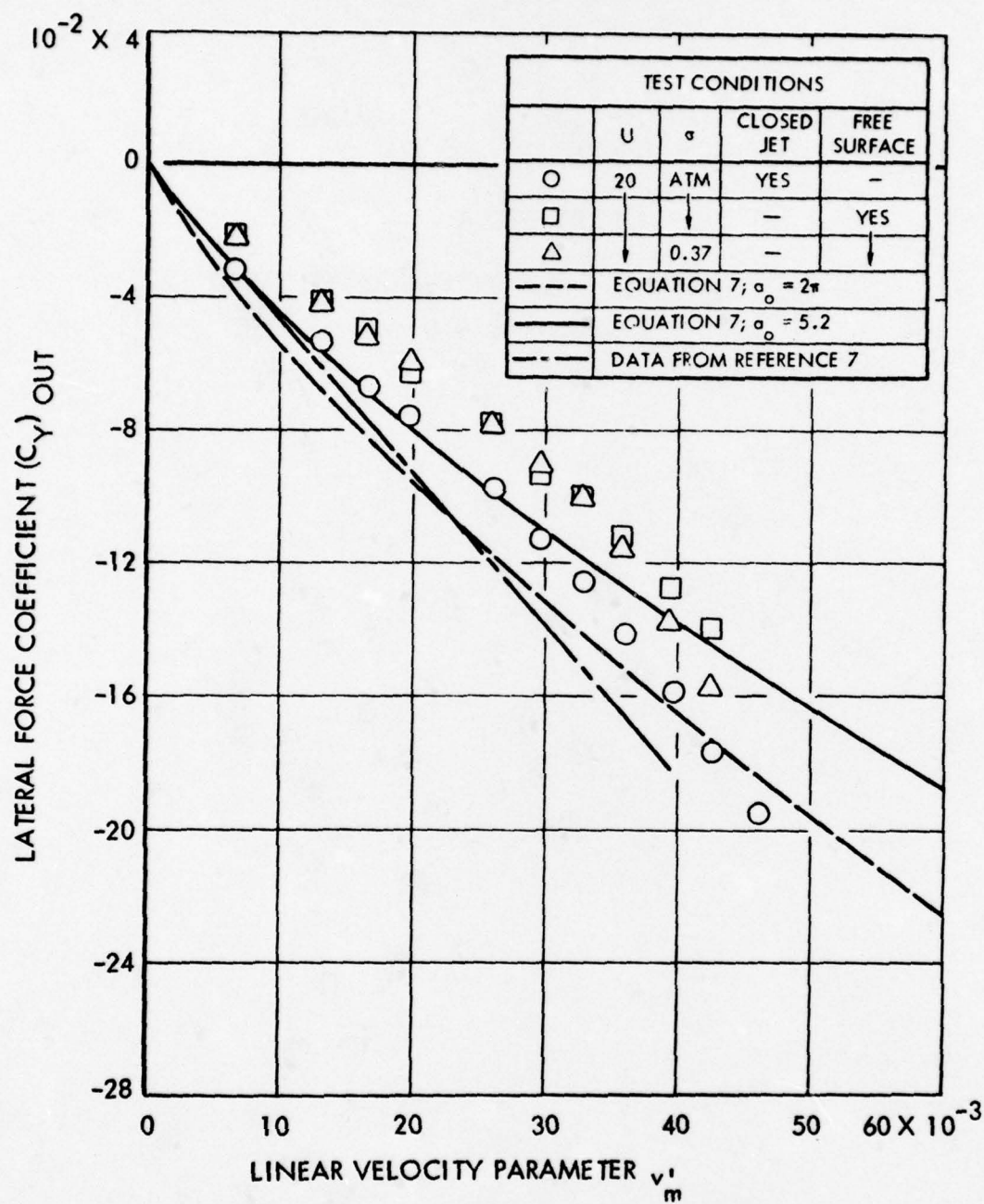
(a) LATERAL FORCE COEFFICIENT

FIGURE 3 – VARIATION OF THE AMPLITUDES OF THE QUADRATURE COMPONENTS
OF LATERAL FORCE AND YAWING MOMENT COEFFICIENTS WITH THE
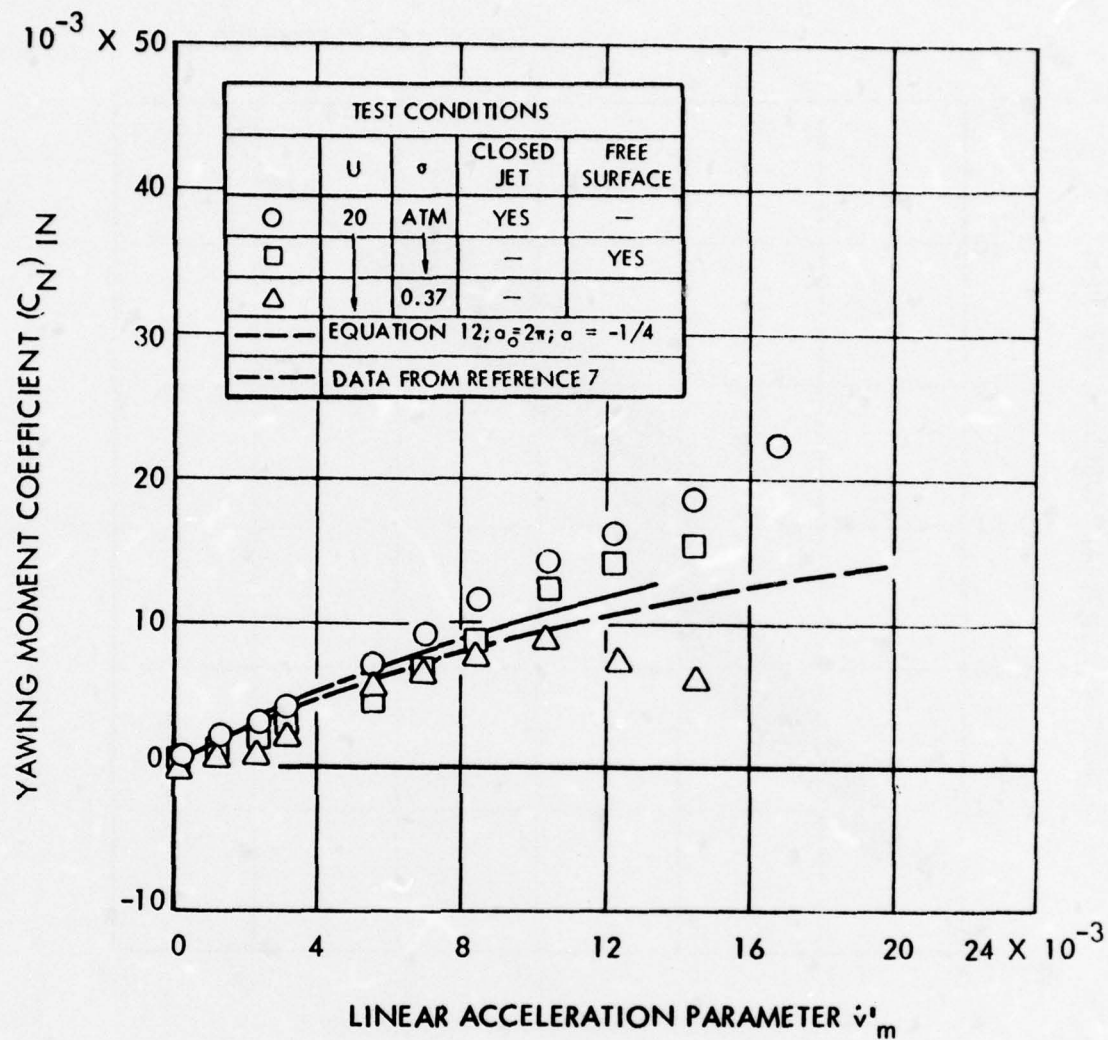LINEAR VELOCITY PARAMETER

(b) YAWING MOMENT COEFFICIENT
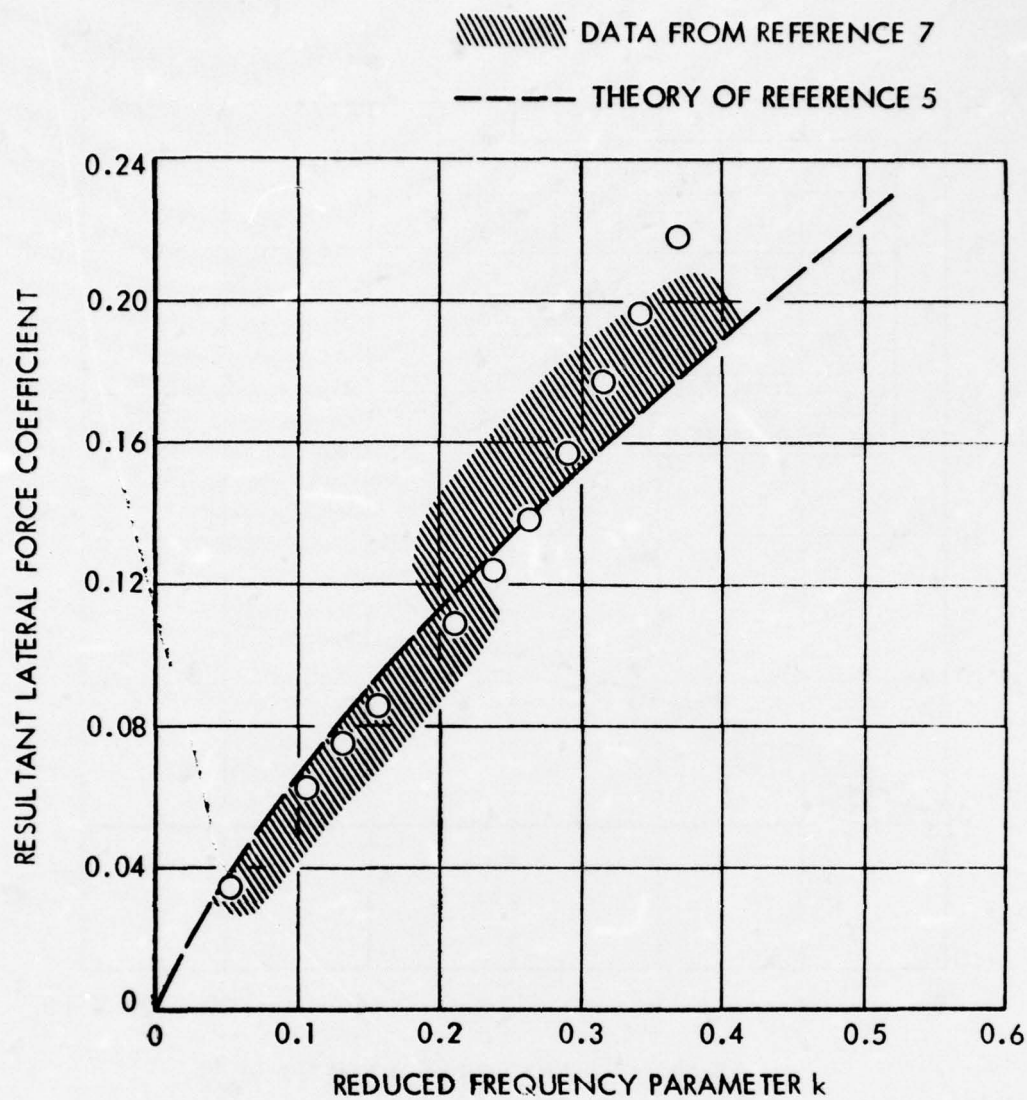
FIGURE 3 - (CONCLUDED)

(a) LATERAL FORCE COEFFICIENT

FIGURE 4 – VARIATION OF THE AMPLITUDES OF THE IN-PHASE COMPONENTS OF
THE LATERAL FORCE AND YAWING MOMENT COEFFICIENTS WITH THE
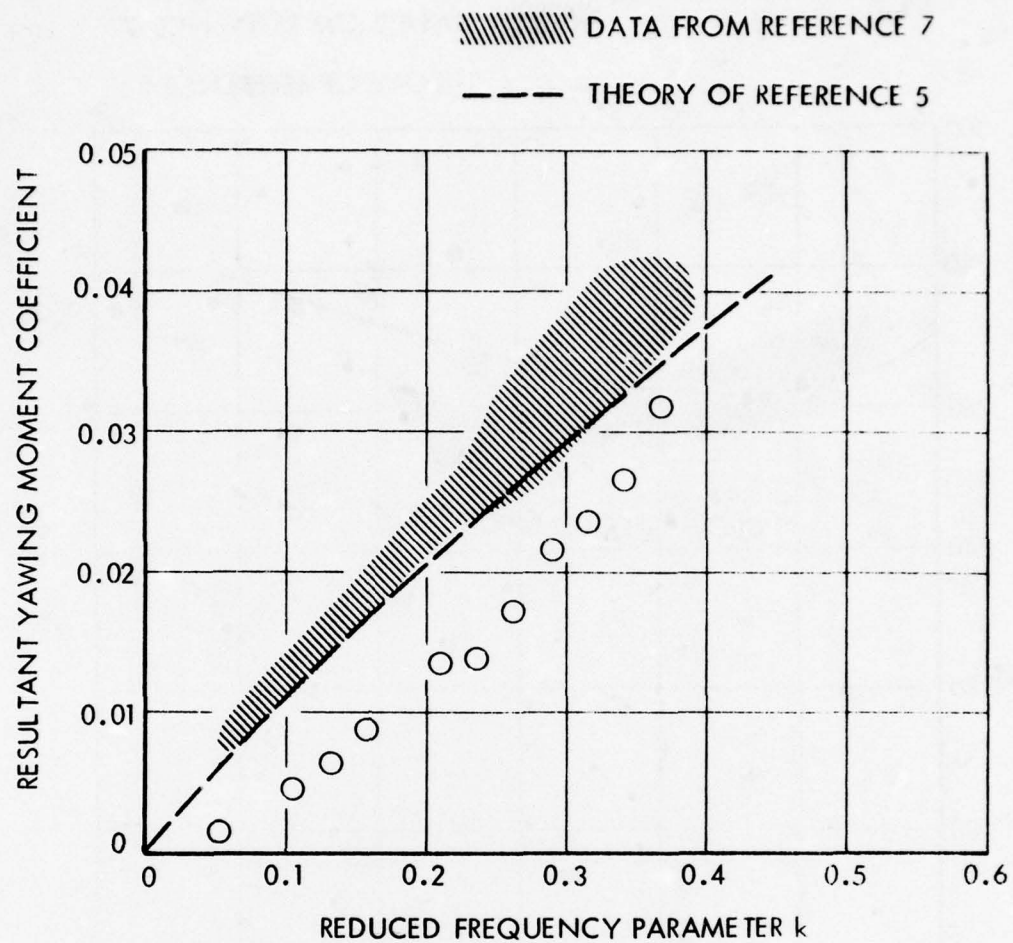LINEAR ACCELERATION PARAMETER

(b) YAWING MOMENT COEFFICIENT

FIGURE 4 – (CONCLUDED)

(a) LATERAL FORCE COEFFICIENT

FIGURE 5 – VARIATION OF THE RESULTANT LATERAL FORCE AND YAWING MOMENT COEFFICIENTS DUE TO PURE SWAYING WITH THE REDUCED FREQUENCY PARAMETER

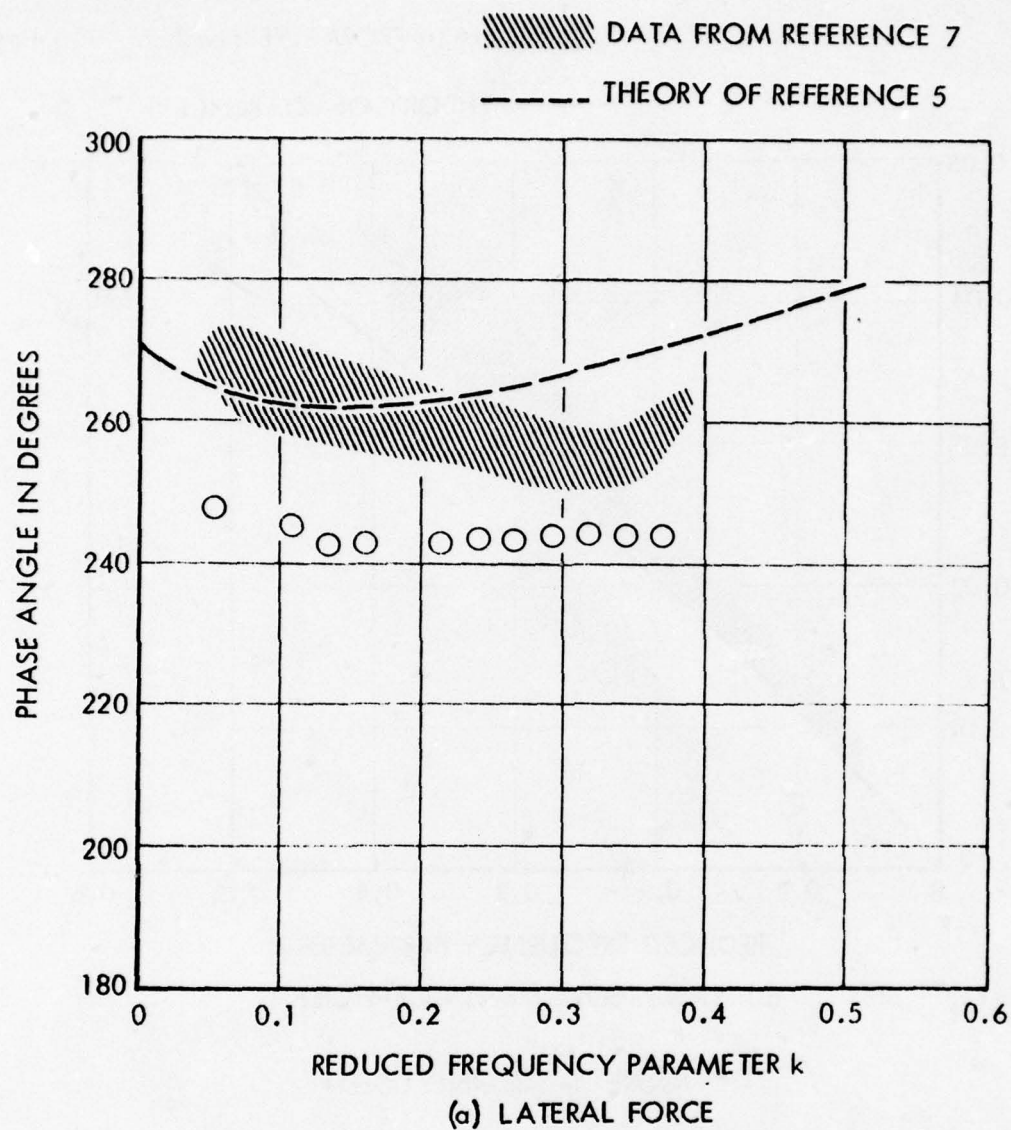(b) YAWING MOMENT COEFFICIENT

FIGURE 5- (CONCLUDED)

FIGURE 6 - VARIATION OF THE PHASE ANGLE BETWEEN THE RESULTANT LATERAL FORCE AND YAWING MOMENT DUE TO PURE SWAYING AND THE LATERAL DISPLACEMENT WITH THE REDUCED FREQUENCY PARAMETER

DATA FROM REFERENCE 7

THEORY OF REFERENCE 5
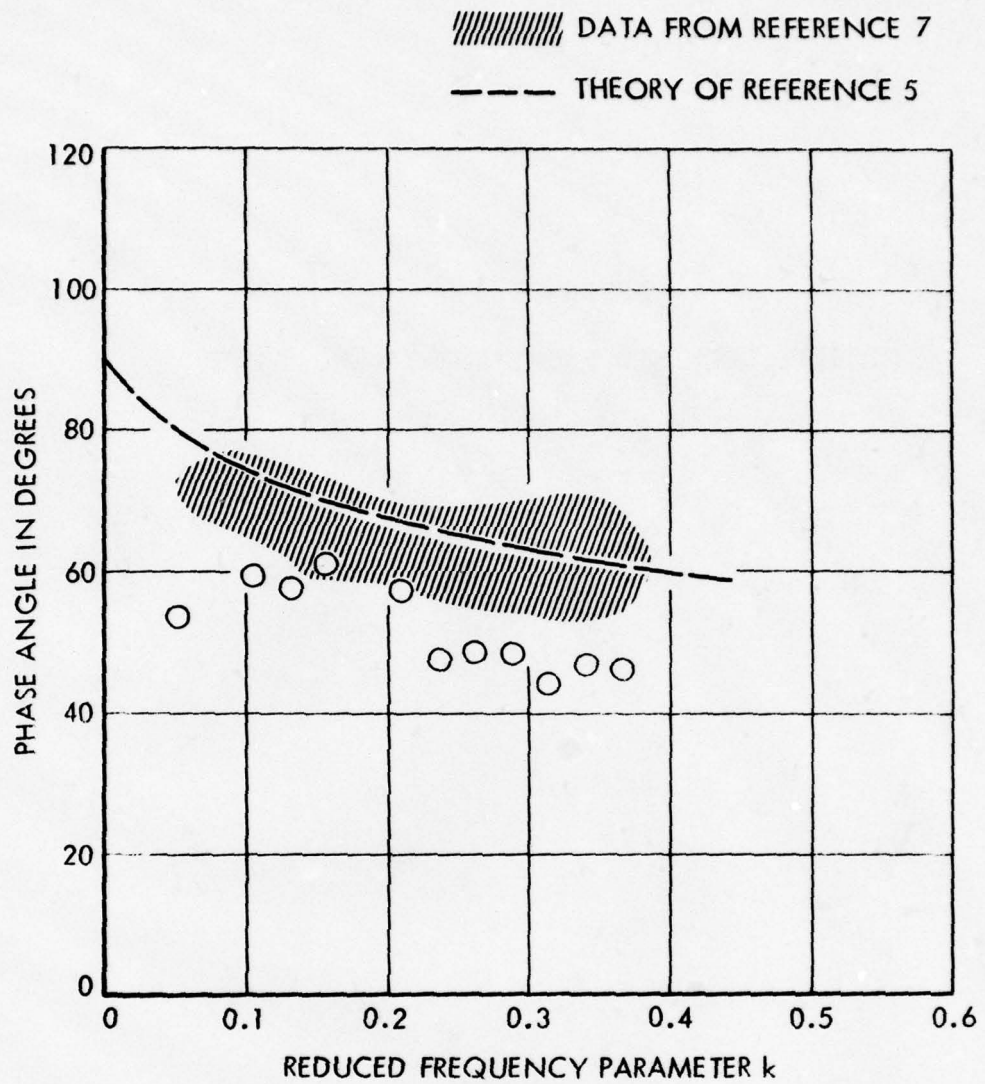
(b) YAWING MOMENT

FIGURE 6 - (CONCLUDED)

APPENDIX B

RESULTS OBTAINED FROM PURE-YAWING TESTS

(Figures 7 - 10)

330

(a) LATERAL FORCE COEFFICIENT

FIGURE 7 – VARIATION OF THE AMPLITUDES OF THE QUADRATURE COMPONENTS OF LATERAL FORCE AND YAWING MOMENT COEFFICIENTS WITH THE ANGULAR VELOCITY PARAMETER

331

TEST CONDITIONS

	U	σ	CLOSED JET	FREE SURFACE
$\bigcirc$	20	ATM	YES	—
$\square$		ATM	—	YES
$\triangle$		0.37	—	YES
– – –	EQUATION 13; $a_o = 2\pi$; $a = -1/4$			
——	EQUATION 13; $a_o = 5.2$; $a = -1/4$			
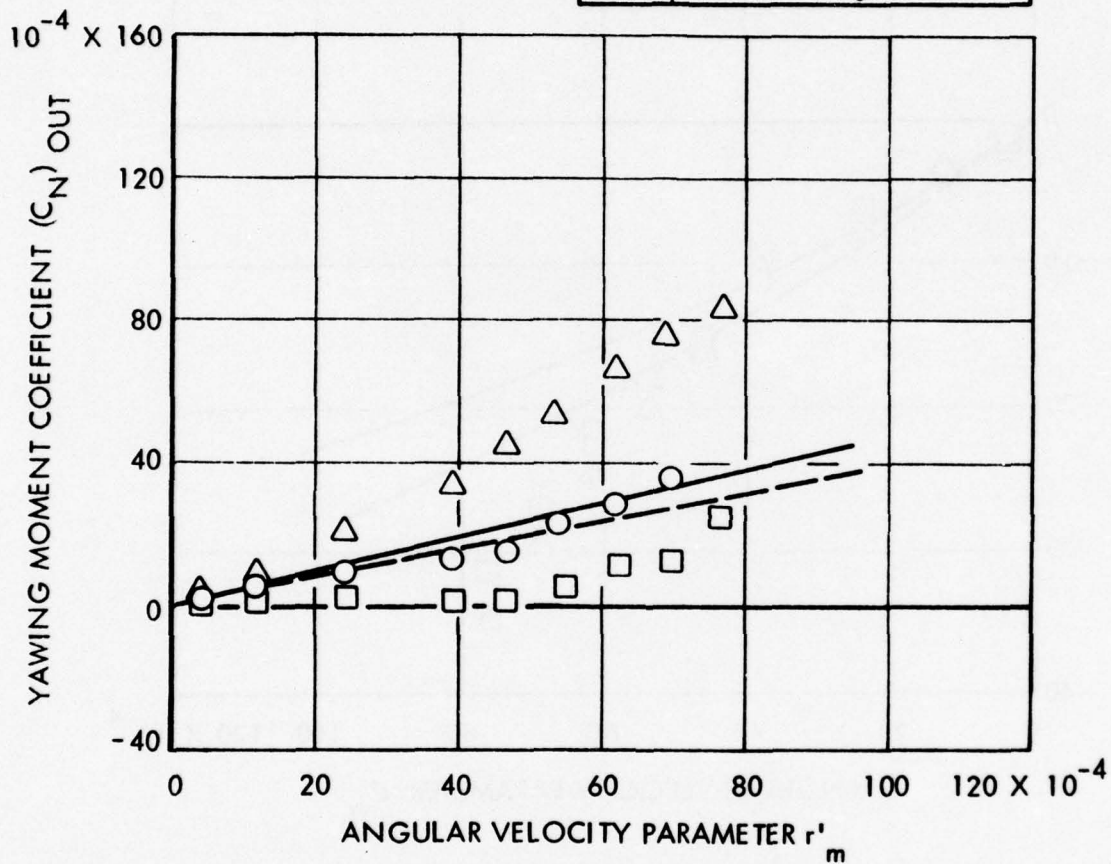
(b) YAWING MOMENT COEFFICIENT

FIGURE 7 - (CONCLUDED)

(a) LATERAL FORCE COEFFICIENT
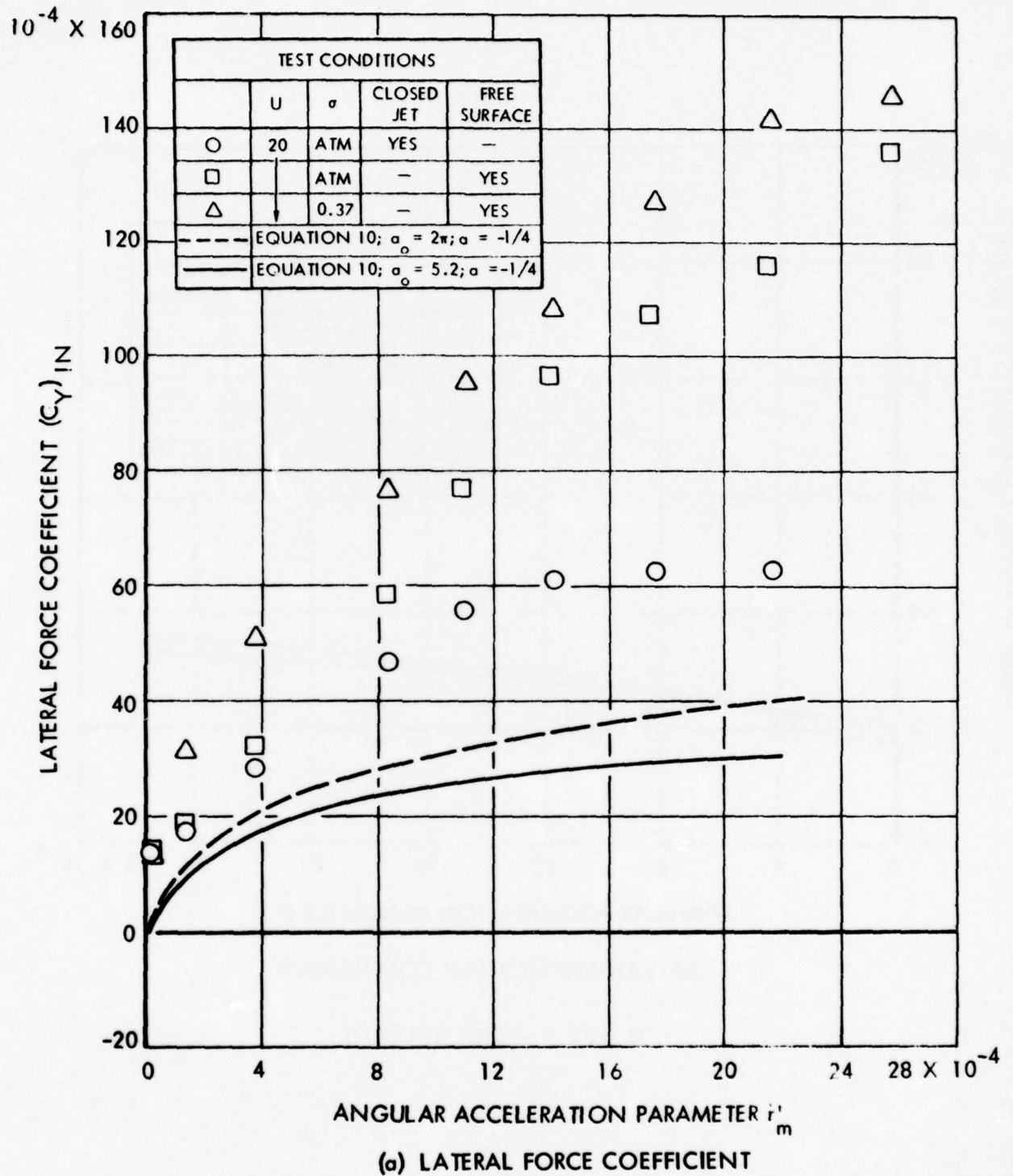
FIGURE 8 – VARIATION OF THE AMPLITUDES OF THE IN-PHASE COMPONENTS OF LATERAL FORCE AND YAWING MOMENT COEFFICIENTS WITH THE ANGULAR ACCELERATION PARAMETERS
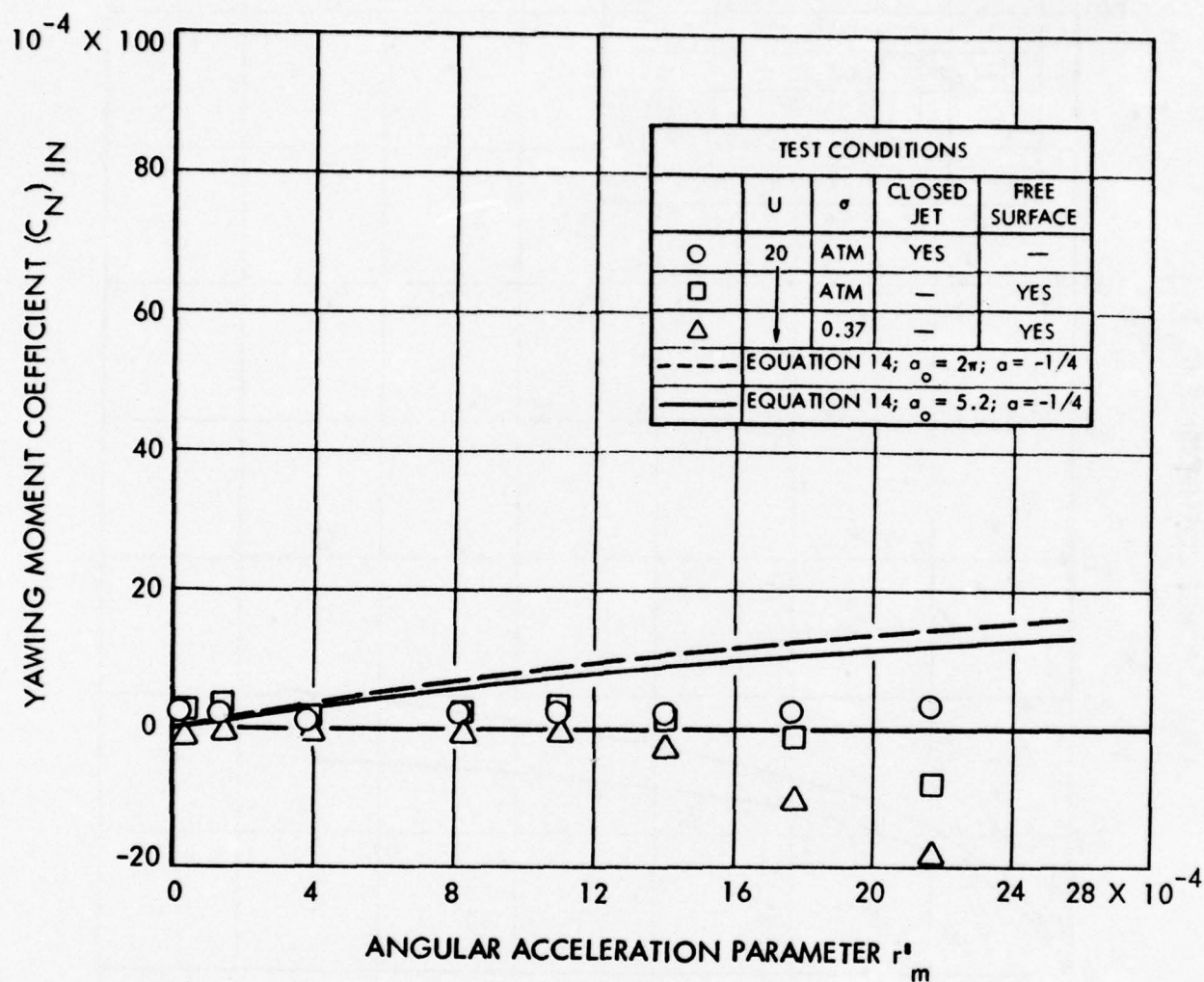
(b) YAWING MOMENT COEFFICIENT

FIGURE 8 - (CONCLUDED)
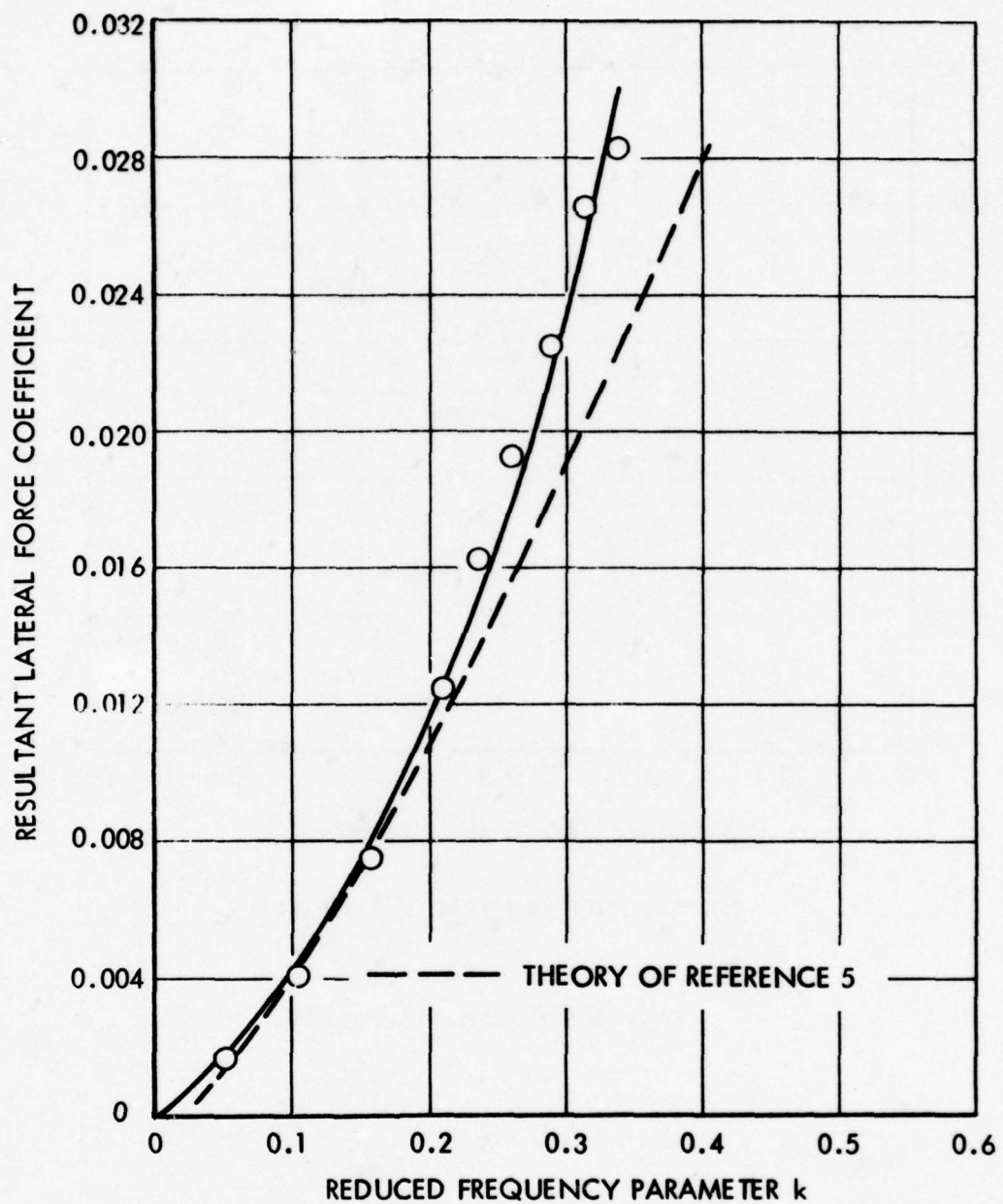
(a) LATERAL FORCE COEFFICIENT

FIGURE 9 - VARIATION OF THE RESULTANT LATERAL FORCE AND YAWING MOMENT COEFFICIENTS DUE TO PURE YAWING WITH THE REDUCED FREQUENCY PARAMETER
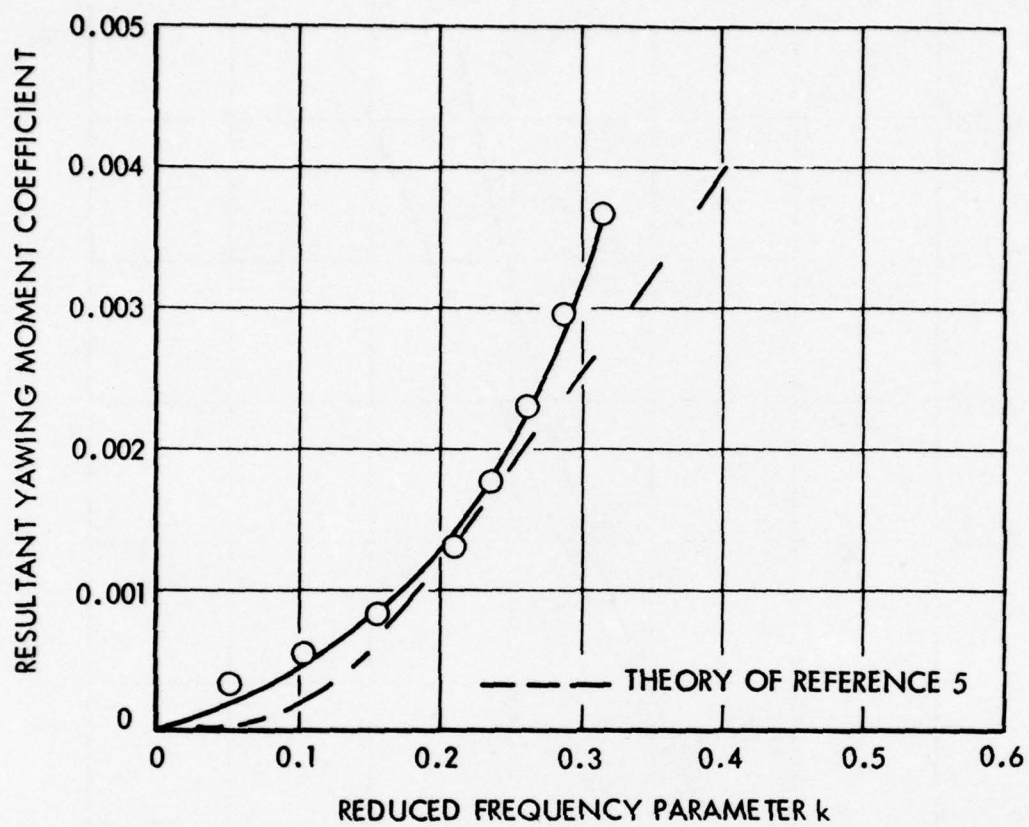
(b) YAWING MOMENT COEFFICIENT

FIGURE 9 - (CONCLUDED)
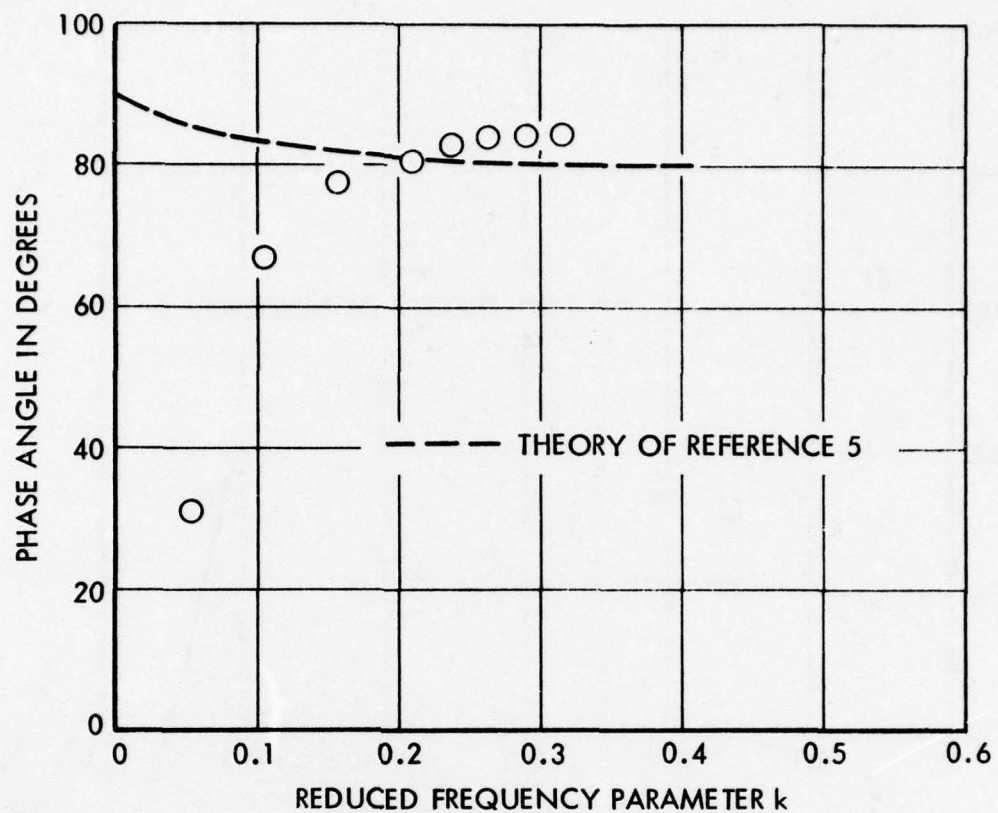
(a) LATERAL FORCE

FIGURE 10 – VARIATION OF THE PHASE ANGLE BETWEEN THE RESULTANT LATERAL
FORCE AND YAWING MOMENT DUE TO PURE YAWING AND THE
ANGULAR DISPLACEMENT WITH THE REDUCED FREQUENCY PARAMETER
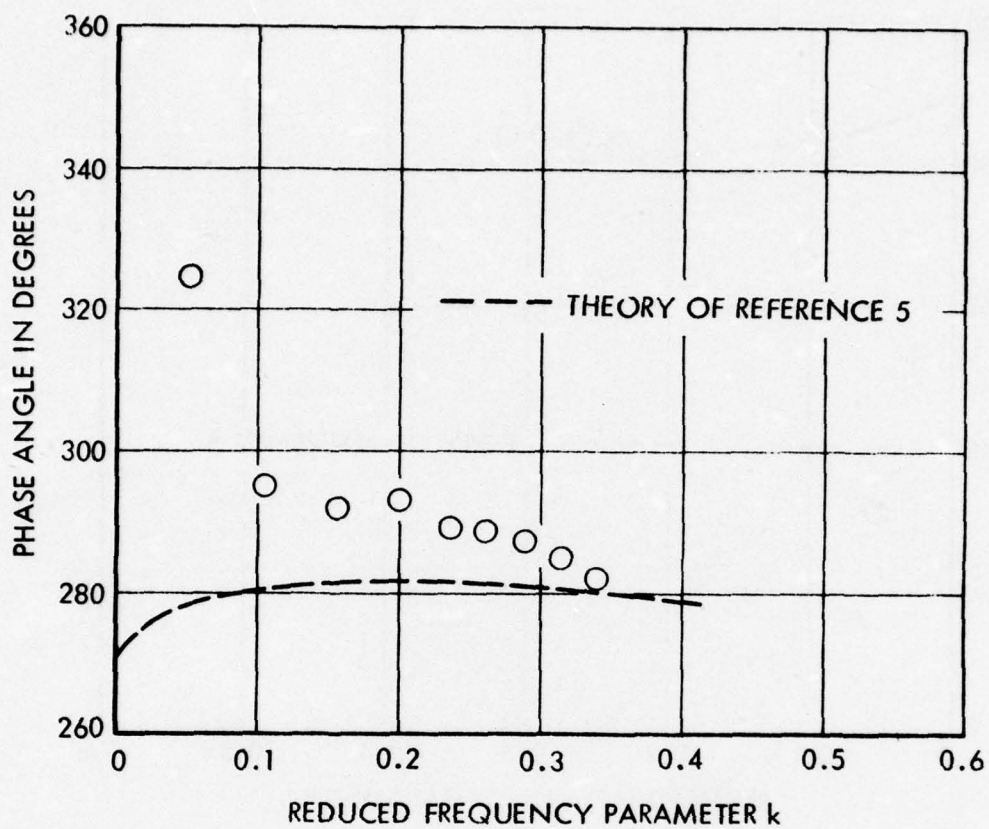
(b) YAWING MOMENT

FIGURE 10 - (CONCLUDED)

REFERENCES

1. Etter, Robert J. and Huang, Thomas T., "An Experimental Investigation of the Static Hydrodynamic Characteristics of Several Simulated, Faired Cables Having Symmetrical NACA Airfoil Sections," HYDRONAUTICS, Incorporated Technical Report 530-1, 1967.

2. Huang, Thomas T. and Etter, Robert J., "Boundary Layer Flow Visualization of Several Simulated Faired Cables Having Symmetrical NACA Airfoil Sections," HYDRONAUTICS, Incorporated Technical Report 530-3, April 1967.

3. Johnson, Virgil E., Jr., and Goodman, Alex, "The HYDRONAUTICS, Incorporated Variable-Pressure, Free-Surface, High-Speed Channel," HYDRONAUTICS, Incorporated Technical Report 229-1, January 1964.

4. Goodman, Alex, "Experimental Techniques and Methods of Analysis Used in Submerged Body Research," Proceedings of Third ONR Symposium on Naval Hydrodynamics, September 1960.

5. Theordorsen, Theodore, "General Theory of Aerodynamic Instability and Mechanism of Flutter," NACA Report 496, 1935.

6. Martin, Milton, "The Stability Derivatives of a Hydrofoil Boat, Part II," HYDRONAUTICS, Incorporated Technical Report 001-10(II), January 1963.

7. Halfman, R. L., "Experimental Aerodynamic Derivatives of a Sinusoidally Oscillating Airfoil in Two-Dimensional Flow," NACA Report 1108, 1952.

8. Chu, W. H., "A Critical Re-Evaluation of Hydrodynamic Theories and Experiments in Subcavitating Hydrofoil Flutter," Southwest Research Institute Project No. 02-1371, Technical Report, June 1964.

9. Abramson, H. N. and Langner, Carl S., "Correlation of Various Subcavitating Hydrofoil Flutter Predictions Using Modified Oscillatory Lift and Moment Coefficients," Southwest Research Institute Project No. 68-1371-2, Technical Report, June 1964.

SESSION 3

FAIRED TOWLINE HYDRODYNAMICS

Bibliography

Summary of Discussion

3.0 <u>FAIRED CABLE HYDRODYNAMICS</u>

    3.1 <u>DESIGN</u>

        3.1.1 Boeing Company D2-23504, Final Report, <u>High-speed towing cable development</u>, CONFIDENTIAL, 31 July 1964

        3.1.2 Boeing Company D2-89924-1, Final Report, <u>Development of High-speed Towing Cables; Underwater Towed Body, Part I</u> CONFIDENTIAL, 12 January 1966

        3.1.3 Boeing Company D2-89924-2, Final Report, <u>Development of High-speed Towing Cables, Underwater Towed Body, Part 2,</u> CONFIDENTIAL, 12 January 1966

        3.1.4 Boeing Company D2-133006-1, Final Report, <u>Tests and Investigations of a High-speed Towed Sonar Cable</u>   June 1966

        3.1.5 Boeing Company D2-133009-2, <u>Cable Towing Test System Critique; Volume II, Cable Performance Analysis</u>, CONFIDENTIAL August 1966

        3.1.6 David Taylor Model Basin Report No. 661, <u>Analysis of Cable and Housing Requirements for a Deep-towed Body at High-speed,</u> by L. Pode, November 1948

        3.1.7 David Taylor Model Basin Report No. C-433, <u>The Development of a Fairing for Tow Cables</u>, by L.F. Fehlner and L. Pode, CONFIDENTIAL, January 1952

        3.1.8 David Taylor Model Basin Report No. C-869, <u>The Development of a Clip-type Fairing for the AN/SQS-17 Towed-sonar System</u>, by T. Gibbons, CONFIDENTIAL, August 1957

        3.1.9 David Taylor Model Basin Report No. C-959, <u>A Recommended Cable-Fairing Design for the Project PHOENIX Towing System,</u> by T. Gibbons, CONFIDENTIAL, May 58

        3.1.10 David Taylor Model Basin Report No. C-1015, <u>Evaluation of Six Types of Cable-fairing for the Ship-towed Sonar Program,</u> by J. Nelligan, CONFIDENTIAL, December 1958

        3.1.11 Goodyear Aircraft Corp. Report GER 8415, Final Engineering Report, <u>Development of an Air-towed Sonar Cable Fairing,</u> CONFIDENTIAL, 15 Dec 1957

        3.1.12 Naval Applied Science Lab Project 9300-54; Technical Memorandum 1, <u>A Study of New Minimum Width Towlines for Large VDS Systems,</u> by C.K. Chatten and J. DiLiberti, CONFIDENTIAL, 4 Sep 1964

        3.1.13 North American Aviation Report C 6-1796/020, <u>Two Dimensional Airfoil Literature Survey,</u> by B.H. Carmichael and D. Meggitt 1 August 1966

3.1.14 North American Aviation SID 65-1279, 1 thru 4; Final Report, High-Speed Towing Cable Development (Phase I-II, Volumes 1-4), CONFIDENTIAL, 29 October 1965

3.1.15 Pneumodynamics Corp., Report TN-SEDU-6634-1, General Design Criteria for Cable-Towed Body Systems Using Faired and Unfaired Cable, by W.M. Ellsworth, Oct 1960

3.1.16 U.S. Rubber Co., Contract N140-(122) 78295B, Final Report, Development of Faired Power Cable. 28 Feb 66

3.1.17 Underwater Sound Laboratory, Pub 765, Guide for Designing Towed Bodies and Towlines for Variable Depth Sonar, by K.T. Patton. 30 June 66

3.1.18 Underwater Sound Laboratory, Technical Memorandum 933-0188-64 A Study of New Minimum-Width Towlines for Large VDS Systems, by D.A. Nichols and S. Gross. 4 Sep 1964

3.2 MODEL TESTS

3.2.1 David Taylor Model Basin Report 1284 (AERO 952), Wind-Tunnel Tests of Two-Dimensional Cable Fairings, by N. G. Ziegler, November 1958

3.2.2 David Taylor Model Basin Report C-756, Wind-Tunnel Tests of Two-Dimensional Faired and Unfaired Sections, by J. T. Matthews. May 1956

3.2.3 David Taylor Model Basin Rept C-855. Wind-Tunnel Tests of Two-Dimensional Faired Cables, Part 1 - Four Cables at Low Reynolds Numbers, by J.T. Matthews. July 57

3.2.4 David Taylor Model Basin Rept C-920, Evaluation of USNUSL Sectional Fairing, by F.W. Johnson and T. Gibbons. Feb 58

3.2.5 David Taylor Model Basin Report C-981 (AERO 921, Part II) Wind-Tunnel Tests of Two-Dimensional Faired Cables. Part II - Additional Tests at Higher Reynolds Numbers, by R. L. Velebny, CONFIDENTIAL, August 1958

3.2.6 David Taylor Model Basin Rept C-1012, The Evaluation of the GAC Fiberglas Sonar Cable Fairing, by T. Gibbons. Nov 58

3.2.7 David Taylor Model Basin Report C-1015, Evaluation of Six Types of Cable-Fairing for the Ship-Towed Sonar Program, by J. Nelligan and T. Gibbons, December 1958

3.2.8 David Taylor Model Basin Hydromechanics Lab, Rept 155-H-01 Experimental determination of the Hydrodynamic Loading Functions for a Special Faired Towcable, by T. Gibbons, and D. Gray. May 66

3.2.9   David Taylor Model Basin. Hydromechanics Lab. Rept 173-H-01
         Drag Characteristics of a Systematic Series of Trailing-
         Type Cable Fairings (DTMB Series B), by J.P. Ramsey and
         T. Gibbons. Aug 66

3.2.10   Great Britain. Admiralty Experiment Labs. Rept 1/57
         Variable Depth ASDIC; the Resistance and Lift of Cable
         Fairing When Inclined to Direction of Flow. SECRET Jan 57

3.2.11   Great Britain. Admiralty Experiment Works Rept 31/58
         Variable Depth ASDIC. Resistance and Lift of Cable Fairing
         When Inclined to Direction of Flow. SECRET July 58

3.2.12   Great Britain. Admiralty Experiment Works Rept 31/59
         Variable Depth ASDIC Resistance and Lift of Modified Cable
         Fairing When Inclined to Direction of Flow. SECRET Aug 59

3.2.13   Great Britain Aeronautical Research Council R&M 599
         The Resistance of Inclined Struts, by C.H.Powell, Mar 1919

3.2.14   Pennsylvania State Univ. ORL Serial NOrd 16598-16
         Water-Tunnel Tests of Cable Fairings and Faired Cables,
         by G. L. Calehuff. 10 Jan 57 CONFIDENTIAL

3.2.15   Pennsylvania State University Ordnance Research Laboratory
         Technical Memorandum 21.3361-28, Water Tunnel Tests of
         Goodyear Cable Fairings, March 1957, by A.F. Lehman
         CONFIDENTIAL 8 May 1957

3.3 STATIC CONFIGURATION ANALYSIS

3.3.1   Canada. Naval Research Est., Dartmouth Report PHx-103
         The Configuration of a Cable Towing a Heavy Submerged Body
         from a Surface Vessel, by M. C. Eames. Nov 1956

3.3.2   Canada. Naval Research Est., Dartmouth, Technical Memorandum
         57/10, Influence of Cable Drag and Body. Weight on the
         Depth and Speed of the Trilby Towed Sonar, by M. C. Eames
         1957

3.3.3   Canada. Naval Research Est., Dartmouth TN FM/66/9 Design
         Curves for Optimum Towing at High Speed, by C.L. Gaul,
         and M. C. Eames. Sep 66

3.3.4   Canada. Naval Research Est., Dartmouth TN Math 66/1
         Configuration of a Cable Towing a Submerged Body, by C.M.
         Mihoff. Mar 66

3.3.5   David Taylor Model Basin Report No. 422 The Tension in a Loop
         of Cable Towed Through a Fluid, by J.G. Thews and L. Landweber.
         June 1936

3.3.6   David Taylor Model Basin Report No. 533 Shape and Tension of a
         Light, Flexible Cable in a Uniform Current, by L. Landweber
         and M. H. Protter. October 1944

344

3.3.7 David Taylor Model Basin Report 687. Tables for Computing the Equilibrium Configuration of a Flexible Cable in a Uniform Stream, by L. Pode, March 1951

3.3.8 David Taylor Model Basin Report 687, Supplement. Cable Function Tables for Small Critical Angles, by L. Pode, Sept 1955

3.3.9 David Taylor Model Basin Report 717, A Method of Determining Optimum Lengths of Towing Cables, by L. Pode, April 1950 Appendix 1, March 1956

3.3.10 David Taylor Model Basin Report 1806. A FORTRAN Program for the Calculation of the Equilibrium Configuration of a Flexible Cable in a Uniform Stream, by E. H. Cuthill, March 1964

3.3.11 David Taylor Model Basin Report C-919. The Towing Configuration of the AN/SQS-17 Sonar System, by C. D. Walton, February 1958

3.3.12 David Taylor Model Basin Report R-33. Tension in a Cable Towing a Heavy Weight Through A Fluid, March 1941

3.3.13 David Taylor Model Basin Report R-37. Orientation and Position of a Heavy Body Suspended in a Uniform Current by a Flexible Cable, August 1941

3.3.14 David Taylor Model Basin. Hydromechanics Lab. Rept 155-H-01 Experimental Determination of the Hydrodynamic Loading Functions for a Special Faired Towcable, by T. Gibbons, and D. Gray. May 66

3.3.15 David Taylor Model Basin. Hydromechanics Lab. Rept. C-069-H-01 Feasibility Study of the Hydromechanic Aspects of an Interim Towed Sonar System for Hydrofoil Craft, by P. K. Spangler May 1965

3.3.16 Edo Corp. Report 5709. The Steady, Rectilinear Towing of a Weightless Hydrofoil-Cable System in a Non-uniform Stream by P. A. Pepper and J. Streich. 26 Jan 1962

3.3.17 Edo Corp. Report 5741. The Equilibrium Configuration of a Towed Hydrofoil-Strut System in Two-Dimensional Steady Turns, by P. A. Pepper and J. Streich. 13 Apr 1962

3.3.18 Edo Corp. Report 5822. The Equilibrium Configuration of a Towed Hydrofoil-Cable System in Two-Dimensional Steady Turns, by P. A. Pepper. 10 Jan 1964

3.3.19 Great Britain. Admiralty Experiment Works. Report 10/51 AME Cable Fairing; Optimum Position of Cable, by L. J. Brooks, March 1953

3.3.20 Great Britain Aeronautical Research Council R&M 1592. The Form of a Heavy Flexible Cable Used for Towing a Heavy Body Below an Aeroplane, by H. Glavert, February 1934

3.3.21 Hydrospace Research Corporation Report 102. Hydrodynamic Design of a Maneuverable Hydrophone Line Array, by J. J. Nelligan CONFIDENTIAL 6 January 1963

3.3.22 Hydrospace Research Corp. Rept 119. Investigation of Hydrodynamic Loading on Faired Towline, by S. M. Gay, A. Brisband and (others) CONFIDENTIAL 17 June 64

3.3.23 Kirkby, J. M. and Stanley, T. J., Configuration and Tension of Cable for Towing Underwater Bodies, Royal Naval Scientific Service Journal V. 12, p. 198-213 CONFIDENTIAL September 1957

3.3.24 Quick, Stanley L., The Shape and Tension of Cables in a Uniform Stream, (Ph.D. Thesis, Polytechnic Institute of Brooklyn), 1962

3.3.25 Rutgers University Contract N70024-1366, Equilibrium and Dynamic Motion of a Towline and a Towed Body, by S. P. Reyle and J. W. Schram June 1966

3.3.26 Sandia Corp Report SC-4219(TR). A Method for Determining the Position of a Towed Vehicle with Respect to the Towing Aircraft, by M. T. Kane and F. G. Blottner. August 1958

3.3.27 United Aircraft Corp Report B 110128-1. Extension of Underwater Towing Cable Theory to High Speeds, by J. W. Clark, Sept 1963

3.3.28 Underwater Sound Lab TM 933-0175-64. Towline Configuration and Forces, by K. T. Patton, CONFIDENTIAL 26 Oct 64

3.3.29 Underwater Sound Lab Technical Memorandum 933-257-64. Derivation of Equations for Maximum VDS Towline Tensions Under Dynamic Conditions, by J. R. Solin. 19 Aug 1964

3.3.30 Whicker, L. F. The Oscillatory Motion of Cable-Towed Bodies, (Ph.D. Thesis, University of California), 1957

3.4 Flutter

3.4.1 Boeing Company Report D2-133006-1. Tests and Investigations of a High Speed Towed Sonar Cable; Final Report June 1966

3.4.2 Canada. Engineering Research Assoc. Report 56-1. Dynamics of Towed Underwater Systems Part 1 Stability of the System, by J. R. Richardson Apr 65

3.4.3 Kaman Aircraft Corp. Report G-69. Dynamic Characteristics of Streamlined and circular cables; Interim Engineering Report. 12 Aug 1954

3.4.4 North American Aviation SID 65-1279, 1 thru 4; Final Report High-Speed Towing Cable Development (Phase I-II, Volumes 1-4) CONFIDENTIAL 29 October 1965

3.5 Divergence

3.5.1 North American Aviation SID 65-1279, 1 thru 4; Final Report
High-Speed Towing Cable Development (Phase I-II, Volumes 1-4)
CONFIDENTIAL   29 October 1965

3.5.2 Naval Underwater Weapons Research and Engineering Station
TM 366. Analytical Investigation of Faired Cable Performance
in a Tethered System, by A. R. Lagasse. July 66

SESSION III. Faired Cable Hydrodynamics

1) It was pointed out that the method of analysis presented in Mr. Calkin's paper neglected the effects of cable curvature on the generation of the hydrodynamic forces. The analysis assumed that the forces on a segment of the towline are independent of their position along the catenary.

The validity of the assumption of superposition of the normal and tangential flows, on which the analysis was based, was also questioned. Mr. Calkins explained that the assumption had been validated initially by theoretical analysis and subsequently had been substantiated by experimental wind tunnel investigations. It was found that for the assumptions made concerning the type of flow, i.e., fully attached laminar or turbulent flow, the method of superposition could be used to predict the forces on a three-dimensional swept wing (towline).

2) Use of a surface plate at the air/water interface to eliminate the towline ventilation cavity was questioned. Dr. Whicker stated that the use of the surface plate eliminated the cavity with no effect on the cable surface angle. However, he pointed out, there were large increases in the towline tension, and the surface plate was discarded as a consequence.

Dr. Whicker was asked whether or not the derived loading functions from the test data were used to compute the tension and depth so that a comparison with the measured values could be made. He replied that this had not been done as yet.

A question was asked on the type of boundary layer that would be expected at the test Reynolds number. Dr. Whicker felt that at the speeds at which the tests were conducted (20 knots) it was expected that the boundary layer would be fully turbulent. This would be due to both the surface condition of the towline, and the type used - that is, a cable with clips and other components that would tend to trip the boundary layer at the cable leading edge.

3) Mr. Folb commented that three-dimensional surface effects were accounted for in fairing model tests on the fairing dynamometer by varying the submergence of the model and plotting the measured forces as a function of depth. As these plots became linear, they were extrapolated to zero depths so that the amount that remains is the so-called free surface or wave-making force. This free-surface force is then subtracted from the total force. The force curve, Mr. Folb explained, becomes linear after a depth of approximately one chord is exceeded.

4) Mr. Gibbons summarized his sea trials as follows:

   a. The depressor used in the tests weighs approximately 150 pounds in water.

   b. Speed was measured with the DTMB knot meter, which is accurate down to 0.2 knots.

c. The tests were conducted under zero sea state conditions.

d. Monitored during the tests were the pitch and roll of the body, the towline angle at the body and at the craft, towline tension at the body and the tow craft, and speed.

A model of the cable used in the sea trials was tested on the fairing dynamometer to measure the normal and tangential loads over the same Reynold's Numbers as were run in the trials. The results of the correlation between this and the sea trial data will be released at a later date.

5. Mr. Goodman was asked about the dependence of the test results on the amplitude of the disturbance. He answered that although amplitude was not varied in the series of tests performed, the test data of Hafner seemed to indicate that there was no marked effect from amplitude.

Mr. Goodman was also asked whether any discernible bending of the models existed during the tests. He replied that these models were constructed of stainless steel, and that essentially no deflection took place. He also pointed out that the tests were conducted on essentially rigid sections so that the results would be applicable to the type of faired towline exemplified by the North American design. The probability of extending these data to an analysis of the flexible Boeing type seems remote at this time, although the possibility of testing a flexible model in the channel was discussed.

SESSION 4
Towed System Sea Trial Evaluation

Mr. C. N. Miller
Navy Electronics Laboratory

High Speed Towing Tests of the Boeing and
North American Towlines

HIGH SPEED TOWING TESTS
OF THE BOEING AND NORTH AMERICAN TOWLINES

by Charles N. Miller
Co-Host
Navy Electronics Laboratory
San Diego, California

ABSTRACT

Under separate contracts with the Navy Electronics Laboratory, the Boeing Company
and North American Aviation produced short lengths of experimental faired towline.
Towing tests in Lake Washington, Seattle, using an instrumented, winged depressor,
verified the predicted frontal area towline drag coefficients, 0.05 and 0.06 re-
spectively, within the limits of experimental error, to a maximum speed slightly
greater than 40 knots.

DESCRIPTION OF THE TOWLINES

The contract awards to Boeing and North American were based on the technical evalua-
tion of twelve proposals received in response to a request for proposals which was
advertised and solicited to some twenty-one corporations. The two design concepts
selected offered distinctly different, promising, and untried approaches to the
solution of the stated performance goals. The NEL goal is an advance in the state-
of-the-art thru the development of a stable, low drag towline to permit VDS opera-
tion from high speed, load sensitive surface vehicles, such as planing craft, hydro-
foils, and hovercraft. The support of two parallel developmental efforts was jus-
tified as a means of increasing the probability of success. As of now, there is
insufficient evidence to make an unequivocal decision regarding the overall super-
iority of one towline over the other. From a hydrodynamic viewpoint, the towlines
are essentially equivalent. Mechanically, each has good and bad features peculiar
to itself.

The Boeing towline:[1]

The fairing shape is a NACA 63A022 section with a chord of 2.64 inches and thick-
ness of 0.58 inches fig. 1. The towline is a composite assembly consisting of an
epoxy bonded glass fiber strength member in the nose portion, with the main body
composed of Hypalon rubber. Two coaxial electrical cables are imbeded in the rub-
ber, and the entire structure is covered with a bonded and rubber impregnated
Dacron jacket. The towline is continuous without any joints or discontinuities
throughout its length. The design ultimate strength was 37,500 pounds minimum.
Development of adequate end fittings proved to be a major technical problem. Work
was discontinued after an end fitting design capable of reliably developing 23,000

lbs ultimate strength was produced, since with the specified safety margins, this was conservative for the anticipated loads during the Lake Washington towing tests. Thirty-two and 116 foot sections were produced for the towing tests. Additionally, a number of shorter samples were produced for fatigue, strength, flexure, and environmental testing.

The North American towline:[2]

This towline is an articulated assembly consisting of rigid, steel links, four feet long. The shape is an NACA 0020 section, of 1.80 inch chord, and 0.36 inch thickness, fig. 1. The forward portion is the tension member and is machined from 17-4 PH stainless steel. The after portion is a polypropylene extrusion. Two coaxial cables are housed in the central cavity formed at the junction between the fairing and strength member. The links are connected with pin joints which provide freedom of chord plane motion still retaining stiffness in torsion, and for bending normal to the chord plane. The design ultimate strength of 25,000 lbs was verified by Laboratory tests. Since the center of tension is aft of the hydrodynamic center, the towline is statically unstable. Stability was assured by adding plastic vanes to every other joint. Fig. 2. As with the Boeing contract, North American provided 32 and 116 foot lengths for tow testing as well as additional samples to verify the design fatigue and tensile strength.

TEST SITE

The towing tests were conducted by Boeing at two locations on Lake Washington, Fig. 3. The land base for the operation was the Boeing factory at Renton, at the extreme southern end of the lake. This was conveniently located only a few hundred yards from the shallow water range, used during towing tests of the thirty-two foot Boeing towline. The 116 foot Boeing towline and both North American towlines were tested about five miles north of the Renton base in water about 150 feet deep. An anchored barge adjacent to the midpoint of the straight line section of the test course was headquarters for operational control for these tests. Data sensed on the towing craft was radioed to the control barge and displayed on a multichannel graphic recorder for use by the test supervisor. The same data was also received by radios on a data van on the closest spot on the lake shore, and tape recorded for subsequent analysis. In addition to serving as a floating basing point for operational control of the tests, and providing logistics support for the towing craft, the barge also supported a vertical array of eight line hydrophone which was employed to obtain radiated acoustic noise data from the tow craft, towline, and depressor. The directivity and spacing of the line hydrophones permitted discrimination between these separate sources. Representatives of NEL were present during all of the tests, and North American engineers were on the site when their towline was being handled or towed.

TOWING CRAFT AND DEPRESSOR

Finding a vehicle suitable for tow testing of these developmental towlines proved to be somewhat of a problem. The goal was to tow the 116 foot lengths to a maximum speed of 45 knots through a range of depression angles from 40 to 70 degrees. (The depression angle is defined as the angle between a longitudinal horizontal through the tow point, and a line from the tow point through the towed depressor.) The most promising craft for this job was Boeing's Hydrodynamic Test System, (HTS). HTS is a hydroplane powered by a J-48 jet engine.[3] Fig. 4. Her top speed is greater than 80 knots, and at a speed of 45 knots, she has excess thrust of about 3500 lbs. Fig. 4 shows a structure in the open space between the pilot's and copilot's stations. This is a force balance and is used to support foil and strut test specimens in the hydrodynamic testing program for which HTS was originally built. To reduce the gross weight and facilitate towline handling, this structure was temporarily removed.

The tow point is approximately amidship and on the centerline, requiring the use of scuba divers for cable attachment. The basic configuration of the depressor is shown in Fig. 5. The wing, tail, and horizontal stabilizer are made of steel. The effective depressor downward lift can be remotely controlled from the tow craft by adjusting the angle of the horizontal stabilizer over a range of 10 degrees. The main body is a hollow metal structure and houses the instrumentation and controls. The cavity is pressurized to 100 psi with dry helium to reduce the chance of water entry. A trailing recovery float is attached at the end of a 250 foot steel cable. This cable was normally kept under slight tension whenever HTS was docked along side the barge to prevent inadvertent rotation of the depressor relative to HTS.

Since the towline strength member and the fairing are integral for both designs, a twist in the strength member would produce a non zero angle of attack of the fairing and a resulting side force. North American engineers pointed out that the Boeing proposed, Hooke's joint between the depressor and the towline would cause the fairing to assume a destabilizing angle of attack whenever the towline was deflected out of the vertical plane in the direction of the tow craft motion. It was North American's suggestion that the depressor and towline be decoupled in yaw by the addition of a swivel at the point of attachment. As an alternate, and partial solution, Boeing recommended canting the roll axis, Fig. 6, which would result in a stabilizing force for all side deflections so long as the forward tilt of the towline never exceeded the angle which would result in the roll axis being tilted down forward. This expedient was adopted and the towing tests were conducted with the roll axis inclined 30 degrees from the normal chord line.

INSTRUMENTATION

The purpose of the towing tests was to verify the predicted stability limits, forces, towline configuration, and radiated acoustic noise. To achieve this, appropriate sensors were located in the depressor, HTS, and the barge. Fig. 7. In the interest of safety the pilot of HTS was provided with a cable tension read out. Other significant measurands were continuously monitored on the barge. Permanent magnetic tape recordings of all data except for radiated noise were made in the shore based data van. The acoustic noise data were recorded on magnetic tape on the barge. Table I identifies the variables which were measured. Except for the measurement of depressor location relative to HTS all of the sensors were

conventional and were employed in a normal fashion. Depressor position was determined acoustically by a system of tri-lateration, Fig. 8. Two hundred and fifty kHz pulses at a repetition rate of 35 pulses per second were transmitted from the depressor and received at two hydrophones on HTS, one located on the outboard edge of each sponson. The horizontal separation of the two receivers was 15 feet. By measurement of the mean transit time of the pulses from the depressor to HTS, the slant range could be determined. This information, coupled with measurement of the time difference of arrival of the same pulse at the two receivers, permitted determination of the cross trail of the depressor. The computations were made automatically by an analog computer and displayed graphically on the barge, and recorded in the data van. Certain limitations of this system should be pointed out. Due to self-noise of HTS and the low acoustic output of the source, the system functioned to a maximum speed of 35 knots with the 32 foot towline, and to only 15 knots with the 116 foot towline. The estimated accuracy of crosstail determination was + 2 feet for the 116 foot towline, with proportionately greater accuracy for the shorter towline. The system is of course sensitive to both yaw and roll of HTS. Since the tests were conducted in the relatively calm waters of a lake, the unsteady motion of HTS had a negligible effect on the system's performance. However, it should be pointed out that scientists at the Defense Research Laboratory, University of Texas, working with U.S. Navy support, have been pursuing the development of similar equipment for the location of VDS bodies towed from ships at sea. In DRL's case, compensation for the complex translational and rotational motions of the towing ship must be made, and are in fact, the major part of the technical problem.[4]

Since the towline contained only two coaxial cables, and there were some eleven variables to be sensed at the depressor, the data was multiplexed. The most convenient method, and one previously developed and currently employed by Boeing in their work for the U.S. Navy on FRESH I, an experimental, jet powered, twin hulled hydrofoil, was frequency multiplexing, using an IRIG standard. The data were radioed from HTS to the barge for "quick look" monitoring, and to the shore data van for permanent recording, as mentioned above. Radiated underwater acoustic noise was measured for the long sections of the Boeing and North American towlines, using an array of eight line hydrophones suspended vertically below the barge.[3] The hydrophones were spaced approximately twelve feet apart so that the upper hydrophones "saw" HTS, and the lower ones "saw" the depressor. Band pass filters restricted the recorded energy to the band from 10 to 30 kHz. At the lower and upper frequency limits, the total beamwidths of the hydrophones to the 3dB points were 11 and 3 degrees respectively.

Determination of the apparent source strength of the towlines required knowledge of the range from the hydrophone string during the recording interval. This was done with an optical ranging system which worked as follows: A surveying transit was modified to provide switching information at these predetermined positions. The three switches were positioned in a horizontal plane 45 degrees apart, as shown, in Fig. 9. HTS was manually tracked by this transit throughout the run. The time duration within the sight lines A to B and B to C were recorded on separate electronic counters. A graph was prepared from which the distance of HTS, measured perpendicular to the barge was obtained. It was assumed that HTS velocity was constant during attainment of optical ranging data. It was not necessary for the HTS track to be parallel to the edge of the barge, since the track position is uniquely determined from the two interval measurements if the assumption of constant velocity is satisfied.

For each day's operation, a test plan was prepared setting forth the specific conditions under which data were to be recorded, each test condition was numbered as an event. For each towline tested, data acquisition was planned for each of the nominal speeds and depressor stabilizer settings of the event matrix shown in Fig. 10. Intermediate data points were to be added at nominal speeds of 10, 20, 30, and 40 knots for certain tests.

As soon as possible after the towline test commenced on each test day, the behavior of the towline was observed at idle speed of HTS and with the depressor stabilized at +4°. Under this reference test condition, a careful check was made for possible towline installation and and instrumentation errors. With the horizontal stabilizer set at +4° (maximum down force) HTS was accelerated slowly to 5 knots and the speed and course stabilized for a minimum of 15 seconds. During this period, data were recorded. Upon satisfactorily completing the 5 knots, +4° event, HTS slowly accelerated to the next test event and stabilized as before. Whenever one of the monitored towline or depressor parameters exceeded the limits set in the daily test plan, the test was immediately stopped and a decision made as to whether to again attempt the called-for test event, to cancel the test event, or to add an intermediate event. Based on the real time display at the barge of the towline/depressor behavior, on course modifications were made to the test plan.

Figures 11 and 12 show the testing matrices which were actually executed during the towline evaluation. For large stabilizer angles, corresponding to maximum towline tension, maximum depth, and maximum angle of depression, towing speed was limited by available HTS thrust. For lower stabilizer angle settings, corresponding to minimum tension, minimum depth, and minimum angle of depression, towing speed was limited by system instability. Instability was sometimes oscillatory and sometimes divergent, and when present appeared in the form of coordinated depressor roll and side trail amplitude in excess of the preset limits. It should be noted that the testing matrix for the longer Boeing towline, indicates that a 95 foot section was tested rather than the 116 foot section which was manufactured. Early in the program this length was inadvertently towed with a 360 degree twist. This accident weakened the upper end requiring the removal of 21 feet, accordingly all data used in analysis were derived from measurements on the 95 and 32 foot sections.

DATA REDUCTION

Data averaged over a one second time period were used for the towline performance calculations. From each test event, which consists of 15 seconds of test data obtained during stabilized HTS speed and headings, a one second period of representative data was selected. The event time listed for the selected event sample was the reference point for the one second period.

From the test magnetic data tape, digitized data were obtained for an eight second period that encompasses the one second of representative data. Processing systems and procedures used for digitizing are described in Ref. 5. An average of the one second digitized sample was calculated and corrected, if necessary, for instrumentation shifts in zero and calibration values. These average data are entered on

data sheets entitled "Tabulations for Calculations." A digital computer program was written to correct these tabulated data for an earth axis reference system and the calculated average total drag coefficient for the tow line and fairings.

The acoustic data were analyzed by playing the magnetic tape recordings through a set of 1/3 octave filters centered at 10, 12.5, 16, 20, 25, and 31.5 kHz, and recording the output on graphic level recorders. The levels were corrected for range, and the beam pattern of the hydrophone. The final results are presented in source level per unit length of towline.

RESULTS

1. Hydrodynamic: The test matrices for the Boeing and North American Aviation towlines delineate the limits of cable performance based on system stability. It should be pointed out that these are system stability limits and not necessarily towline stability limits. In fact, there is evidence that with proper yaw de-coupling at the attachment of the towline to the depressor, these limits could be advanced to higher speeds and shallower depression angles. Using the Lake Washington test data, Boeing computed the towline drag per foot for normal incidence at 45 knots for their towline 6, 7, 8. Using the available test data and slightly different computations, NEL made an independent assessment of towline drag.[9] Finally, the test data were given to North American Aviation and they made their own calculations of towline drag.[10] The range of results are summarized below:

Estimated 45 knot drag per foot at normal incidence

based on Lake Washington tests

	minimum	maximum
Boeing towline	14.2 lbs	15.1 lbs
North American towline	10.4 lbs	12.3 lbs

2. Acoustic: The amount of acoustic data are very limited. The primary purpose of the towing tests was to measure drag and system stability It was agreed to gather acoustic data on a non-interference basis. Data were only obtained on some of the higher speed runs with the 95 foot Boeing towline and the 116 foot North American towline. In these runs, data from the lower hydrophones appeared to be dominated by depressor noise, and data from the upper hydrophones contained mainly noise from HTS. Among the data which appeared valid, there were large variations from event to event. Within the limits of variability, both towlines appeared to be about equal as noise sources. Fig. 13. is a plot of noise versus speed for the Boeing and North American towlines. The single data point for the 5/16 inch wire rope was obtained by Boeing using HTS and the same measuring, re-cording, and analysis equipment used for the two faired towlines.

SUMMARY

Two faired towlines of radically different design have been successfully towed to speeds in excess of 40 knots and have exhibited lower drag than any previously tested designs. Within experimental error the normal drag computed from the experimental test data agrees with the predicted drag based on best currently available theory. System instability was exhibited at increasing speed and decreasing angles of towline depression. This is believed to be the result of roll-yaw coupling between the depressor and towlines, and probably could be reduced or eliminated by redesign of the towline-depressor attachment.

REFERENCES

(1) Boeing Document D2-89924-1, Final Report, Development of High-Speed Towing Cables/Underwater Towed Body, 12 January 1966, CONFIDENTIAL

(2) North American Aviation Documents, SID 65-1279-1 (Vol. I), SID 65-1279-2 (Vol. II), Final Report, High Speed Towing Cable Development, 29 October 1965, CONFIDENTIAL

(3) Boeing Document D2-89921-1, High Speed Towing Tests, March 1966, Unclassified

(4) University of Texas, Defense Research Laboratory, Quarterly Progress Report No. 5, Contract NObsr-93126, U.S. Navy Bureau of Ships, 31 March 1966, CONFIDENTIAL

(5) Boeing Document D2-84138-1, TDPC AMSO Data Processing Systems & Procedures January 1966, Unclassified

(6) Boeing Document D2-89921-2, High Speed Towing Tests. Test Results of NEL-2-B-Series Cables, March 1966 CONFIDENTIAL

(7) Boeing Document D2-89921-3, High Speed Towing Tests, Test Results of NEL-3-NA-Series Cables, March 1966, CONFIDENTIAL

(8) Boeing Document D2-133009-2, Cable Towing Test System Critique Cable Performance Analysis, August 1966 CONFIDENTIAL

(9) NEL Technical Memorandum 990, A Preliminary Evaluation of the High-Speed Towing Capability of: FRESH I, H.S. DENISON, PC(H), September 1966 CONFIDENTIAL

(10) North American Aviation Document C6-2525/020, Evaluation of Test Results of NAA High-Speed Tow Cable, October 1966 CONFIDENTIAL

TABLE 1. VARIABLES MEASURED.

Variable	Range	Sensor
ON HTS		
Boat trim angle	$\pm 30°$	Vertical gyro
Cable tension	0-7500 lbs.	Strain gage
Cable inclination angle	$0-90°$	Pot.
Cable azimuth	$\pm 10°$	Pot.
Q	0-40 PSI	Strain gage pressure transducer
Slant range	0-150 ft.	Ultrasonic transducers
Side trail	± 50 ft.	Ultrasonic transducers
AT DEPRESSOR		
Body pitch angle	$\pm 15°$	Vertical gyro
Body roll angle	$\pm 30°$	Vertical gyro
Cable tension	0-7500 lbs.	Strain gage
Cable inclination	$0-90°$	Pot.
Body depth	14.7-70 PSIA	Strain gage transducer
Q Total	14.7-70	Strain gage transducer
Body yaw rate	$\pm 30°/sec$	Yaw rate gyro
Stabilizer angle	$\pm 5°$	Pot.

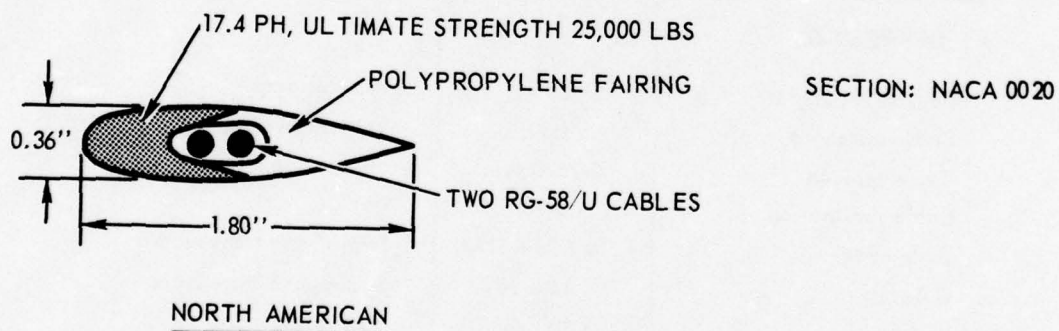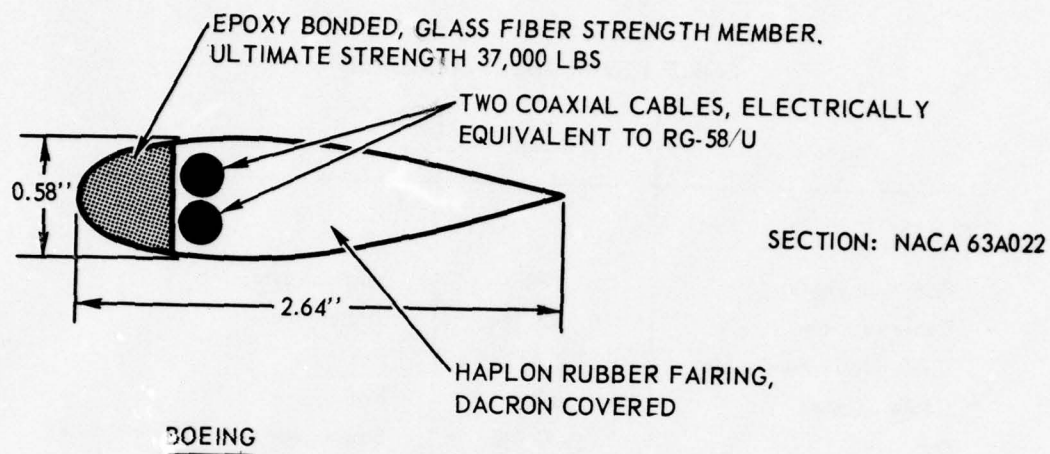Figure 1. Boeing and North American towline sections.
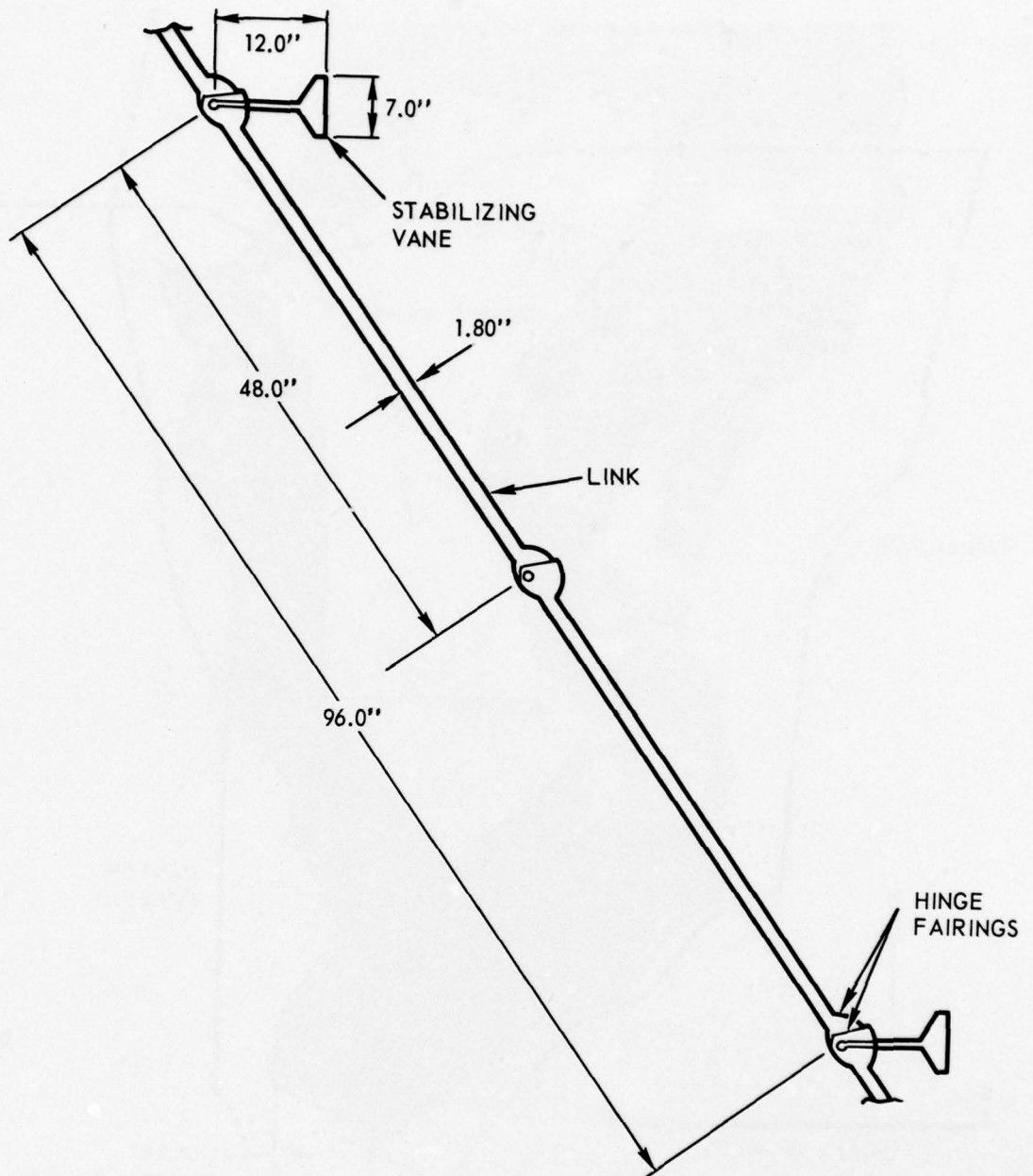
Figure 2. *North American towline, showing stabilizing fins at every other joint.*

363

SEATTLE

FLOATING BRIDGE

DEEP WATER COURSE

INSTRUMENT BARGE

SUNSET HIGHWAY

RANIER AVE.

MERCER ISLAND

SHALLOW WATER COURSE

N

RENTON FREEWAY

0   1   2
SCALE OF MILES

BOEING RENTON DIVISION

OPERATING BASE

RENTON
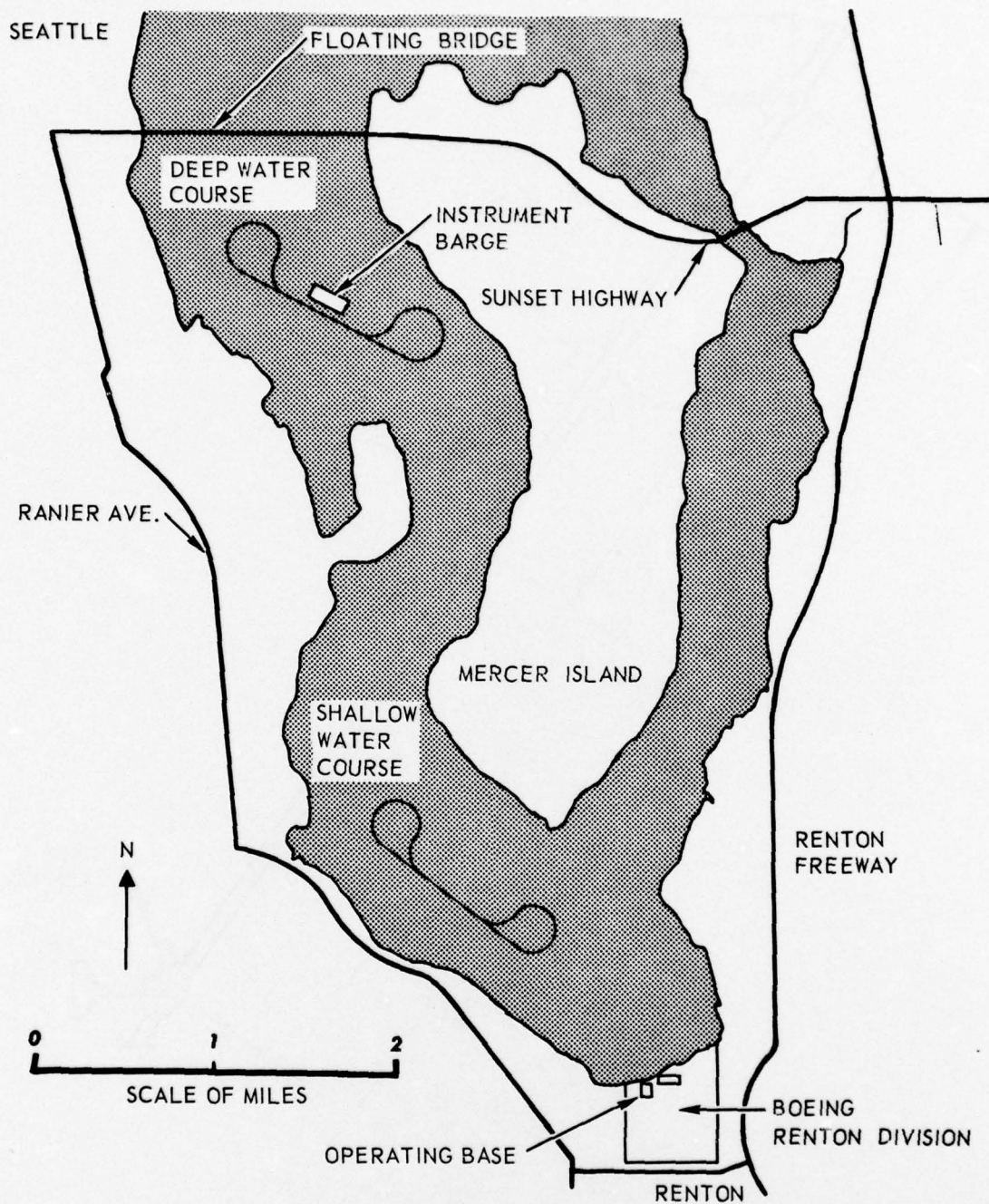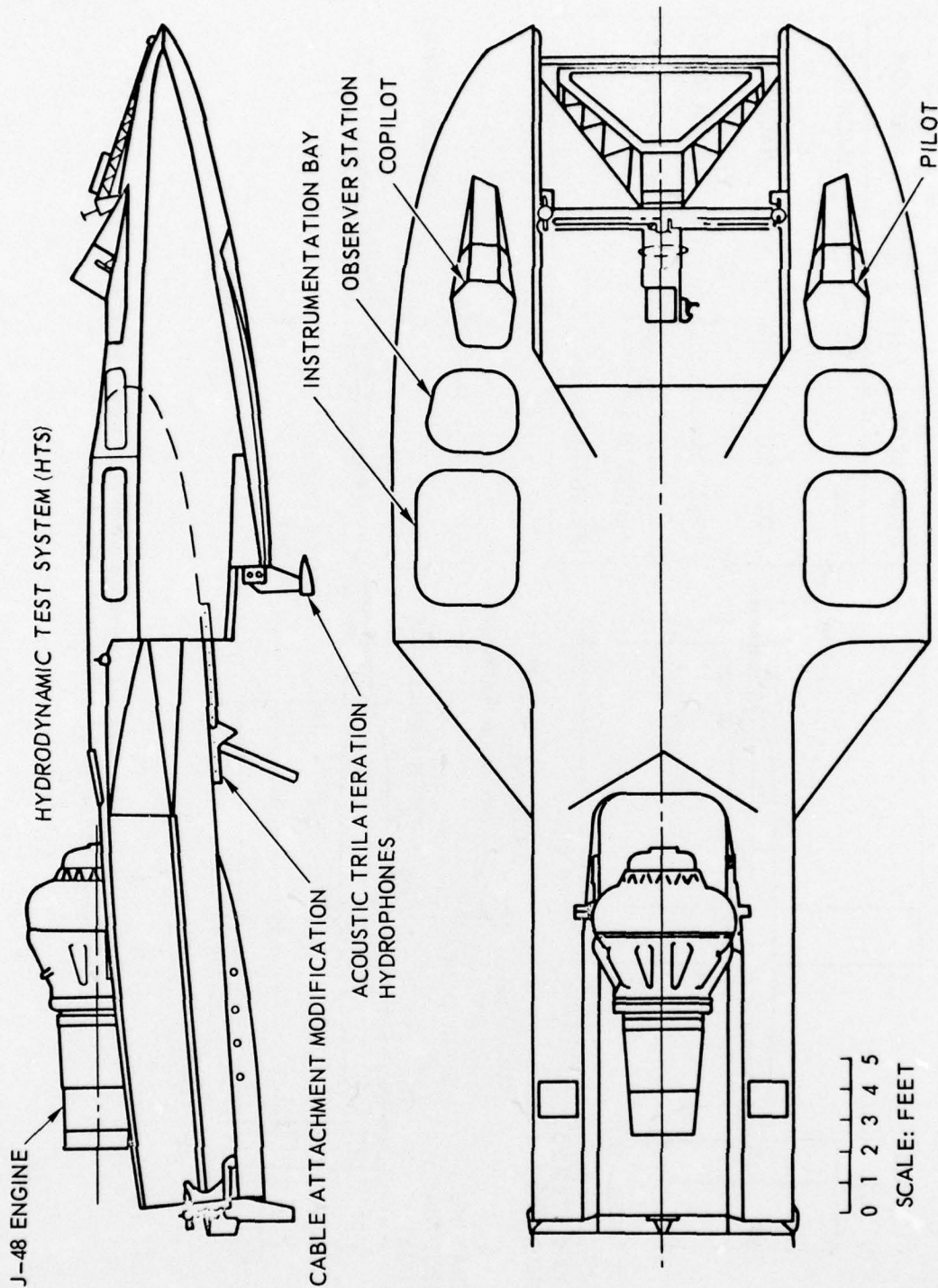
Figure 3. Test area.

Figure 4. HTS (Hydrodynamic Test System). The Boeing hydroplane used for towing the Boeing and North American developmental towlines.

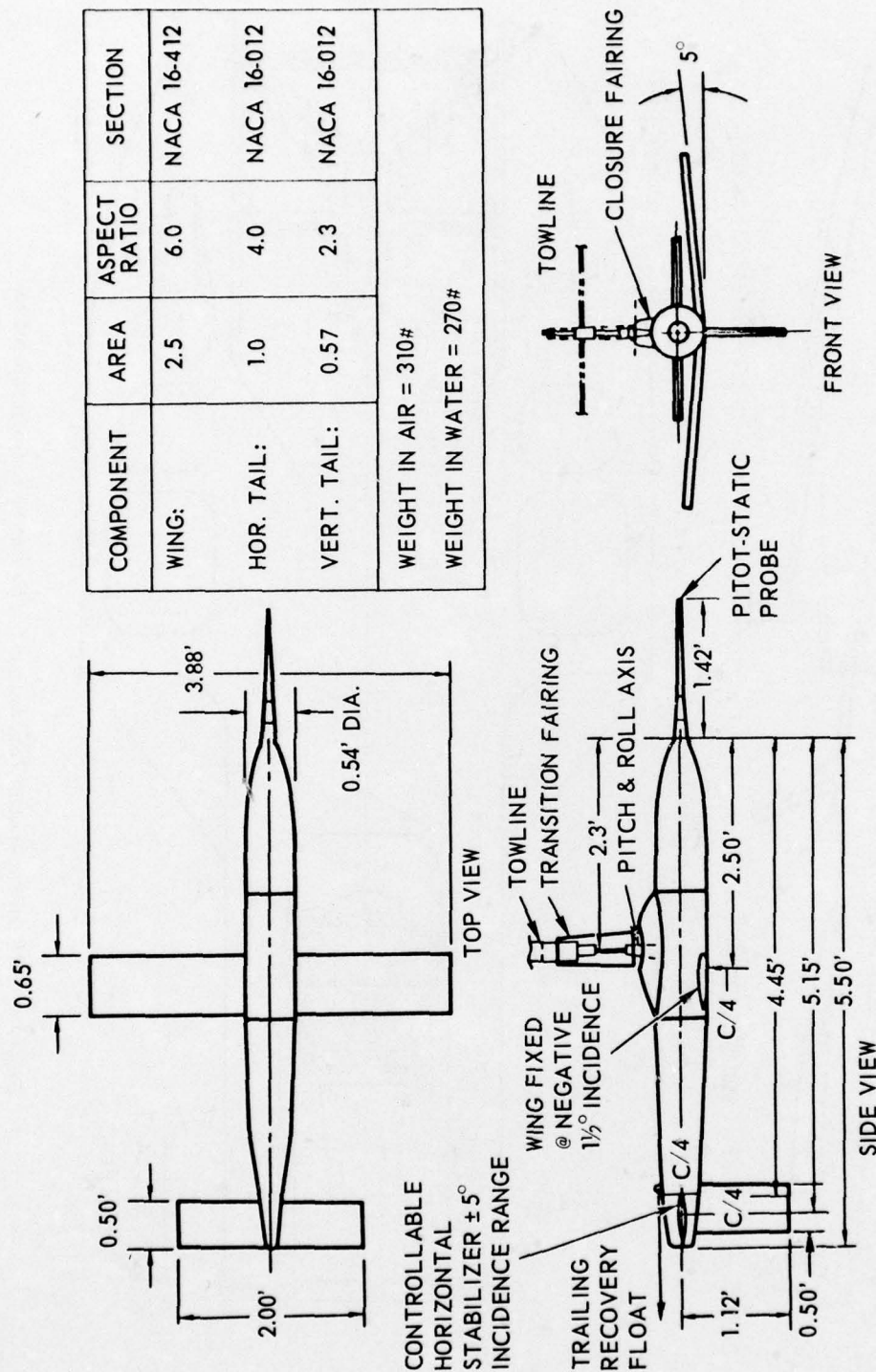| COMPONENT	AREA	ASPECT RATIO	SECTION
WING:	2.5	6.0	NACA 16-412
HOR. TAIL:	1.0	4.0	NACA 16-012
VERT. TAIL:	0.57	2.3	NACA 16-012

WEIGHT IN AIR = 310#
WEIGHT IN WATER = 270#

Figure 5. Towed depressor. Wing and empennage are made of steel. Instrumentation and controls are housed in pressurized cavities within body.
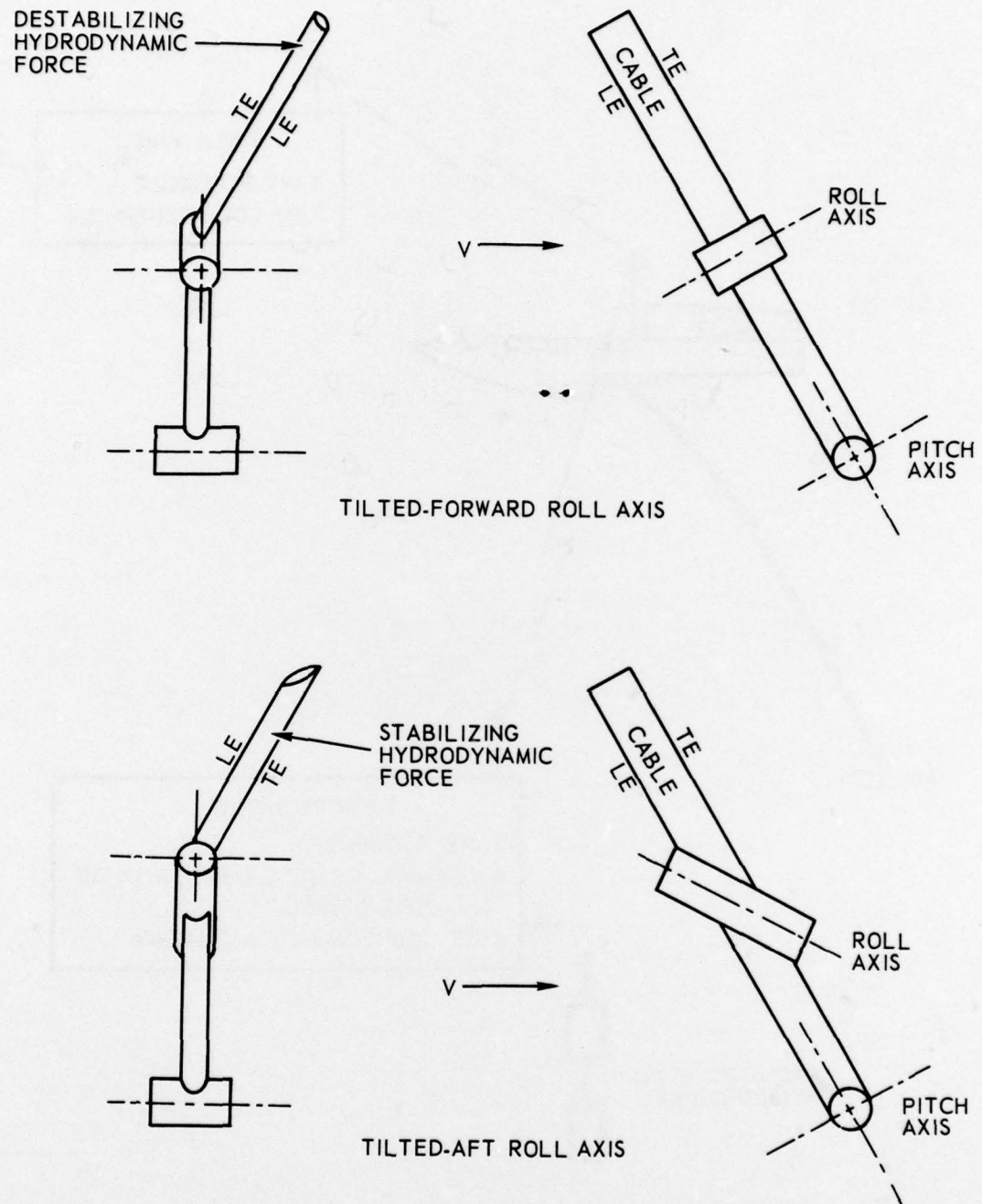
Figure 6. Effect of roll axis orientation on sway-angle divergence.
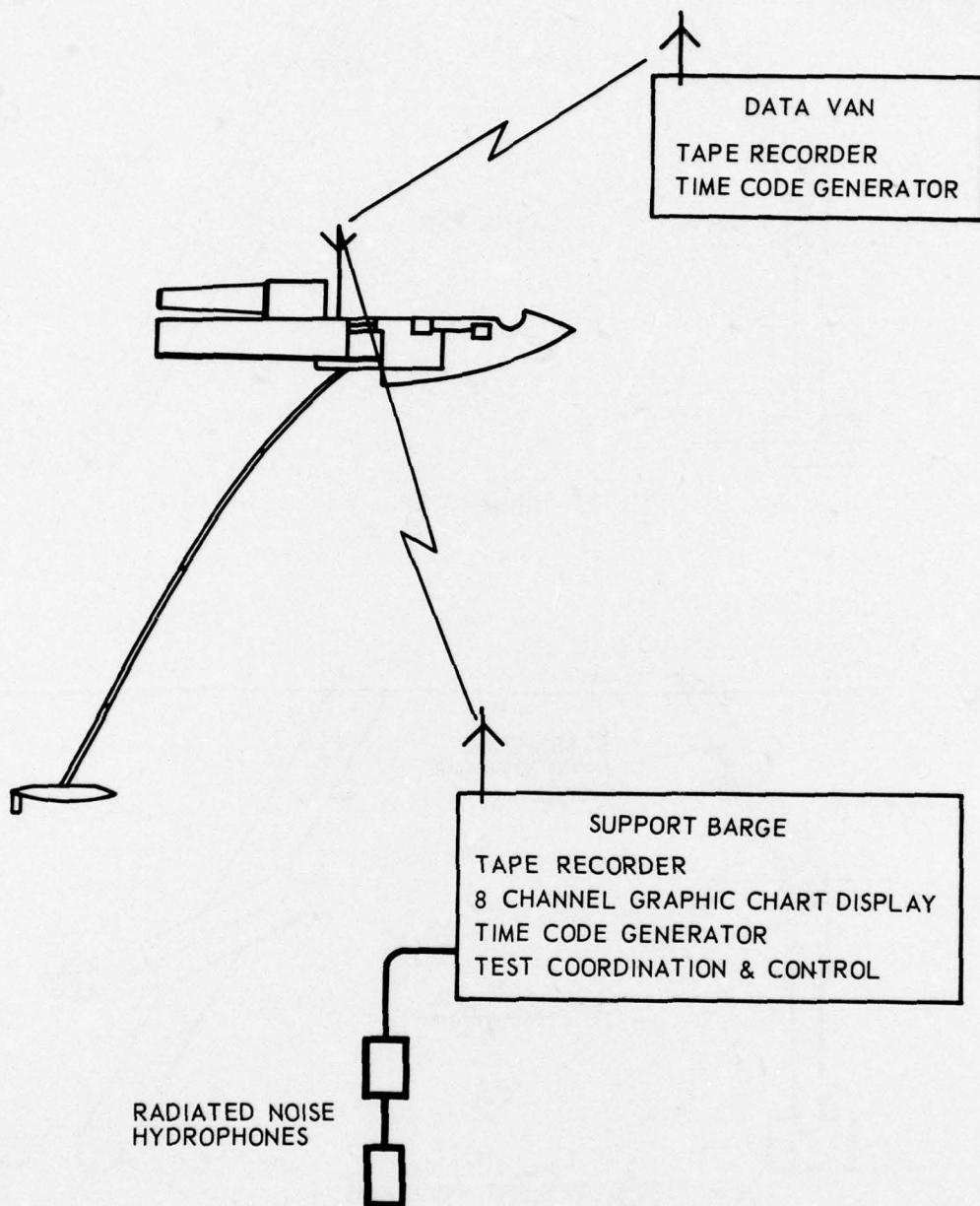
Figure 7. General arrangement for monitoring and recording tow test data.

MEASURE:
    Y – DEPTH, STATIC PRESSURE
    r_1 & r_2, ACOUSTIC

CALCULATE:

$$r \approx \frac{r_1 + r_2}{2}$$

$$X - TRAIL = \sqrt{r^2 + y^2}$$

$$Z - CROSS\ TRAIL \approx \frac{r(r_2 - r_1)}{S}$$
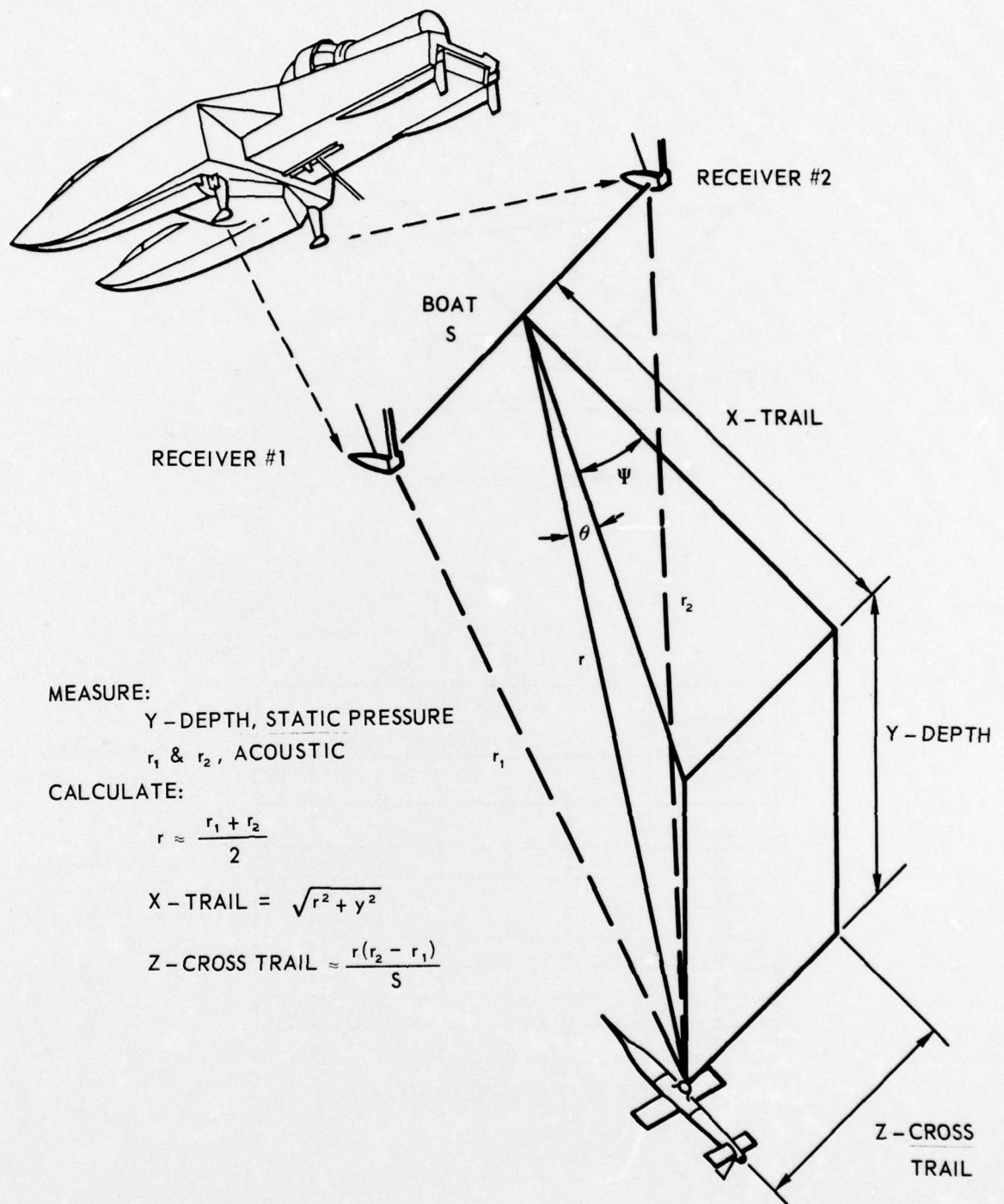
Figure 8. Acoustic trilateration system for determination of depressor position relative to HTS.

369
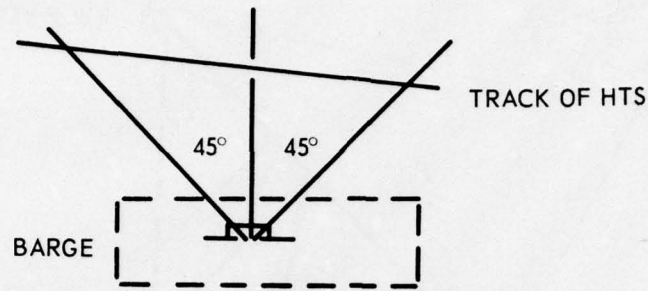
Figure 9. Optical ranging system

Depressor Stabilizer Setting, Degrees	Nominal HTS Speed – Knots					
	Idle	5	15	25	35	45
+4						
+3						
+2						
+1						
0						
−1						
−2						
−3						

FIGURE 10. TEST EVENT MATRIX.

Depressor Stabilizer Setting, Degrees	Nominal HTS Speed – Knots								
	Idle	5	15	20	25	30	35	40	45
+4	•	•	•		•		•	Thrust lim.	
+3	•	•	•		•		•		
+2	•	•	•		•		•	•	
+1	•	•	•	•		•	•	•	
0	•	•	•	•	•	•	•	•	
−1	•	•	•	•	•	•			
−2	•	•	•	•	•			Stability limited	
−3	•	•	•	•					

(a) Boeing 32 foot towline.

Depressor Stabilizer Setting, Degrees	Nominal HTS Speed – Knots								
	Idle	5	15	20	25	30	35	40	45
+4	•	•	•		•		•	Thrust lim.	
+3	•	•	•		•				
+2	•	•	•		•				
+1	•	•	•		•				
0	•	•	•				Stability limited		
−1	•	•	•						
−2	•	•	•						
−3	•	•							

(b) Boeing 95 foot towline.

FIGURE 11. TESTING MATRICES FOR BOEING TOWLINE.

Depressor Stabilizer Setting, Degrees	Nominal HTS Speed – Knots									
	Idle	5	10	15	20	25	30	35	40	45
+4	•	•	•	•	•	•	•	•	Thrust lim.	
+3	•	•	•	•	•	•	•	•	•	
+2	•	•	•	•	•	•	•	•	•	
+1	•	•	•	•	•	•				
0	•	•	•	•	•	•				
−1	•	•	•	•	•	•		Stability limited		
−2	•	•	•							
−3	•	•	•							

(a) North American, 32 foot towline.

Depressor Stabilizer Setting, Degrees	Nominal HTS Speed – Knots									
	Idle	5	10	15	20	25	30	35	40	45
+4	•	•	•	•	•	•	•	•	Thrust lim.	
+3	•	•	•	•	•	•	•	X		
+2	•	•	•	•	•	•	•	X		
+1	•	•	•	•	•	•	•	X		
0	•	•	•	•	•	•	•			
−1	•	•	•	•	•	•	•	Stability limited		
−2	•	•	•	•	•	•				
−3	•	•	•	•						

X – Cancelled due to pairing damage

(b) North American, 116 foot towline.

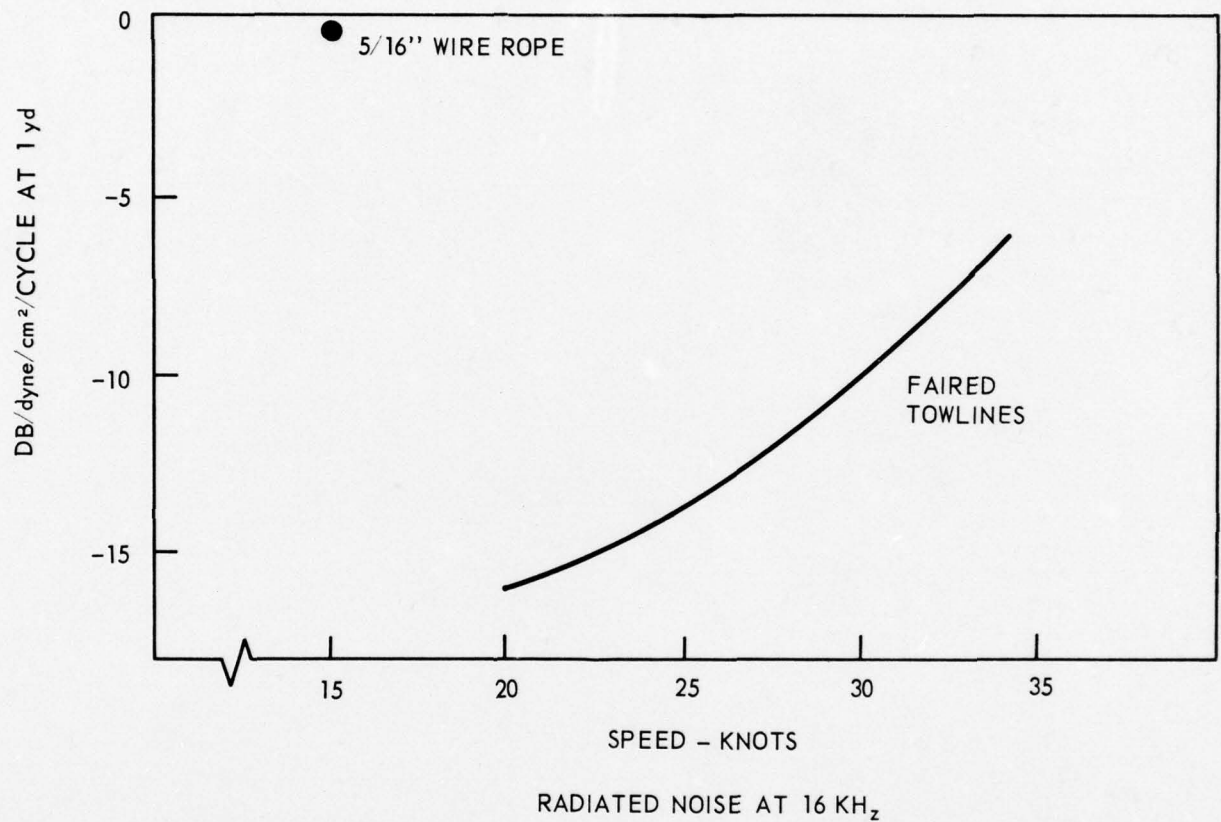FIGURE 12. TESTING MATRICES FOR NORTH AMERICAN TOWLINE.

Figure 13. Radiated noise per yard. Curve is mean value for Boeing and North American towlines, since the differences were negligible. Data point for 5/16" wire shown for comparison.

SESSION 4

TOWED SYSTEM SEA TRIAL EVALUATION

Bibliography

4.0 TOWED SYSTEM SEA TRIAL EVALUATION

4.1 Boeing Co. D2-23504. High-Speed Towing Cable Development, Final Report. 31 July 1964

4.2 Boeing Co. D2-89921-1. High Speed Towing Tests; Test Methods and Procedures March 1966

4.3 Boeing Co. D2-89921-2, Volumes 1-2. High Speed Towing Tests; Test Results of NEL-2-B Series Cables CONFIDENTIAL (Volume 2, Analog Data Unclassified) March 1966

4.4 Boeing Co. D2-89921-3, Volumes 1-2 High Speed Towing Tests; Test Results of NEL-3-NA Series Cables, CONFIDENTIAL (Volume 2, Analog Data, Unclassified) March 1966

4.5 Boeing Co. D2-89921-3, Volumes 1-2 High Speed Towing Tests; Test Results of NEL-3-NA Series Cables, CONFIDENTIAL (Volume 2, Analog Data, Unclassified) March 1966

4.6 Boeing Co. D2-133009-1. Cable Towing Test System Critique; Volume I, History and Experience August 1966

4.7 Canada. Naval Research Est., Dartmouth Tech Note FM/65/6 Quarter Scale Trilby Body - Model II - Towing Trials, by L. A. Byckler. Feb 65

4.8 David Taylor Model Basin Report C-905. Towing Characteristics of the 1/4-Scale AN/SQA-S Sonar Body, by L. F. Whicker and T. Gibbons, CONFIDENTIAL, January 1958

4.9 David Taylor Model Basin Report C-1172 An Investigation of the 1/3 Scale AN/SQS-17 Variable-Depth-Sonar Body Based on Constrained-Model and Calm-Water Cable-Towing Tests, by S.M.Y.Lum. May 1960

4.10 Great Britain Admiralty Experiment Works Report 36/58 Over Stern V.D.A. pull in Towing Cable When Ship Turns. August 1958

4.11 Great Britain Admiralty Underwater Weapons Est. Tech Note 109/63 Assessment of Stability and Drag of Certain Underwater Bodies when Towed in Line Ahead Formation, by E. H. Constable. Jan 63

4.12 Hydrospace Research Corporation Report 102 Hydrodynamic Design of a Maneuverable Hydrophone Line Array, by J. J. Nelligan CONFIDENTIAL 6 January 1963

4.13 Hydrospace Research Corp. Rept 119. Investigation of Hydrodynamic Loading on Faired Towline, by S. M. Gay, A Brisbane and (others). 17 June 64

4.14 Mine Countermeasures Station, Panama City, Fla. Data Report 5414(GD-5)-14 The AN/SQS-15 Variable Depth Sonar Evaluation Status and General Test Outline. 18 June 1954

4.15 Navy Mine Defense Lab Rept i-105 Towed Underwater Vehicle System, by W. R. Sherman. Aug 66

4.16 North American Aviation Report C6-2525/020 Evaluation of Test Results of NAA High-Speed Tow Cable CONFIDENTIAL 19 October 1966

4.17 Navy Research Lab Letter Report No. C-4000-18A/52. Ship Towed Sonar; Interim Report of Recent Field Trials of Towed Sonar for Small, Slow Speed Ships, by I. Cook. CONFIDENTIAL 17 January 1952

4.18 Tracor, Inc. Document 64-108-C Experimental Study of the Attitude Behavior of the AN/SQA-10 VDS Fish, by K. L. Oehler. 14 Jan 1964

4.19 Underwater Sound Lab TM 933-168-63 Effect of Towed-Body Mass on Slack Towline Effects, by F. B. Rakoff. 21 June 63

4.20 Underwater Sound Lab Technical Memorandum 933-0119-63 Cold Weather Tests of AN/SQA-10 VDS Towline Fairing, by R. I. Welsh. 18 June 1963

4.21 Underwater Sound Lab TM 933-0255-65 AN/SQA-11 Towline Curves and Fairing Comprehensive Forces, by K. T. Patton. 10 Nov 65 CONFIDENTIAL

4.22 Underwater Sound Lab TM 933-448-65 Experiment Concerning Towline Kiting, by S. M. Rupinski. 16 Sep 65

4.23 Underwater Sound Lab TM 1230-070-60 Results of Tests of the B.F.G. Rubber-meehanite Fairing on the USS MALOY (EDE-791) by R.W.Pierce. 8 May 60

5.0 GENERAL

5.1 ASW Systems Project Office. Report of the Comprehensive Review Group; Variable Depth Sonar. 15 Apr 65

5.2 Boeing Co. Report D2-89925-1 Endurance and Seakeeping Characteristics of ASW Hydrofoil Ships with Towed Variable Depth Sonar. 2 Dec 65

5.3 Canada. Naval Research Est., Dartmouth Report PHx-95. The Canadian Variable Depth Sonar Project, by J. G. Retallack (and others) July 1955

5.4 Canada, Naval Research Establishment, Dartmouth. Tripartite Seminar on Hydromechanics of High Speed Towing, 18-22 October 1965 CONFIDENTIAL

5.5 David Taylor Model Basin. HML C-069-H-01. Feasibility Study of the Hydromechanic Aspects of an Interim Towed Sonar System for Hydrofoil Craft, by P. K. Spangler May 65

5.6 David Taylor Model Basin. Hydromechanic Aspects of Towing Problems, by G. B. Springston. 25 Sep 1963

5.7 David Taylor Model Basin Report C-958 Proceedings of the first tripartite Conference on Hydrodynamics of Ship-Towed, Cable-Body Systems, by W. M. Ellsworth, M. C. Eames and W. D. Chesterman. May 1958

5.8 General Dynamics. Convair. Feasibility Study on Application of Towed Sonar to Advanced Hydrofoil Craft, Phase 1 Report: Parametric and Pre-design Studies. n.d.   5/27/63

5.9 Grumman Aircraft Engineering Corp. Report M23.17, Part 1 AG(EH) Towed Towed Sonar Study, part 1 - Hydrodynamic Considerations, by T. B. Street. 30 Sep 1963 CONFIDENTIAL

5.10 Naval Air Defense Command Report NADC-AW-6229 Research and Development Program for Airborne Towed Vehicles. 8 Jan 1963.

5.11 Navy Electronics Lab TM 959 Status Review of the NEL Faired Cable Design Program, by D. E. Calkins 11 July 66 CONFIDENTIAL

5.12 Navy Electronics Lab TM 990 Preliminary Evaluation of the High-Speed Tow Capability of: FRESH-I, H.S. DENISON, PC(H). 20 Sep 66 by D. E. Calkins CONFIDENTIAL

5.13 Telephonics Corp. Report NR281-019 Study of a Towed Sonar System at Depths 600 feet to 1000 feet at 25 knots Ships Speed. CONFIDENTIAL

5.14 Underwater Sound Lab Report 532 Variable Depth Sonar - A Summary Report to 1962. 4 Jan 1962 CONFIDENTIAL